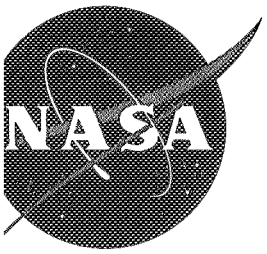

NASA Conference Publication 3332
Volume I

hirteenth Workshop for Computational Fluid)ynamic Applications in Rocket Propulsion nd Launch Vehicle Technology

N. Williams, Compiler

Proceedings of a workshop held at
Huntsville, Alabama
April 25–27, 1995

March 1996

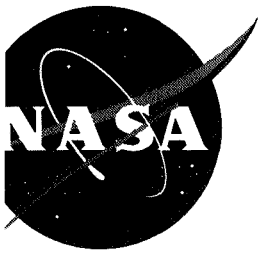

NASA Conference Publication 3332
Volume I

hirteenth Workshop for Computational Fluid ynamic Applications in Rocket Propulsion nd Launch Vehicle Technology

V. Williams, Compiler
rshall Space Flight Center • MSFC, Alabama

tional Aeronautics and Space Administration
ırshall Space Flight Center • MSFC, Alabama 35812

Proceedings of a workshop held at
Huntsville, Alabama
April 25–27, 1995

March 1996

THIRTEENTH WORKSHOP FOR COMPUTATIONAL FLUID DYNAMIC APPLICATIONS IN ROCKET PROPULSION AND LAUNCH VEHICLE TECHNOLOGY – VOLUME I

TABLE OF CONTENTS

TABLE OF CONTENTS (Continued)

THIRTEENTH WORKSHOP FOR COMPUTATIONAL FLUID DYNAMIC APPLICATIONS IN ROCKET PROPULSION AND LAUNCH VEHICLE TECHNOLOGY – VOLUME II

TABLE OF CONTENTS

TABLE OF CONTENTS (Continued)

Orbital Sciences Corporation OSC

Rockwell

X–34

Small Reusable Booster

Cooperative Agreement
No. NCC 8–75

X-34 System Concept is a Multi-Purpose, Reusable Commercial Launch Vehicle

Orbital Sciences Corporation

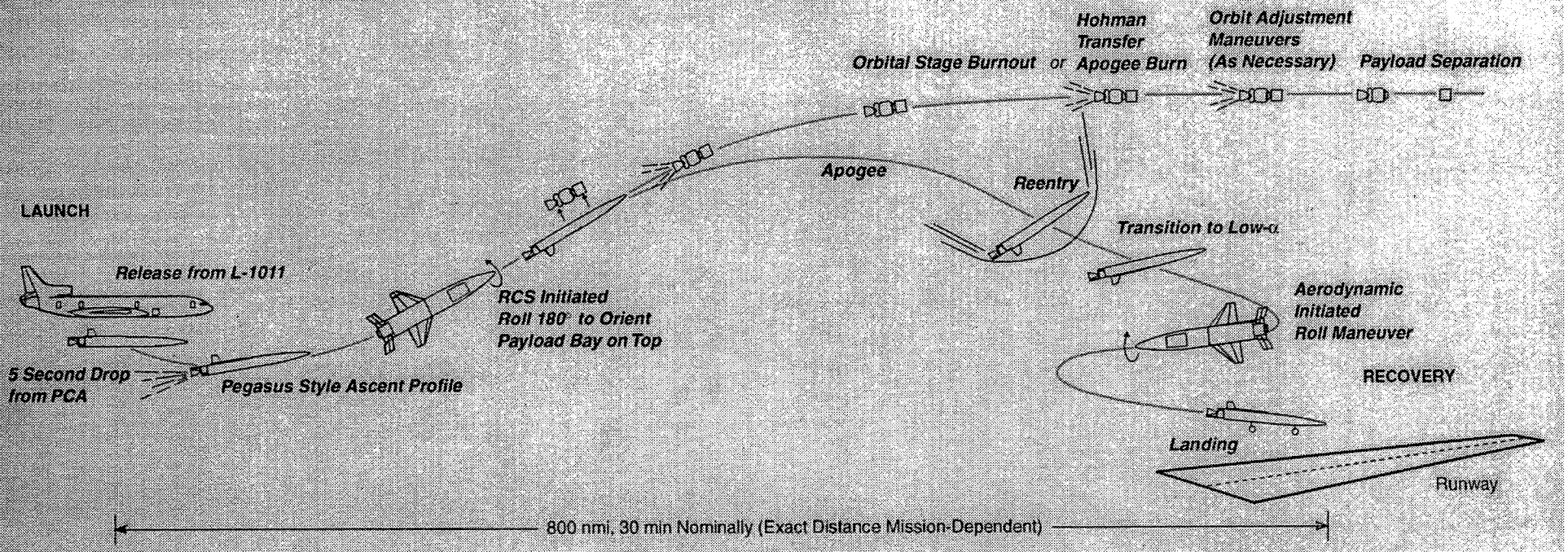

950328.08

L-1011 Launched Configuration

Orbital Sciences Corporation

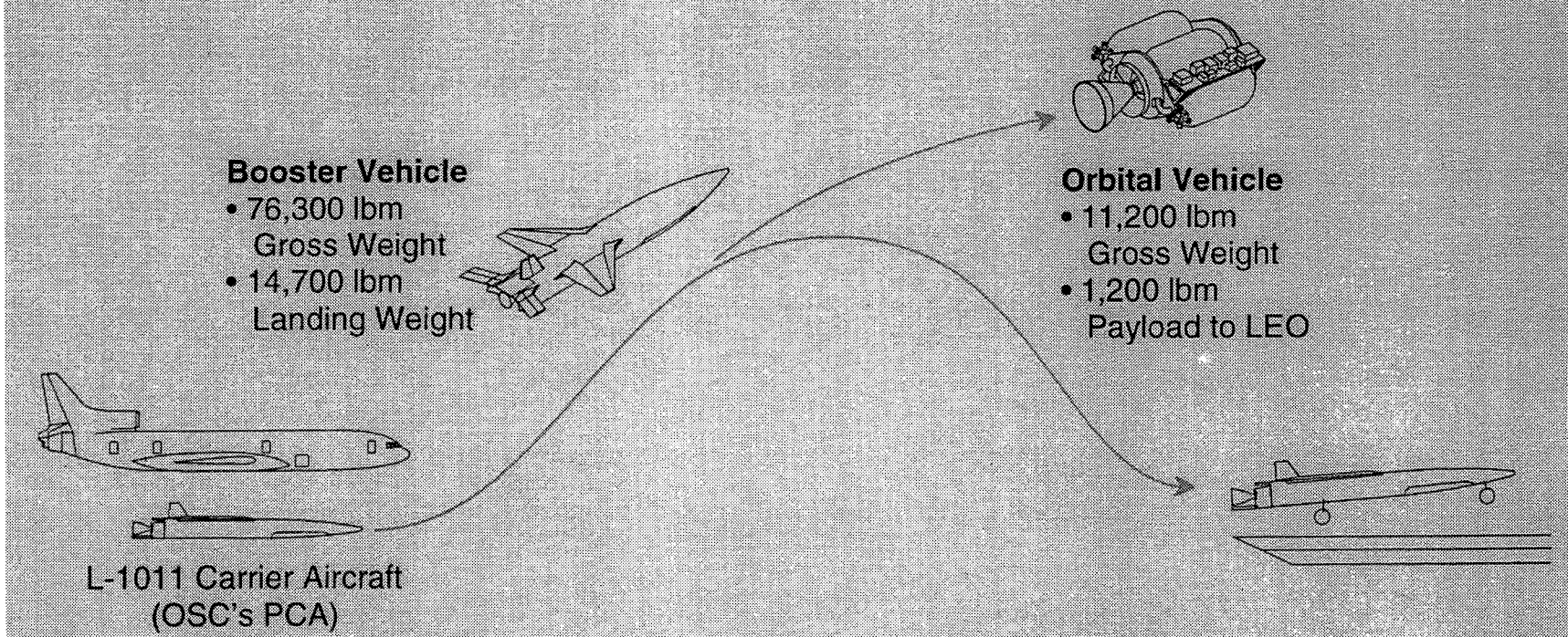

950328.11

B-747 Launched Configuration

Orbital Sciences Corporation

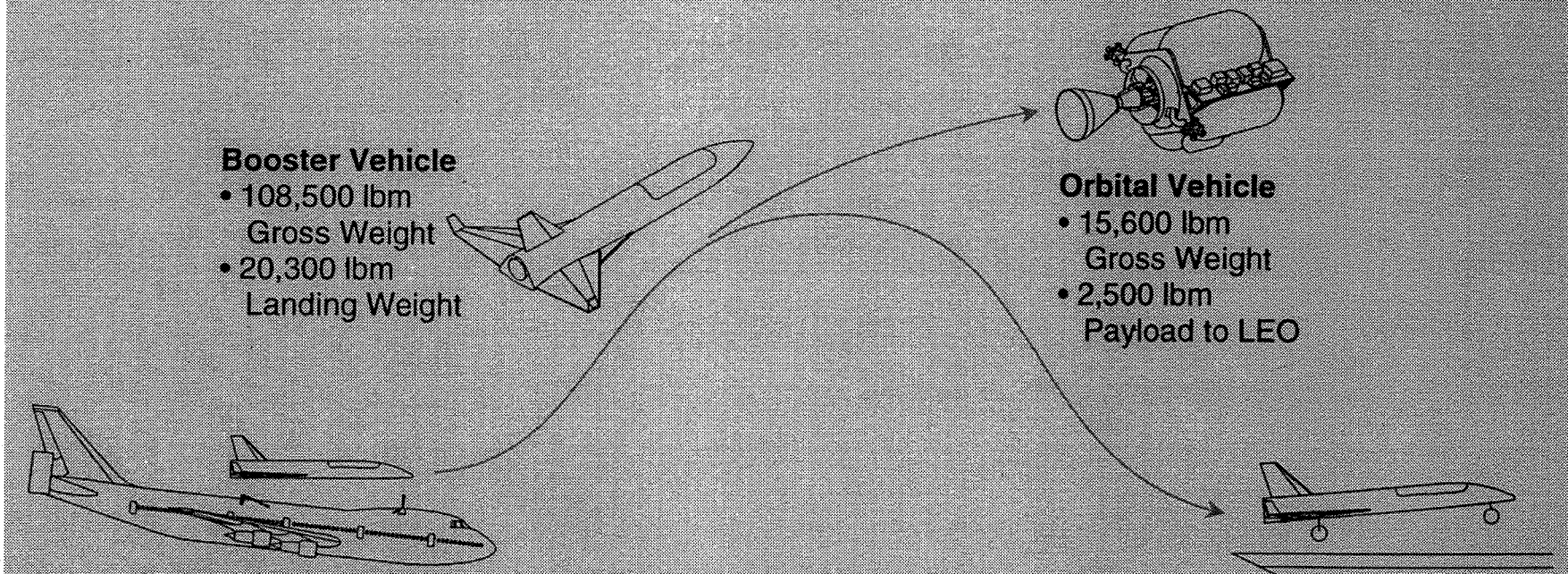

L-1011 Launched Configuration

Sciences Corporation

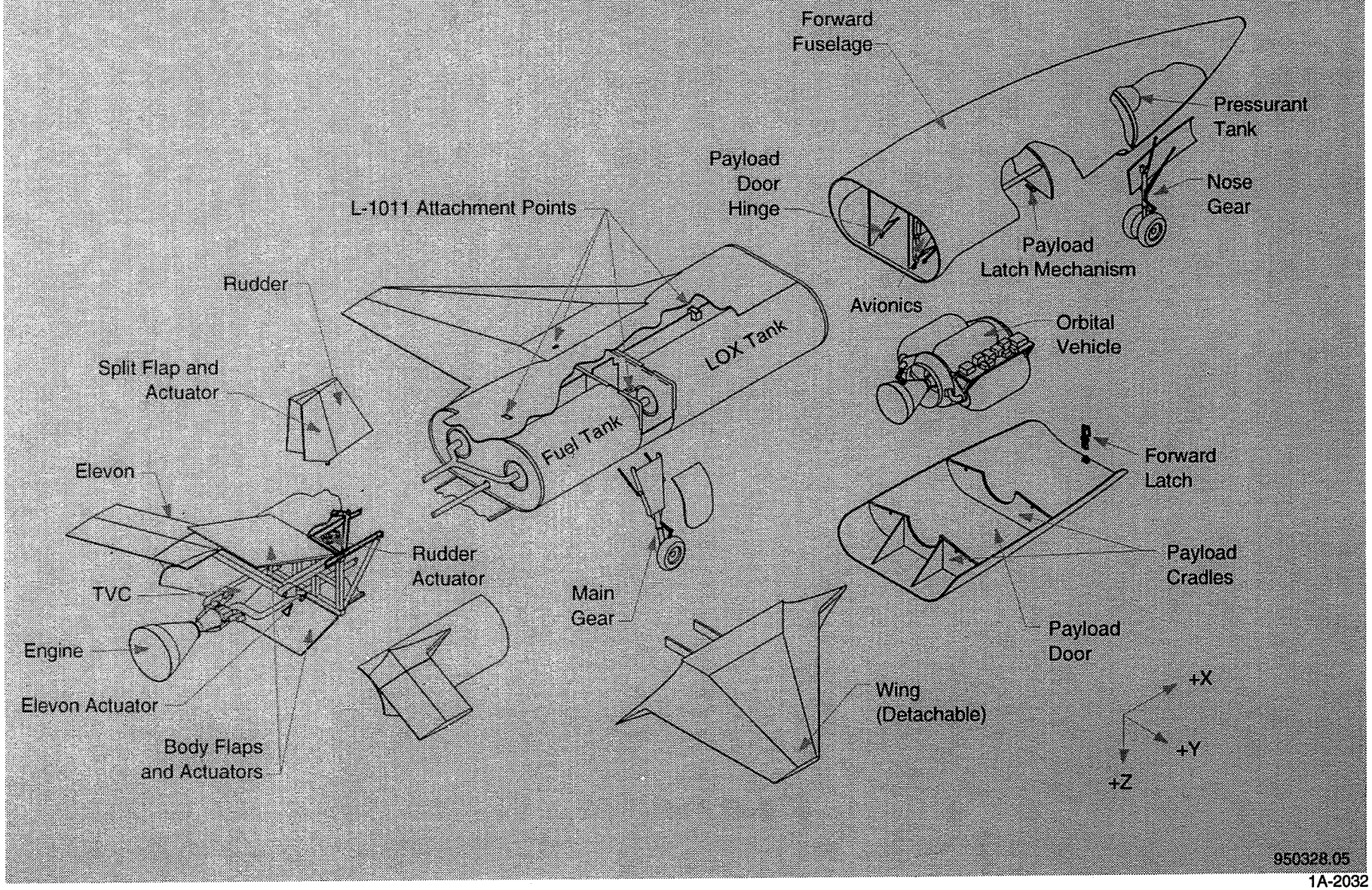

950328.05

1A-2032

B-747 Launched Configuration

Orbital Sciences Corporation

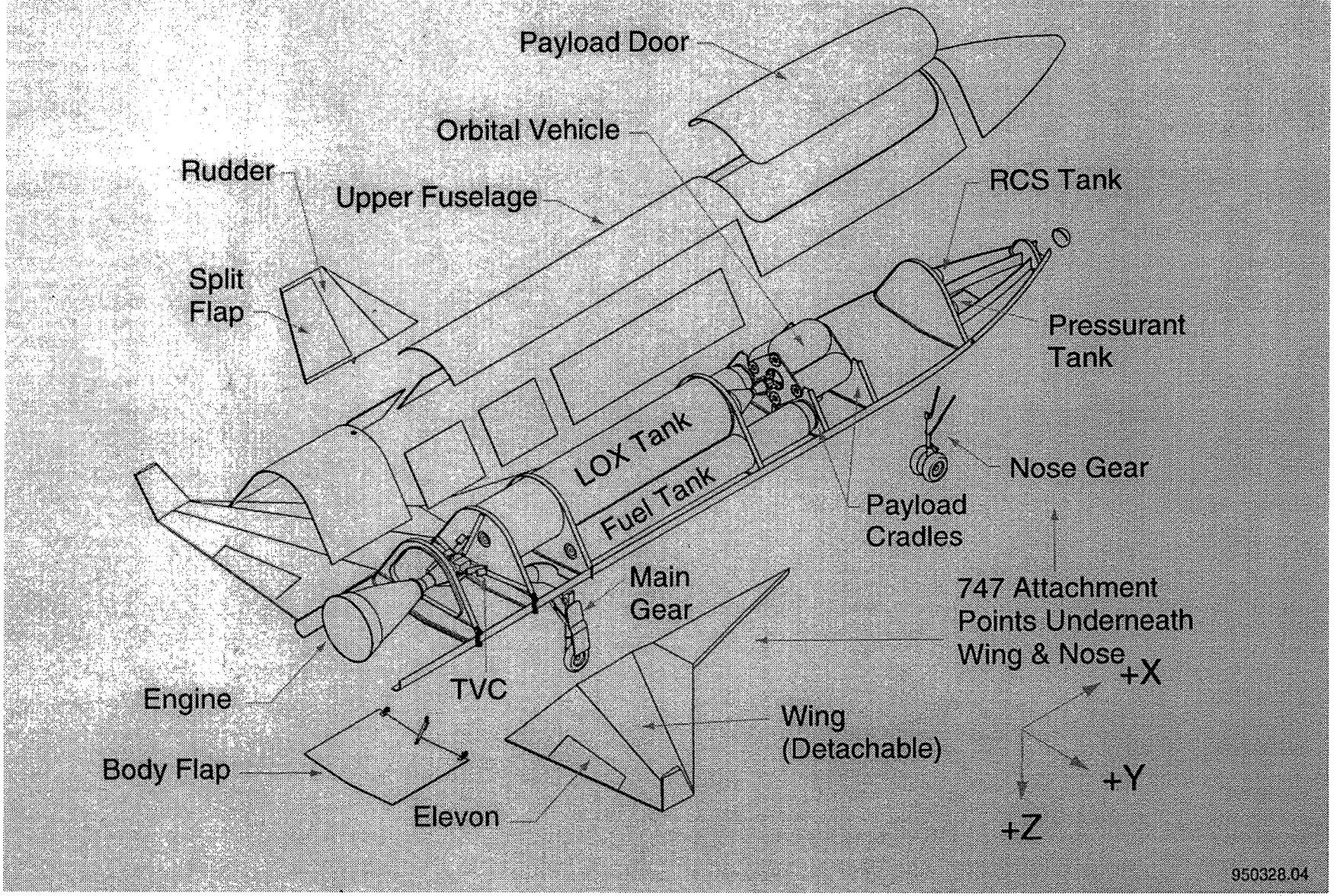

950328.04

1A-2033

Summary of X-34 Data

Sciences Corporation

	L-1011 Launched Configuration	B-747 Launched Configuration
Weight at Separation (Including Payload)	76,300 lb	108,500 lb
Landing Weight	14,700 lb	20,300 lb
Length	72 ft	88 ft
Wing Span	34 ft	50 ft
Fuselage Max Width	11 ft	13 ft
Orbital Vehicle Weight	11,200 lb	15,600 lb
Orbital Payload	1,200 lb	2,500 lb
Orbital Payload Volume	200 ft^3	550 ft^3

950328.06

1A-2036

X-34 Industry/Government Partnership Structure

Orbital Sciences Corporation

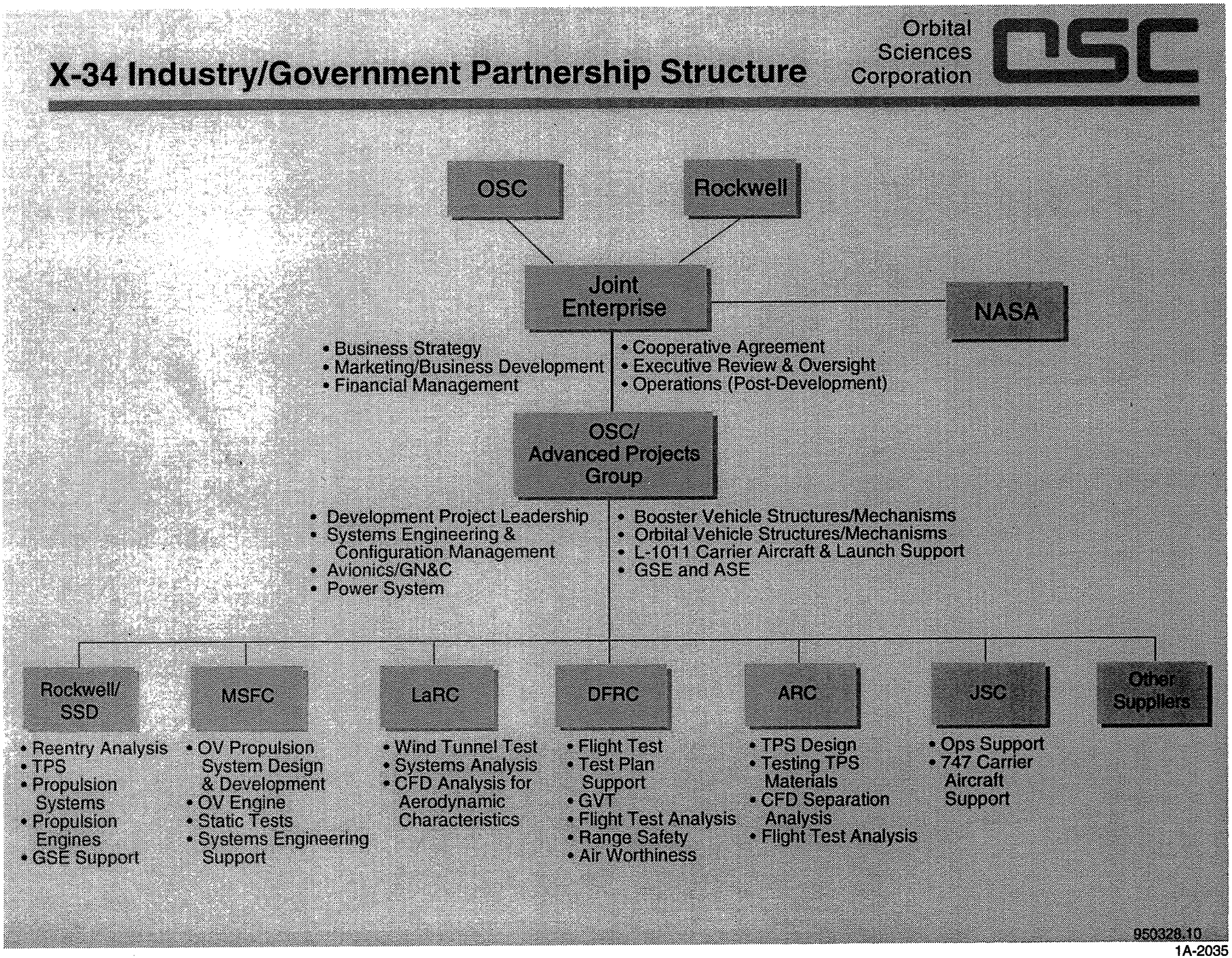

950328.10

1A-2035

Our X-34 Program Schedule Reflects an 18 Month Advance Start

Orbital Sciences Corporation

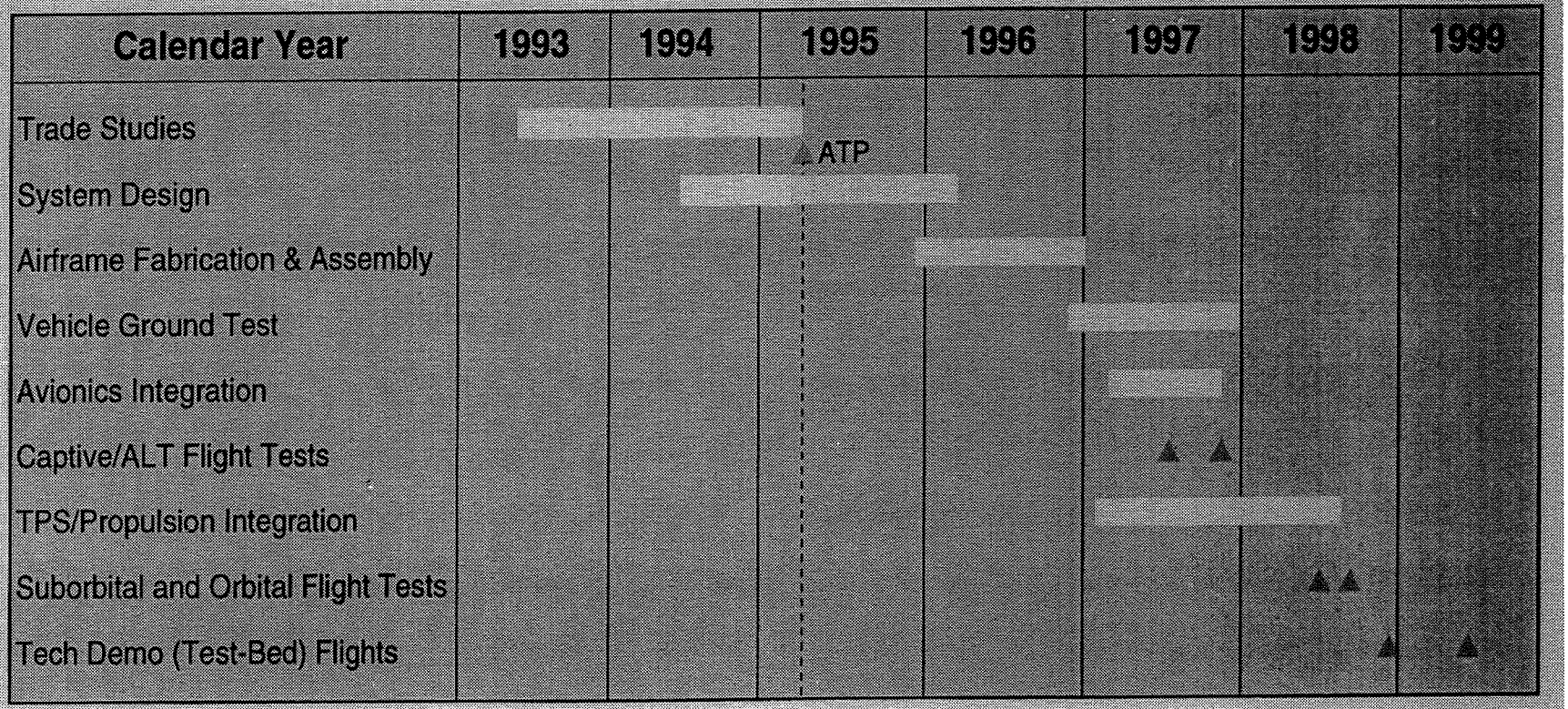

950328.07

1A-2034

X-34/747 SEPARATION CFD

AMES RESEARCH CENTER

APPLIED COMPUTATIONAL AERODYNAMICS BRANCH

Neal M. Chaderjian
Ph: (415) 604-4472, E-mail: nealc@nas.nasa.gov

Technical Approach

Static CFD validation, extrapolation to static flight conditions and dynamic separation maneuver using the Reynolds-averaged Navier-Stokes (RANS) equations.

- Compute three static wind-tunnel cases to validate RANS simulation with experimental data. Also, carry out one fine-grid computation to further assess solution accuracy and solution independence of grid.

- Recompute three previous static cases at flight conditions. (Remove any modeling of wind-tunnel walls and increase Reynolds number to flight conditions.) This provides extrapolation of wind-tunnel conditions to actual flight conditions.

- One RANS simulation of a 5 second separation maneuver. Compute carrier aircraft /X-34 trajectories and pitch angle by coupling dynamic CFD with three-degree-of-freedom flight-dynamic equations.

NASA Ames X-34 CFD Separation

B747 Surface Grids

CODE: Overflow/Navier-Stokes

Grid Communication: Chimera/Overset Interpolation

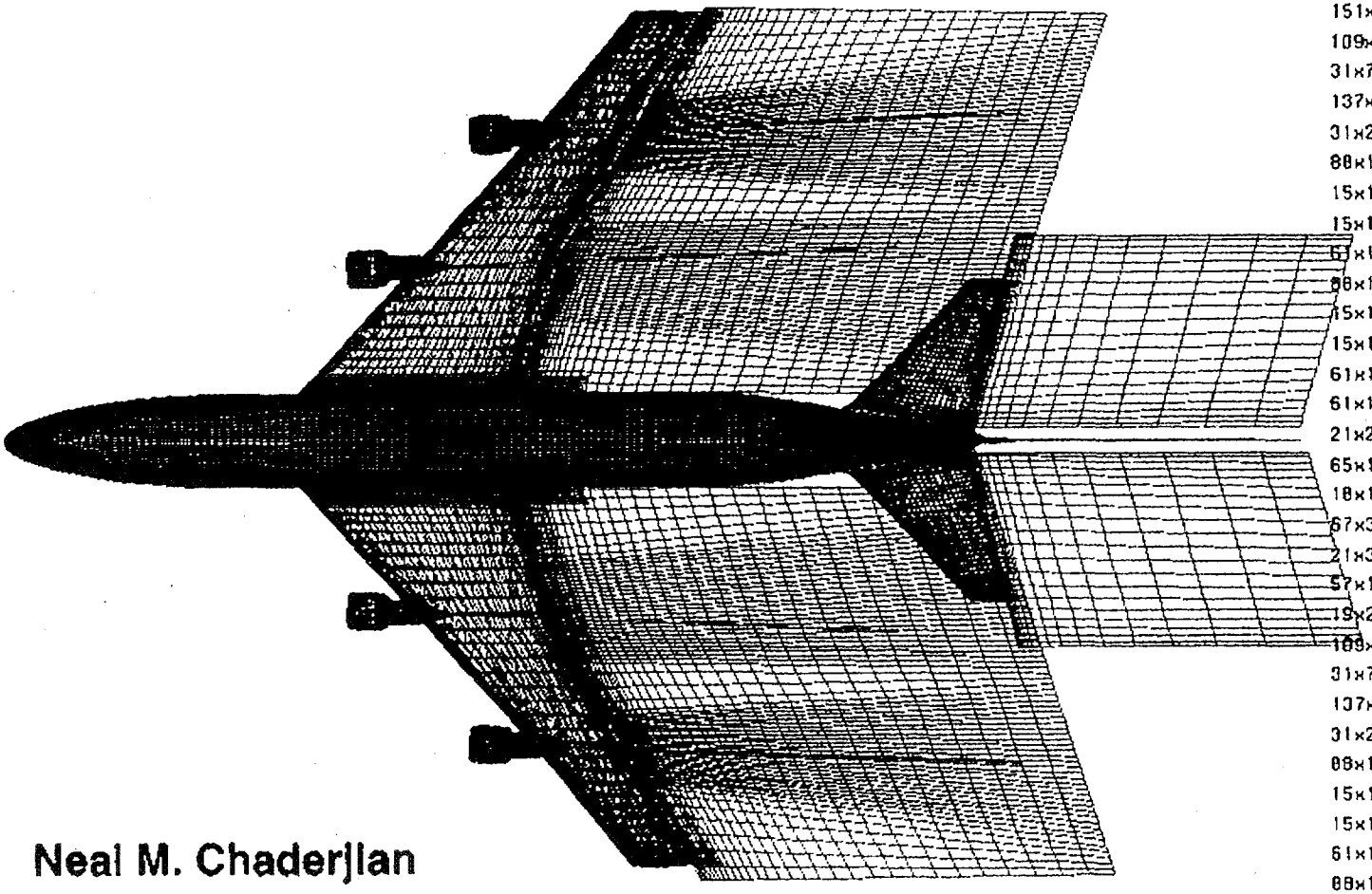

151x121x61	GRID 1
109x35x61	GRID 2
31x71x41	GRID 3
137x21x31	GRID 4
31x21x45	GRID 5
88x17x45	GRID 6
15x17x31	GRID 7
15x17x31	GRID 8
61x17x35	GRID 9
88x17x45	GRID 10
15x17x31	GRID 11
15x17x31	GRID 12
61x17x35	GRID 13
61x18x45	GRID 14
21x21x45	GRID 15
65x14x45	GRID 16
18x14x21	GRID 17
87x34x41	GRID 18
21x31x43	GRID 19
57x13x41	GRID 20
19x21x31	GRID 21
109x35x61	GRID 22
31x71x41	GRID 23
137x21x31	GRID 24
31x21x45	GRID 25
88x17x45	GRID 26
15x17x31	GRID 27
15x17x31	GRID 28
61x17x35	GRID 29
88x17x45	GRID 30
15x17x31	GRID 31
15x17x31	GRID 32
61x17x35	GRID 33
18x14x21	GRID 34
87x34x41	GRID 35
21x31x43	GRID 36

Neal M. Chaderjian

Page intentionally left blank

Reusable Launch Vehicle (RLV) Propulsion Technology

Jimmy Lee
NASA/MSFC

April 25, 1995

Vertical takeoff SSTO

Lifting Body SSTO

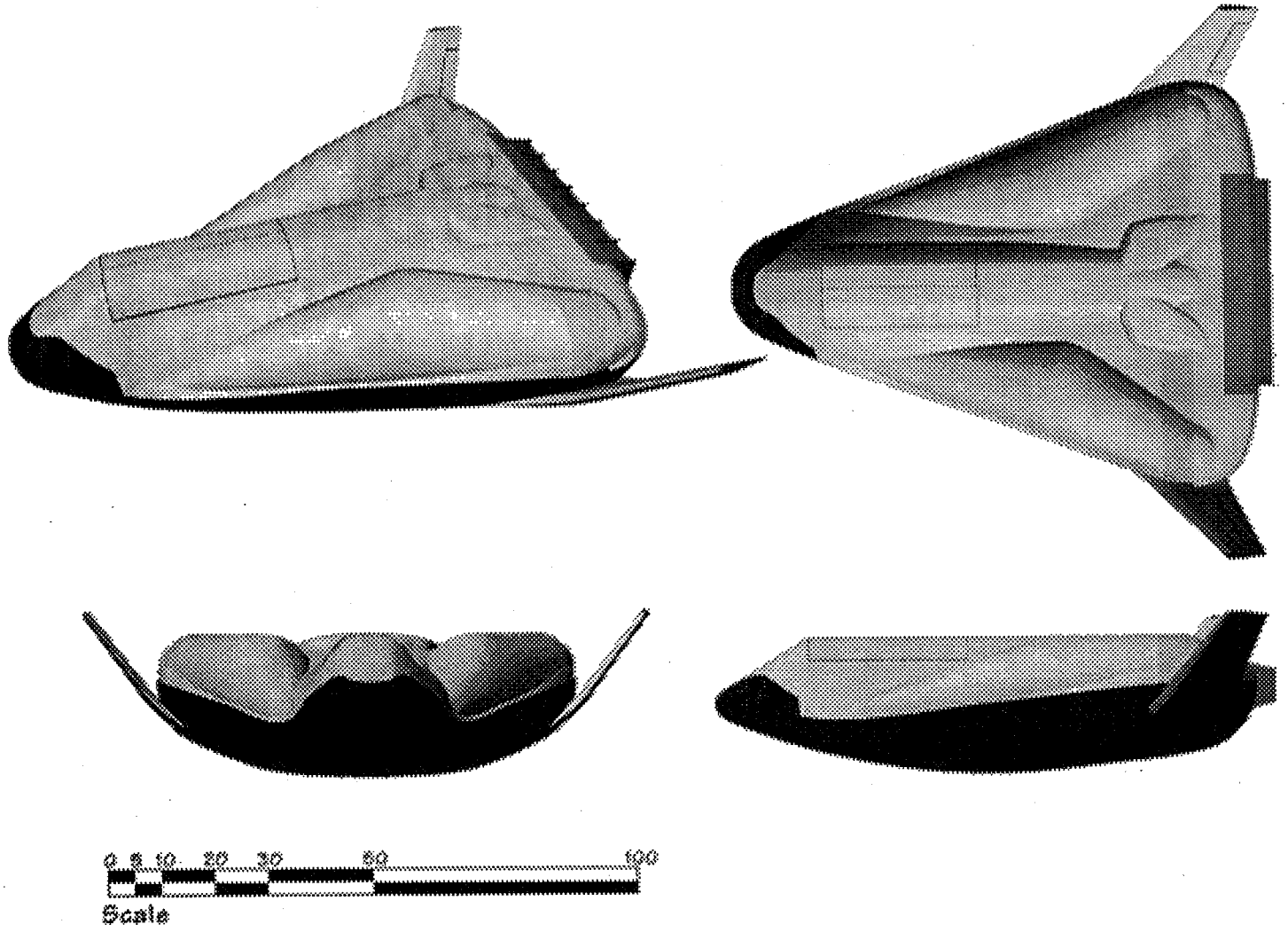

Reusable Launch
Vehicle Propulsion
Technology

Winged RLV
0 5 10 20 30 50
Scale
USA
United States

RLV Engine Requirements / Attributes

Quantitative Operability Design Requirements

• Minimum Flight Hardware MTBR	20 flights / 10,000 seconds
• Minimum Flight Hardware Life Limits	60 flights / 30,000 seconds
• Fault Detection / Isolation to an LRU	0.25 hours / 1 manhour
• Maximum Scheduled Engine Maintenance	16 hours elapsed / 64 manhours
• Maximum Time to Replace LRU	4 hours / 8 manhours
• Maximum Time to Replace Engine	8 hours elapsed / 32 manhours
• Minimum Engine Reliability (via test & analysis)	0.999
• Minimum Engine Hardware HCF Life Factor*	1.15 on endurance
• Minimum Engine Hardware LCF Life Factor*	10X on life

* Issue of fracture control

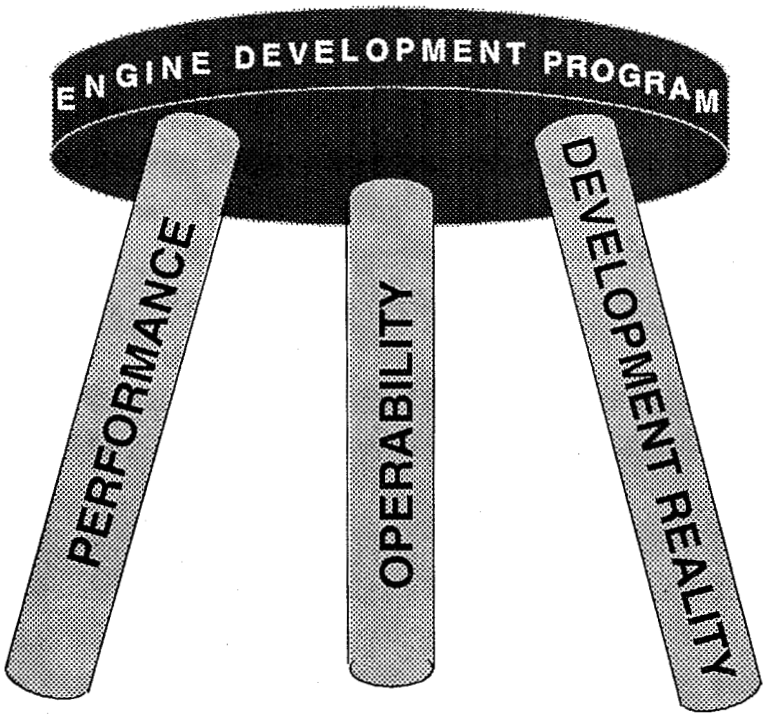

Any New Rocket Engine Development Program*Must* Maintain an Even Balance Between Performance, Operability and Development Reality...

Engine System Trade-Offs

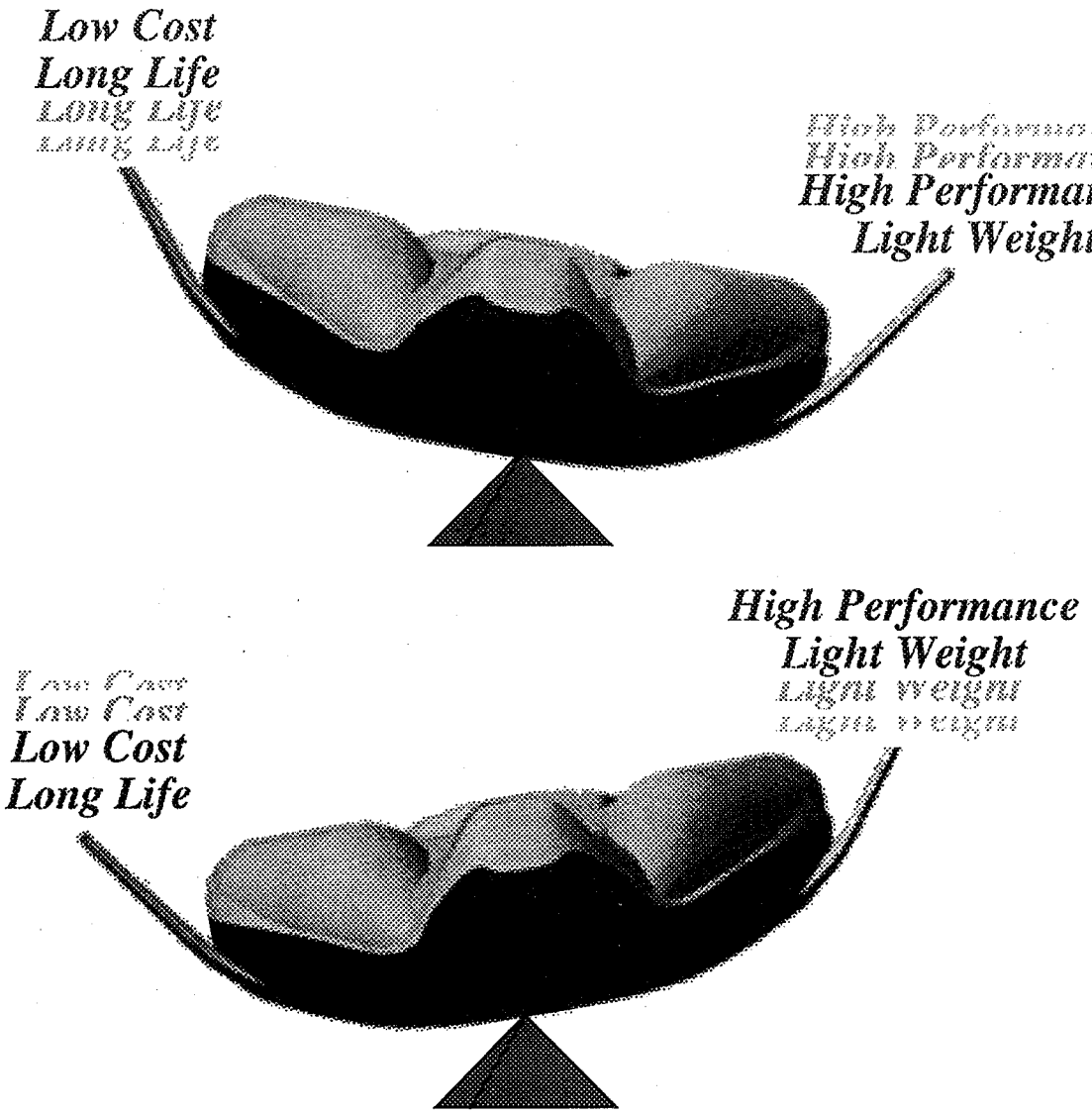

Emphasis is on Balance of Design Requirements Between:

- **Operability**
- **Performance**
- **Weight**
- **Cost**

Baseline Technology Program Supports Proposed Engine System Concepts

- **Bipropellant Systems**
  - RD-0120 (Aerojet)
  - DUAL BELL (Rocketdyne)
  - LINEAR AEROSPIKE (Rocketdyne)
- **Tripropellant Systems**
  - RD-0120 DERIVED (Aerojet)
  - RD-704 (Pratt & Whitney)
  - BELL ANNULAR (Rocketdyne)

Tripropellant Engines

Tripropellant Engine Options

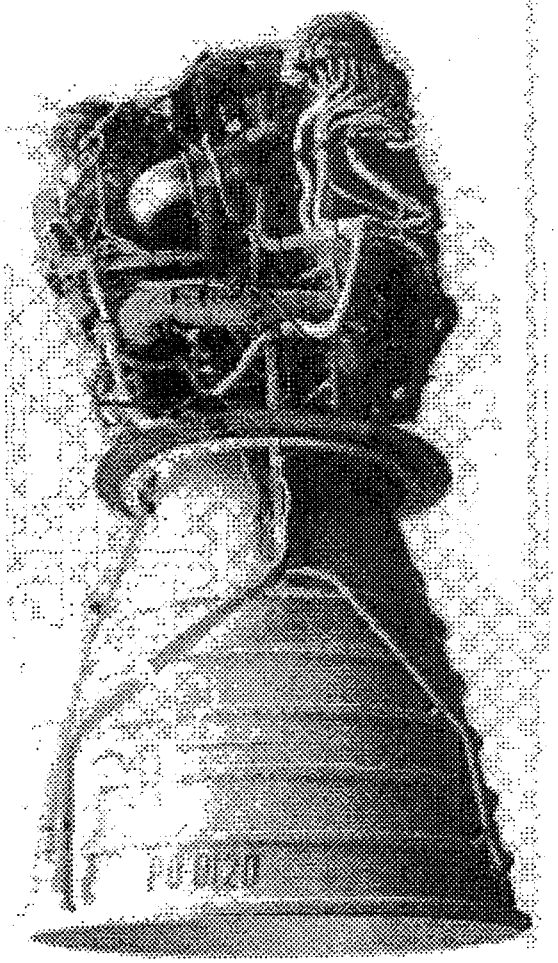

AEROJET/CADB
RD-0120 Derivative Engine

- Staged Combustion Cycle
- Fuel Rich Preburner
- Tripropellant Preburner
- Common Chamber Bell
- Fixed Expansion Ratio
- RD-0120 Heritage

Tripropellant Engine Options

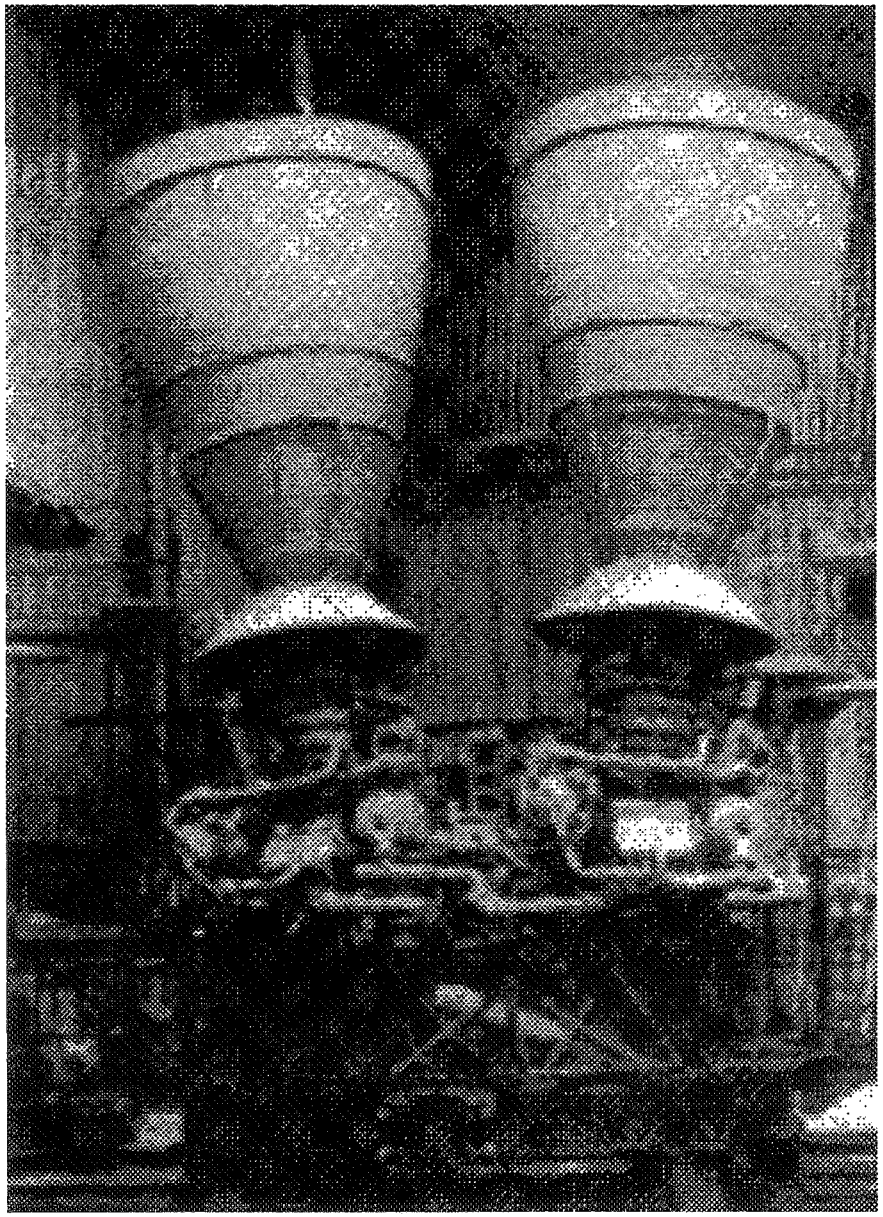

P&W/NPO ENERGOMASH RD-704 Engine

- Fixed Expansion Ratio
- Common Chamber Bell
- Tripropellant Main Injector
- Ox Rich Preburner
- Staged Combustion Cycle
- RD-170 Heritage

RD-701 Mock-up Shown

Tripropellant Engine Options

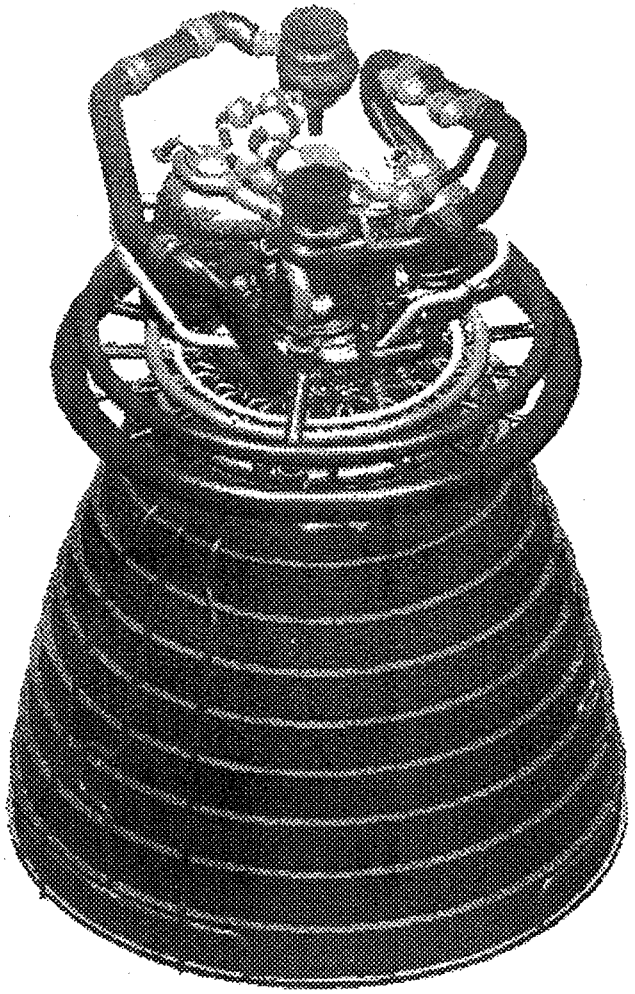

ROCKETDYNE
Bell Annular Engine

- Staged Combustion Cycle
- Fuel Rich Preburner
- O2/H2 Core
- O2/RP-1 Annular Combustor
- Dual Chamber/Common Bell
- Dual Expansion Ratio

Bipropellant Engines

Bipropellant Engine Options

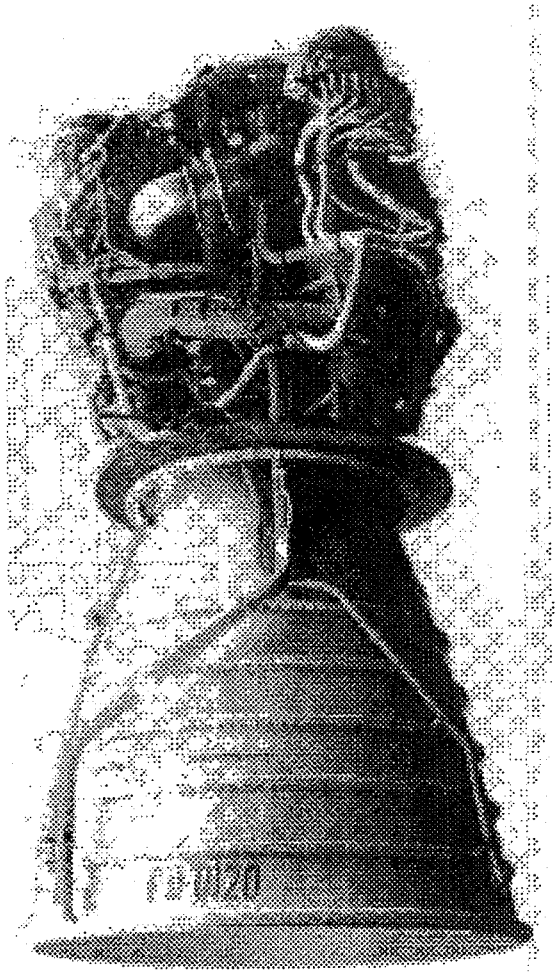

AEROJET/CADB RD-0120 Engine

- Staged Combustion Cycle
- Fuel Rich Preburner
- Common Chamber Bell
- Fixed Expansion Ratio

Bipropellant Engine Options

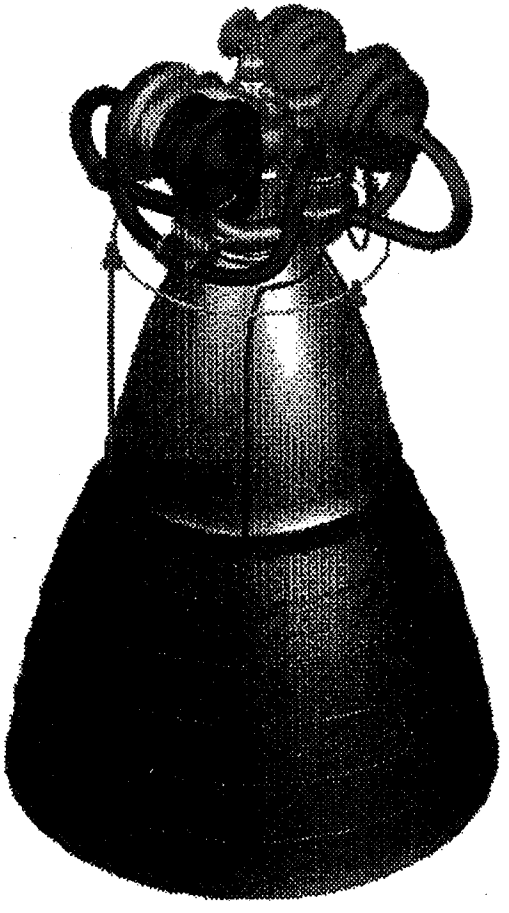

ROCKETDYNE
Dual Bell Engine

- **Full Flow Staged Combustion Cycle**
- **Ox Rich Preburner**
- **Fuel Rich Preburner**
- **Dual Expansion Ratio**

Bipropellant Engine Options

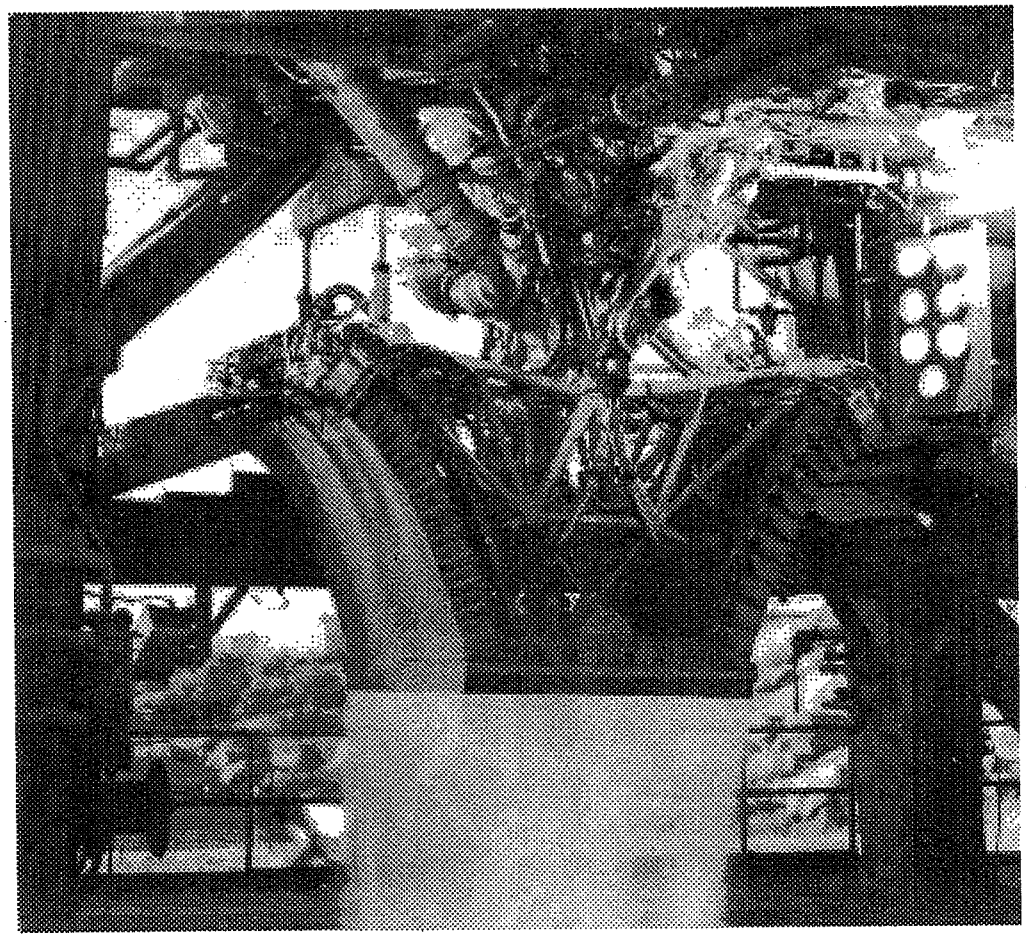

ROCKETDYNE
Linear Aerospike Engine

- Staged Combustion Cycle
- Ox Rich Preburner
- Modular Combustion Chambers
- Conformal/Segmented Altitude Compensating Nozzle
- Variable Expansion Ratio

Inherent Characteristics

TRIPROPELLANT

- SINGLE INJECTOR/CHAMBER
  - Coupled Propellant Systems
  - Potential Hydrocarbon Performance Improvement
- LOX/LH2 CORE/LOX/RP-1 AUGMENTED
  - Decouples Lox/LH2 and Lox/RP-1 Systems
  - Dual Throat Areas

BIPROPELLANT

- STAGED COMBUSTION CYCLE
  - Historic Thrust/Weight ~ 66
  - Hydrogen Is Difficult To Pump
- AEROSPIKE
  - Optimizes Boattail Area
  - Inherent Altitude Compensating Capability

Programmatics

RLV Technology Development & Demonstration Strategy

Base Technology Program

- **Reusable Cryogenic Tank**
- **Graphite Composite Primary Structures**
- **Advanced Thermal Protection**
- **Advanced Propulsion**
- **Avionics / Operable Systems**

Flight Demonstration Program

DC-XA
- Operations
- Advanced Technology

Advanced Technology Demonstrator (ATD)
- Operations
- Mass Fraction

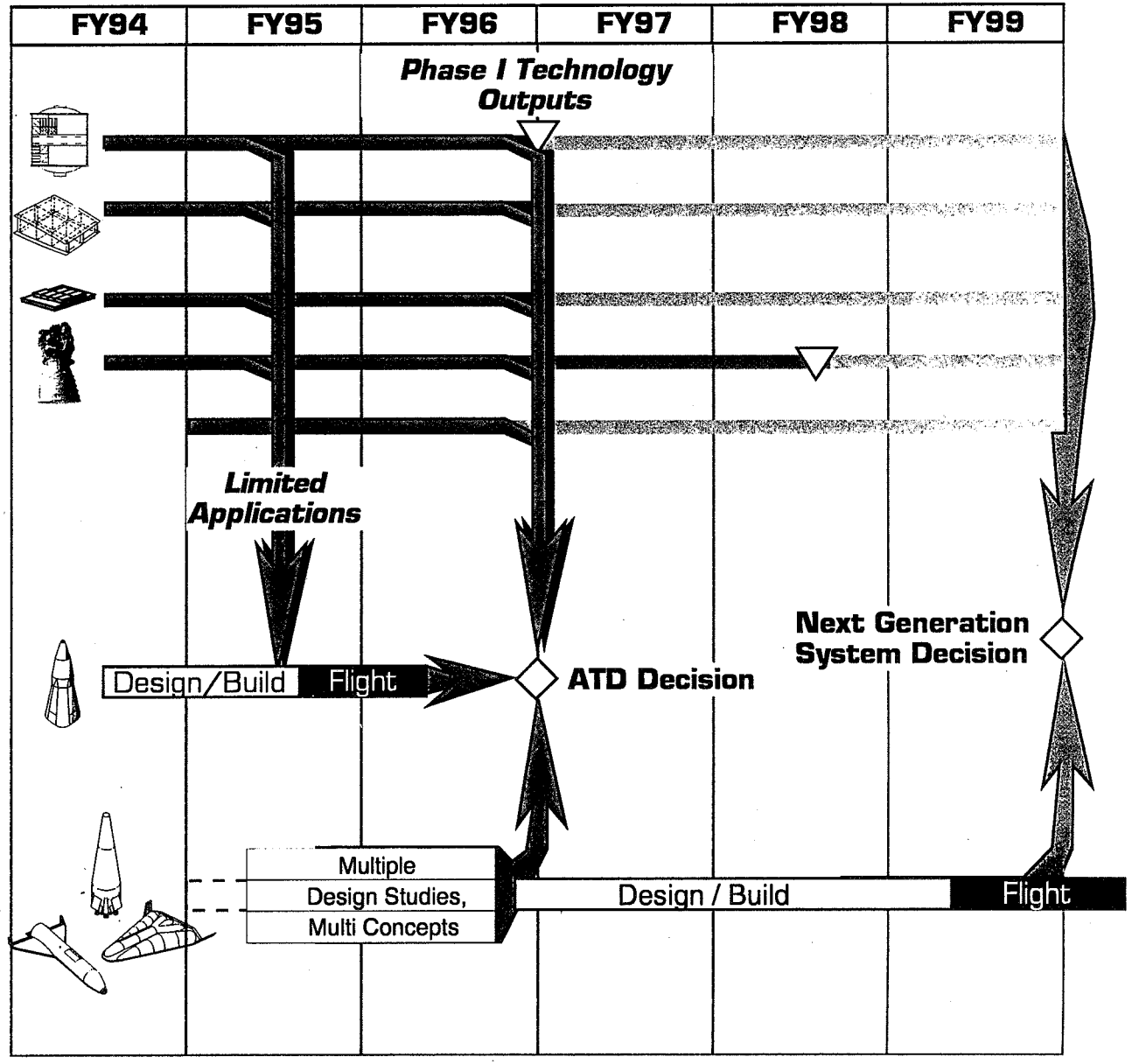

Propulsion Technology Schedule & Products

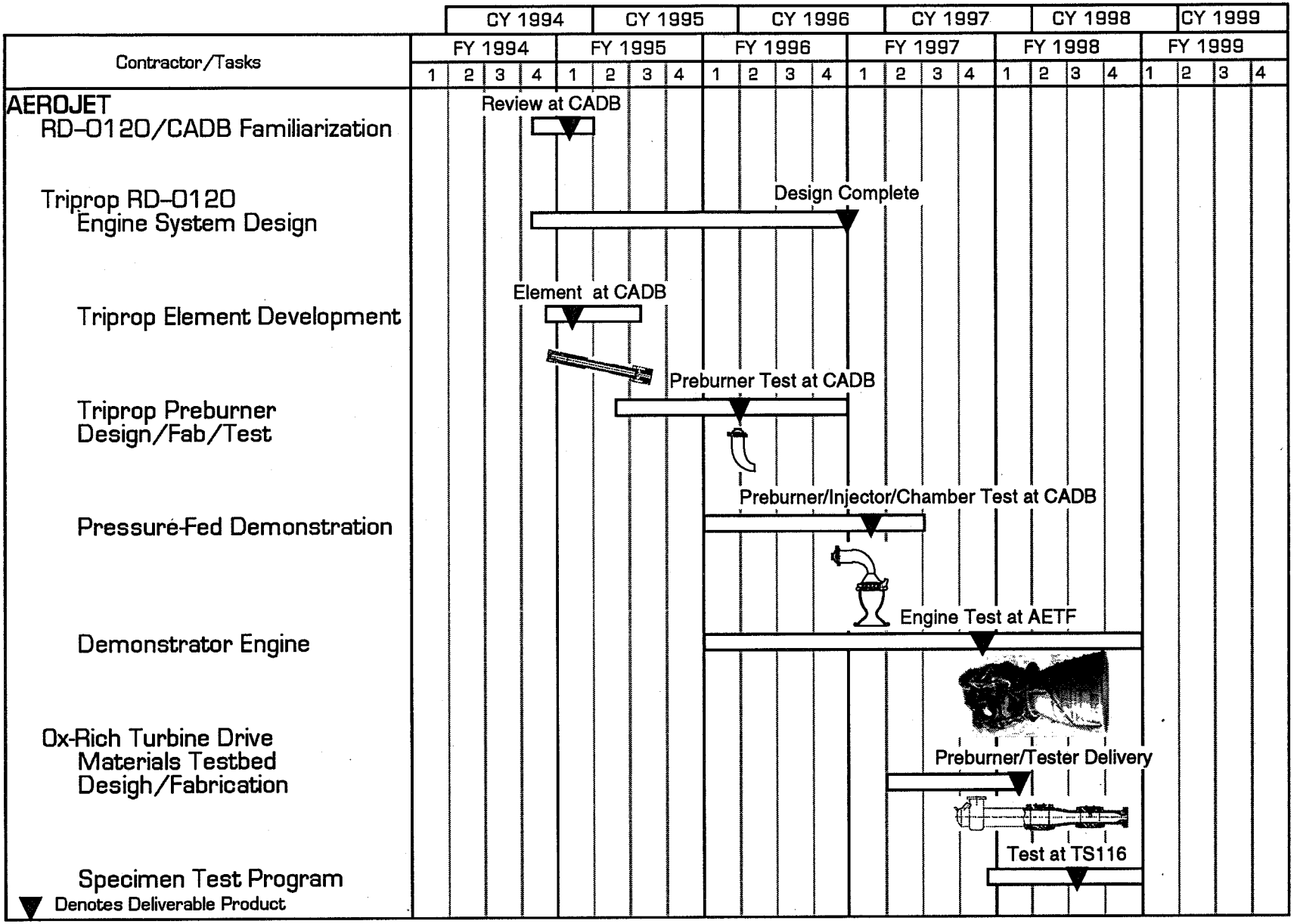

Propulsion Technology Schedule & Products

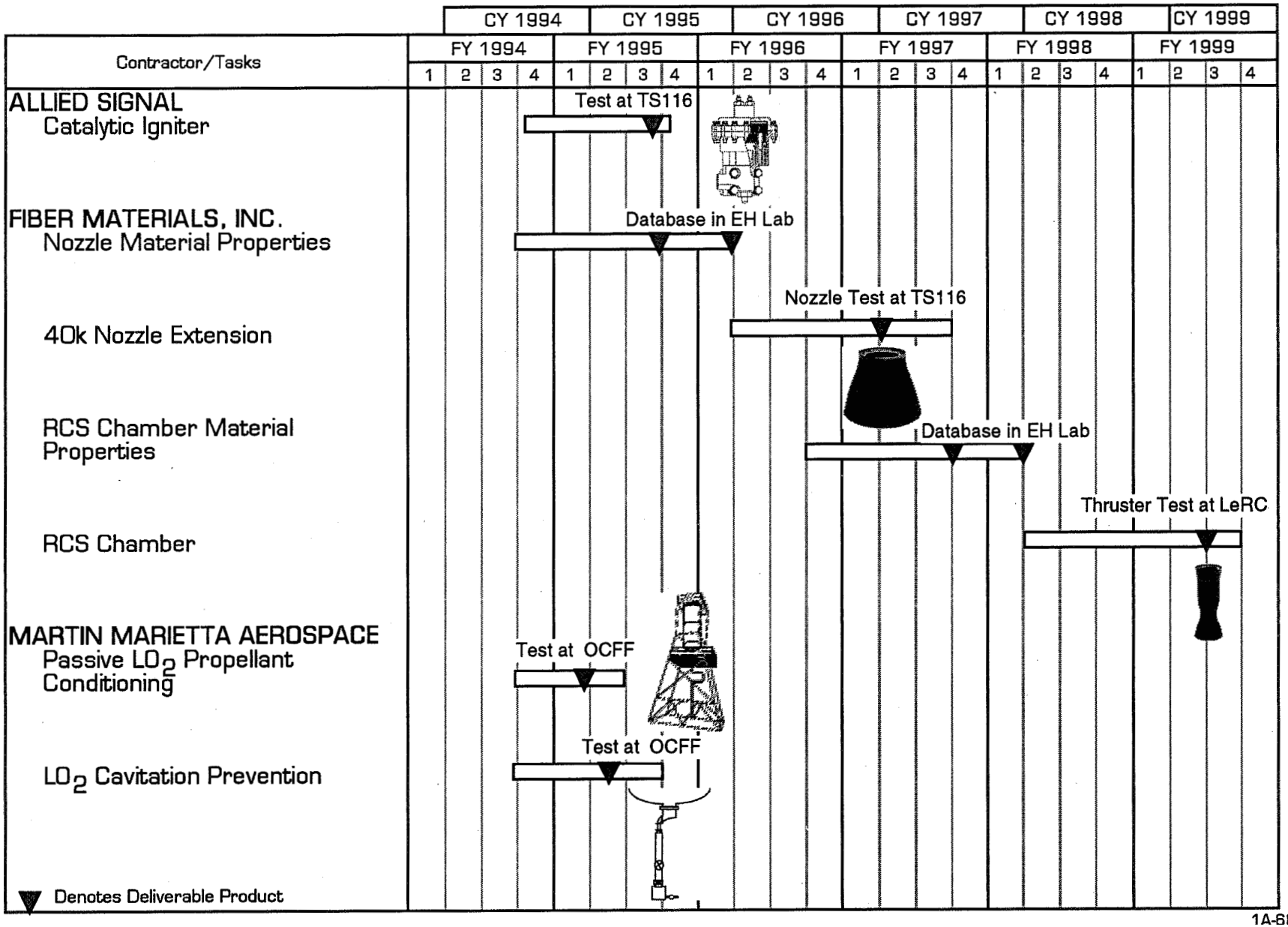

Propulsion Technology Schedule & Products

Contractor/Tasks	CY 1994 / FY 1994				CY 1995 / FY 1995				CY 1996 / FY 1996				CY 1997 / FY 1997				CY 1998 / FY 1998				CY 1999 / FY 1999			
	1	2	3	4	1	2	3	4	1	2	3	4	1	2	3	4	1	2	3	4	1	2	3	4
MARTIN MARIETTA AEROSPACE																								
RP-1 Pressurization			Test at TS116 ▼																					
Russian Kerosene			Test at TS116 ▼																					
MCDONNELL DOUGLAS																								
Liq-Gas H_2 Conversion																								
O_2/H_2 APU																								
Composite Feedline / Valve Body			Fabricate at PEC ▼																					
H2 Leak Detection System (In-House)			Design/Fab at EB Lab ▼																					
Integrated Pallet Test							Test at TS500 ▼				DC-XA Flight ▼													
PRATT & WHITNEY																								
Russian Technology Assessment			Review at NPOE ▼																					
19 Element Triprop Injector Optimization			Russian Tests Complete ▼																					
19 Element Triprop Injector Demonstration							Test at TS116 ▼																	

▼ Denotes Deliverable Product

Propulsion Technology Schedule & Products

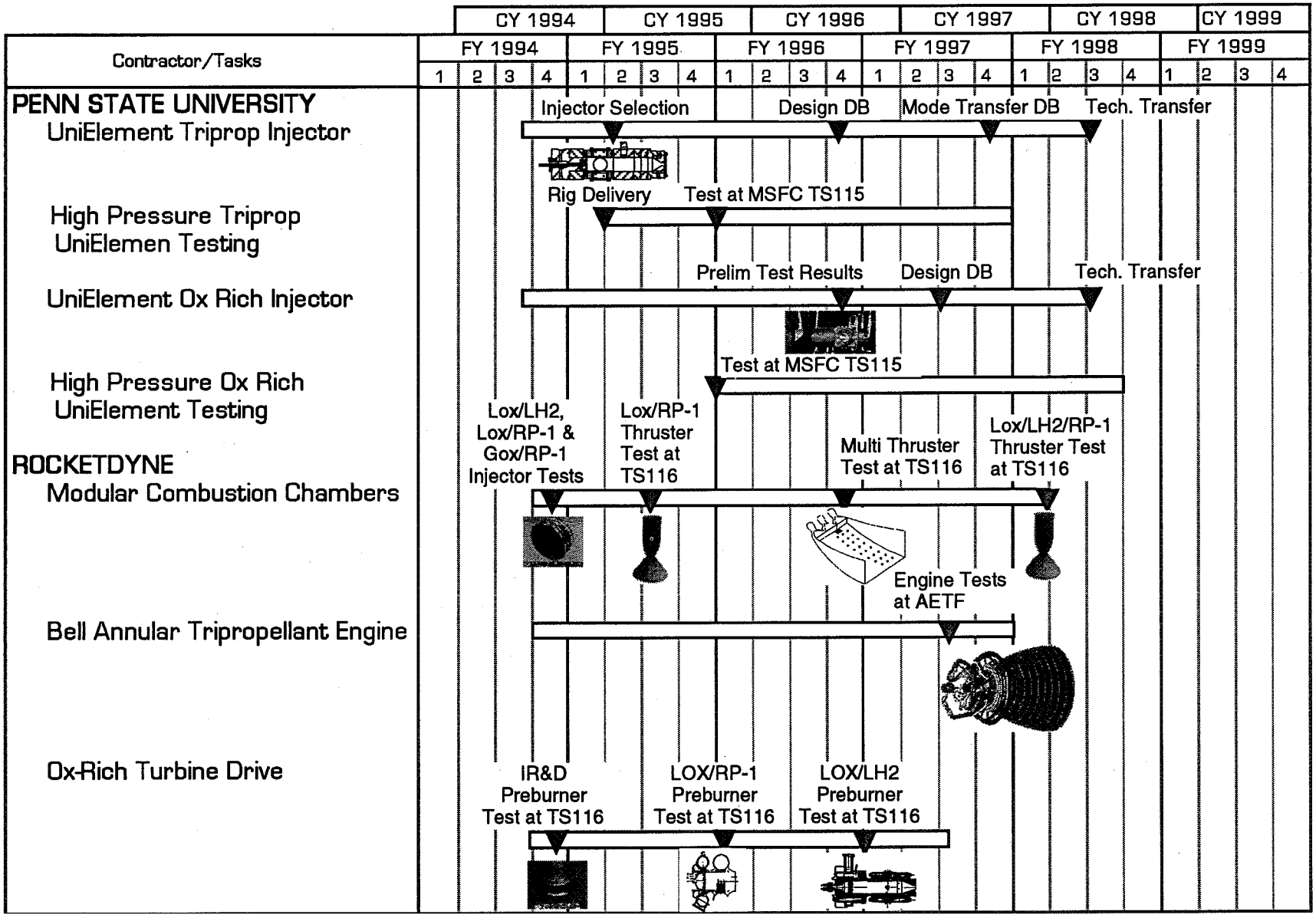

Propulsion Technology Schedule & Products

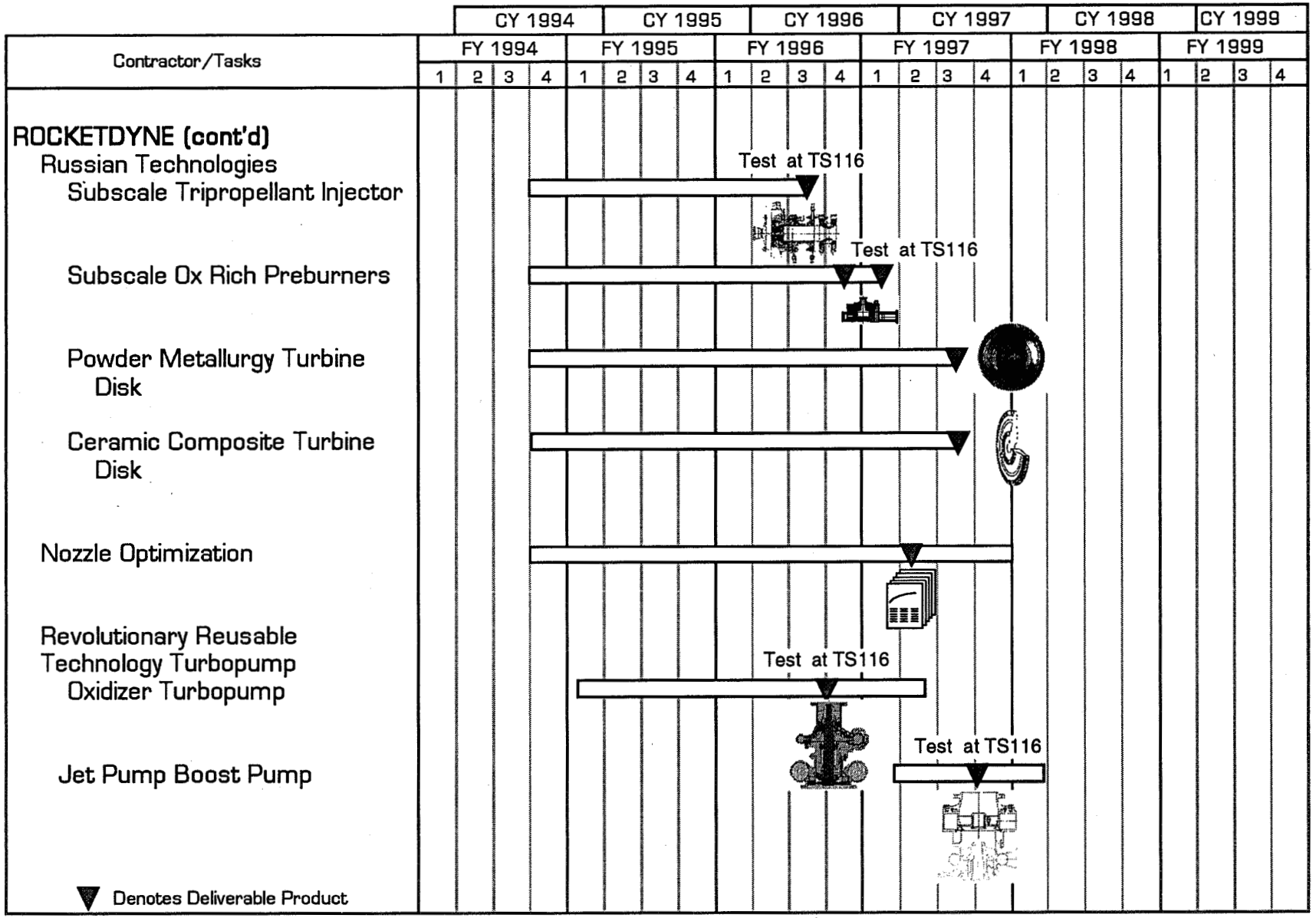

Propulsion Technology Schedule & Products

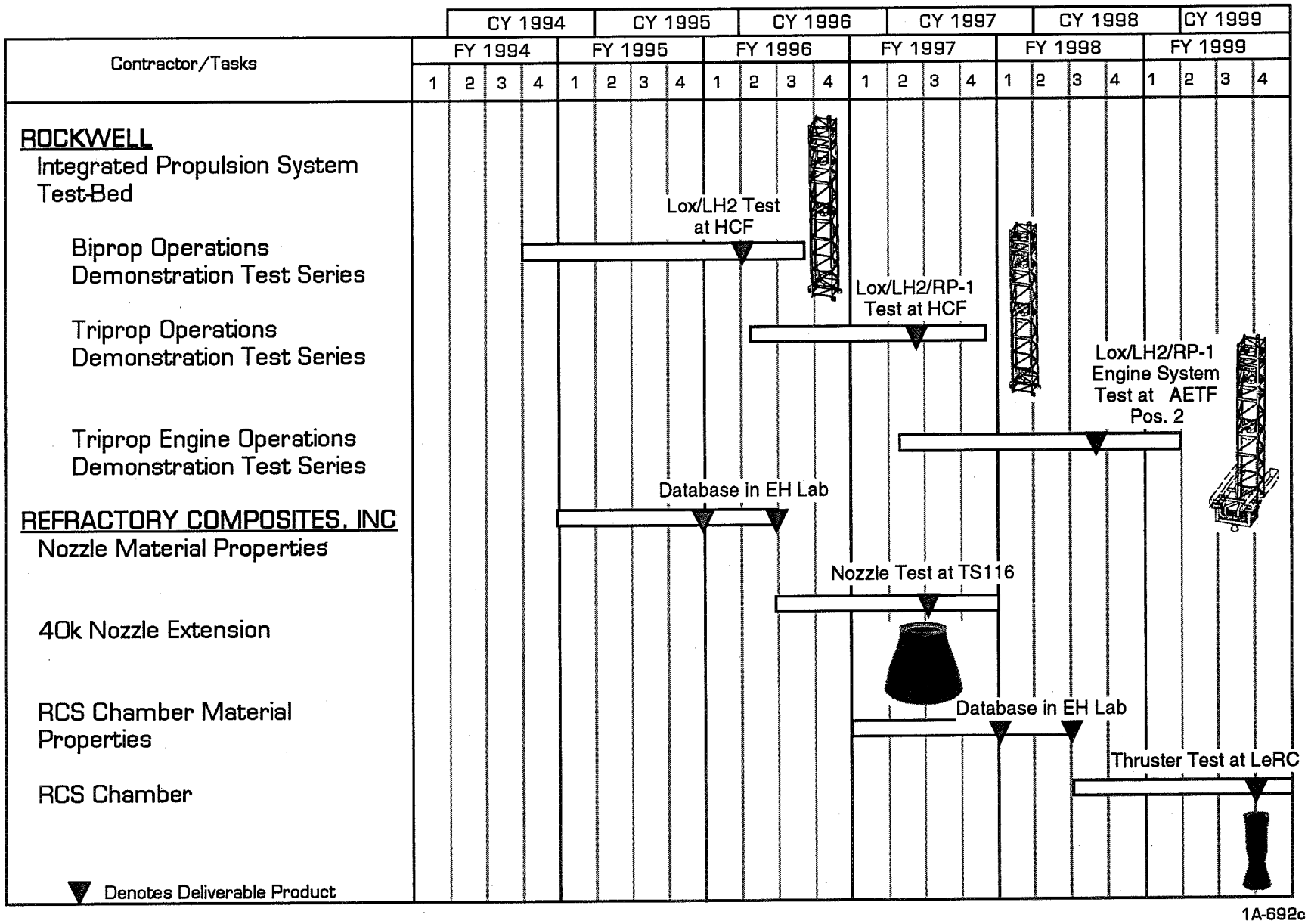

1A-692c

Technology Program Updates

Cooperative Agreements Are Renewed Each October

An Assessment Process Is Being Established
- Industry Driven
- Assessment Results Available By August Of Each Year

Technology Tasks That Are Supported By Vehicle Concepts And Offer Significant Payoff Will Be Maintained

Page intentionally left blank

Overview of MSFC

CFD Activities

Presented to:
13th Workshop for CFD
Applications in Rocket
Propulsion and Launch Vehicle Tech.
April 25, 1995

Paul McConnaughey
Chief, CFD Branch
Fluid Dynamics Div.
NASA MSFC

Overview

- **Objectives of CFD at MSFC**
- **Representative Current Activities**
  - Shuttle flight and development program supporting applications
  - Advanced Propulsion Technology analyses
  - X-33 and X-34
  - Technology Utilization and Transfer
- **Future Directions**
  - Programs
  - CFD Technology
- **Summary**

Objectives of CFD at MSFC

- **Support MSFC programs with CFD analysis**
  - Flight
  - Development
  - Technology
- **Facilitate CFD technology development and transfer**
  - CFD Consortium for Applications in Propulsion Technology
  - Cooperative agreements and in-house complimentary tasks
  - Contracted efforts with industry, SBIR, and universities
  - Coordination of activities with other NASA and DoD centers

An engineering analysis tool to support hardware design and development

Representative Flight/Development Program Supporting Applications

- **Space Shuttle Main Engine (SSME) Program**
  - LPOTP bearing analysis
  - SSME Block I and Block II Isp loss
- **Alternate Turbopump Development (ATD) Program**
  - Fuel pump 6N+/- alpha frequency vibration
    - impeller inlet flow
    - inlet guide vane analysis
  - Fuel pump interstage diffuser housing erosion
- **Reusable Solid Rocket Motor (RSRM)**
  - NBR Stiff inhibitor problem assessment
  - Nozzle manufacturing defect flow assessment
  - Joint defect clogging assessment
  - Gimbaled nozzle cold flow simulations
  - Pressure spike investigation/slag accumulation prediction

Representative Flight/Development Program Supporting Applications (continued)

- **Gravity Probe B**
  - Nozzle performance predictions and test
  - He slosh for control dynamics
- **RD-170 Emission Predictions**
  - Flight predictions for environmental assessment
    - hydrocarbon chemistry
    - thermal NOx

Advanced Propulsion Technology Analyses

- **SIMPLEX Turbopump Development**
  - Turbine stage and disk analysis
  - Pump stage analysis (flange to flange)
- **P&W Advanced Liquid-Hydrogen Turbopump**
  - Radial inflow turbine stage and volute analysis
  - Pump stage analysis (flange to flange)
- **Rocketdyne RS 2000 D-1 Bell Annular Tripropellant Engine**
  - Modular thruster analysis and shape optimization
  - Bell Annular nozzle flow interaction analysis
  - Nozzle conjugate heat transfer for mode 2
  - RP-1 combustion model development

Advanced Propulsion Technology Analyses

- **Penn State Tripropellant Injector Analysis**
  - LOX/RP1/H2 injector analysis
    - gas/gas/gas
    - liquid/liquid/gas
  - Hydrogen/oxygen gas/gas injector benchmark
- **Composite Nozzle Design Analysis (FMI/RCI)**
  - Conjugate heat transfer analysis
  - design iterations through flow, thermal, stress
- **SR-71 Linear Aerospike Flight Test Simulation (LADC/Rocketdyne)**
  - Aerospike benchmark and slipstream assessment
  - Body and base pressure predictions
- **Revolutionary Reusable Technology Turbopump (Rocketdyne)**

X-33 - Lockheed Advanced Development Company

- **Plume/aero Interaction**
- **Base Flow Environments**
- **Loads Analysis**

X-33 - McDonnell Douglas/The Boeing Company

- **Base Flow Environments**
  - DC-X cold flow test and hot fire
  - X-33 cold flow tests and hot fire
  - RLV environments

X-33 - Rockwell Space Division

- **Base Flow Environments**

X-34 - Orbital Sciences Corporation

- **Upper Stage Engine Development**
  - Turbomachinery design analysis
  - Ablative nozzle and combustion devices design analysis
  - Design point currently in work

Technology Utilization and Transfer

- **Space Act Agreements**
  - General Motors/Saginaw Division
    - Power steering analysis and cold flow test
  - North American Marine Jet
    - Water jet design analysis
- **Interagency Agreement**
  - David Taylor Naval Weapons Lab
    - Impeller analysis and cavitation modeling
- **NASA Aerospace Industry Technology Reinvestment Program**
  - Computational Aeroacoustics Analysis System (CAAS)
    - Joint code and system development project
    - Rocketdyne, Ford, MacNeal-Schwendler, MSFC, LaRC
    - Aeroacoustics analysis for aerospace, automotive, and commercial applications

Future Directions - Programs

- **Continue work on**
  - X-33 and X-34 Cooperative agreements
  - Shuttle development issues as required
    - ATD fuel pump
    - SSME Phase II, Block II
- **Greater emphasis on**
  - joint government/industry initiatives
  - CFD in early phases of programs
- **Programs will continue to be focused on hardware development**
  - Limited resources for CFD development
  - Applications must 'buy' their way into programs

Future Directions - CFD Technology

- **Continue work with**
  - Block structured grids/solvers (GASP, FDNS)
  - Chimera (OVERFLOW)
  - Adaptive Methods (SAGE)
- **Assessment of Finite Element Codes/Methods**
  - interdisciplinary analyses
  - CAAS development for commercialization
- **Greater emphasis on**
  - Distributed and parallel computing
  - Reacting and multiphase flows

Summary

- **CFD has made significant progress in supporting programs at MSFC**

- **Emphasis within industry and MSFC continues to be cooperative agreements and joint ventures**
  - Hardware design applications
  - Obtain benefits from past and current investment in CFD technology development

CFD Consortium for Applications in Propulsion Technology (CFD CAPT)

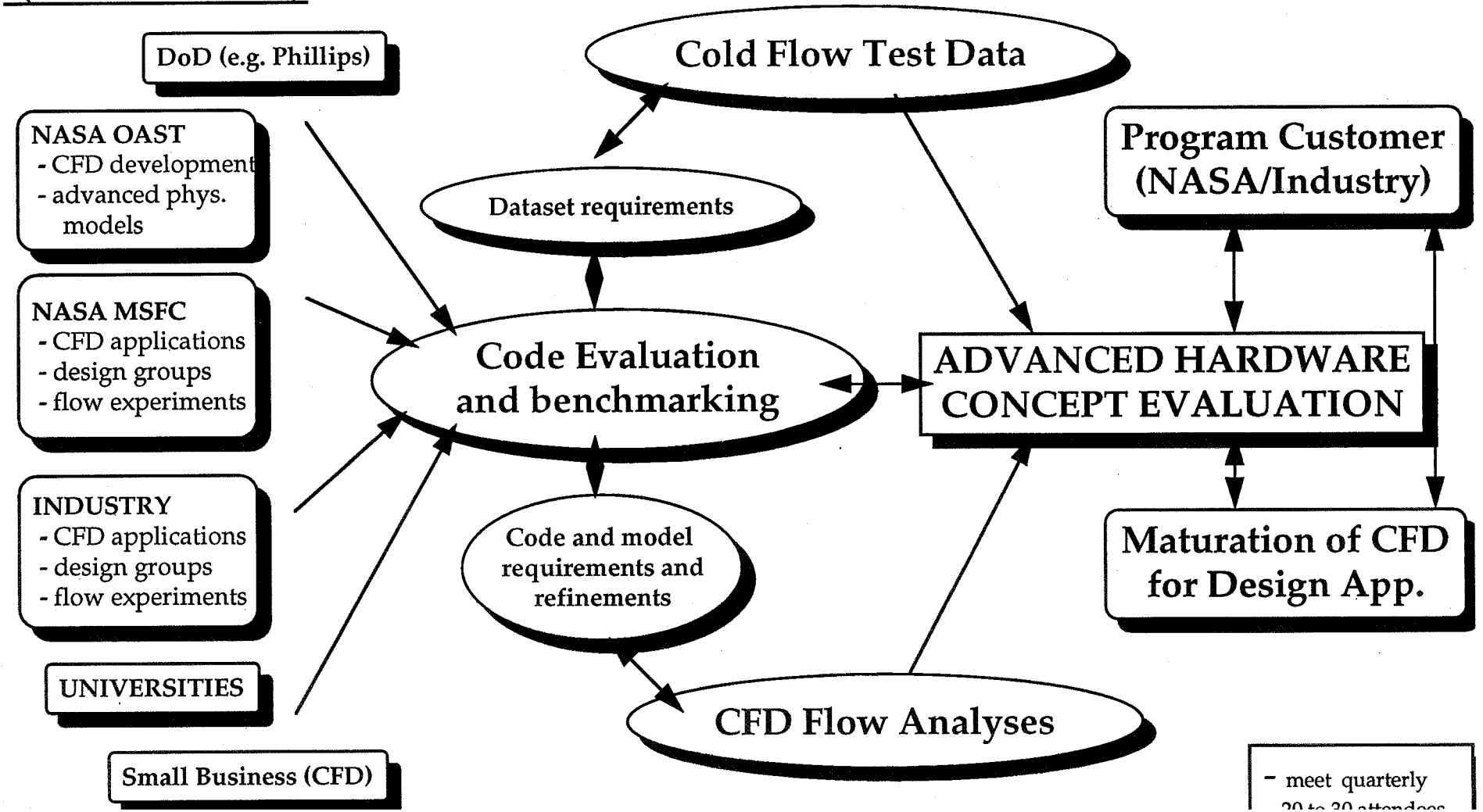

Codes in use at MSFC

- **Grid generation codes**
  - GENIE++, EAGLEVIEW, general, interactive, 3-D (MSU , MSFC)
  - CAGI, CAD interface for GENIE++, (MSU, MSFC)
  - GEN2D, interactive 2-D (Sverdrup, MSFC)
  - HYPGEN, hyperbolic volume grids (ARC)
  - SAGE, 3-D grid adaption (ARC)

- **Flow Solvers**
  - OVERFLOW, compressible, real gas flows, (AR C)
  - GASP, compressible, reacting flows, (Aerosoft, LaRC, MSFC)
  - FDNS, wide Mach range, reacting flows (ESI, SECA, MSFC)

- **Post Processing / Graphics codes**
  - PLOT3D, FAST
  - FAST, interactive 3-D, animation capability

Page intentionally left blank

CFD Analysis of the ATD HPFTP Inlet Guide Vanes

R. Garcia
R. Williams

NASA/MSFC

13th Workshop for CFD Applications in Rocket Propulsion and Launch Vehicle Technology
MSFC, AL
April 25-27, 1995

CFD Analysis of the ATD HPFTP Inlet Guide Vanes

Computational Fluid Dynamics Branch
Fluid Dynamics Division
Structures and Dynamics Laboratory
George C. Marshall Space Flight Center

Overview

- Problem Background
- Objectives and Approach
- Axisymmetric Results
- 3D Results
- Summary/ Conclusions

ATD HPFTP Cross Section

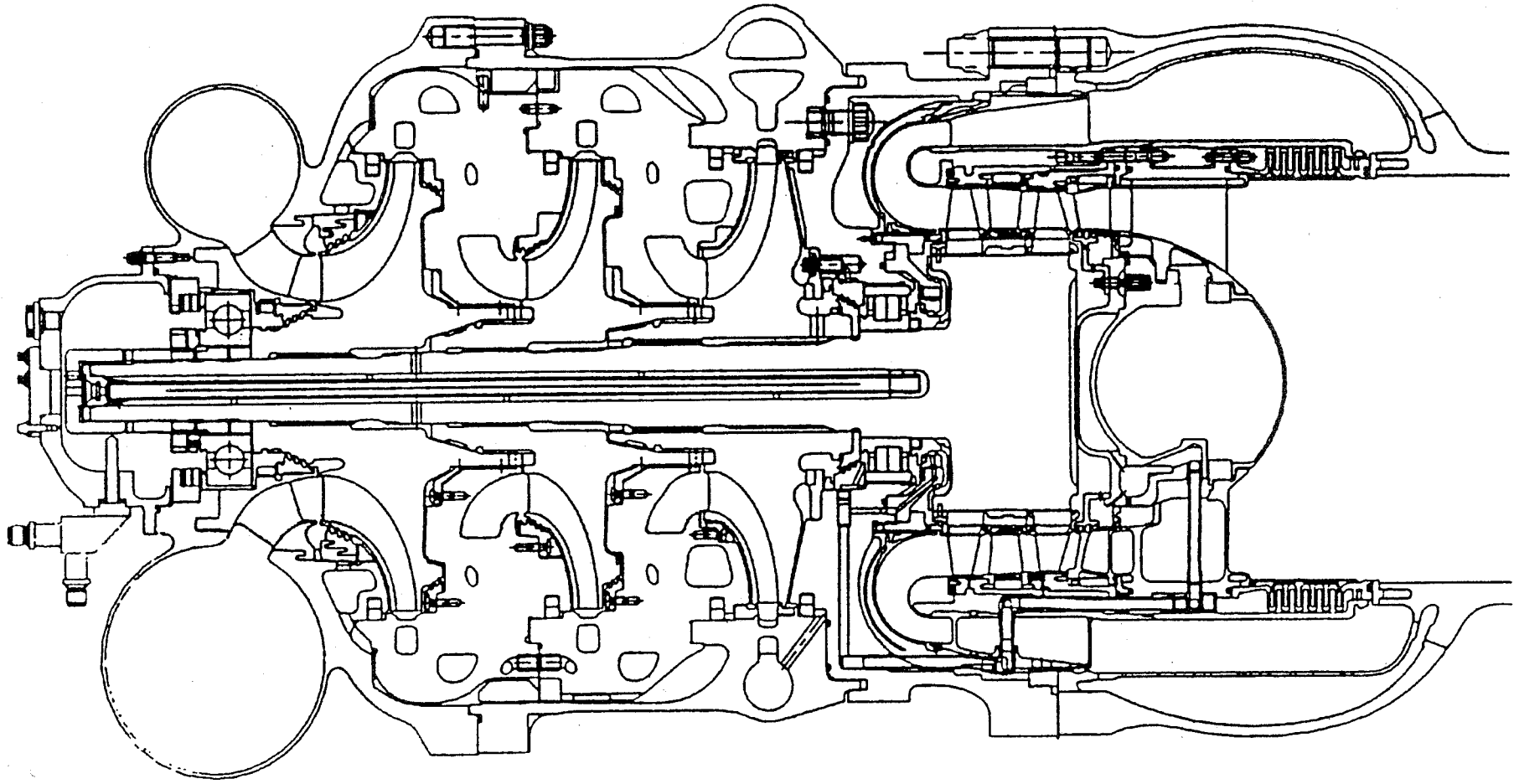

Problem Background

- **Testing of the ATD HPFTP Revealed Anomalous Frequency (alpha)**
  - High level (6-9gs) amplitudes in the 60 - 100 Hz range
    - » **Sidebands about six time synchronous frequency (6N)**
      - * the three impellers have 6-full blades
    - » **Signal cleanest on pump-end accelerometers**
      - * also sensed by high response pressure sensors
    - » **Signal processing indicated signal source potentially in area where cavitation is present**
- **Several Theories Proposed, Including Flow Instability/Irregularity in the Inlet, Upstream of the 1st Stage Impeller**
- **CFD Analysis Requested to Support the Investigation**

National Aeronautics and Space Administration

CFD Analysis of the ATD HPFTP Inlet Guide Vanes

Computational Fluid Dynamics Branch
Fluid Dynamics Division
Structures and Dynamics Laboratory
George C. Marshall Space Flight Center

6N and Side Bands
(from accelerometer)

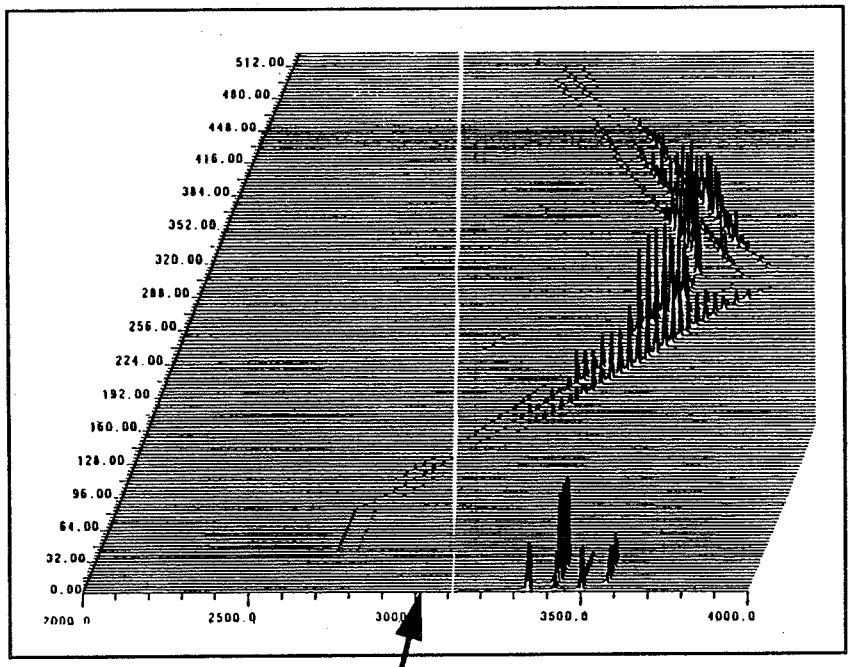

Alpha Frequency
(from p-measurement)

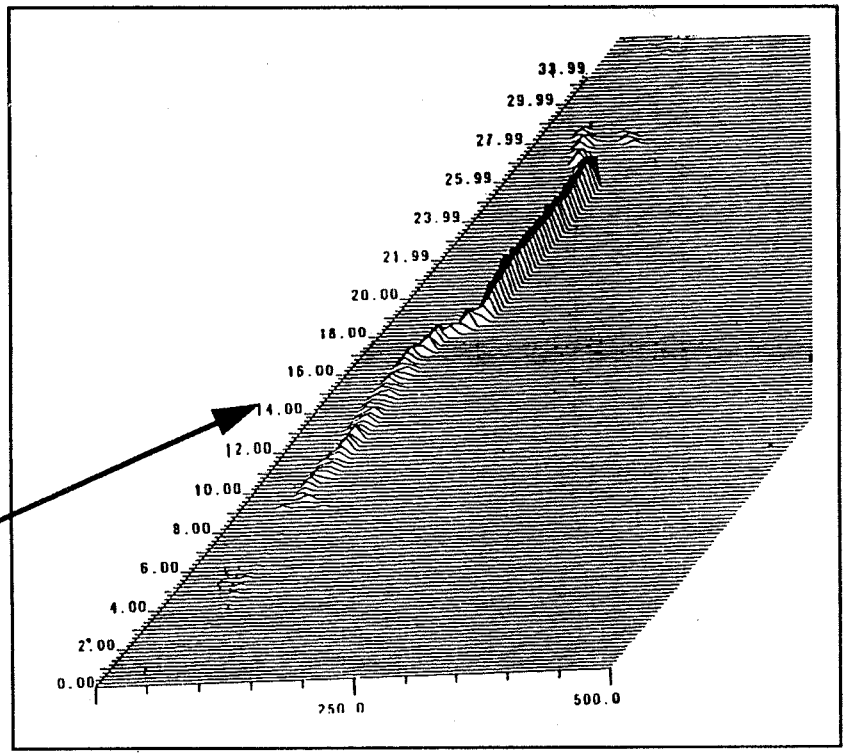

Plots cover changes in power level and in pump inlet pressure

CFD Analysis of the ATD HPFTP Inlet Guide Vanes

Computational Fluid Dynamics Branch
Fluid Dynamics Division
Structures and Dynamics Laboratory
George C. Marshall Space Flight Center

Objective

- **Inlet Flow Path is Complex**
  - Volute, 15 inlet guide vanes, 2 parasitic flow entry points
- **The Inlet & the 1st Stage Impeller tested in Water in 1987**
  - Testing for inlet performance and impeller suction capability
  - Flow-vis indicated at least one inlet guide vane (igv) was separated
  - Significant circumferential flow angle variation at the igv inlet
  - Parasitic flows modeled but not as per the final design
- **CFD Analysis Performed to Determine the Flow in the IGV**
  - Establish a current baseline
  - Assess design modifications as required to eliminate the alpha frequency

Pump-End Flow Circuit

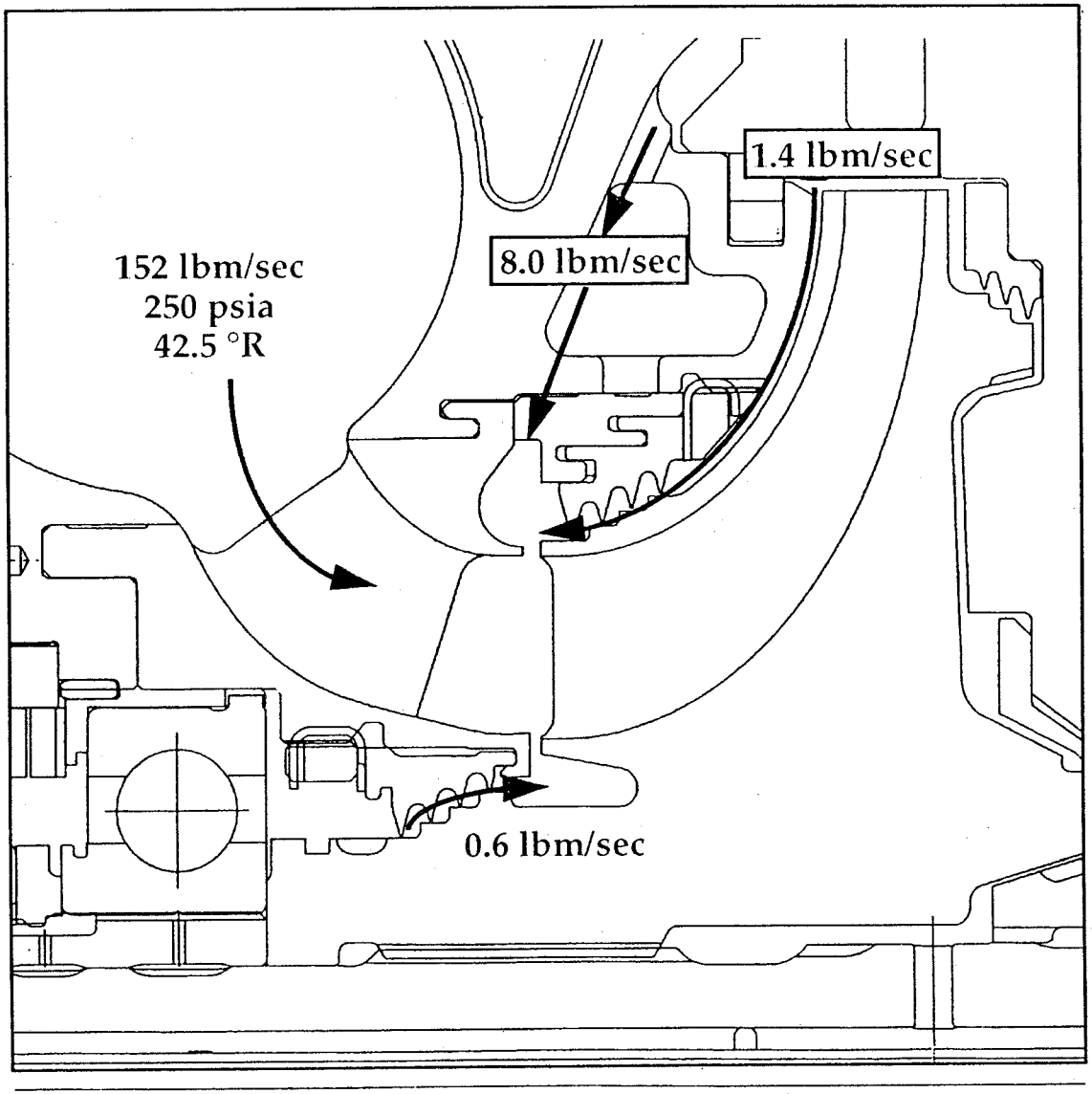

CFD Analysis of the ATD HPFTP Inlet Guide Vanes

Computational Fluid Dynamics Branch
Fluid Dynamics Division
Structures and Dynamics Laboratory
George C. Marshall Space Flight Center

Approach

- **Use Axisymmetric Model to Assess Profile Geometry and Parasitic Flows Reentry**
  - Main flow = 152 lbm/sec, 250 psia, 42.5 °R
  - Shroud cavity flow = 8.0 lbm/sec from impeller back-face, 1.4 from impeller front-face
  - Hub cavity flow = 0.6 lbm/sec from bearing coolant circuit
- **Use 3D IGV Analysis to Assess the Circumferential Variations**
  - Main flow only: 152 lbm/sec
  - Analyze one "representative" channel
  - Vary inlet swirl angle over extremes measured on the water rig
- **Provide Flow Conditions at the Impeller Inlet**

Approach (continued)

- **Generated Axisymmetric Grid Using GRIDGEN**
  - Allows for establishing connectivity across blocks
    - » **facilitates manipulation of grid size and point distribution**
  - Grids typically 4000 to 6000 points
- **Generated 3D IGV Grid Using TIGER**
  - Used same profile geometry as the axisymmetric grid
  - Obtained vane geometry from IGES file
    - » **TIGER finds the intersection between the vane and the profile walls**
  - Used 20K grid and 60K grid
- **Used FDNS3D for All Cases**
  - 1.5 YMP-CPU hrs for Axisymmetric, 5.0 YMP-CPU hrs for 3D cases
- **Postprocessed Using PLOT3D, FAST, XMGR, and Custom Codes**

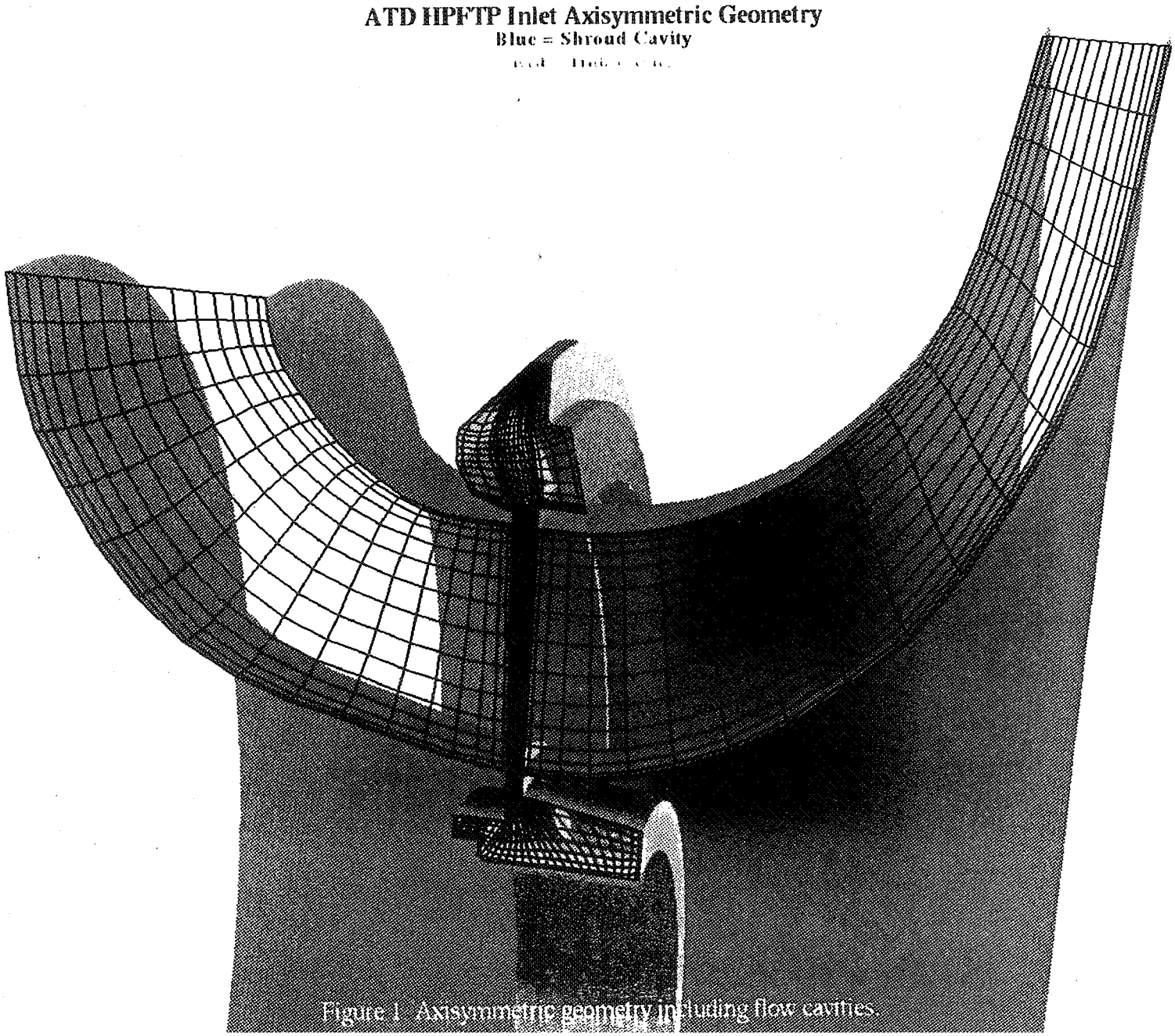

Figure 1. Axisymmetric geometry including flow cavities.

ATD HPFTP Inlet Guide Vane Geometry: Sample of Coarse Grid

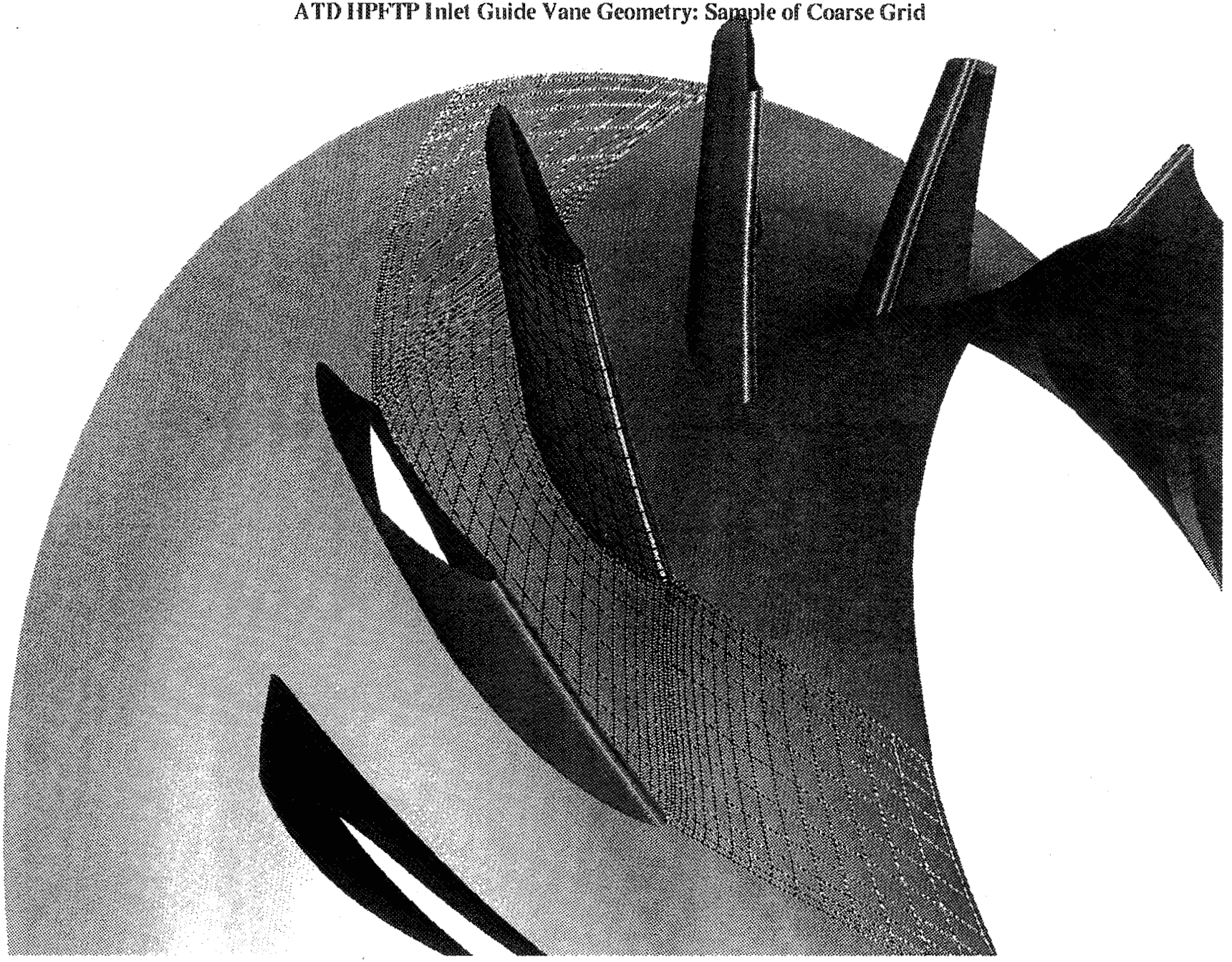

Axisymmetric Results

- **No Flow Irregularities Due To the Profile Geometry**
  - Main flow only
- **Parasitic Flows Reentry Causes Separation at the Impeller Inlet**
  - Separation not significantly affected by swirl velocity
  - Separation leads to blockage and decrease in static pressure
  - Separation eliminated if parasitic flow reduced to <4.0 lbm/sec (from 9.4)
- **Shroud Cavity Flow Circuit Modified**
  - Impeller back-face leakage routed to the inlet volute
  - Leakage from the shroud cavity into the main flow reduced to 1.6 lbm/sec
  - Flow rate through the igv increased by 7.2 lbm/sec
- **Results Show That the Separation is Eliminated, Pressure Increased**
- **Testing on TTB Showed That Alpha Was Affected by Modification**
  - Not measurable at low Nss, frequency shifted at high Nss values

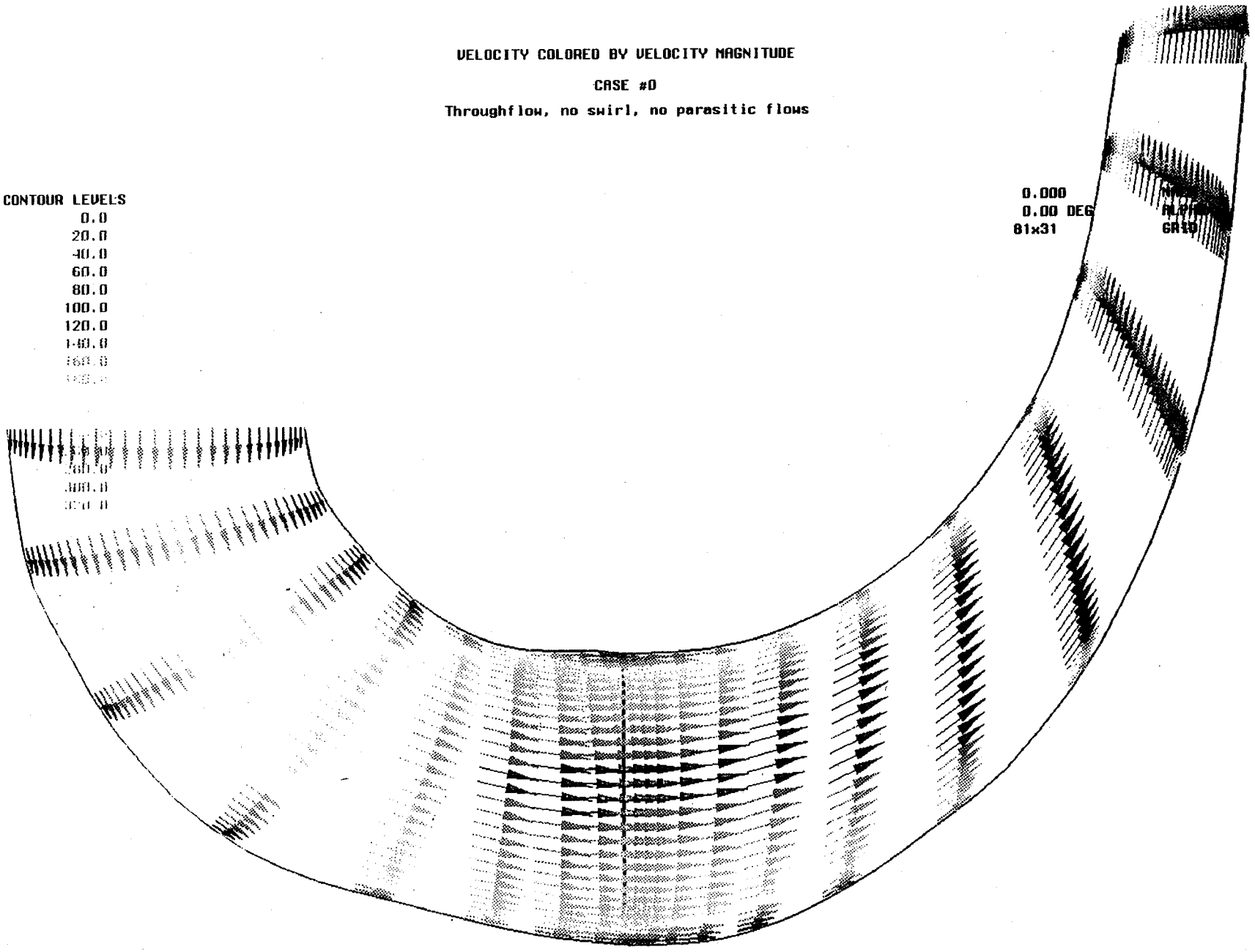
VELOCITY COLORED BY VELOCITY MAGNITUDE
CASE #0
Throughflow, no swirl, no parasitic flows
CONTOUR LEVELS
0.0
20.0
40.0
60.0
80.0
100.0
120.0
140.0
0.000
0.00 DEG
81x31

fdnsq.2.img

VELOCITY COLORED BY VELOCITY MAGNITUDE
CASE #6
Throughflow, swirl, baseline flows, grid sensitivity
CONTOUR LEVELS
0.0
12.5
25.0
37.5
62.5
75.0
87.5
100.0
112.5
125.0
137.5
150.0
162.5
175.0
187.5
200.0
212.5
225.0
237.5
250.0
262.5
275.0
287.5
300.0
312.5
325.0
337.5
350.0
362.5
375.0
387.5
400.0
0.000
MACH
0.00 DEG
ALPHA
93x31
GRID 1
21x21
GRID 2
21x21
GRID 3
37x41
GRID 4
56x16
GRID 5

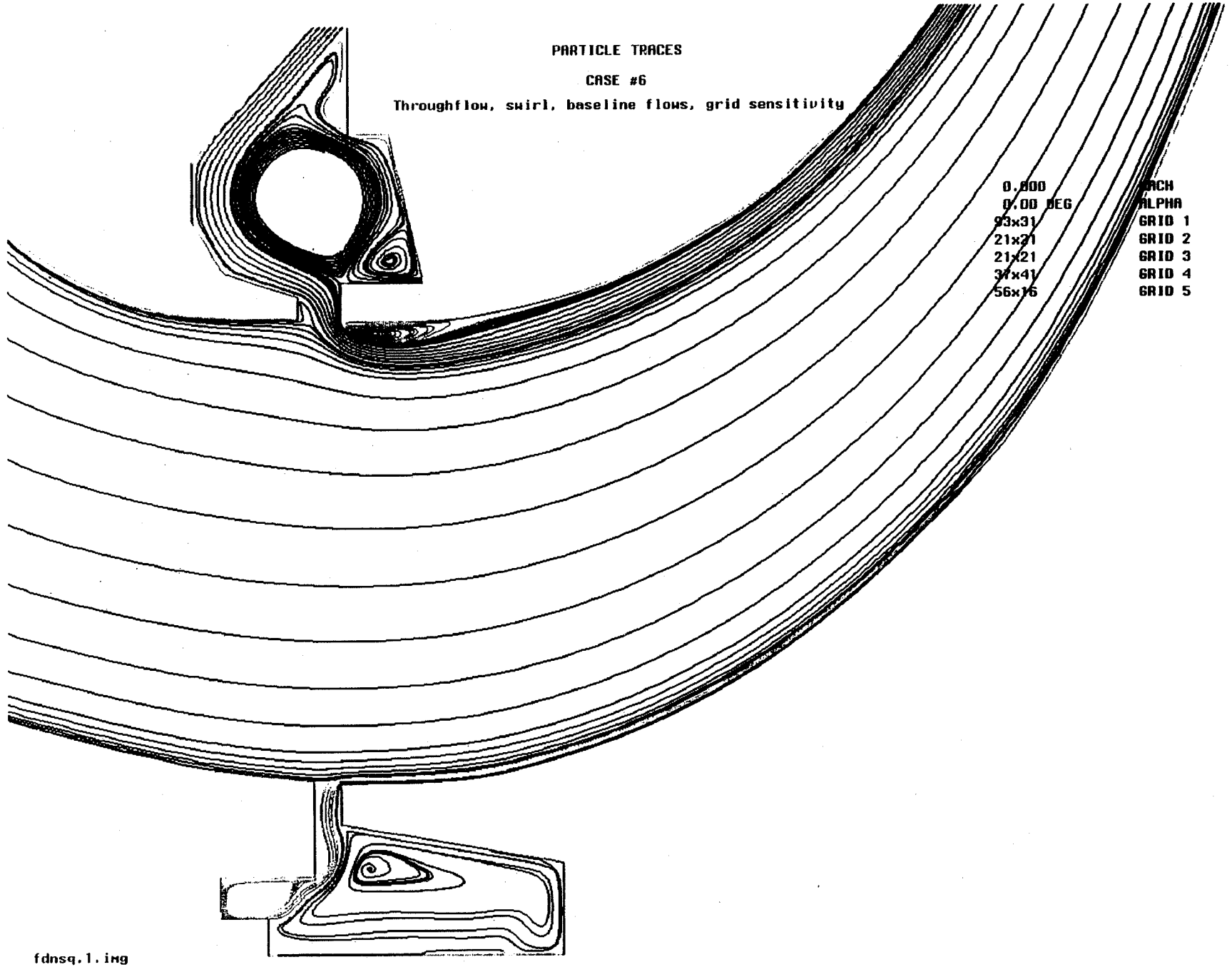
PARTICLE TRACES
CASE #6
Throughflow, swirl, baseline flows, grid sensitivity
0.800
0.00 DEG
93x31
21x21
21x21
31x41
56x16
MACH
ALPHA
GRID 1
GRID 2
GRID 3
GRID 4
GRID 5
fdnsq.1.img

Pump-End Flow Circuit: Modified

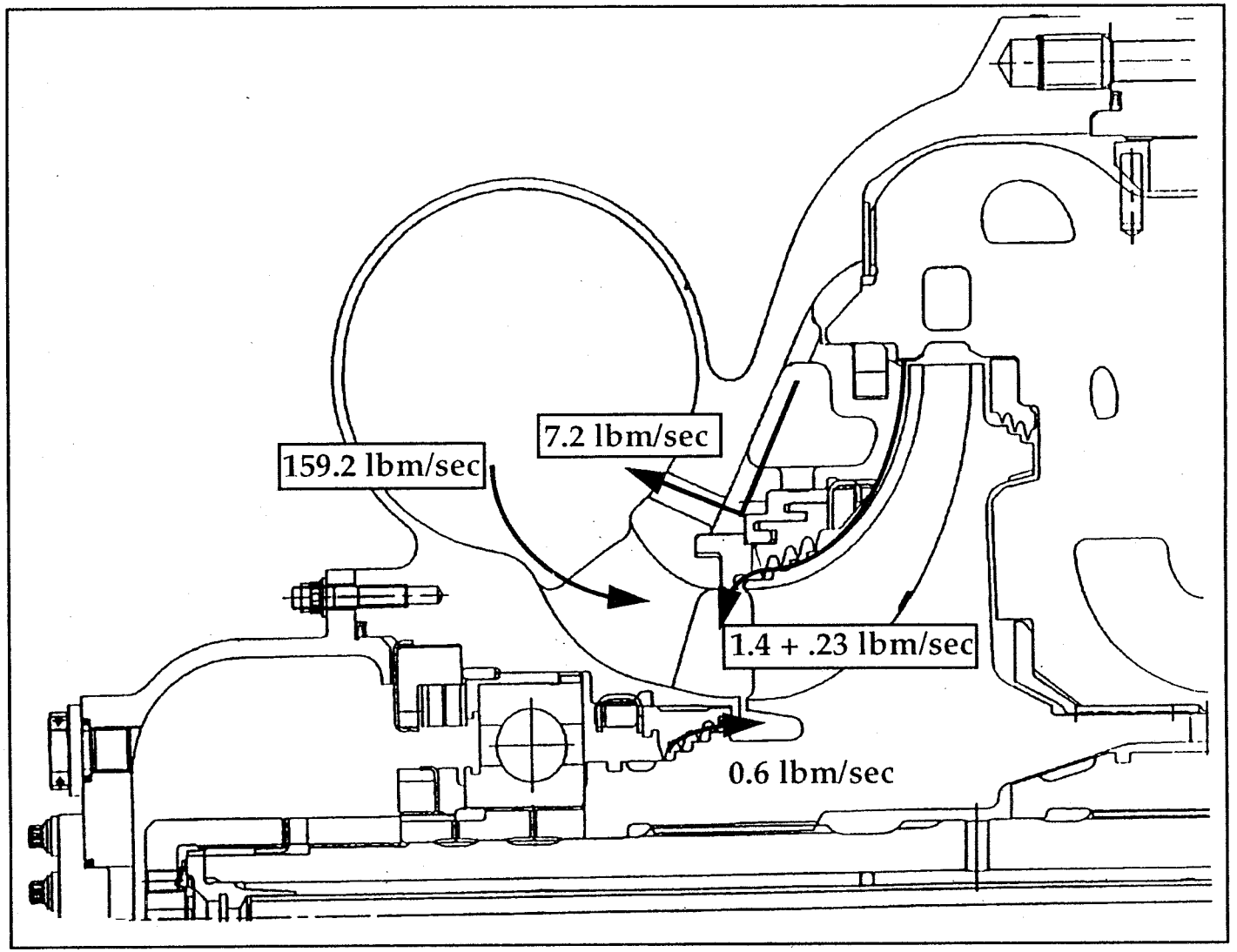

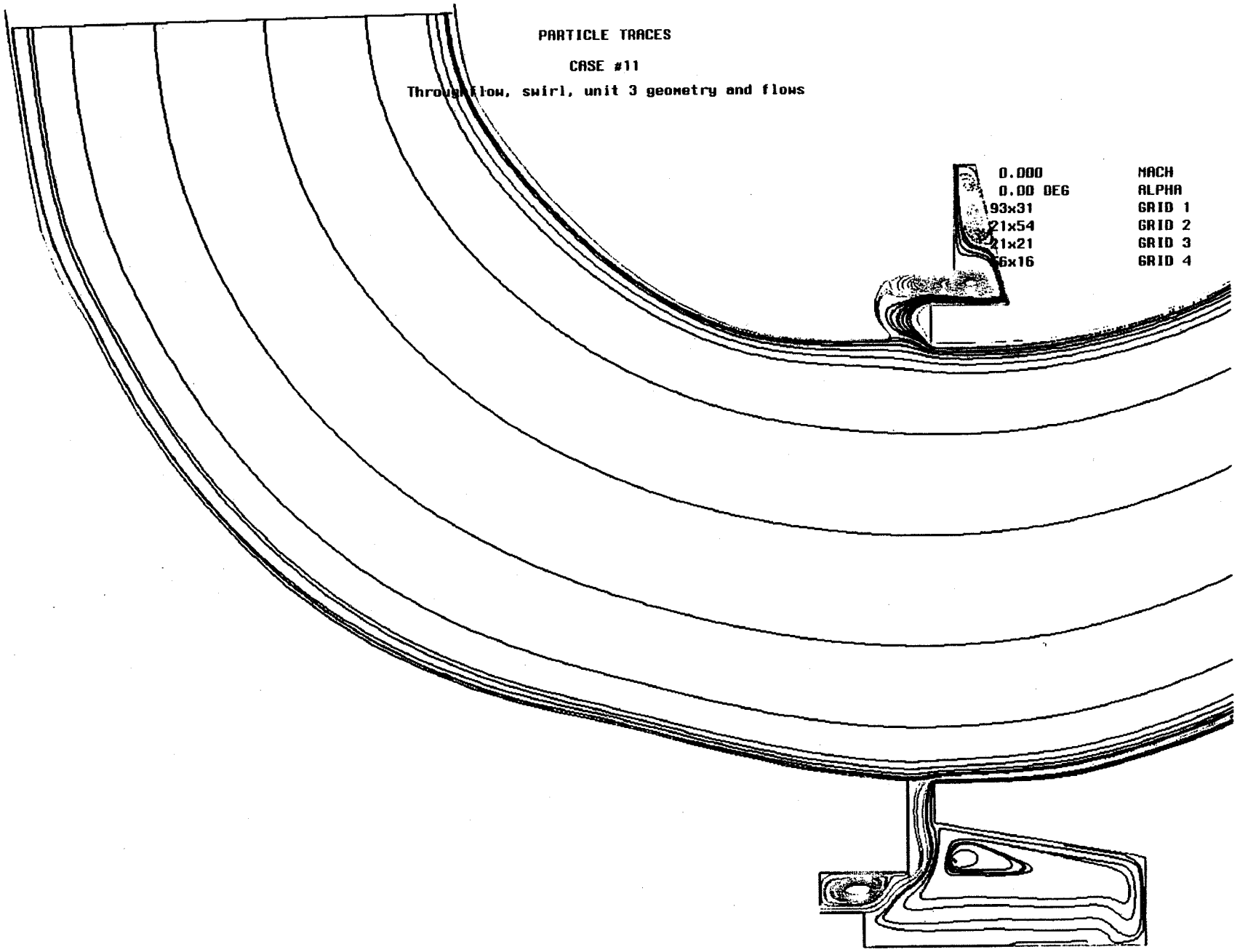
PARTICLE TRACES
CASE #11
Through flow, swirl, unit 3 geometry and flows
0.000 MACH
0.00 DEG ALPHA
193x31 GRID 1
121x54 GRID 2
121x21 GRID 3
96x16 GRID 4

fdnsq.1.img

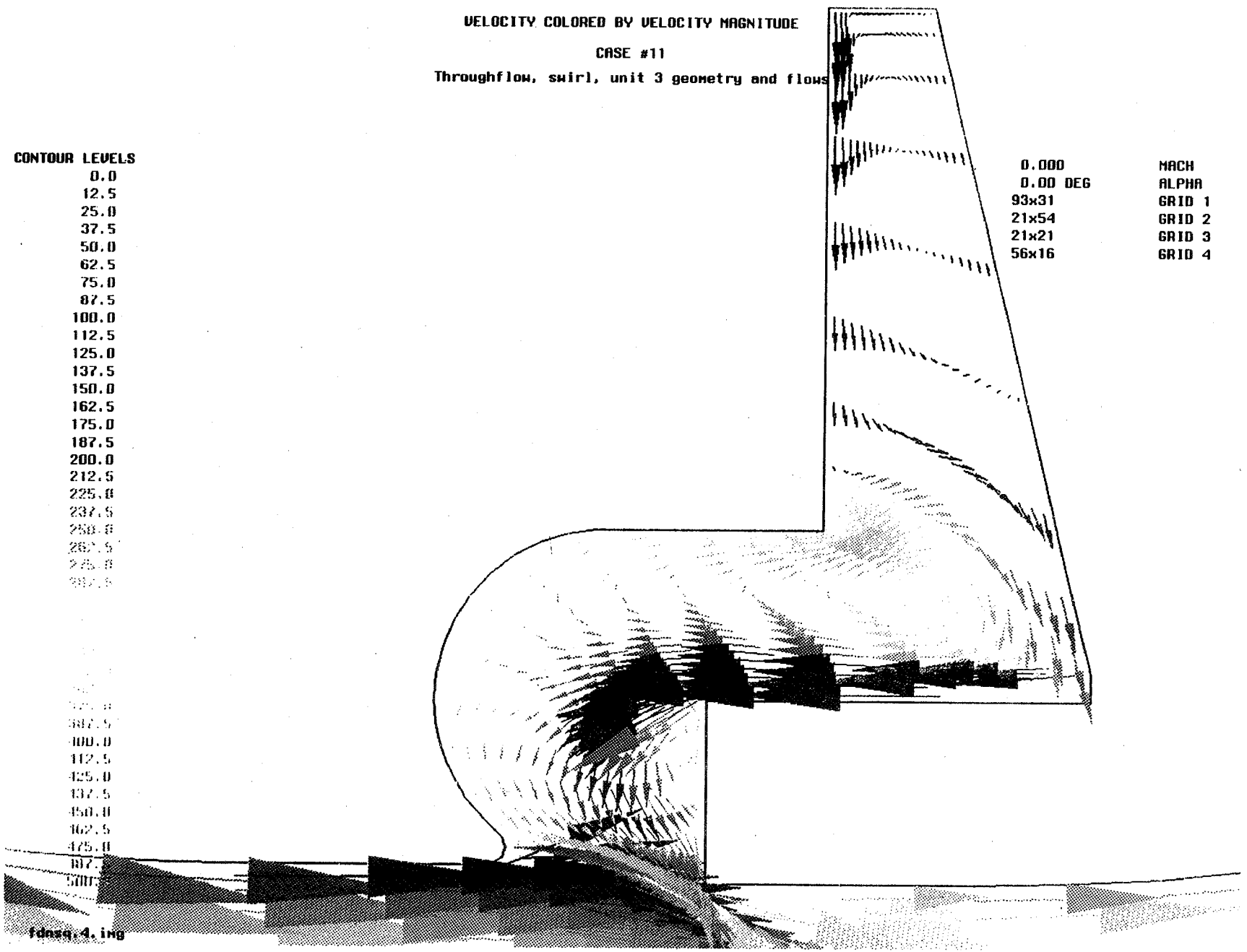
VELOCITY COLORED BY VELOCITY MAGNITUDE
CASE #11
Throughflow, swirl, unit 3 geometry and flows
CONTOUR LEVELS
0.0
12.5
25.0
37.5
50.0
62.5
75.0
87.5
100.0
112.5
125.0
137.5
150.0
162.5
175.0
187.5
200.0
212.5
225.0
237.5
250.0
262.5
275.0
287.5
300.0
312.5
325.0
337.5
350.0
362.5
375.0
387.5
400.0
412.5
425.0
437.5
450.0
462.5
475.0
487.5
500.0
0.000 MACH
0.00 DEG ALPHA
93x31 GRID 1
21x54 GRID 2
21x21 GRID 3
56x16 GRID 4
fdnsq.4.ing

Axisymmetric Results: Impeller Inlet Plane

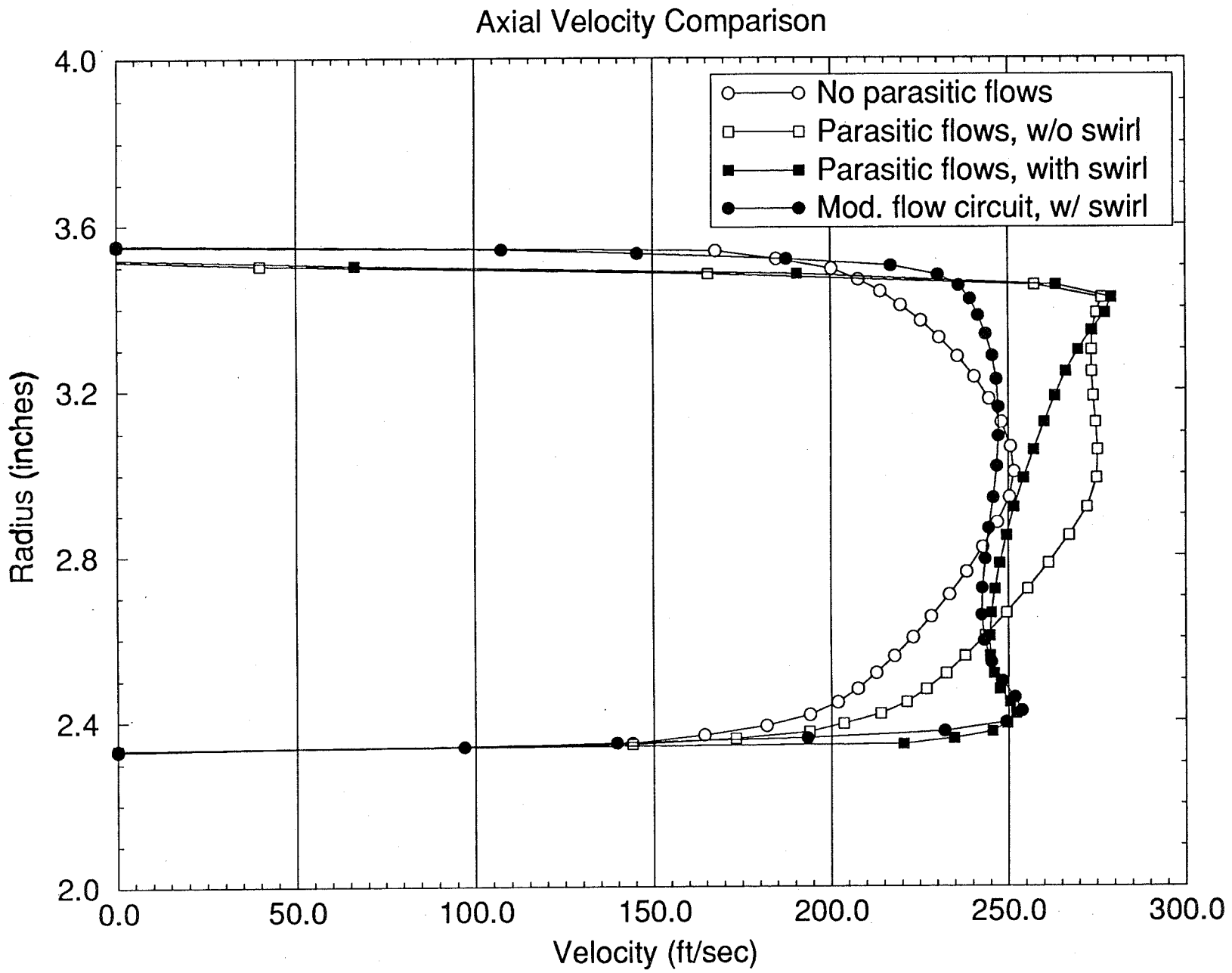

Axisymmetric Results: Impeller Inlet Plane

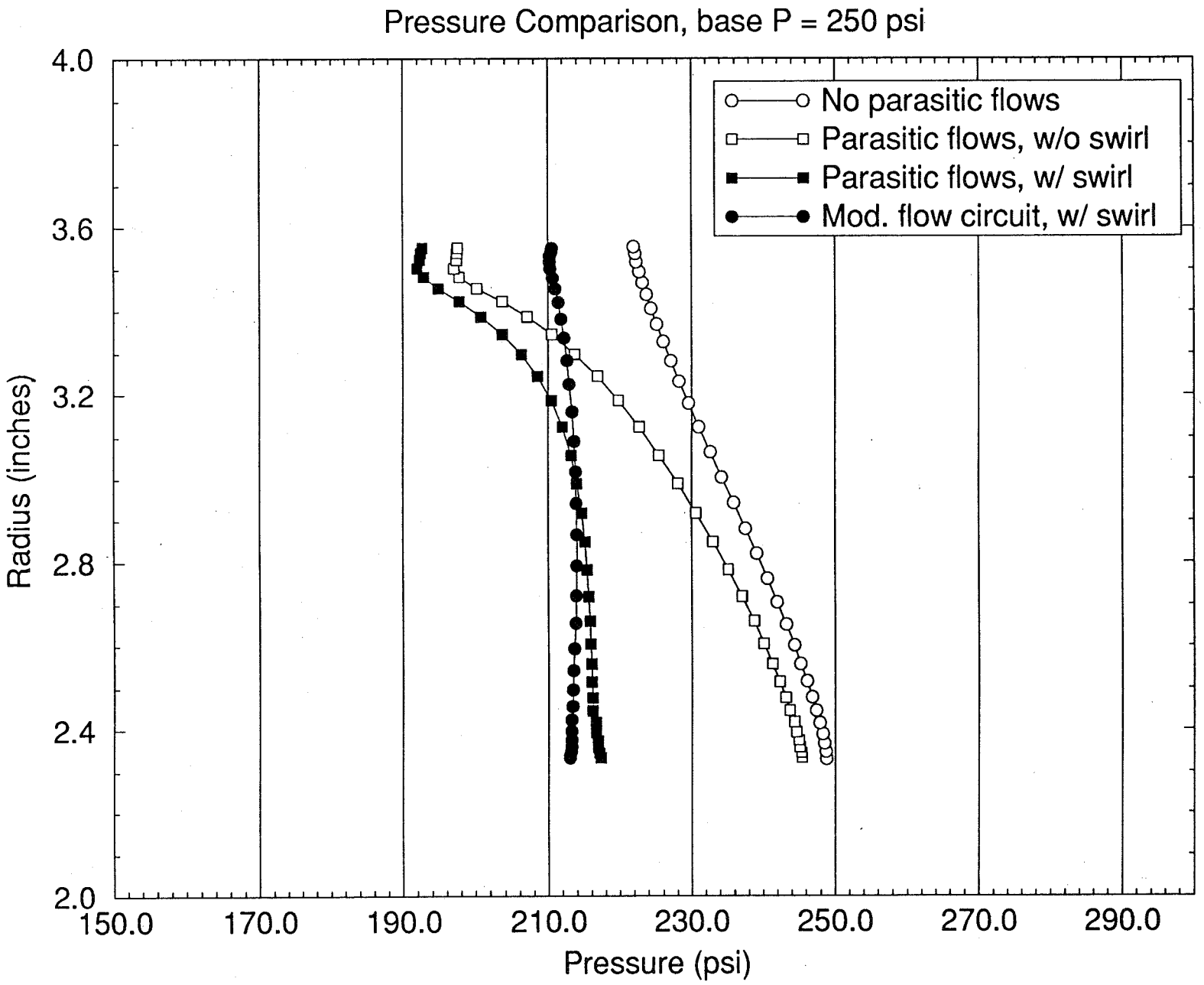

3D Results

- **Coarse Grid (20K points) Used to Model 3 Inlet Swirl Angle Cases**
  - 25, 35, and 45 degrees at the inlet to the domain
    - » **Swirl angle constant from inner to outer wall**
  - Repeated the low swirl angle case with a varying profile from inner to outer wall
    - » **better simulation of the 295 degree location on the water rig**
- **The 35 and 45 Degrees Cases Resulted in Well Behaved Flow Patterns**
  - No separations
  - Moderate adverse to favorable pressure gradient on the suction surface
  - Small secondary flows due to moderate vane loadings

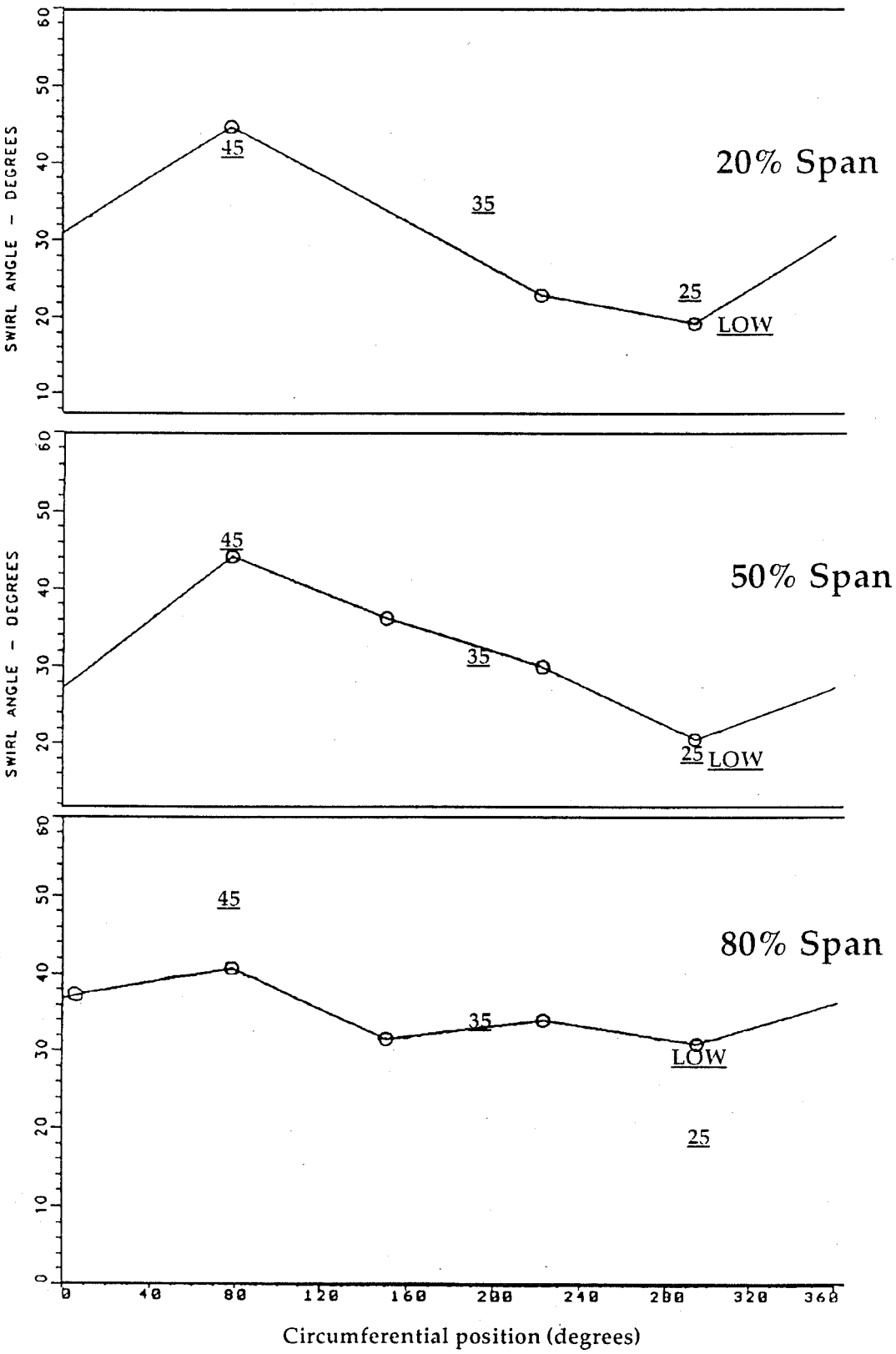

ATD HPFTP Inlet Water Rig Data
IGV Leading Edge Swirl Angle Variation

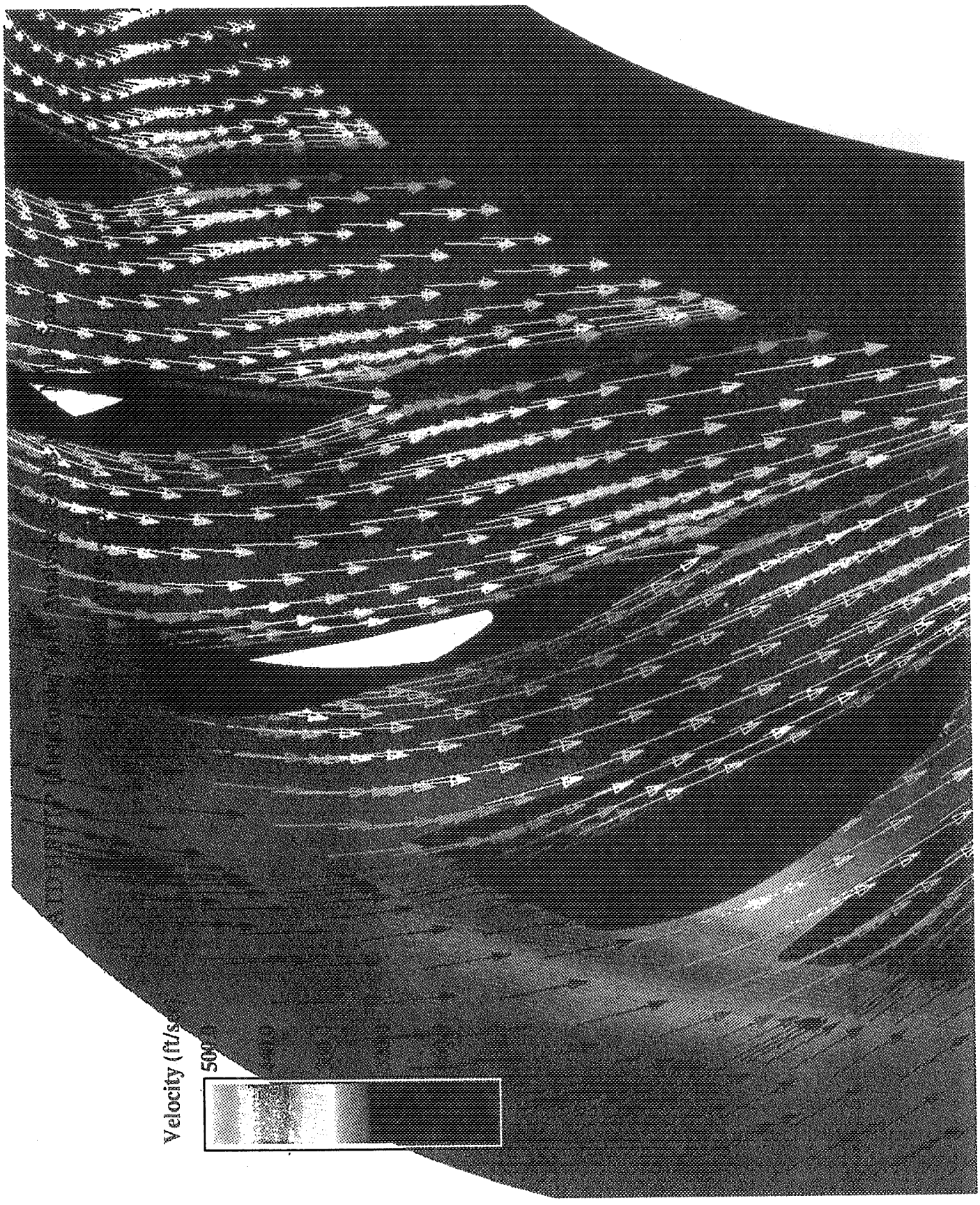
Velocity (ft/s

Inlet Swirl Angle = 35
Pressure (psi)
280.0
260.0
240.0
220.0
200.0
180.0

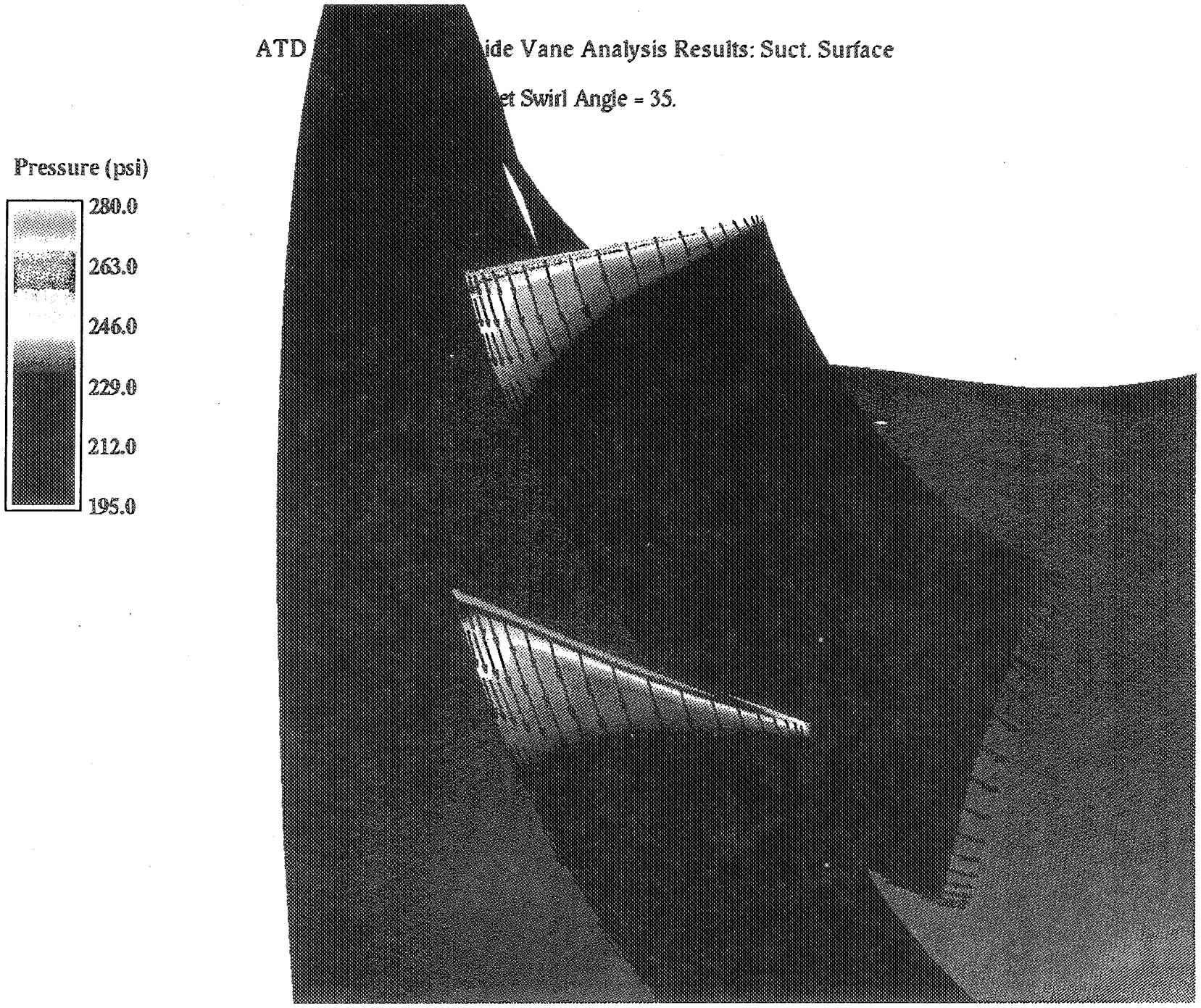
ATD
ide Vane Analysis Results: Suct. Surface
et Swirl Angle = 35.
Pressure (psi)
280.0
263.0
246.0
229.0
212.0
195.0

3D Results (continued)

- **The 25 Degree and "Low" Swirl Angle Cases Yielded Qualitatively Similar Results**
  - High vane inlet incidence angles = high vane loading
  - Vane loadings produce strong secondary flows and adverse pressure gradient
  - Suction surface separated in both cases
    - » **much more so in the 25 degree case**
  - Large vane-to-vane flow variations at the impeller inlet
- **Low Swirl Angle Cases Yielded Negative Incidence at the Impeller Hub, and Largest Incidence at the Impeller Mid-Span**
- **Low Swirl Angle Cases Yielded the Lowest Static Pressure at the Impeller Inlet**
  - Pressure adjusted circumferentially per the water rig data

ATD HPFTP Inlet Guide Vane Anal
Inlet Swirl Angle
Pressure (psi)
260.0
248.0
236.0
224.0
212.0
200.0

Velocity (ft/s

Particle Traces For the 25 Degrees Inlet Swirl Case
Particles Dropped Near the Hub

red = dropped at the l.e.; blue = dropped at the t.e.

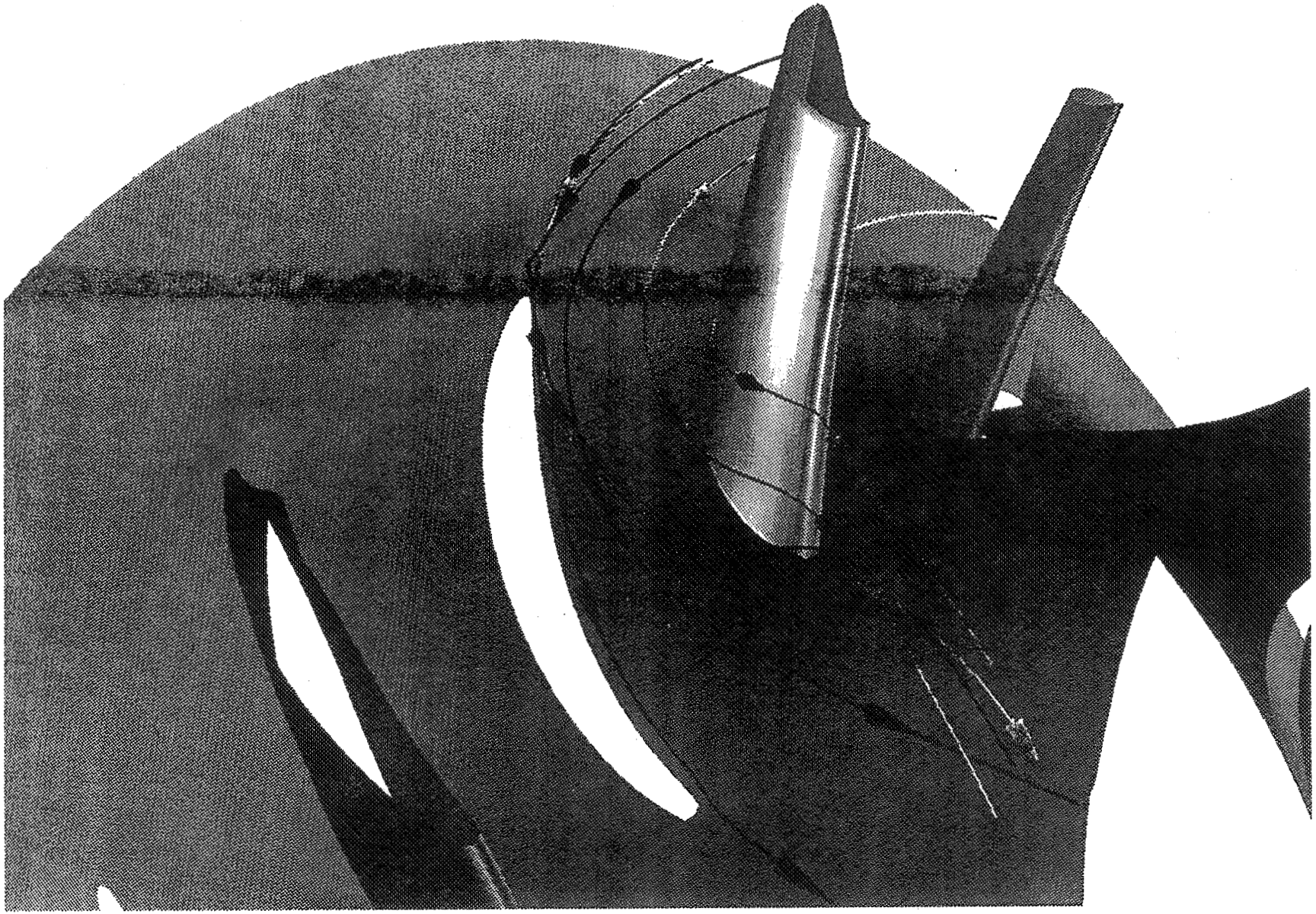

Particle Traces for the 25 Degrees Inlet Swirl Case
Particles Dropped Near Suction Surface
Particles projected to the plane adjacent to the vane

Particle Traces For the 25 Degrees Inlet Swirl Case
Particles Dropped Near Pressure Surface
particles constrained to the plane adjacent to the vane

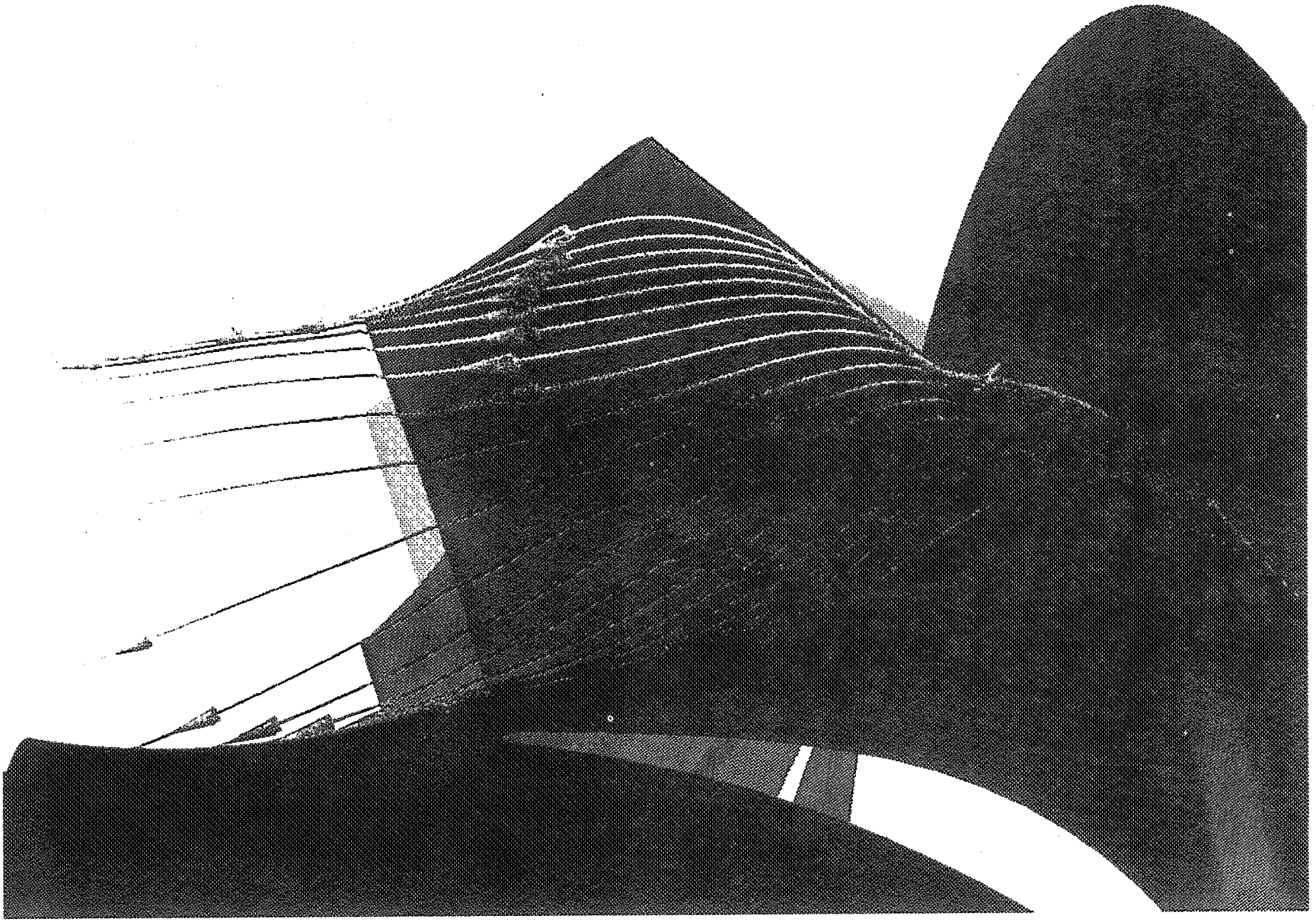

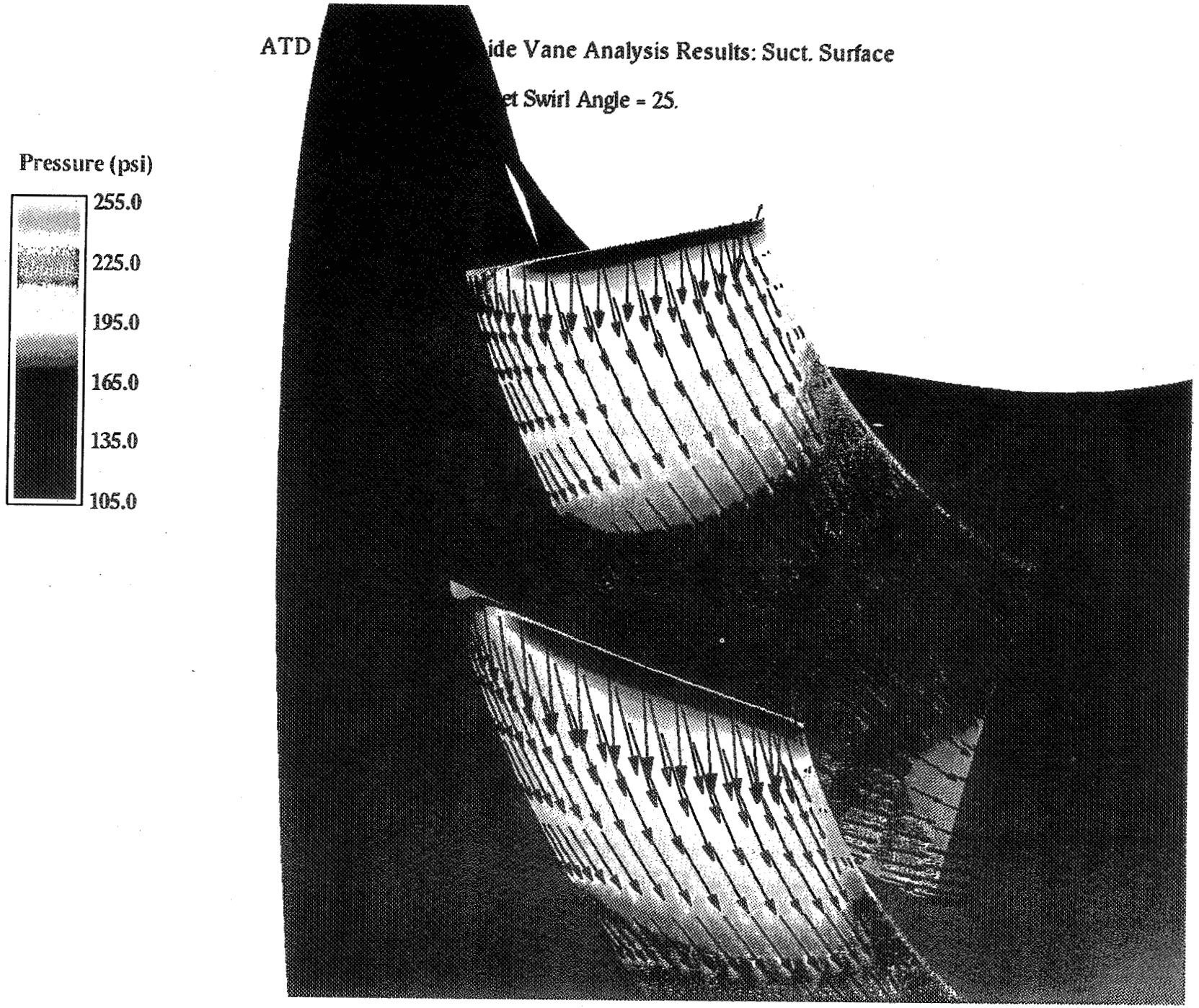
ATD
ide Vane Analysis Results: Suct. Surface
et Swirl Angle = 25.
Pressure (psi)
255.0
225.0
195.0
165.0
135.0
105.0

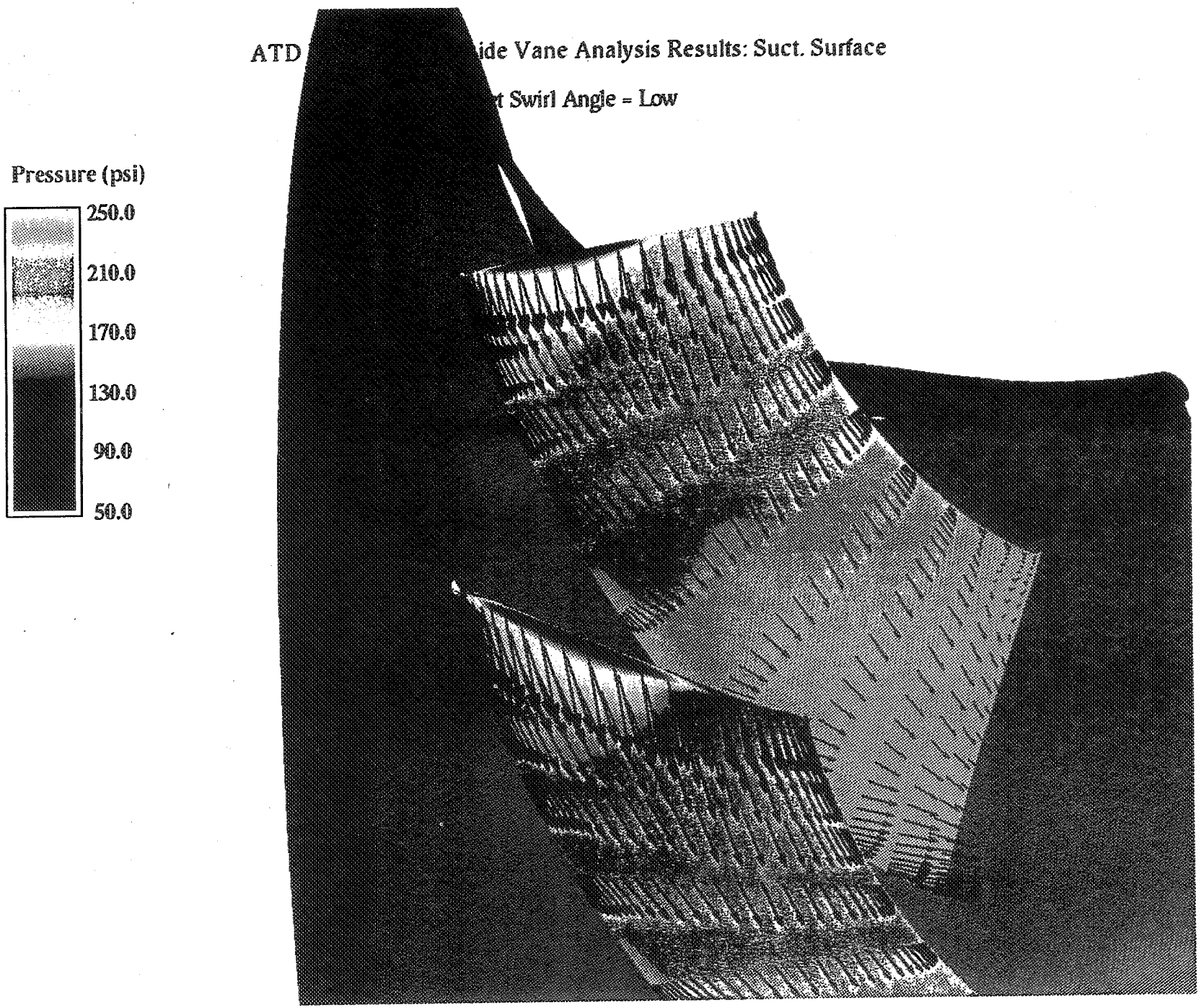
ATD ide Vane Analysis Results: Suct. Surface
t Swirl Angle = Low
Pressure (psi)
250.0
210.0
170.0
130.0
90.0
50.0

ATD HPFTP Inlet Guide Vane Analysis Results: Impeller Inlet

Inlet Swirl Angle = 25

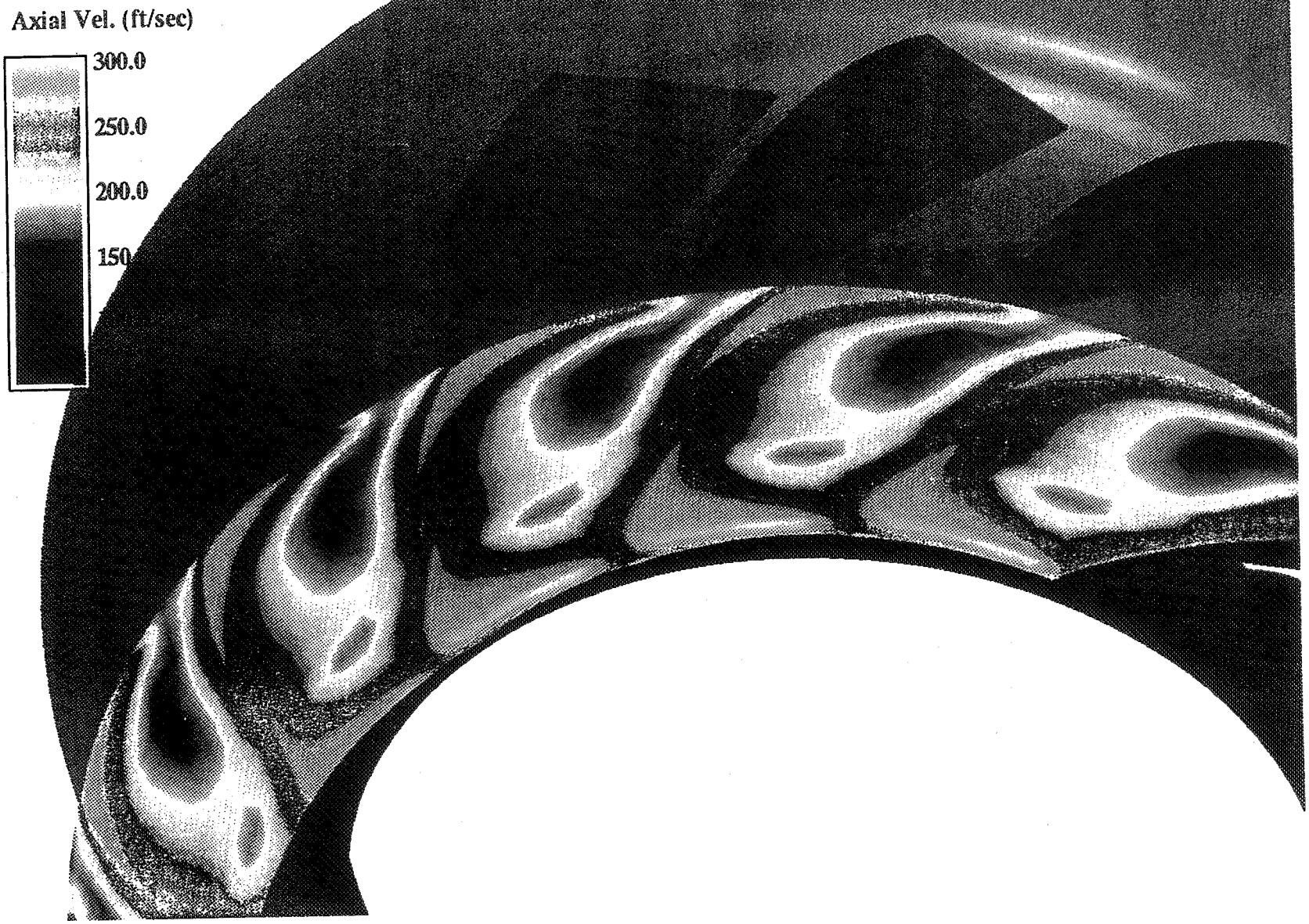

ATD HPFTP Inlet Guide Vane Analysis: Swirl Angle = 25

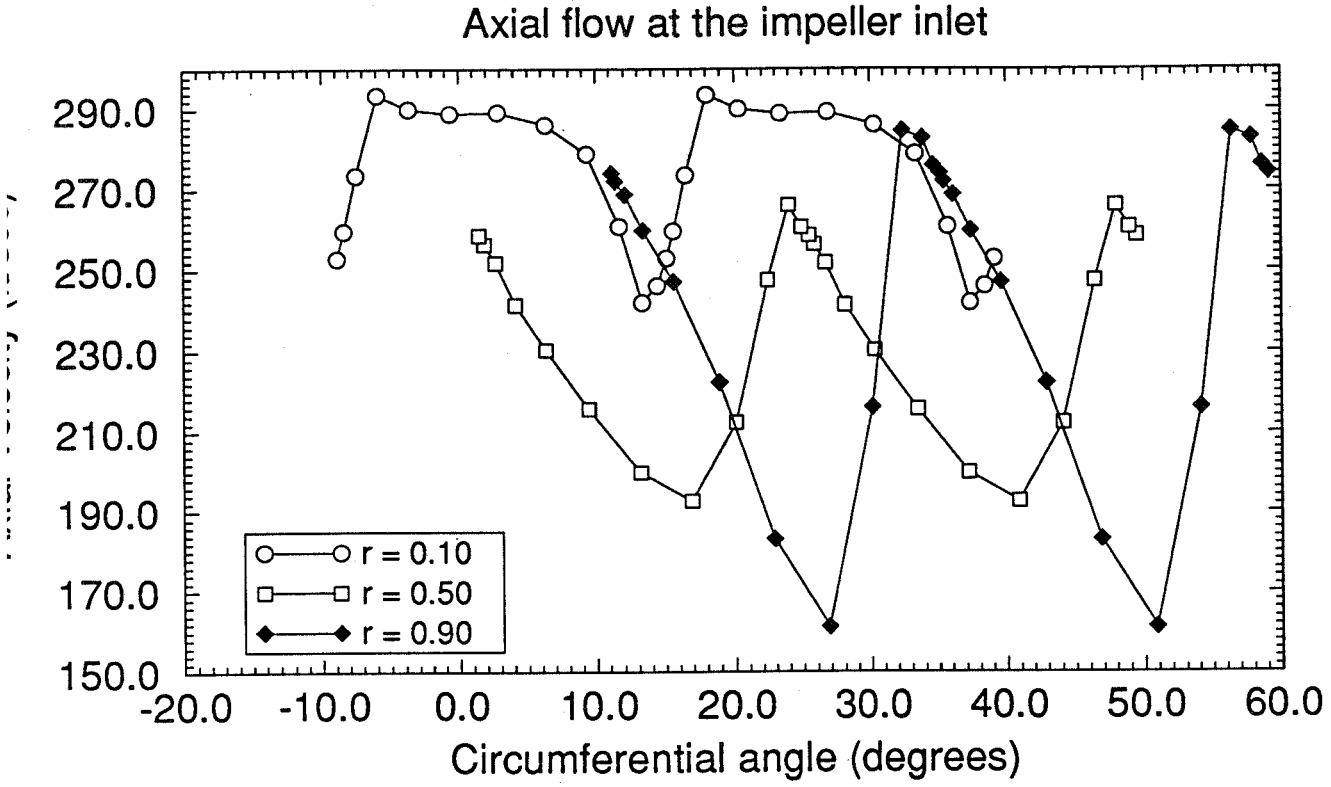

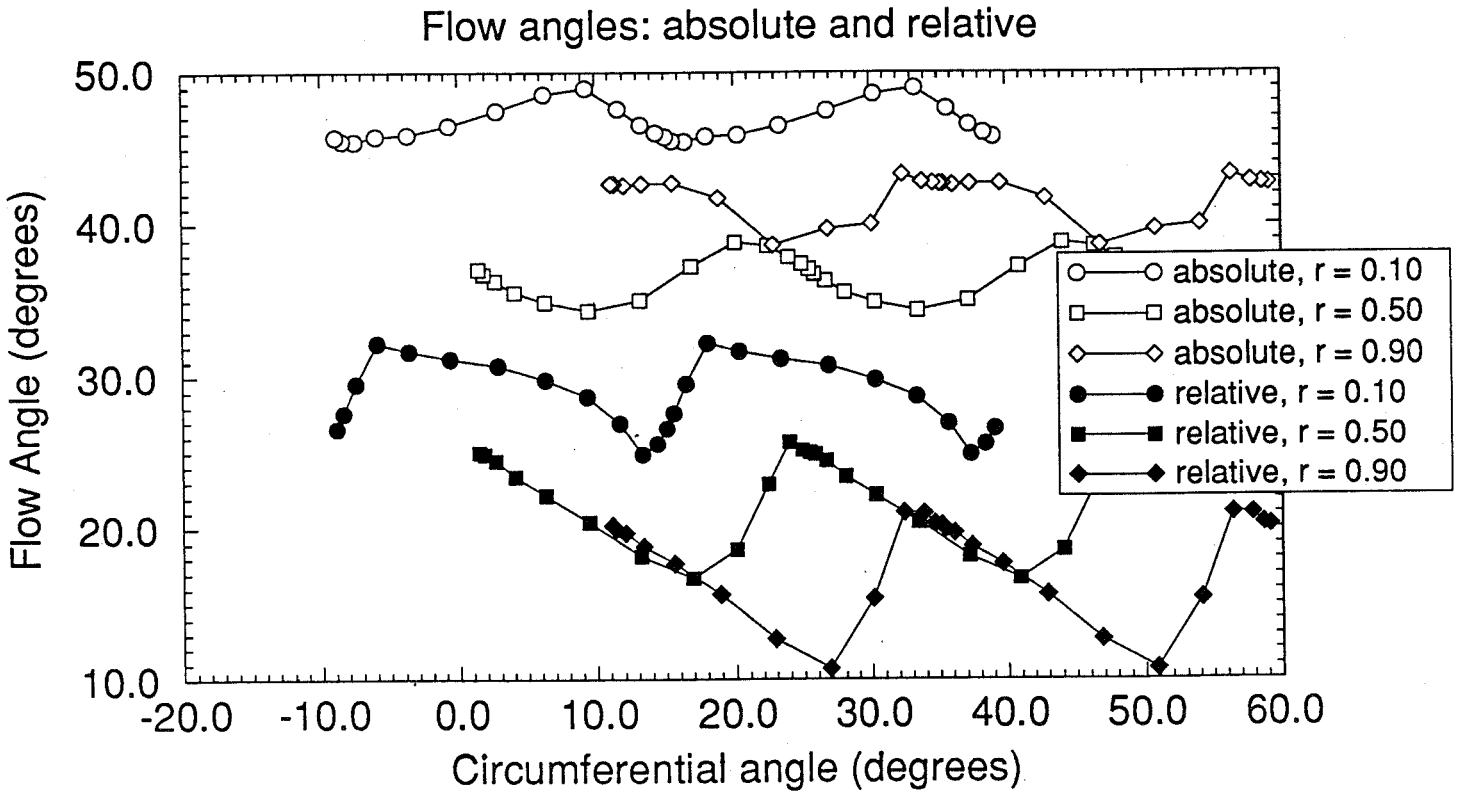

ATD HPFTP Inlet Guide Vane Analysis

Axial flow at the impeller inlet

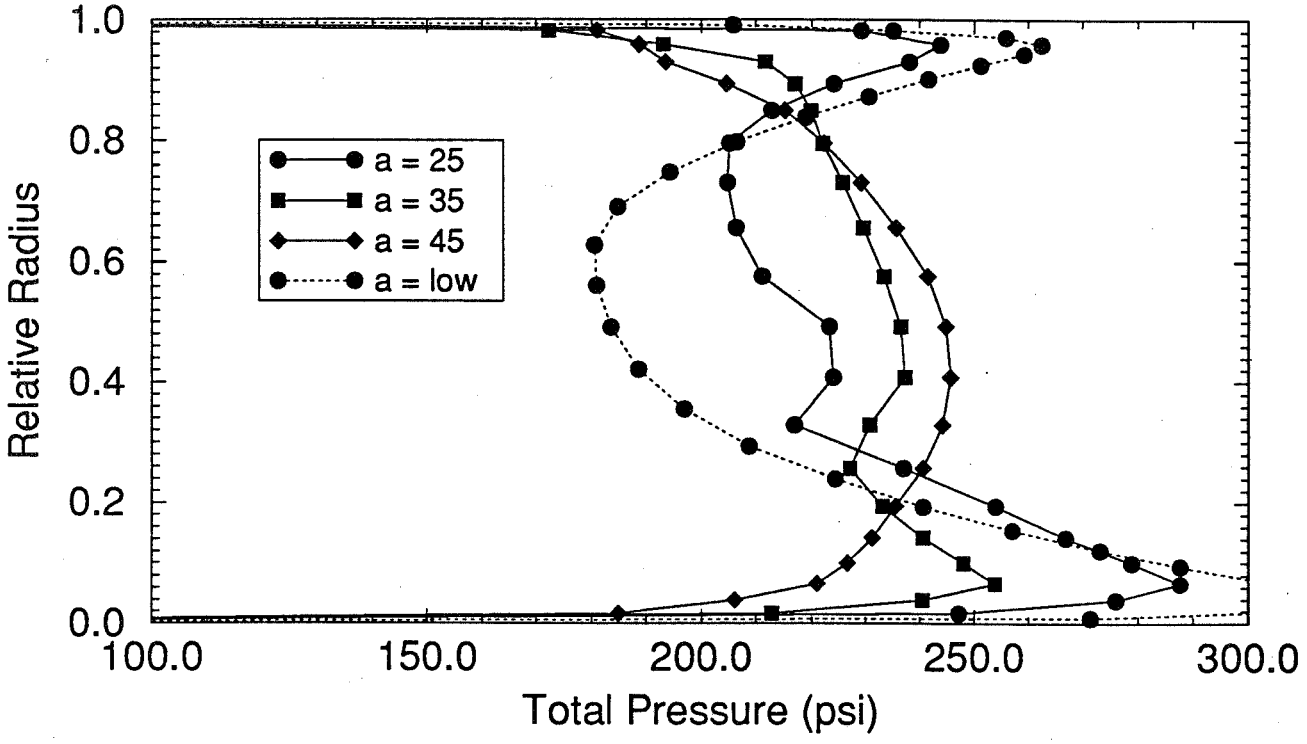

Flow angles: absolute and relative

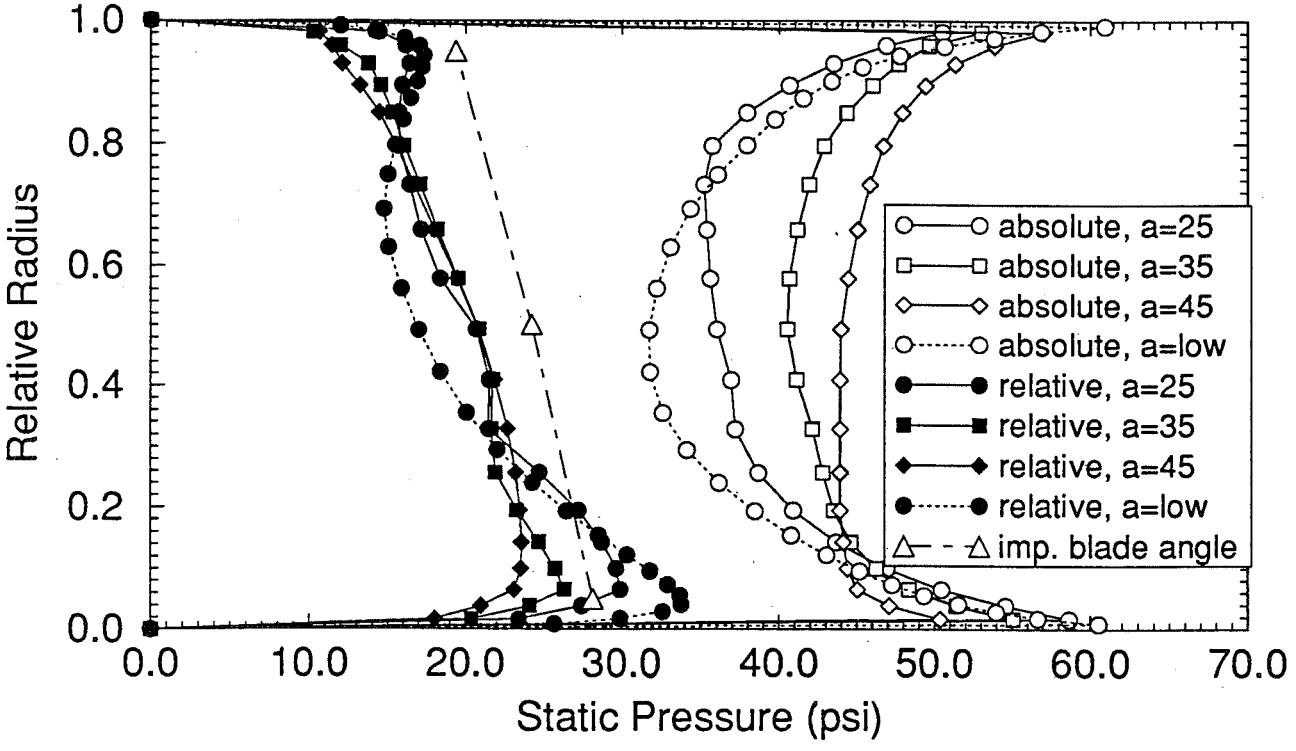

ATD HPFTP Inlet Guide Vane Analysis

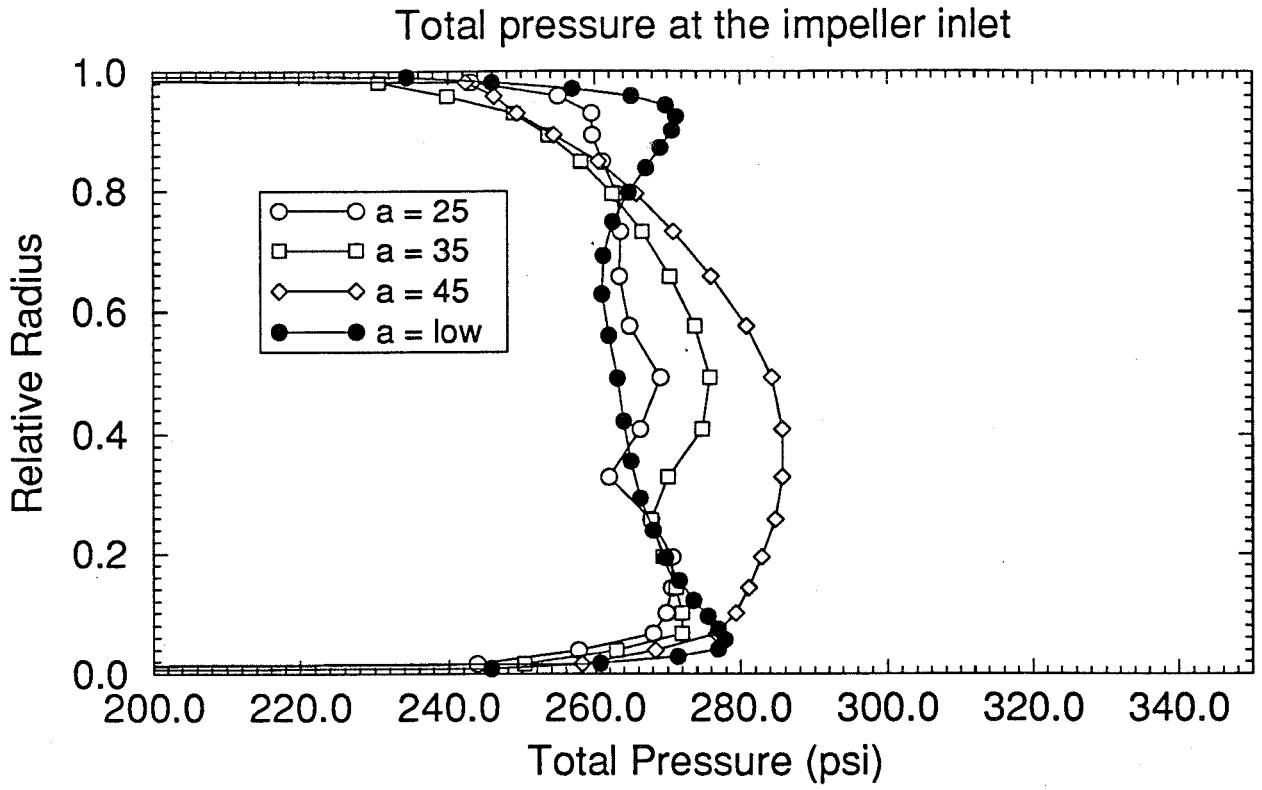

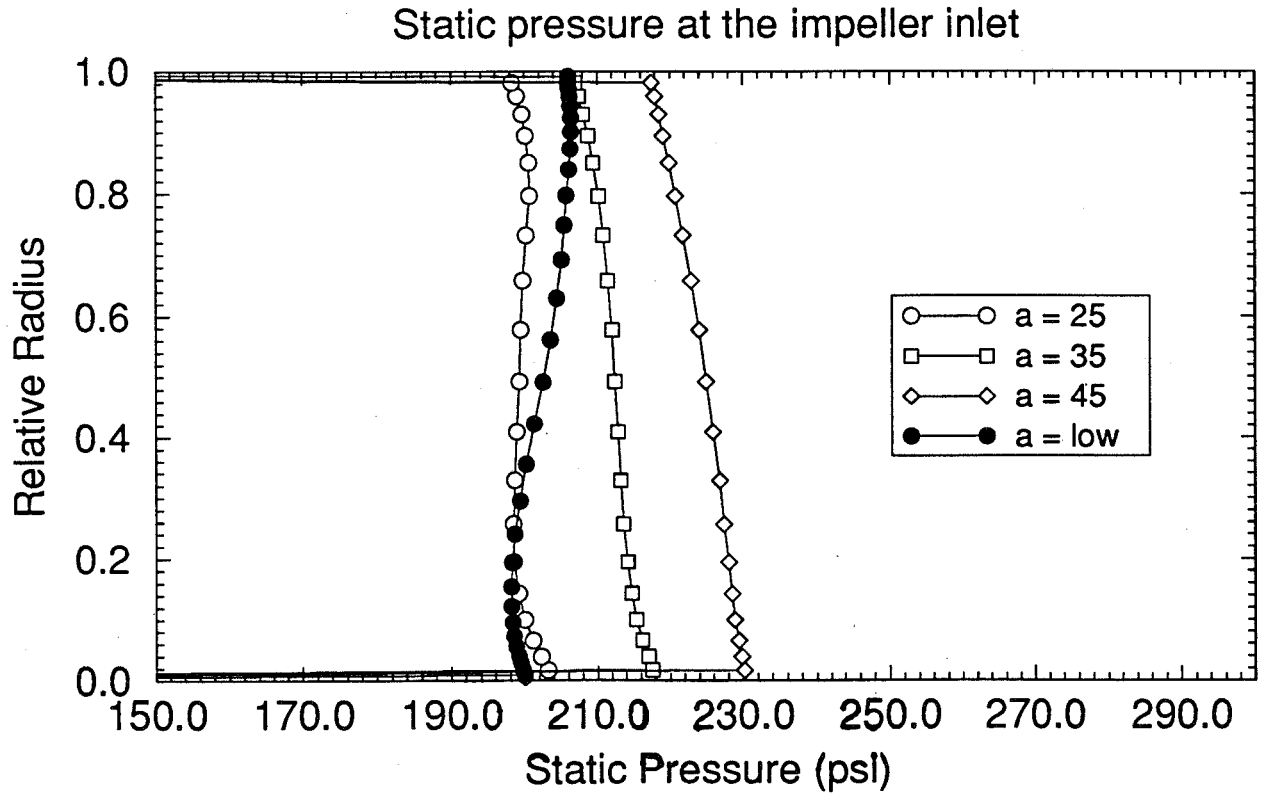

Summary/Conclusions

- **CFD Analysis Used to Support the ATD HPFTP Alpha Frequency Investigation**
- **Axisymmetric Analyses Showed Need For Modifying the Parasitic Flow Circuit**
  - Modified circuit showed improvement over the baseline in hot-fire test
- **3D Analyses of the IGV Indicates Significant Flow Variation Circumferentially at the Impeller Inlet**
  - Lowest static pressure coincident with the highest incidence angle variation along the span

Dynamic Water Flow Tests Using Four-Bladed Axial Flow Inducers

Tom Nesman, and Wayne Bordelon
Fluid Dynamics Division
National Aeronautics and Space Administration, MSFC
Marshall Space Flight Center, AL 35812

Dr. Jen Jong
AI Signal Research, Inc.
3322 South Memorial Parkway. Suite 67
Hunstsville, AL 35801

Abstract

Unsteady fluid mechanisms in pumping systems have the potential of causing high amplitude vibrations in rocket engines. An inducer flow test series using water was conducted to investigate this type of mechanism. The mechanisms of interest are generated by flow through an unshrouded four-bladed inducer. High frequency signal analysis was utilized to determine dynamic characteristics of the flow associated with various inducer blade angles, radial tip clearances, and blade chords. The test was conducted at NASA's Marshall Space Flight Center where the inducer test leg was constructed for this type of testing.

The high frequency characteristics of inducer cavitation were a special focus of the water flow test. Typically, rocket engine turbomachines are required to pump at suction specific speeds near head fall off to achieve the desired efficiency and to perform over the range of varying inlet pressures experienced during boost to orbit. Under these conditions pump inducers are likely to experience local cavitation that can degrade performance and introduce unsteady oscillations to the feed system. The cavitation characteristics observed on these tests followed a fairly repeatable sequence. At relatively high inlet pressure, small cavitation clouds are present behind each of the four inducer blades. The second type of cavitation occurred when the inlet pressure was lowered until two symmetric cavitation clouds appeared behind alternate blades. A third type of cavitation occurred just before head fall-off with two alternate blade cavitation clouds of different size. Distinct pressure oscillation frequencies are associated with each type of cavitation. Oscillations show up as synchronous frequency multiples, non-synchronous anomalous frequencies, as narrow band random signals, or as broadband random noise.

Five different inducer designs were tested. Fluctuating pressure throughout the model and strain on the blade surfaces were measured and correlated to operating parameters and visual observations of the flow. Several digital signal processing techniques were used to analyze the high frequency data. Spectral analysis was performed on all high frequency measurements and plotted as an isospectral plot that showed relative amplitude and frequency versus suction specific speed. A topographical map of the blade fluctuating strain was made to identify the forced response of the blade as a function of chord and suction specific speed. In addition, a new technique called coherent phase wide band demodulation, was used to account for the relative cavitation intensity. The coherent phase wide band demodulation uses the physical modulation relationship between the broadband cavitation noise and unsteady flow oscillations to recover the hidden periodicity buried in the broadband signal of the measured fluctuating pressure. The magnitude of the recovered periodic is used as an indication of relative cavitation severity.

Using the water flow model, the inducer test leg facility was capable of providing suction specific speeds over a wide operational range. This allowed detailed definition of the operational parameters as well as investigation of potential fluid oscillation mechanisms. High frequency signal processing techniques were used to analyze the fluid oscillations with emphasis on cavitation. This presentation provides a synopsis of the observed fluid dynamic behavior in terms of signal characteristics and typical pump operating parameters.

George C. Marshall Space Flight Center
Fluid Dynamics Division

Dynamic Water Flow Tests Using Four-Bladed Axial Flow Inducers

Workshop for CFD Applications in Rocket Propulsion and Launch Vehicle Technology

Tom Nesman and Wayne Bordelon
Fluid Dynamics Division - NASA - MSFC

Dr. Jen Jong
AI Signal Research, Inc.

Introduction

- Unsteady fluid mechanisms in pumping systems have potential of causing high amplitude vibrations in rocket engines
- Inducer flow test series using water conducted to investigate this type of mechanism
- Mechanisms of interest generated by flow through an unshrouded four-bladed inducer
- High frequency signal analysis used to determine dynamic characteristics of flow associated with various inducer blade angles, radial tip clearances, and blade chords
- Test conducted at NASA's Marshall Space Flight Center where inducer test loop constructed for this type of testing

Four Blade Unshrouded Inducer

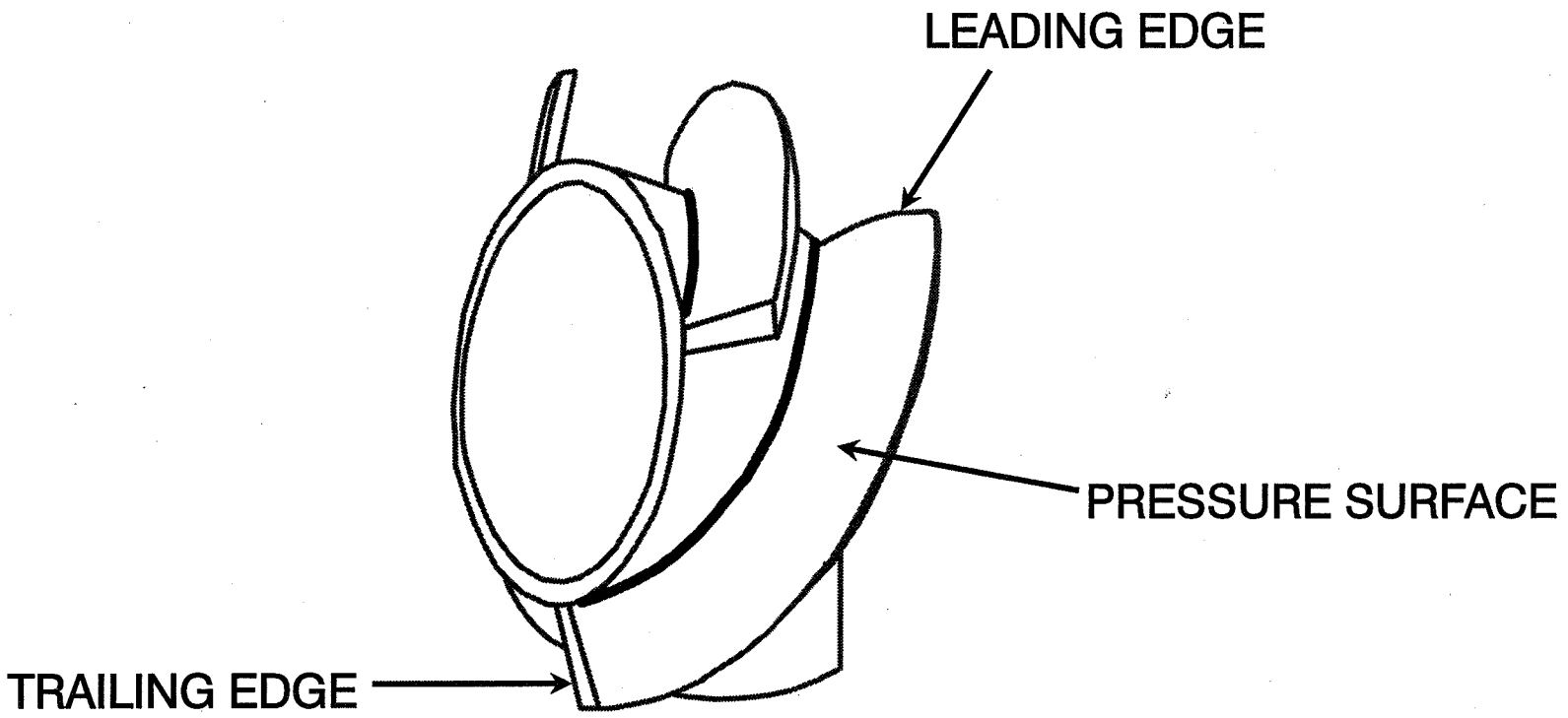

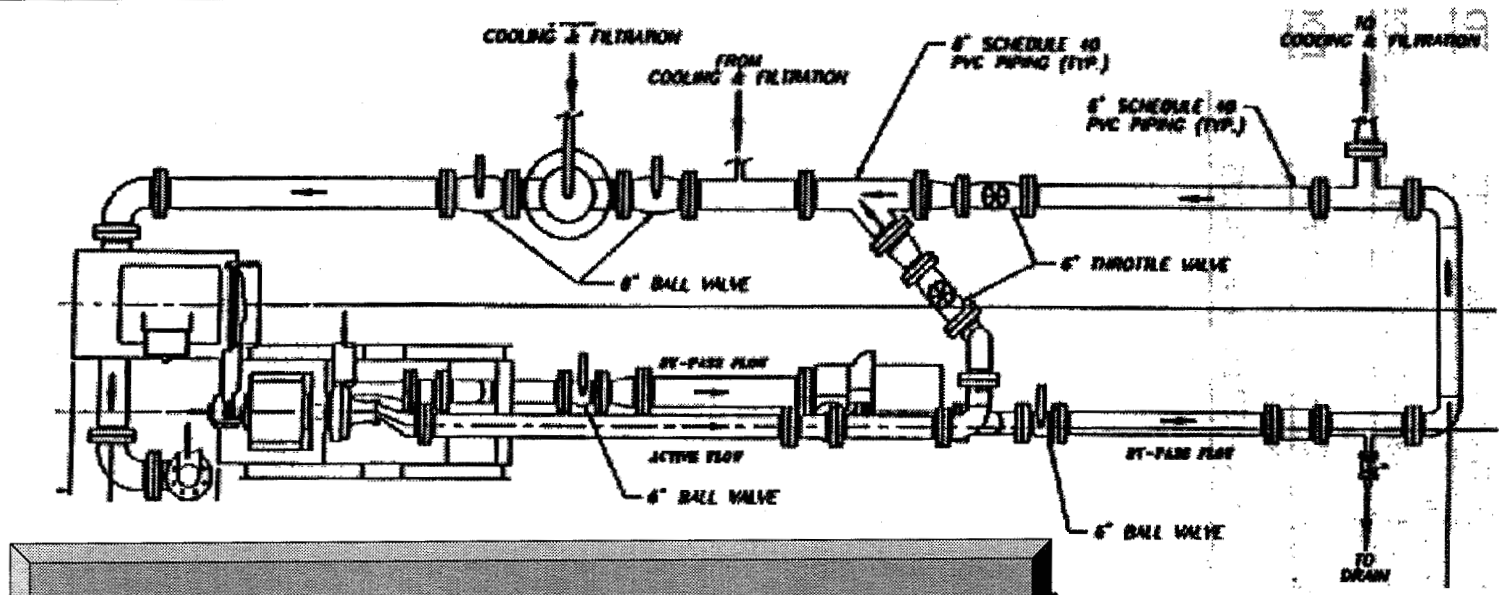

Inducer Test Loop (NASA-MSFC)

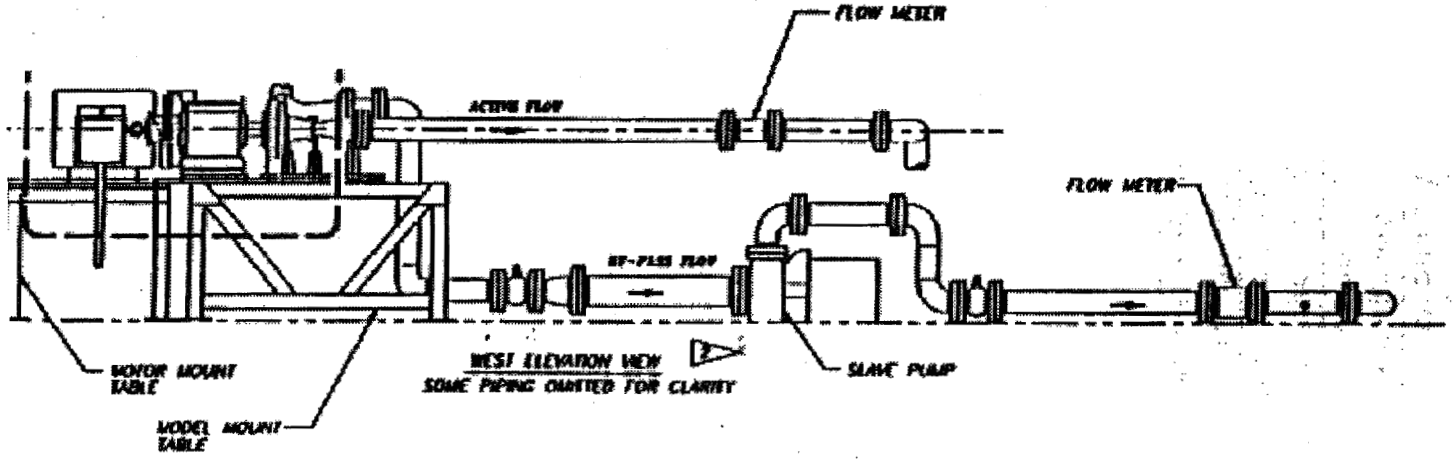

General Characteristics

- Focus --- high frequency characteristics of inducer cavitation
- Rocket engine turbomachines pump at suction specific speeds near head fall off to achieve desired efficiency and to perform over range of varying inlet pressures experienced during boost to orbit
- Under these conditions pump inducers are likely to experience local cavitation
  - Degrades performance
  - Introduces oscillations to feed system
- Cavitation characteristics observed
  - At relatively high inlet pressure, small cavitation clouds are present behind each of four inducer blades
  - Second type of cavitation occurs when inlet pressure is lowered until two symmetric cavitation clouds appeared behind alternate blades
  - Third type of cavitation occurs just before head fall-off with two or four cavitation clouds of different size
  - After head fall-off, surging cavitation is observed
- Distinct pressure oscillation frequencies are associated with each type of cavitation
  - Synchronous frequency multiples, 1N, 2N, 4N ...
  - Broadband random noise
  - Narrow band random signals
  - Non-synchronous anomalous frequencies

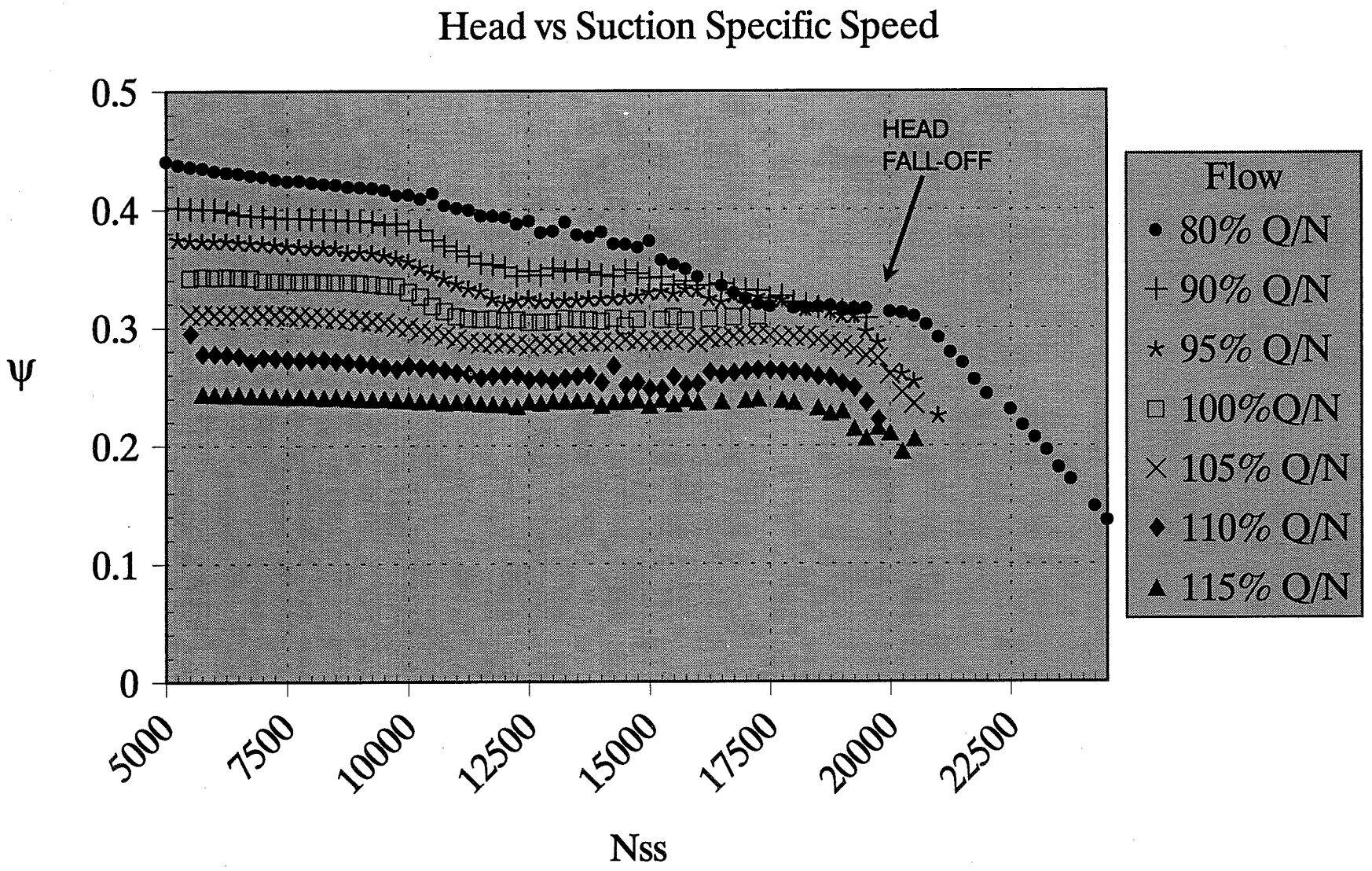
Head vs Suction Specific Speed
HEAD
FALL-OFF
Flow
80% Q/N
90% Q/N
95% Q/N
100%Q/N
105% Q/N
110% Q/N
115% Q/N
ψ
0.5
0.4
0.3
0.2
0.1
0
5000
7500
10000
12500
15000
17500
20000
22500
Nss

Procedure

- Five different inducer designs tested
- Four different inducer tip clearances tested (.005", .010", .020", .030")
- Suction ramp at fixed speed and flowrate
- Oscillatory data measured and correlated to operating parameters and visual observations of flow
  - Fluctuating pressure throughout model
  - Acceleration on housing and shaft support
  - Strain on the blade surfaces
- Several digital signal processing techniques used to analyze high frequency data
  - Isoplot of relative amplitude and frequency versus time
  - Composite rms of blade fluctuating strain as function of chord and suction specific speed.
  - Coherent phase wide band demodulation
    - Uses physical modulation relationship between broadband cavitation noise and unsteady flow oscillations
    - Recovers hidden periodicity buried in broadband signal
    - Magnitude of recovered periodic is indication of relative cavitation severity

Table of Inducer Builds

Designation	Leading Edge ß	Blade Length
Instrumented Baseline	17.6°	Full
Baseline	17.6°	Full
Build 2	15.6°	Full
Build 3	14.6°	Full
Build 4	14.6°	Trailing Edge Cutback
Build 5	15.6°	Trailing Edge Cutback
Instrumented Build 3	14.6°	Full

Typical Suction Ramp

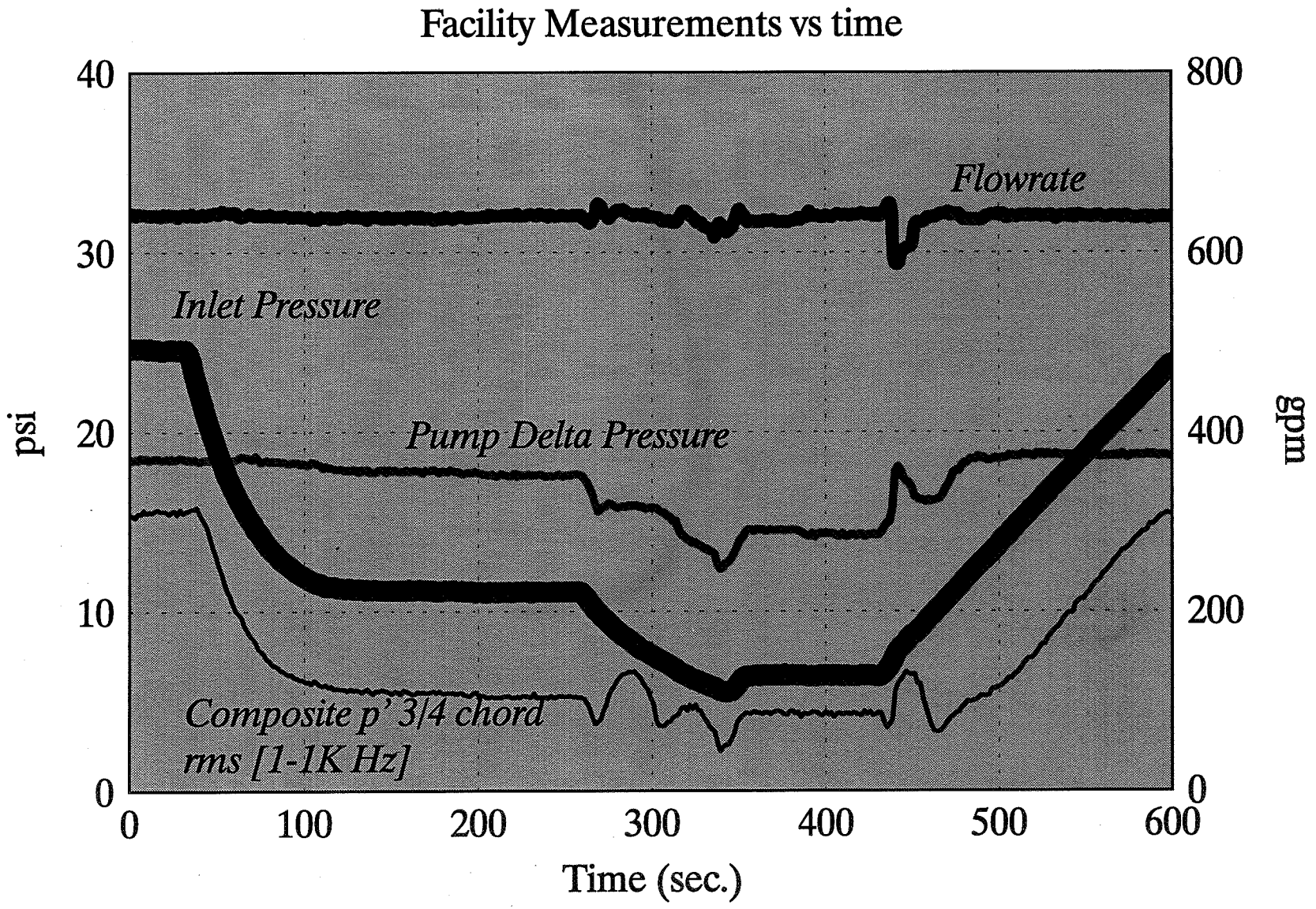

Instrumentation Locations

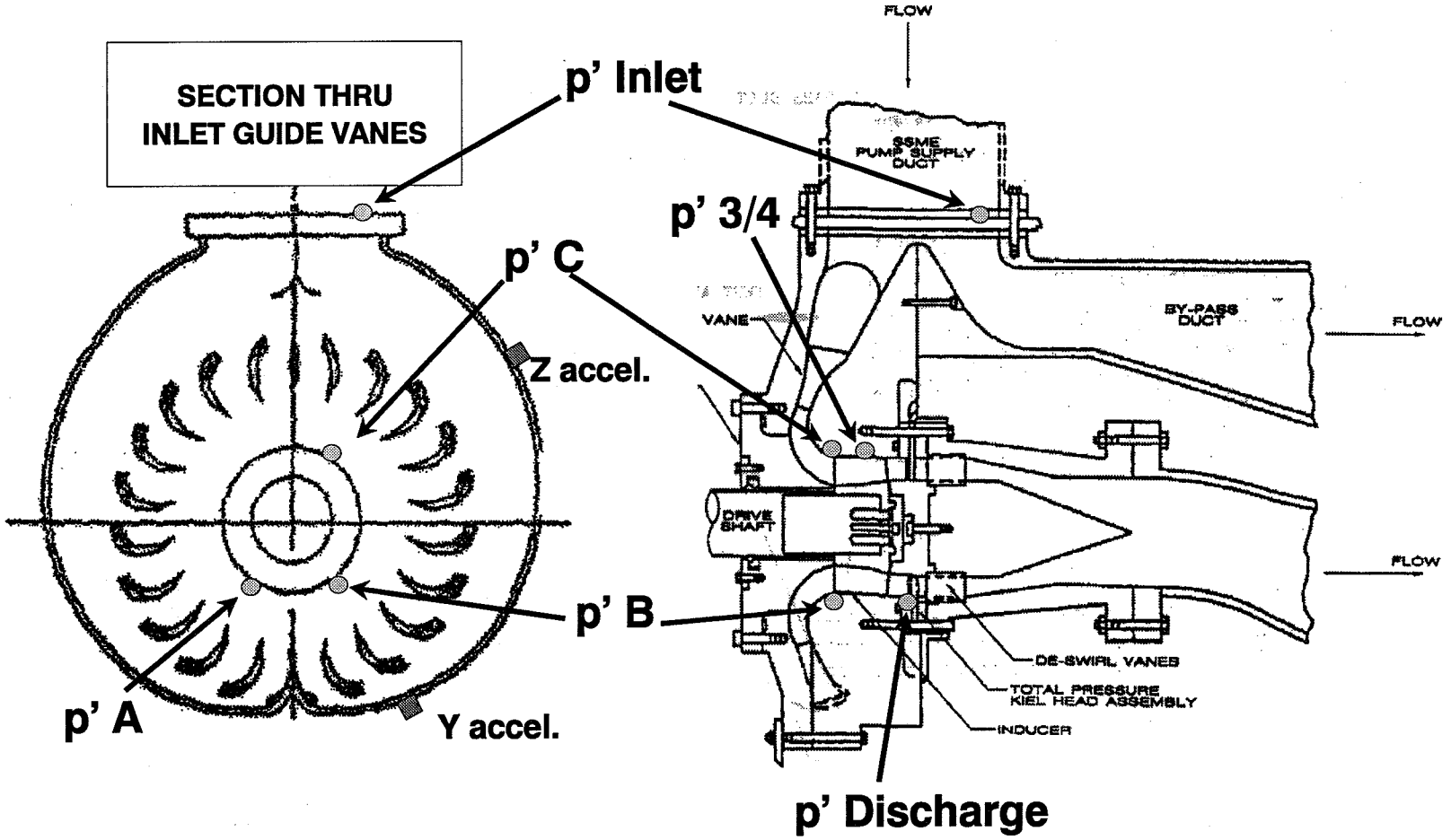

Instrumented Inducer Strain Gages

George C. Marshall Space Flight Center
Fluid Dynamics Division

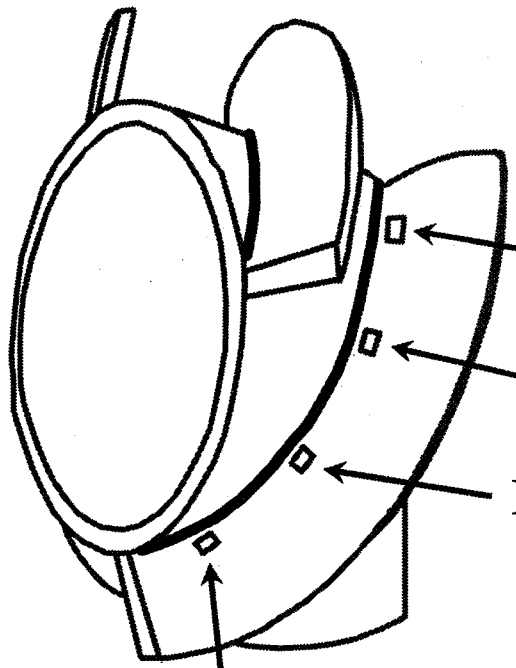

#- : blade number
PS : pressure side
SS : suction side
LE : leading edge
TE :trailing edge
-S : semiconductor
-F : foil

Table of Strain Gage Locations

Blade 1	Blade 2	Blade 3	Blade 4
1-PSLE-S	2-SSLE-S	3-PSLE-F	4-PSLE-S
1-PS38-S	2-PS38-S	3-PS38-S	4-PS38-S
1-PS60-S	2-PS60-S	3-PS60-S	4-PS60-F
1-PSTE-S	2-SSTE-S	3-PSTE-F	4-PSTE-S

Results

- 1.4 N anomalous frequency
  - Replicated with baseline inducer
  - Alternating blade cavitation
  - Eliminated in modified inducers
- 4 cavitation regimes
  - Tip cavitation
  - Alternate blade cavitation
  - Asymmetric cavitation
  - Surging
- Synchronous p' amplitude
  - Parameter variation
  - Inducer blade tip
  - Inducer discharge

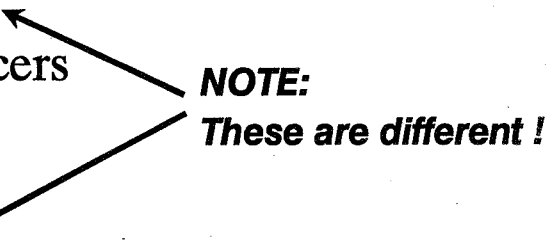

1.4N Anomalous Frequency

Baseline Inducer Discharge p' PSD Isoplot

ITL-1 55/1 - 100% Q/N - 4200 rpm
ß=17.6° - .01" clearance
Full blade

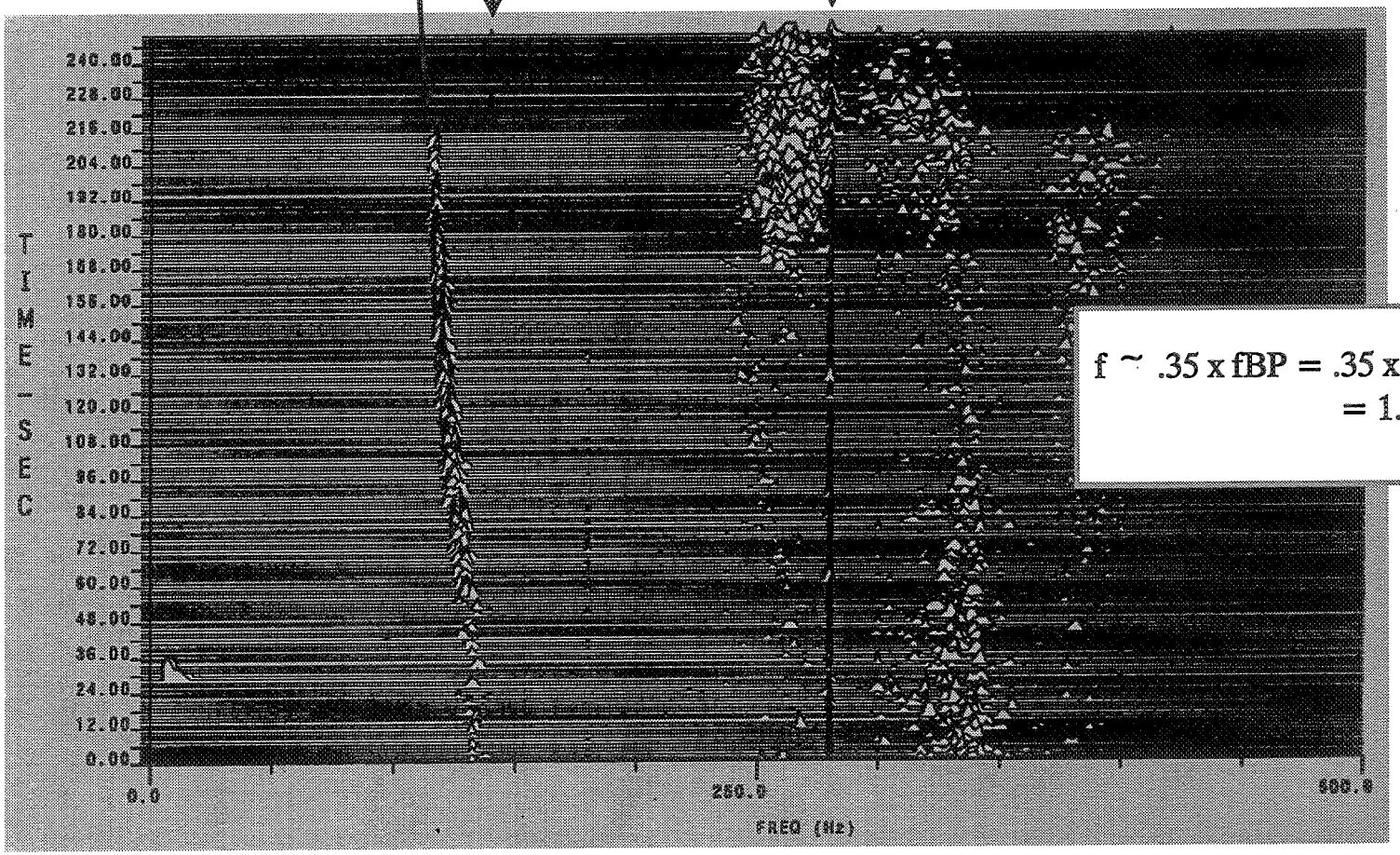

f ~ .35 x fBP = .35 x 4N
= 1.4 N

Build 3 Inducer Discharge p' PSD Isoplot

ITL-2 127/0 - 90% Q/N - 4200 rpm
ß=14.6° - .01" clearance
Full blade

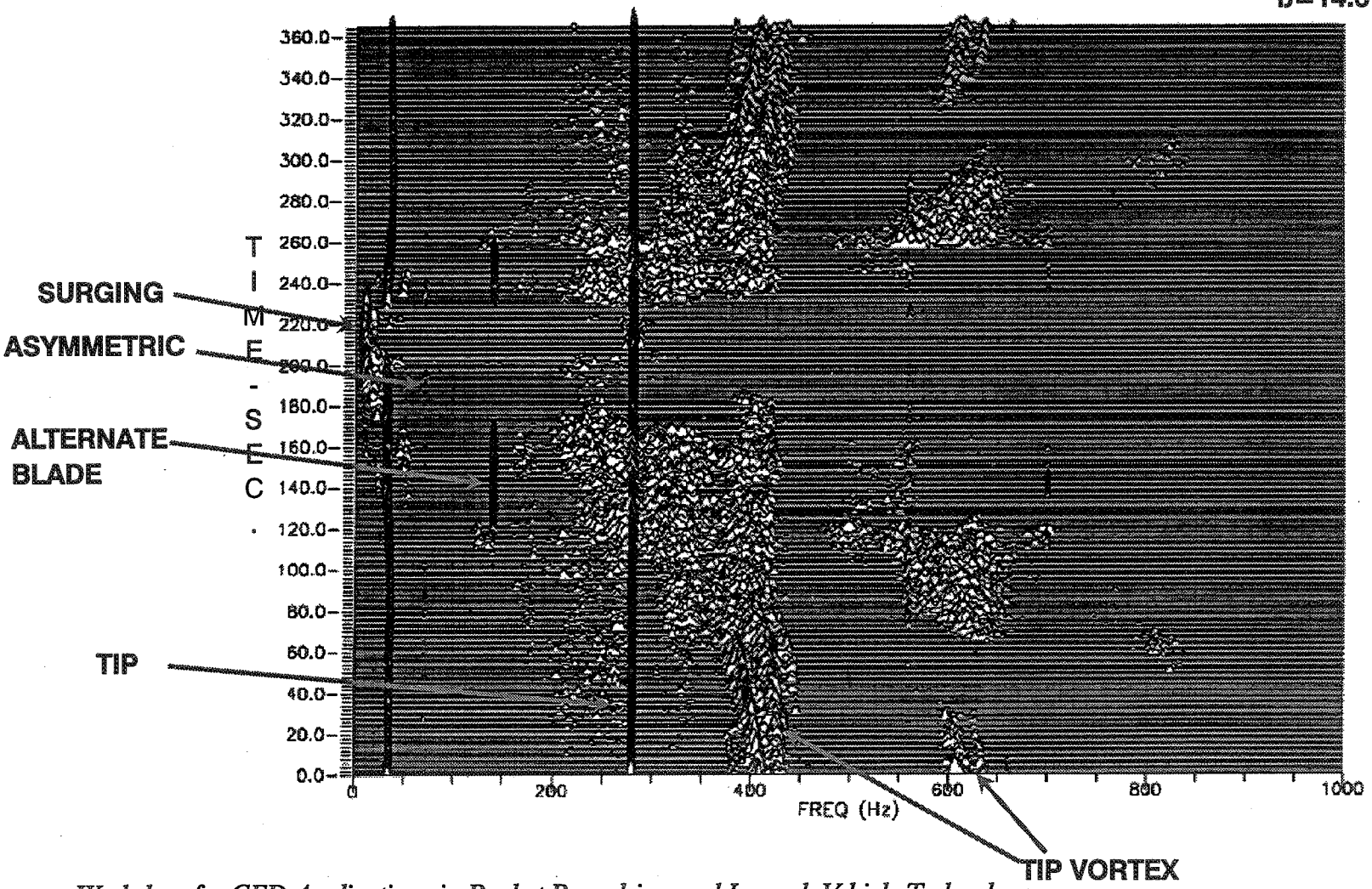

Cavitation Description

George C. Marshall Space Flight Center
Fluid Dynamics Division

Tip Cavitation

- Cavitation cloud behind each blade
- Strong blade passage signature (4N)
  - p' (strongest at tip and 3/4 chord)
  - acceleration (volute housing)
- 5000 < Nss < 9000

Alternate Blade Cavitation

- Cavitation cloud behind two opposite blades only
- High amplitude 2N
  - p'
  - accelerometers
- Coincident "dip" in Head vs Nss curve
- 10,000 < Nss < 15,000

Asymmetric Cavitation

- 2 or 4 cavitation clouds of different size
- 14,000 < Nss < 15,000
- Occurs again at higher Nss at discharge

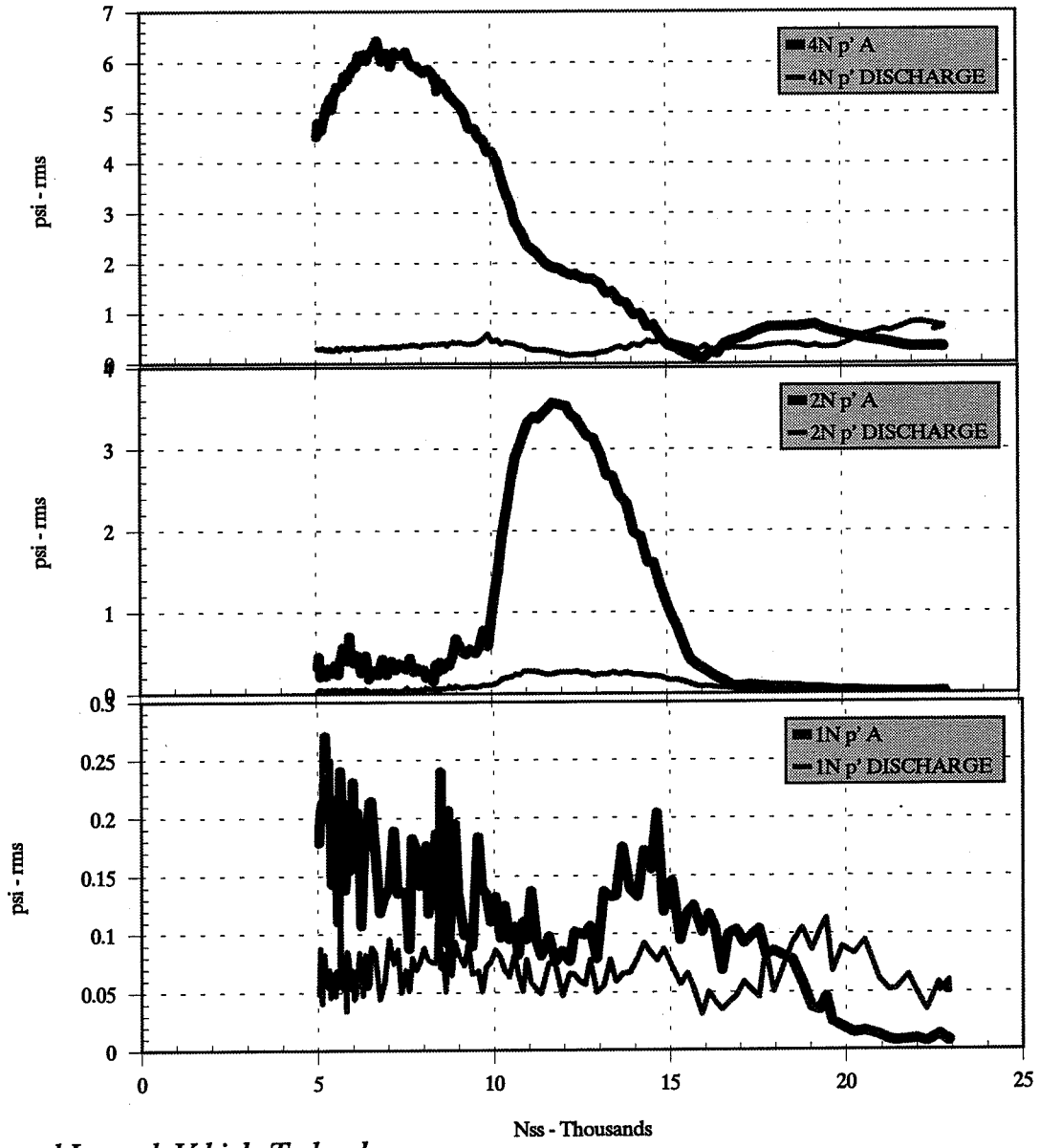

14.6 .030 Full Blade 100%Q/N
ITL-6 40/1
microstrain rms [1-1000 Hz]

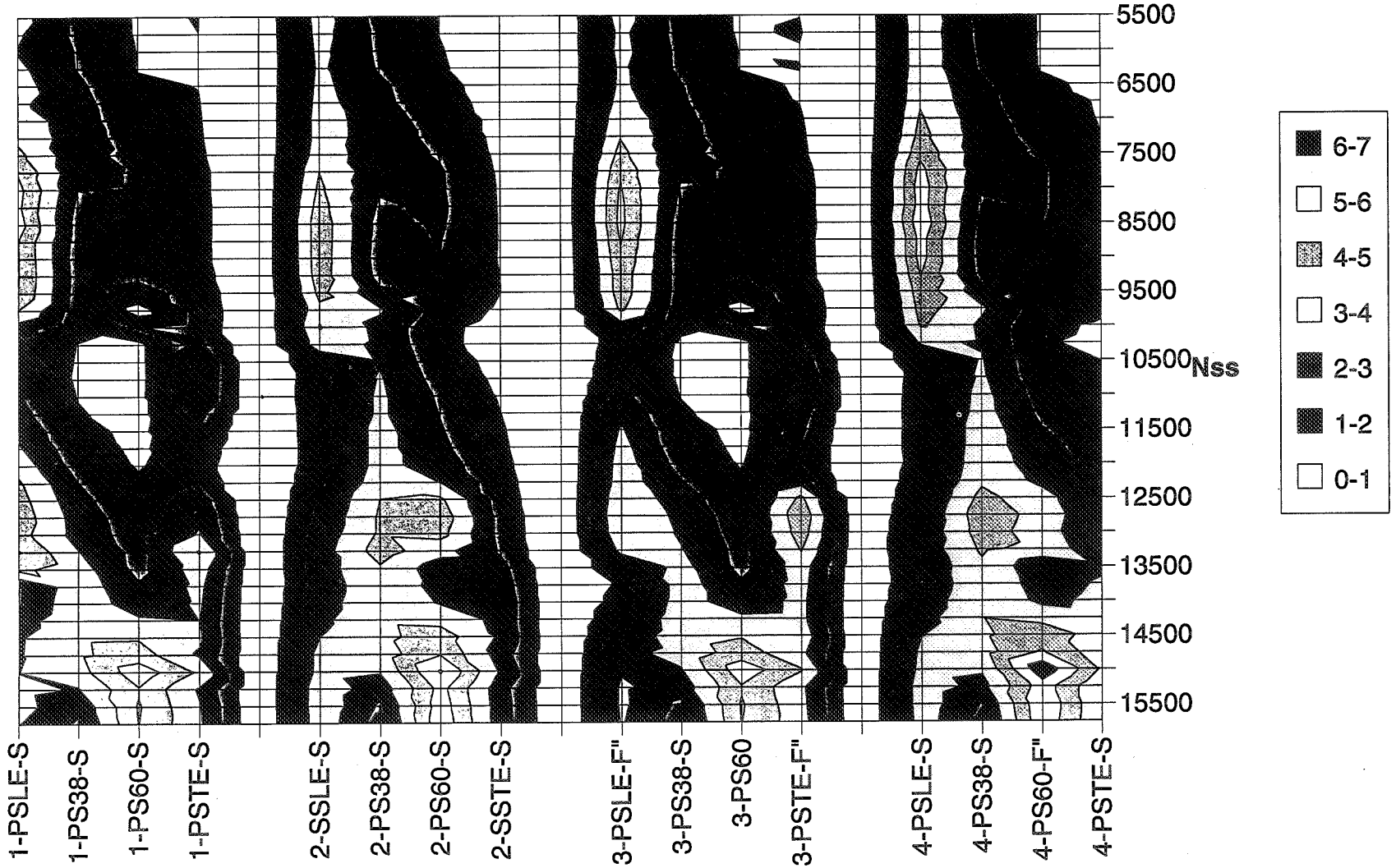

III

Overall Blade Fluctuating Strain: Composite RMS [1-1000 Hz]

George C. Marshall Space Flight Center
Fluid Dynamics Division

100% Q/N - 4200 rpm - ß=14.6° - .03" Clearance - Full blade

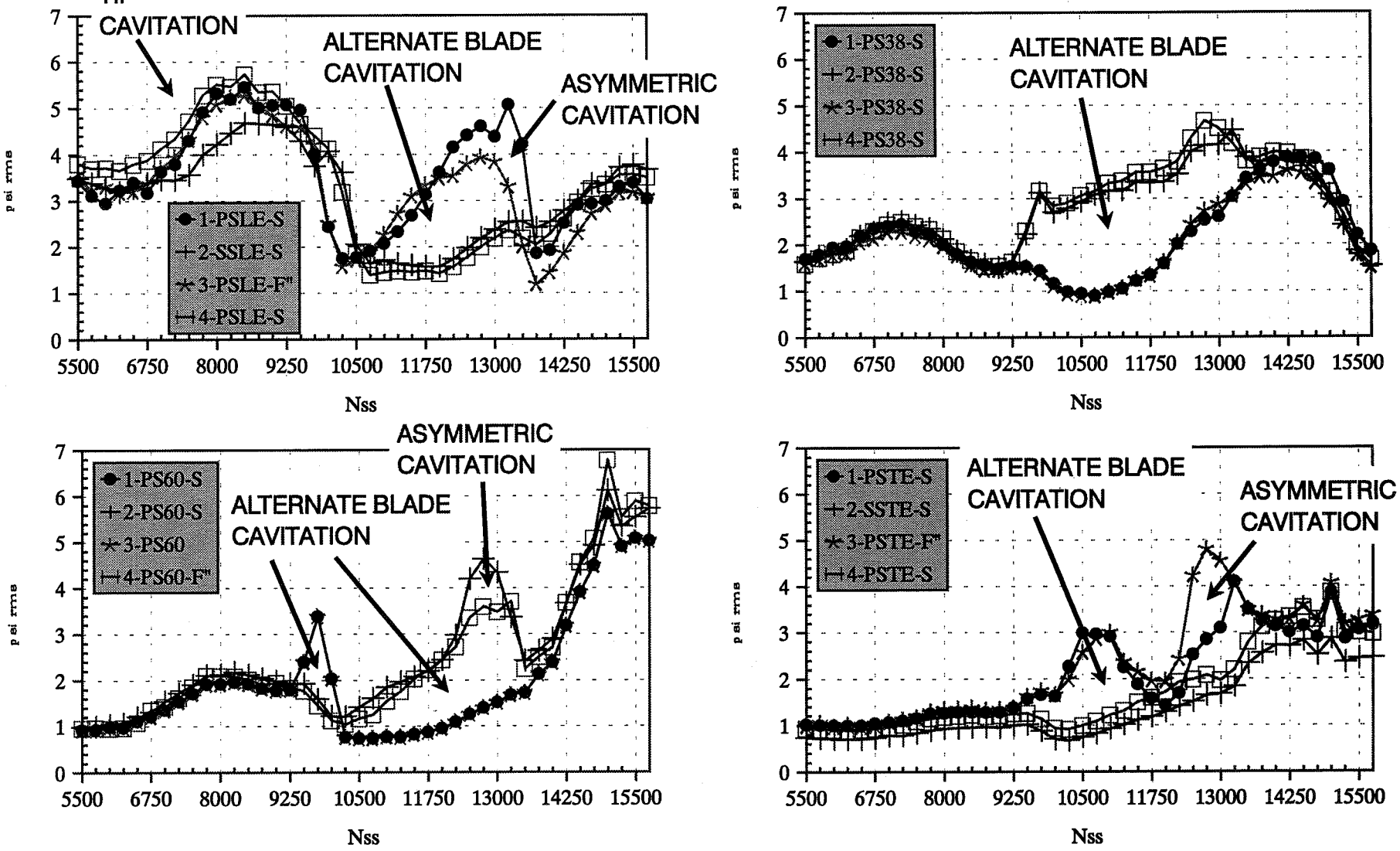

Cavitation Modulation: 3/4 Chord p' Measurement

George C. Marshall Space Flight Center
Fluid Dynamics Division

Cavitation noise:
Contained in high frequency noise floor
Multiple transient events (popping)
Frequency of events is controlled by unsteady flow

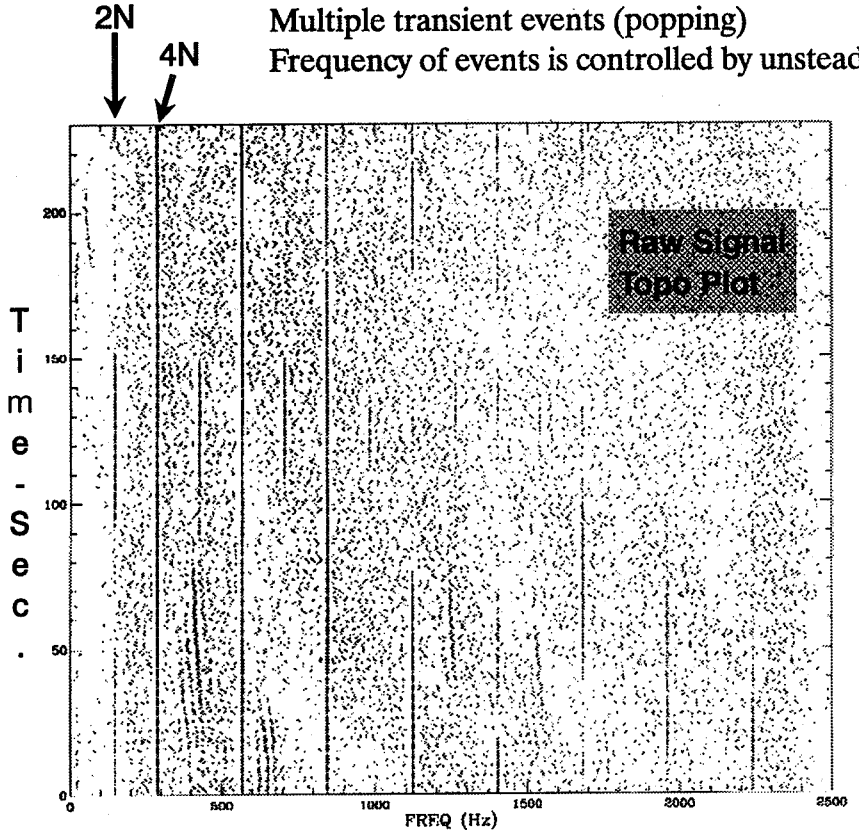

ITL-7 16/1 - 100% Q/N - 4200 rpm
ß=15.6° - .03" clearance
Trailing edge cutback

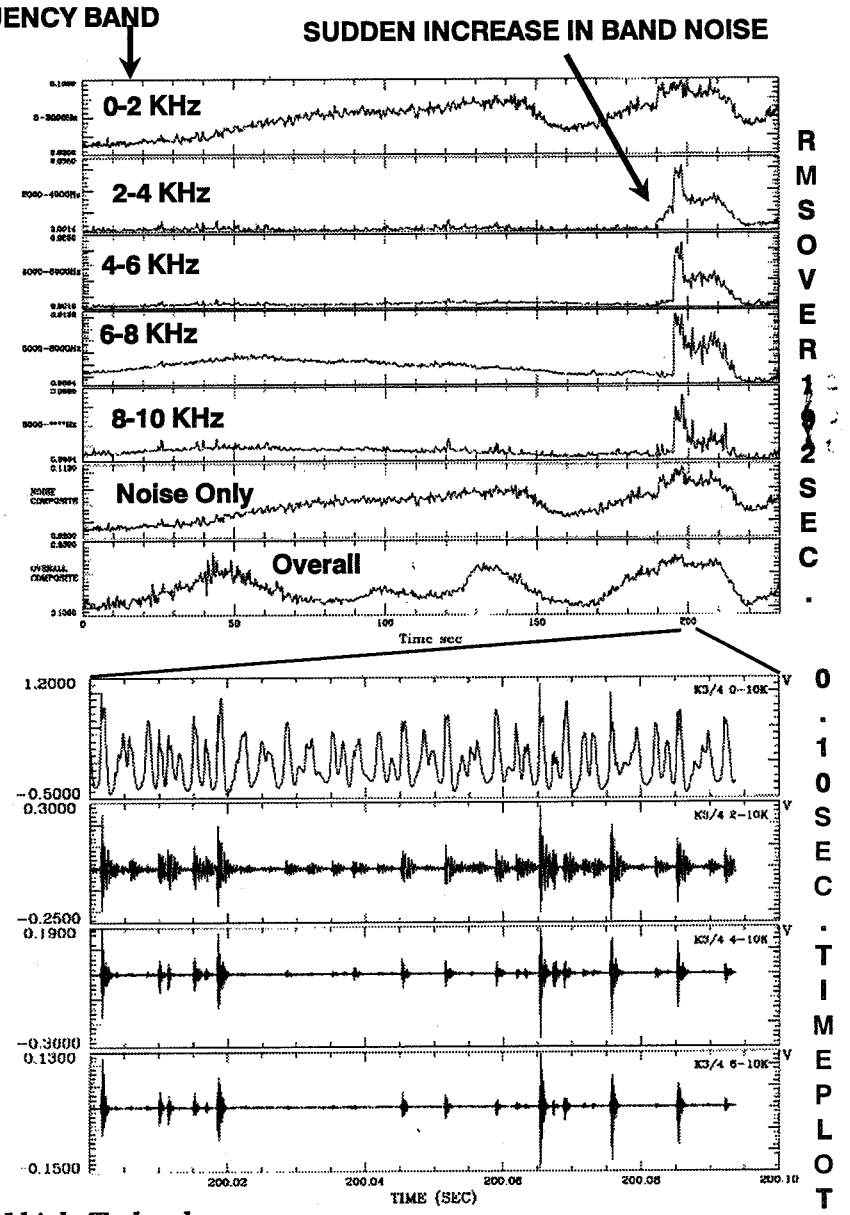

Cavitation Modulation: 3/4 Chord p' Measurement

Cavitation Detection

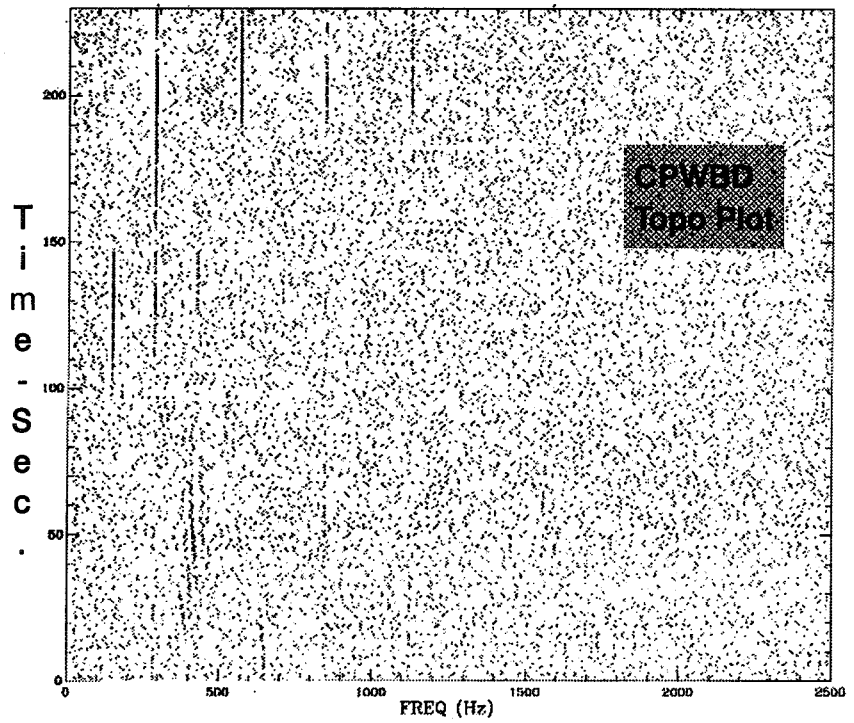

- Use modulation relationship between broadband cavitation noise and unsteady flow oscillations
- Wide band demodulation
  - Envelope bandpassed signal
  - Magnitude is proportional to cavitation intensity
  - Requires knowledge of frequency band carrying signal (or trial and error)
  - Easily corrupted by extraneous periodicities in analysis frequency band
- Coherent phase wide band demodulation (CPWBD)
  - Uses phase information to recover modulation from broadband signal
  - Apriori knowledge of frequency band not necessary
  - Not affected by extraneous periodicities in data

Frequency lines in CPWBD topo plot are periodics that modulate cavitation noise

Inducer Tip p' Parameter Variation

George C. Marshall Space Flight Center
Fluid Dynamics Division

Effect of ß angle on tip synchronous oscillations

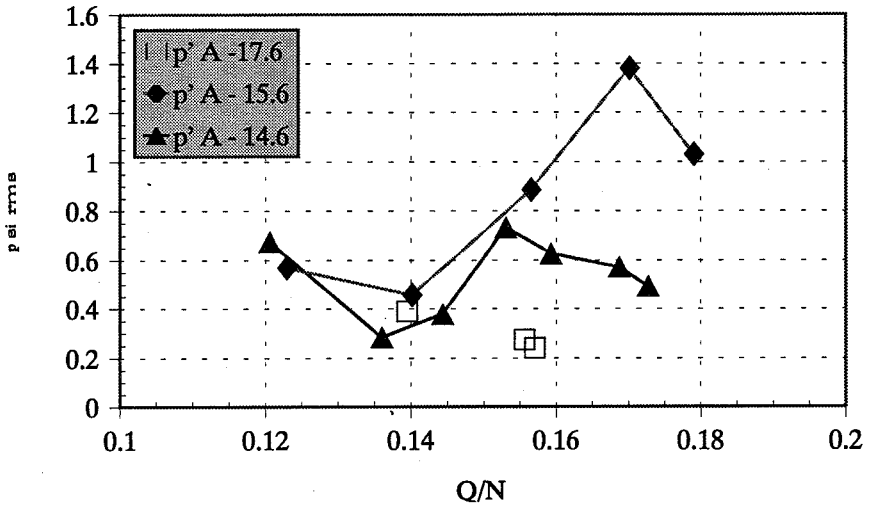

Effect of trailing edge cutback on tip synchronous oscillations

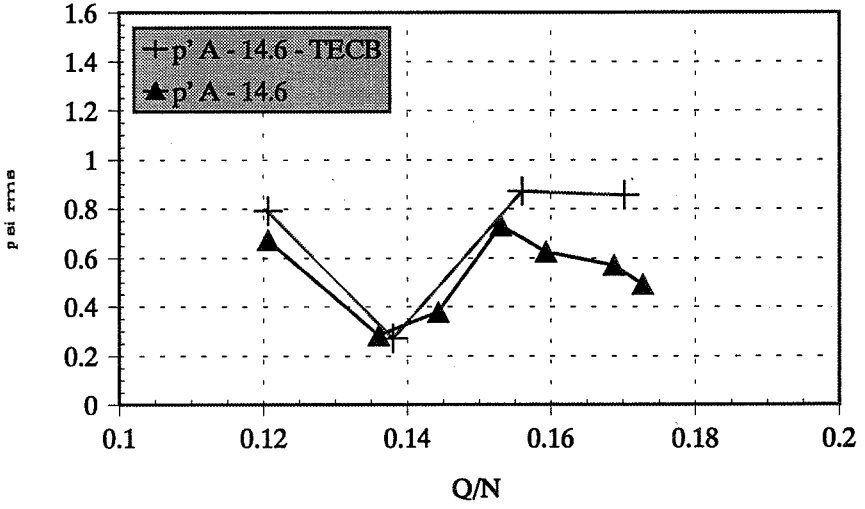

Effect of clearance on tip synchronous oscillations

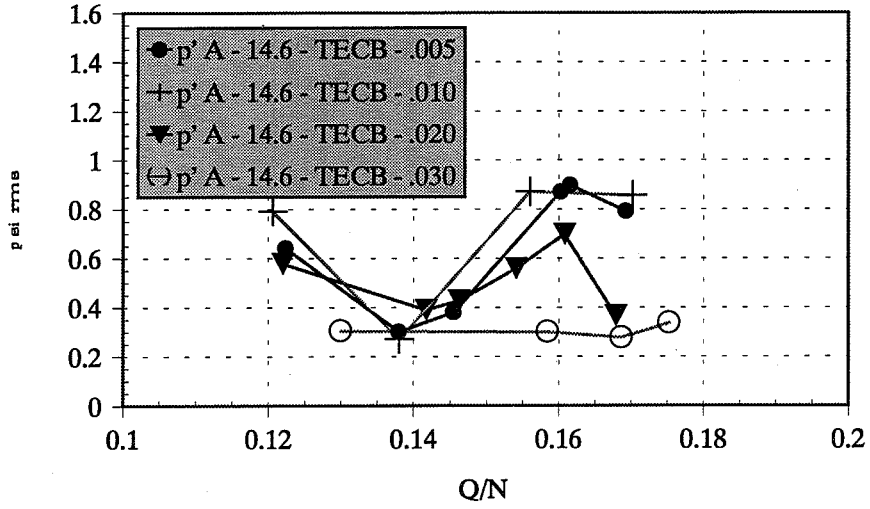

Discharge p' Parameter Variation

George C. Marshall Space Flight Center
Fluid Dynamics Division

Effect of ß angle on discharge synchronous oscillations

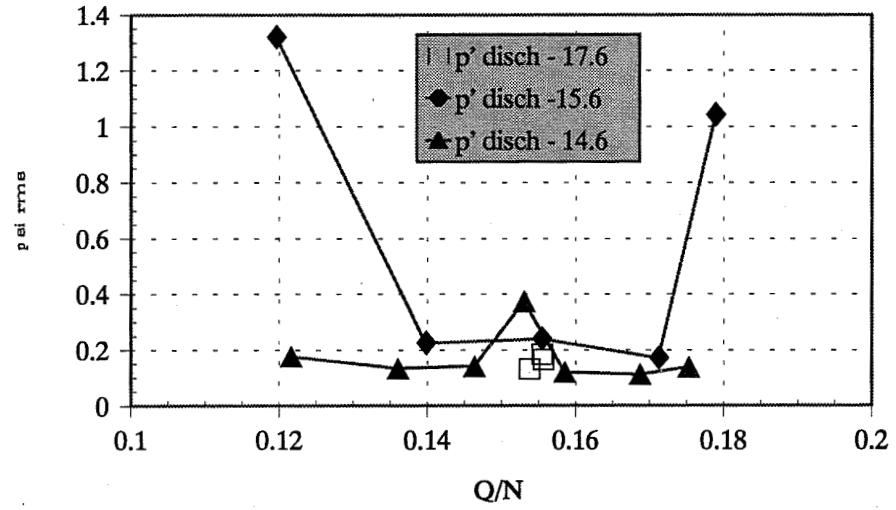

Effect of trailing edge cutback on discharge synchronous oscillations

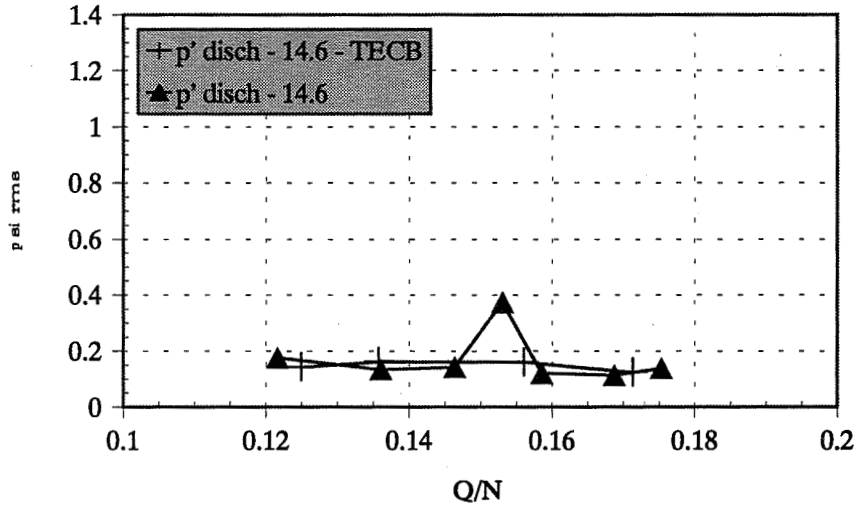

Effect of clearance on discharge synchronous oscillations

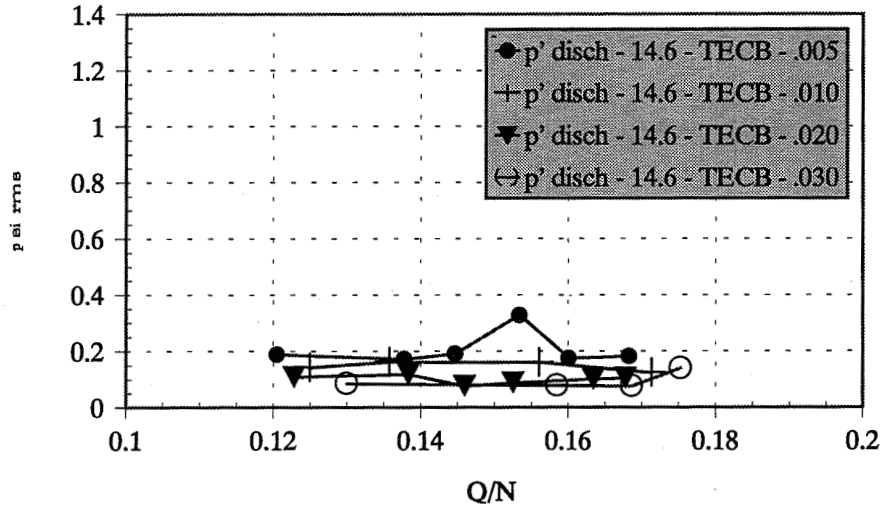

Summary

- Water flow model + inducer test loop facility capable of providing suction specific speeds over wide operational range
- Allows detailed definition of operational parameters as well as investigatin of potential fluid oscillation mechanisms
- High frequency signal processing techniques used to analyze fluid oscillations with emphasis on cavitation
- Presentation provides a synopsis of observed fluid dynamic behavior in terms of signal characteristics and typical pump operating parameters

Page intentionally left blank

Influence of Tip Clearance and Reynolds Number on the Flow in the ADP Inducer

Joan G. Moore and John Moore

Mechanical Engineering Department
Virginia Polytechnic Institute and State University
Blacksburg, Virginia 24061-0238

ABSTRACT

Calculations of three-dimensional turbulent flow in the Rocketdyne Advanced Development Program (ADP) rocket pump inducer showed significant backflow and recirculation upstream of the leading edge at design and below design flow rates. The influence of the tip clearance on the recirculation has been studied computationally by varying the shroud boundary condition and the tip clearance in the inducer. The results showed that the tip clearance has only a small effect on the leading edge backflow.

Rocket pumps are initially tested in air or water at Reynolds numbers well below those for liquid hydrogen flow. Calculations over a wide range of Reynolds number show the changes in overall performance due to variations in blade and shroud shear.

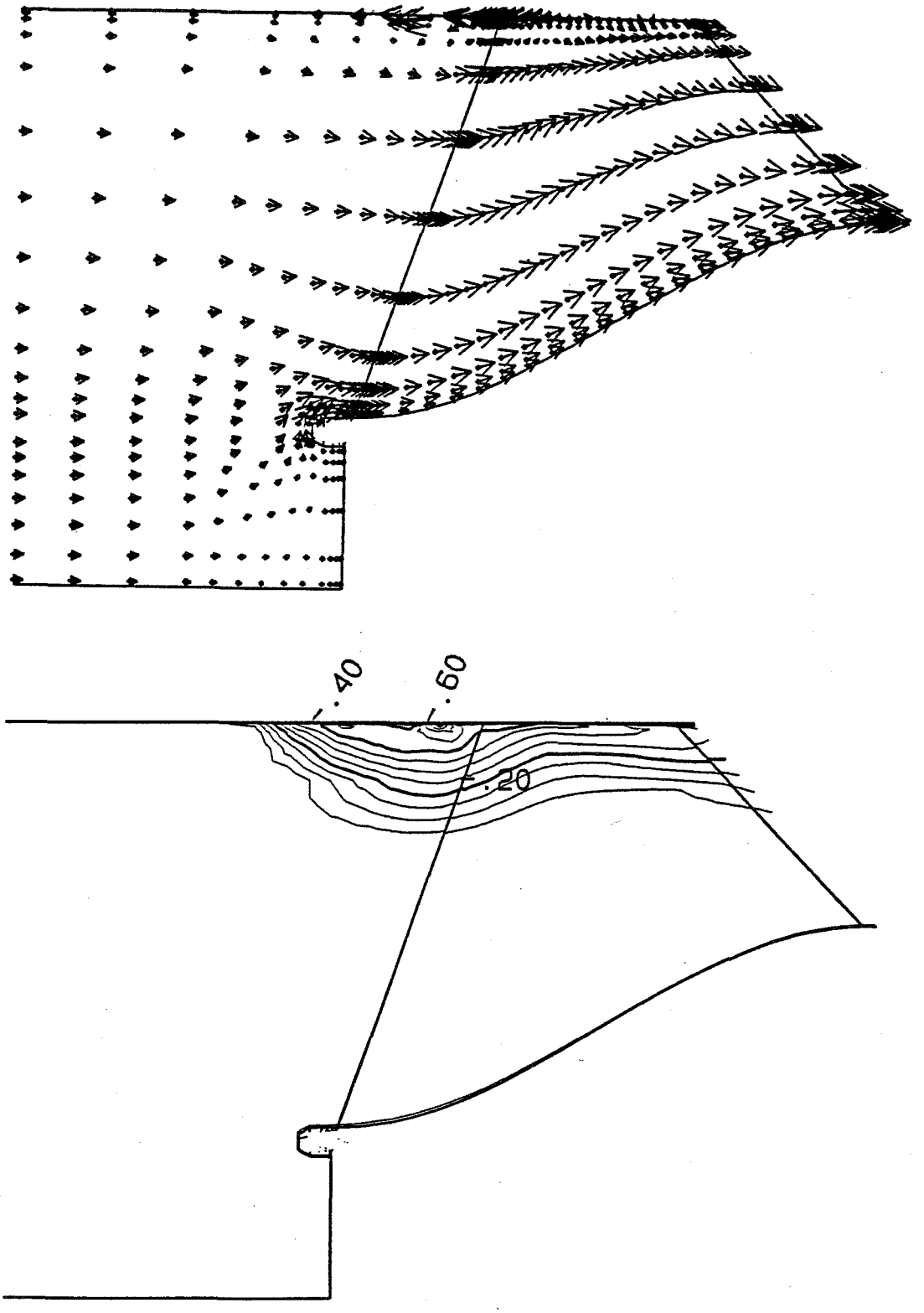

ADP inducer, design flow rate. Stationary shroud, 0.01 inch tip gap.
Mid passage velocity vectors and rotary stagnation pressure, P*.
Note leading edge tip vortex.

ADP Inducer 0.01 inch tip gap, stationary shroud

Vectors at 94% of blade height

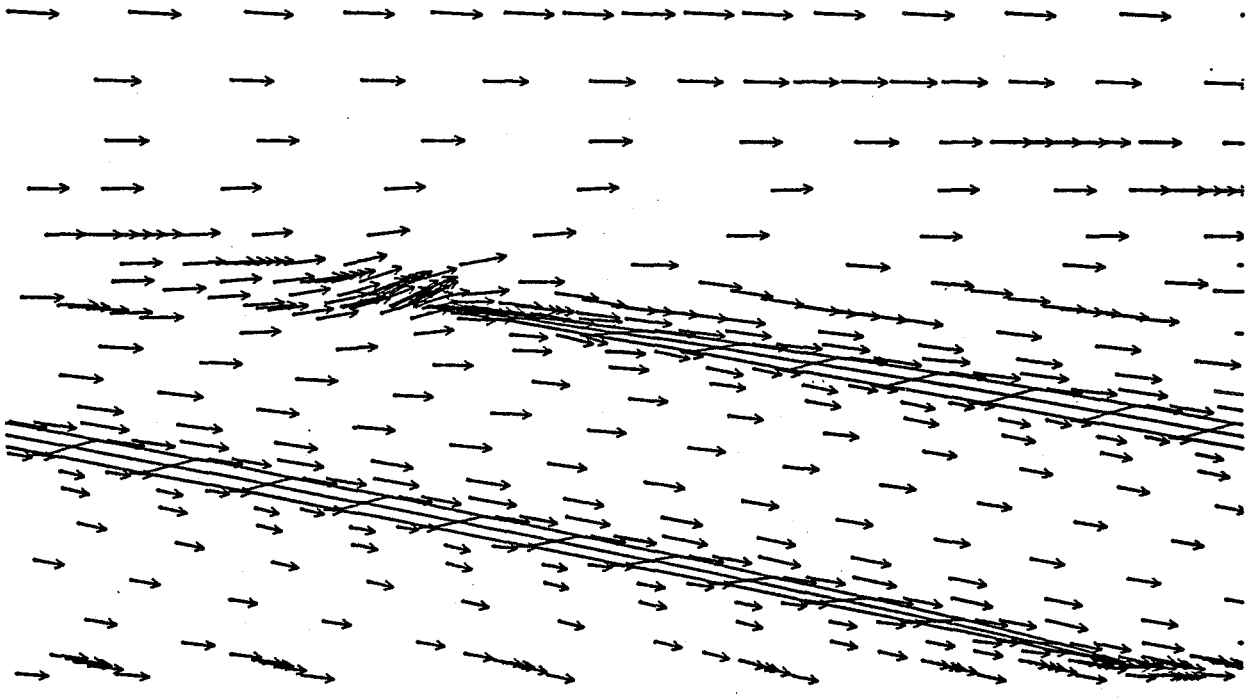

Velocity vectors at 94% of blade height show incidence at leading edge.

ADP Inducer 0.01 inch tip gap, stationary shroud

Vectors near shroud wall

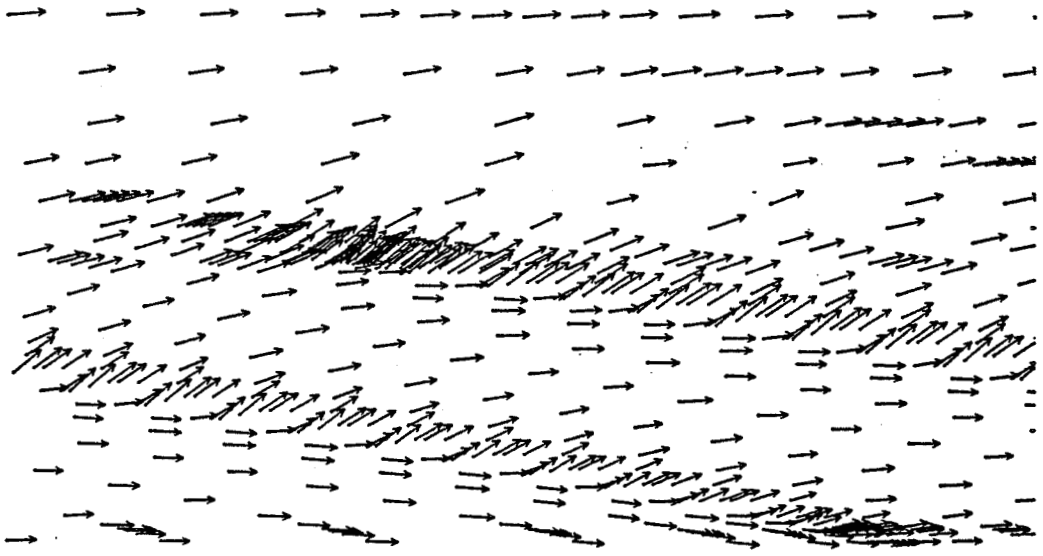

ADP Inducer 0.01 inch tip gap, stationary shroud

Vectors at blade tip height

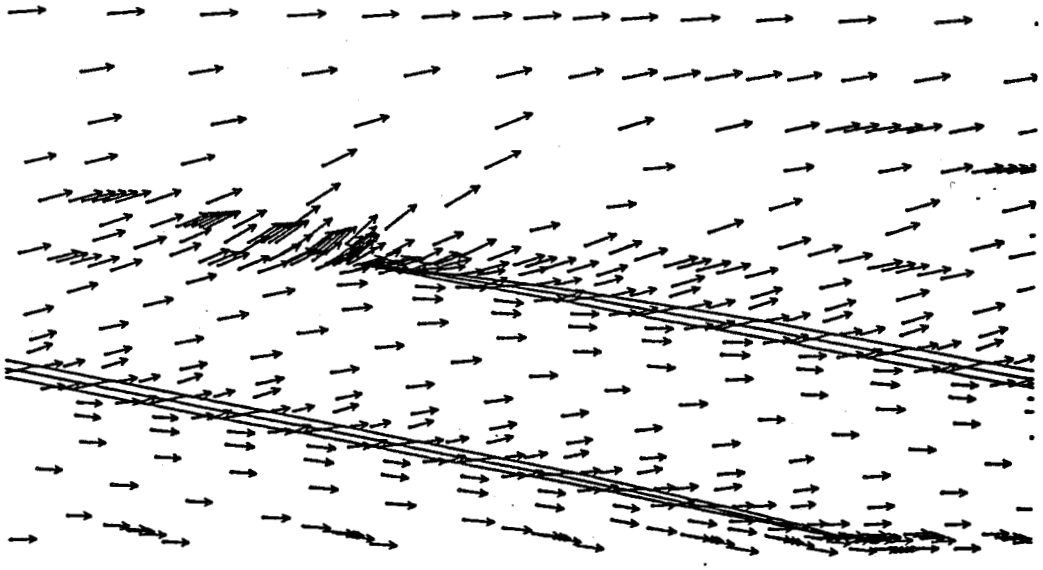

Velocity vectors show tip leakage flow flowing back into the leading edge vortex.

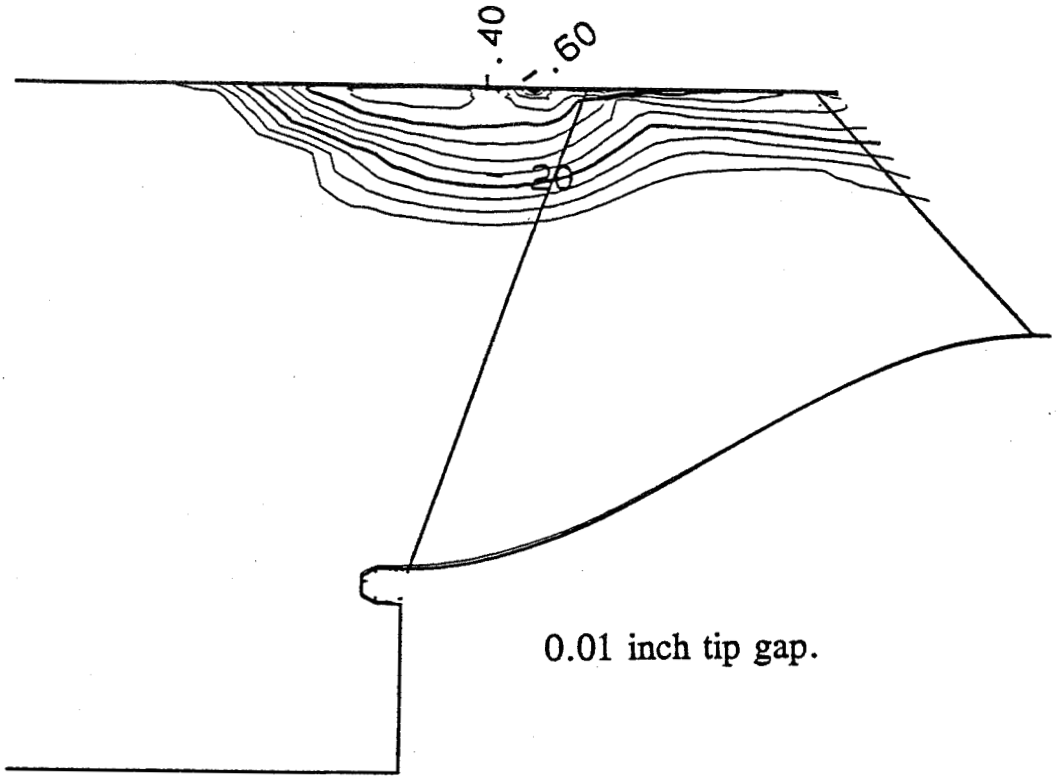

0.01 inch tip gap.

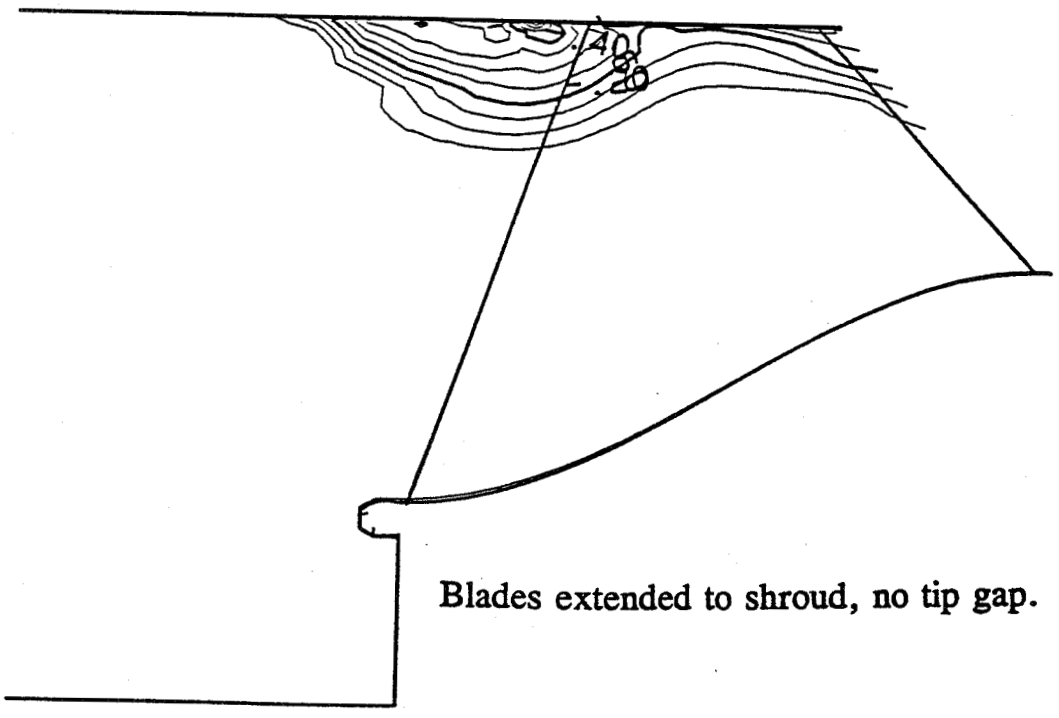

Blades extended to shroud, no tip gap.

ADP inducer, design flow rate.
Inviscid shroud over the inducer, stationary shroud up and downstream of inducer,
Rotary stagnation pressure, P*, at mid-passage.

Backflow / Mass Flow Rate

——— tip gap, stationary shroud

- - - - - - - tip gap, inviscid shroud

——— — no gap, inviscid shroud

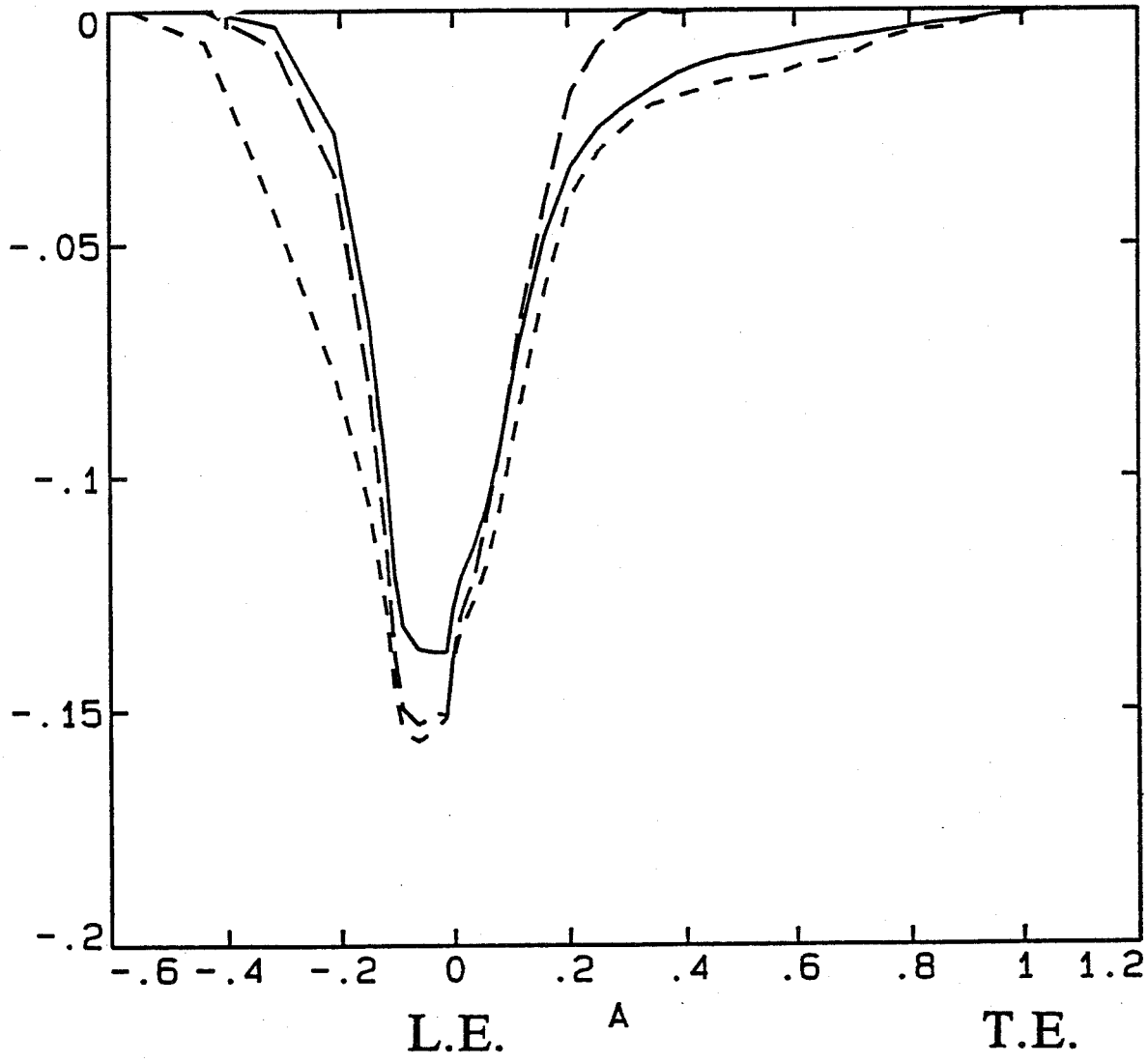

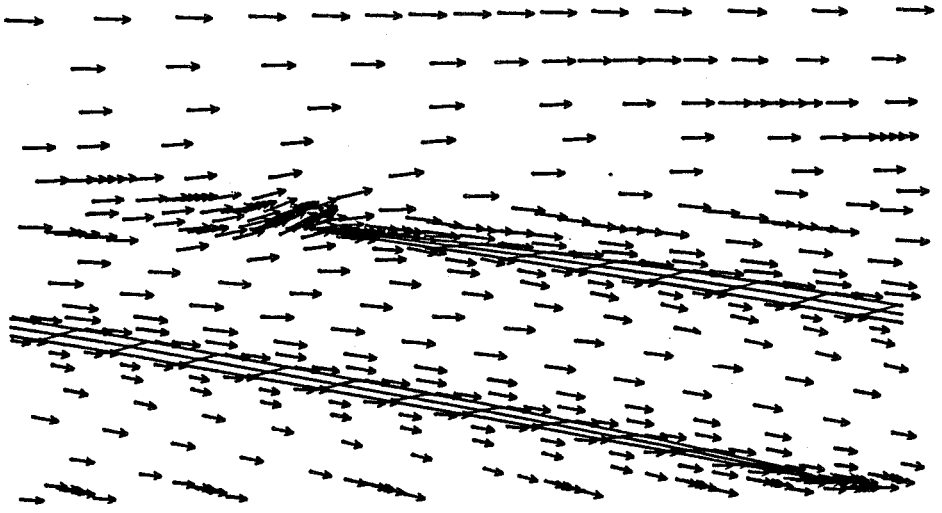

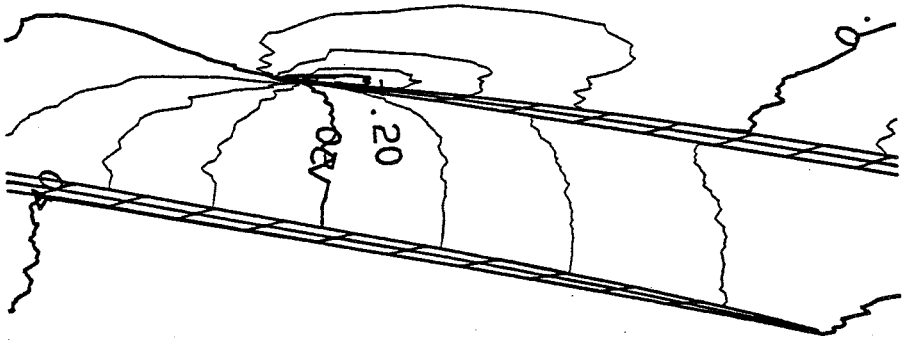

ADP inducer, design flow rate. Blades extended to shroud, no tip gap.
Inviscid shroud over the inducer, stationary shroud up and downstream of inducer,
Static pressure, P, and velocity vectors at 94% of blade height.

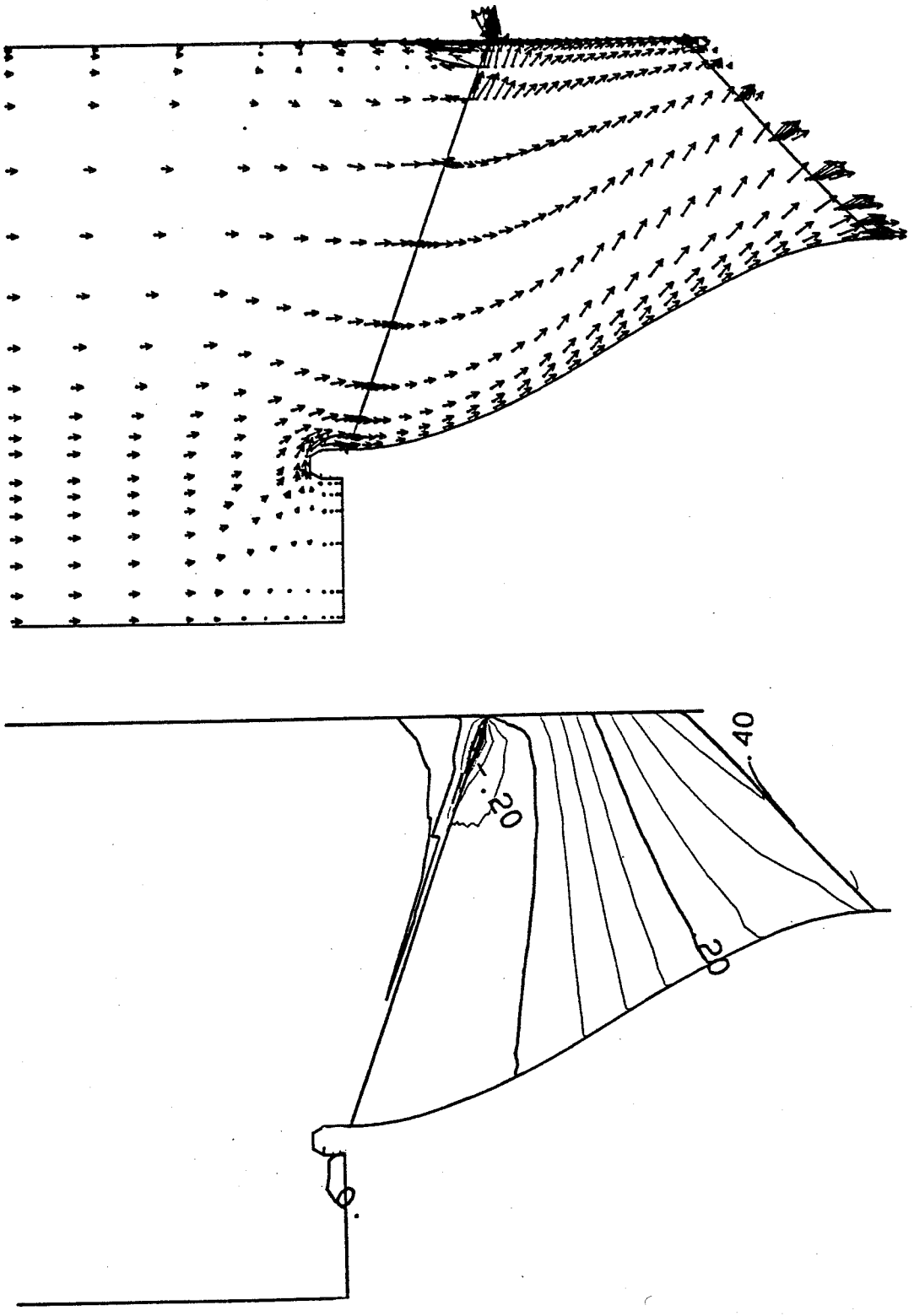

ADP inducer, design flow rate. Blades extended to shroud, no tip gap.
Inviscid shroud over the inducer, stationary shroud up and downstream of inducer,
Static pressure, P, and velocity vectors near suction surface.

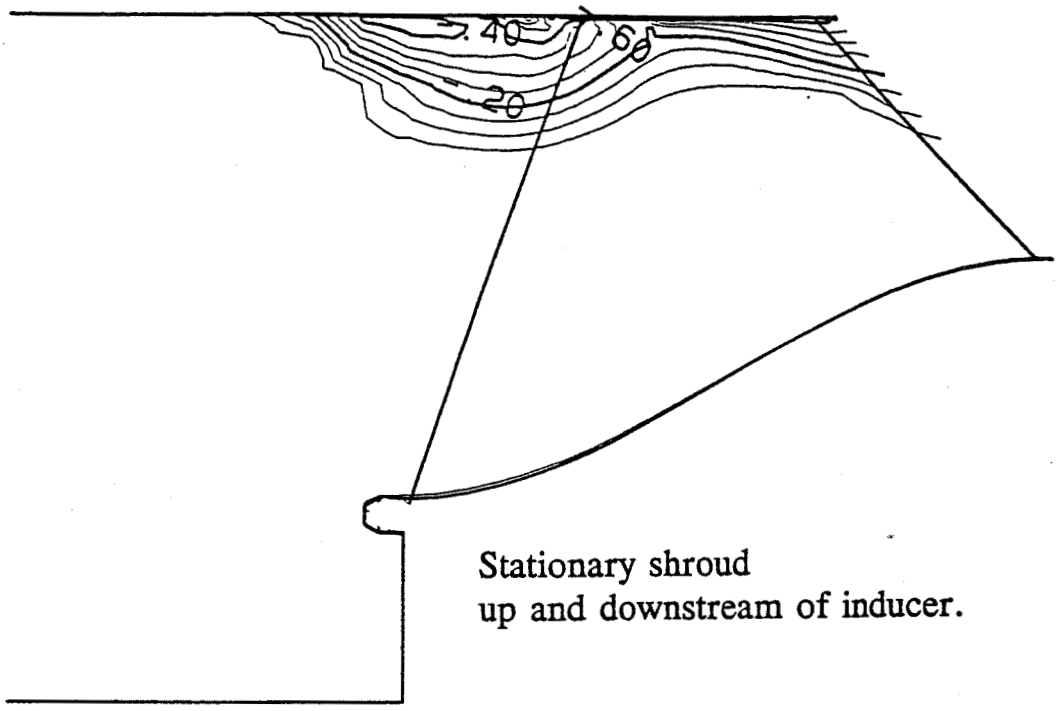

Stationary shroud
up and downstream of inducer.

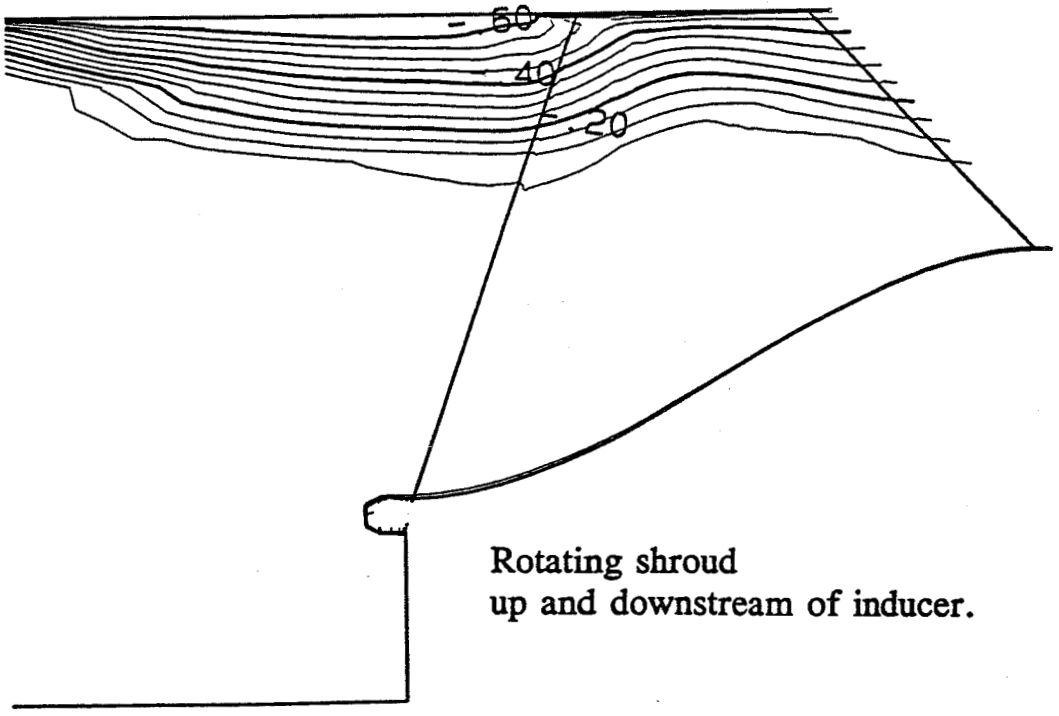

Rotating shroud
up and downstream of inducer.

ADP inducer, design flow rate.
Blades extended to shroud, no tip gap, rotating shroud on inducer,
Rotary stagnation pressure, P*, at mid-passage.

Leading Edge Tip Vortex

Tip Leakage ?

Incidence ?

Test case - ADP inducer 100% design flow rate

5 Calculations

with/without Tip Clearance

Different Shroud Boundary Conditions

1. Stationary shroud wall inlet to exit, 0.01 inch tip clearance (water test)
2. Inviscid shroud wall over inducer, 0.01 inch tip clearance
3. Inviscid shroud wall over inducer, blades extended to shroud, no tip gap
4. Rotating shroud wall over inducer, no tip gap
5. Rotating shroud wall inlet to exit, no tip gap

Conclusions

Leading edge tip vortex caused by incidence

Enhancement due to tip leakage is not large

If calculations with tip leakage cannot be run

Use inviscid shroud on inducer

Use stationary shroud up and down stream

Calculations Varying the Reynolds Number

Design Flow Rate

$$Re = \frac{\rho U_{tip} D_{tip}}{\mu_\ell}$$

S.E.P. Ariane 5 Inducer

$Re = 110 \times 10^6$	(~ liquid hydrogen)
$Re = 11 \times 10^6$	(~ water test)
$Re = 1.1 \times 10^6$	air test

Rocketdyne ADP Inducer

$Re = 77 \times 10^6$	(~ liquid hydrogen)
$Re = 7.7 \times 10^6$	water test
$Re = 0.77 \times 10^6$	(~ air test)

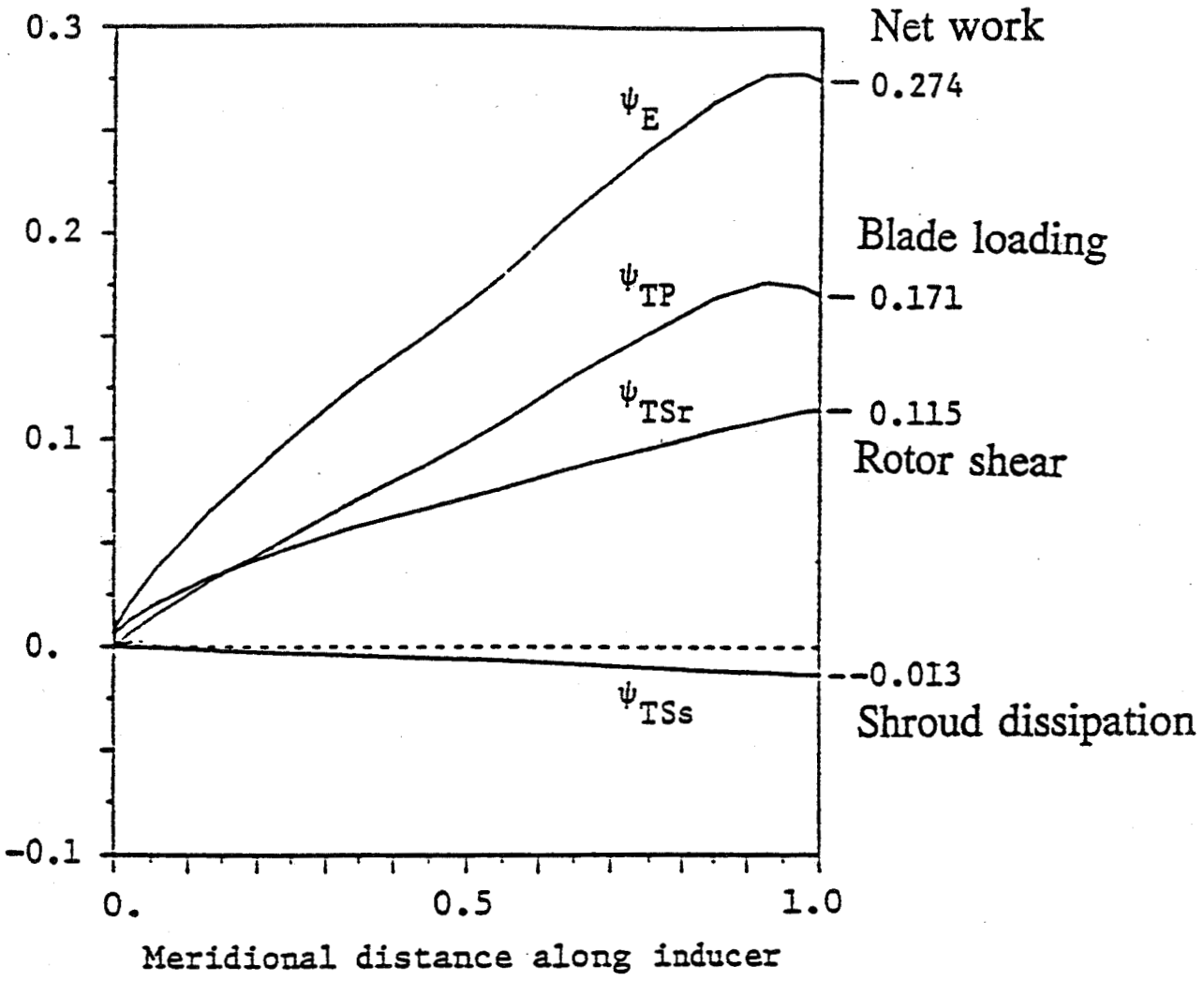

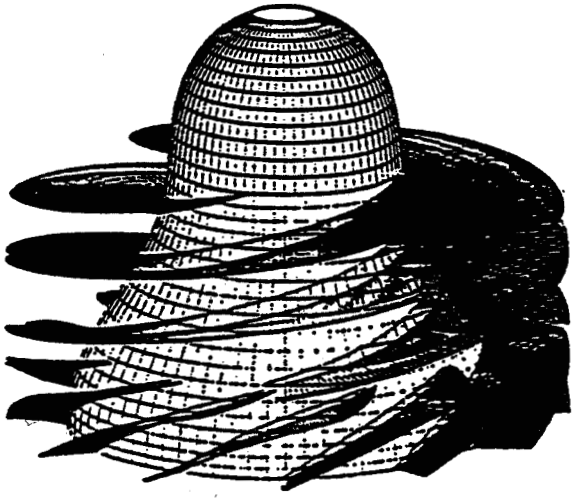

Contributions to work input, air test of Ariane 5 LH2 inducer.

Reynolds number effects?

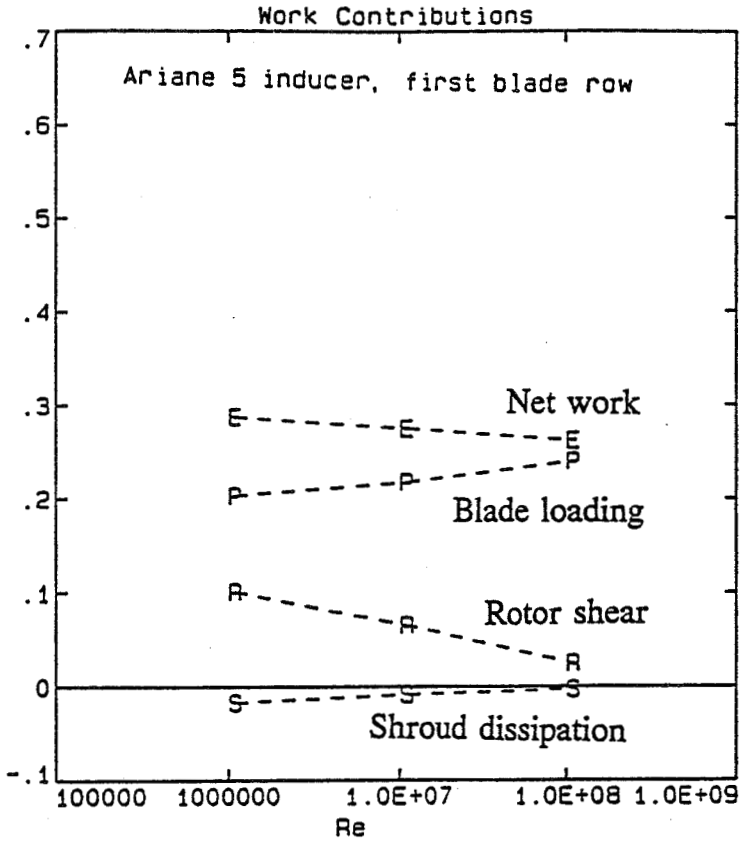
Work Contributions
Ariane 5 inducer, first blade row
.7
.6
.5
.4
.3
.2
.1
0
-.1
Net work
Blade loading
Rotor shear
Shroud dissipation
100000
1000000
1.0E+07
1.0E+08
1.0E+09
Re

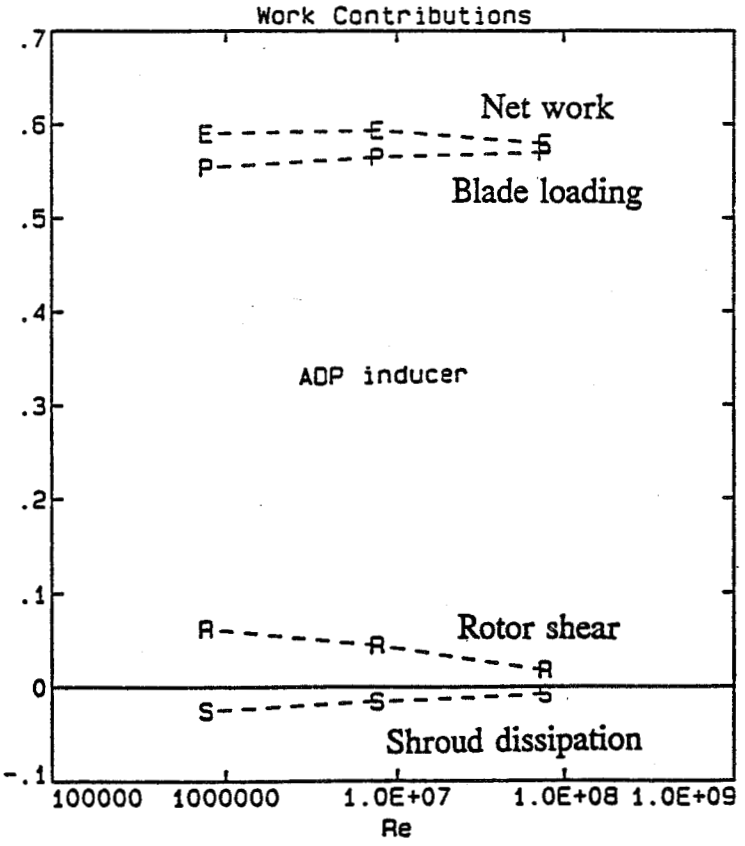
Work Contributions
.7
.6
.5
.4
.3
.2
.1
0
-.1
Net work
Blade loading
ADP inducer
Rotor shear
Shroud dissipation
100000
1000000
1.0E+07
1.0E+08
1.0E+09
Re

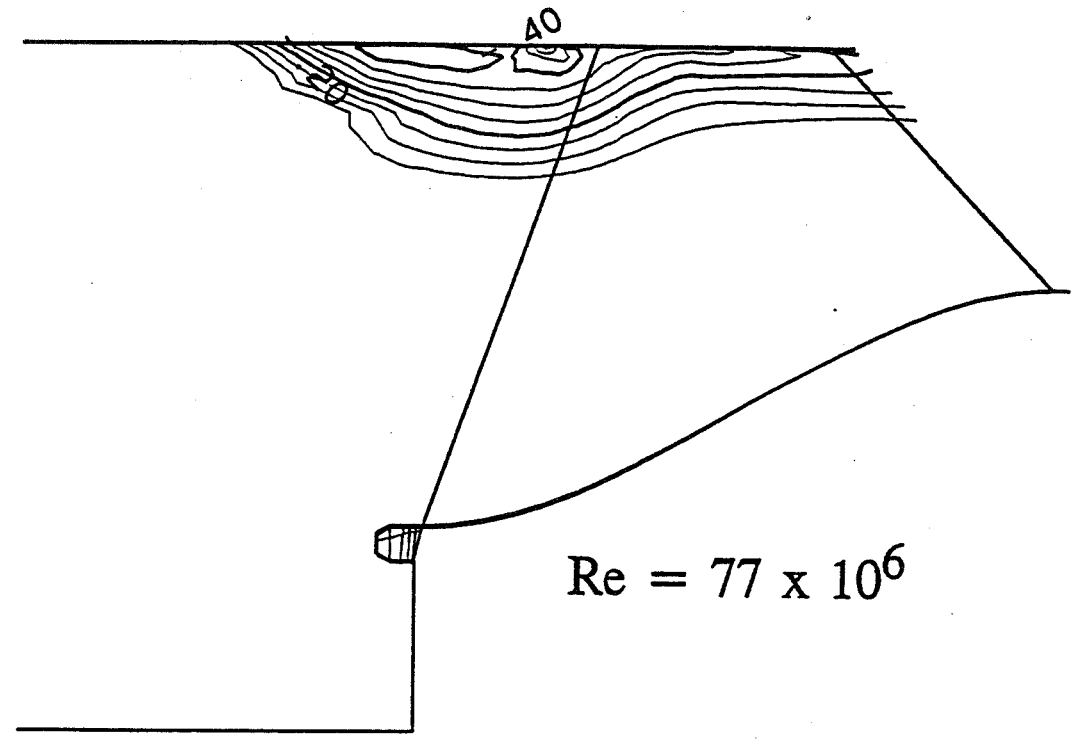

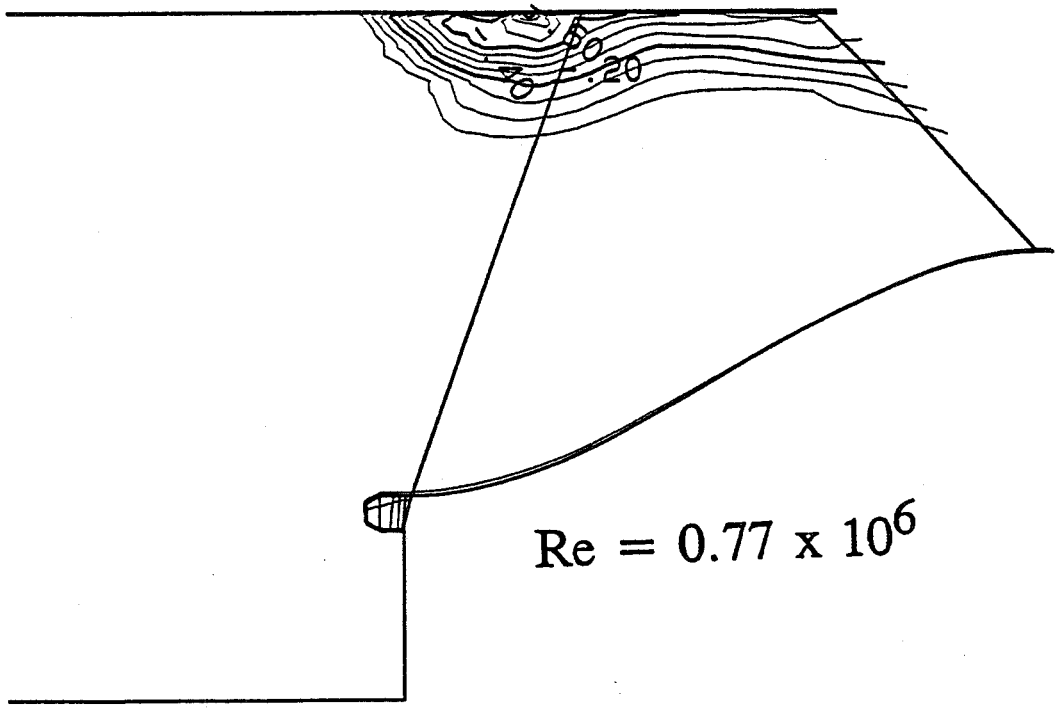

ADP inducer, design flow rate. Stationary shroud, 0.01 inch tip gap.

Rotary stagnation pressure, P*, at mid-passage.

Mass-Averaged Rotary Stagnation Pressure

ADP Inducer, 100% design flow rate

$$Re = \frac{\rho U_{tip} D_{tip}}{\mu_t}$$

-------- Re = 77 x 10^6

——— Re = 7.7 x 10^6 (water test)

– – – – – Re = 0.77 x 10^6

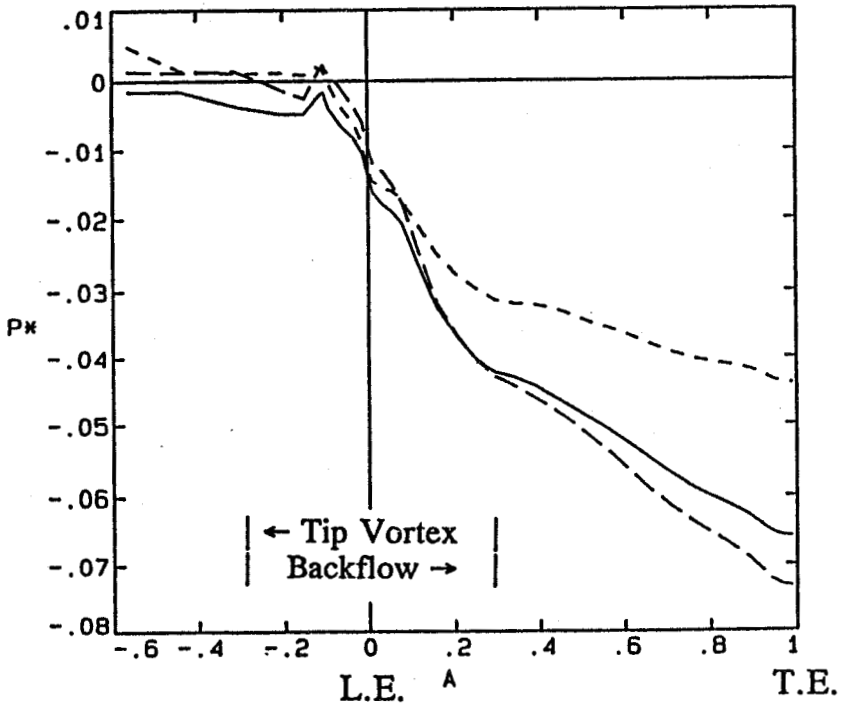

Reynolds Number Dependence of Losses, -P*, to inducer exit

Re	Total -	Vortex =	Difference
$77x10^6$	0.043	0.026	0.170
$7.7x10^6$	0.065	0.032	0.033
$0.77x10^6$	0.073	0.031	0.042

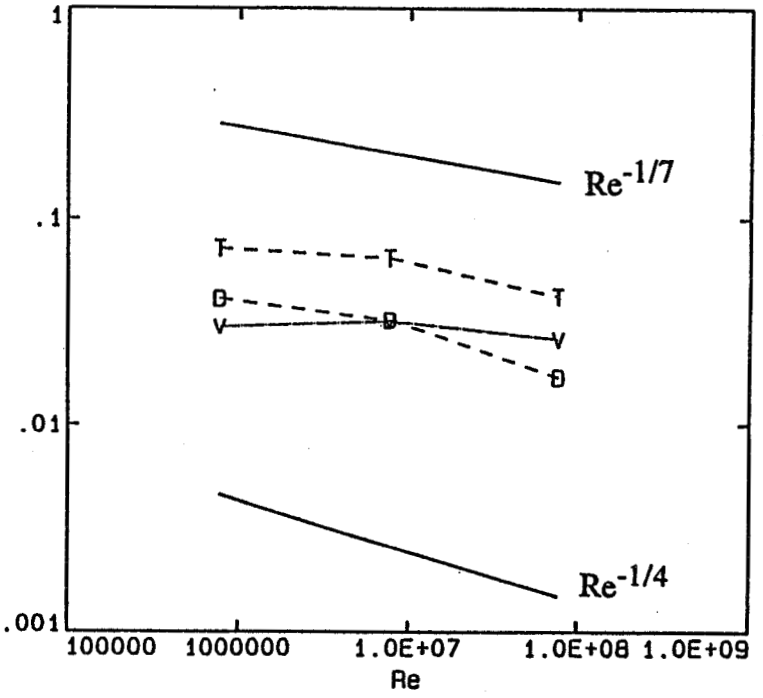

ADP inducer

Reynolds Number Dependence,
to inducer exit

Re	$1-\eta$	ψ_{TSr}	ψ_{TSs}
77×10^6	0.087	0.018	0.008
7.7×10^6	0.134	0.045	0.016
0.77×10^6	0.160	0.062	0.026

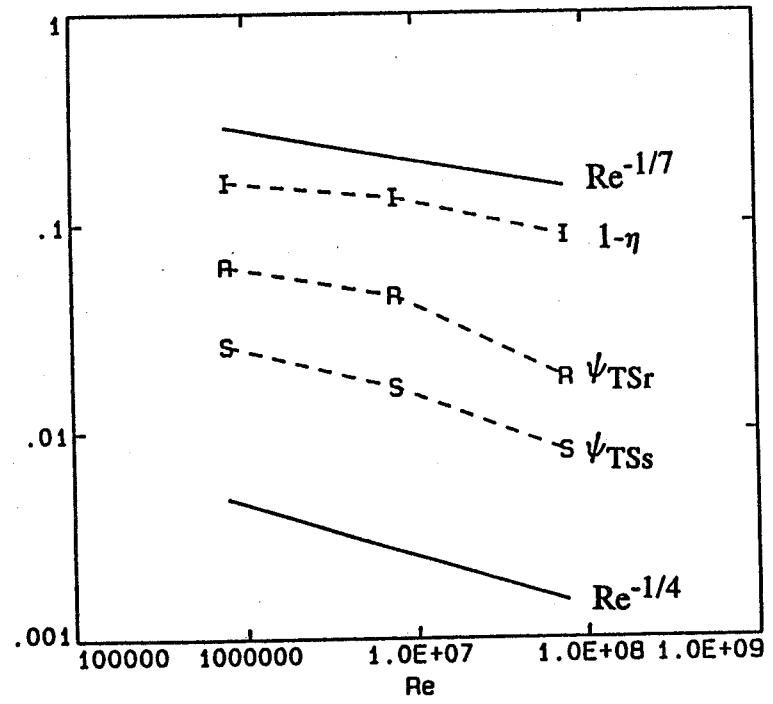

ADP inducer

Reynolds Number Dependence

Conclusions

Ariane 5 inducer, first blade row

Work due to rotor shear $\simeq$ 40% of total work inducer:

low Re air test

low blade loading

ADP inducer, design flow rate

Leading edge vortex increases in size with increase in Re

Leading edge vortex losses independent of Re

$\simeq$ 1/2 of total loss for water test Re

Remaining losses, rotor and shroud torques:

have expected Re dependence

between $Re^{-1/7}$ to $Re^{-1/4}$

CFD Analysis In The Design of A Water-Jet-Drive System

R. Garcia

NASA/MSFC

13th Workshop for CFD Applications in Rocket Propulsion and Launch Vehicle Technology
MSFC, AL
April 25-27, 1995

National Aeronautics and
Space Administration

CFD Analysis In The Design of A Water-Jet-Drive System

Computational Fluid Dynamics Branch
Fluid Dynamics Division
Structures and Dynamics Laboratory
George C. Marshall Space Flight Center

Overview

- **Introduction/Objectives**
  - Technology Utilization Office
  - North American Marine Jet Request
- **Approach**
  - Geometry Generation, Grid Generation
  - CFD Code
  - Postprocessing
- **Results**
  - Baseline + 4 Parametric Cases
  - Final Design
- **Summary/ Conclusions**

Introduction

- **Technology Utilization (TU) Office at MSFC Promotes Technology Transfer to Industry**
  - Informs Industry of NASA Technology and Expertise
  - Accepts & Evaluates Requests for Technical Support from Industry
  - Coordinates Joint NASA - Industry Research and Technology Application
- **Program Goal is to Make U.S. Industry More Competitive**
- **Use of Government Manpower and Facilities "Free-of-Charge" Limited to Requests Meeting Certain Criteria**
  - Project Must Provide a Direct Benefit to NASA

Introduction (continued)

- **North American Marine Jet (NAMJ) Requested NASA Assistance in Development of a Water-Jet-Drive System in the 350-500 Hp Range**
  - Market Niche Controlled by Foreign Manufacturer
  - Potentially a Large Market Demand

- **NAMJ Requested Impeller Analysis Support, and Instrumentation and Testing Information**

- **MSFC Interested in Expanding Turbomachinery Data Base and Analytical Experience**
  - Developing Tools to Streamline CFD Analysis at MSFC

- **MSFC Has and Continues to Demonstrate the Value of Applying CFD in the Design Process**

WATER-JET-DRIVE SYSTEM SCHEMATIC

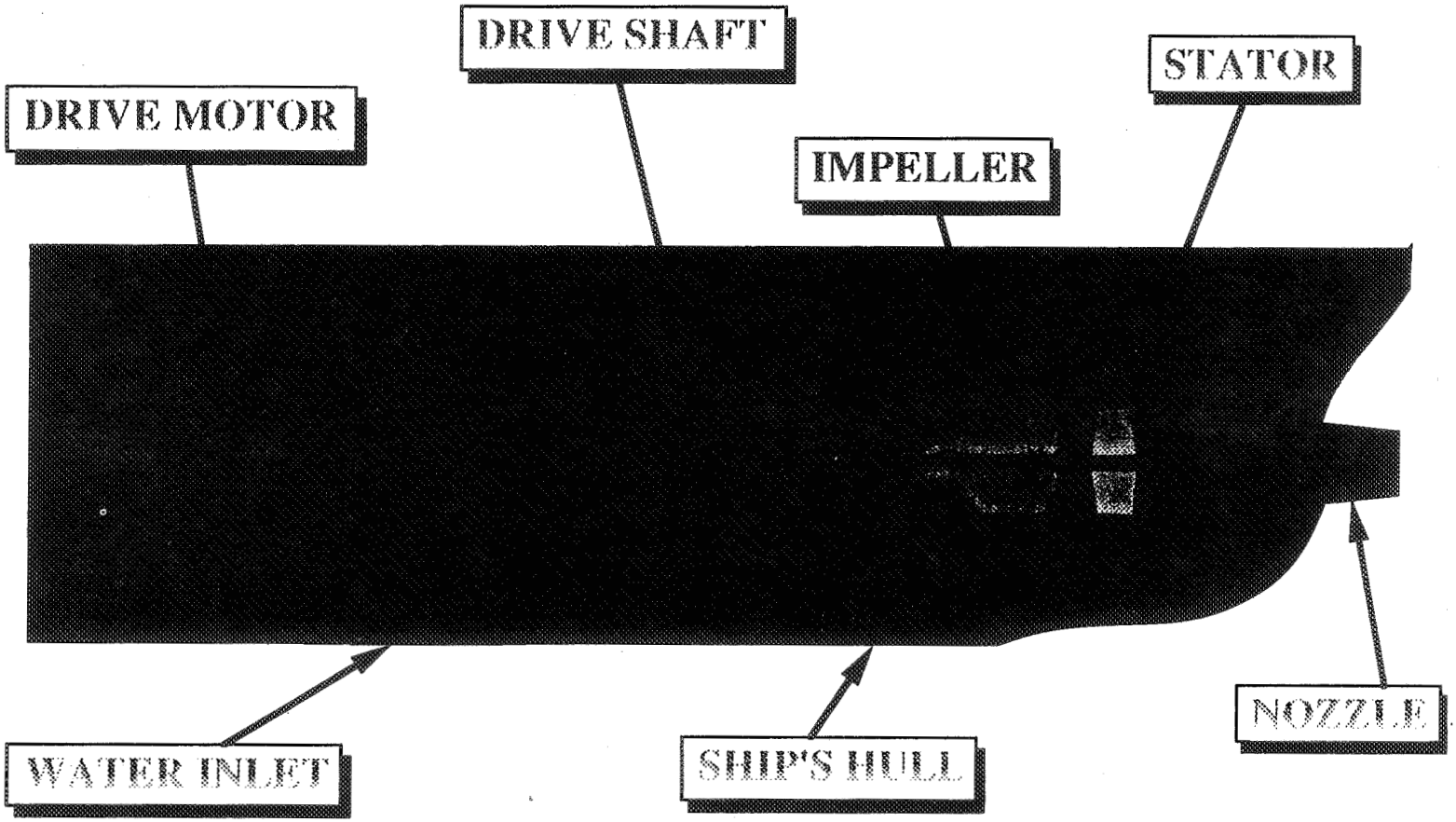

National Aeronautics and
Space Administration

CFD Analysis In The Design of A Water-Jet-Drive System

Computational Fluid Dynamics Branch
Fluid Dynamics Division
Structures and Dynamics Laboratory
George C. Marshall Space Flight Center

Objectives

- **Use CFD to Analyze an Impeller Design Supplied by NAMJ**
  - Perform Parametric Study to Evaluate Sensitivity of Baseline Design to Geometric Parameters
  - Only Relative Differences Valid
    - -- Makes Simplified Modeling Possible
  - Apply Lessons Learned to a New (Final) Design
- **Streamline MSFC's Pump CFD Analysis Procedure**
  - Improve Blade Geometry Generation tools
  - Gain Experience With New Grid Generation Tool
  - Debug New Version of CFD Code

CFD Analysis In The Design of A Water-Jet-Drive System

Computational Fluid Dynamics Branch
Fluid Dynamics Division
Structures and Dynamics Laboratory
George C. Marshall Space Flight Center

Approach

- **Acquire Baseline Geometry from Drawings**
  - Tedious; Geometry Not Completely Defined

- **Use Geometry Generator to Create Impeller Definition**
  - Create the Camber Line and Blade Thickness Distribution
    - -- Facilitates Varying the Blade Shape in Subsequent Analyses
  - Create Additional Blade Profiles
  - Create Hub and Shroud Contours

- **Use TIGER Grid Generator to Create Grids**
  - MSU - LRC Developed Grid Generator for Turbomachinery Applications
  - Acceptable Grids Can Be Generated in Less Than 1 Hour
  - Single Block Grids, 101 * 21 * 21 (typical)
    - -- Ignore Tip Clearance
    - -- Full Blade Only

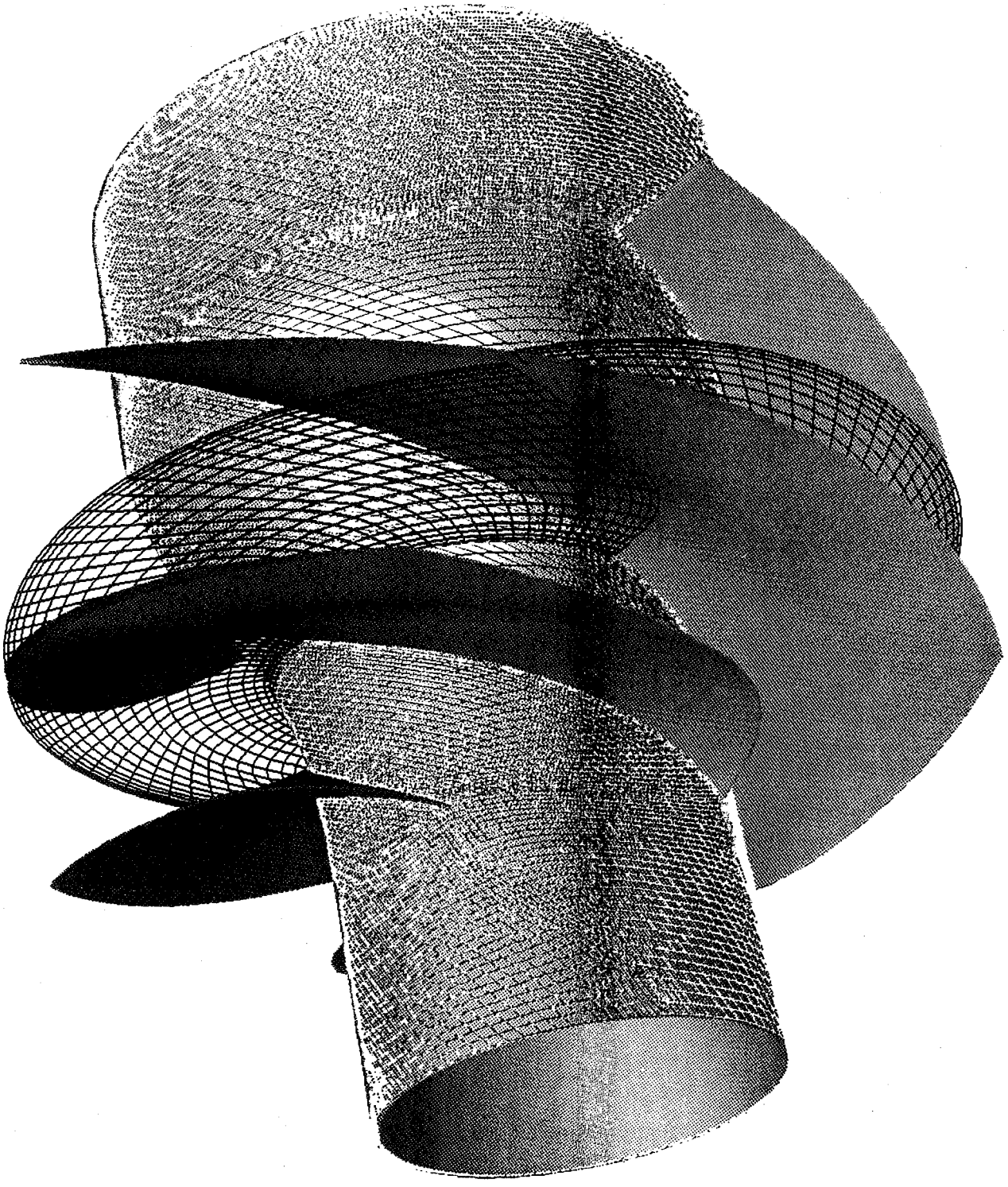

Approach (continued)

- **Use FDNS3D to Obtain the Flow Field**
  - Pressure-Based, Predictor-Corrector Algorithm
  - Crank-Nicholson Time Discretization
  - Central Difference with Artificial Dissipation Spatial Discretization
  - Linearized System Solved Using a Modified Stone's Solver or *Conjugate Gradient Solver*

- **Solutions Postprocessed Using FAST and Custom Codes**
  - Efficiency and Head Rise
  - Inlet and Exit Hub-to-Shroud Flow Angle Distributions
  - Blade-to-Blade Velocity Distributions at Selected Radial Planes

National Aeronautics and Space Administration

CFD Analysis In The Design of A Water-Jet-Drive System

Computational Fluid Dynamics Branch
Fluid Dynamics Division
Structures and Dynamics Laboratory
George C. Marshall Space Flight Center

	← Parametrics on the Baseline →					← Final Design →	
case #	1 (baseline)	2	3	4	5	6	7
rpm	2800	2800	2800	2800	2800	2600	2600
tip flow coefficient	.259	.181	.259	.259	.259	.171	.137
tip blade angle							
inlet	13.1	13.1	13.1	20.8	16.3	12.9	12.9
exit	24.1	24.1	29.5	28.6	24.1	32.2	32.2
hub-to-tip radius ratio							
inlet	.185	.185	.185	.185	.185	.400	.400
exit	.525	.525	.525	.525	.525	.700	.700
full blade tip solidity	1.38	1.38	1.27	0.75	0.92	1.66	1.66
leading edge sweep	9.1	9.1	9.1	21.5	21.5	25.6	25.6

National Aeronautics and Space Administration

CFD Analysis In The Design of A Water-Jet-Drive System

Computational Fluid Dynamics Branch
Fluid Dynamics Division
Structures and Dynamics Laboratory
George C. Marshall Space Flight Center

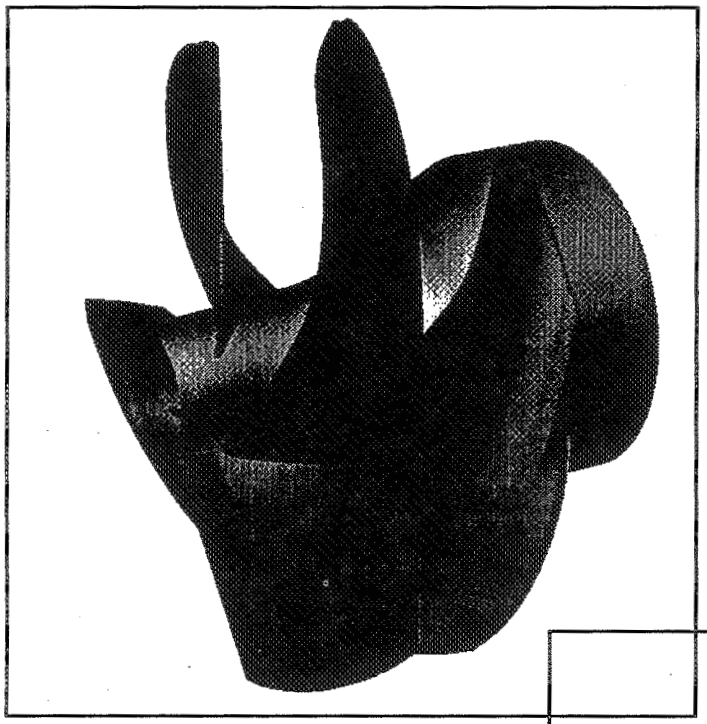

Case #1

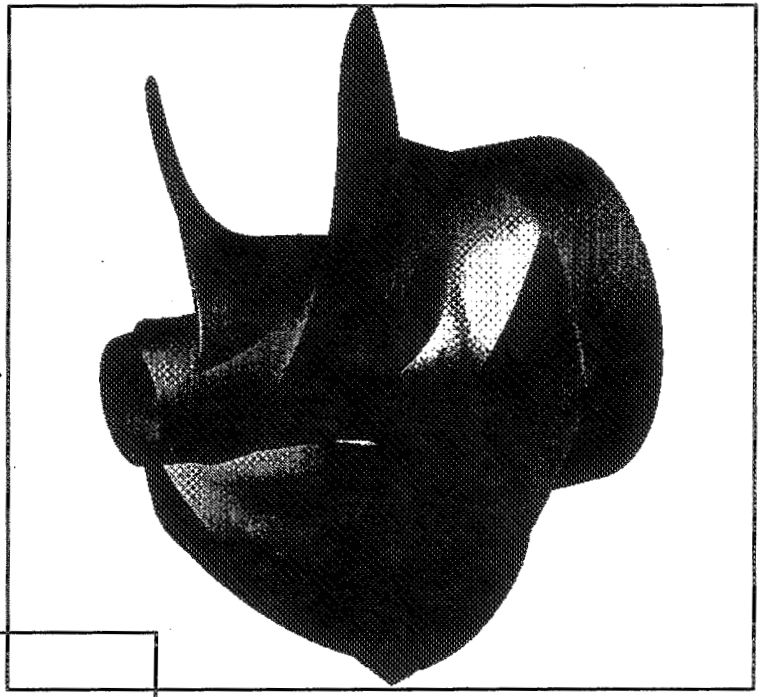

Case #4

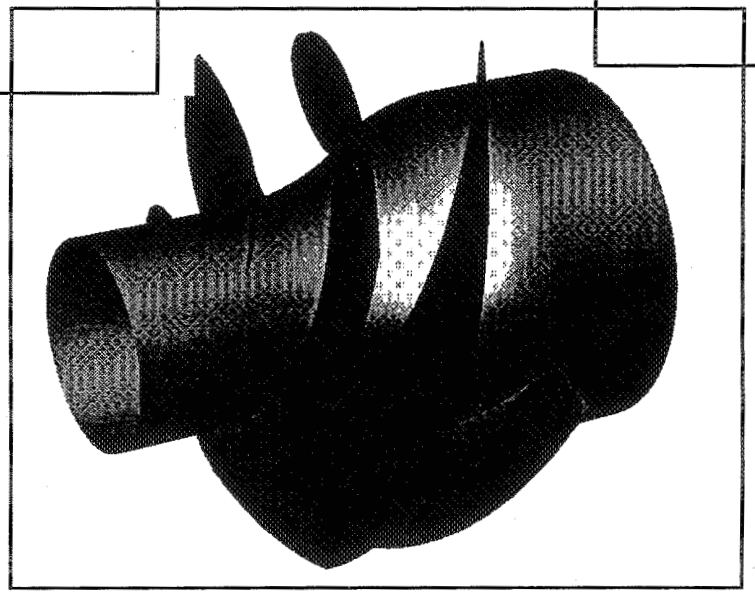

Case #6

CFD Analysis In The Design of A Water-Jet-Drive System

Computational Fluid Dynamics Branch
Fluid Dynamics Division
Structures and Dynamics Laboratory
George C. Marshall Space Flight Center

Results

- **Identified a Flow Coefficient Problem in the Baseline Impeller (Case #1)**
  - As Provided by NAMJ
  - Negative Incidence Over Most of the Leading Edge

- **Parametric Case #2 Evaluated Reduced Flow Coefficient (-30%)**
  - Significant Improvement in Performance

- **Parametric Case #3 Evaluated the Effect on Increased Camber**
  - Increased Efficiency and Head Rise

° **Parametric Case #5 Evaluated Effect of Increased Leading Edge Sweep**
  - Sweep increased from 9.1 to 21.5 degrees
  - Effectively Increased Blade Angle at the Tip
  - Small Increase in Efficiency and Pressure Rise

Results (continued)

- **Parametric Case #4 Evaluated Re-profiled Blades (MSFC)**
  - Inlet Tip Angle Increased, Sweep of Case #5 Retained
  - Efficiency +25%, Head Coefficient +28%
  - Ideal Specific Thrust Increased by 10% over the Baseline

- **Parametric Case #6 Involved a Complete Redesign Accounting for Updated System Requirements (Consultant)**
  - Blade Incidence Set Similar to Case #4
  - Increased Hub-to-Tip Radius Ratio, Solidity, & Camber
  - Efficiency +48%, Head Coefficient +85%
  - Ideal Specific Thrust Increased by 4% over the Baseline

- **Parametric Case #7 Evaluated the Redesign Impeller at 80% of Design Flow**
  - No Adverse Flow Features Identified

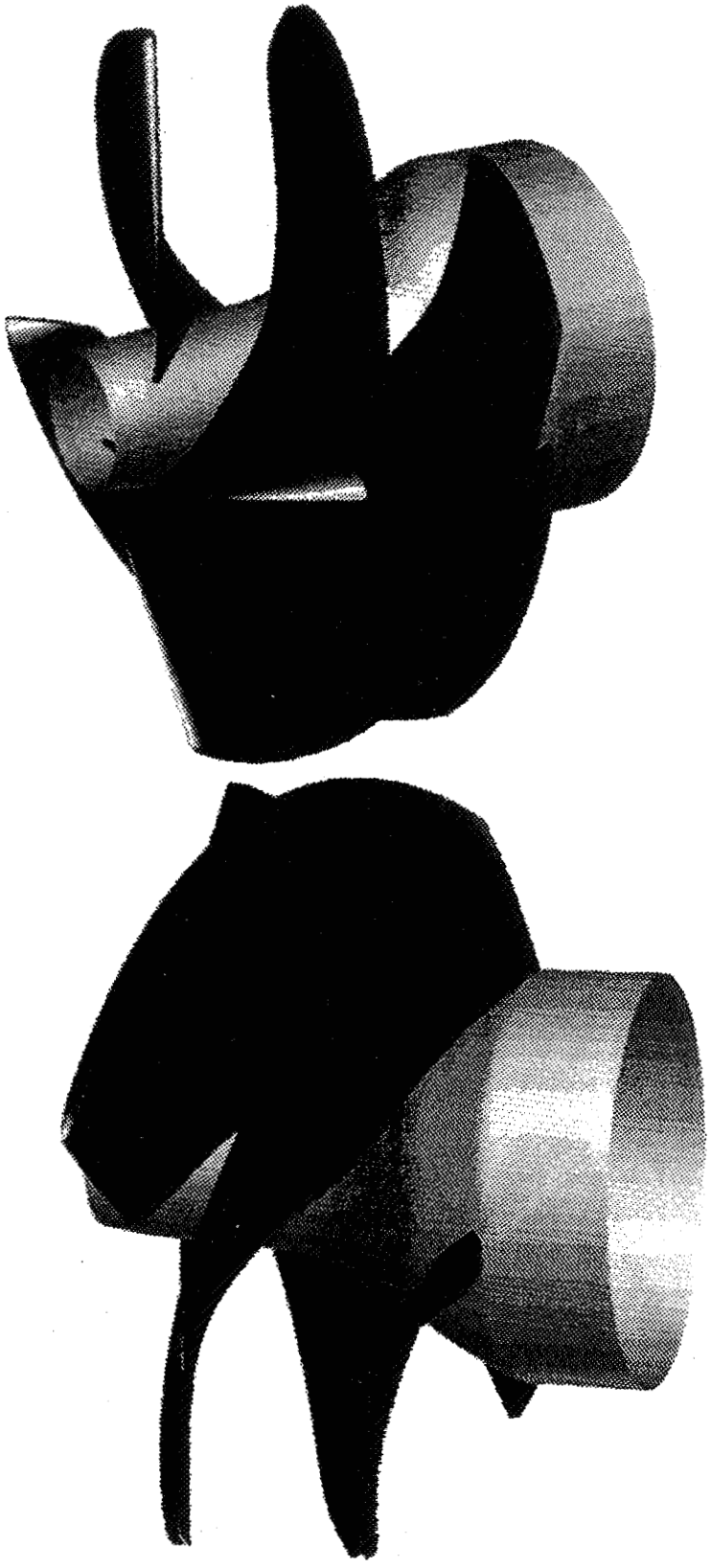

Figure 1. Baseline impeller geometry, blades colored by pressure

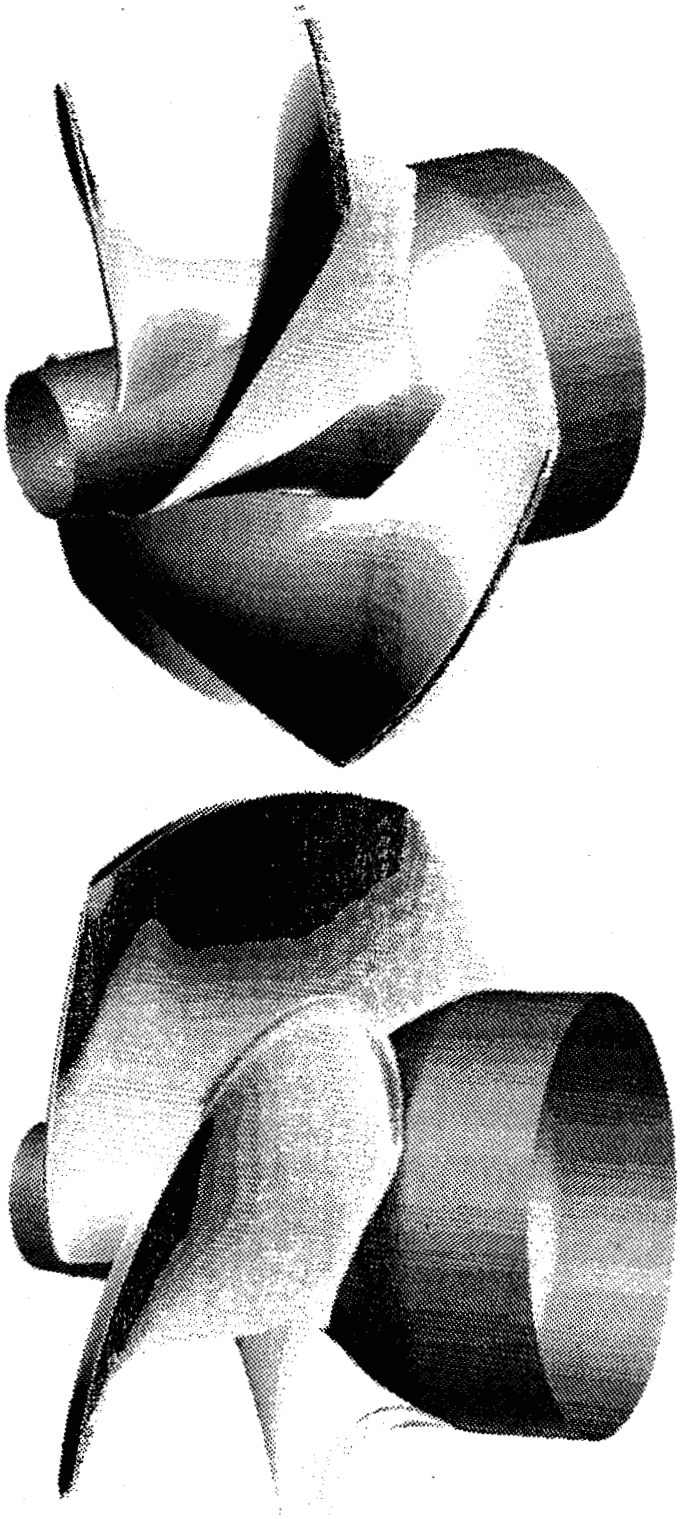

Figure 4. Interim impeller geometry (case #4), blades colored by pressure

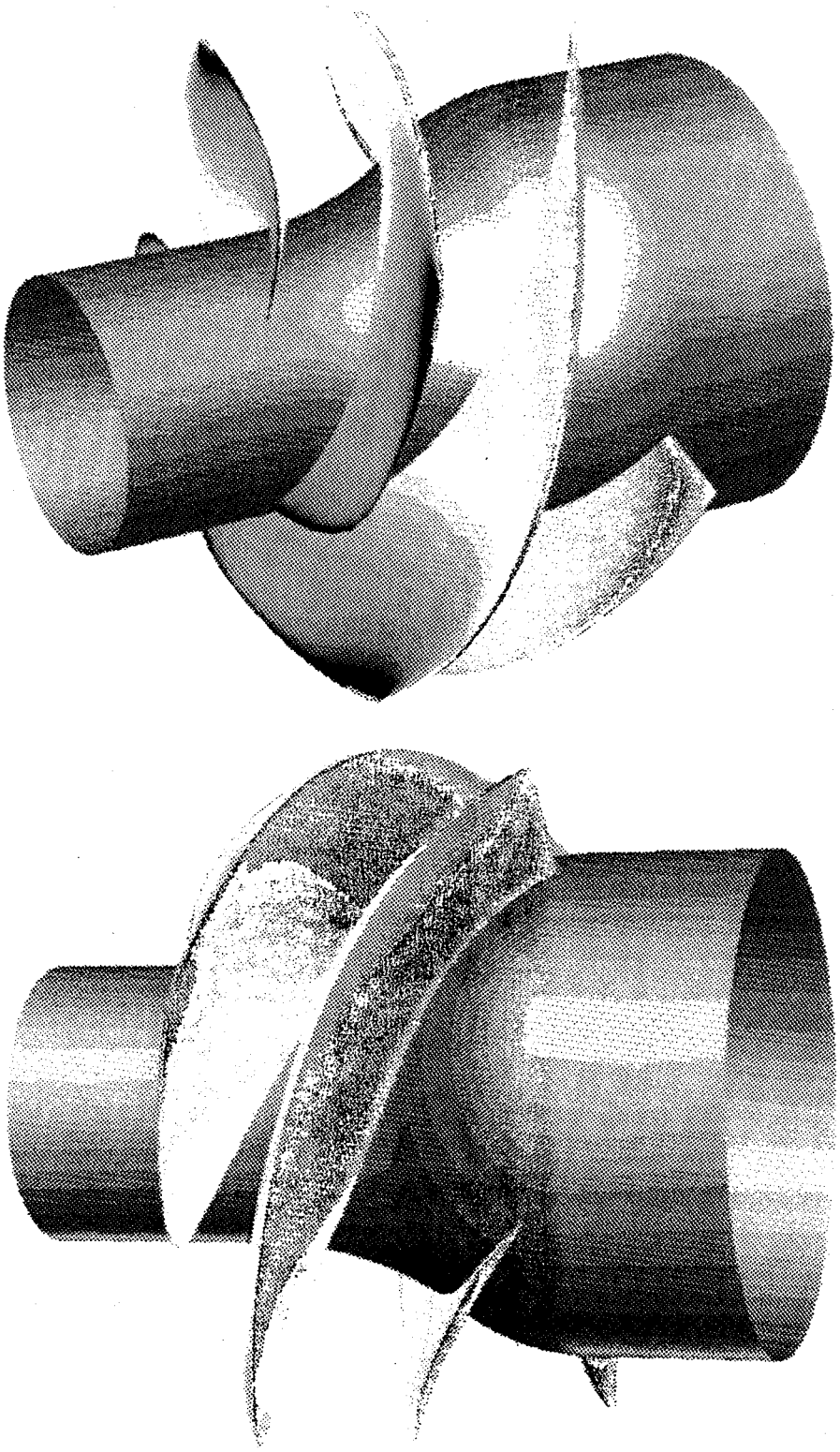

Figure 7. Final impeller geometry (case #6c), blades colored by pressure

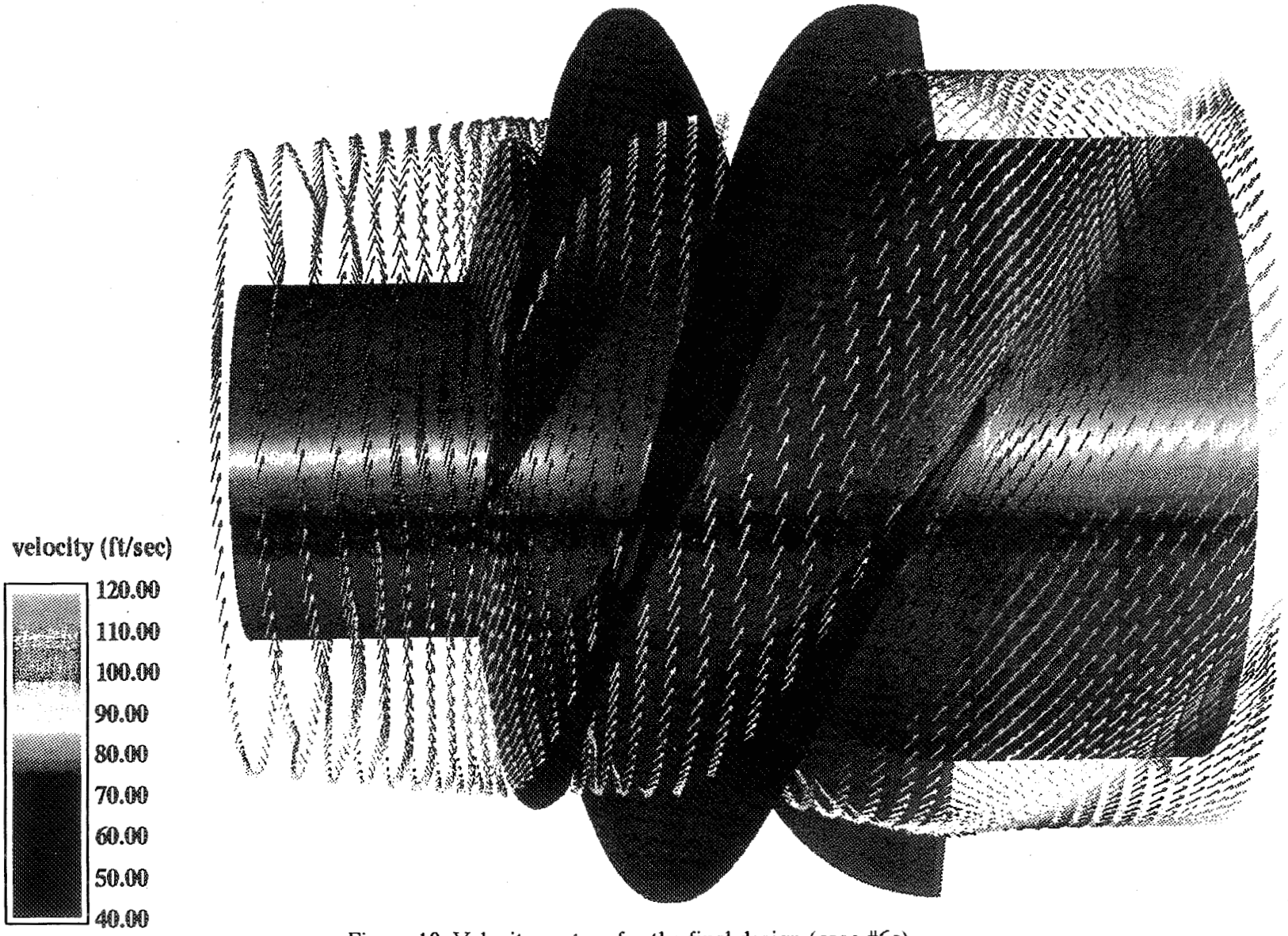

Figure 18. Velocity vectors for the final design (case #6c)
on a plane near the blade midspan

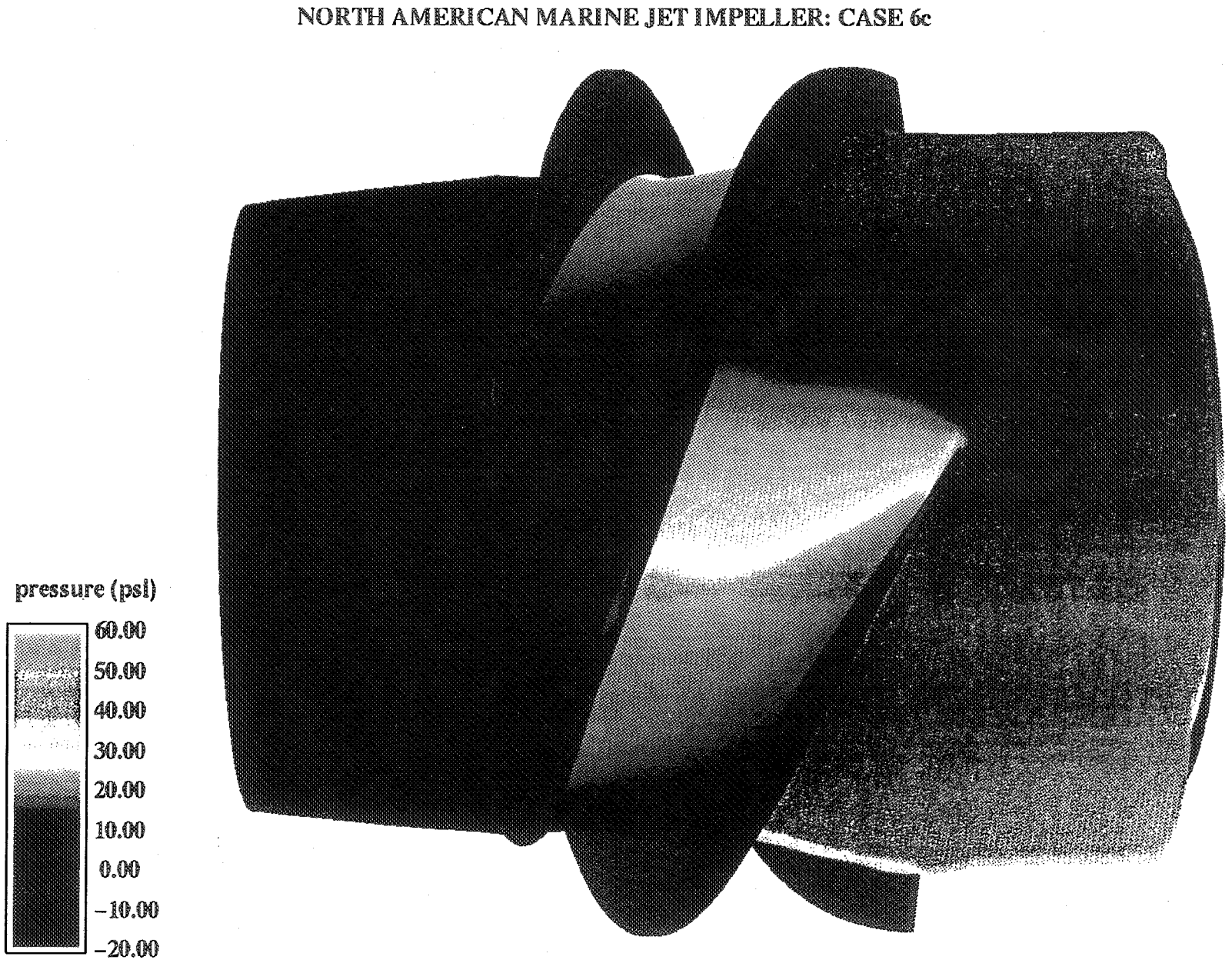

Figure 22. Pressure contours for the final design (case #6c on a plane near the blade midspan

NORTH AMERICAN MARINE JET IMPELLER: CASE 6c

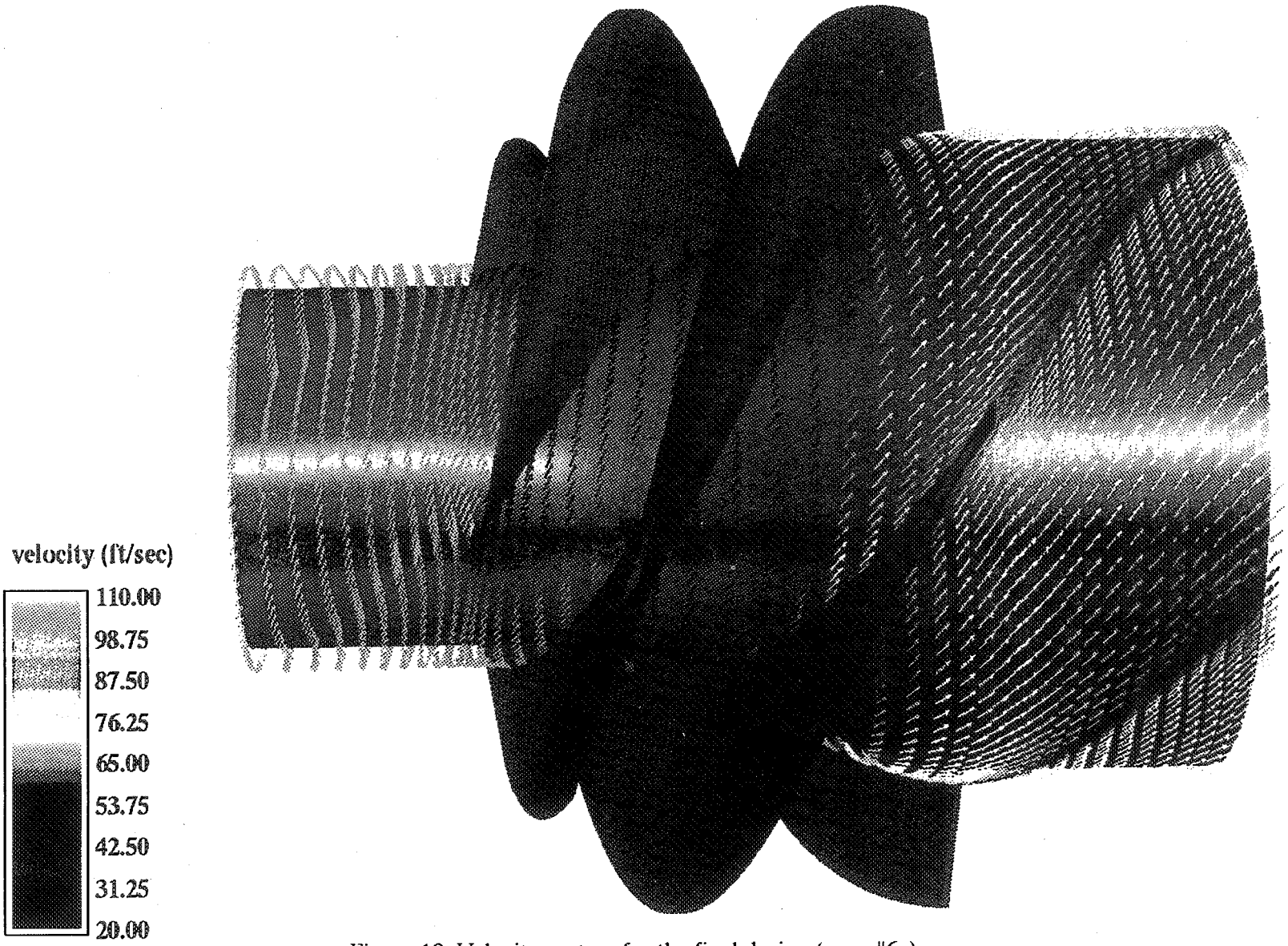

Figure 19. Velocity vectors for the final design (case #6c)
on a plane near the hub

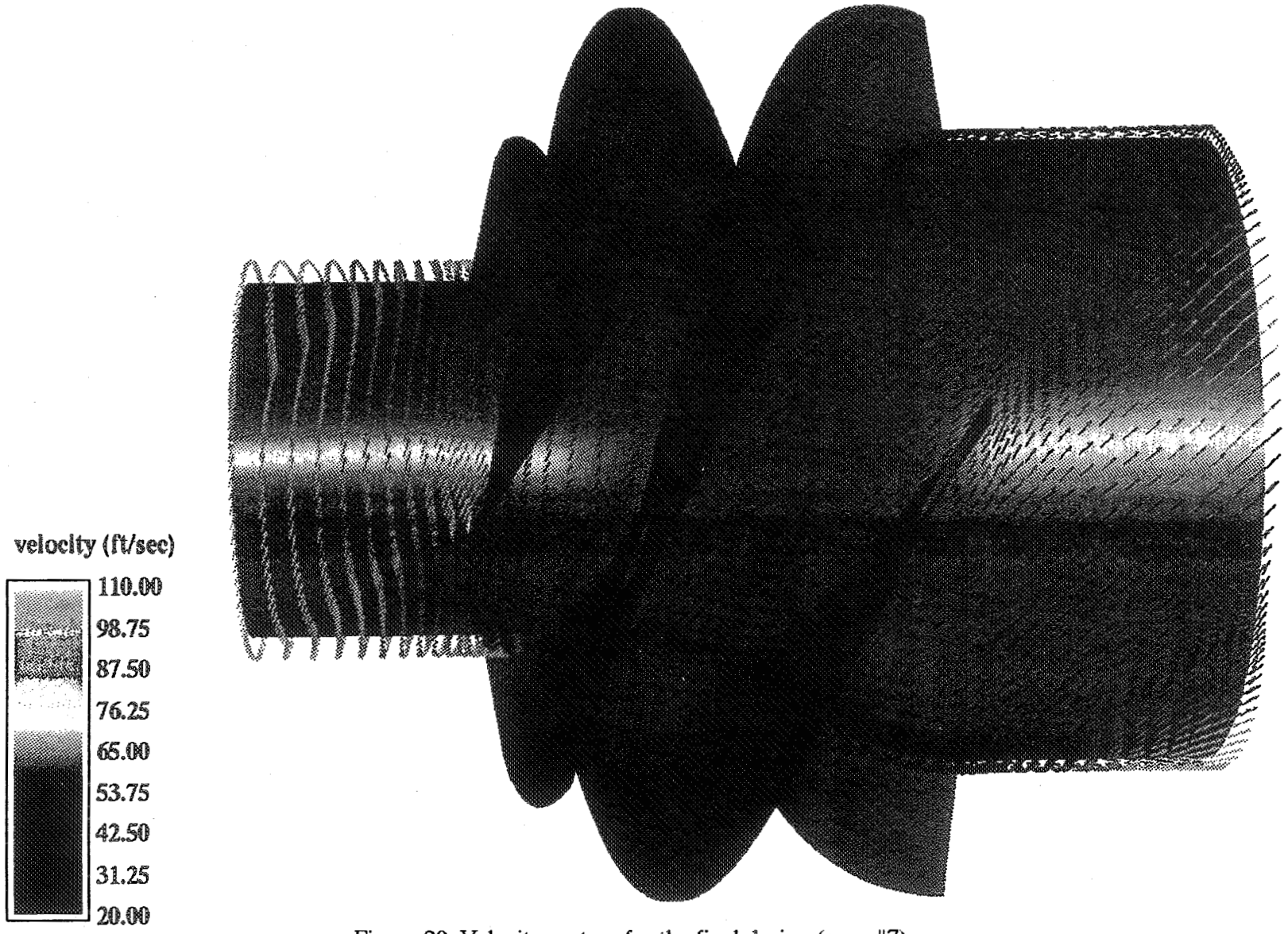

Figure 20. Velocity vectors for the final design (case #7)
on a plane near the hub

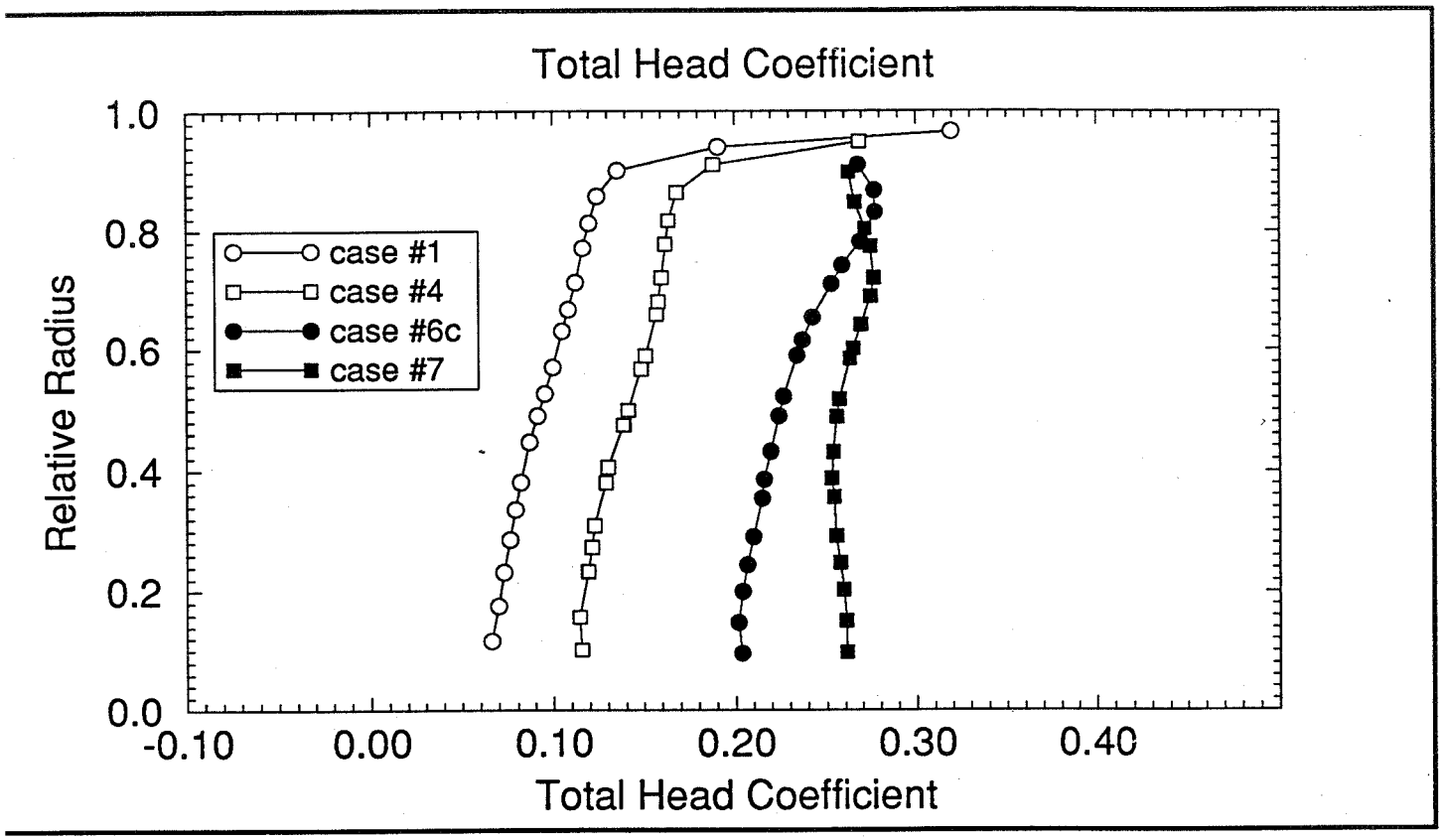

Figure 11. Radial distribution of total head coefficient rise (head/tip velocity squared

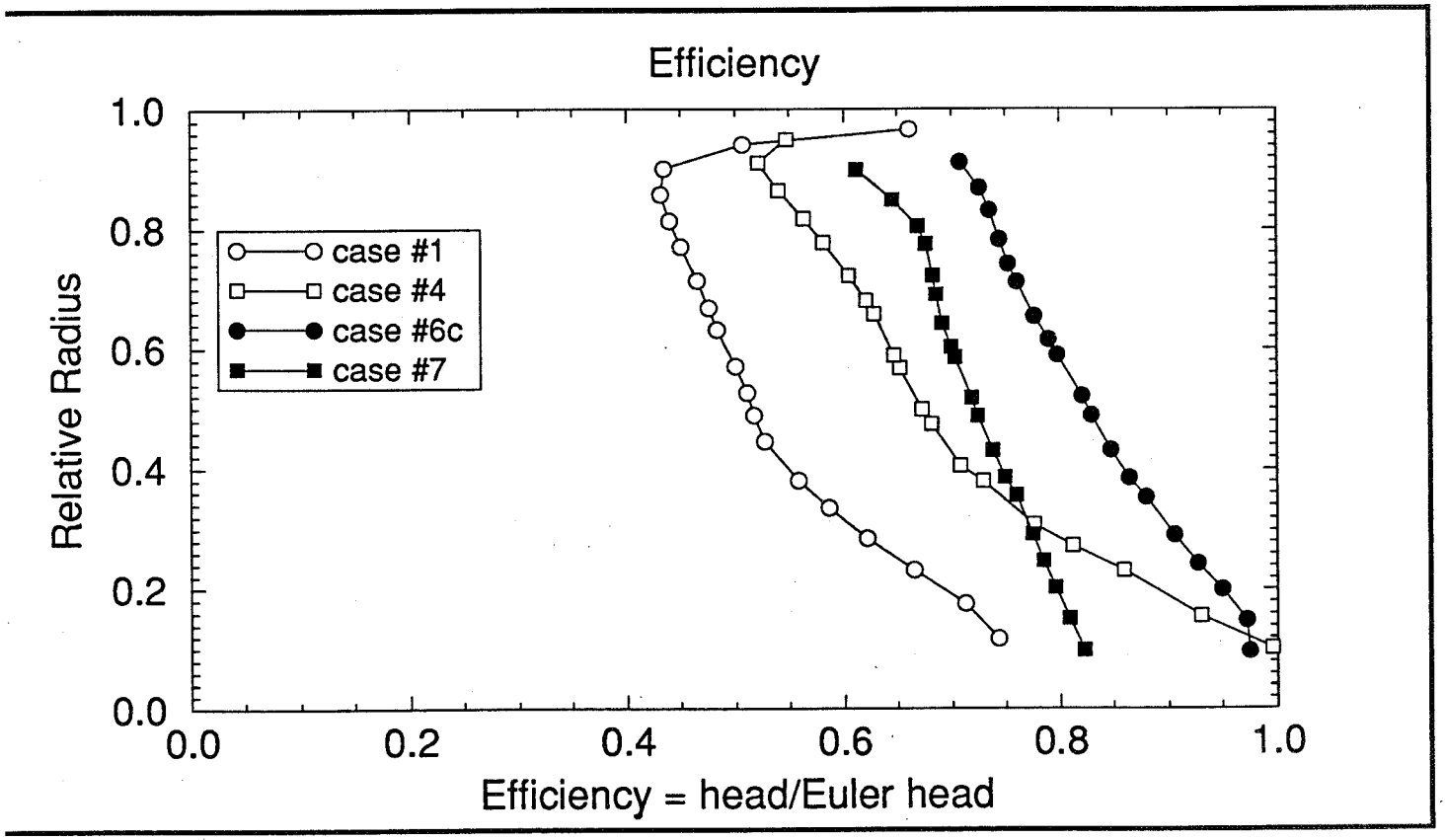

Figure 12. Radial distribution of efficiency (actual head rise/Euler head rise)

Nondimensional Impeller Performance

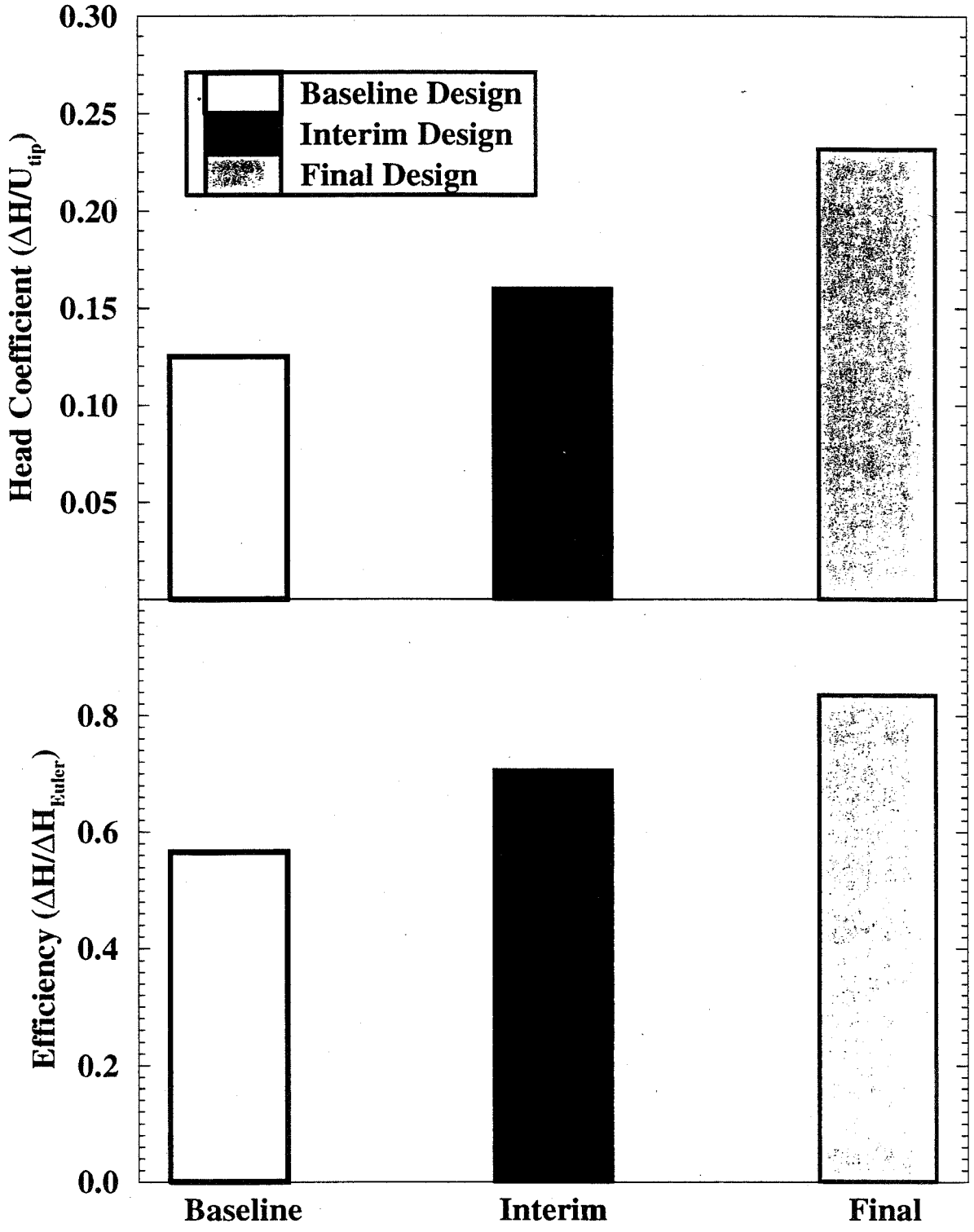

"Equivalent Power" Impeller Performance

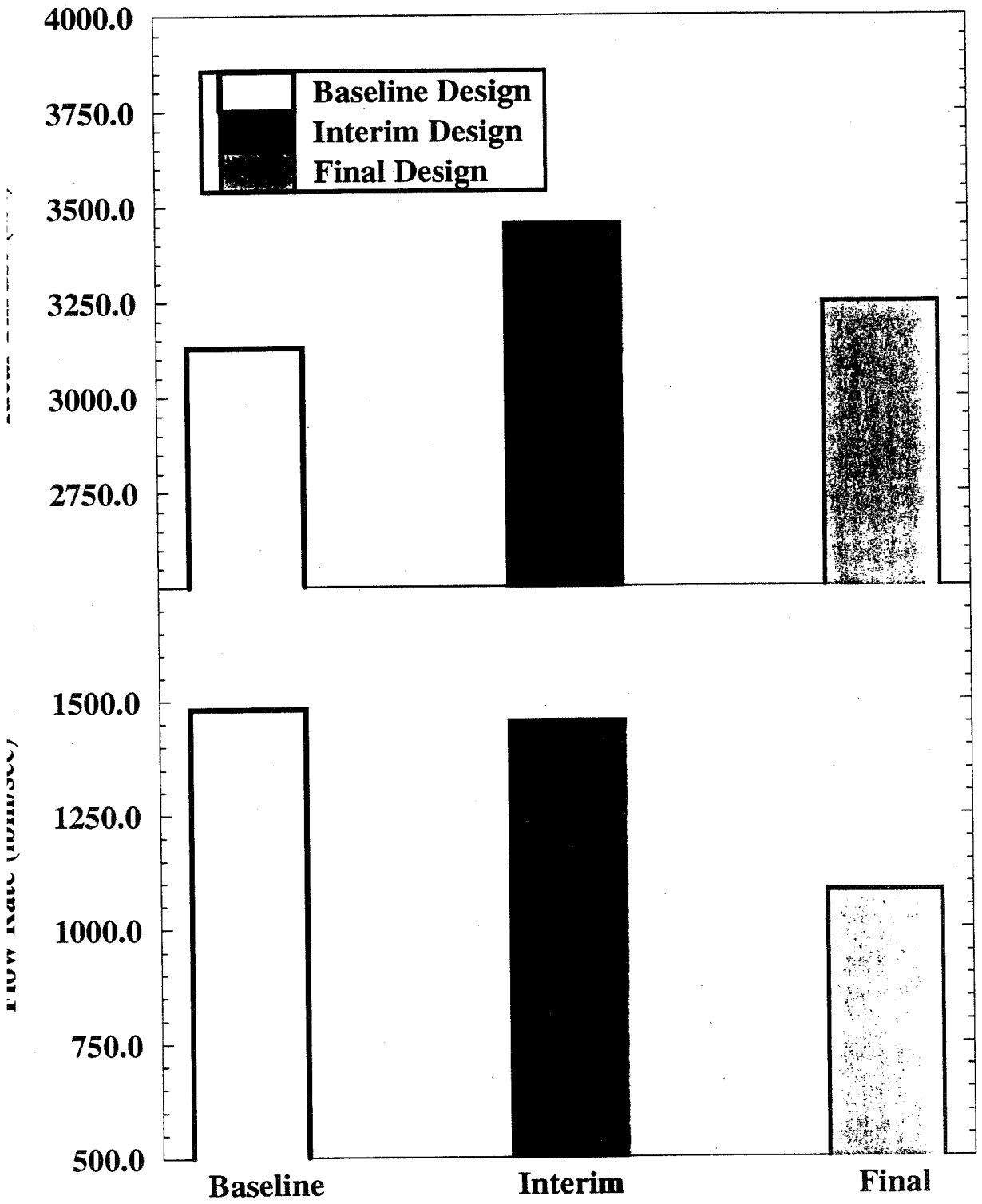

Summary/Conclusions

- **TU Office Assisting the Transfer of NASA Technology to Industry**
  - Information and Expertise
- **NAMJ Final Design Significantly Better Performance Than Baseline**
  - CFD Supported Design Phase in Timely Manner
  - Final Design Benefited From Insight Acquired From Parametric Cases
  - CFD Geometry File Used to Generate a Prototype Casting Mold
  - Prototype to be Tested by NAMJ
- **MSFC Streamlined its Turbomachinery Analysis Procedure**
  - Improvements Made to Geometry and Grid Generators
  - New Solver in FDNS3D Verified
  - Turbomachinery Data Base Expanded

PROCESS DEMONSTRATION AND REACT CODE VALIDATION FOR SHROUDED INDUCER OPERATION AT AND OFF DESIGN

Maria Subbaraman
Rotating Machinery Fluid Dynamics

Ed Ascoli
CFD Technology Center

Rocketdyne, Canoga Park, California

13th Workshop for CFD
Applications in Rocket Propulsion
Huntsville, Alabama
April 25-27, 1995

Rockwell Aerospace
Rocketdyne

OBJECTIVES

- Integrate CFD into design process
  - Demonstrate link between CAD geometry data bases and CFD analysis tools
  - Validate Rocketdyne Elliptic Analysis Code for Turbomachinery (REACT) for shrouded inducers

APPROACH

- EXISTING GEOMETRY
  - Inducer geometries existed in CATIA
- RAPID MESH GENERATION
  - CAD geometry input to RAGGS (Rockwell Automated Grid Generation System)
  - RAGGS based templates used to generate meshes
- 3-D ANALYSIS
  - Multi-zone steady state REACT with k-e model
  - Apollo and Sun workstations
- VALIDATION AGAINST TEST DATA

Page intentionally left blank

CAD Link to CFD Mesh Tools

- Geometry created in CAD system
  - CATIA
  - pro/E
- Blade surface representation output in appropriate format
  - CAD IGES surfaces
  - Point Arrays from CAD or T/M codes
- CAD output read into RAGGS
- Once in RAGGS format, can either
  - Use General RAGGS capability to interactively create mesh
  - Use RAGGS based templates to semi-automate mesh generation for blade passage configurations

BLADE PASSAGE TEMPLATES

- Mesh generation templates designed for blade passage configurations (axial, radial, mixed)
- Template tools (written in Fortran and Unix shell programming language)
    - Interface with and employ RAGGS batch utilities
    - Incorporate Logic Branching and Artificial Intelligence
    - At any stage template results can be interactively viewed and enhanced using RAGGS interactive tools
- Mesh generation times for inducer configuration
    - Months - PATRAN-2, circa 1990 (first inducer grid)
    - Days - RAGGS (without templates)
    - Hours - New Grid using Templates
    - Minutes - Grid modifications with Templates

REACT VALIDATION

- Axial inducer geometry
    - Shrouded
    - Leakage over shroud
- Two mesh sizes
    - 20K grid points
    - 64K grid points
- Validated against test data at and off-design
    - Hub-to-tip distributions of
        - Discharge flow velocity
        - Absolute flow angle
        - Static and total pressures

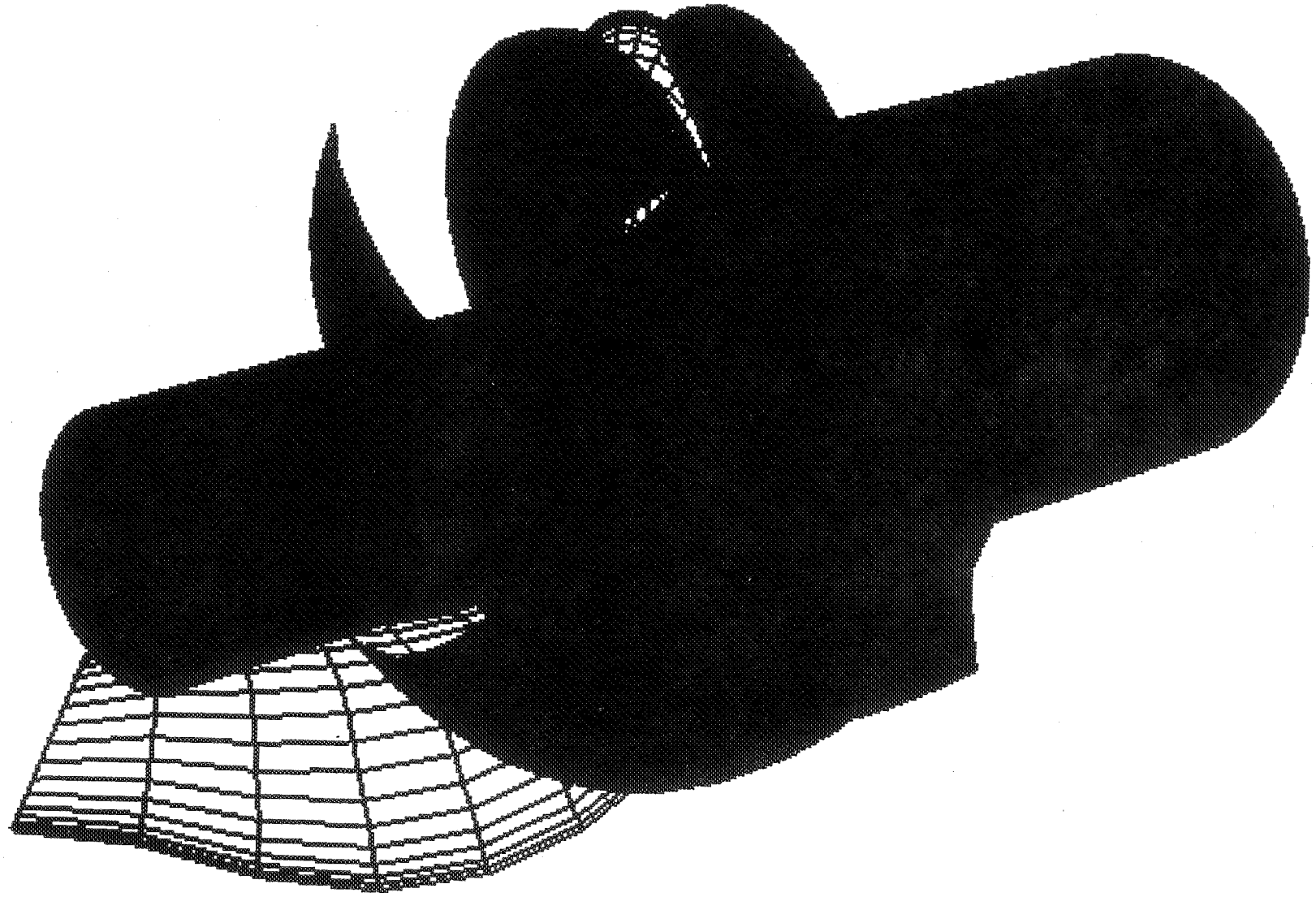

Rockwell Aerospace
Rocketdyne

20 K Mesh

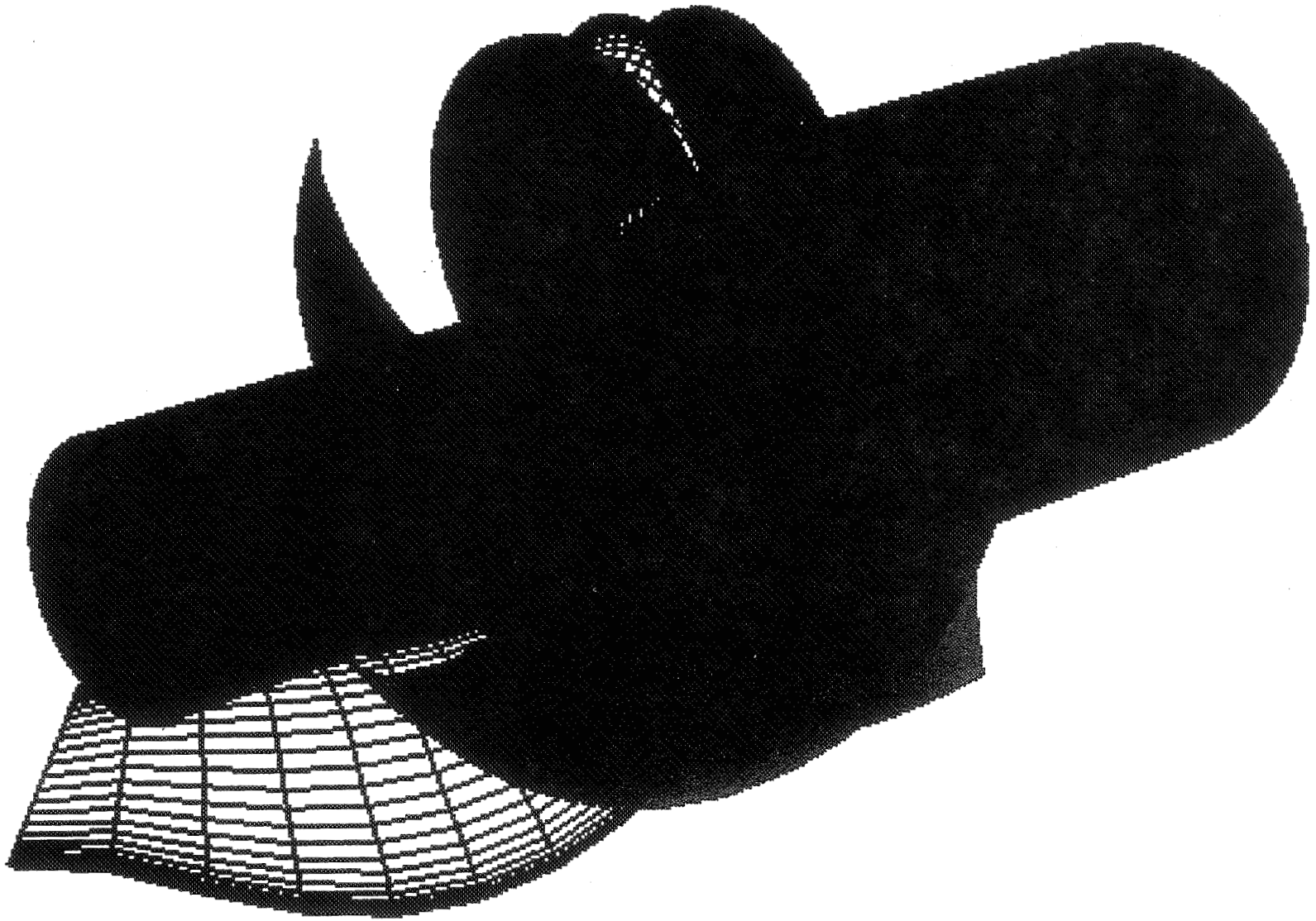

Rockwell Aerospace
Rocketdyne

64 K Mesh

SHROUDED INDUCER WITH FLOW RECIRCULATION

CFD MODEL

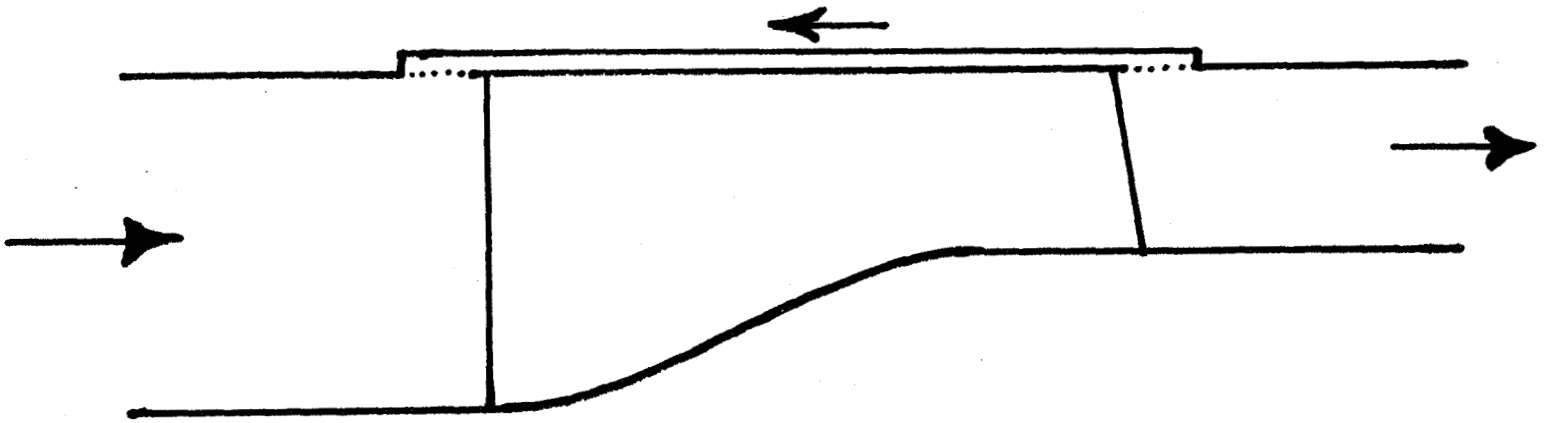

Total and Static Discharge Pressure (at 95% Design Flow)

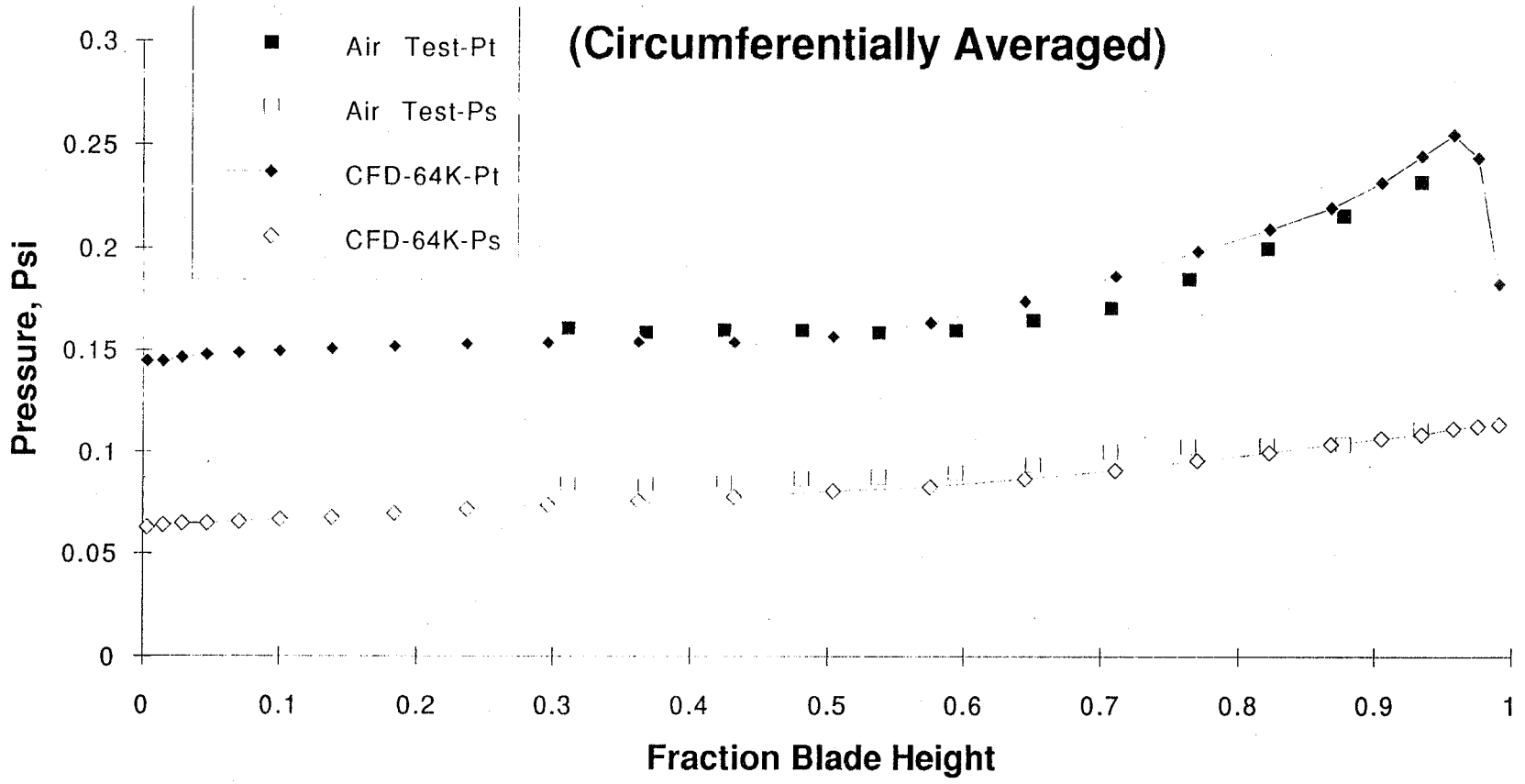

Rockwell Aerospace
Rocketdyne

Discharge Flow Angle Distribution at 104% Design Flow

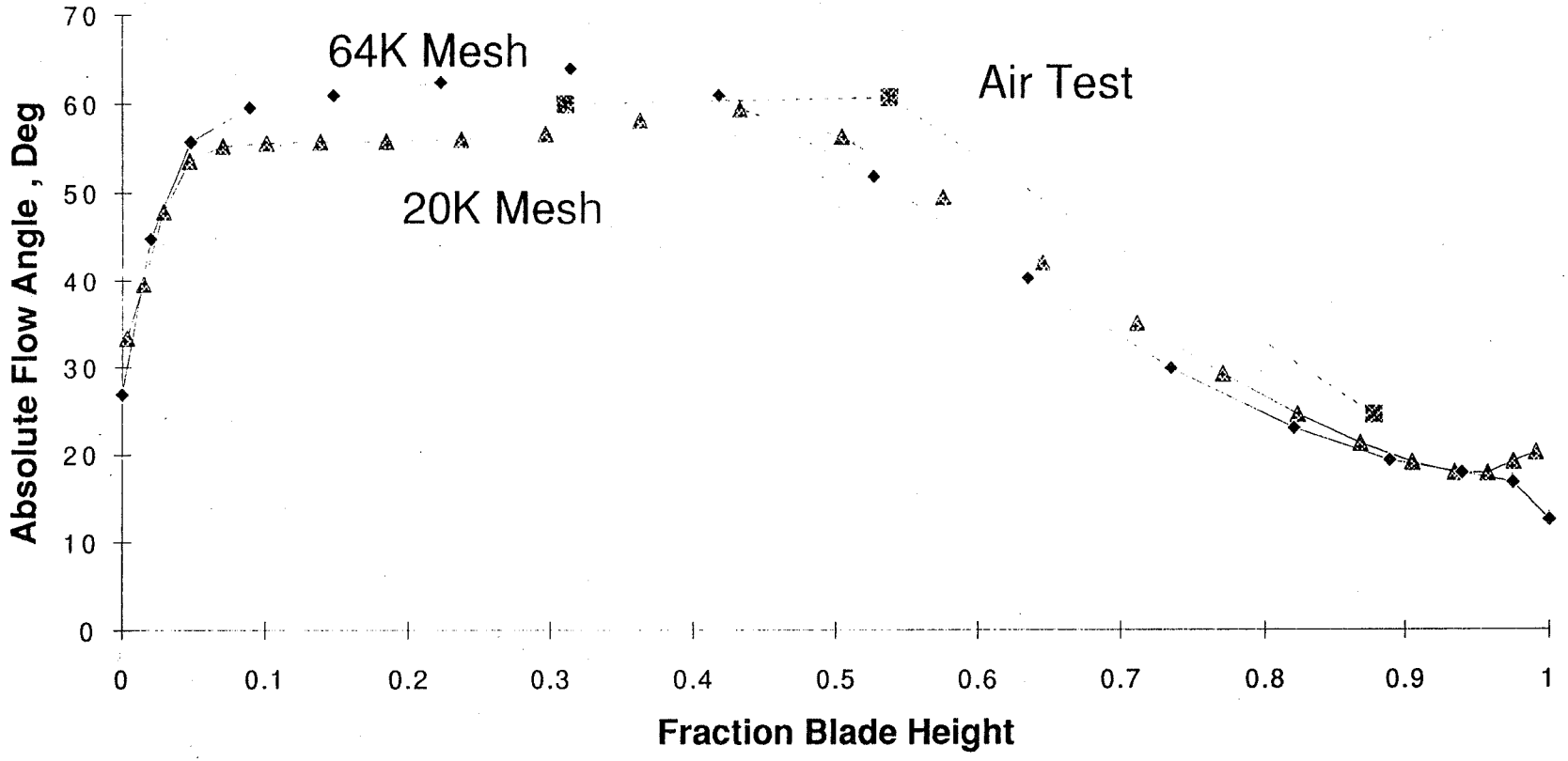

Rockwell Aerospace
Rocketdyne

Discharge Flow Angle Distribution (at 85% Design Fl ow)

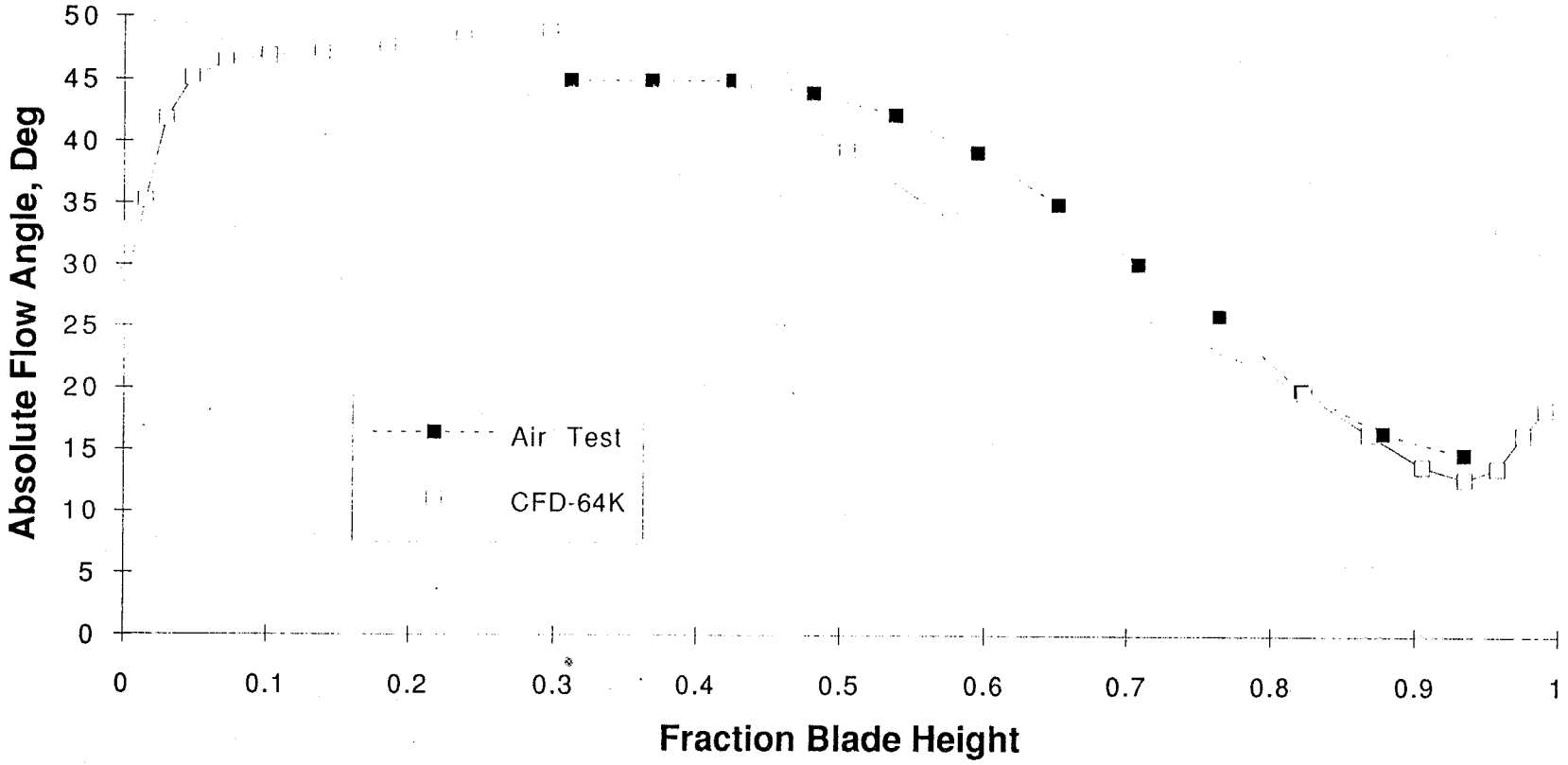

Rockwell Aerospace
Rocketdyne

Relative Stagnation Pressure
Inducer
Discharge
Inducer
Inlet

Rotary Stagnation Pressure

Rotary Stagnation Pressure
1.0
0.5
0.0

SUMMARY

- CAD-RAGGS Template process link demonstrated
- Effectiveness of RAGGS Templates demonstrated
    - Save time
    - Facilitate grid optimization
- REACT validated for shrouded inducer geometry
    - Excellent agreement with test data
        - Design point
        - Off-design

Page intentionally left blank

Numerical Simulation of the Unsteady Flow Field in an Integrated Centrifugal Impeller-Vaned Diffuser System

by
Leonard Walitt
Titan Research and Technology Division of the Titan Corpration

Abstract

A new computer code, called STARZONE, has been developed for turbomachinery applications. STARZONE solves the time-dependent, turbulent Navier-Stokes equations for three-dimensional flow. This code utilizes a third order accurate state-of-the-art total variational diminishing (TVD) operator for integrating the Euler equations of motion and timestep splitting for inclusion of viscous and Reynolds stress terms. A full second order closure turbulence model is embodied in STARZONE. The STARZONE computer code also employs adaptive zoning to efficiently zone regions of high gradients. Finally, STARZONE is a multi-block code, which permits the flow interaction of a rotor block with a stator block. All the blades can be included for the rotor block and all the vanes can be included for the stator block. The blade/vane counts need not be the same.

STARZONE has been applied to an impeller-vaned diffuser system composed of 17 impeller blades and 19 diffuser vanes. The impeller exit diameter is 24.25 inches and the impeller rotates at 14,970 r.p.m.. The diffuser has variable geometry and the working medium is air. Two cases have been studied. The first has a mass flow rate of 13.72 kg/sec, while the second has a mass flow rate of 12.10 kg/sec. The diffuser throat is smaller for the second case. It has been observed experimentally that the compressor flow is unstable for both cases.

The numerical simulation for the first case indicated that the flow separated at the impeller suction surface leading edge, near the hub, and remained separated throughout the inducer region. In the vaneless space between the impeller blades and the diffuser vanes there are flow asymmetries present. Due to vaneless space asymmetries, pressure distributions along the pressure and suction surfaces of a diffuser vane vary from one diffuser vane to another. In addition, there is flow separation at the diffuser vane leading edge. The calculated stage total pressure ratio matched the measured value.

Time histories of the mass flow rate were studied for the first case at the interface surface between the rotating impeller block and the stationary diffuser block and at the exit of the diffuser. The double amplitude of the mass flow rate time history at the diffuser exit was 9.1 percent of the mass flow rate upstream of the impeller and its frequency was 1435 hz. Let us consider the diffuser vanes as a set of rectangular cavities relative to the impeller. Under this scenario the calculated frequency is within 5 percent of the first harmonic resonant frequency for a rectangular cavity.

The numerical simulation for the second case produced some interesting fluid mechanical results. The flow exiting the impeller impacts the lower surface of a diffuser vane away from its leading edge. This causes an expansion around the leading edge of the vane and along the upper surface of the vane. The diffuser vanes then act as convergent-divergent nozzles to the flow preventing its complete diffusion.

NUMERICAL SIMULATION OF THE UNSTEADY FLOW IN AN INTEGRATED CENTRIFUGAL IMPELLER-VANED DIFFUSER SYSTEM

L. Walitt

Titan Research and Technology Division
Titan Corporation
Chatswoth, California

Computational Fluid Dynamics Branch
Fluid Dynamics Division
Structures and Dynamics Division
Science and Engineering Directorate
Marshall Space Flight Center

Workshop for CFD Applications in Rocket
Propulsion and Launch Technology
Huntsville, Alabama
April 25-27, 1995

TOPICS TO BE PRESENTED

- O STARZONE COMPUTER CODE
  - --History
  - --Features of Computer code
  - --Fields of Application of Computer code
- O DESCRIPTION OF PROBLEM
  - --Impeller-Vaned Difffuser Geometry
  - --Finite Difference Mesh
  - --Compressor Performance Map
  - --Cases Studied
    - ---Case r117
    - ---Case r118
- O IMPELLER-VANED DIFFUSER NUMERICAL RESULTS FOR CASE R117
  - --Overall Flow Fields
  - --Vaneless Space and Diffuser Vane Flow Fields
  - -- Unsteady Flow Field Effects
    - ---resonance
  - -- Effects of Adaptive Zoning on Flow Fields
    - ---inducer region
    - ---diffuser region
  - -- Summary of Principal Results
- O IMPELLER-VANED DIFFUSER NUMERICAL RESULTS FOR CASE R118
  - --Overall Flow Fields
  - --Vaneless Space and Diffuser Vane Flow Fields
  - --Unsteady Flow Field Effects
  - -- Summary of Principal Results

FEATURES OF STARZONE COMPUTER CODE

O MULTI-BLOCK STRUCTURE

---code structured with independent blocks of cells which communicate through Interface surfaces

O ARBITRARY-LAGRANGIAN-EULERIAN MOTION OF CELLS IN EACH BLOCK

--- rotating block can communicate with stationary block
--- rotor-stator and stator-rotor
--- multiple stages of a compressor or turbine

O TOTAL VARIATIONAL DIMINISHING (TVD) ALGORITHM

--- accurate representation of shock waves

O AUTOMATIC ADAPTIVE ZONING

--- efficiently exploits available mesh points
--- accurately defines regions of high gradients

O SECOND ORDER TURBULENCE MODELING

--- transition
--- higher order correlation's of turbulent fluctuations

O FINITE RATE CHEMISTRY INCLUDING TURBULENT CHEMISTRY/ COMBUSTION MODELS

--- unmixedness and temperature spottiness models

O MUTIPHASE LIQUID AND SOLID/LIQUID PARTICLE PHYSICS

--- particle transport and particle/gas micro physics

O AERODYNAMIC DESIGN OPTIMIZATION ALGORITHM

--- optimize aerodynamic shape to maximize a performance parameter

FIELDS OF APPLICATION OF STARZONE

O ROTOR FLUID DYNAMICS

---calculate steady flow field in a compressor impeller or turbine rotor
---calculate the unsteady rotating stall in a compressor rotor accounting for all the blades

O UNSTEADY ROTOR-STATOR INTERACTIONS

---calculate the interaction of a compressor impeller and its vaned diffuser
----all impeller blades and all diffuser vanes accounted for
---calculate the interaction of a turbine nozzle cascade with the turbine blading
---- all nozzle vanes and all turbine blades included

O STEAM TURBINE LATE STAGE EROSION DUE TO DROPLETS

---calculate condensation of water vapor in a steam turbine
--- include slip between droplets and water vapor

O ACOUSTIC RADIATION FROM A TURBOMACHINE

---second order turbulence model calculates the two-point turbulent fluctuation correlation's required for sound propagation

O CHEMICAL REACTIONS IN A TURBINE INCLUDING PARTICLE PHYSICS

--- finite rate chemistry
--- unmixedness and temperature spottiness

O COMBUSTION

--- gasoline engine combustion integrated with intake manifold and exhaust manifold fluid mechanics
--- diesel engine combustion including fuel droplet micro physics and the formation of the fuel vapor
--- turbine engine combustion including pre whirl

Finite Difference Mesh for Centrifugal Impeller-Diffuser System

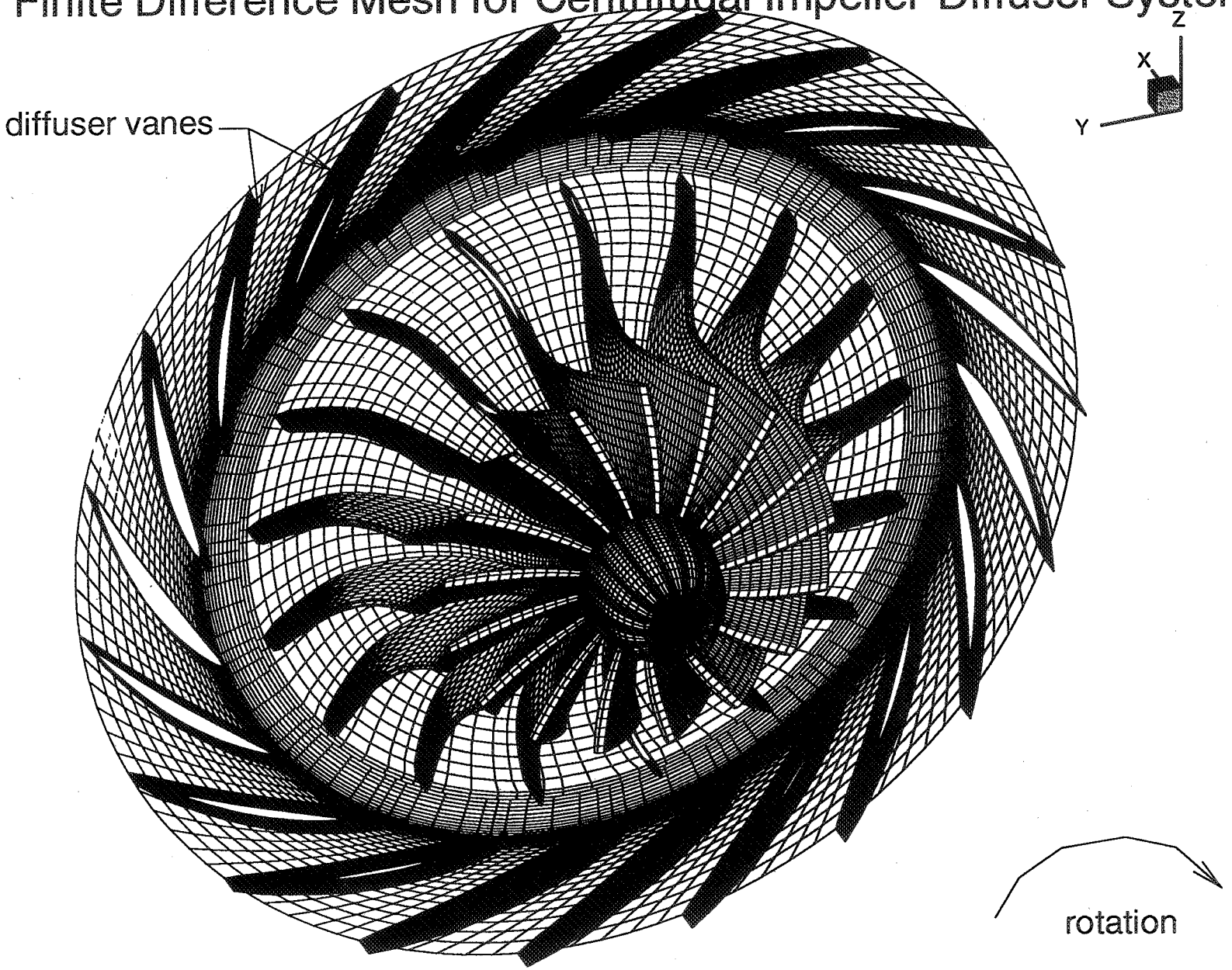

INLET T = 35 DEG C
INLET P = Ø.99 BARA
REL HUM = 53%

COMPLETE CURVES

CURVE	DGV	IGV	Case
● A	Ø	Ø	Y117
● B	-1.5	Ø	Y118
C	"	2Ø	
D	"	4Ø	
E	-6.Ø	4Ø	
F	"	6Ø	
G	Ø	2Ø	
H	-1Ø.Ø	2Ø	

SURGE POINTS

POINT	DGV	IGV
1	Ø	-1Ø
2	+6	Ø
3	-6	Ø
4	-1Ø	Ø
5	-14	Ø
6	-1Ø	Ø
7	-14	75
8	-12	75

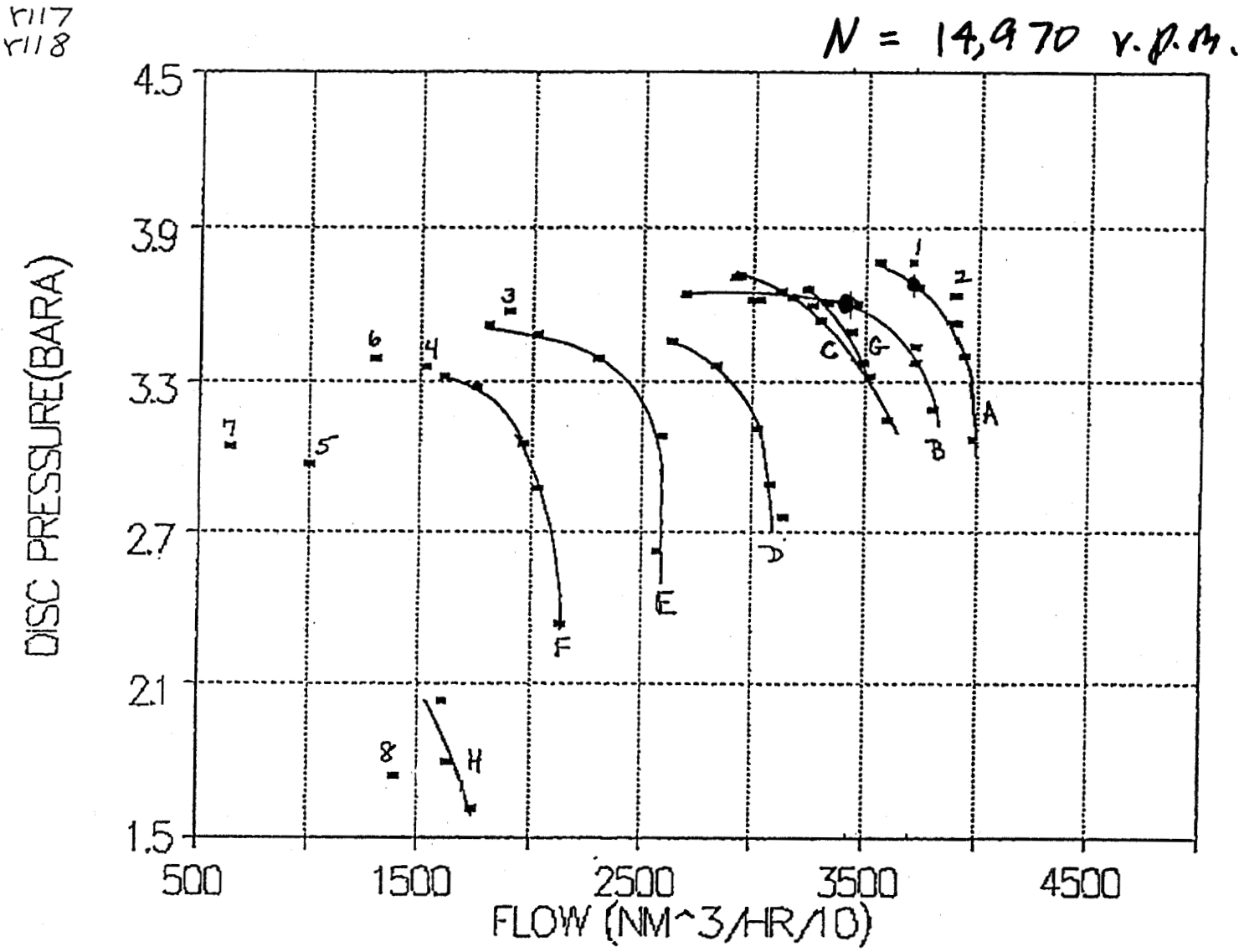

CASES ANALYSED

Case No.	IGV Angle (deg.)	DGV Angle (deg.)	Inlet Flow (icfm)	Inlet Flow (nm**3/hr)	Inlet Flow (kg/sec)	P_{te}/P_{to}
r117	0.0	0.0	26,000	37,121	13.72	3.70
r118	0.0	-1.5	24,000	34,265	12.10	3.62

Mach Number Field in the Rotor-Stator Regions at a Time of 2.95 ms

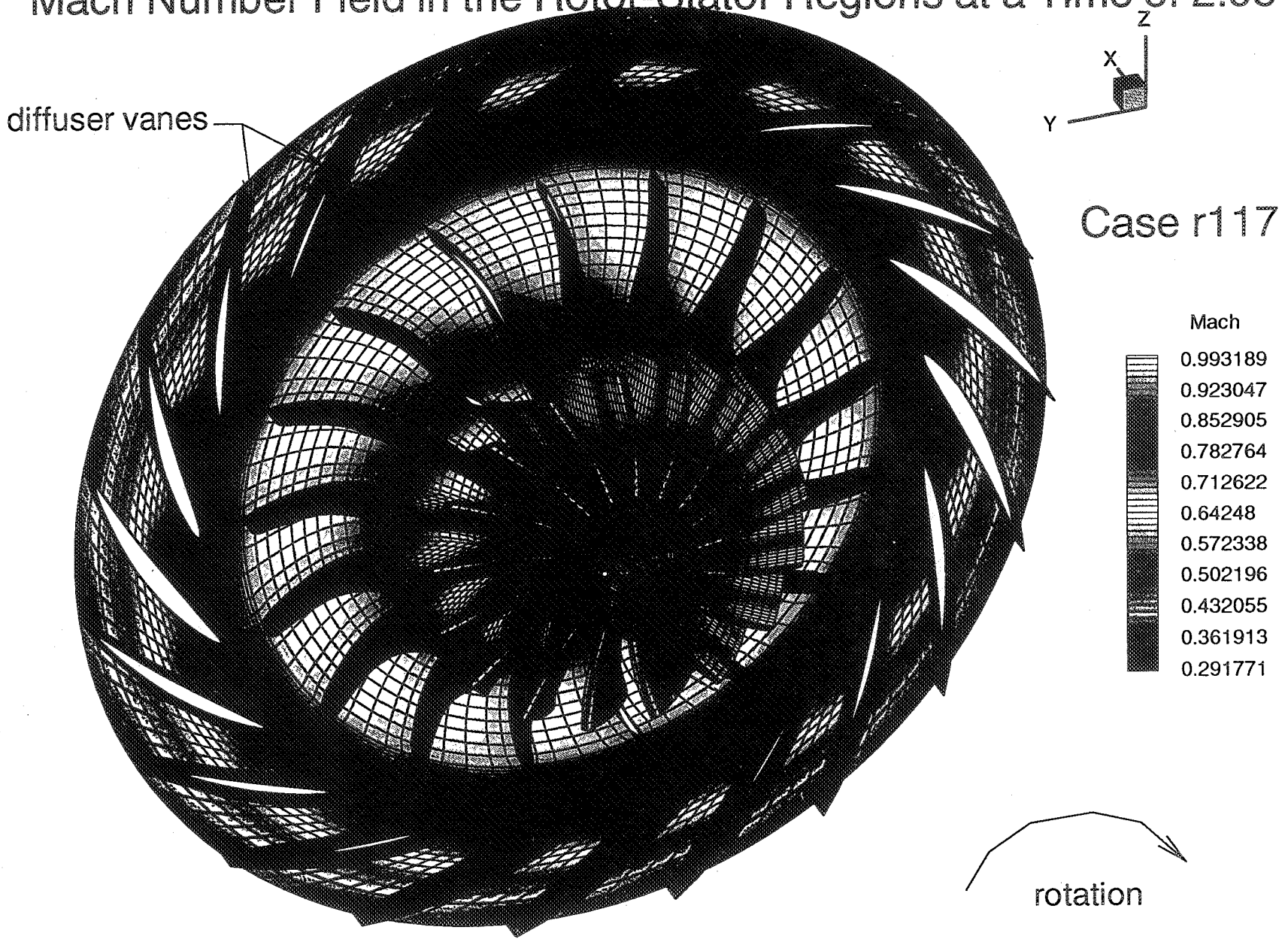

Pressure Field in the Rotor-Stator Regions at a Time of 2.95 ms

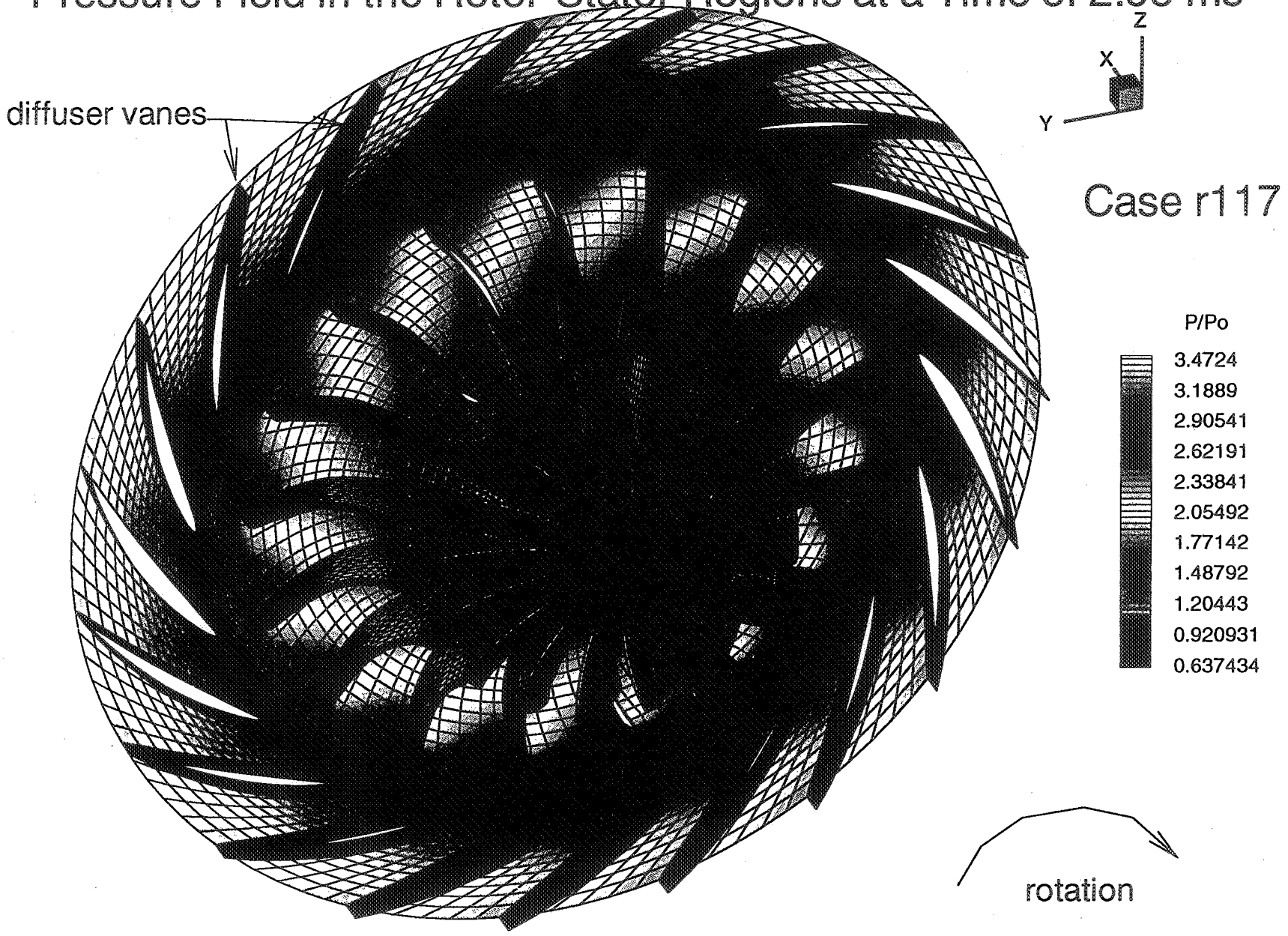

COMPARISON OF MEASURED AND CALCULATED TOTAL PRESSURE RATIOS

Case	$(P_{te}/P_{to})_m$	$(P_{te}/P_{to})_c$	Percent Error	Me
r117	3.70	3.67	.8	0.350
r118	3.62	3.71	2.4	0.425

Mach Numbers in the Diffuser Shroud at a Time of 2.95 ms

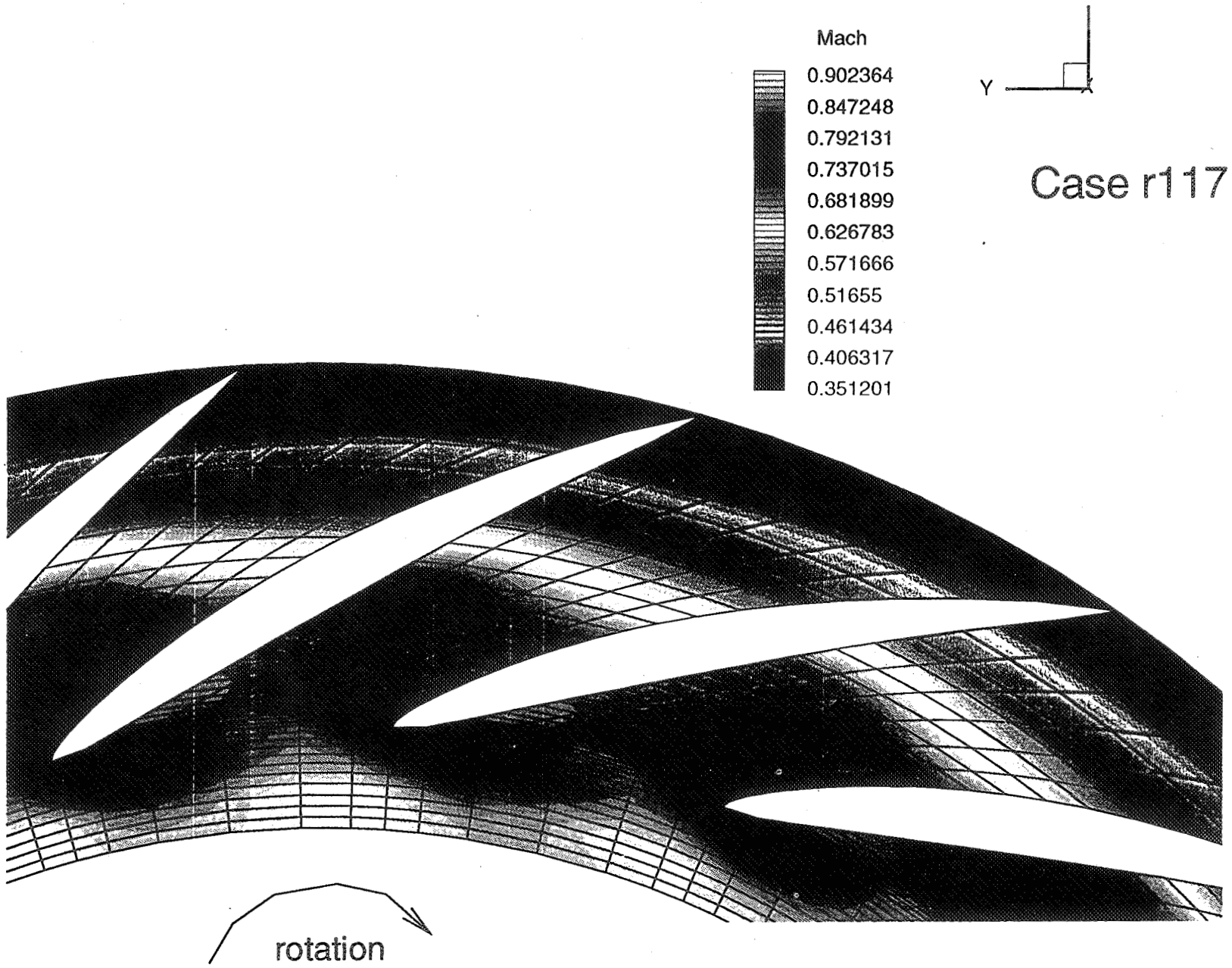

Pressure Field in the Diffuser Shroud at a Time of 2.95 ms

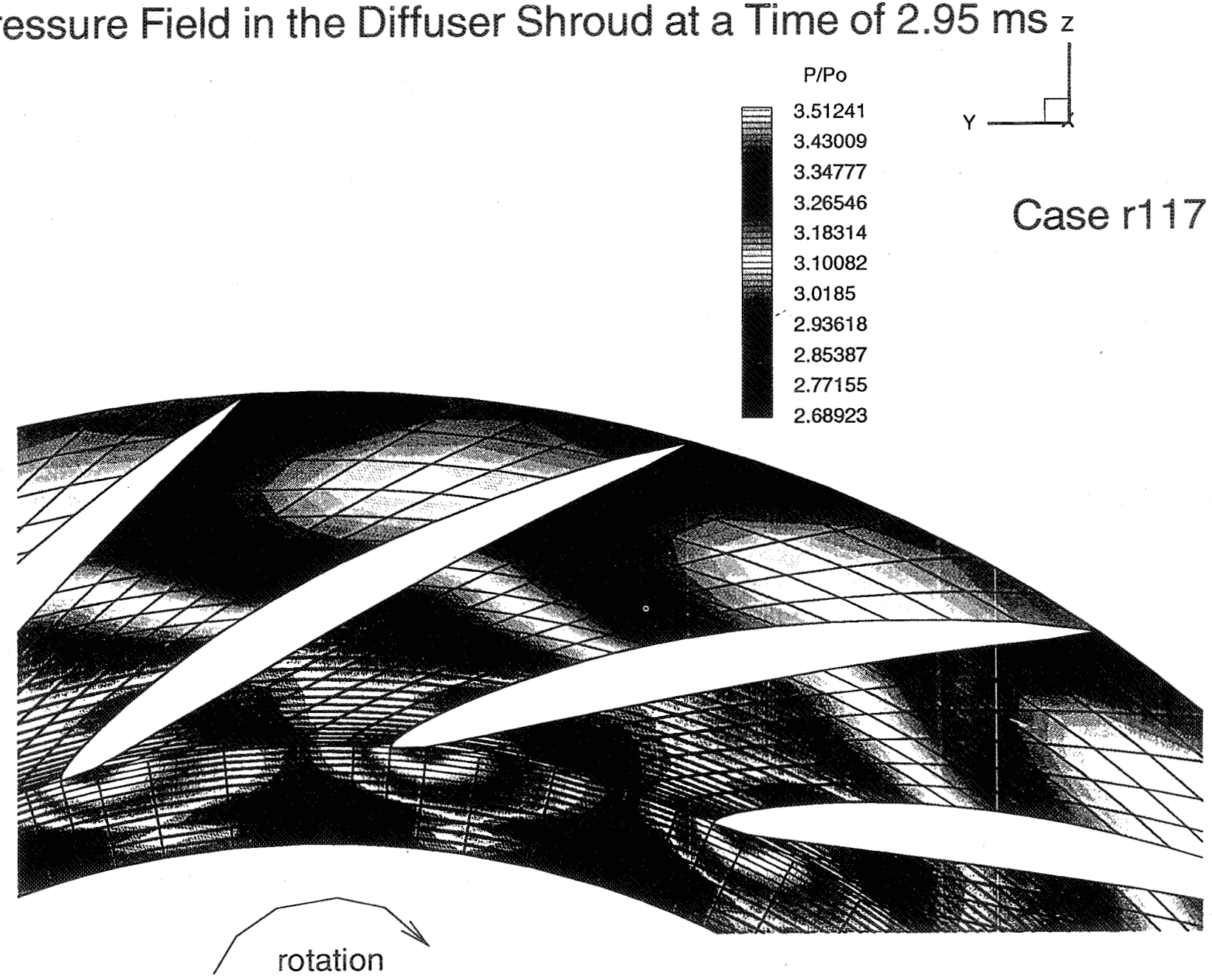

Pressure Field in the Diffuser Shroud at a Time of 2.95 ms

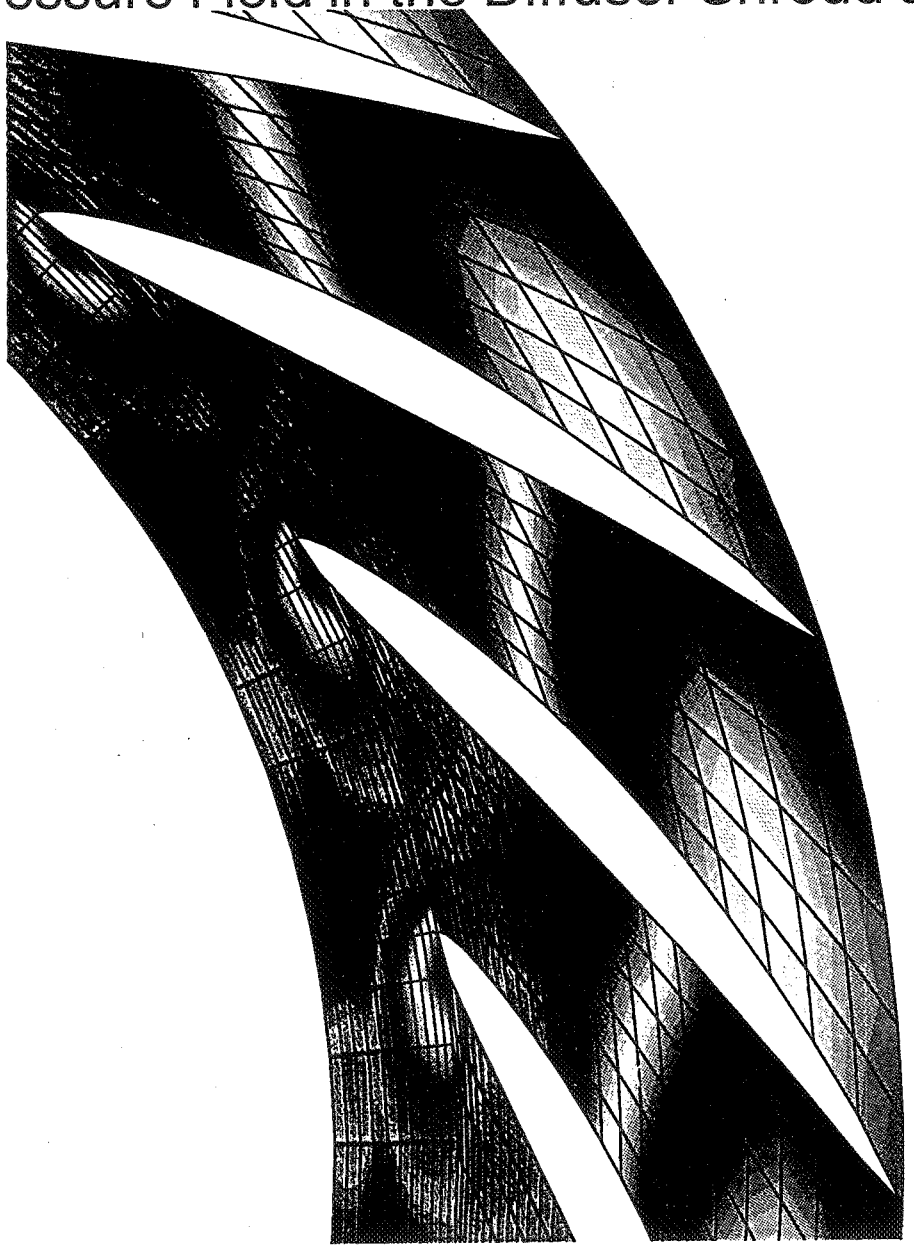

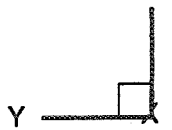

Case r117

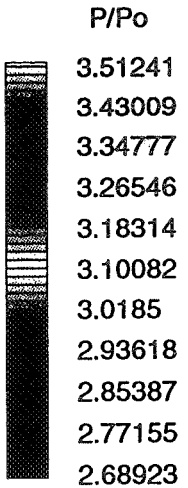

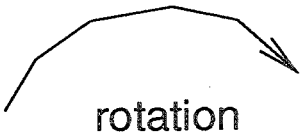

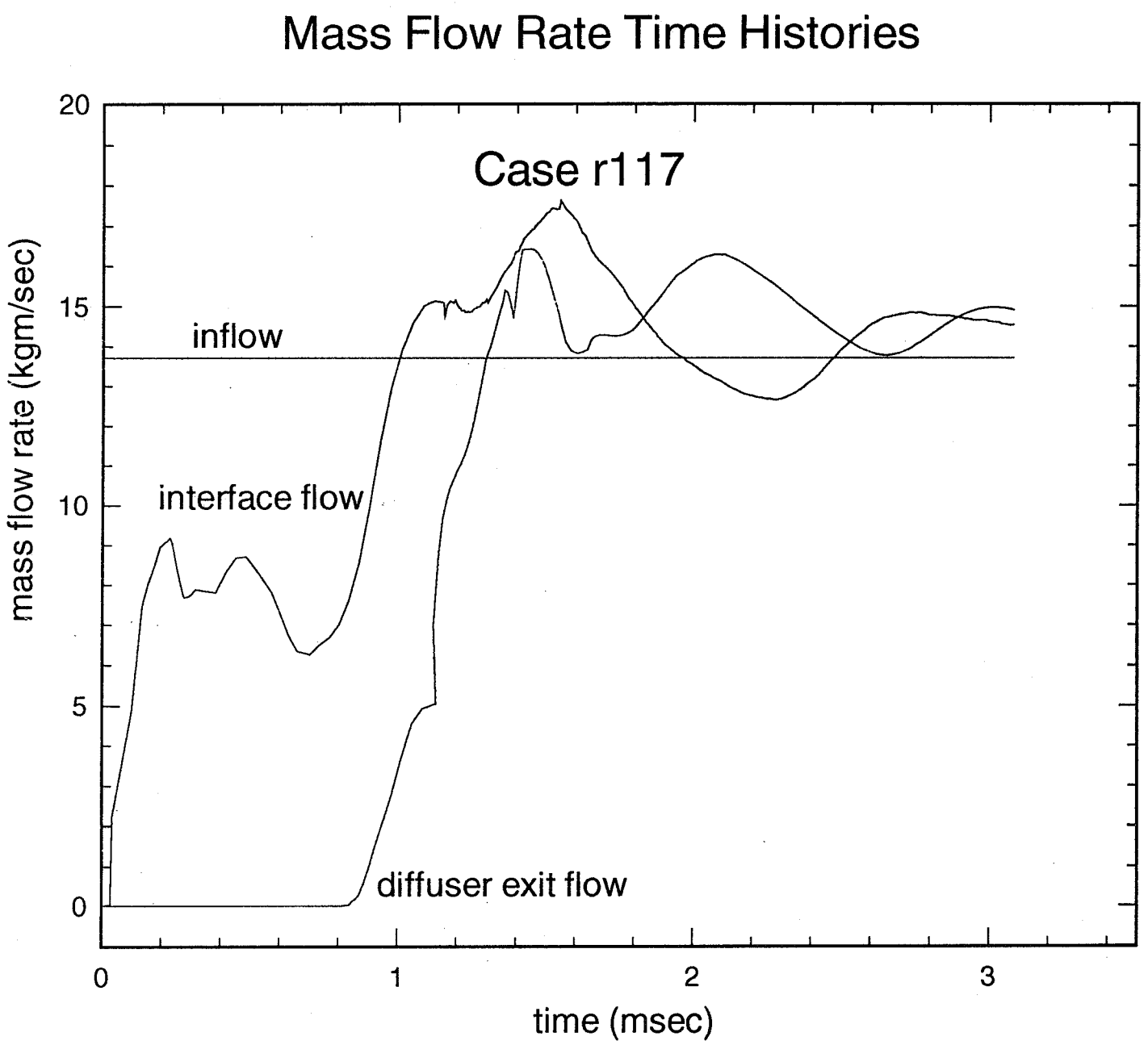
Mass Flow Rate Time Histories
Case r117
inflow
interface flow
diffuser exit flow
mass flow rate (kgm/sec)
time (msec)
0
5
10
15
20
0
1
2
3

Mesh in the Diffuser Shroud Region

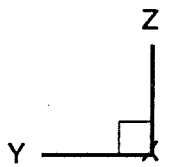

Case r117

region in red defines
rectangular cavity
H = 1.772 inches
L = 5.5 inches

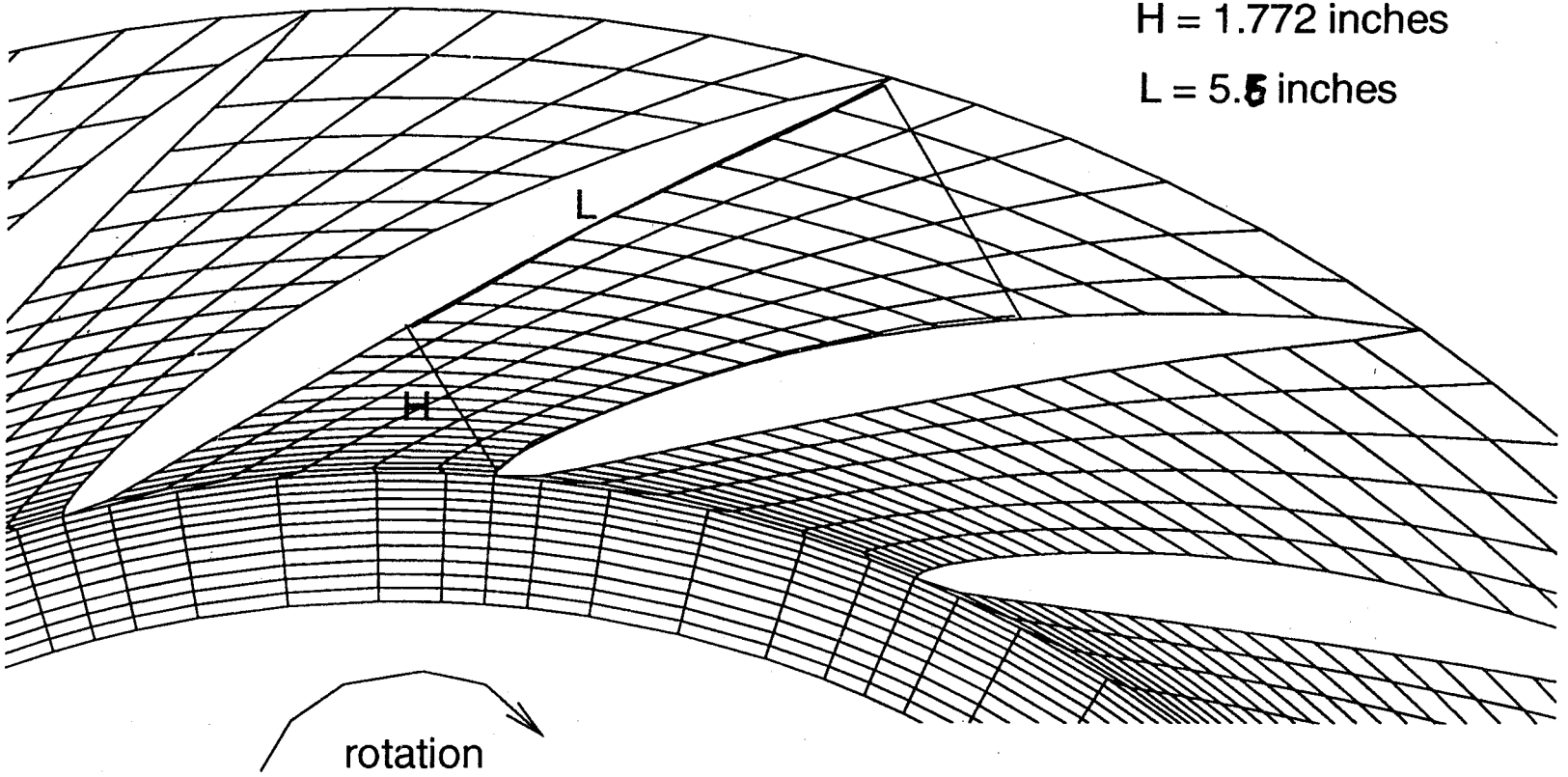

Table 2: Comparison of Mass Flow Rate Frequencies with Resonant Frequencies for a Rectangular Cavity of Length L and Height H

L= 5.63 inches
H= 1.77 inches

Case	Interface Frequency (hz)	Diffuser Exit Frequency (hz)	First Harmonic Frequency for a Rectangular Cavity (hz)	Percent Difference
r117	1035	1435	1510	5

Meridional Mesh Showing Cross Sectional Surfaces Analysed

Case r117

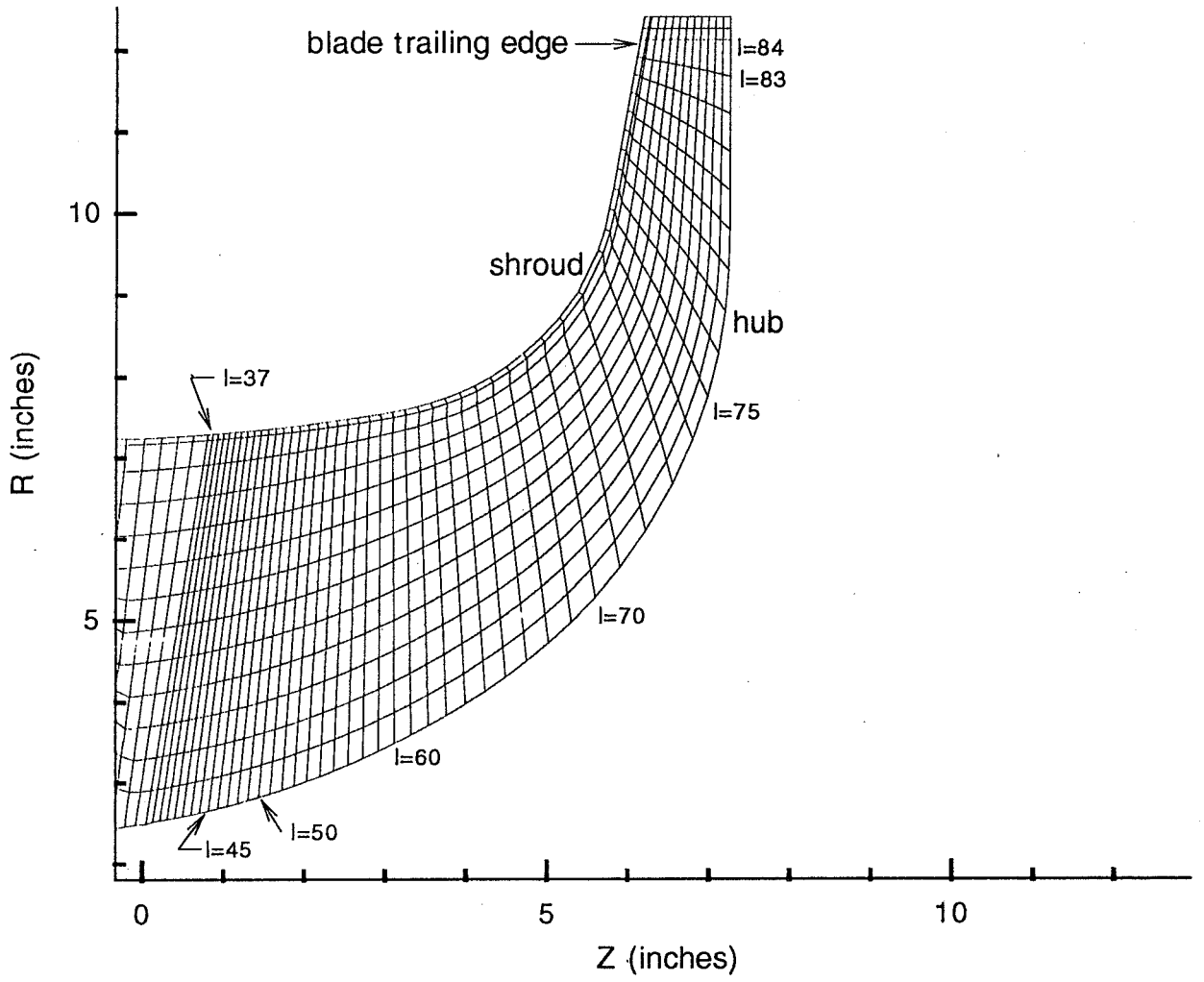

Mass Flux in Cross Sectional Surfaces at a Time of 3.205 ms

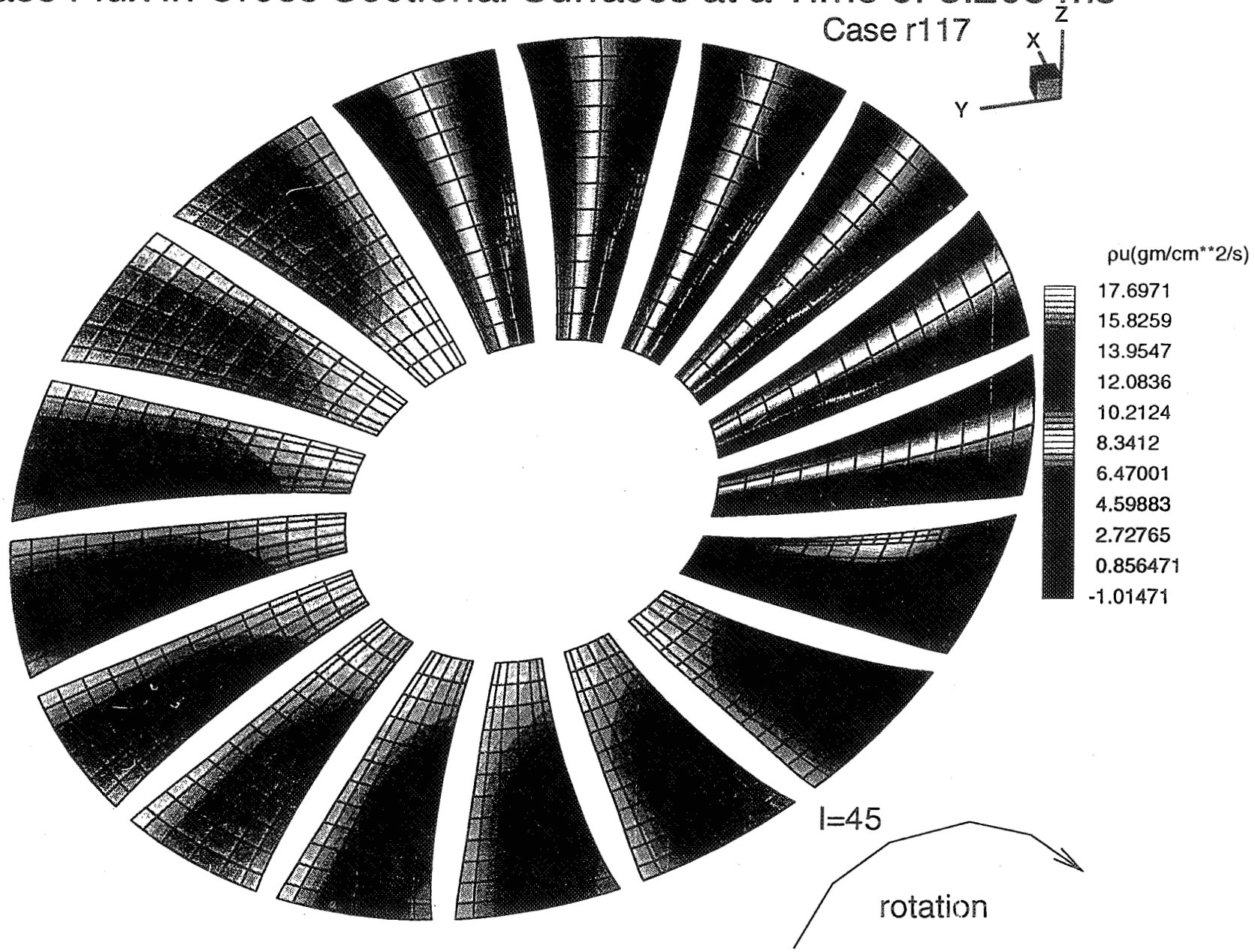

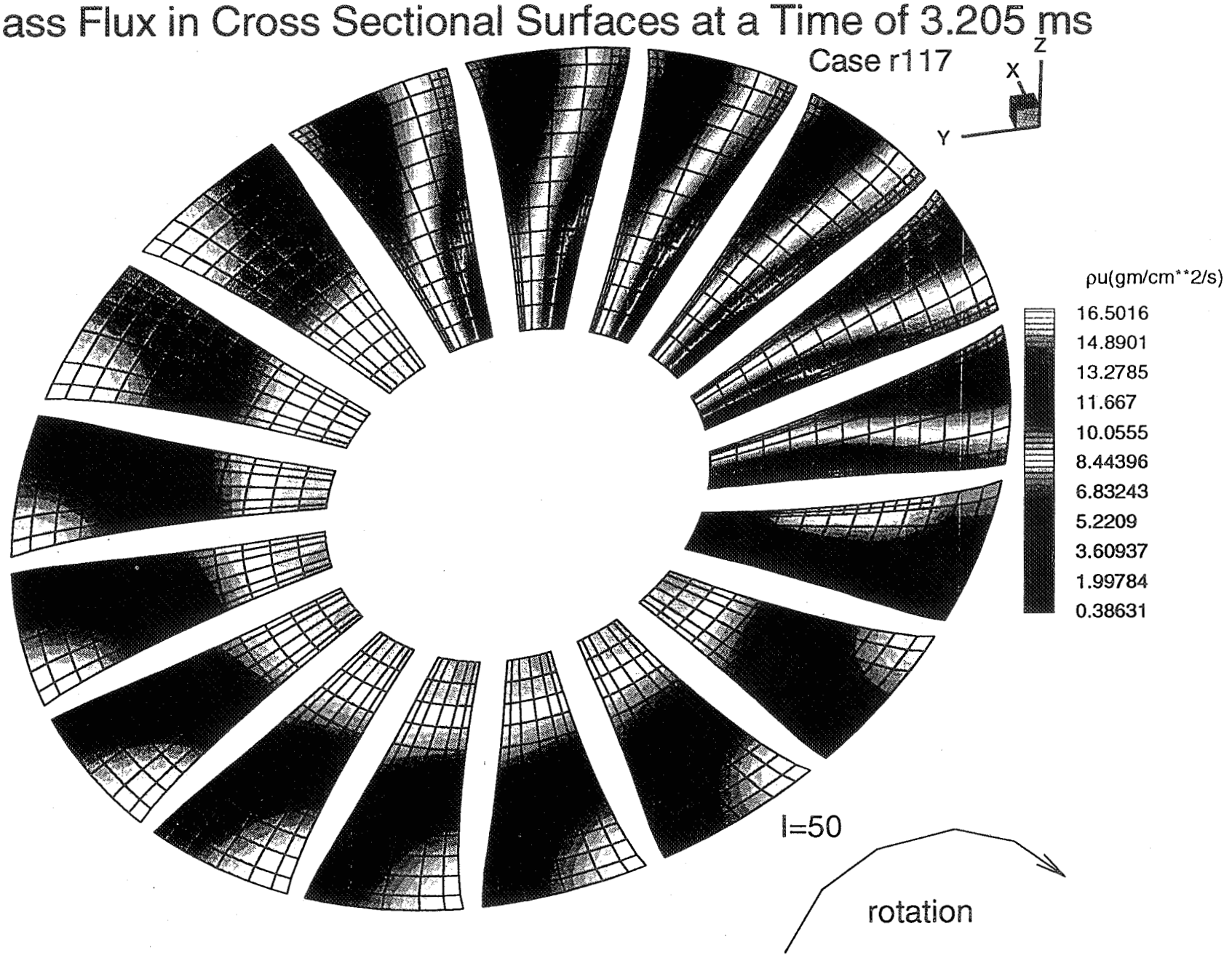
Mass Flux in Cross Sectional Surfaces at a Time of 3.205 ms
Case r117
Z
X
Y
ρu(gm/cm**2/s)
16.5016
14.8901
13.2785
11.667
10.0555
8.44396
6.83243
5.2209
3.60937
1.99784
0.38631
I=50
rotation

Mass Flux in Cross Sectional Surfaces at a Time of 3.205 ms

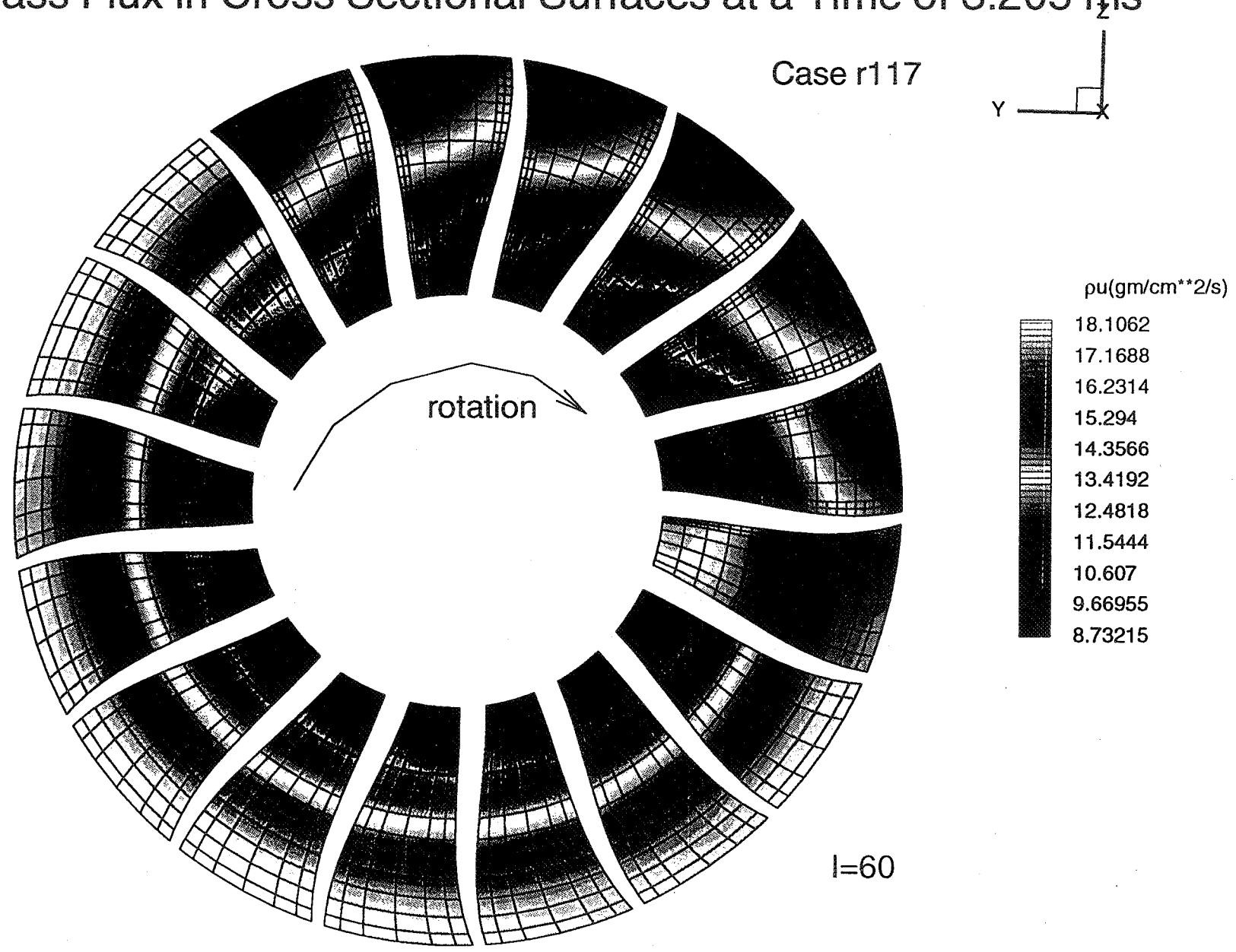

Pressure Ratio on the Diffuser Vanes at a Time of 3.205 ms

Case r117

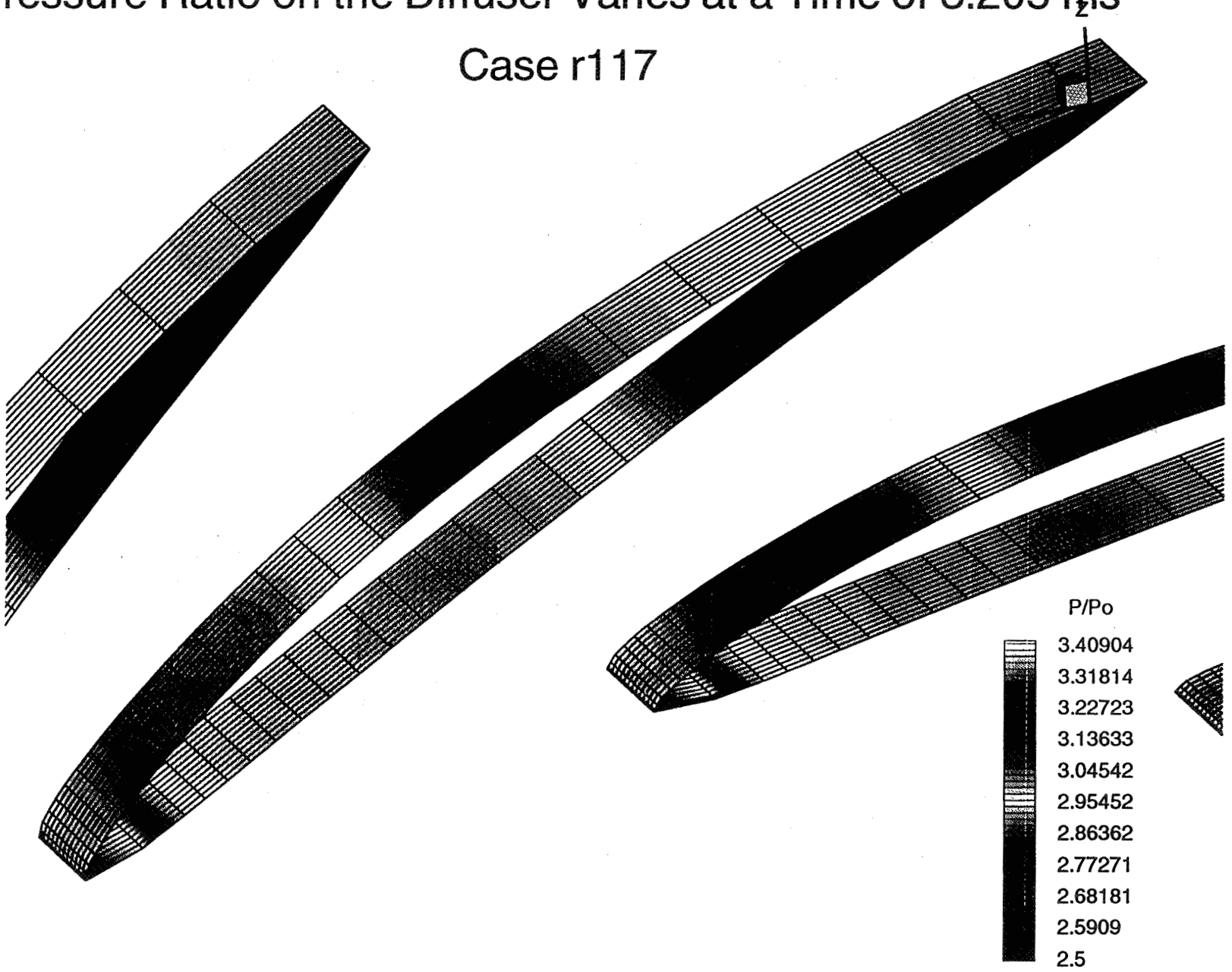

Mach Number on the Diffuser Vanes at a Time of 3.205 ms

Case r117

PRINCIPAL RESULTS FOR CASE R117

O Calculated Total Pressure Ratio across the Stage in Accord with the Measured Total Pressure Ratio

O Inducer Flow Separates at Suction Surface Leading Edge, near the Hub, and Remains Separated Throughout Inducer Region.

O Principal Part of Pressure Loading Across Impeller Blades takes Place Near the Tip of Blades in the Inducer Region.

O Asymmetries are Present in the Vaneless Space between the Impeller Blades and the Diffuser Vanes.

O Due to Vaneless Space Asymmetries, Pressure Distributions along the Pressure and Suction Surfaces of a Diffuser Vane Vary from one Diffuser Vane to Another.

O The Flow in the Leading Edge Region of Each Diffuser Vane Separates Due to a Mismatch in Flow Angle of the Incident Flow from the Impeller and the Vane Geometric Angle.

O Diffuser Vanes act as Cavities to the Flow Exiting the Impeller Blades Causing Resonance

Mach Number Field in the Rotor-Stator Regions at a Time of 6.73 ms

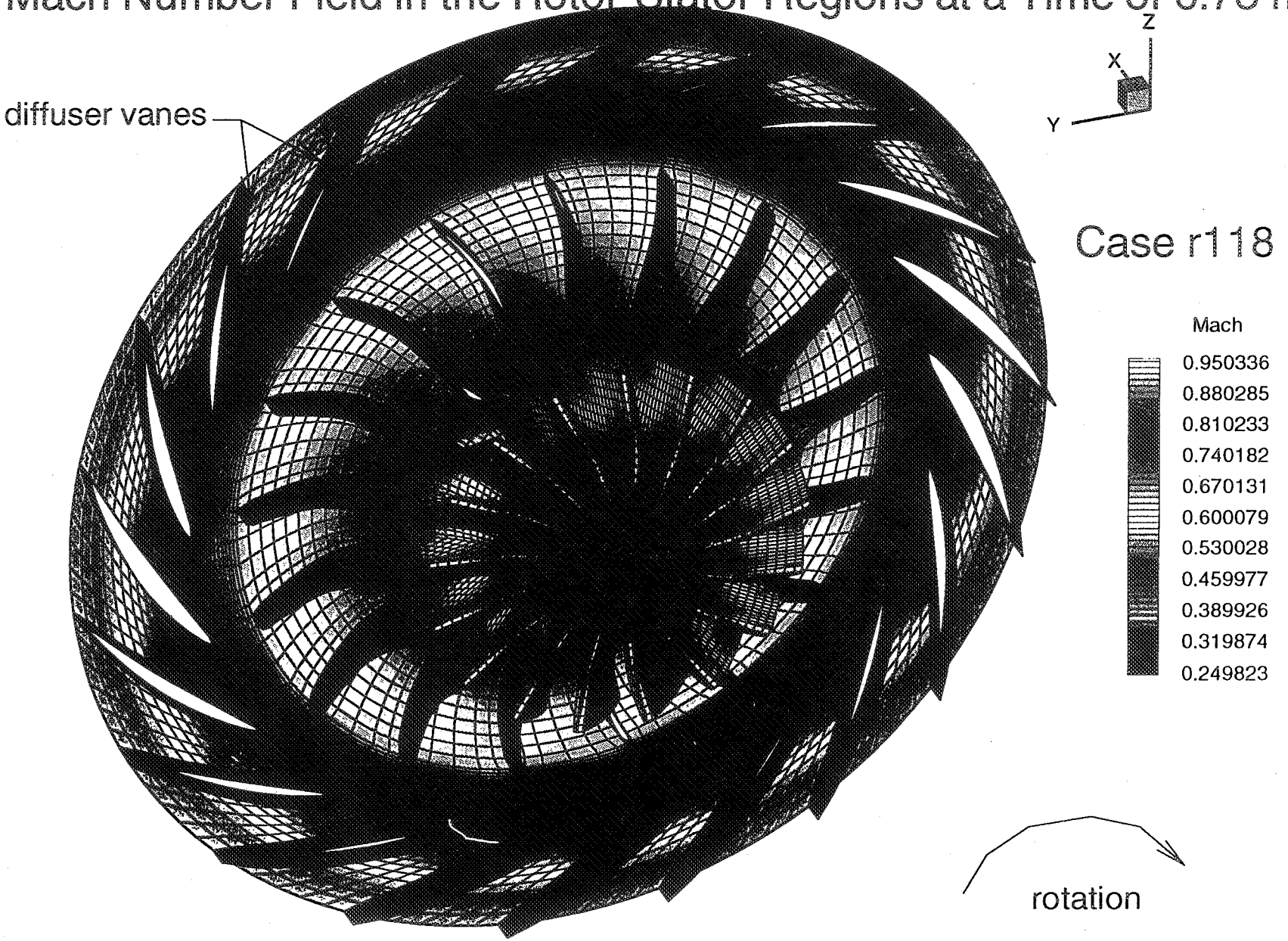

Pressure Field in the Rotor-Stator Regions at a Time of 6.73 ms

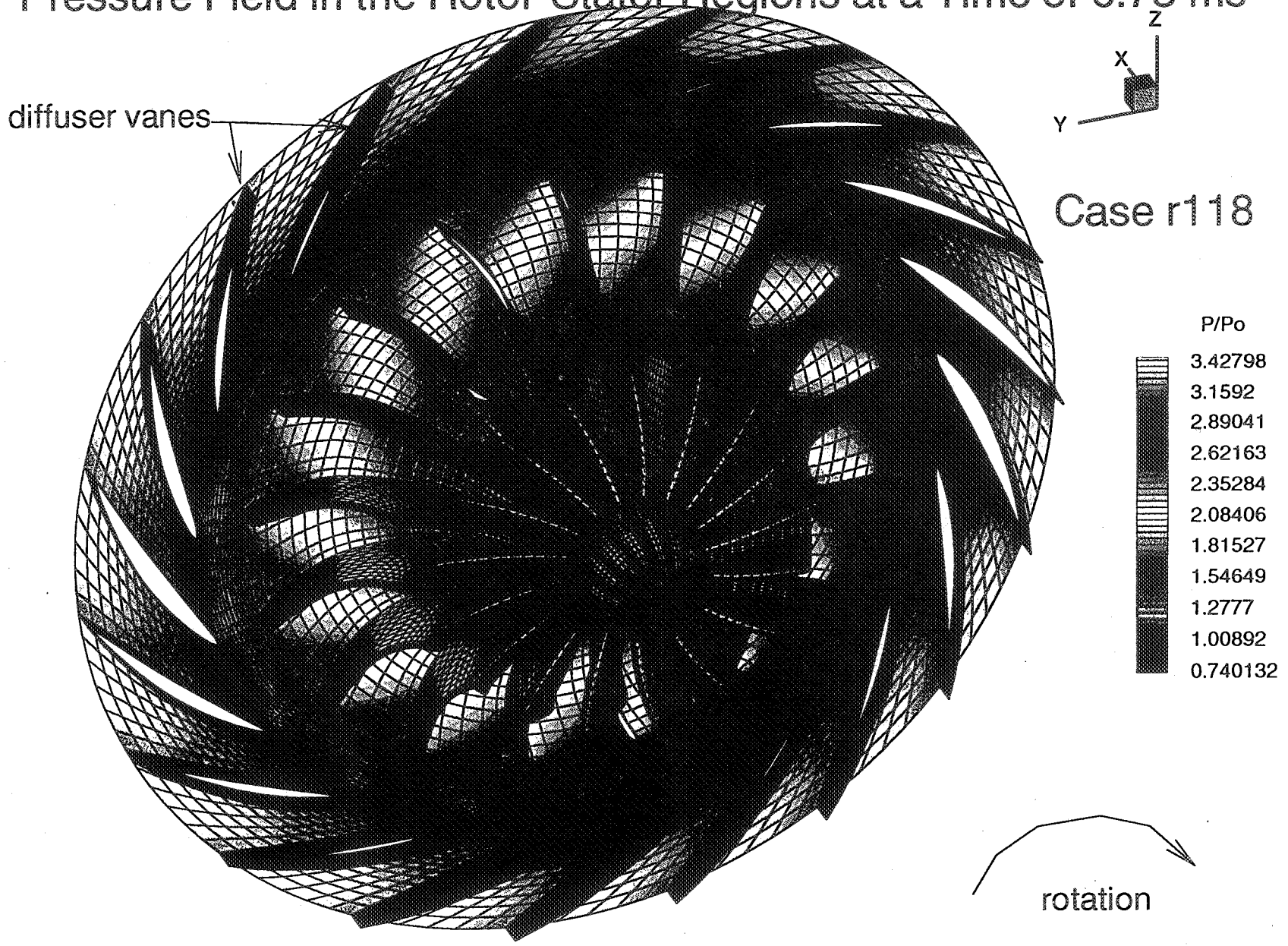

COMPARISON OF MEASURED AND CALCULATED TOTAL PRESSURE RATIOS

Case	$(P_{te}/P_{to})_m$	$(P_{te}/P_{to})_c$	Percent Error	M_e
r117	3.70	3.67	.8	0.350
r118	3.62	3.71	2.4	0.425

Mach Number Field in the Diffuser Shroud at a Time of 6.73 ms

Case r118

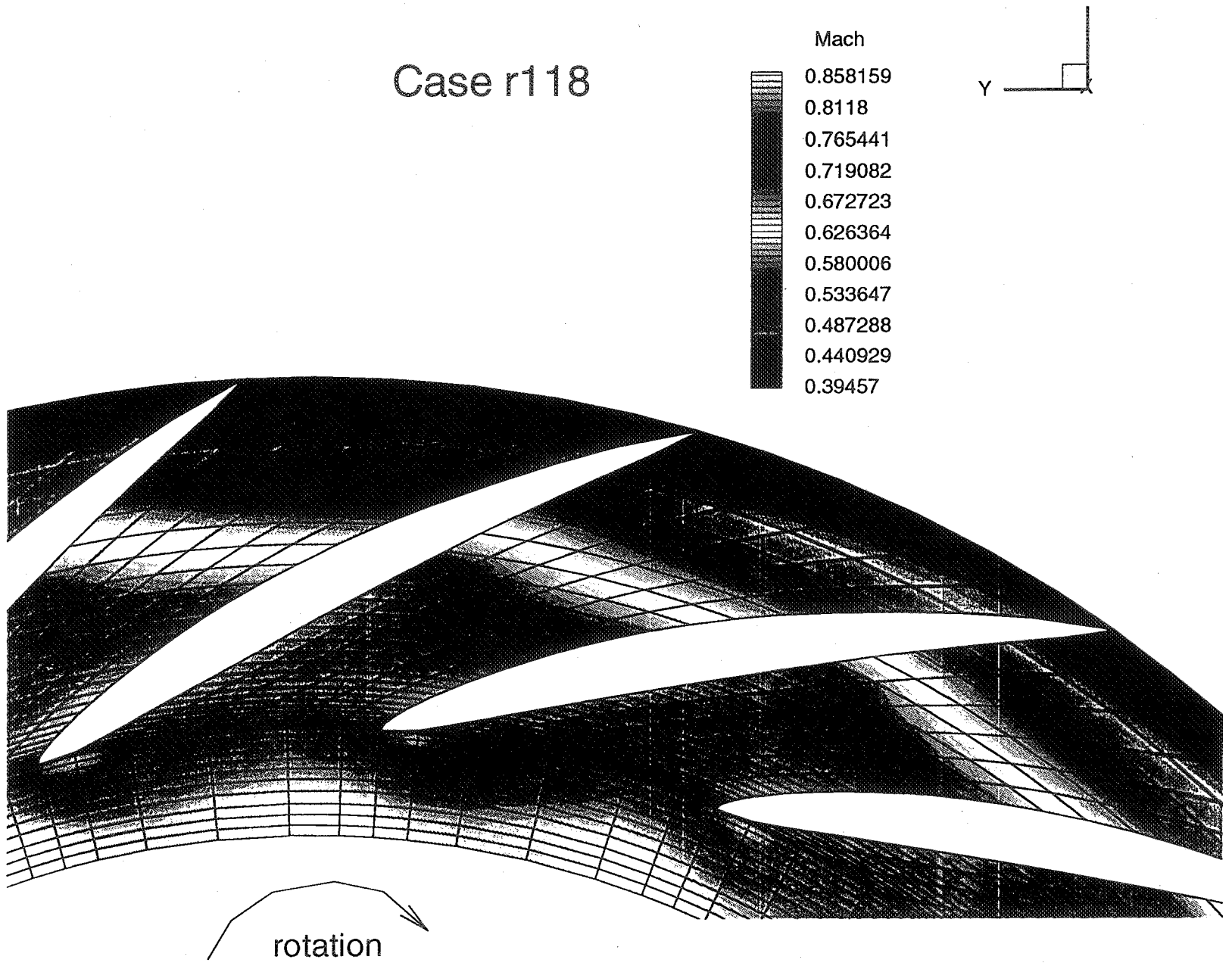

Pressure Field in the Diffuser Shroud at a Time of 6.73 ms

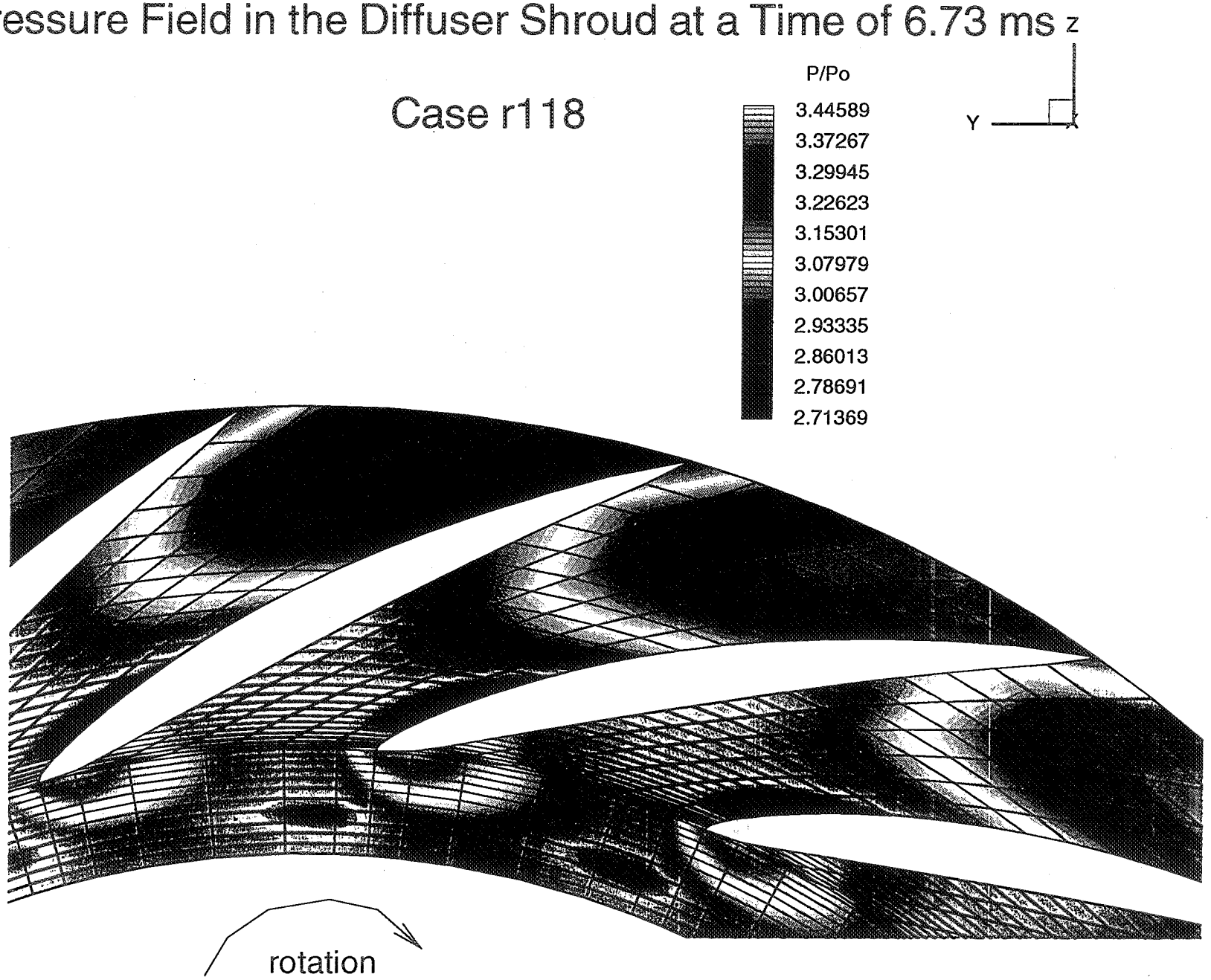

Turbulent Intensities in the Diffuser Shroud at a Time of 6.73 ms

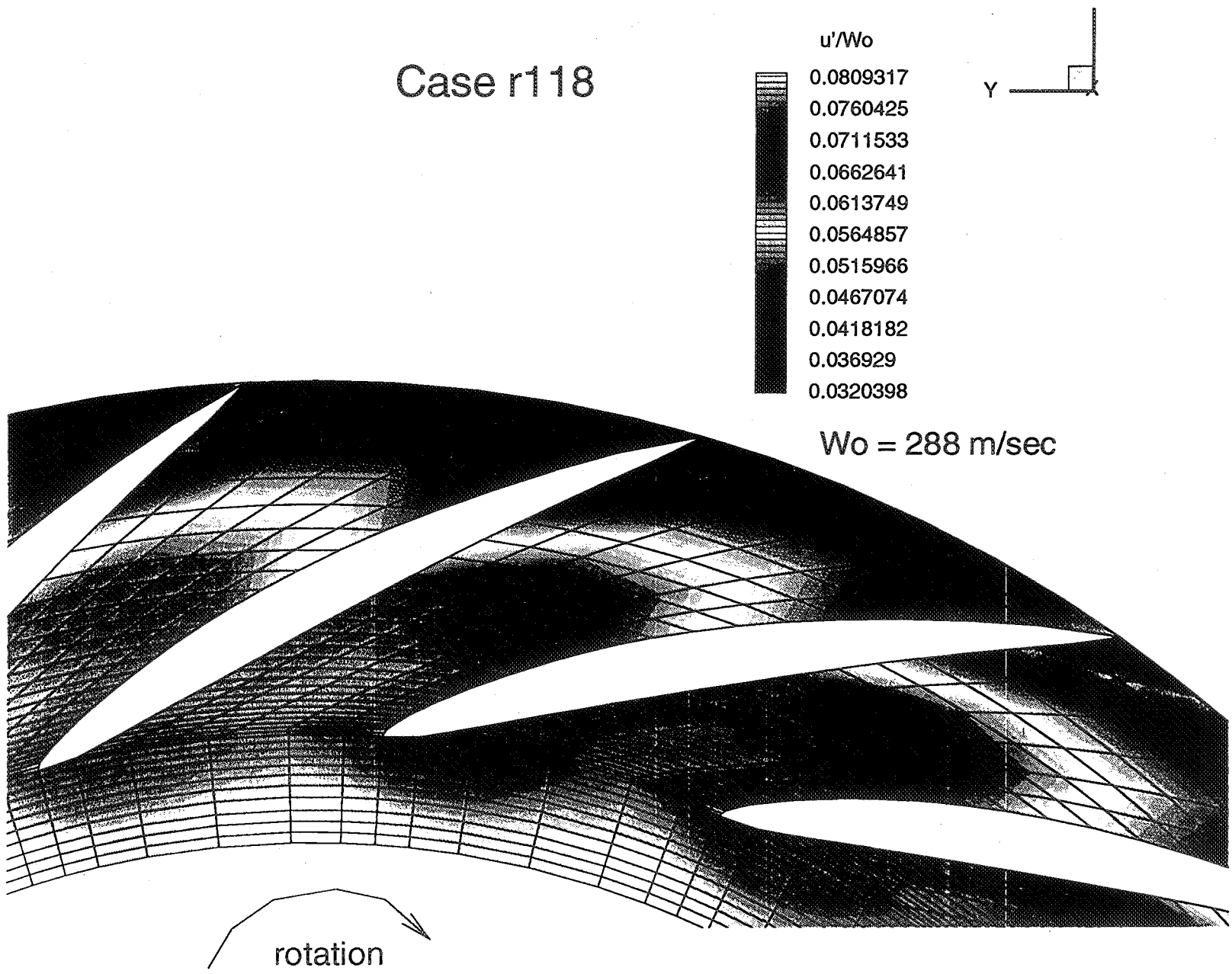

Turbulent Intensity in the Diffuser Shroud at a Time of 2.95 ms

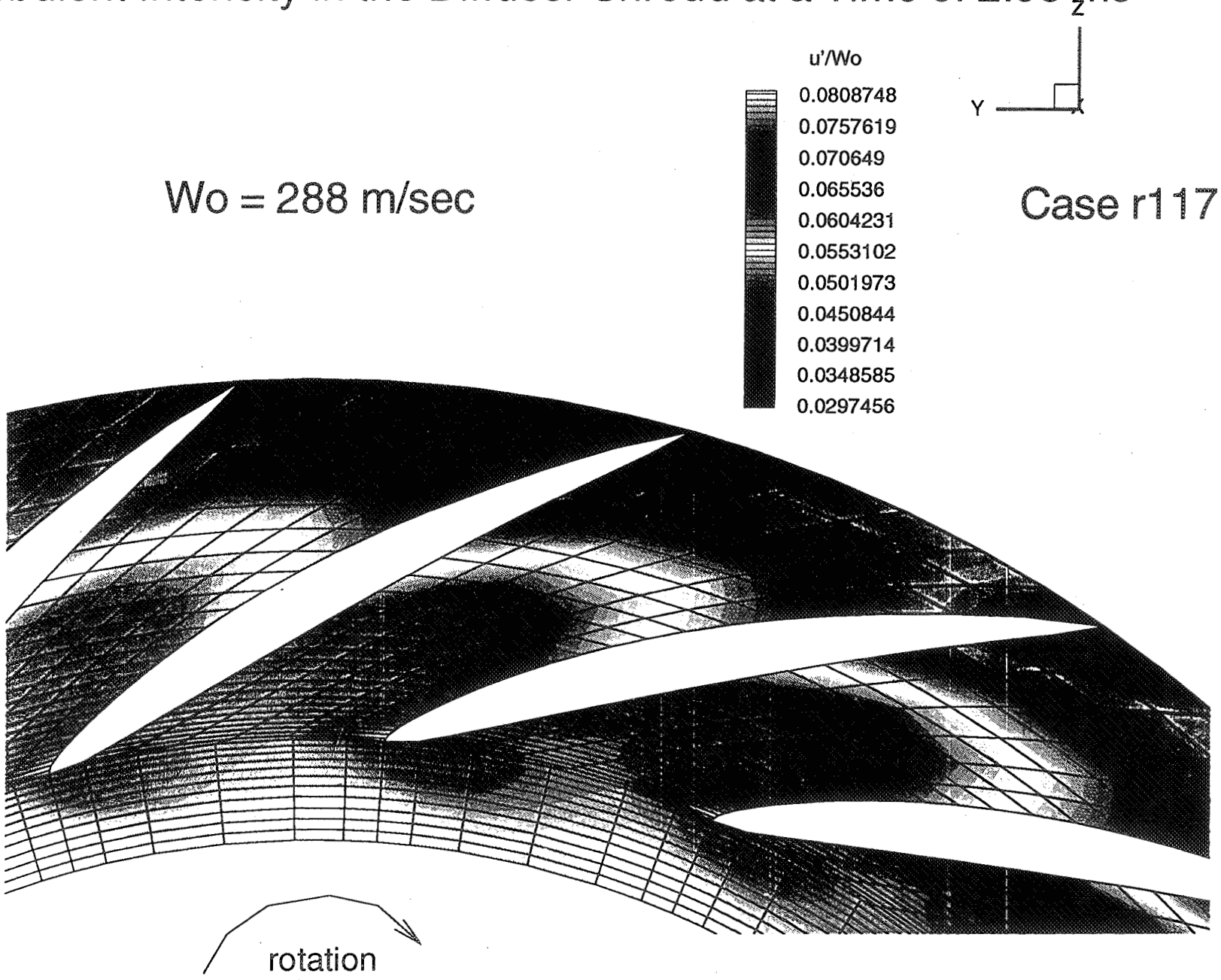

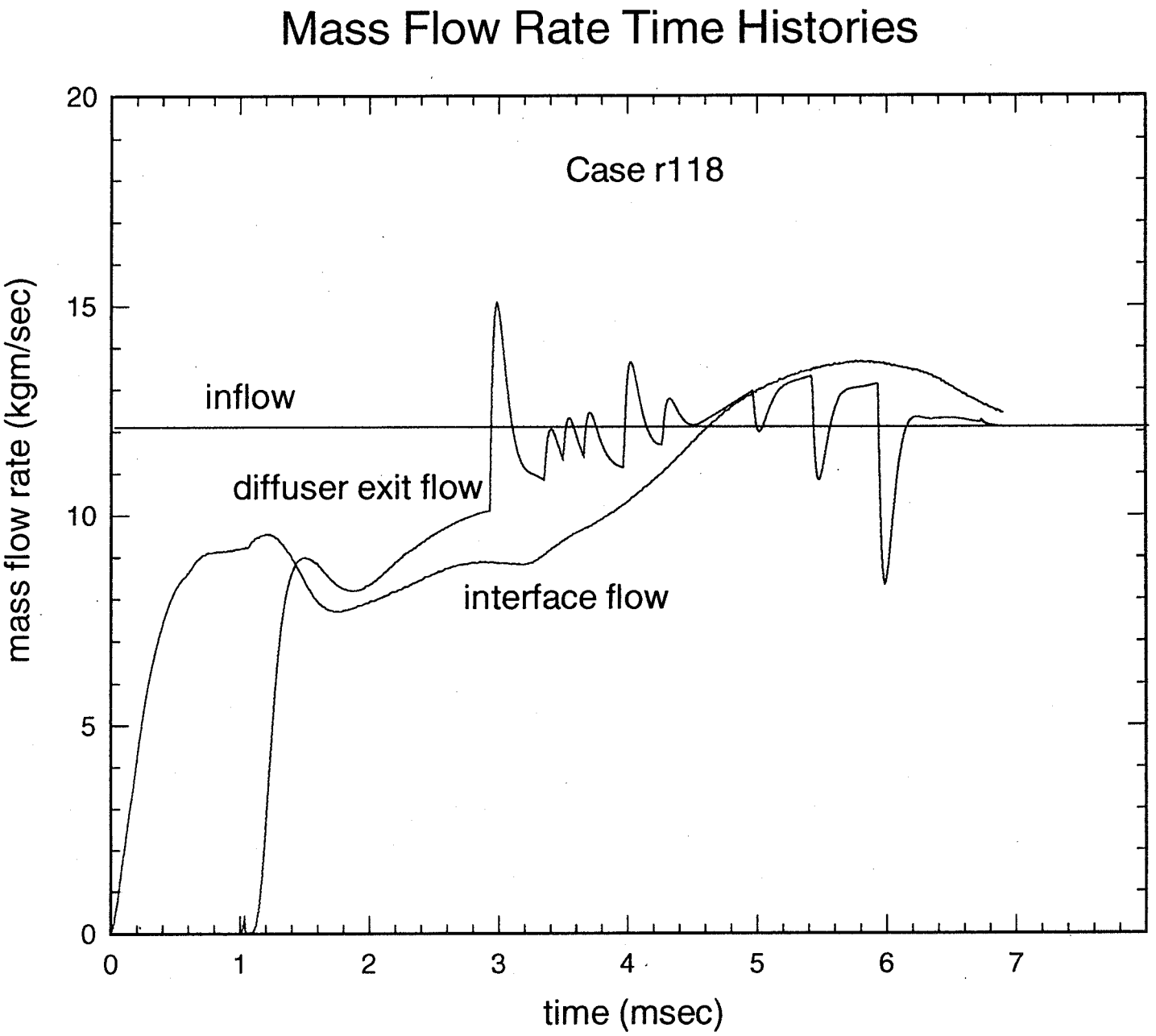
Mass Flow Rate Time Histories
Case r118
inflow
diffuser exit flow
interface flow
mass flow rate (kgm/sec)
time (msec)
0
5
10
15
20
0
1
2
3
4
5
6
7

PRINCIPAL RESULTS FOR CASE R118

O Calculated Total Pressure Ratio across the Stage is in Accord with the Measured Total Pressure Ratio.

O Asymmetries are Present in the Vaneless Space between the Impeller Blades and the Diffuser Vanes.

O Due to Vaneless Space Asymmetries, Pressure Distributions along the Pressure and Suction Surfaces of a Diffuser Vane Vary from one Diffuser Vane to Another.

O The Flow in the Leading Edge Region of Each Diffuser Vane Separates Due to a Mismatch in Flow Angle of the Incident Flow from the Impeller and the Vane Geometric Angle.

O The Diffuser Vanes act as Convergent- Divergent Nozzles to the Flow Preventing its Complete Diffusion. Thus, the Exit Mach Number is Higher and Exit Pressure is Lower for Case r118 Relative to Case r117.

O The Turbulent Intensity in the Diffusers is Higher in Case r118 than in Case r117. Thus, the Turbulent Noise is Higher in Case r118. This Result is in Accord with Observations in the Field.

Page intentionally left blank

NUMERICAL SIMULATION OF DIFFUSER FLOW

WEI-CHUNG CHEN
ED ASCOLI
ANTHONY H.J. EASTLAND

APRIL 25, 1995

CFD WORKSHOP
APPLICATION IN ROCKET PROPULSION
HUNTSVILLE, ALABAMA
APRIL 25-27, 1995

Rockwell Aerospace
Rocketdyne

NUMERICAL SIMULATION OF DIFFUSER FLOW

- **BACKGROUND AND MOTIVATION**
  - VALIDATE CFD CODE FOR TYPICAL ROCKET ENGINE DIFFUSER FLOW
  - AIR TEST DATA AVAILABLE FOR SSME PREBURNER PUMP DIFFUSER
  - WATER TEST DATA WILL BE AVAILABLE FOR CONSORTIUM PUMP VANE-ISLAND DIFFUSER

- **APPROACH**
  - COMPARE CFD RESULTS WITH TEST DATA OVER WIDE RANGE OF OPERATING CONDITIONS
  - USE CFD AS DESIGN TOOL AT EARLY DESIGN STAGE

NUMERICAL SIMULATION OF DIFFUSER FLOW

BASIC FEATURES OF TWO DIFFUSERS

I.D.	SSME DIFFUSER	CONSORTIUM DIFFUSER
TYPE	CIRCULAR ARC VANE DIFFUSER	VANE-ISLAND DIFFUSER
AREA RATIO	2.8:1	2.5:1
INLET ANGLE	9.9°	10.1°
OUTLET ANGLE	10.8°	38.0°
INLET DIAMETER (IN)	5.44	9.8
OUTLET DIAMETER (IN)	6.80	13.515
NO. OF BLADES	11	11
STRUCTURAL SOLIDITY	LESS THAN 50%	MORE THAN 50%
SHAPE	CURVED CHANNEL IN BLADE TO BLADE PLANE	STRAIGHT CHANNEL

NUMERICAL SIMULATION OF DIFFUSER FLOW

SSME DIFFUSER

- **FLOW SOLVER**
  - REACT3D WITH K-E TURBULENCE MODEL AND WALL FUNCTION
- **BOUNDARY CONDITIONS**
  - INLET B.C. BASED ON PUMP PERFORMANCE PREDICTION PROGRAM AT IMPELLER EXIT
  - ZERO GRADIENT APPLIED TO OUTLET B.C.
  - BLADE TO BLADE PERIODICITY APPLIED TO BOTH INLET AND OUTLET
  - NON-SLIP APPLIED TO THE END WALLS AND BLADE SURFACES
- **CFD GRID**
  - ALGEBRAIC GENERATED H-GRID
  - GRID SIZE 10K~20K
- **TEST ARTICLE**
  - 9 DESIGNS 77 TESTS COMPLETED AT AIR TEST RIG
  - OVERALL DIFFUSER STATIC PRESSURE RECOVERY MEASURED OVER 0.0 TO 150% DESIGN FLOW

PREBURNER PUMP REDESIGN
FOR LARGE THROAT MCC ENGINE
TESTER DESIGN

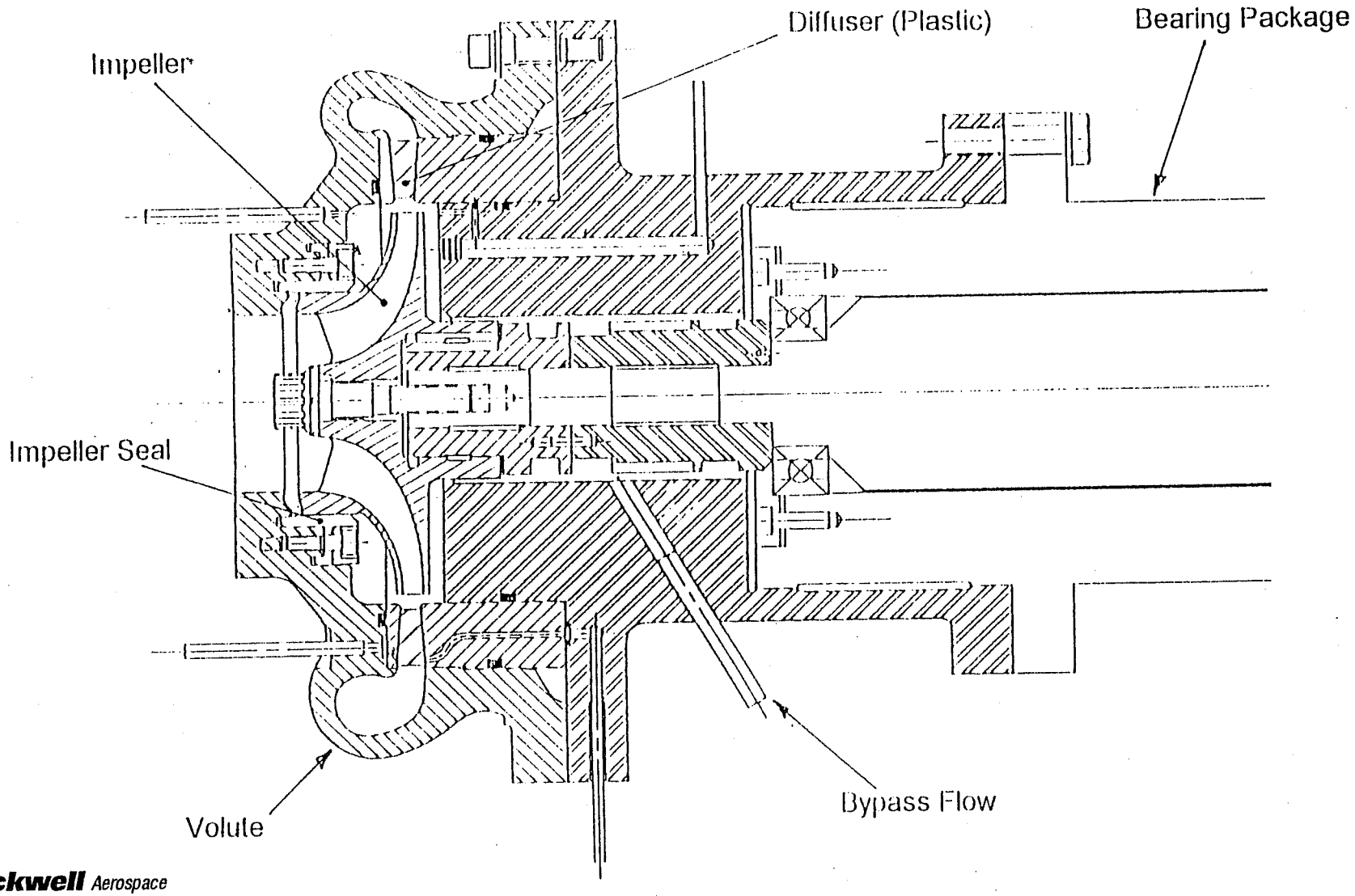

SSME RADIAL DIFFUSER

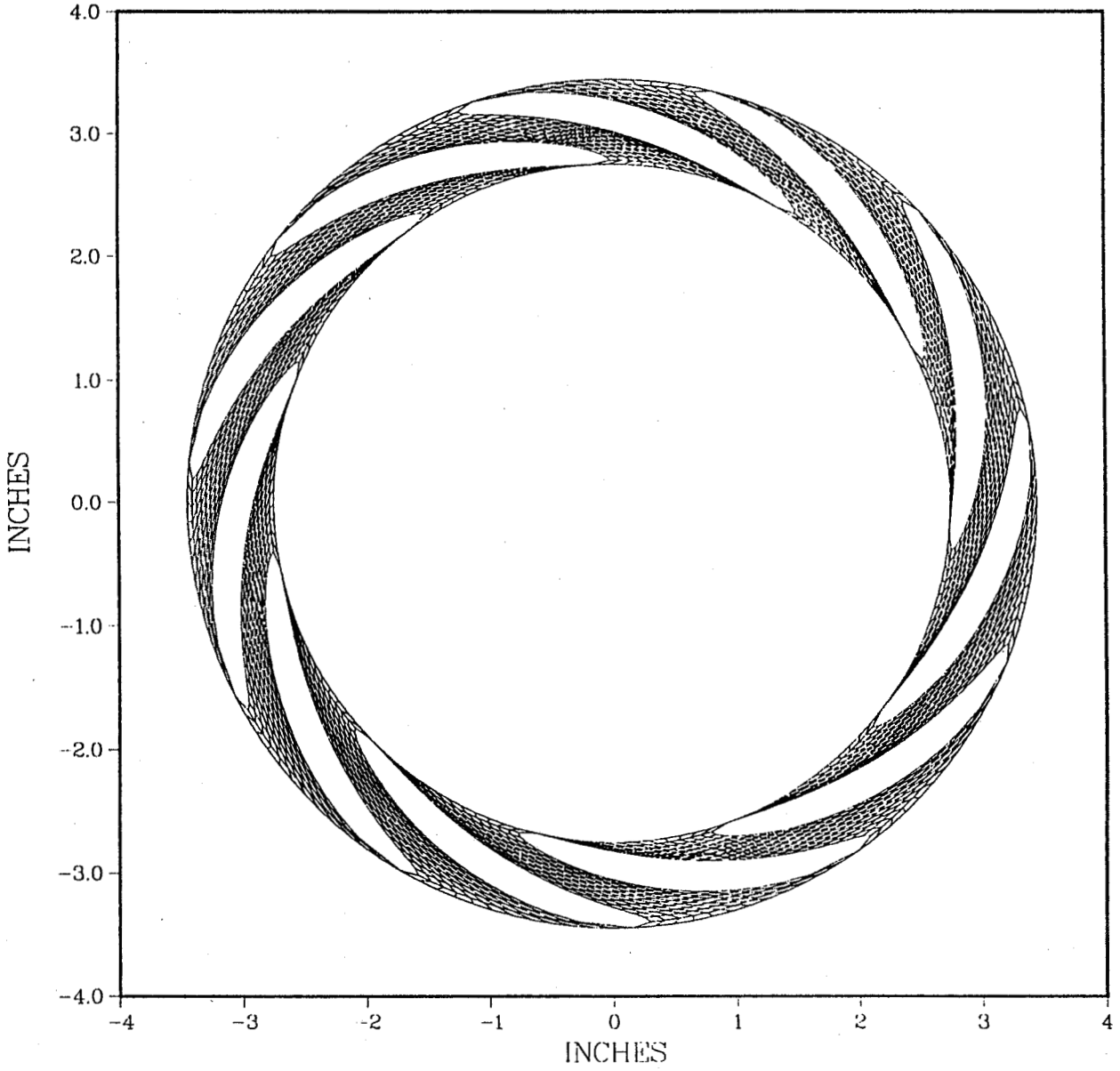

SSME RADIAL DIFFUSER

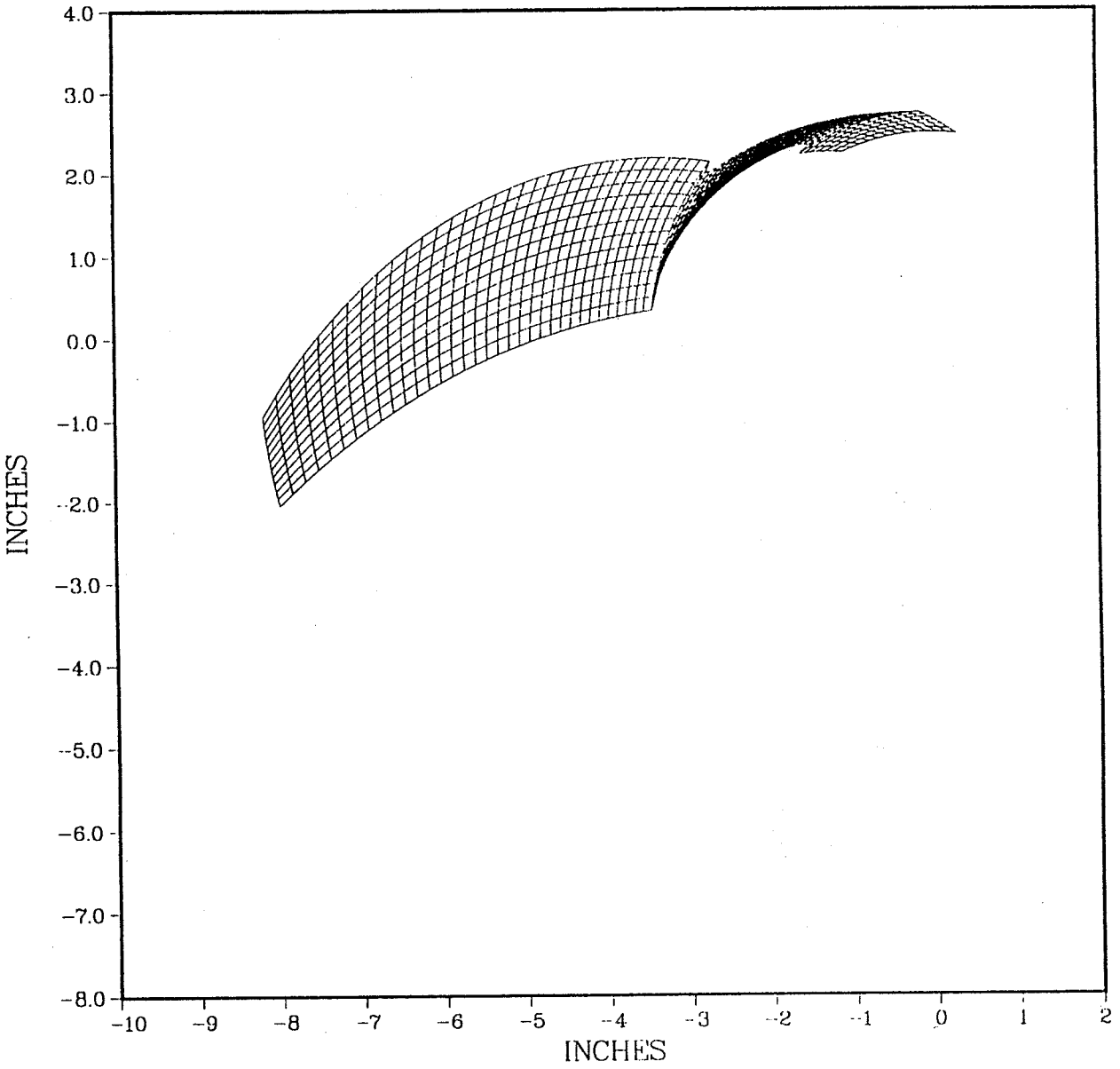

SSME HPOTP PREBURNER DIFFUSER
MAX. PRESSURE RECOVERY

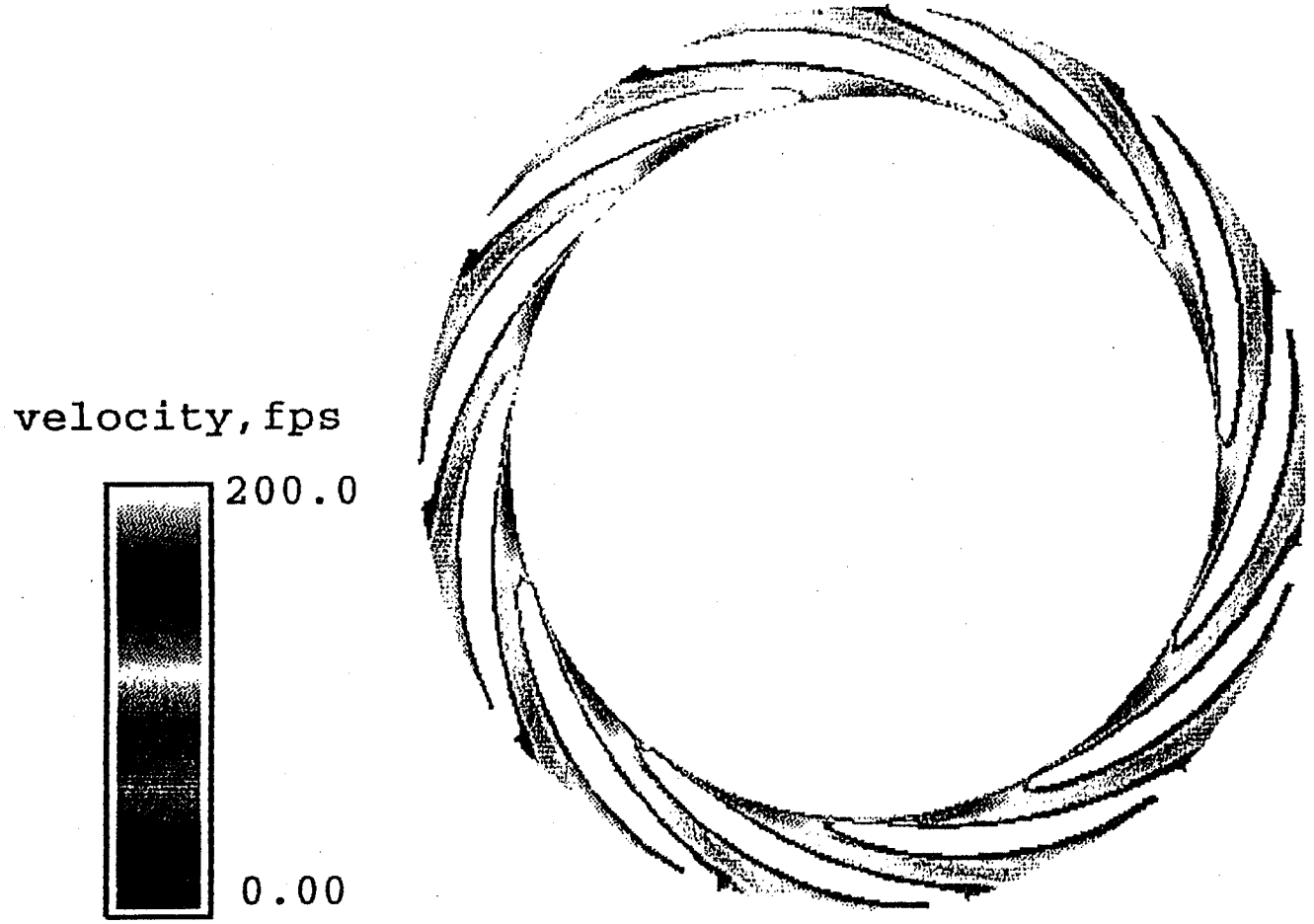

SSME HPOTP PREBURNER DIFFUSER
MAX. PRESSURE RECOVERY

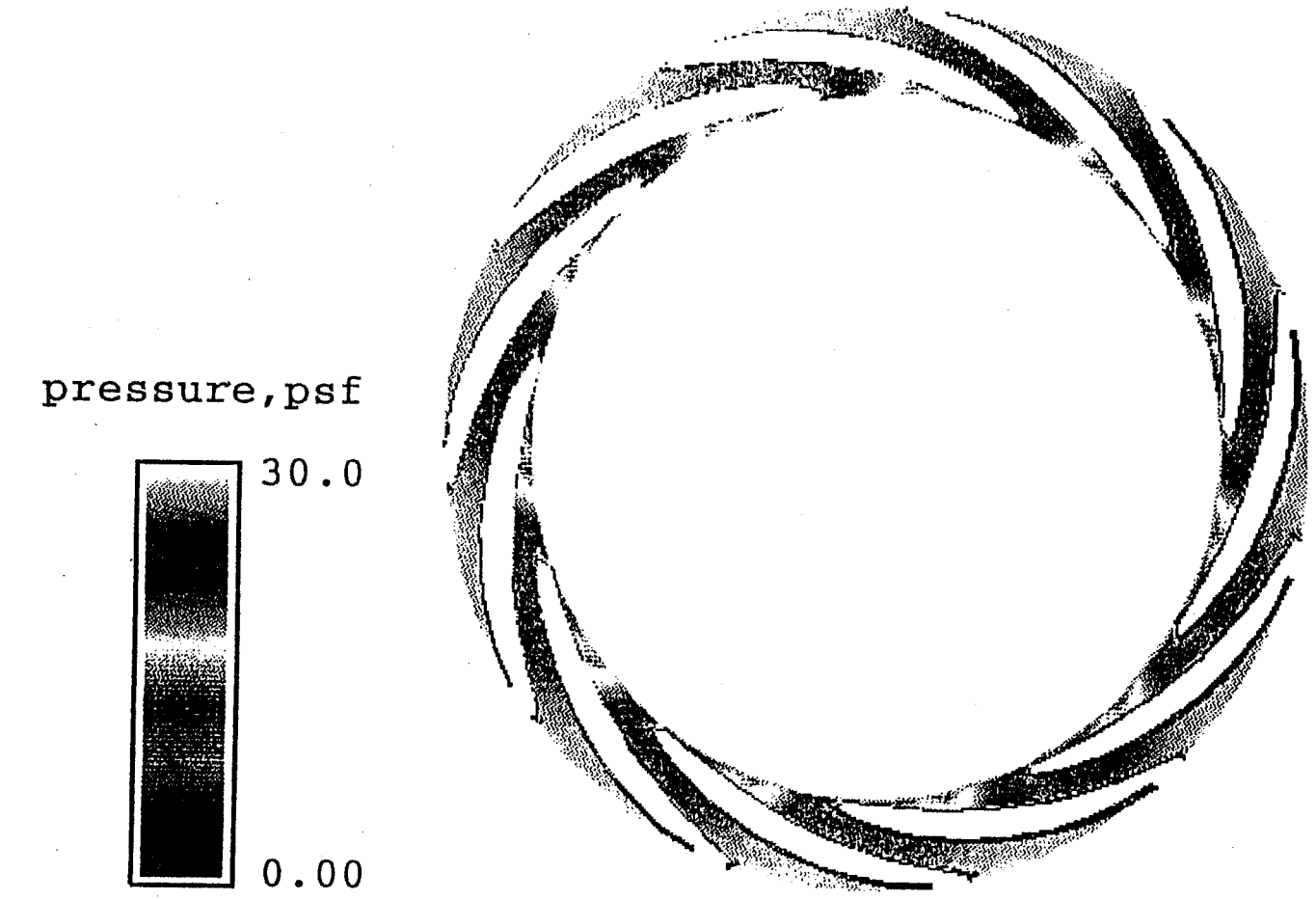

SSME HPOTP PREBURNER PUMP AIR TEST
DIFFUSER PRESSURE RISE (AVERAGE)

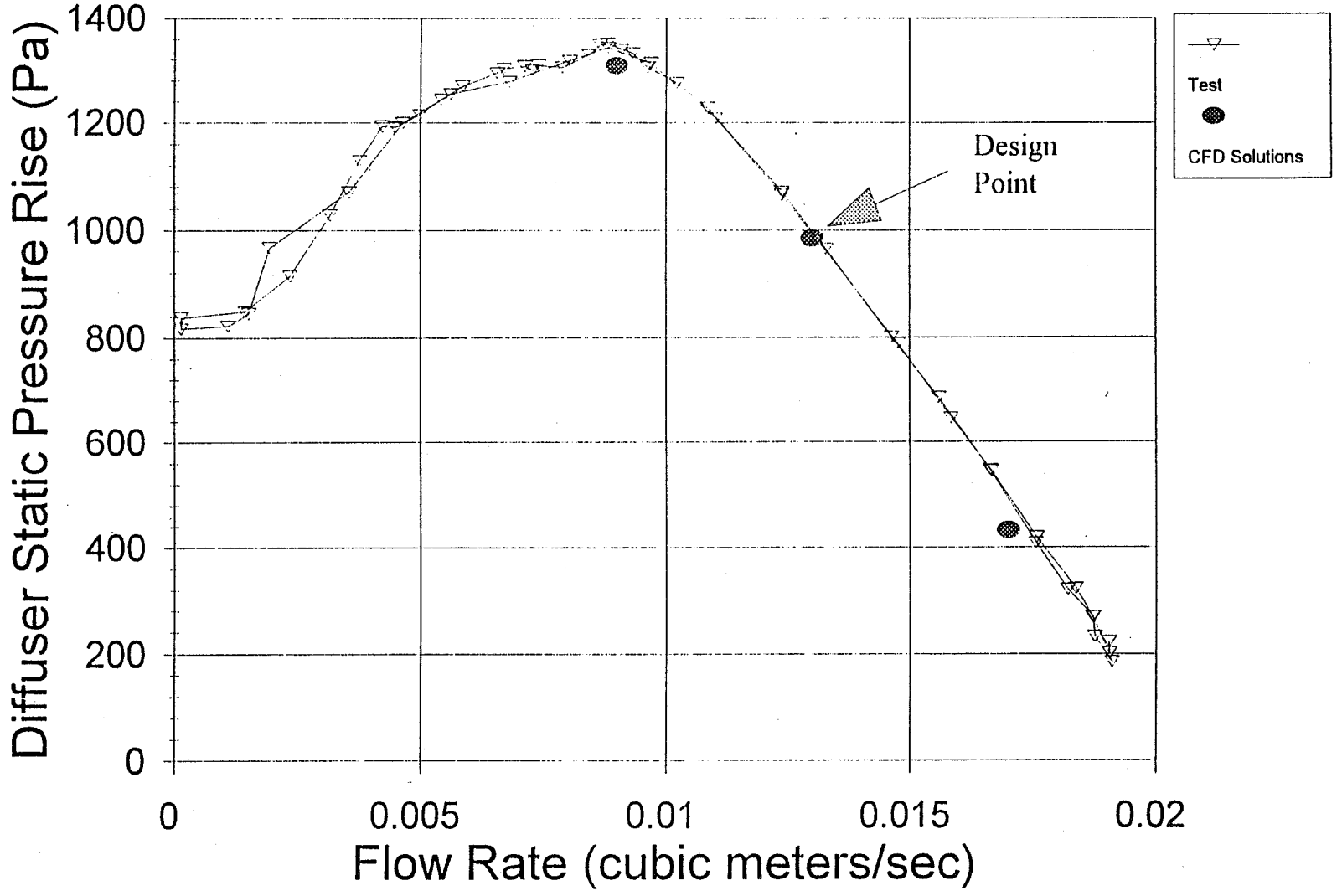

NUMERICAL SIMULATION OF DIFFUSER FLOW
CONSORTIUM DIFFUSER

- **BACKGROUND**
  - VANE-ISLAND TYPE DIFFUSER SELECTED FOR GREATER STRUCTURAL SOLIDITY
  - VELOCITY RATIO 4.4 REQUIRED BETWEEN STAGES
    - VELOCITY RATIO 2.2 SELECTED FOR UPCOMER DESIGN

- **DESIGN APPROACH**
  - OPTIMIZE DIFFUSER CONFIGURATION THROUGH CFD
  - CONFIRM PERFORMANCE THROUGH WATER TEST

CONSORTIUM 2 STAGE FUEL PUMP

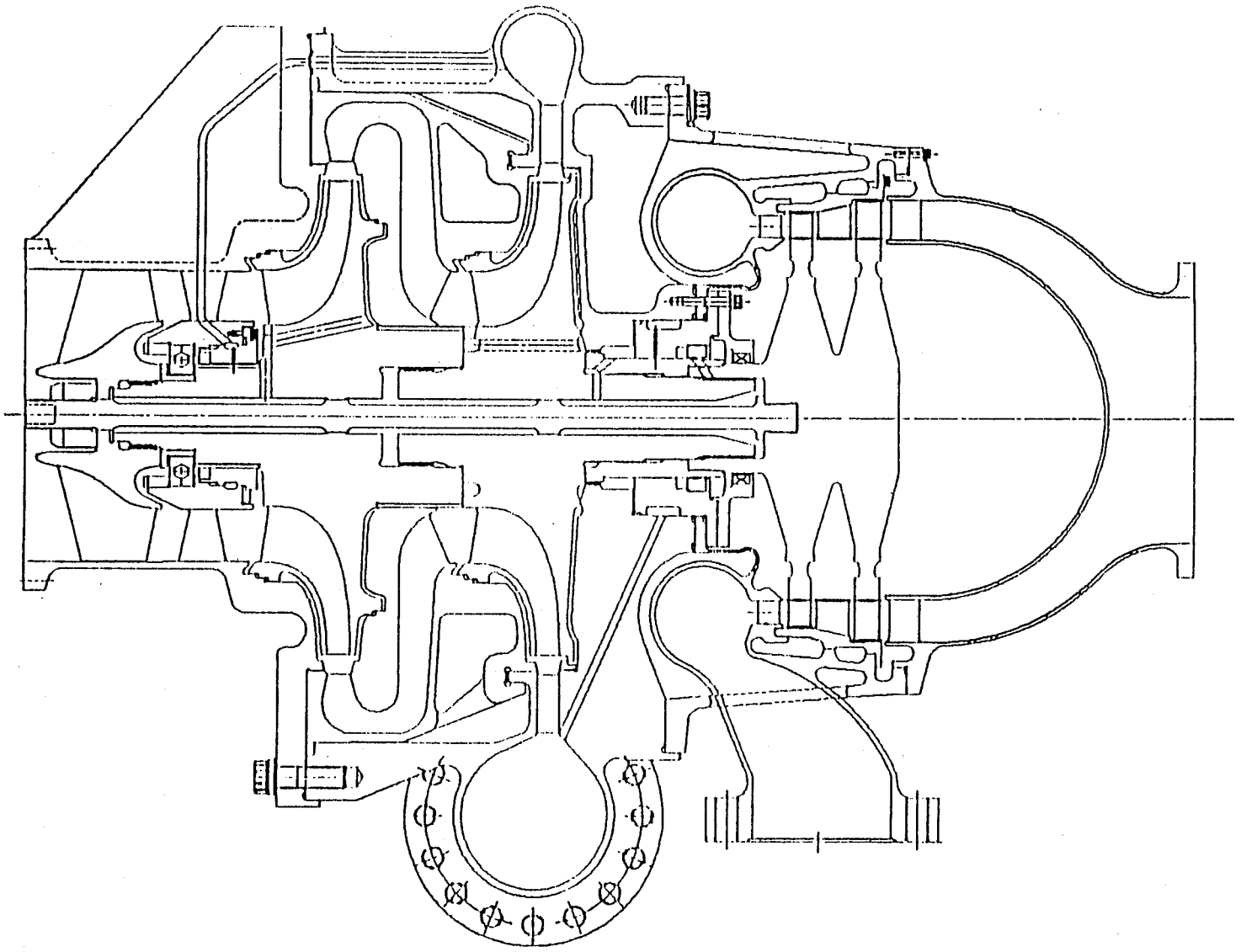

NUMERICAL SIMULATION OF DIFFUSER FLOW

- **FLOW SOLVER**
  - REACT3D AND STARCD
- **BOUNDARY CONDITIONS**
  - INLET B.C. BASED ON CFD RESULTS AT IMPELLER EXIT
  - OUTLET B.C.
    - PERIODICITY WITH SUDDEN EXPANSION TO SIMULATE TESTER
    - PIPE FLOW TYPE (W/O SUDDEN EXPANSION) TO SIMULATE 1ST STAGE UPCOMER DIFFUSER
- **CFD GRID**
  - ALGEBRAIC GENERATED H-GRID
  - GRID SIZE 65K~105K
- **TEST ARTICLE**
  - WILL BE TESTED IN WATER TEST RIG
  - DETAILED VELOCITY DISTRIBUTION MEASURED WITH 3-D LASER VELOCIMETER
  - STATIC PRESSURE MEASURED ALONG BOTH END WALLS AND BLADE SURFACES

HYDRODYNAMIC DESIGN OF ADVANCED PUMP COMPONENTS
ADVANCED PUMP DIFFUSER
LASER SURVEY LOCATIONS

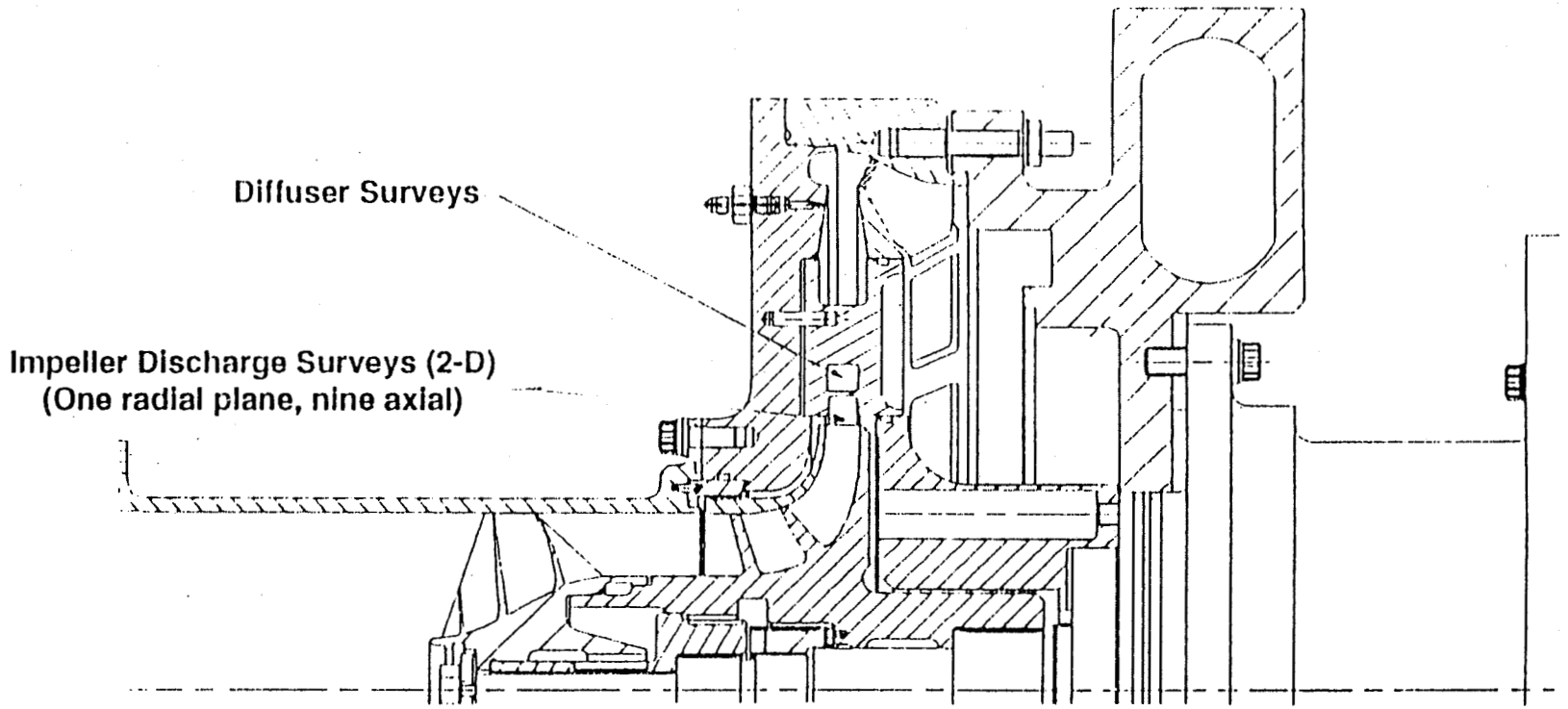

ADVANCED PUMP DIFFUSER
TARGET LASER SURVEY LOCATIONS

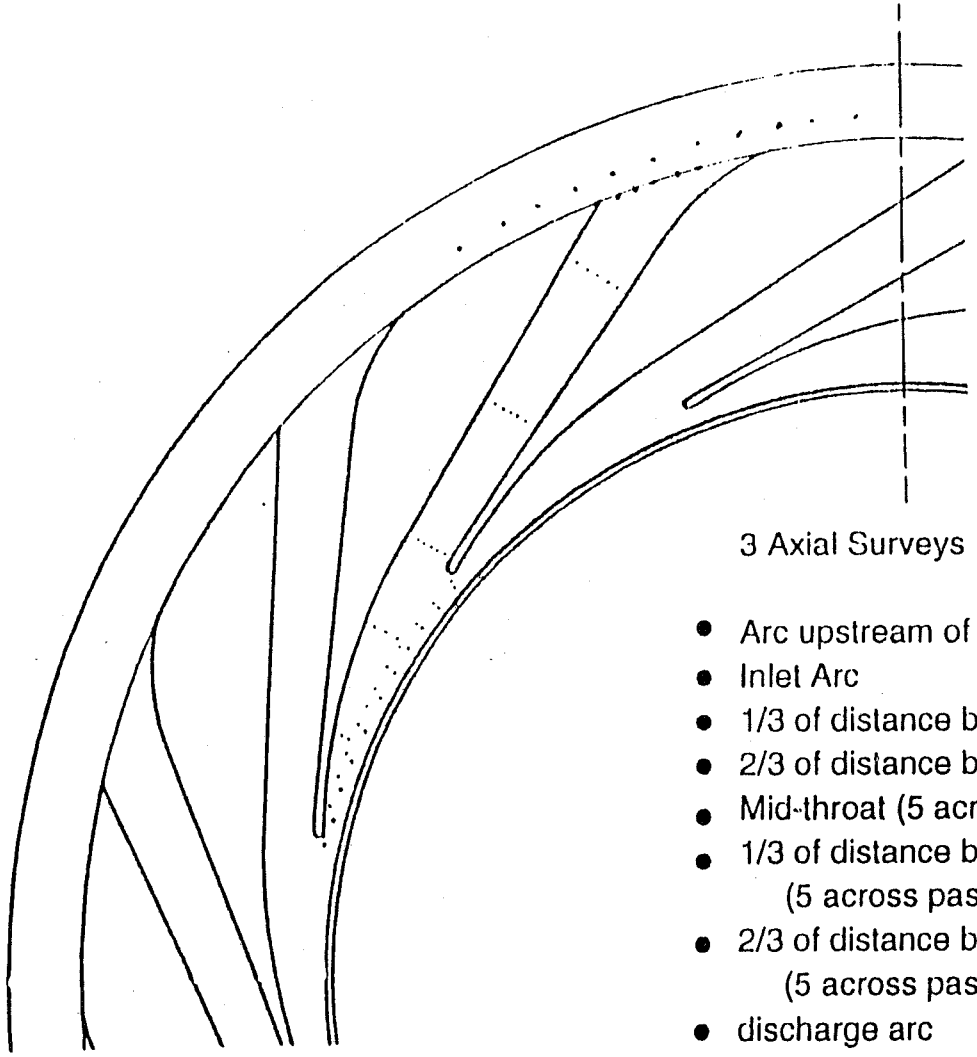

3 Axial Surveys

- Arc upstream of inlet
- Inlet Arc
- 1/3 of distance between inlet arc and mid-throat
- 2/3 of distance between inlet arc and mid-throat
- Mid-throat (5 across passage)
- 1/3 of distance between mid-throat and discharge arc (5 across passage)
- 2/3 of distance between mid-throat and discharge arc (5 across passage)
- discharge arc
- vane-to-vane downstream of discharge arc

NASA CONSORTIUM BASELINE DIFFUSER
CFD GRID AND FLOW SOLVER

PARAMETER CASES	GRID SIZE	ZONE NO.	ORDERO F DIFF.	DIFFUSER UPSTREAM WALL	DIFFUSER DOWNSTREAM GEOMETRY	FLOW SOLVER	COMMENT	I.D.
1	105K	3	2ND	NO SLIP	WITH SUDDEN EXPANSION	REACT3D	SIMULATE TESTER	TESTER
2	65K	3	2ND	NO SLIP	NO SUDDEN EXPANSION	REACT3D	SIMULATE CONTINUOUS CROSSOVER	DIF2
3	65K	3	2ND	SLIP	NO SUDDEN EXPANSION	REACT3D	SIMILIAR TO CASE 2 WITH BETTER L.E. DEFINITION	DIFC
4	65K	3	1ST	NO SLIP	NO SUDDEN EXPANSION	REACT3D	SIMILIAR TO CASE 2 WITH BETTER L.E. DIFINITION	DIFB
5	65K	1	1ST	NO SLIP	NO SUDDEN EXPANSION	STARCD	SAME AS CASE 2	STARCD

ADVANCED PUMP DIFFUSER
MERIDIONAL PLANE (TESTER)

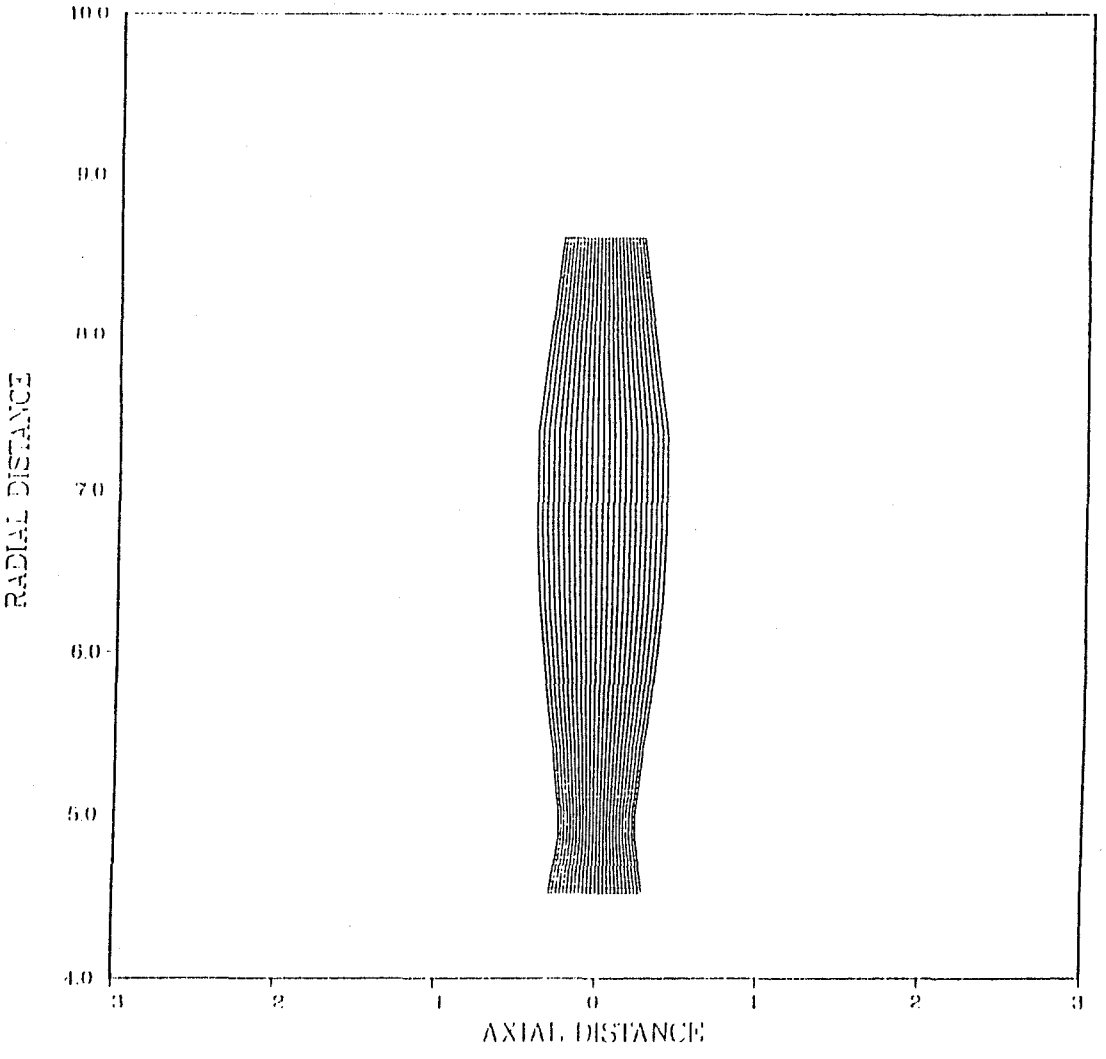

ADVANCED PUMP DIFFUSER
BLADE-TO-BLADE CFD GRID (TESTER)

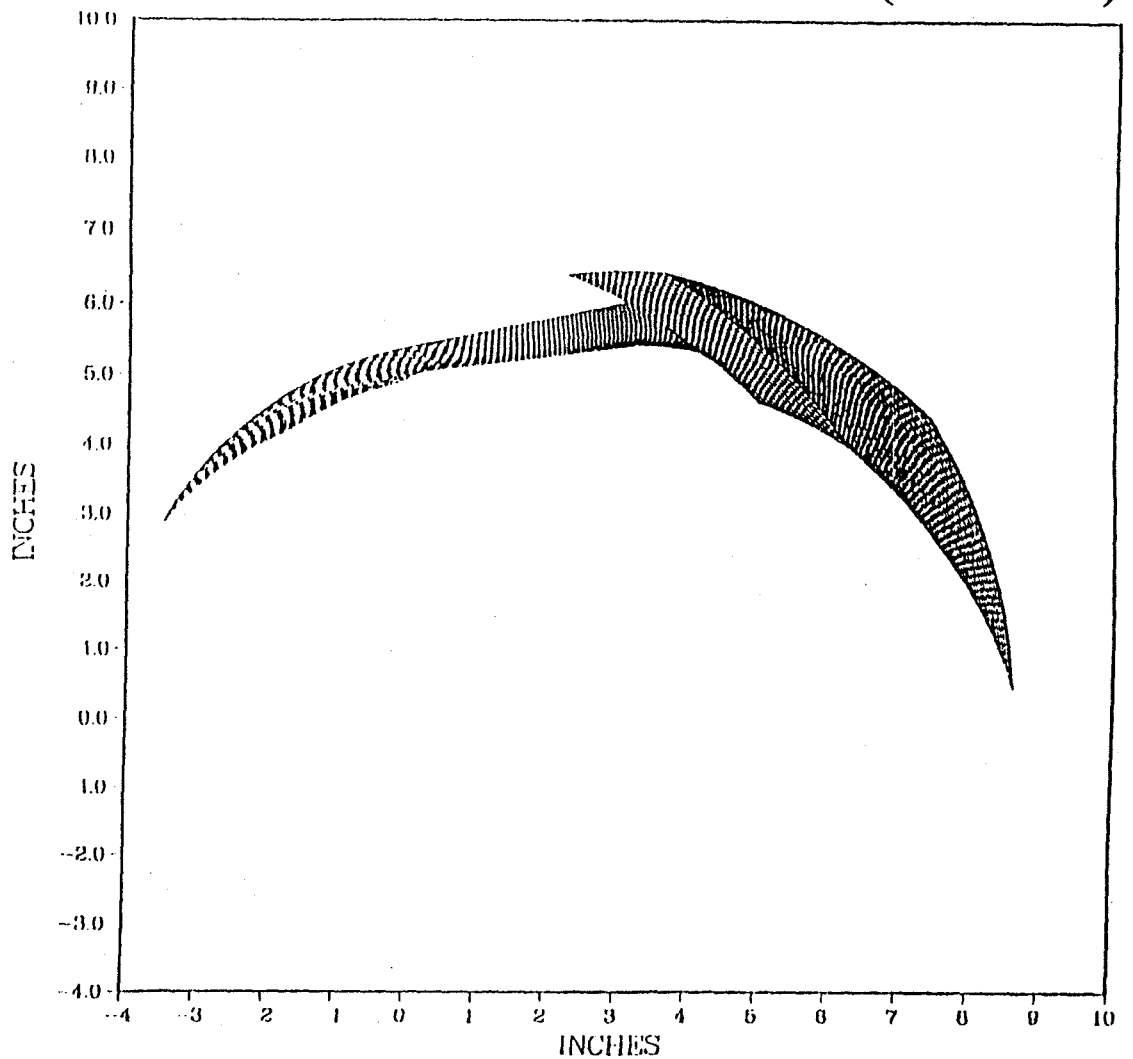

Rockwell Aerospace
Rocketdyne

ADVANCED PUMP DIFFUSER
MERIDIONAL GRID (DIF2)

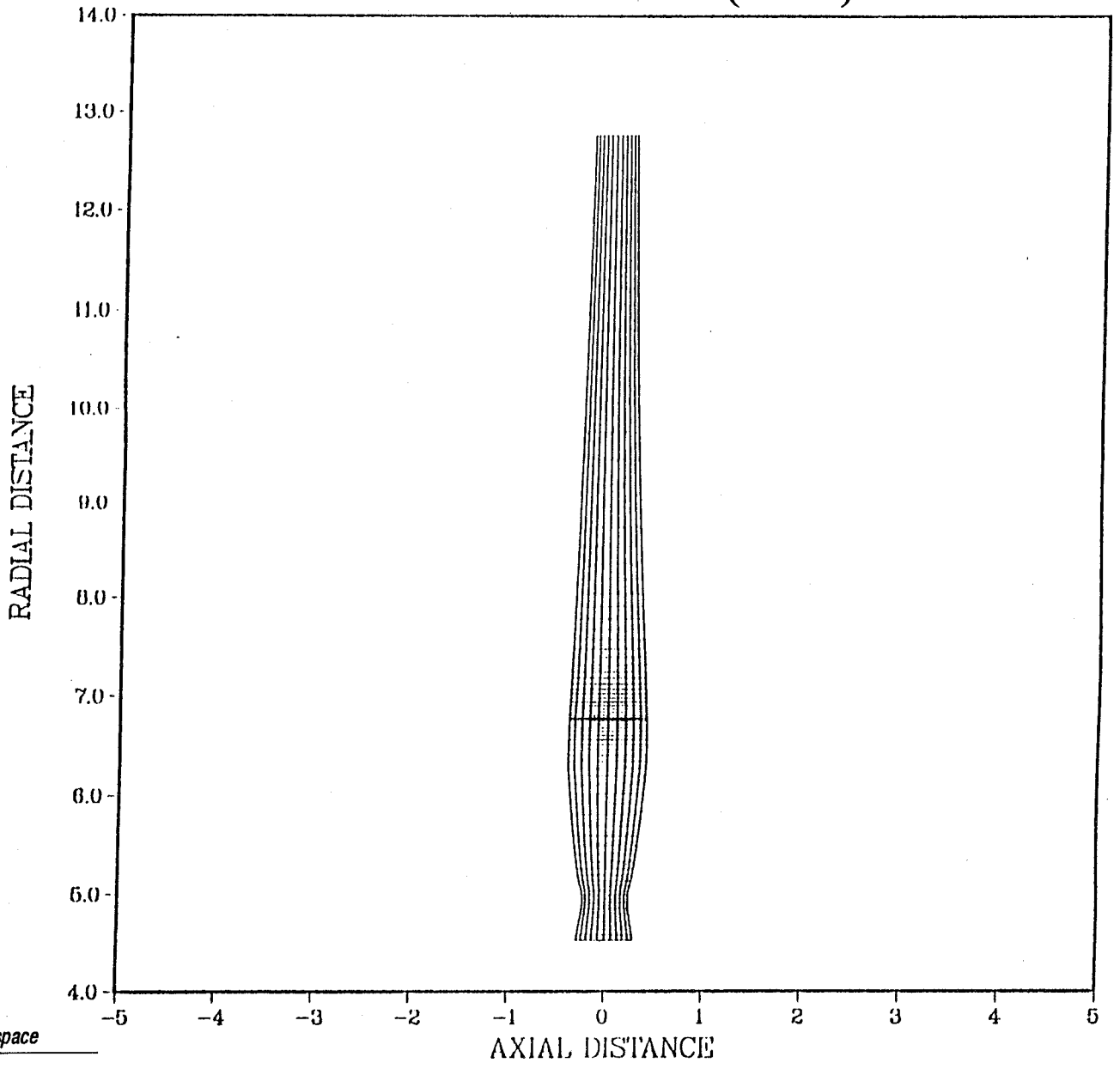

ADVANCED PUMP DIFFUSER
BLADE-TO-BLADE CFD GRID (TESTER)

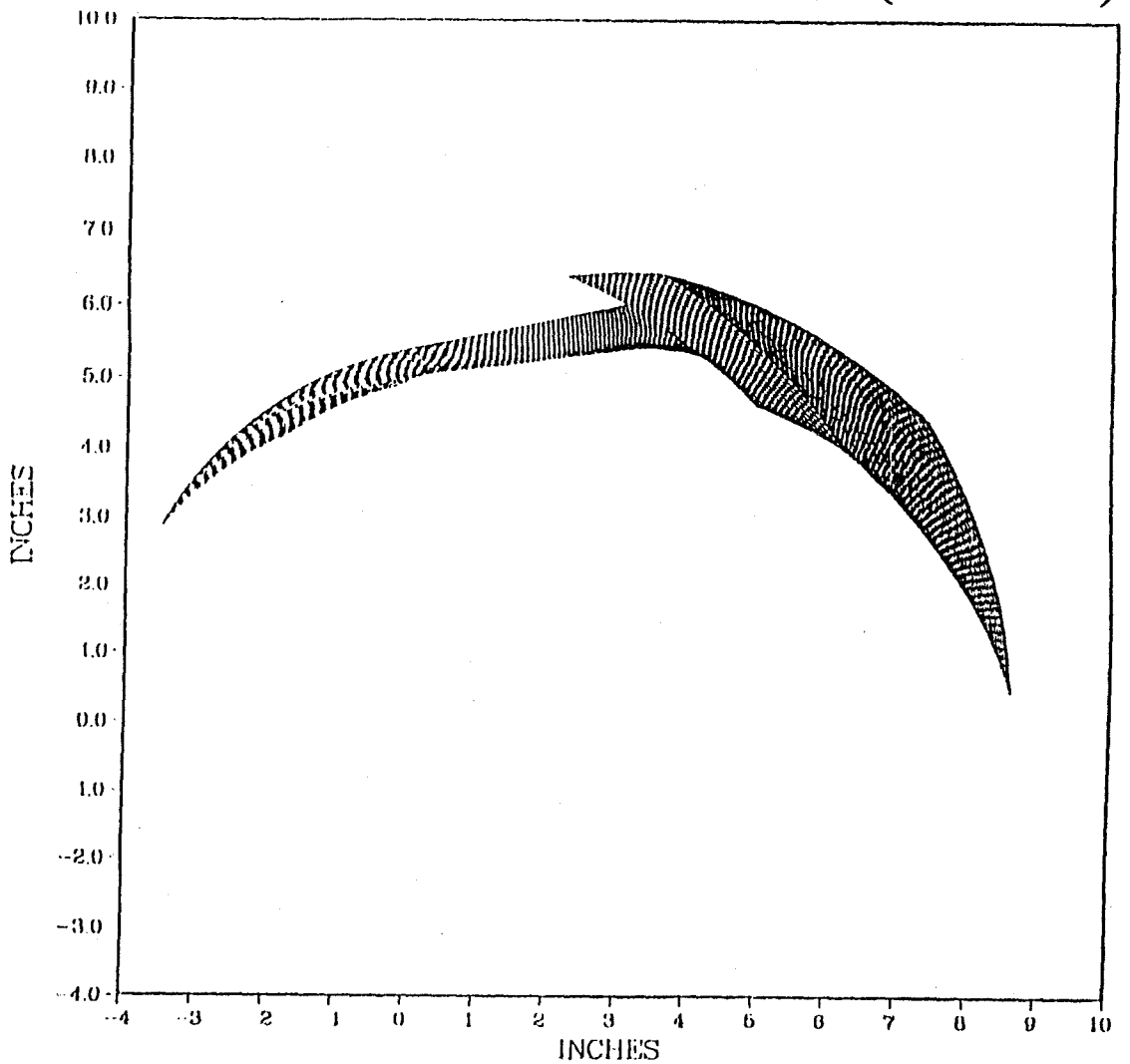

Rockwell Aerospace
Rocketdyne

NASA CONSORTIUM BASELINE DIFFUSER
PRELIMINARY RESULTS

- **COMPARISON OF CASE 1 AND CASE 2 (W/ EXIT SUDDEN EXPANSION VS. W/O)**
  - PRESSURE RECOVERY COEFFICIENT SLIGHTLY IMPROVED FOR SUDDEN EXPANSION (C_p= 0.67 VS. 0.64)
  - BOTH ACHIEVE UNIFORM AND SMOOTH STATIC PRESSURE RECOVERY
  - LOW ENERGY REGION AT MIDSECTION OF PRESSURE SIDE

- **COMPARISON OF CASE 2 (NO SLIP) AND CASE 3 (SLIP)**
  - LOW ENERGY FLOW SHIFTED TOWARD PRESSURE SIDE T.E. FOR SLIP CONDITION
  - INCIDENCE ANGLE INCREASED FOR SLIP CONDITION

NASA CONSORTIUM BASELINE DIFFUSER
PRELIMINARY RESULTS (CONTINUED)

- **COMPARISON OF CASE 4 (REACT3D; 1ST ORDER) AND CASE 5 (STARCD; 1ST ORDER)**
  - SIMILAR SOLUTIONS OBTAINED
  - SMALL DIFFERENCE IN SHAPE OF LOW ENERGY REGION TOWARD PRESSURE SIDE T.E.
  - SMALL DIFFERENCE MAY COME FROM κ-ε VALUE AT INLET BOUNDARY

- **COMPARISON BETWEEN EMPIRICAL AND CFD RESULTS**
  - CFD PREDICTION OF DIFFUSER η=0.75, EMPIRICAL PREDICITION η=0.70
  - CFD PREDICTION OF C_p = 0.63, EMPIRICAL PREDICTION C_p = 0.59

CONSORTIUM VANEISLAND DIFFUSER
VELOCITY FIELD
NO SUDDEN EXPANSION (DIF2)

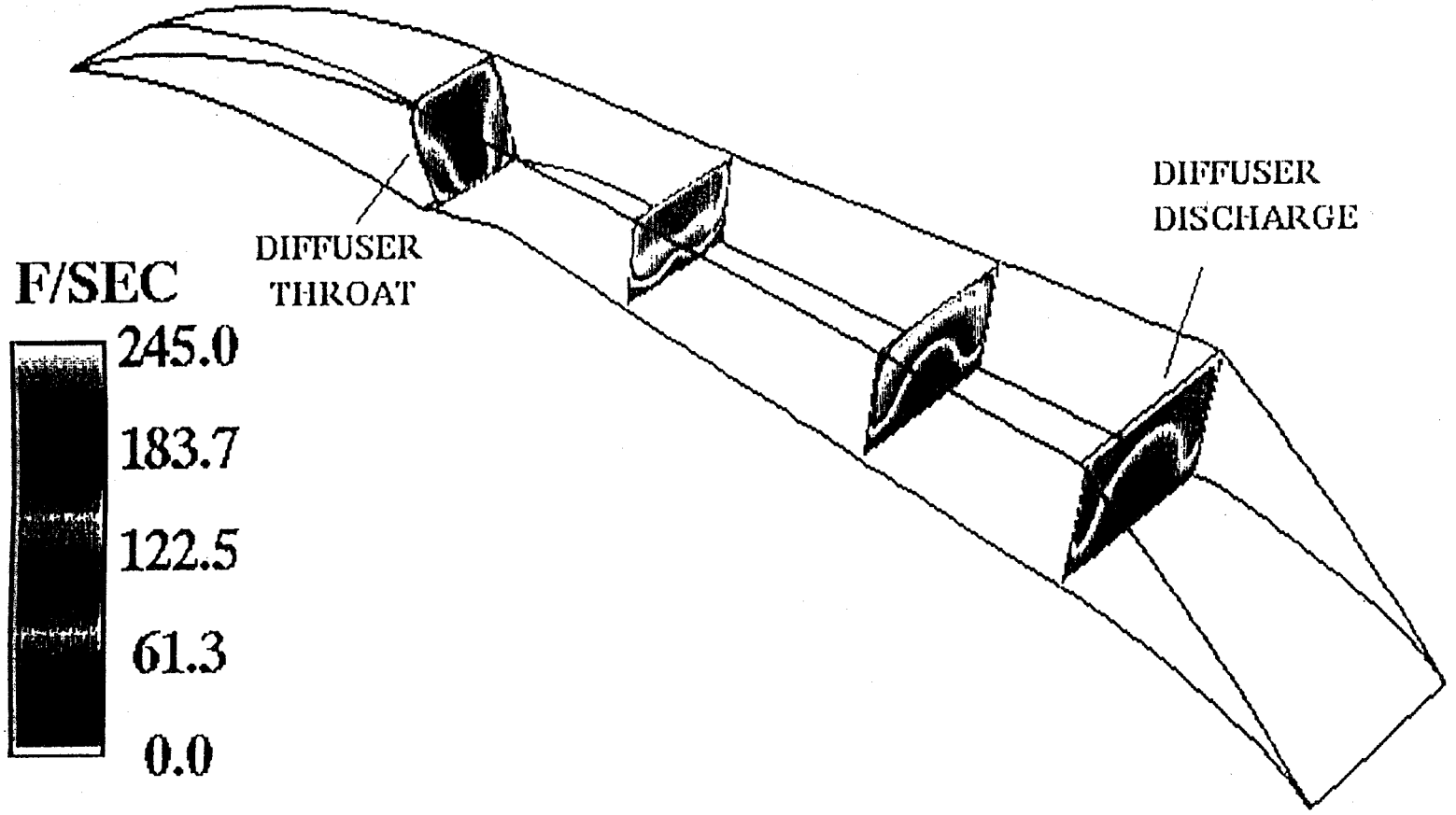

CONSORTIUM VANEISLAND DIFFUSER
STATIC PRESSURE FIELD
TESTER

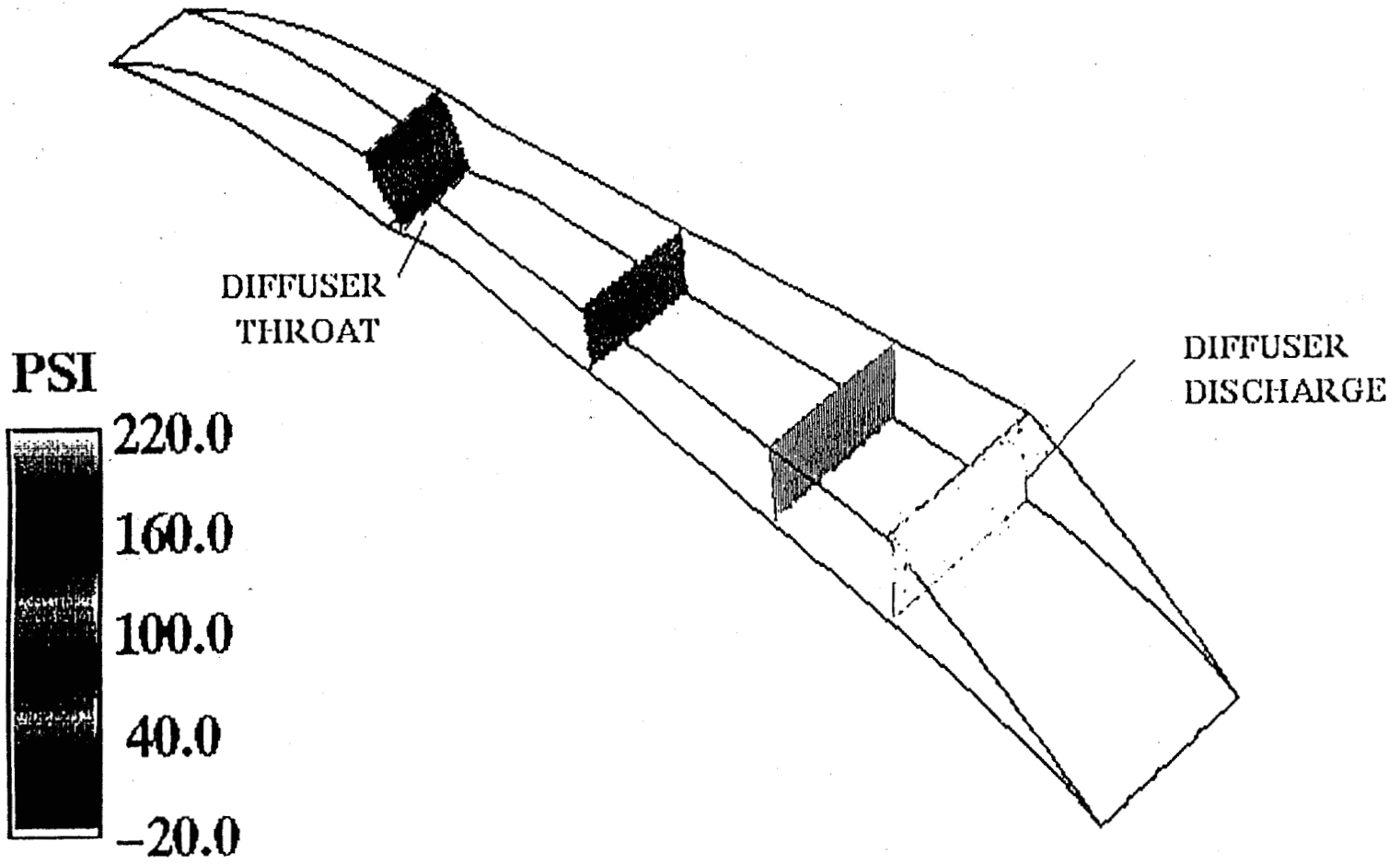

Rockwell Aerospace
Rocketdyne

CONSORTIUM VANEISLAND DIFFUSER
STATIC PRESSURE FIELD
NO SUDDEN EXPANSION (DIF2)

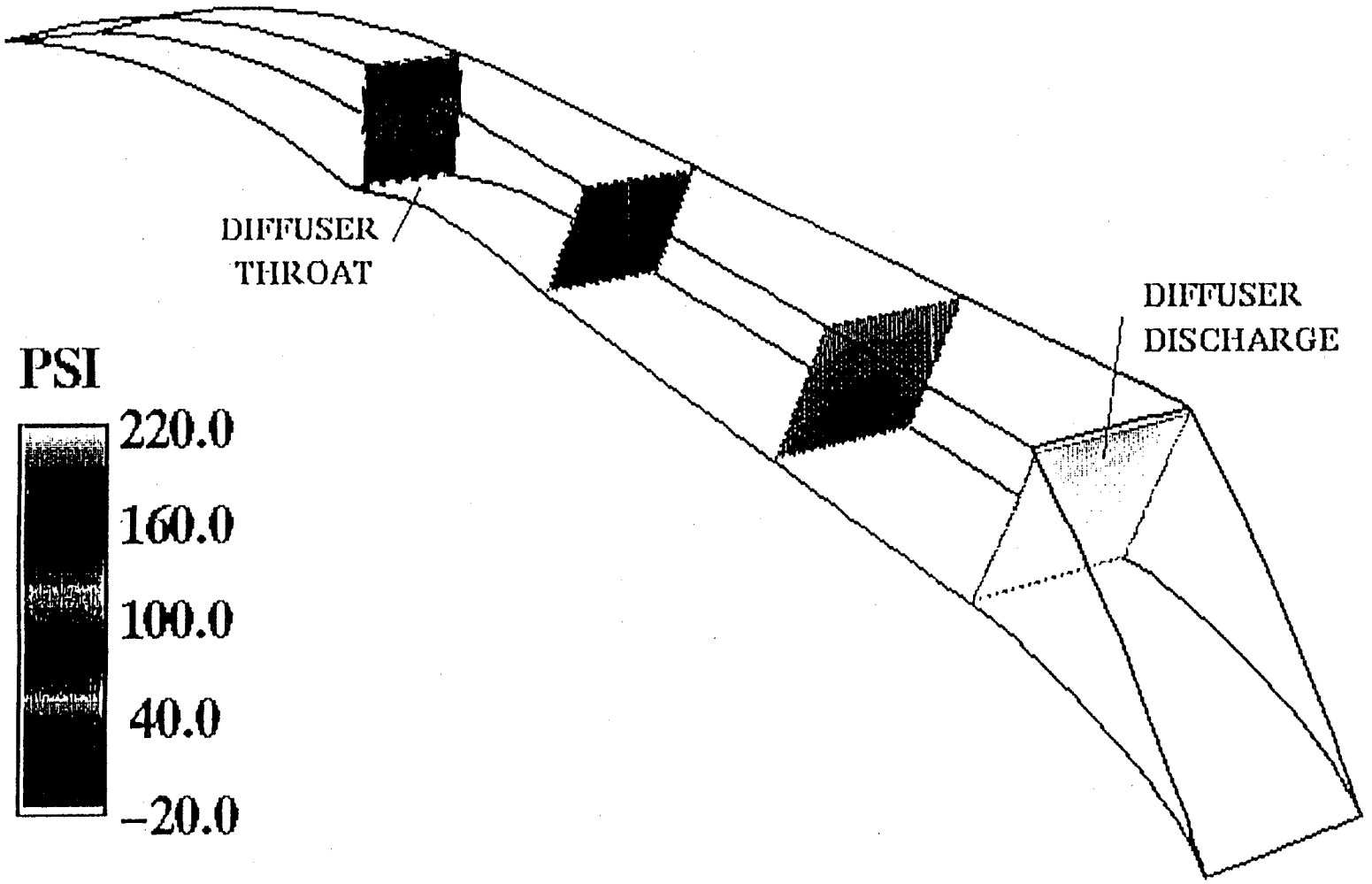

Rockwell Aerospace
Rocketdyne

CONSORTIUM VANEISLAND DIFFUSER
TOTAL PRESSURE FIELD
TESTER

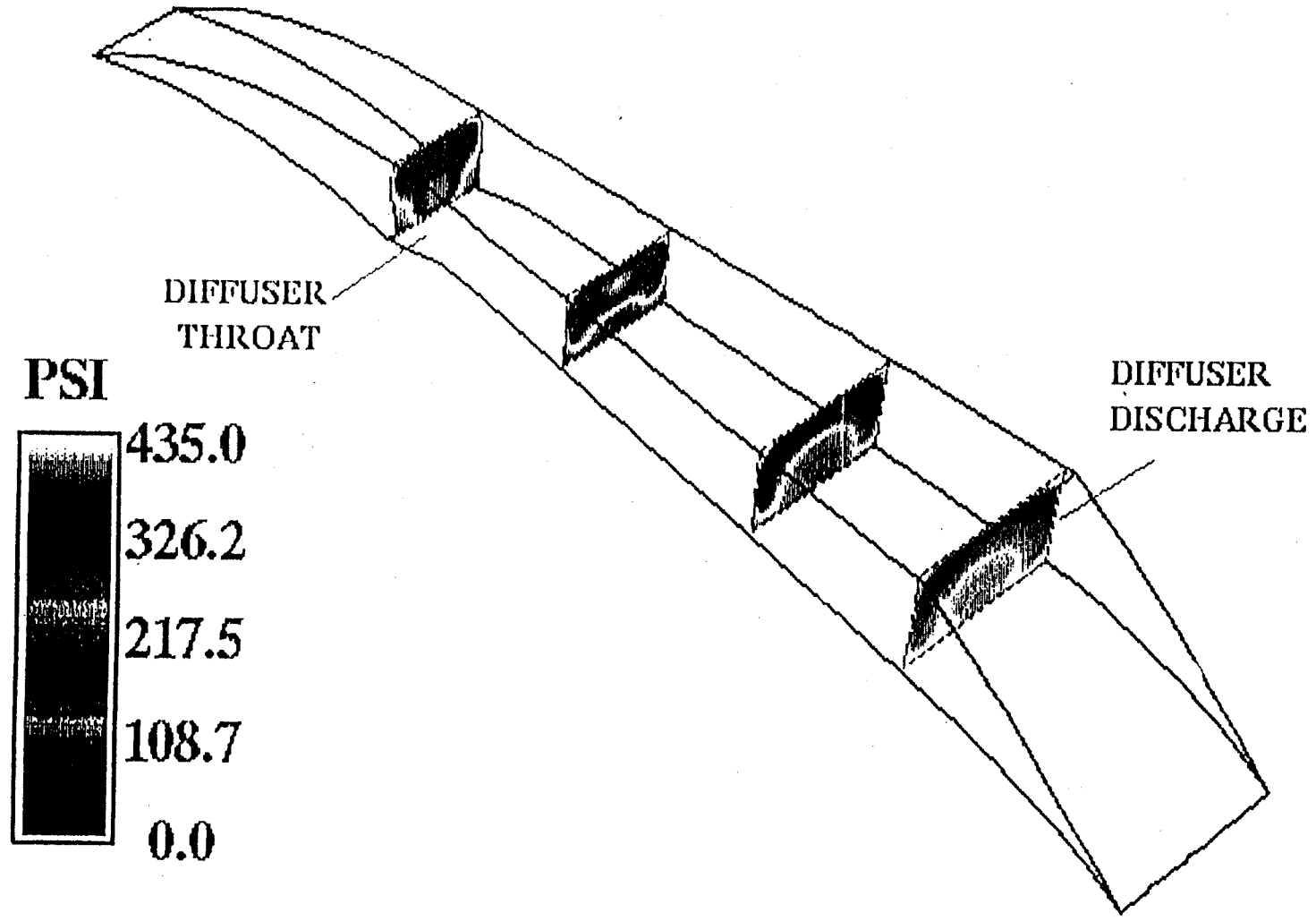

Rockwell Aerospace
Rocketdyne

CONSORTIUM VANEISLAND DIFFUSER
TOTAL PRESSURE FIELD
NO SUDDEN EXPANSION (DIF2)

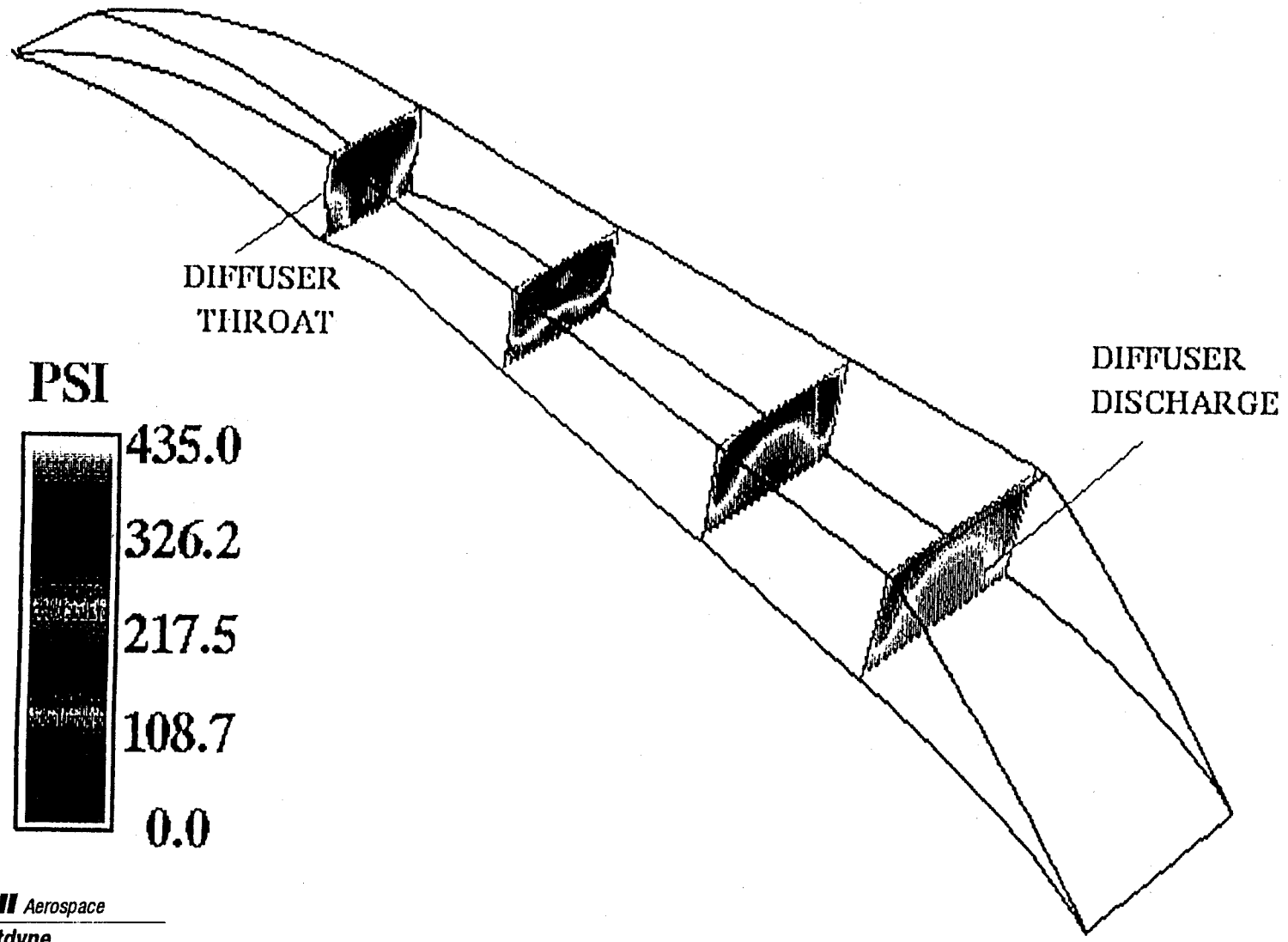

Rockwell Aerospace
Rocketdyne

CONSORTIUM VANEISLAND DIFFUSER BLADE-TO-BLADE VELOCITY FIELD TESTER

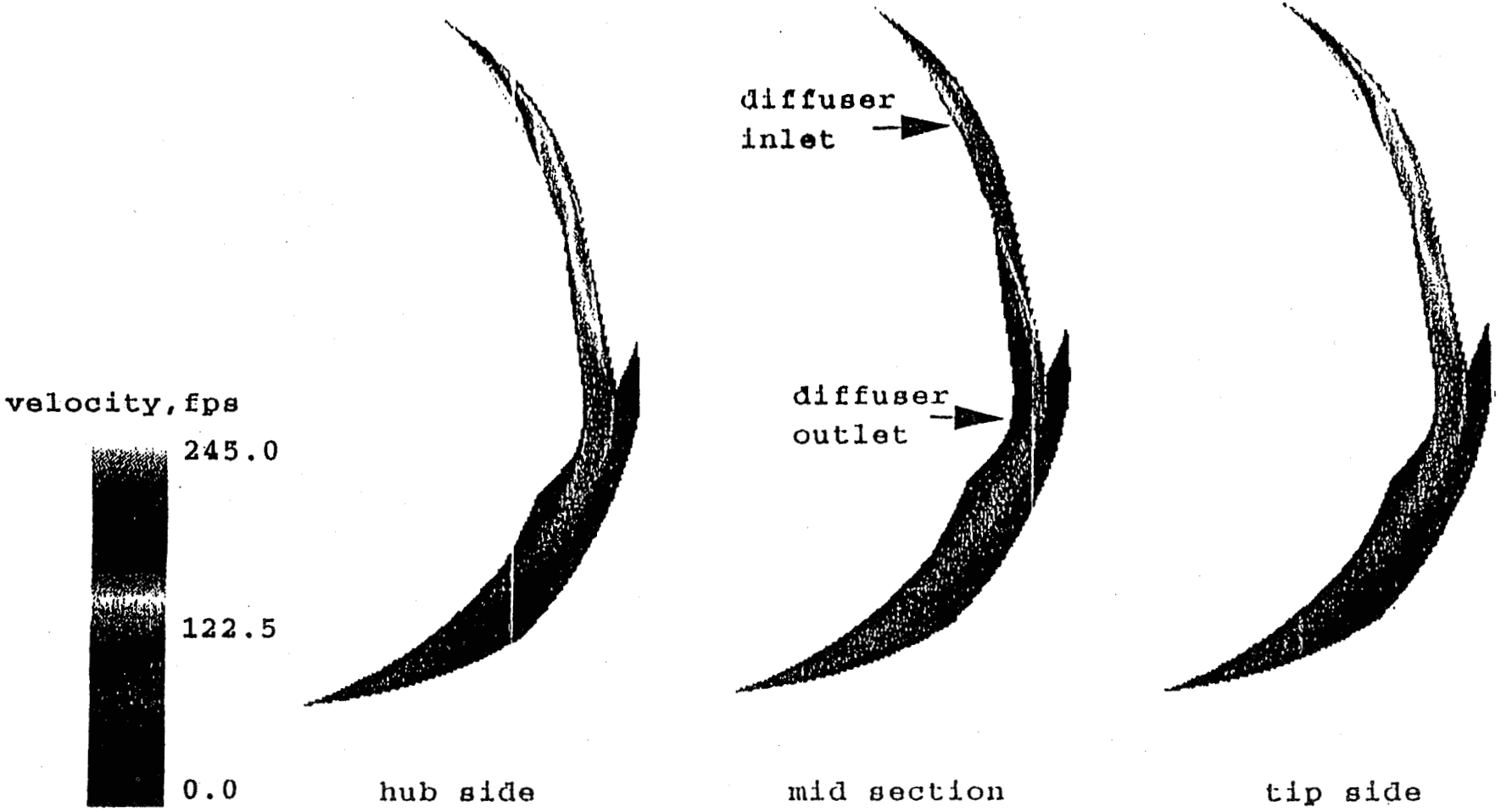

Rockwell Aerospace
Rocketdyne

CONSORTIUM VANEISLAND DIFFUSER
BLADE-TO-BLADE VELOCITY FIELD
NO SUDDEN EXPANSION (DIF2)

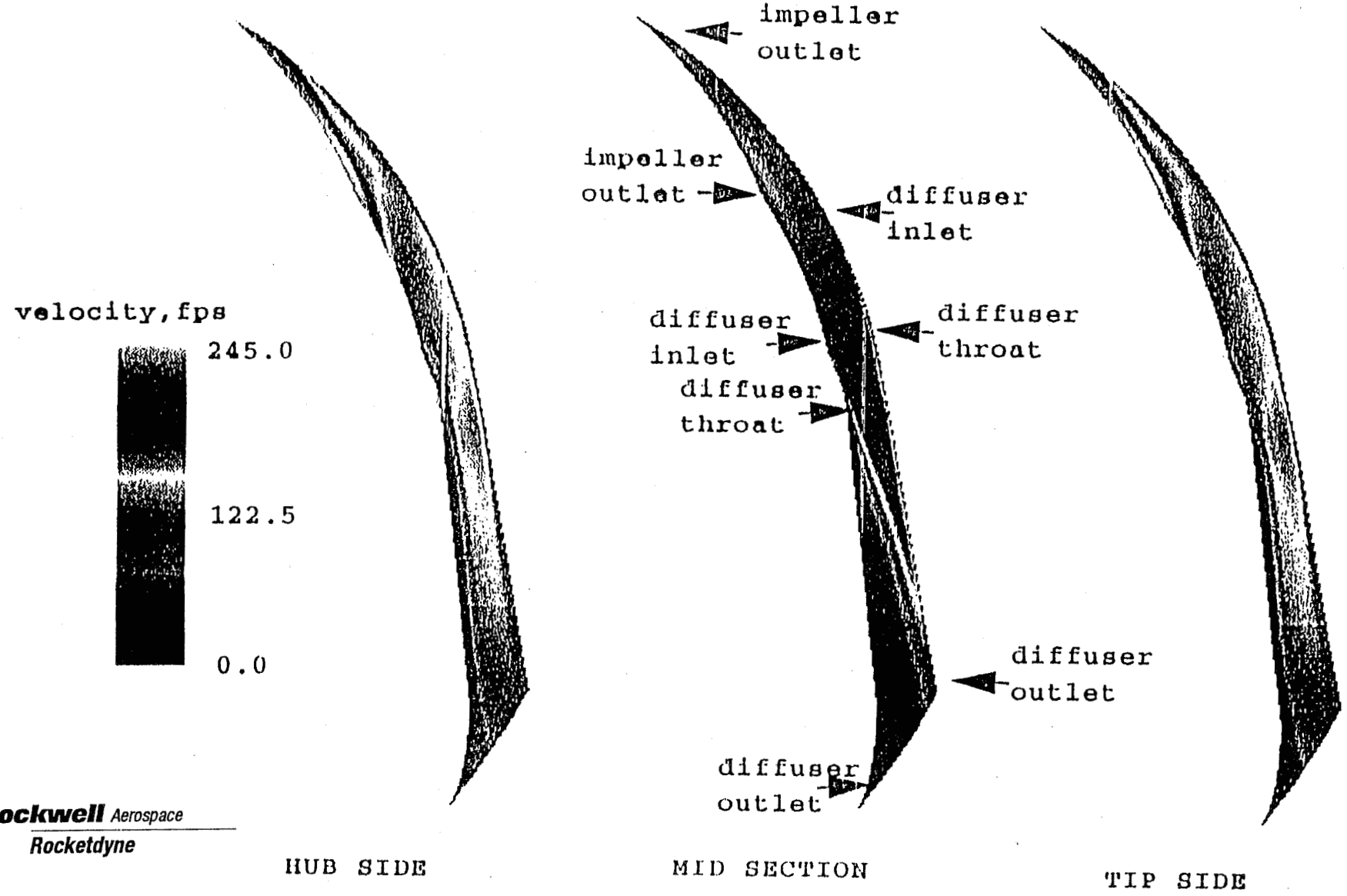

Rockwell Aerospace
Rocketdyne

CONSORTIUM VANEISLAND DIFFUSER BLADE-TO-BLADE PRESSURE FIELD TESTER

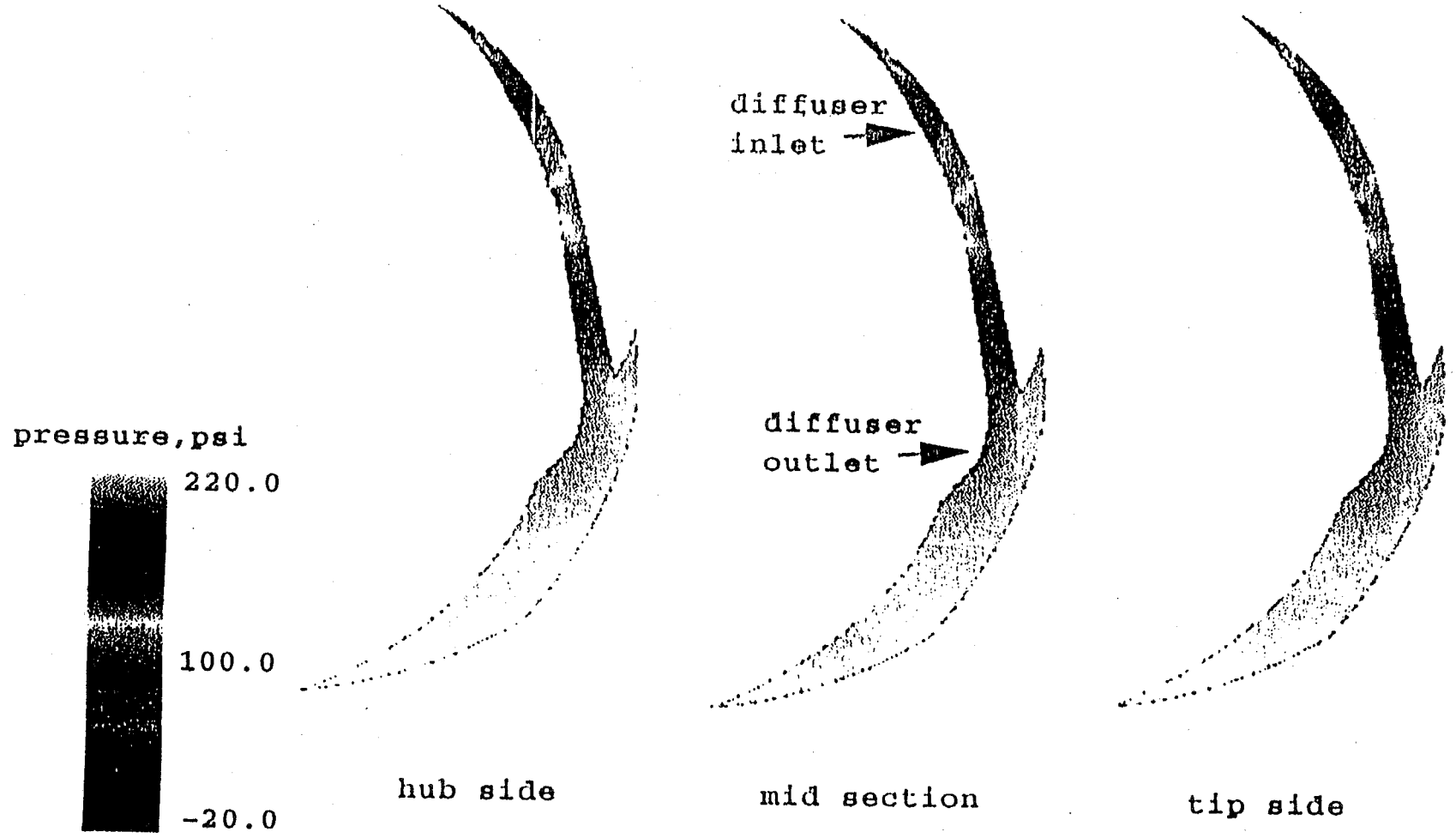

Rockwell Aerospace
Rocketdyne

CONSORTIUM VANEISLAND DIFFUSER
BLADE-TO-BLADE PRESSURE FIELD
NO SUDDEN EXPANSION (DIF2)

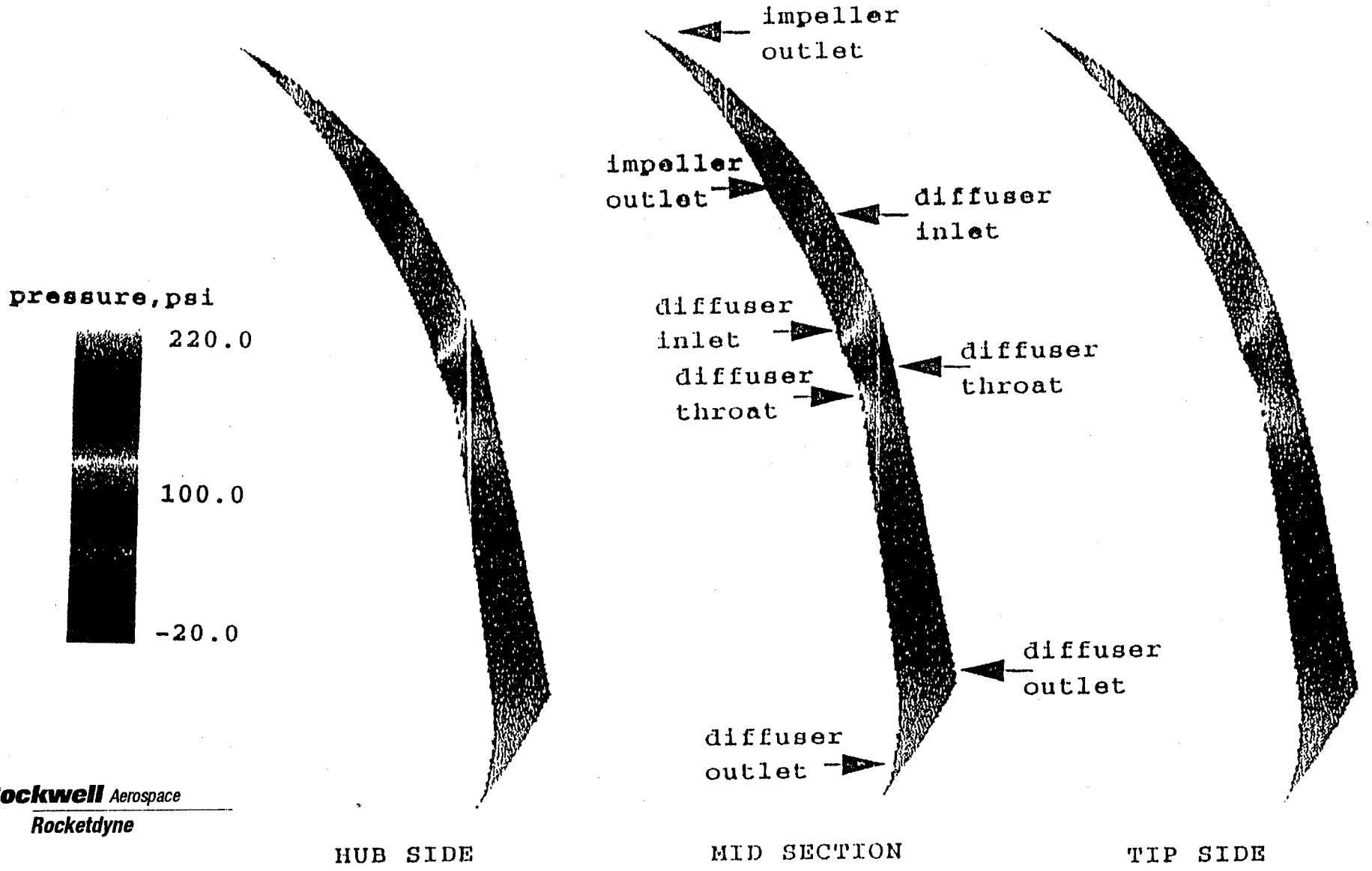

Rockwell Aerospace
Rocketdyne

CONSORTIUM VANEISLAND DIFFUSER
STATIC PRESSURE FIELD
DIFC-SLIP

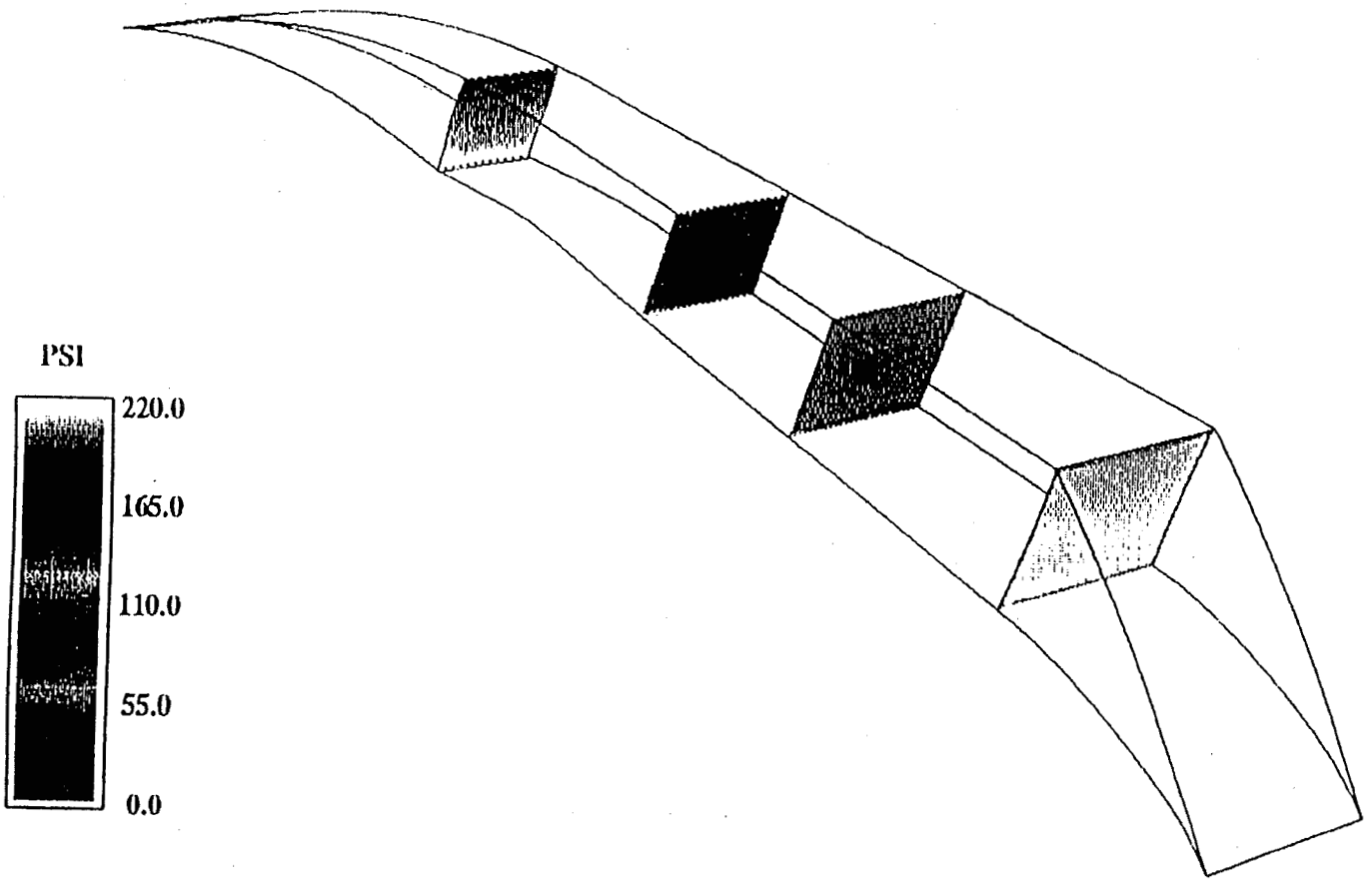

CONSORTIUM VANEISLAND DIFFUSER
VELOCITY FIELD
DIFC-SLIP

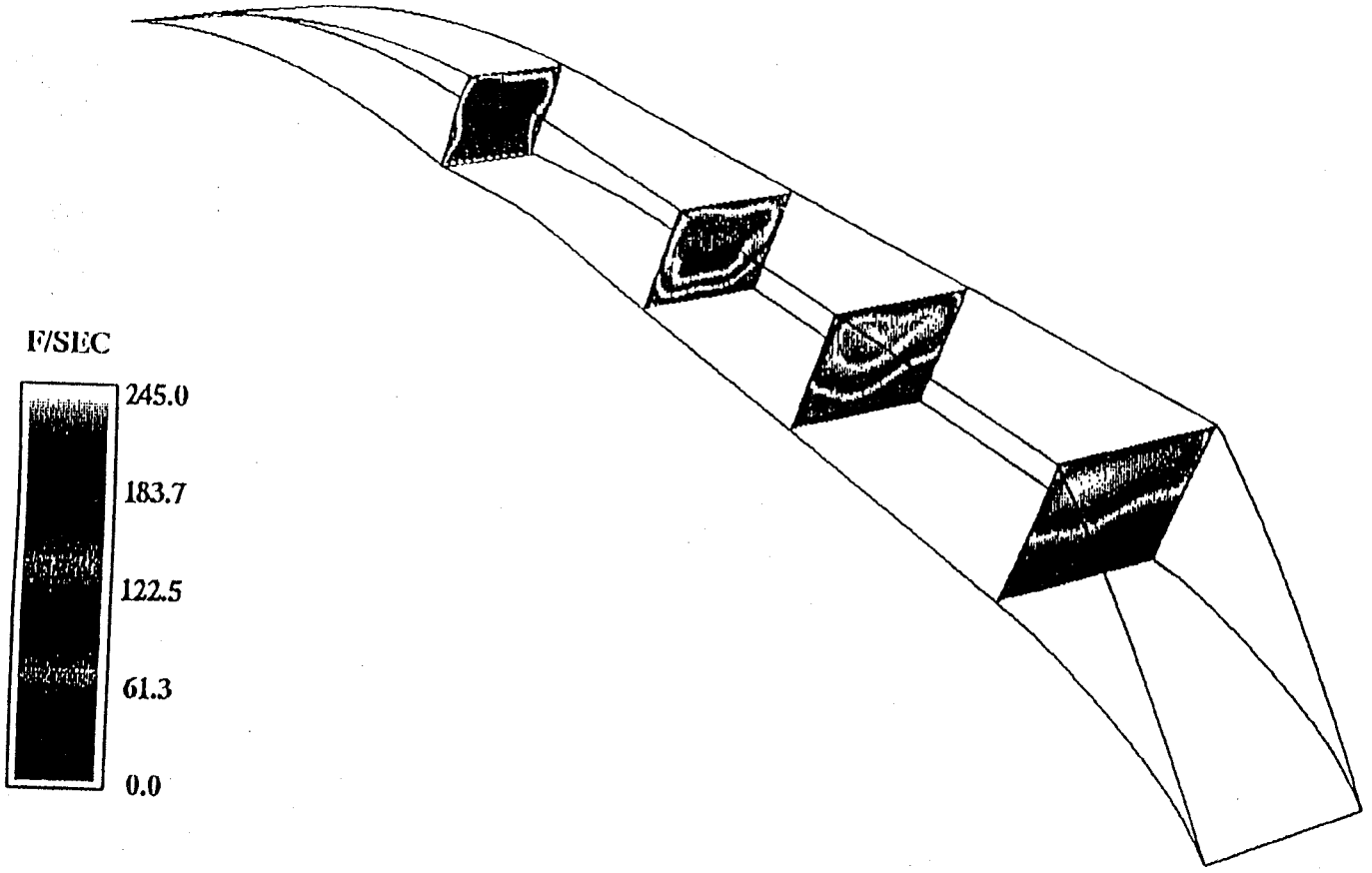

Rockwell Aerospace
Rocketdyne

CONSORTIUM VANEISLAND DIFFUSER
STATIC PRESSURE FIELD
DIFB-1ST ORDER

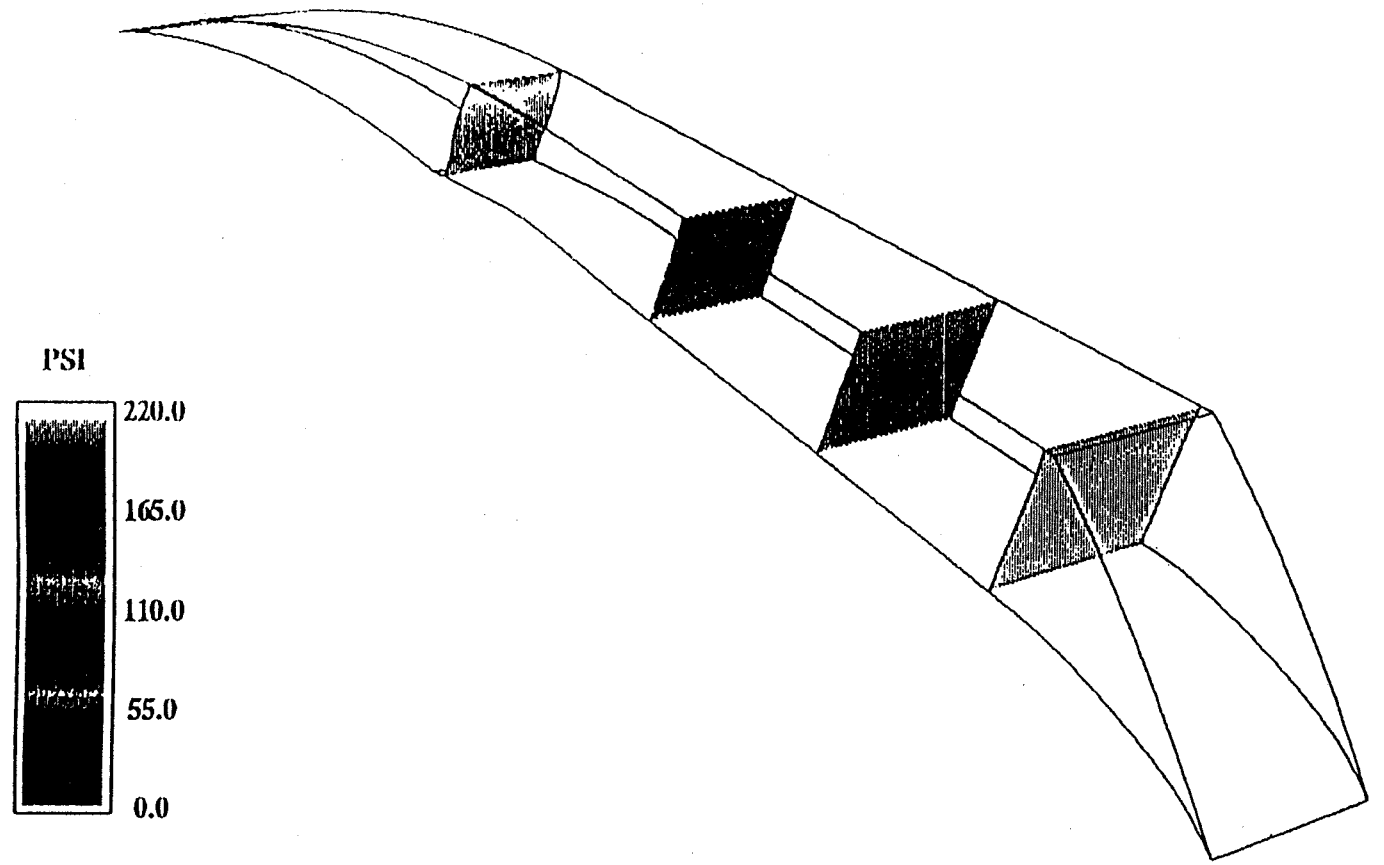

CONSORTIUM VANEISLAND DIFFUSER
VELOCITY FIELD
DIFB-1ST ORDER

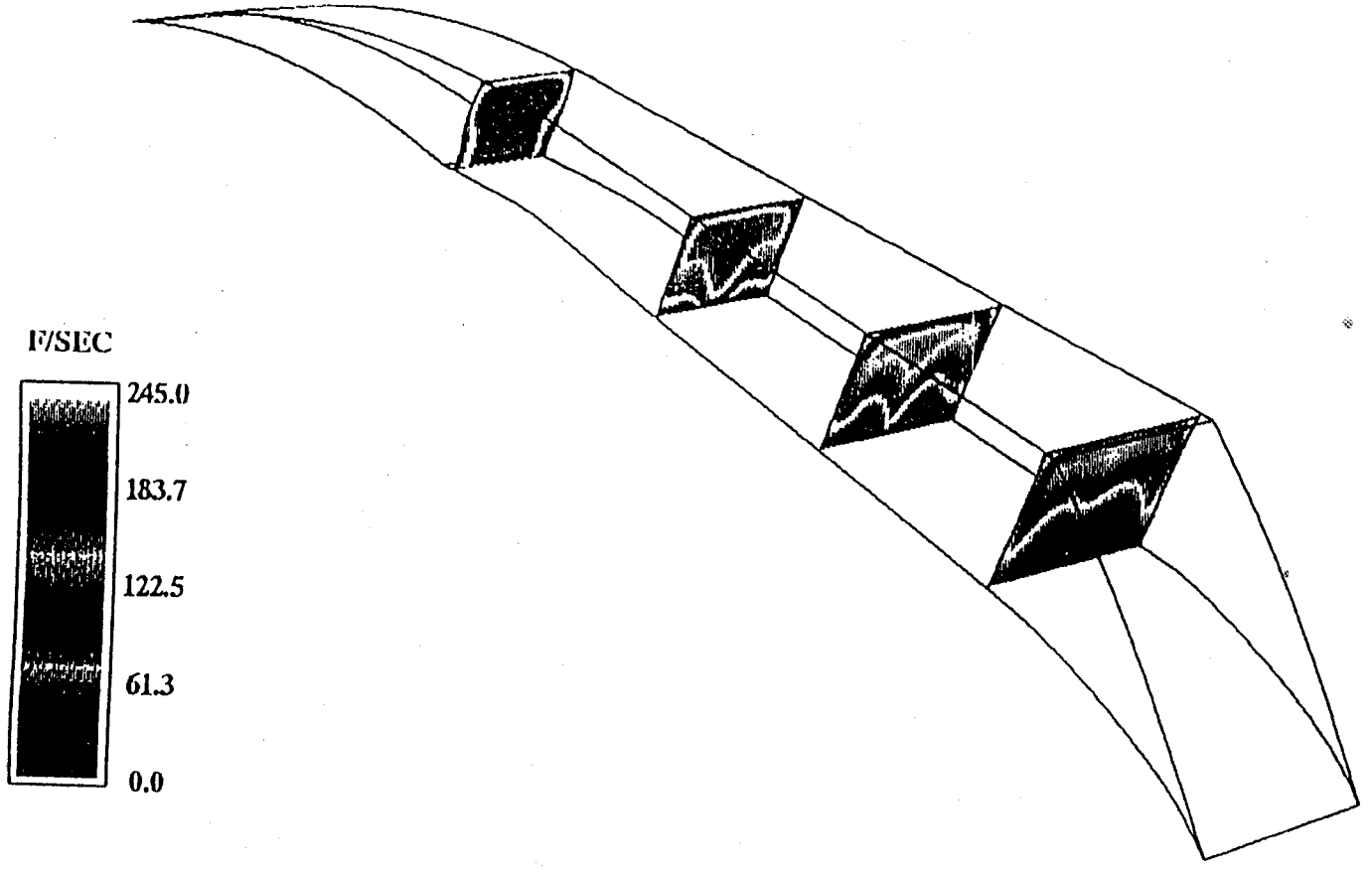

STAR-CD 1ST ORDER SOLUTION
VELOCITY

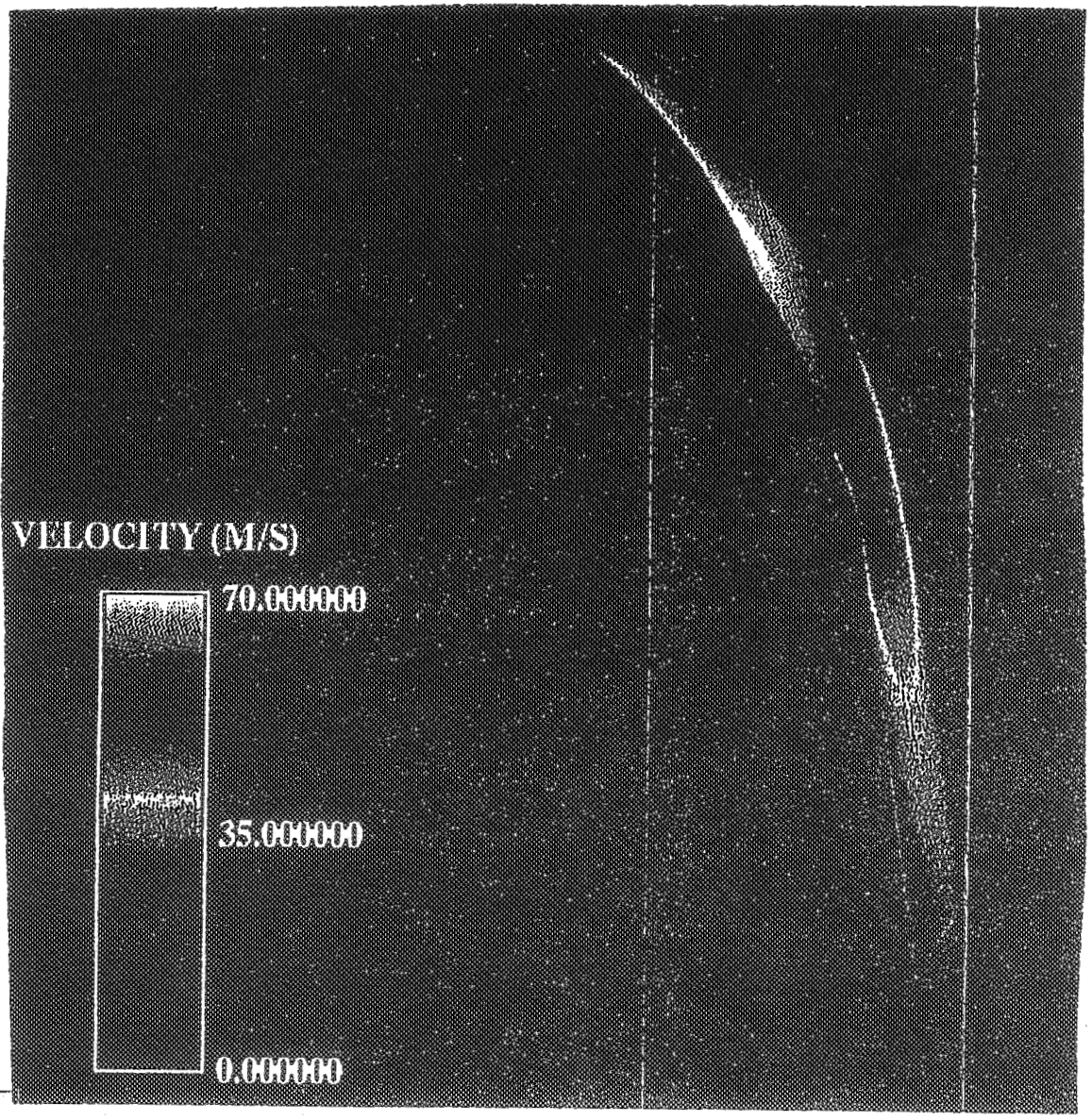

REACT3D 1ST ORDER SOLUTION
VELOCITY

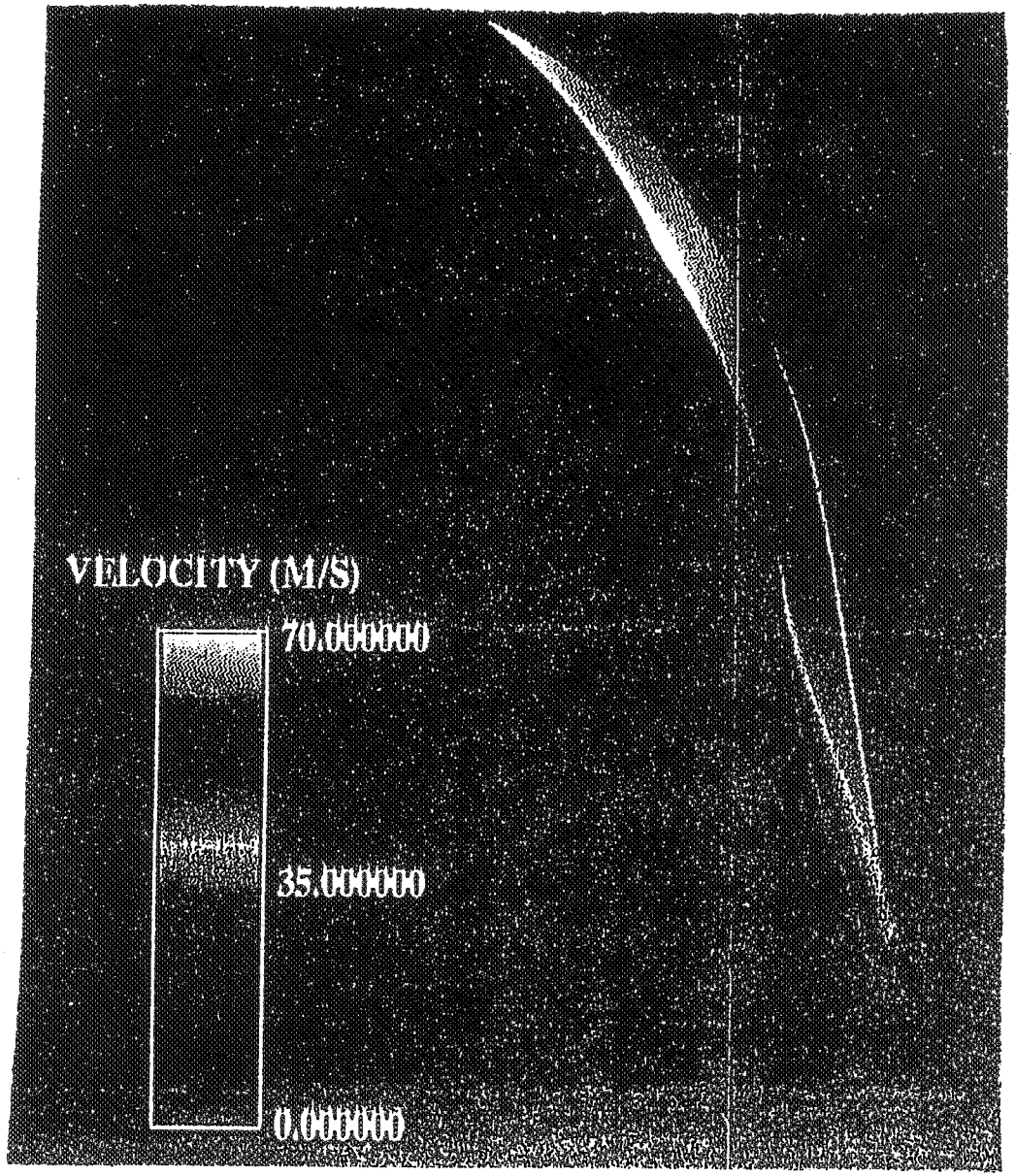

Rockwell Aerospace
Rocketdyne

REACT3D 1ST ORDER SOLUTION
VELOCITY

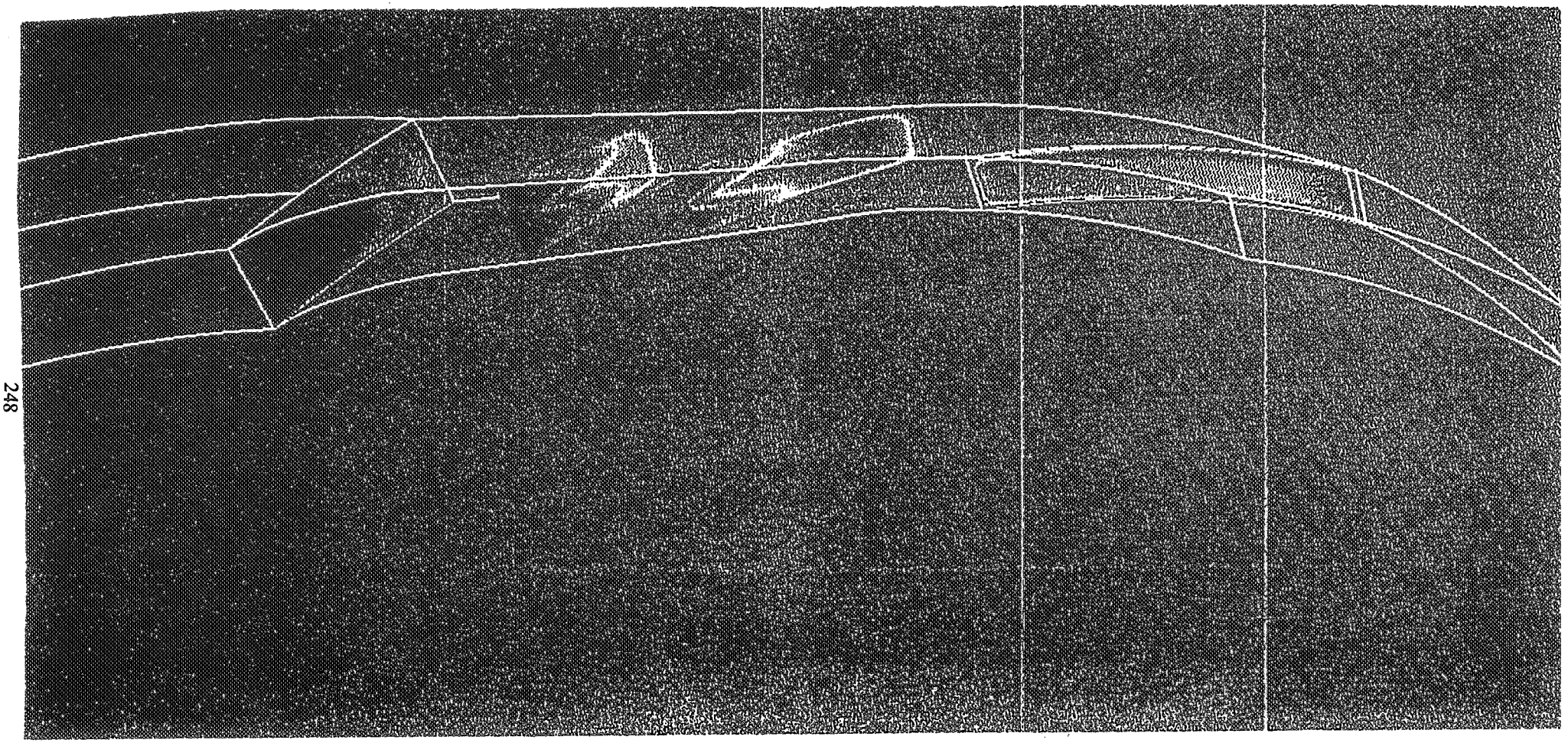

STAR-CD 1ST ORDER SOLUTION
VELOCITY

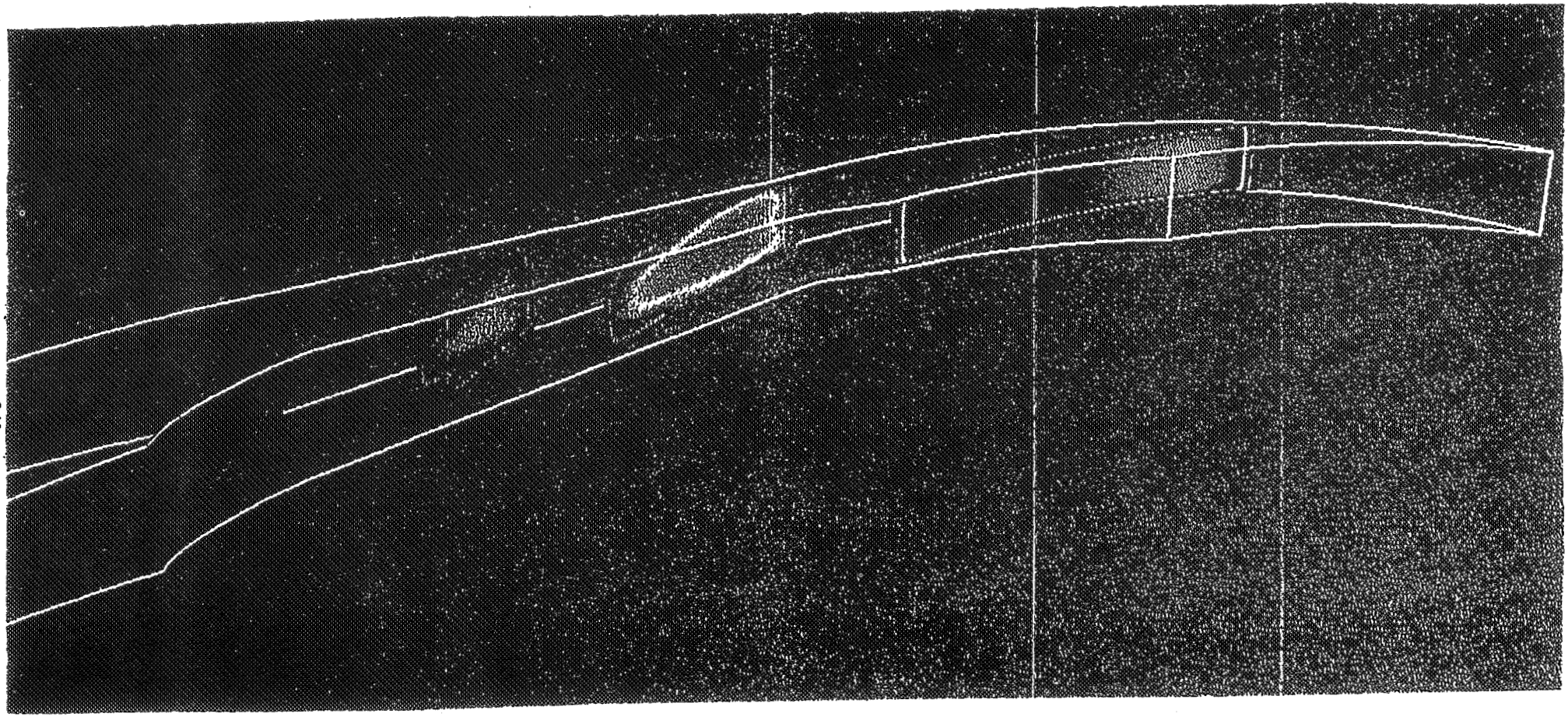

NUMERICAL SIMULATION OF DIFFUSER FLOW

- **RADIAL FLOW DIFFUSERS HAVE BEEN SUCCESSFULLY ANALYZED WITH REACT3D AND STARCD**
- **DOUBLE CIRCULAR ARC DESIGN**
  - COMPARISON WITH AIR TEST DATA INDICATES GOOD AGREEMENT OVER WIDE FLOW RANGE (DESIGN AND OFF-DESIGN CONDITIONS)
- **VANE-ISLAND DESIGN**
  - SIMILAR FLOW FEATURES PREDICTED BY BOTH REACT AND STARCD
  - VALIDATION DATA TO BE PROVIDED BY WATER TESTS
- **ALGEBRAIC GENERATED H-GRID PROVIDES FAST TURNAROUND TIME DURING INITIAL DESIGN STAGE**
  - GRID DEPENDENCY STUDY NECESSARY TO DEFINE GRID RESOLUTION REQUIREMENTS
- **USING CFD AS A DIFFUSER DESIGN TOOL APPEARS FEASIBLE EVEN IN EARLY DESIGN STAGES**

ZERO SIDE FORCE VOLUTE DEVELOPMENT

P.G. Anderson, Ron Franz, R.C. Farmer
SECA, Inc.
Huntsville, AL

Y.S. Chen
ESI
Huntsville, AL

C.E. Brennen, R.V. Uy
California Institute of Technology
Pasadena, CA

ABSTRACT

To reduce the hydrodynamic forces from the centrifugal impeller/volute interaction which act on the impeller of a turbopump, and consequently on the rotor bearings, for a wider range of flow coefficient than just design, a computational design tool for the volute was developed. A computational fluid dynamics (CFD) code, FDNS3D, was used to simulate the flow in the volute and to evaluate potential changes in the volute geometry. An analytic model developed by Adkins and Brennen to simulate two-dimensional flow in a cross-sectional plane of a pump was employed to initialize the flowfield calculation and as an option to simulate the flow within the impeller.

Geometry describing planar cross-sections and the midplane contour is used to construct the volute grid. A subset of these geometry variables are then used as the independent variables in an optimization procedure to minimize the force on the impeller. To reduce the computation time, the Adkins model was used to simulate the impeller exit flow.

A volute which had been tested at the California Institute of Technology was simulated. An improved geometry was postulated and analyzed. The CFD solution indicated that the improvements could be realized. A volute of this geometry was constructed and tested at Caltech's turbopump laboratory. Results of this test and their interpretation are presented as a validation for the CFD volute design evaluation.

1995 CFD Workshop
NASA/MSFC

ZERO SIDE FORCE VOLUTE DEVELOPMENT

P.G. Anderson, Ron Franz, R.C. Farmer
SECA, Inc.
Huntsville, AL

Y.S. Chen
ESI
Huntsville, AL

C.E. Brennen, R.V. Uy
California Institute of Technology
Pasadena, CA

OBJECTIVE:

Develop a CFD model to design a volute which minimizes hydrodynamic side loads on the impeller over a wide range of flow rates.

APPROACH:

Use the FDNS code to develop the CFD model.

Use the Adkins/Brennen pump model to expedite the solution.

Design a volute with this methodology.

Verify the design experimentally.

VOLUTE DESIGNS
FOR MINIMIZING RADIALLY UNBALLANCED FORCES

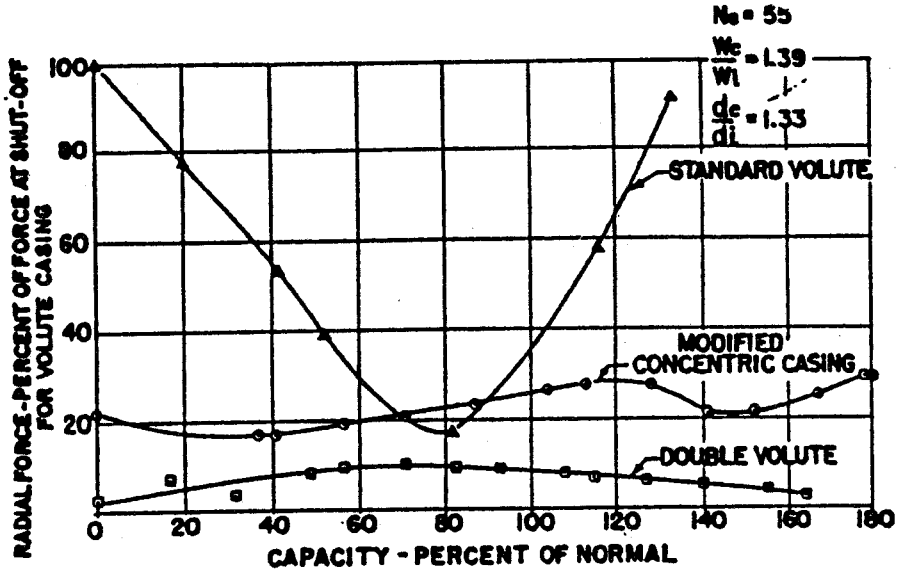

Comparison of the effect of three casing designs on radial force for $N_s = 55$

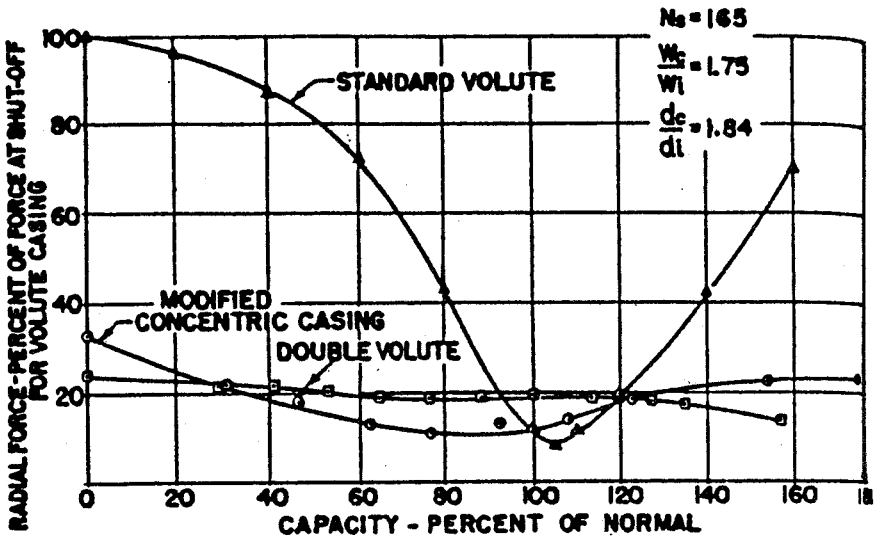

Comparison of the effect of three casing designs on radial fora for $N_s = 165$

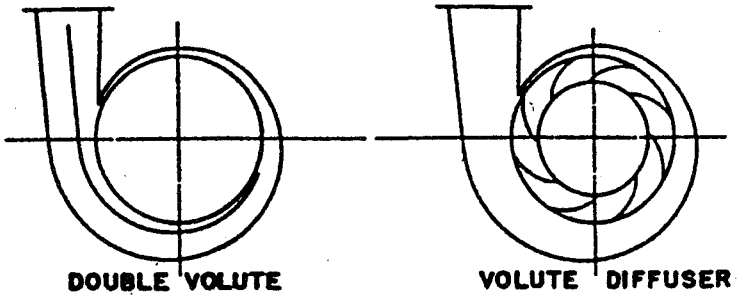

IMPELLER X

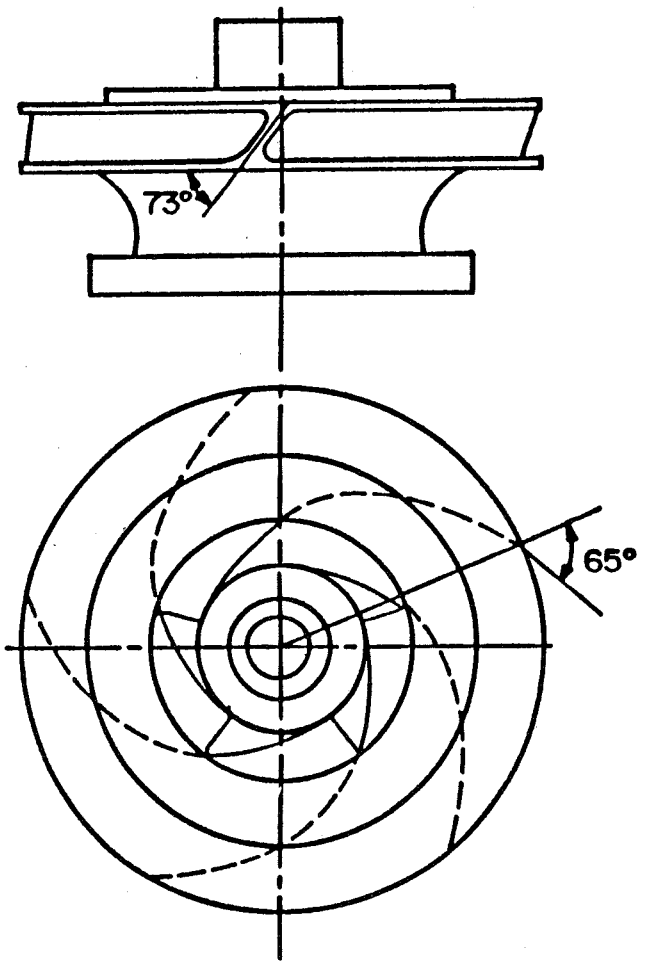
73°
65°

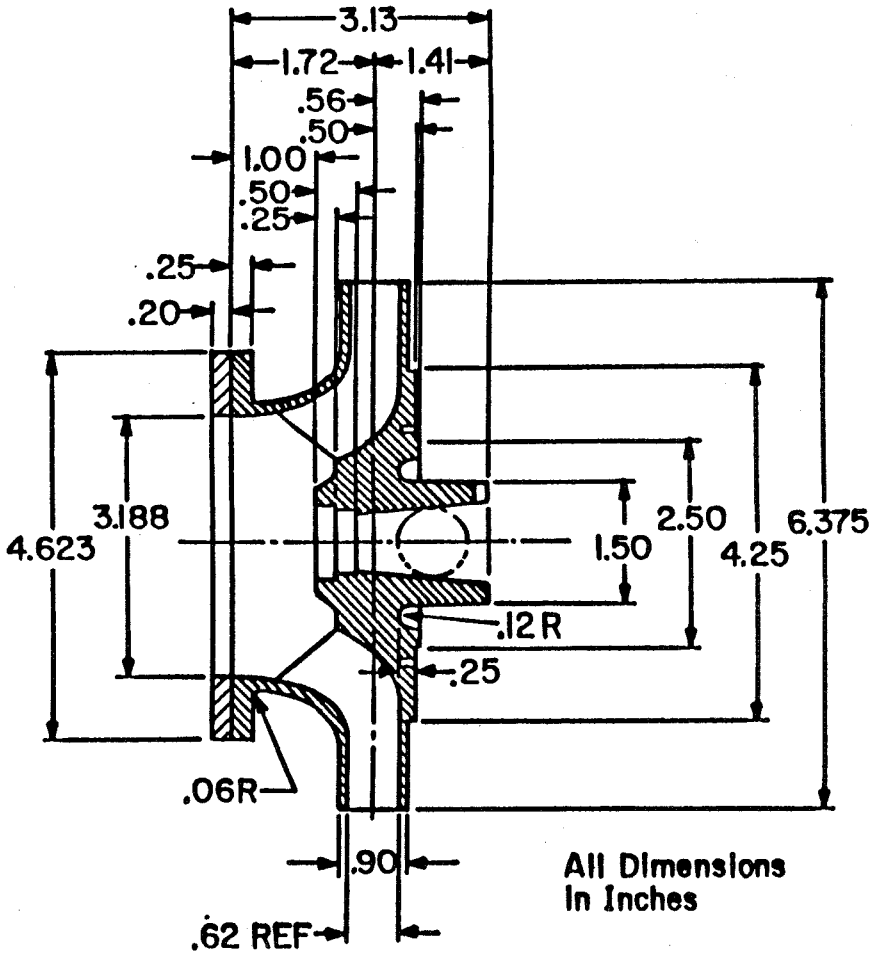
3.13
1.72
1.41
.56
.50
1.00
.50
.25
.25
.20
4.623
3.188
1.50
2.50
4.25
6.375
.12 R
.25
.06R
.90
.62 REF
All Dimensions
In Inches

VOLUTE A

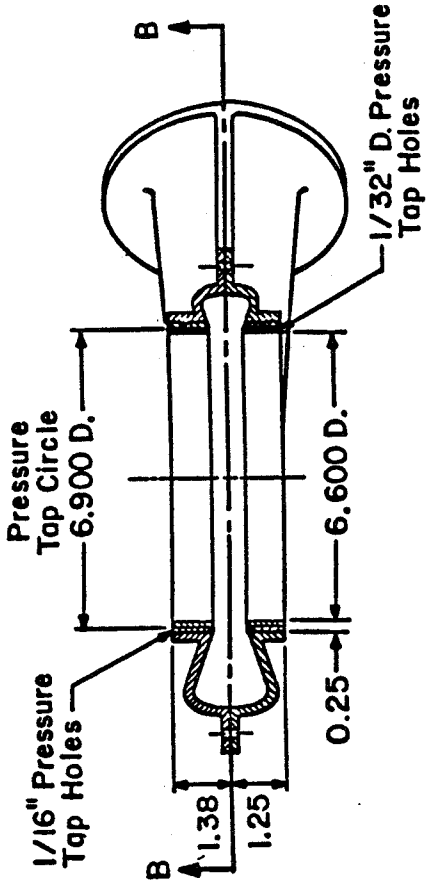

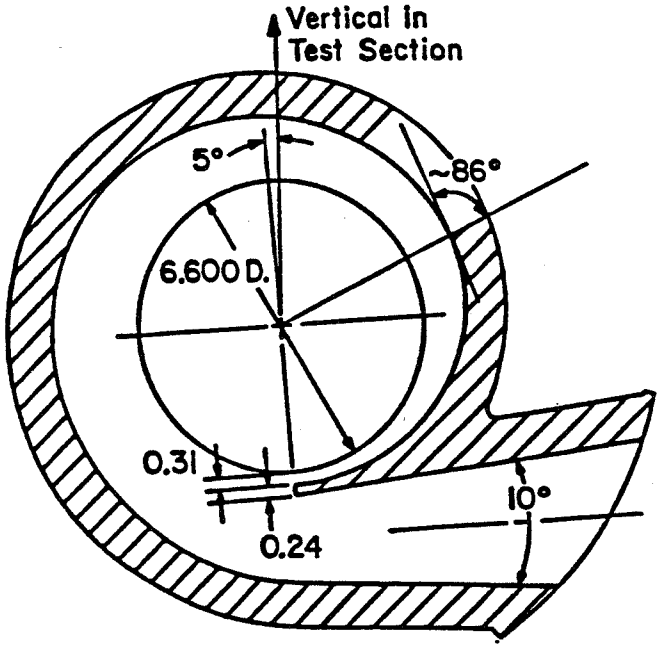

Section B-B

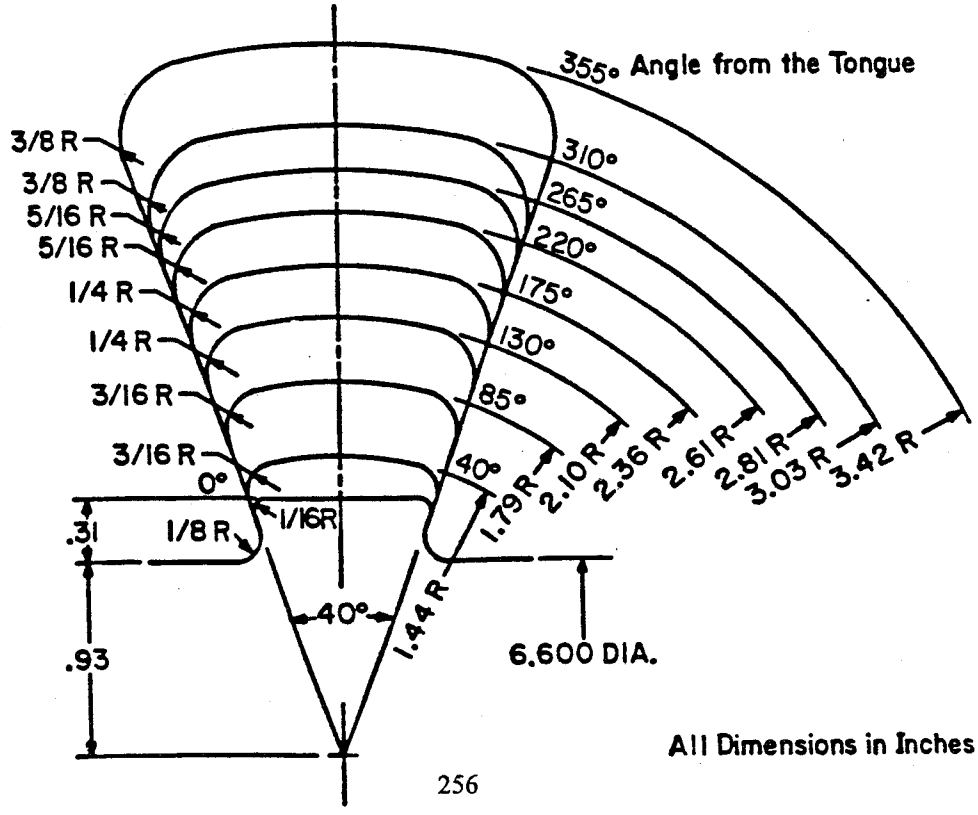

All Dimensions in Inches

GEOMETRY OF A CENTRIFUGAL PUMP IMPELLER

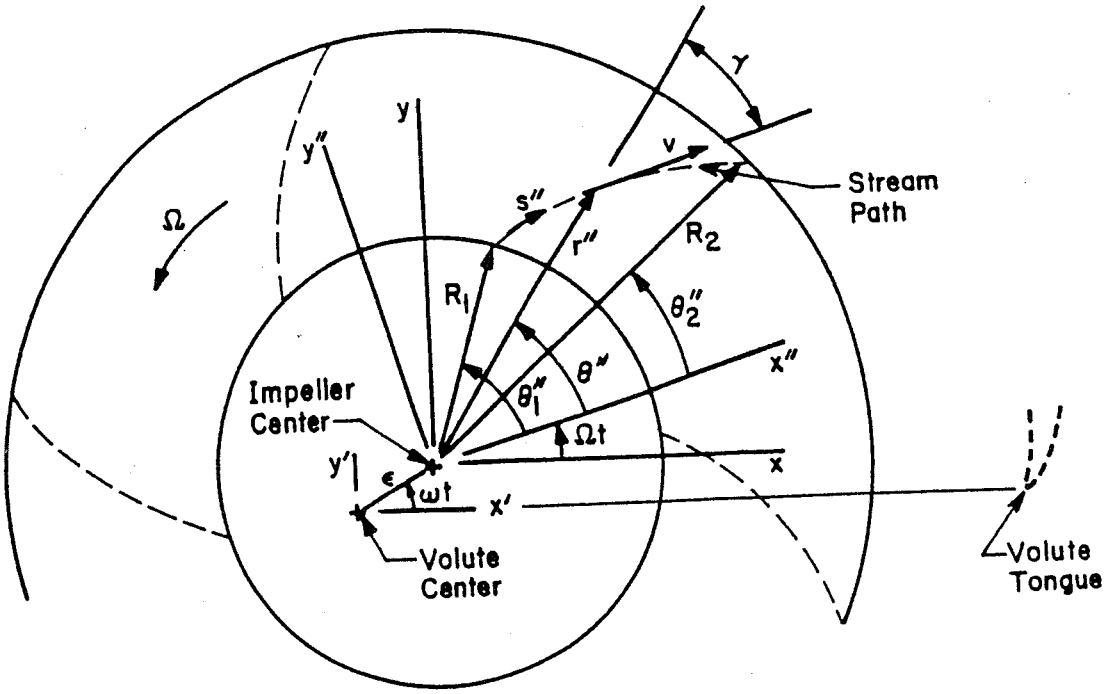

Adkins/Brennen Impeller Model (centered)

The impeller model equation at the impeller/volute interface with no inlet swirl is

$$2\phi \ln\frac{r_2}{r_1} \sec^2 \gamma \frac{d\beta}{d\theta} + \phi^2 \sec^2 \gamma \beta^2 + \frac{p(r_2,\theta)-p_{t1}}{\frac{1}{2}\rho(\Omega r_2)^2} - 1 = 0$$

Periodicity requires $\beta(0)=\beta(2\pi)$ and continuity $\frac{1}{2\pi}\int_0^{2\pi} \beta \, d\theta = 1$.

$$v_r = \frac{\phi \Omega r_2^2 \beta(\theta_2)}{r}$$

$$r_1 \le r \le r_2$$

$$\frac{v_\theta}{v_r} = -\tan \gamma$$

$$\phi = \frac{Q}{2\pi r_2^2 b_2 \Omega}$$

where

b_2	width of impeller discharge passage
p_1, p_2	impeller inlet, exit static pressure
p_{t1}	impeller inlet total pressure
Q	volume flow rate
r_1, r_2	impeller inlet, exit radius
v_r, v_θ	radial, azimuthal velocity relative to the impeller
$\beta(\theta)$	impeller relative velocity perturbation function
γ	impeller relative flow spiral angle
θ	angle measured in the stationary frame from the tongue in the direction of impeller rotation
ρ	fluid density
ϕ	flow coefficient
Ω	radian frequency of the impeller rotation

PARAMETERS TO DESCRIBE A VOLUTE CROSS-SECTION

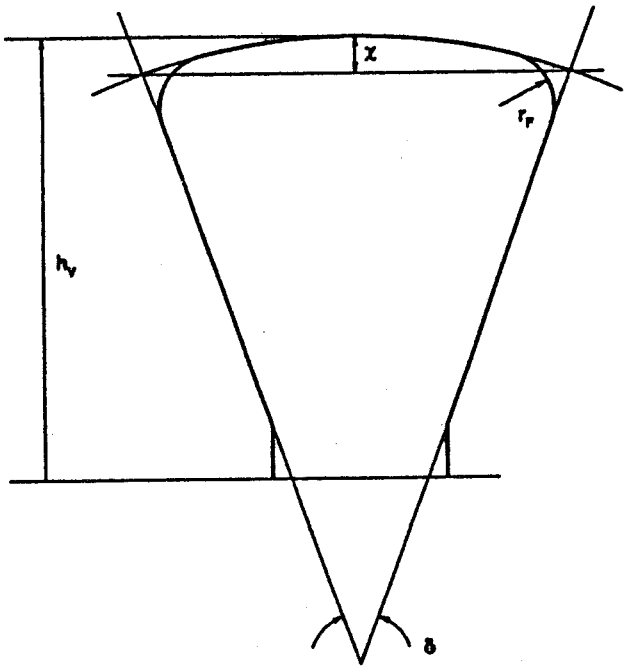

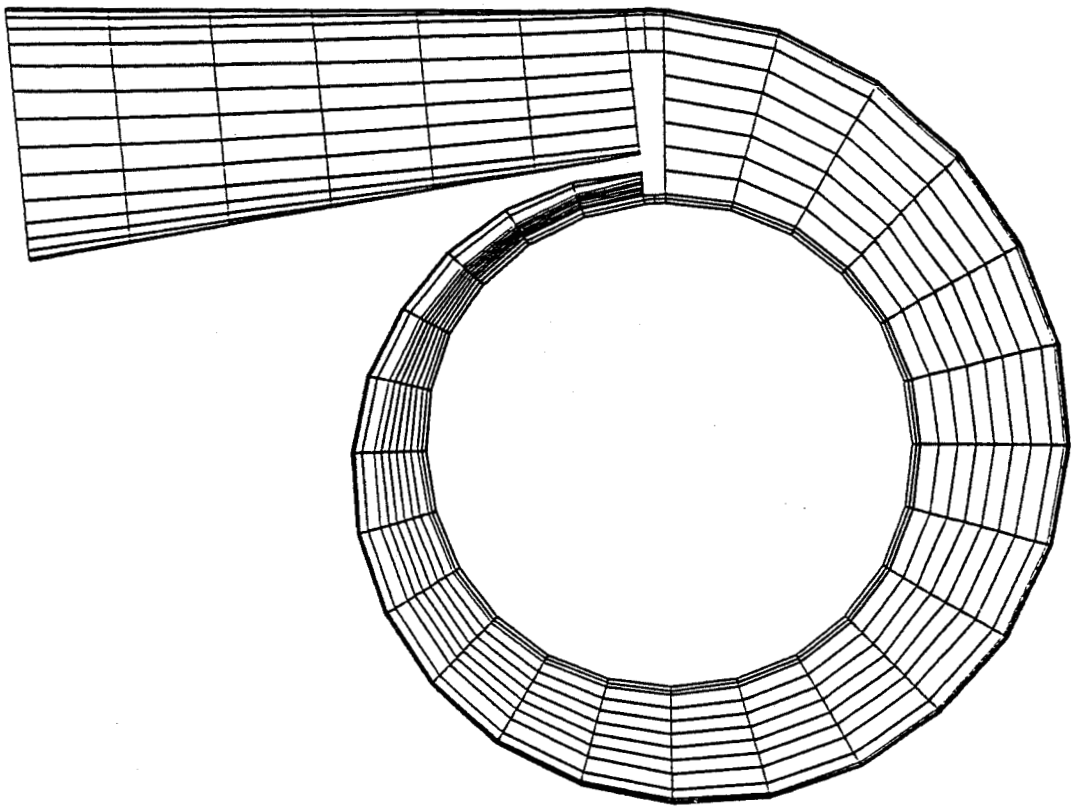

Volute surface, excluding the tongue region.

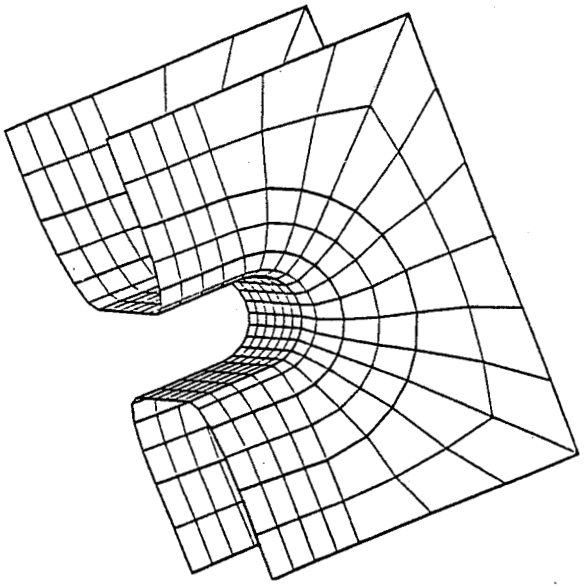

An illustration of generating the tongue surface.

EXTERIOR SURFACE OF VOLUTE GRID

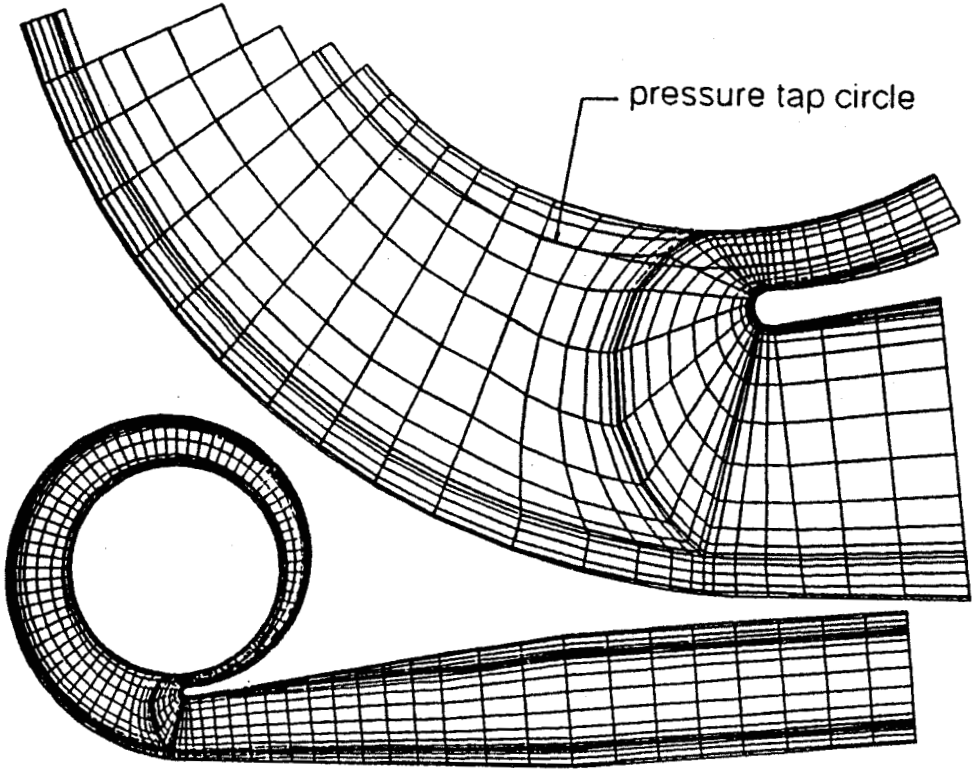

Volute Grid, With Pressure Tap Circle Indicated

FULLY COUPLED BASELINE SOLUTION

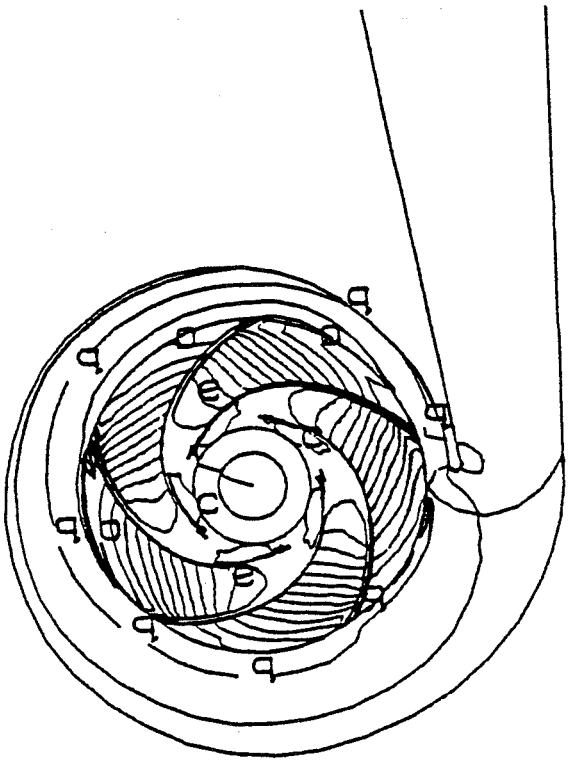

XMIN=-1.57E+01
XMAX= 1.67E+01
YMIN=-5.18E+00
YMAX= 2.25E+01

Color-Map:

a	9.7348E+01
b	9.8595E+01
c	9.9843E+01
d	1.0109E+02
e	1.0233E+02
f	1.0358E+02
g	1.0483E+02
h	1.0607E+02
i	1.0732E+02
j	1.0857E+02
k	1.0982E+02
l	1.1106E+02
m	1.1231E+02
n	1.1356E+02
o	1.1481E+02
p	1.1605E+02
q	1.1730E+02
r	1.1855E+02
s	1.1979E+02
t	1.2104E+02
u	1.2229E+02

Pressure contours φ=.092.

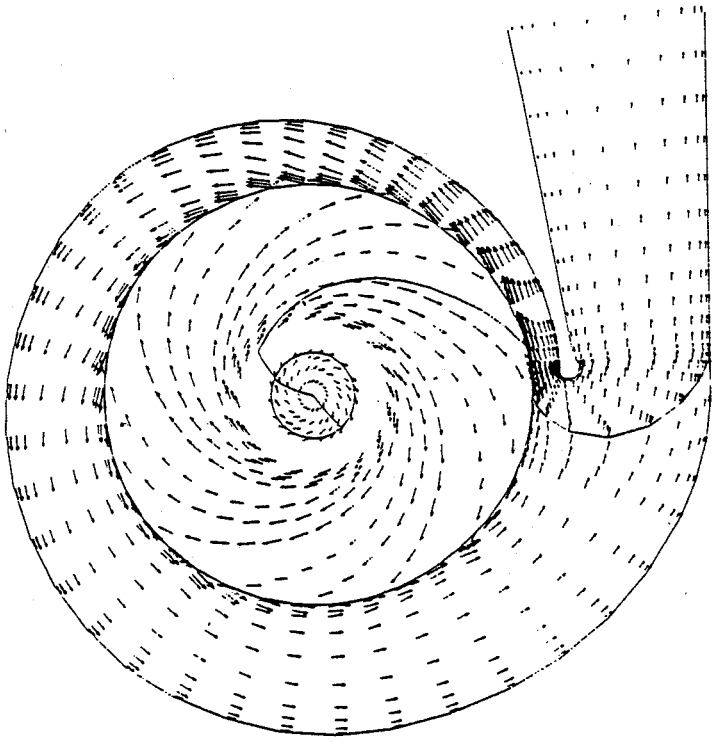

XMIN=-5.96E+00
XMAX= 7.02E+00
YMIN=-5.18E+00
YMAX= 5.88E+00

Color-Map

a	0.0000E+00
b	2.9183E-01
c	5.8367E-01
d	8.7551E-01
e	1.1673E+00
f	1.4591E+00
g	1.7510E+00
h	2.0428E+00
i	2.3347E+00
j	2.6265E+00
k	2.9183E+00
l	3.2102E+00
m	3.5020E+00
n	3.7938E+00
o	4.0857E+00
p	4.3775E+00
q	4.6694E+00
r	4.9612E+00
s	5.2530E+00
t	5.5449E+00
u	5.8367E+00

Velocity vectors φ=.092.

FULLY COUPLED BASELINE SOLUTION

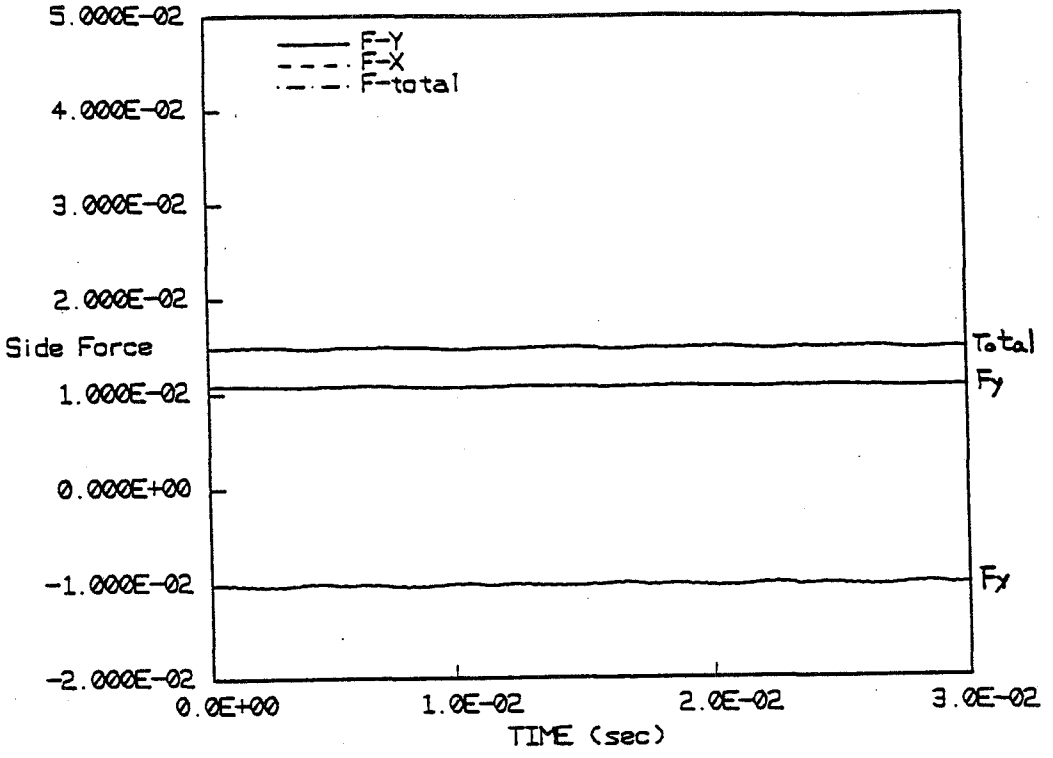

Force, magnitude and components, iteration history.

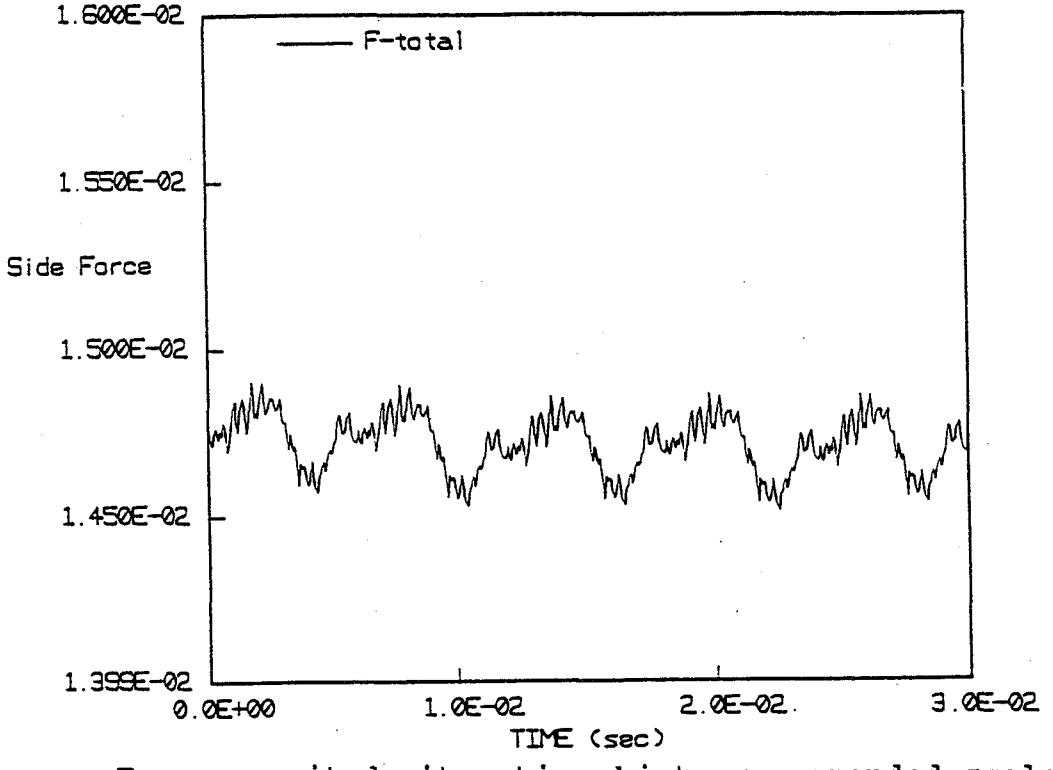

Force magnitude iteration history, expanded scale.

FULLY COUPLED BASELINE SOLUTION

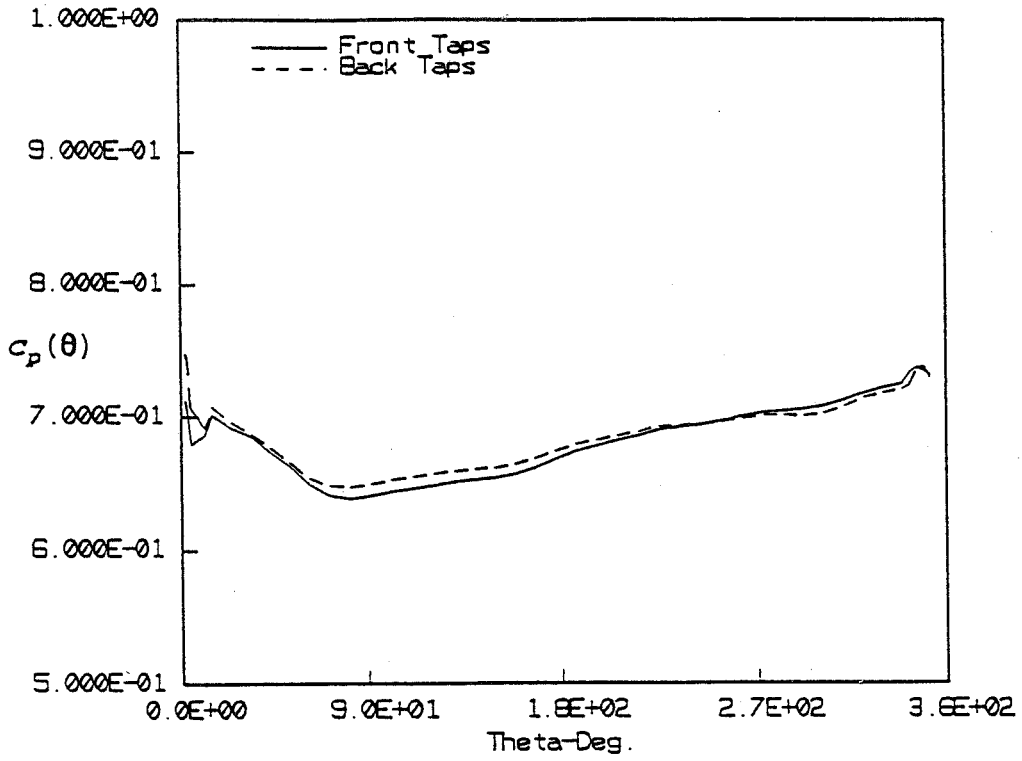

Pressure profile in the volute, φ=.092.

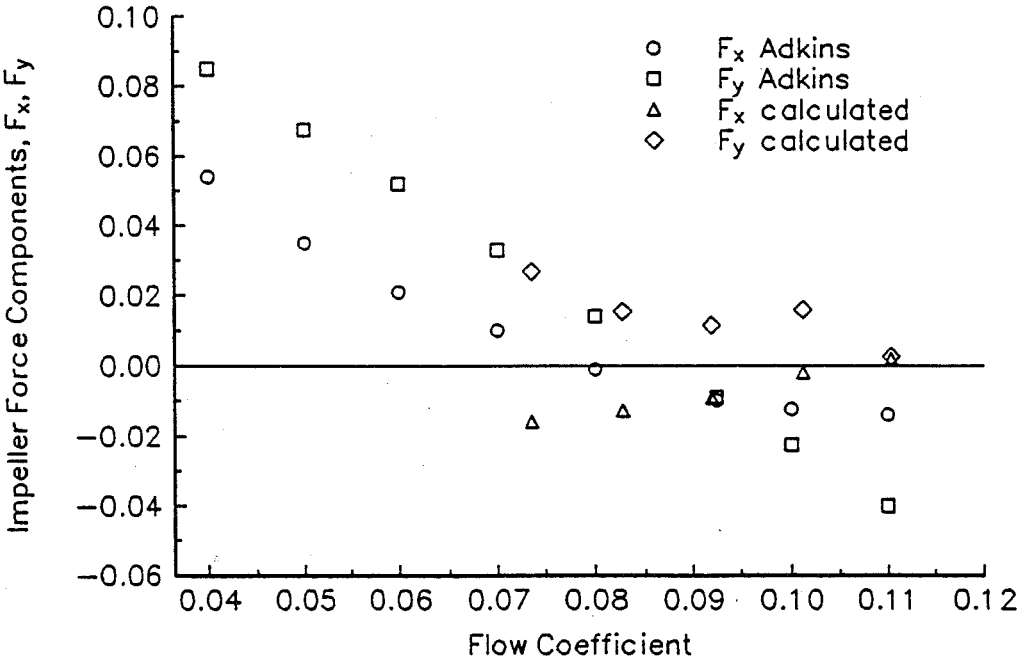

Force components as a function of flow coefficient.

CFD VOLUTE SOLUTION
WITH ADKINS/BRENNEN IMPELLER MODEL

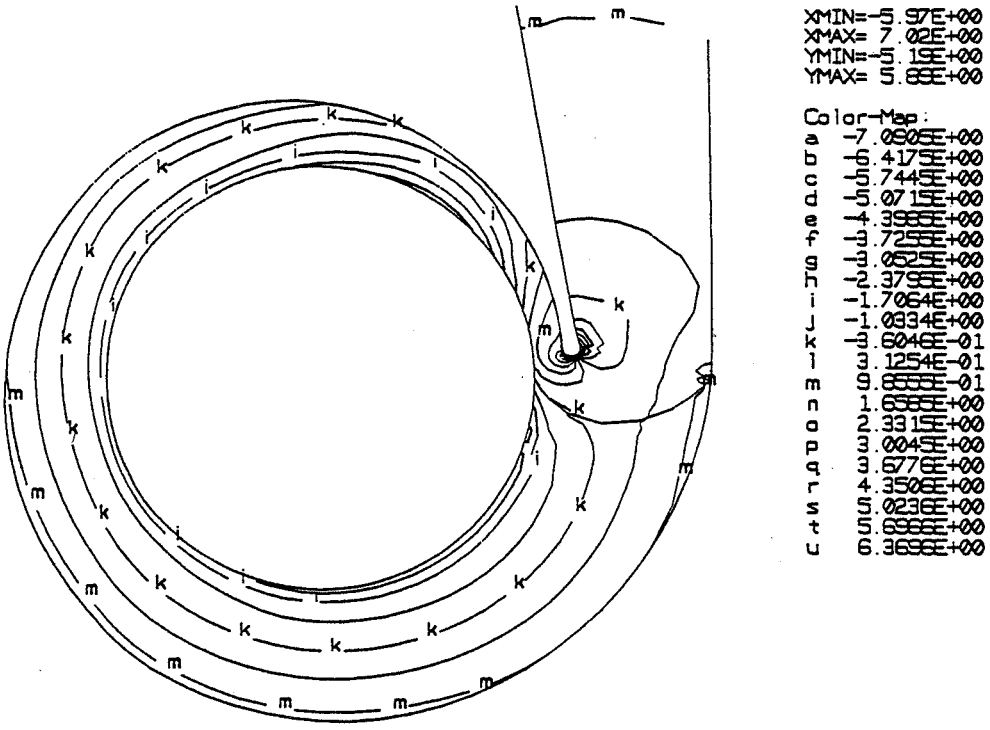

Pressure contours ϕ=.092.

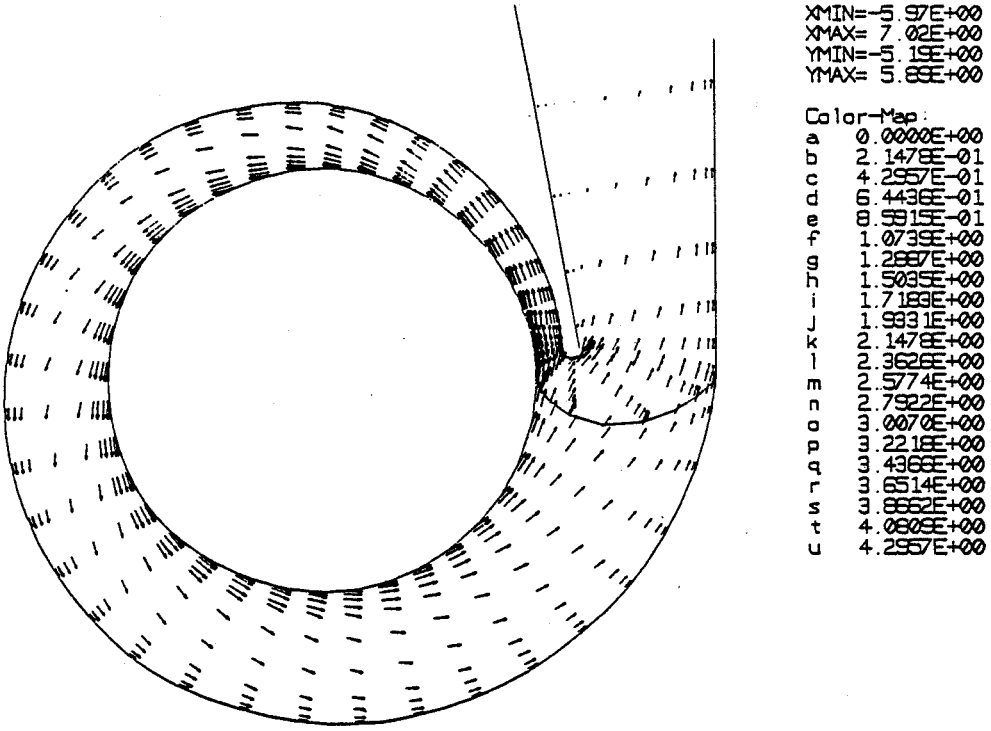

Velocity vectors ϕ=.092.

CFD VOLUTE SOLUTION
WITH ADKINS/BRENNEN IMPELLER MODEL

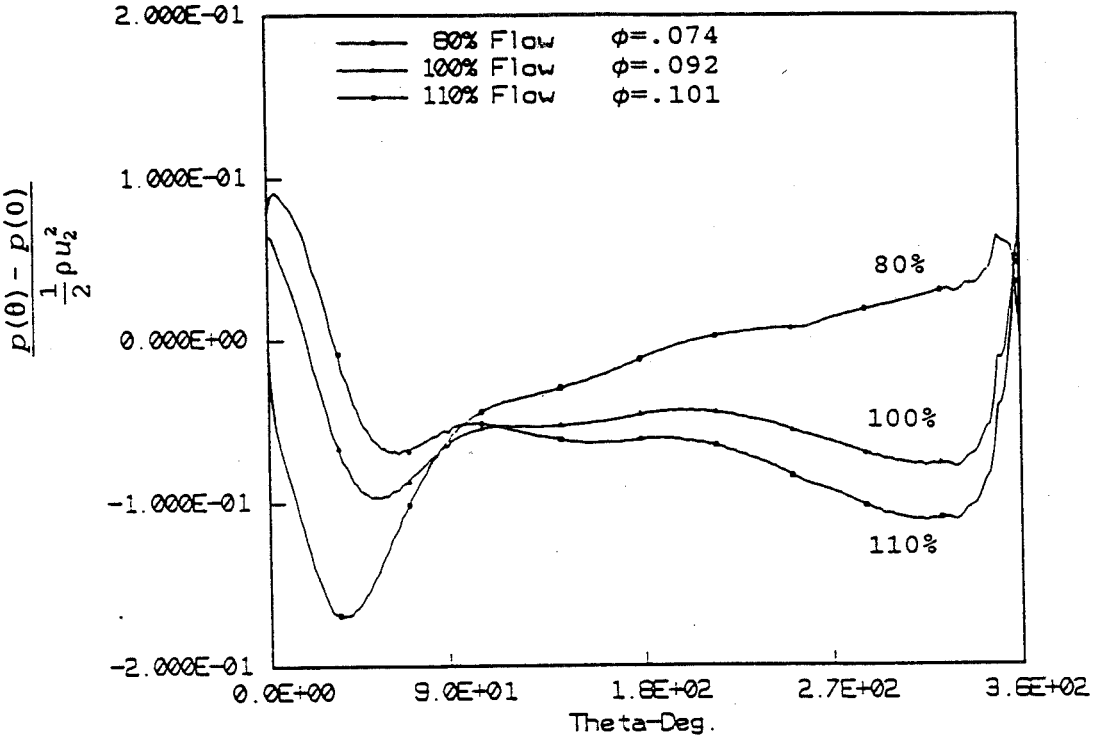

Volute pressure profile, from computation.

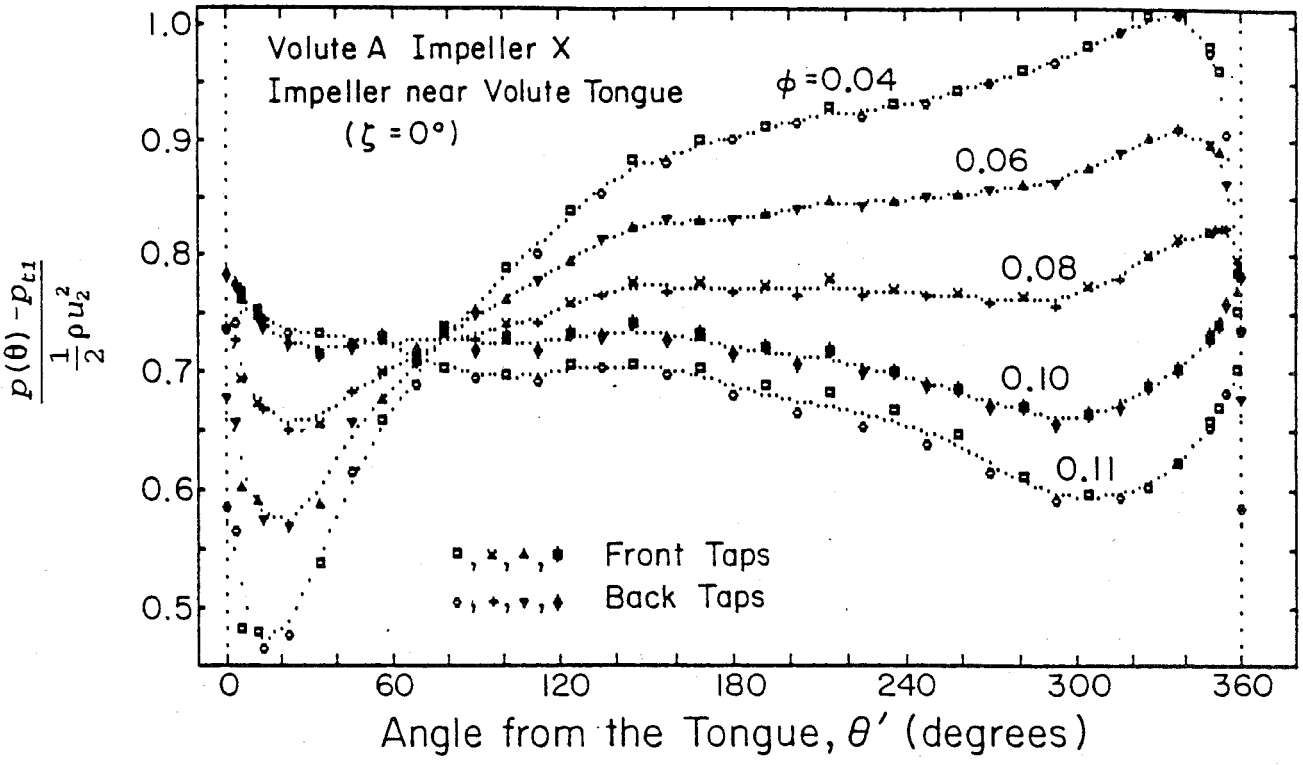

Volute pressure profile, from experiment (Adkins 1986).

CFD VOLUTE SOLUTION
WITH ADKINS/BRENNEN IMPELLER MODEL

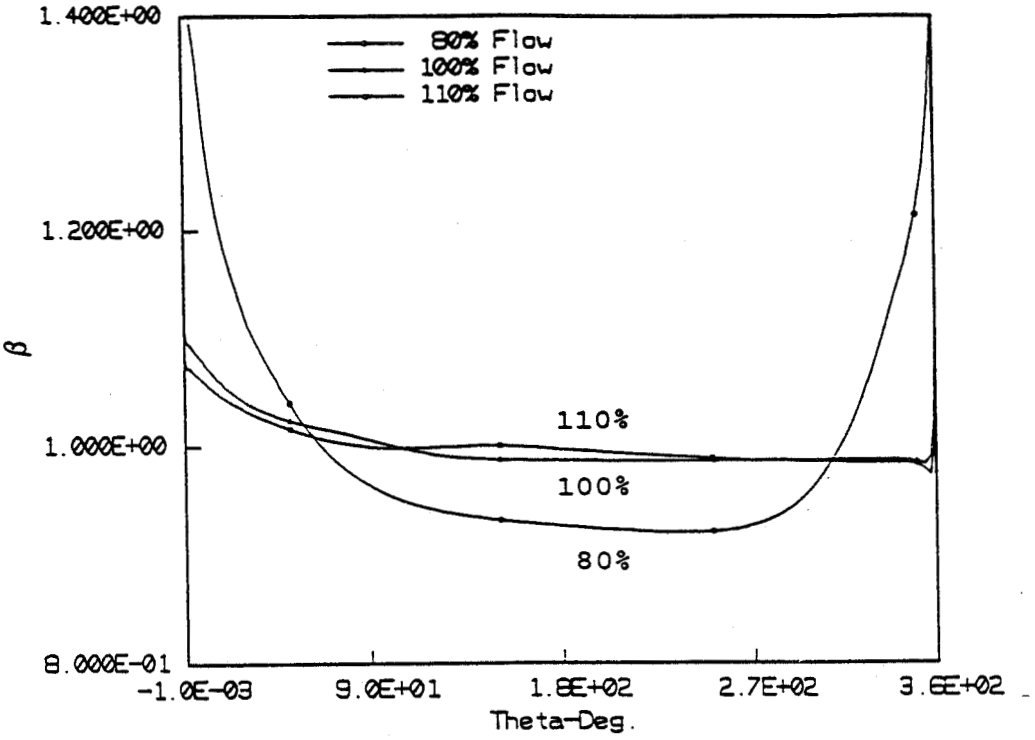

Relative velocity magnitude perturbation function, from computation.

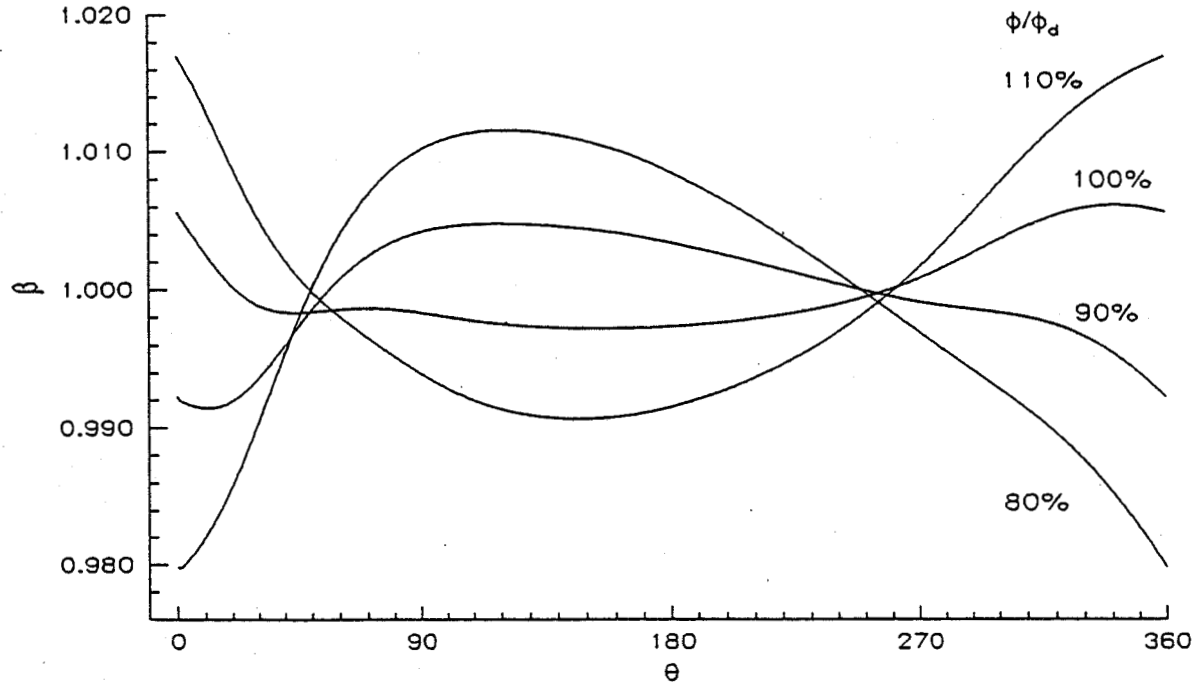

Relative velocity magnitude perturbation function, using Adkins' impeller/volute model.

CFD VOLUTE SOLUTION
WITH ADKINS/BRENNEN IMPELLER MODEL

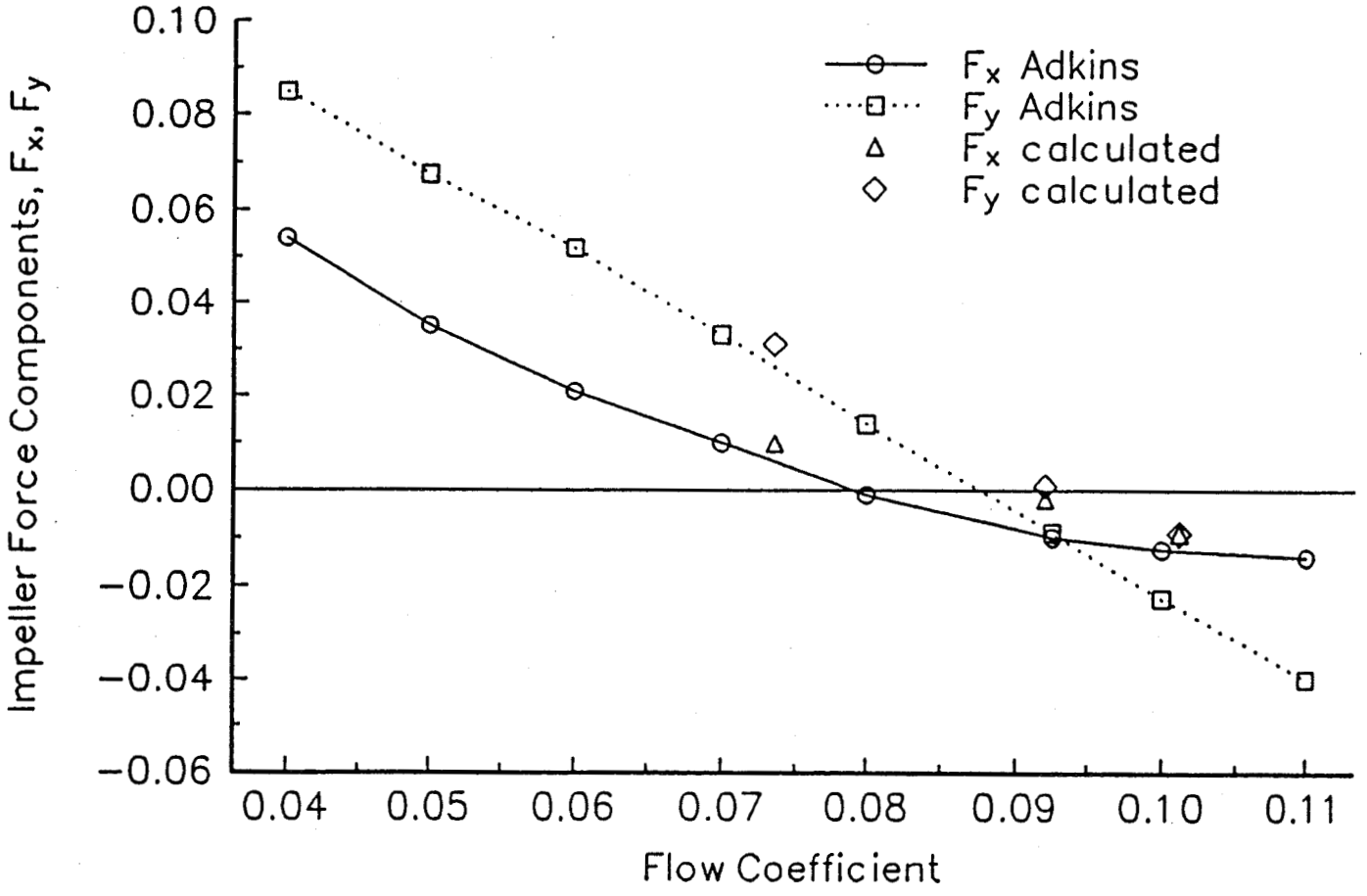

Force components as a function of flow coefficient.

CONTOUR VARIATIONS

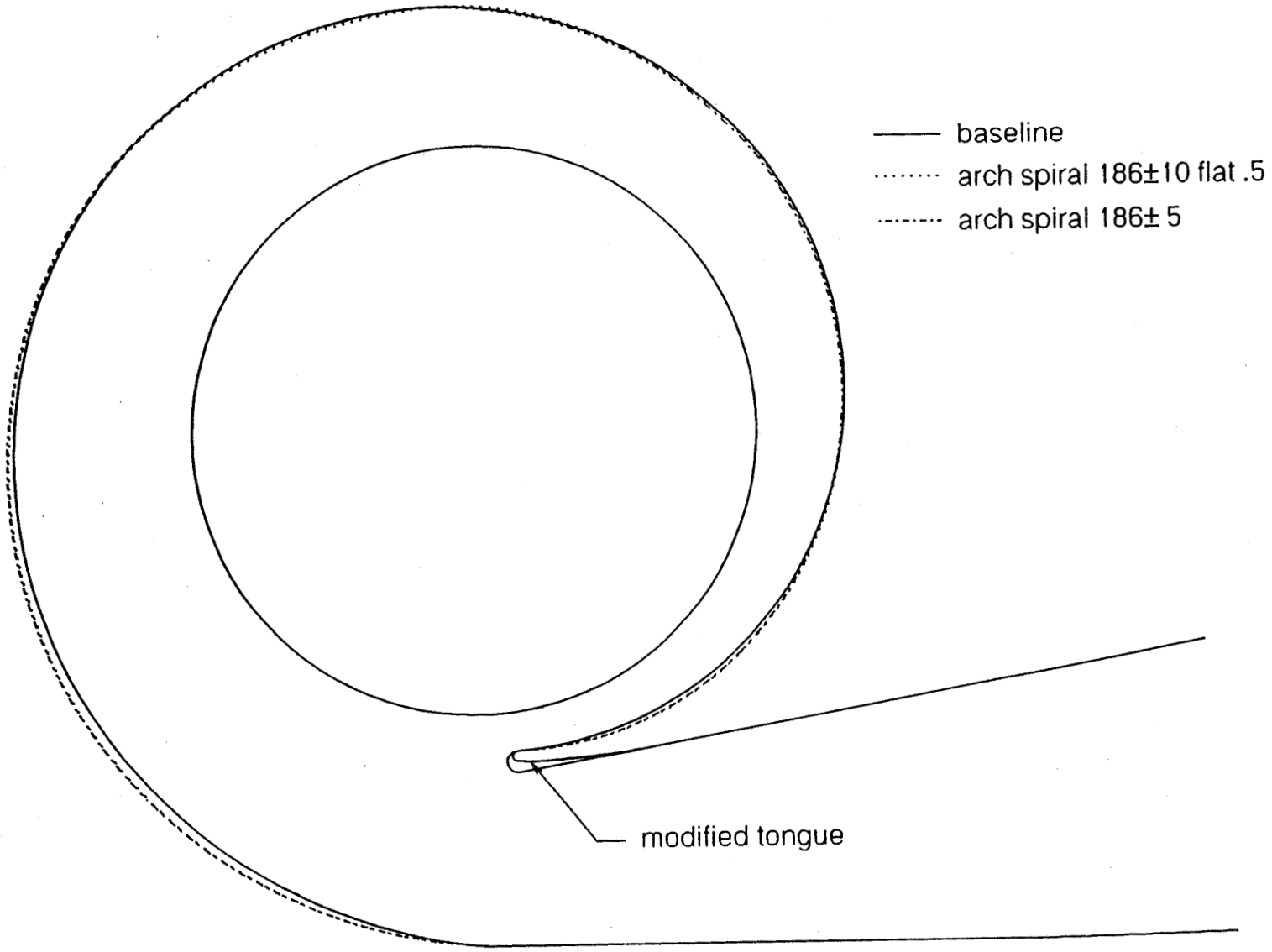

SPIRAL VARIATIONS

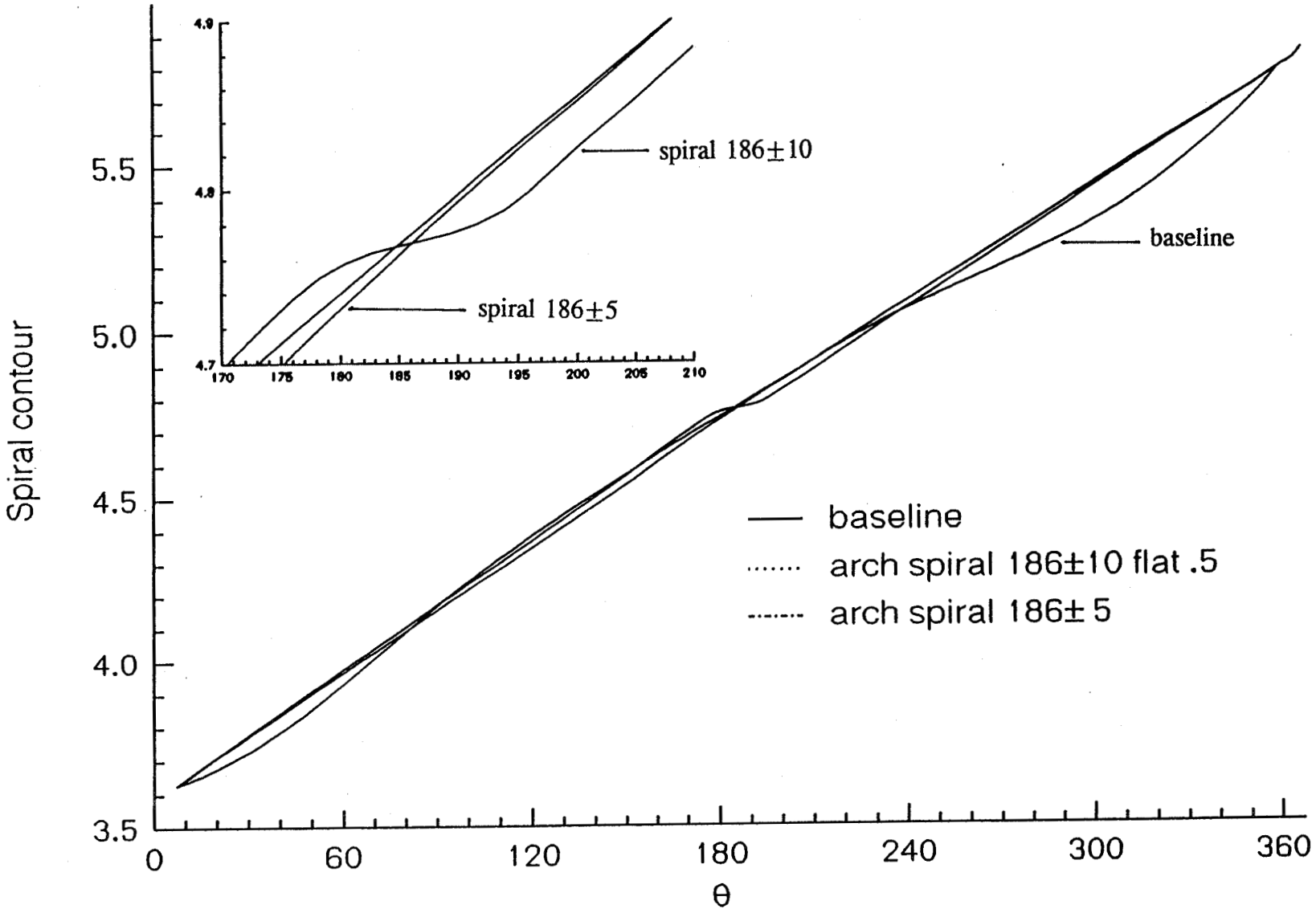

AREA VARIATIONS

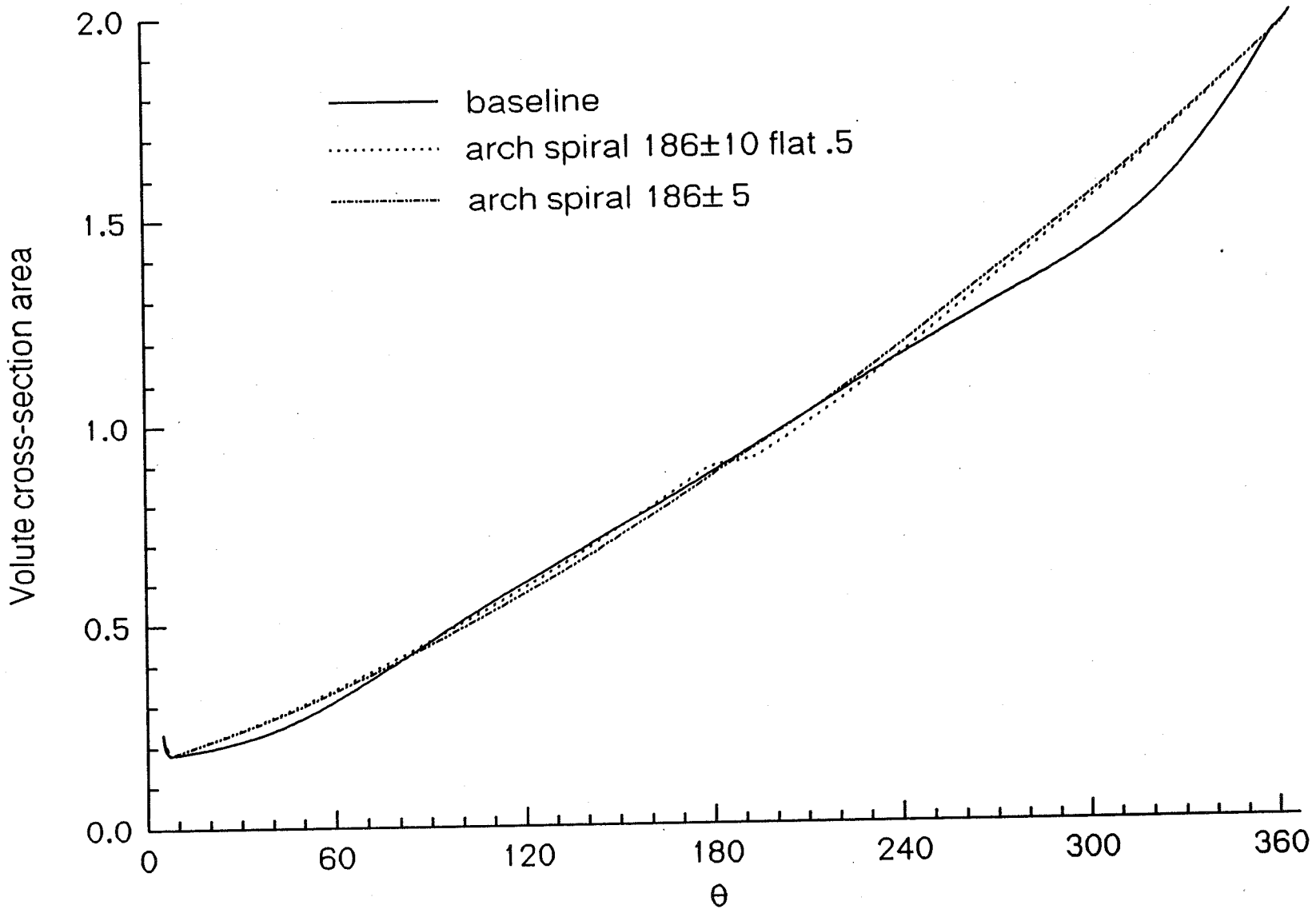

DERIVATIVE OF AREA VARIATIONS

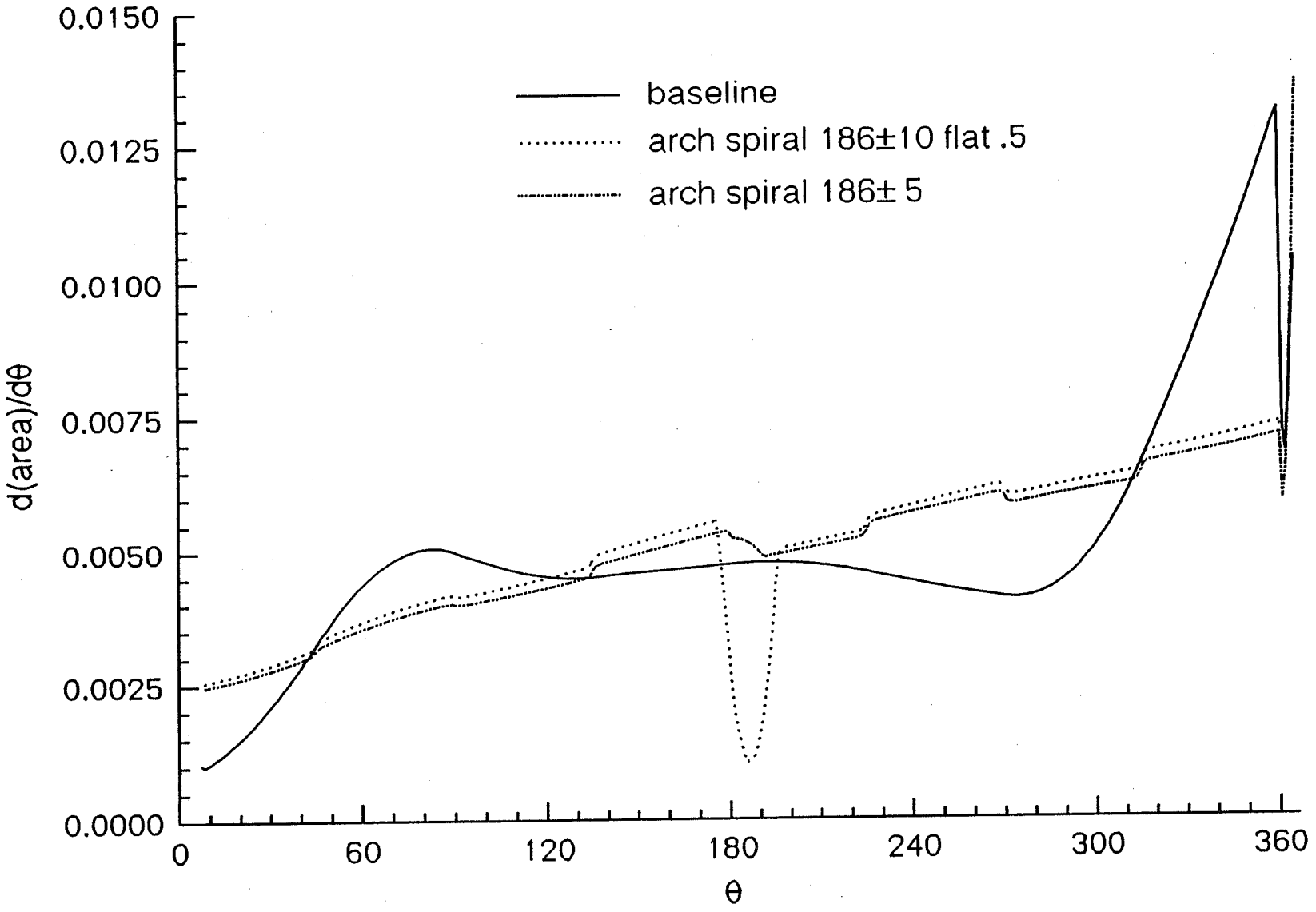

GEOMETRY VARIATION EFFECTS

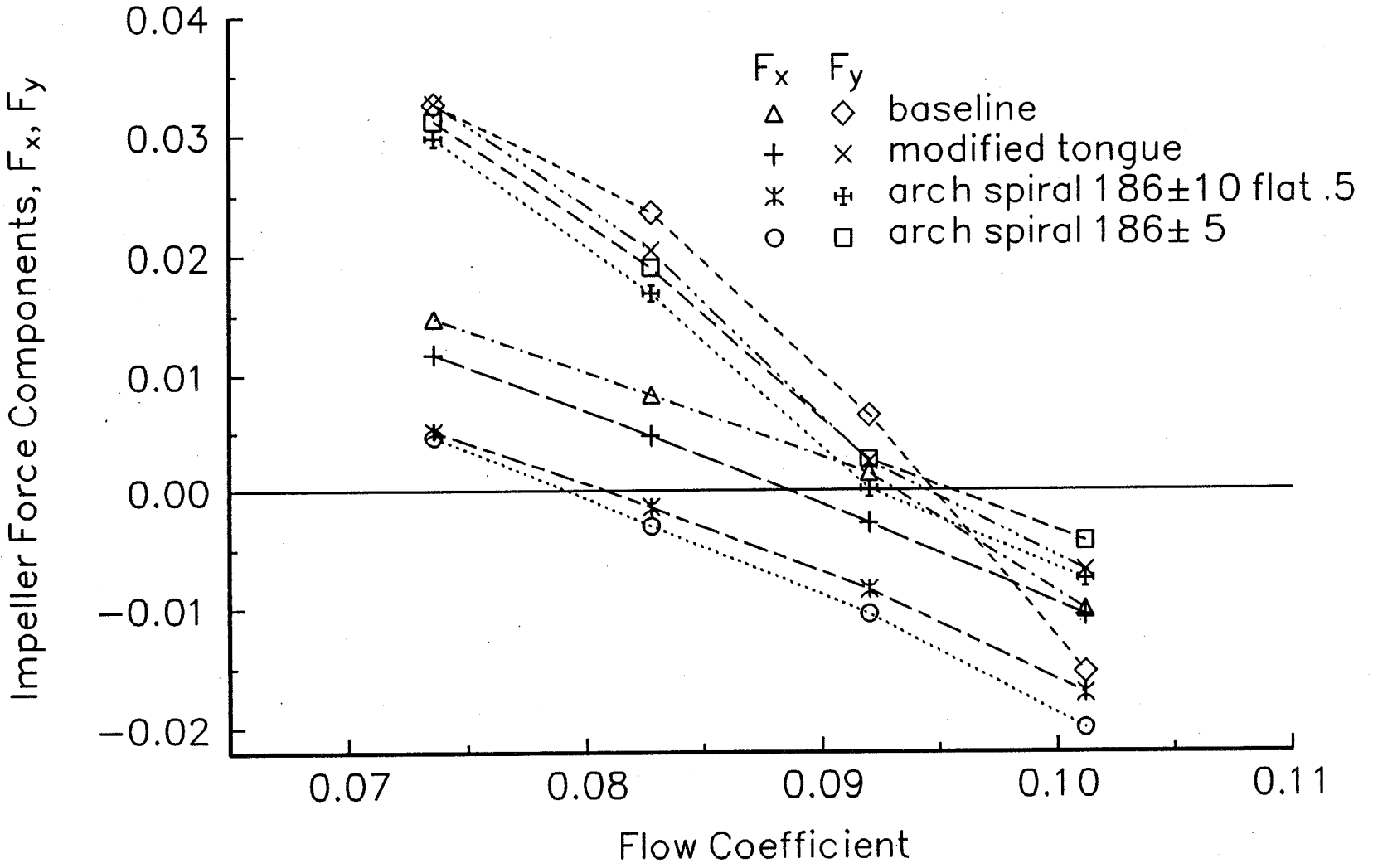

RADIAL FORCES VS. FLOW COEFFICIENT

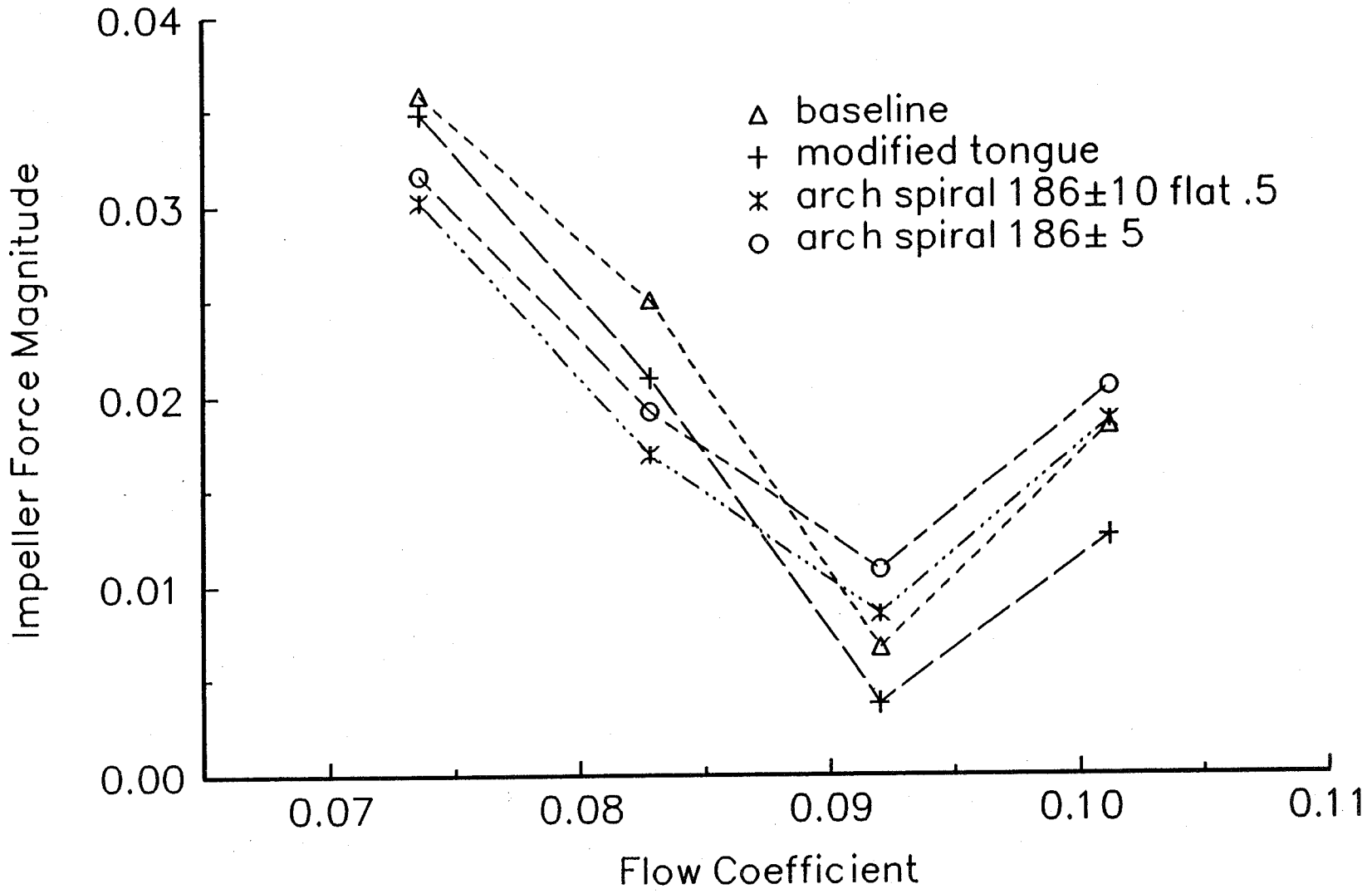

PUMP MODEL PREDICTIONS COMPARED TO CALTECH EXPERIMENTS

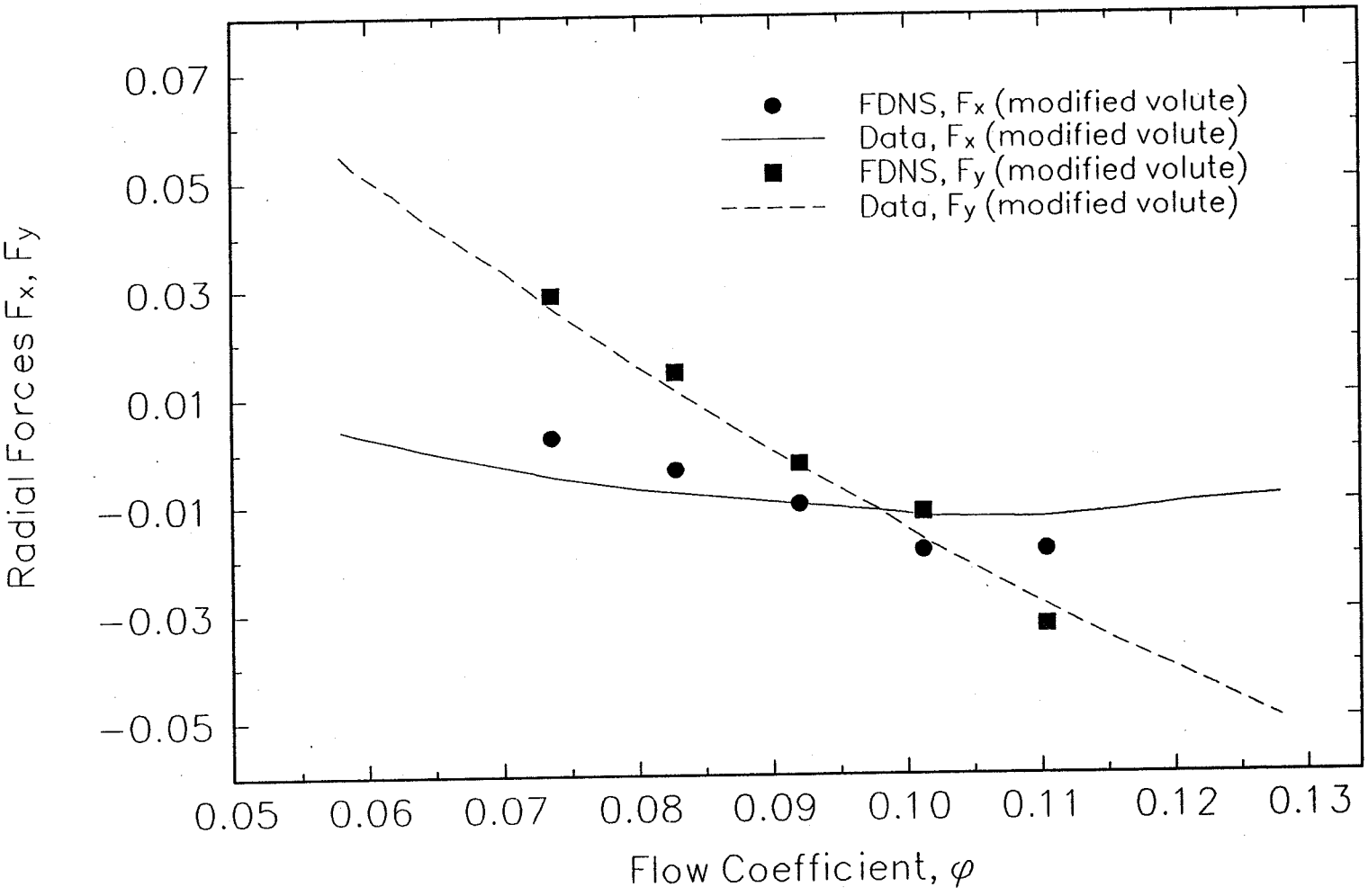

MODIFIED VOLUTE COMPARED TO VOLUTE A

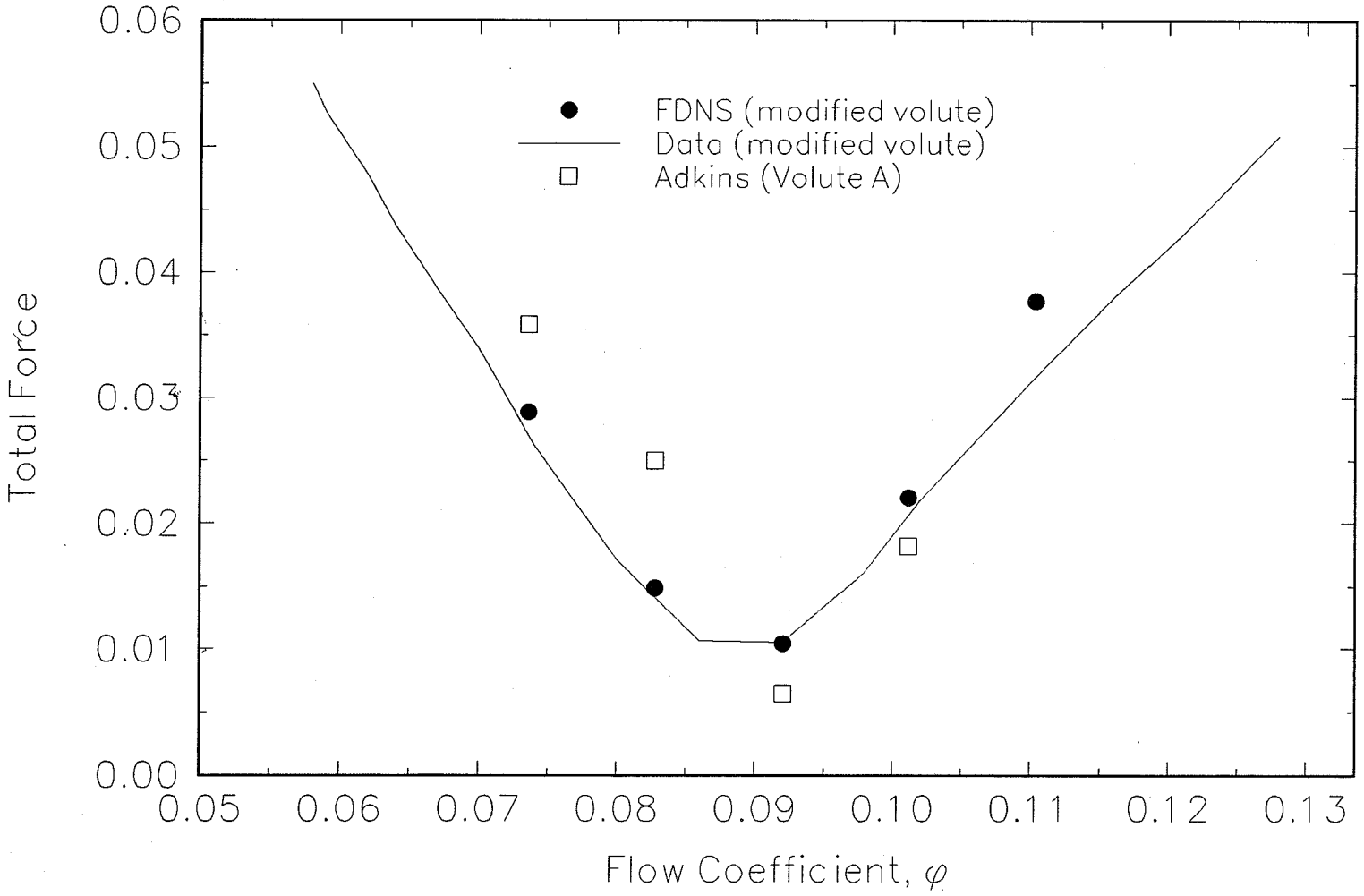

CONCLUSIONS:

(1) A useful volute grid generator was developed.

(2) Coupled impeller/volute CFD solutions are feasible, but faster solution methods should be used for parametric studies.

(3) The Adkins/Brennen impeller model coupled to the CFD volute model provides a practical design tool for optimizing volute geometries. One fully coupled impeller/volute solution should be made for each impeller configuration at the design point.

(4) The model described in (3) was used to design a volute and experiments validated the design.

(5) The design methodology can be used to minimize or set to a prescribed value the radial forces on a pump by controlling volute geometry.

RECOMMENDATIONS:

(1) The grid generator should be extended to provide an option for providing the volute surface in an IGES format.

(2) The CFD pump model should be exercised to describe a wide range of volute configurations.

(3) The model should be applied to studies of vaned volutes, vaned diffusers, and cross-over ducts.

(4) The model should be extended to treat impeller/volute rotordynamic interactions.

Page intentionally left blank

Computational Analysis of Volutes

E. D. Lynch
CFD Technology Center
Rocketdyne Division, Rockwell International

ABSTRACT

Volutes have an important influence on the performance of rocket engine turbines because of the requirement for efficient collection of the turbine influx and efflux. However, because of the complex nature of volute geometries, volute analysis has received relatively less attention than analysis of the turbine rotor.

This paper presents a methodology for the analysis of volutes, focusing on the analysis of exit volutes where the high subsonic entrance Mach numbers (i.e., ca. M = 0.8) lead the effects of compressibility to play an important role. To treat the complex volute geometries, a multizone numerical framework was combined with an accurate scheme for translating the CAD geometry and an appropriate grid topology near the tongue lip (viz., a "fan" grid). The RAGGS (Rockwell Automated Grid Generation System) code was instrumental in the rapid processing of a reasonable grid. The multizone and compressibility capabilities were upgrades from the existing REACT (Rocketdyne Elliptic Analysis Code for Turbomachinery) incompressible code which employs a conjugate-gradient-based, pressure-correction-scheme, solution advancement methodology with allowance for a rotating coordinate system reference frame. A second-order, fully-upwind discretization of the density was adopted in the pressure correction equation, and variable density and viscosity effects were incorporated. In the multizone framework an option for global iteration between the zones was created to prevent pressure waves from building up at the zonal boundaries. This feature proved especially important when large entrance swirl increased the flowfield communication between the zones.

This paper presents preliminary three-dimensional, compressible, full Navier-Stokes results for the exit volute at the outlet of the Gas Generator Oxidizer Turbine. Interpretations of the results of this calculation are then made to yield unique insights into volute operation.

COMPUTATIONAL ANALYSIS OF VOLUTES

E. D. Lynch

CFD Technology Center

Rocketdyne Division,
Rockwell International

Thirteenth Workshop for CFD

Applications in Rocket Propulsion
and Launch Vehicle Technology

Huntsville, Alabama

April 25-27, 1995

NEEDS FOR VOLUTE ANALYSIS

- **EFFICIENT COLLECTION OF TURBINE FLOW ESSENTIAL FOR BEST OVERALL PERFORMANCE**

- **VOLUTE FLOWS ARE THREE-DIMENSIONAL AND COMPLEX**
  - LARGE SWIRL GENERATES SIGNIFICANT SECONDARY FLOWS
  - COMPRESSIBILITY EFFECTS SIGNIFICANT FOR TURBINE EXIT VOLUTE (ENTRANCE M ~ 0.8)

- **RELATIVELY LITTLE 3-D CFD ANALYSIS PERFORMED TO DATE**

VOLUTE GEOMETRY AND FLOW CONDITIONS

- **EXIT VOLUTE DESIGN FOR GAS GENERATOR OXIDIZER TURBINE**
- **INFLOW CONDITIONS**
  - TURBINE EXIT/VOLUTE ENTRANCE MACH NUMBER ~ 0.8
  - SWIRL VELOCITY 3.7 TIMES AXIAL VELOCITY
- **EXIT VIA COLLECTION DUCT (EXTENDED TO ALLOW ZERO GRADIENT EXIT BOUNDARY CONDITION)**
- **CONDITIONS REPRESENTATIVE OF TYPICAL EXIT VOLUTE**

REACT CODE METHODOLOGY FOR VOLUTE ANALYSIS

- **PRESSURE CORRECTION METHODOLOGY**
- **FULL NAVIER–STOKES ANALYSIS WITH k-ε TURBULENCE MODEL**
- **MULTIPLE ZONE TREATMENT**
  - EXPLICIT UPDATE BETWEEN ZONES
  - INCLUSION OF TRANSIENT TERMS TO MITIGATE ZONES ADVANCING AT DIFFERENT SPEEDS
- **COMPRESSIBILITY EFFECTS**
  - ENERGY EQUATION SOLVED TO ALLOW FOR VARIABLE DENSITY AND VISCOSITY
  - DENSITY COMPONENT TO PRESSURE CORRECTION TREATED
  - PRESSURE CORRECTION EQUATION SOLVED WITH BICONJUGATE SOLVER—CONJUGATE GRADIENT INAPPLICABLE
- **3-ZONE GRID (121,000 POINTS) GENERATED WITH ROCKWELL AUTOMATED GRID GENERATION SYSTEM (RAGGS) FROM CAD GEOMETRY FILE**

VARIOUS ISSUES ENCOUNTERED DURING ANALYSIS

- FLOW SOLUTION IN SMALL GRID CELLS (e.g., NEAR TONGUE) UNPHYSICALLY ACCELERATED BY RELAXATION METHOD — NUMERICAL INSTABILITIES GENERATED
- STRONG PRESSURE PULSES MOVE AROUND RACETRACK DURING STARTUP TRANSIENTS CAUSING WAVE-LIKE STRUCTURES TYPICAL OF ROTATING FLOWS
- HAMMER SHOCKS FROM EXIT BOUNDARY CONDITION RELATIVELY SEVERE AT START DUE TO HIGH MACH NUMBER
- PRESSURE WAVES TEND TO CONSOLIDATE AT ZONAL BOUNDARIES
- SWIRL & CENTRIFUGAL FORCES INDUCE RADIAL PRESSURE GRADIENT AND SET UP STRONG SECONDARY CIRCULATION
- TONGUE ACTS AS POOR AIRFOIL INDUCING COMPRESSION AND REEXPANSION

SOLUTIONS IMPLEMENTED TO ADDRESS NUMERICAL ISSUES

- **INCLUDE TRANSIENT TERMS IN RELAXATION EQUATIONS**
  - PREVENT ZONES FROM CONVERGING AT WIDELY DIFFERENT SPEEDS
  - PREVENT SOLUTION IN SMALL CELLS FROM BEING ARTIFICIALLY ACCELERATED
- **UNDERRELAX EXIT FLOW CONDITION TO AMELIORATE HAMMER SHOCKS**
- **INITIALLY ADD DISSIPATION TO PRESSURE EQUATION TO SMOOTH OUT PRESSURE DISTURBANCES**
- **ADD LOCAL DISSIPATION NEAR TONGUE AND FAN TO PREVENT LOCAL INSTABILITIES**

EXIT VOLUTE GRID

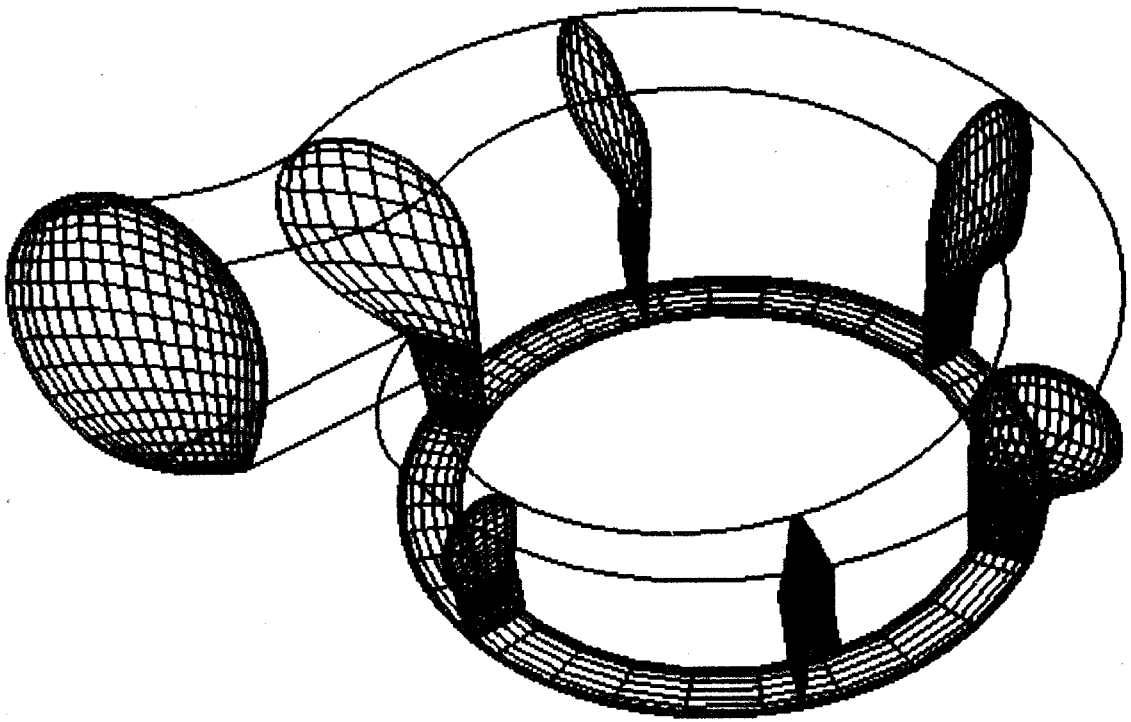

EXIT VOLUTE ANALYSIS

PARTICLE TRACES

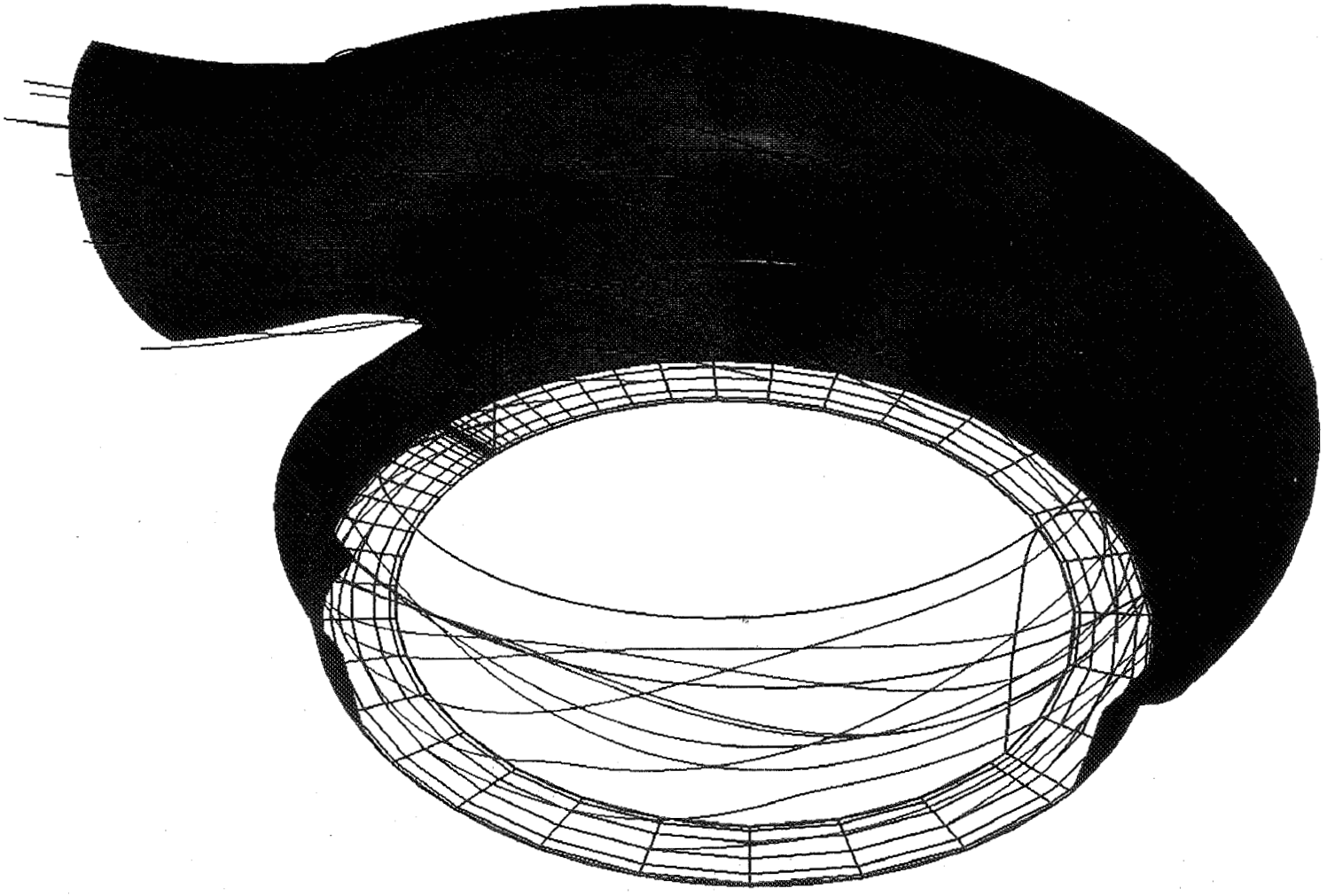

EXIT VOLUTE ANALYSIS

PRESSURE CONTOURS

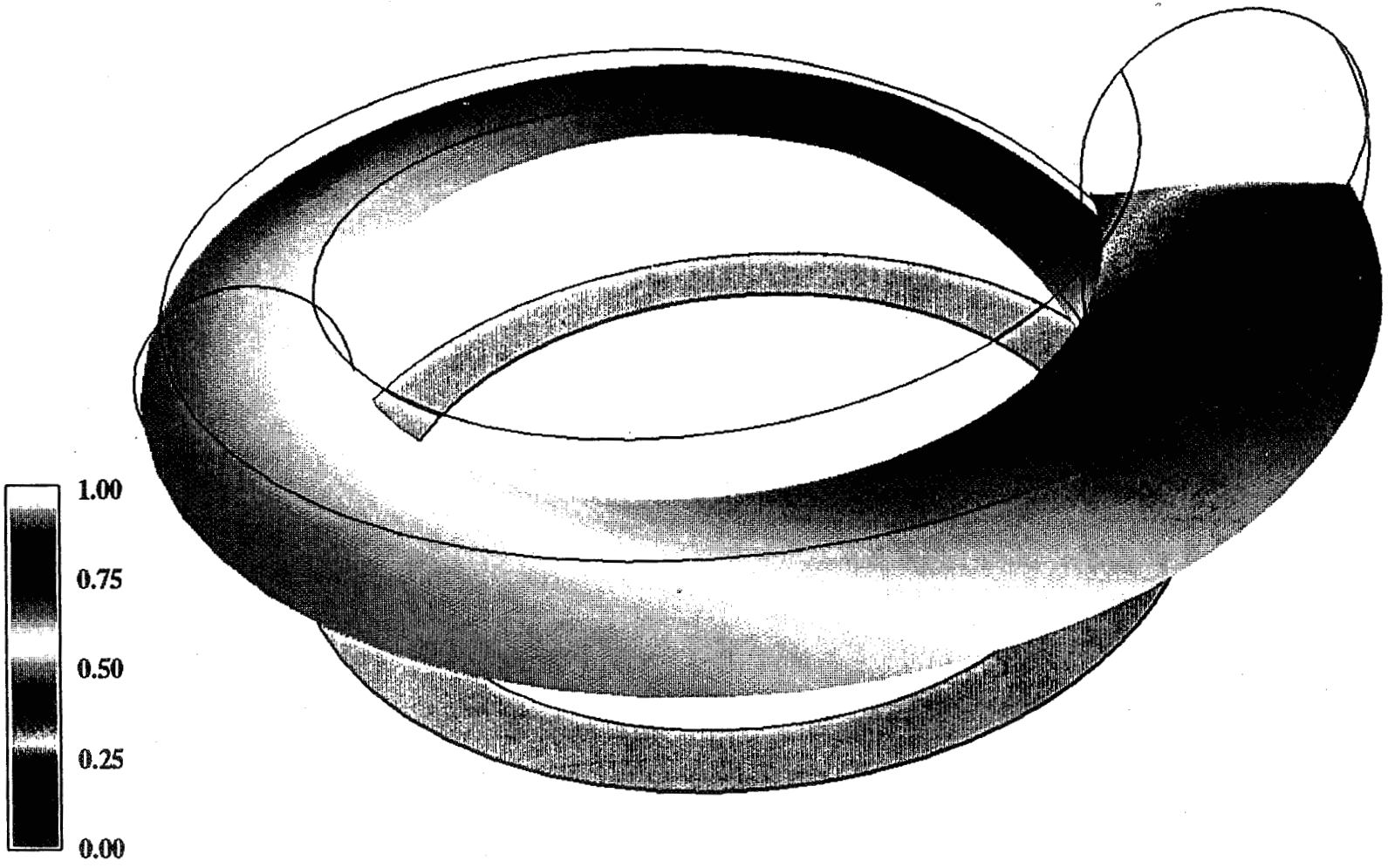

Rockwell Aerospace
Rocketdyne

EXIT VOLUTE ANALYSIS

VELOCITY CONTOURS

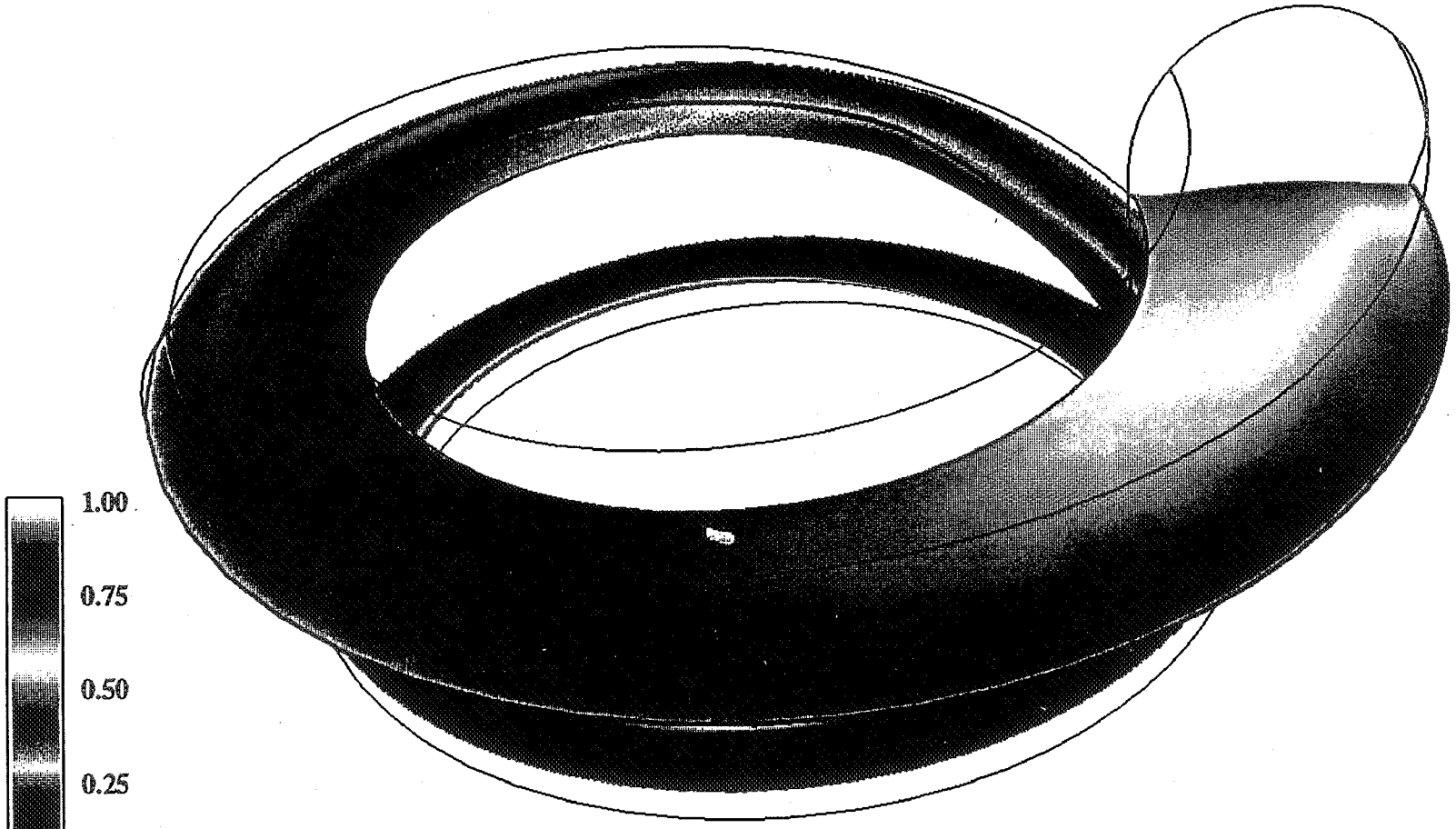

Rockwell Aerospace
Rocketdyne

CFD Technology Center

SUMMARY

- **REACT CODE UPGRADED TO MODEL EXIT VOLUTE**
  - COMPRESSIBILITY
  - TRANSIENT TERMS TO TREAT MULTIPLE ZONES WITH STRONG INTERZONAL INFLUENCE
  - SOLUTION APPROACH DEVELOPED

- **PRELIMINARY EXIT VOLUTE RESULTS OBTAINED**
  - PRESSURE GREATER ON OUTSIDE WALL DUE TO CENTRIFUGAL EFFECTS
  - VELOCITY DECREASES WITH DUCT EXPANSION
  - VORTICAL SECONDARY FLOW ESTABLISHED IN TOP VOLUTE RACETRACK
  - SOME PARTICLES APPEAR TO GET TRAPPED IN SECONDARY FLOW

3-D COMPUTATIONAL FLUID STRUCTURE INTERACTION (FSI) FOR TURBOMACHINERY: METHODOLOGY DEVELOPMENT FOR CALCULATION OF ROTORDYNAMIC FLOWS

13th WORKSHOP FOR CFD APPLICATIONS TO ROCKET PROPULSION
MARSHALL SPACE FLIGHT CENTER
APRIL 25-27, 1995

M. Williams*, W. Chen+, L. Brozowski+, A. Eastland+, M. Sindir*

+ Advanced Rotating Machinery
* CFD Group

Rockwell Aerospace
Rocketdyne

AGENDA

- **Background**
- **Objective**
- **Status**
- **Basic Numerical Methodology**
- **Results And Comparison With:**
  - Daily & Nece
  - Cyl-in-Cyl Damping And Added Mass
  - Texas A&M Centered Seal
  - Texas A&M 50% Static Eccentric Seal
  - Texas A&M 50% Dynamic Eccentric Seal
  - Cal Tech Impeller Shroud
- **Concluding Remarks**

BACKGROUND

- **Stable Turbomachinery Operation Depends On The Damping Of The Rotor Motion**
- **Currently, Rotordynamic Stability Parameters Are Estimated By Using Bulk Flow Theories And Small Perturbation Assumptions (e.g. Black, Childs)**
  - Larger Uncertainty in Predicting Impeller Shroud Force Coefficients
  - Limited Use As Design Tool

- **Navier-Stokes Based Methodologies For Rotordynamic Calculations Have Been Developed (e.g., Dietzman et al., Przekwas et al, Bashkarone et al.)**
  - These Methodologies Also Utilize A Small Perturbation Assumption
- **What's Involved In Navier-Stokes Rotordynamic Flow Calculations ?**
  - Moving Rotor, Eccentricity
  - Unsteady, Incompressible Viscous Flow
  - 3-D Geometries With Large Area Changes
  - Time-Periodic Rotor Shaft Forces

EXAMPLE OF ROTOR RESPONSE MODEL (PRAGENAU)

ROTORDYNAMIC FLOW FORCES ARE REPRESENTED BY K AND C COEFFS.; THESE FLOW COEFFICIENTS MUST BE KNOWN TO PREDICT ROTORDYNAMIC STABILITY

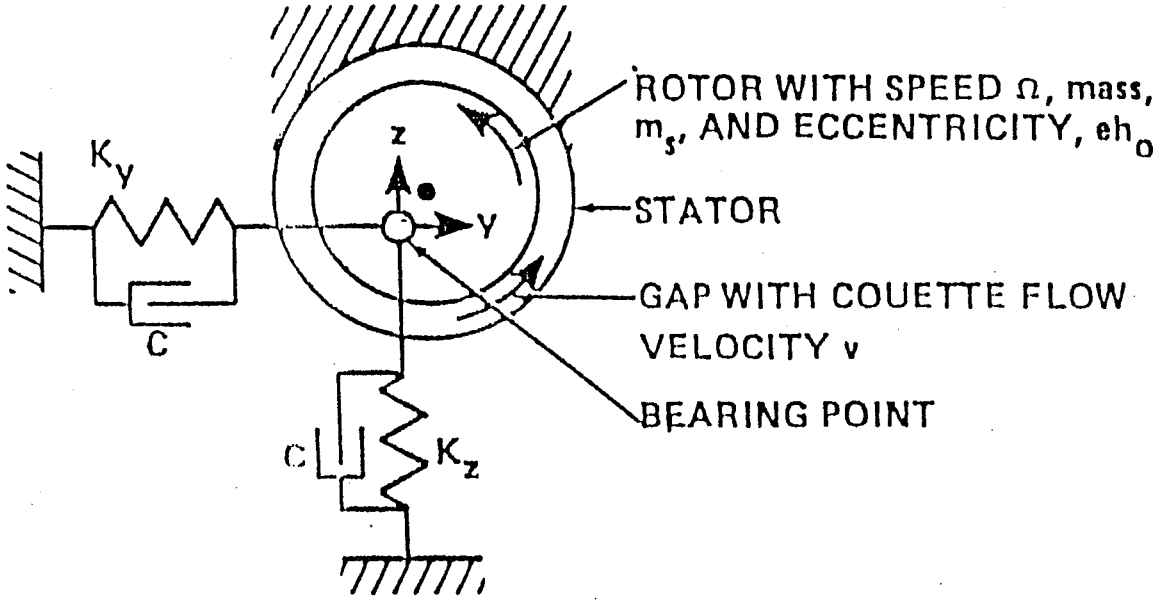

$$\begin{Bmatrix} y \\ z \end{Bmatrix} = \begin{bmatrix} K_z + sC + s^2 m_s & -c\Omega C \\ c\Omega C & K_y + sC + s^2 m_s \end{bmatrix} \begin{Bmatrix} F_y \\ F_z \end{Bmatrix} D^{-1}$$

OBJECTIVE

- **A Navier-Stokes Based Methodology For The Calculation Of Rotordynamic Parameters Is Needed**
  - To Increase The Generality Of The Methodology, It Should Allow For Relatively Large Rotor Motions And It Should Not Rely On Bulk And Couette Flow Assumptions
- **The Objective Of The Current Effort Is To Build On Rocketdyne's 2-D Fluid-Structure Interaction (FSI) Work And Develop A Time-Accurate Navier-Stokes Scheme For Rotordynamic Flows (With Arbitrary Rotor Motion)**

STATUS

- **Small Scale Effort (~8 hrs/week)**
- **Basic Methodology For 3-D Rotordynamic Flow Calculations Implemented**
  - 3-D Scheme Builds On Previous In-House 2-D FSI Work
    - Goal Is To Include Same Basic Features As Previous 2-D FSI Scheme
    - 2-D FSI Scheme
      - Initially Used Hybrid Finite-Difference Stencil
      - Then Implemented Full Unstructured Mesh Scheme
      - Moving Boundaries
      - Time-Accurate Incompressible Viscous Flow
- **Systematic Methodology Validation Started**
  - Comparison With Steady-State Daily & Nece
  - Comparison With Basic Added Mass And Damping
  - Preliminary Comparison With Test Data For Representative Seal And Shroud Configuration
- **Accuracy and Code Speed Assessment Underway**
  - Mesh Density Requirements
  - Workstation Computing Efficiency

3-D ROTORDYNAMIC FLOW METHODOLOGY
(Enigma/FSI)

- Time Implicit Scheme For Unsteady Incompressible Viscous Flow
- Batina's Dynamic Mesh Movement Algorithm
- Rigid Body Motion And Moving Boundaries
- Successive Iteration Used To Satisfy Governing Equations At Each Time Level
- Helmholtz Pressure Method Used To Enforce Incompressibility (Combination Of Psuedo-Compressibility And Projection Scheme)

METHODOLOGY (CONCL'D)

- **Mesh Vertex Finite-Difference Stencil With Arbitrary Node ID**
  - No Need For Multi-zone Interpolation
  - Governing Equations Solved At Each Interior Flow Node
  - Can Model 3-D Geometries Of Interest

DAILY & NECE

- **Test Data (ASME J. Eng. , 1960)**
  - Enclosed Rotating Disk Within A Water Filled Cylindrical Cylinder
  - Rotor Radius = a = 0.25m
  - Shaft Radius = 0.0254m
  - Rotation = 71.3 rad/s
  - Cavity Dimensions, s/a = 0.0637

- **Flow Calculation**
  - 21 x 61 x 20 Flow Mesh
  - Steady-State Flow Mode
  - Turbulent Flow
  - Compared Swirl and Radial Flow Velocities To Daily & Nece
    - Pumping Action And Swirl Velocity Predicted
    - Good Agreement with Previous 2-D Axisymmetric Calculation (ASME J. Turbo., 1991)

DAILY & NECE FLOW GEOMETRY

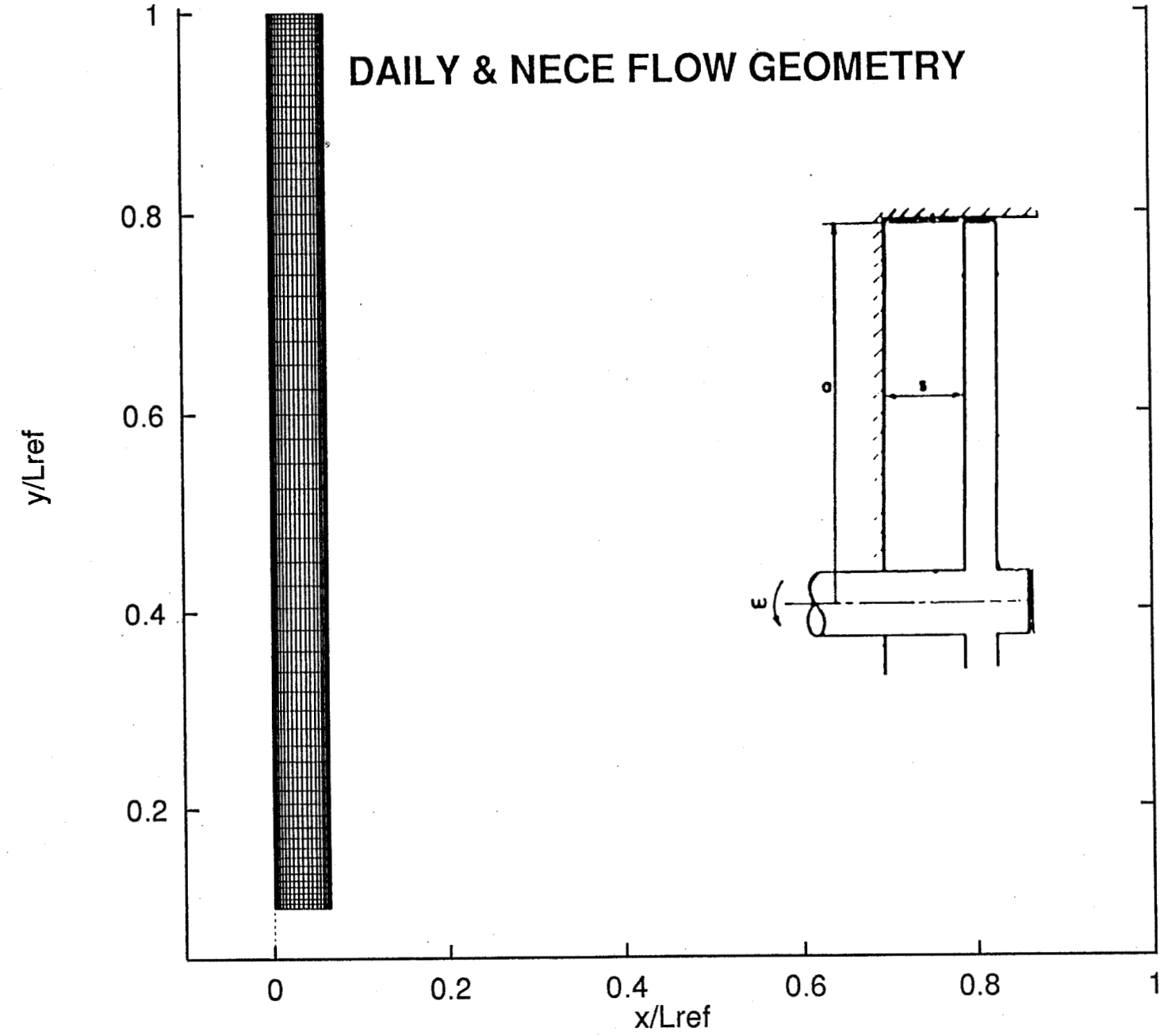

COMPARISON OF COMPUTED VELOCITIES WITH DAILY & NECE TEST DATA

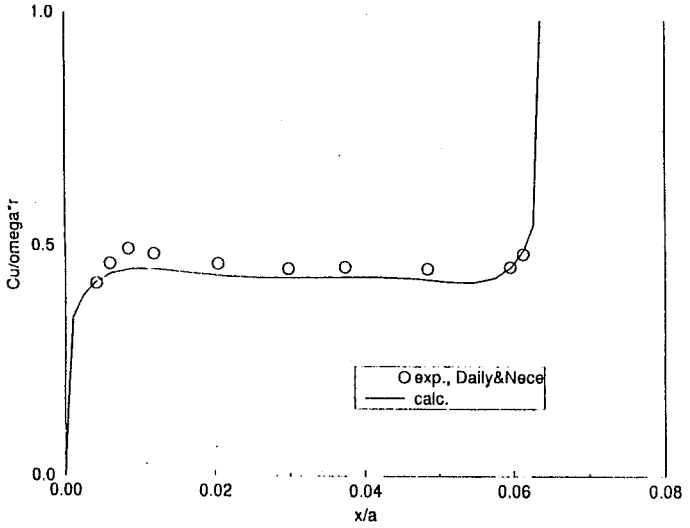

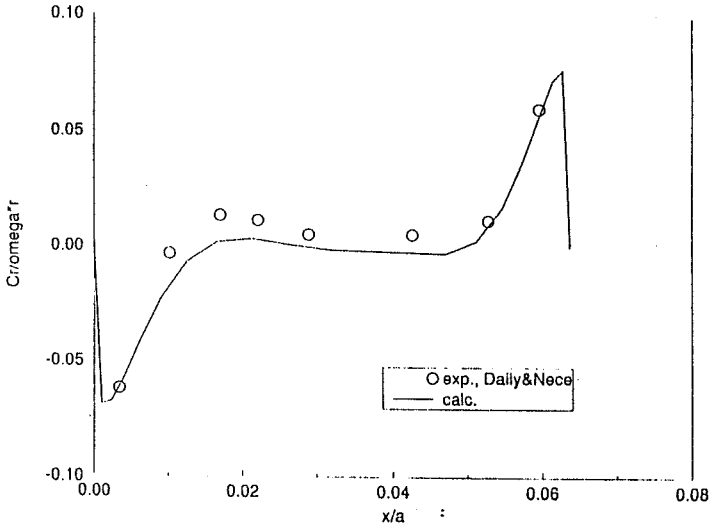

ADDED MASS AND DAMPING OF A CYLINDER WITHIN A FLUID FILLED CYLINDER

- **Flow Configuration**
  - Cylinder-Within-Water Filled Cylinder
  - Inner Cylinder Radius = 12.7mm
  - Outer Cylinder Radius = 63.5mm
  - Theoretical Solution By Chen et al. (ASME J. Appl. Mech., 1976)

- **Flow Calculation**
  - 6x21x20 Flow Mesh
  - Time Dependent Laminar Flow
  - Inner Cylinder Moving
  - Force Coefficients Were Calculated By Imposing A Harmonic Motion On The Inner Cylinder And Decomposing The Resultant Time-Periodic Force Acting On The Inner Cylinder
  - Added Mass And Damping Show Good Agreement With Chen et al.; Damping Tends To Be Over Predicted

FLOW GEOMETRY FOR ADDED MASS AND DAMPING

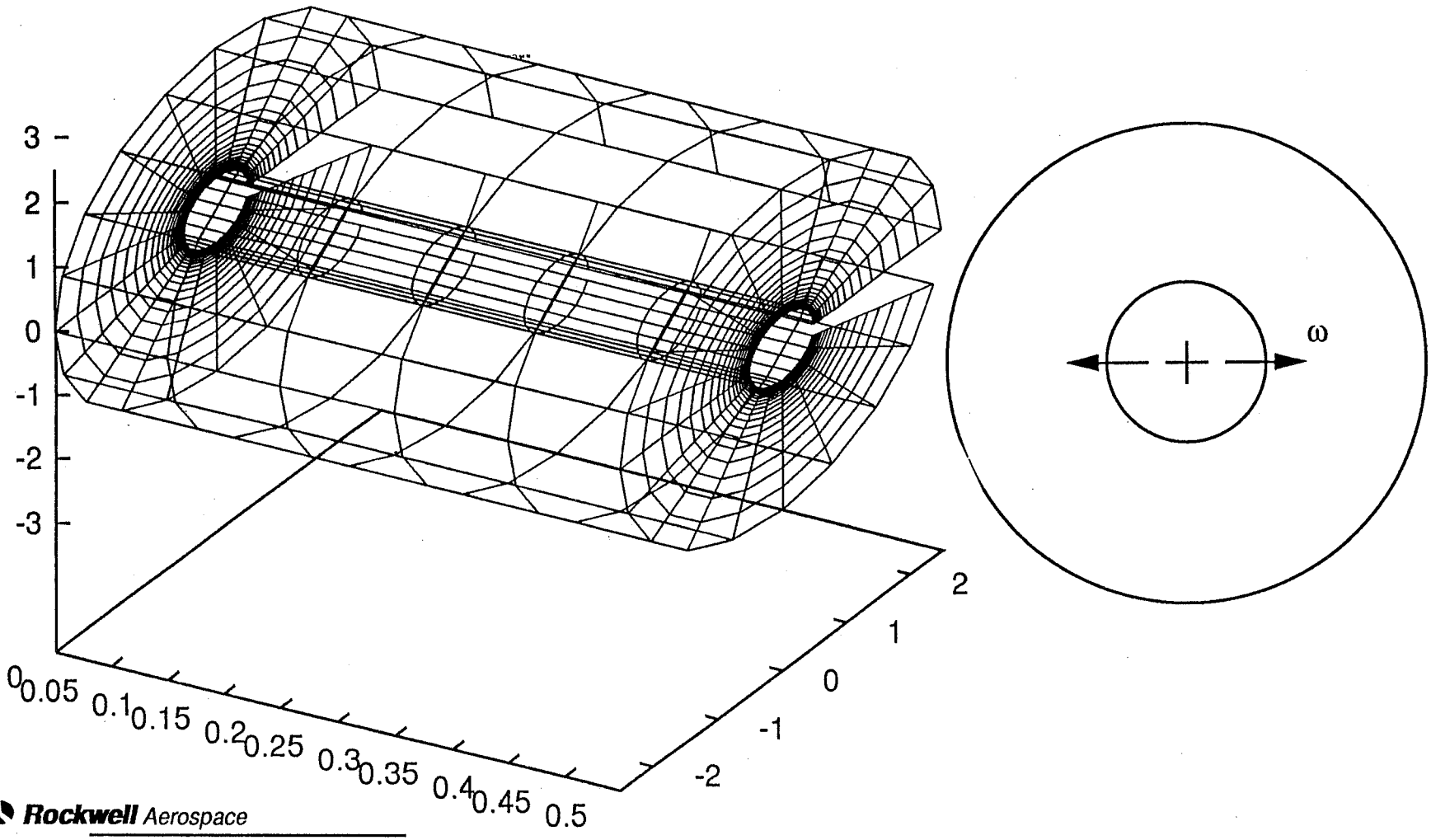

Rockwell Aerospace
Rocketdyne

COMPUTED DRAG FORCE HISTORY FOR f = 1.59 Hz MOTION AND ADDED MASS AND DAMPING

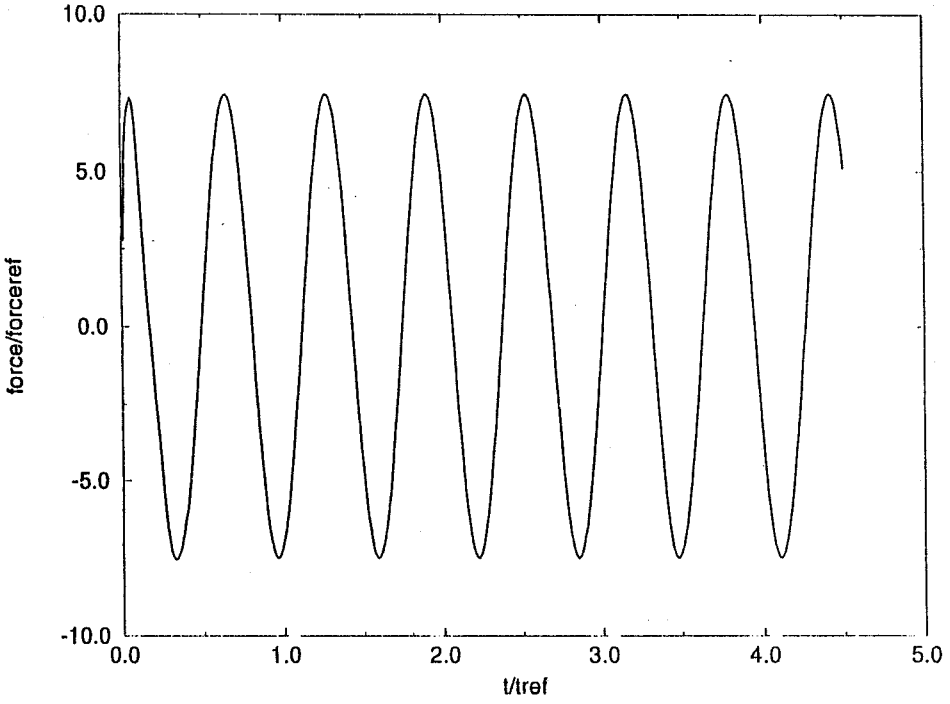

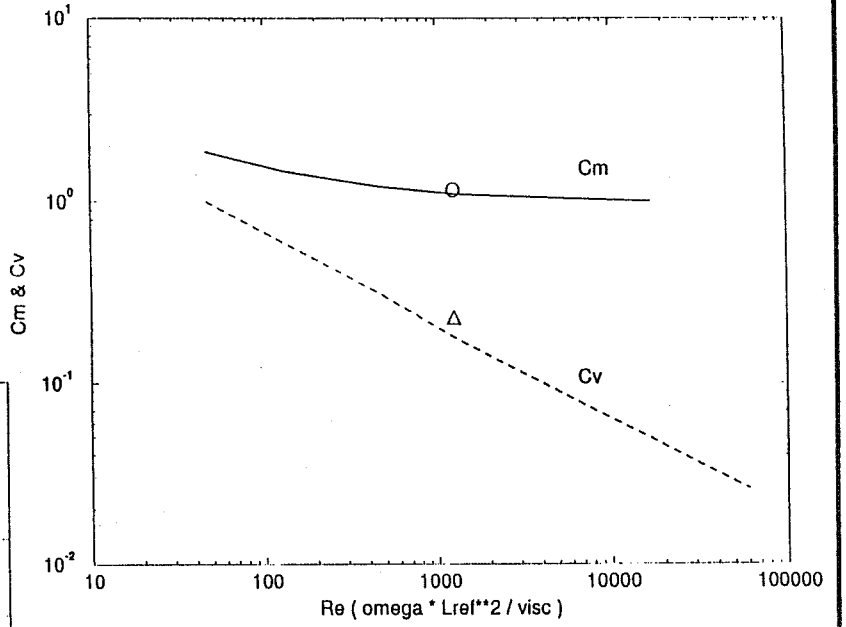

CENTERED SEAL

- **Test Data (Texas A&M, Morrison et al.)**
  - Seal Clearance = 1.27mm
  - Length-To-Clearance Ratio = 29.4
  - Mass Flow Rate = 0.00486 m**3/s
  - Shaft Rotation = 3600 rpm

- **Flow Calculations**
  - Steady-State Flow Mode
  - Turbulent Flow
  - Grid Refinement In Azimuth Direction
    - Grid 1: 1 Node Per 36deg In Azimuth (13070 Total Nodes)
    - Grid 2: 1 Node Per 22.5deg (20912)
    - Grid 3: 1 Node Per 18deg (26140)
  - Compared Seal Exit Axial And Azimuthal Flow Velocities To Test Data
  - Agreement Is Good
  - For Clarity, Contour Plots Shown With Exaggerated Clearance

CENTERED SEAL FLOW GEOMETRY

Texas A&M Seal Rig Composite Drawing

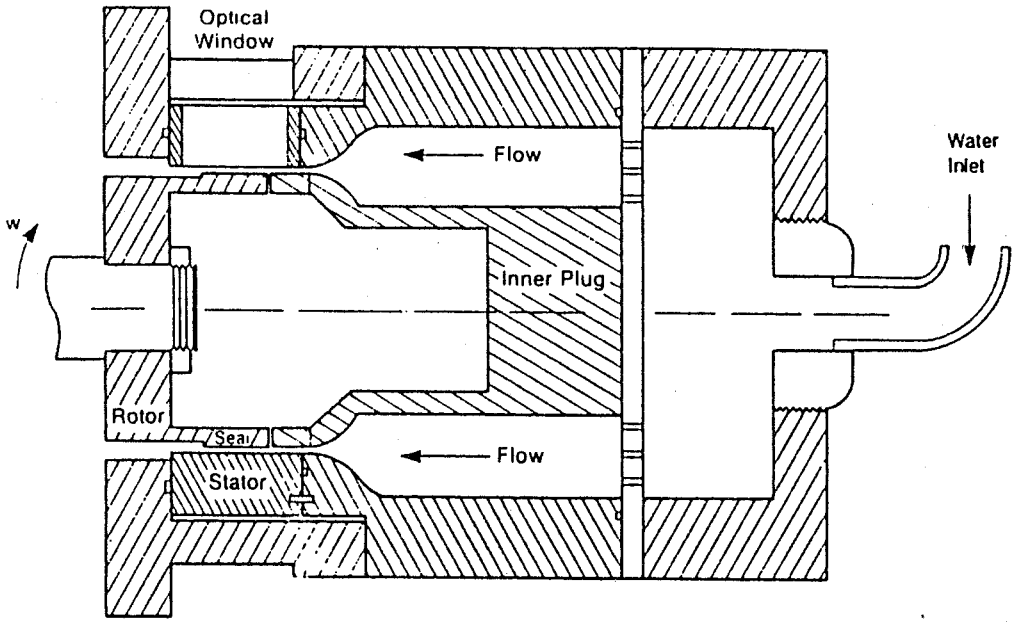

CENTERED SEAL FLOW MESH (AXIAL PLANE)

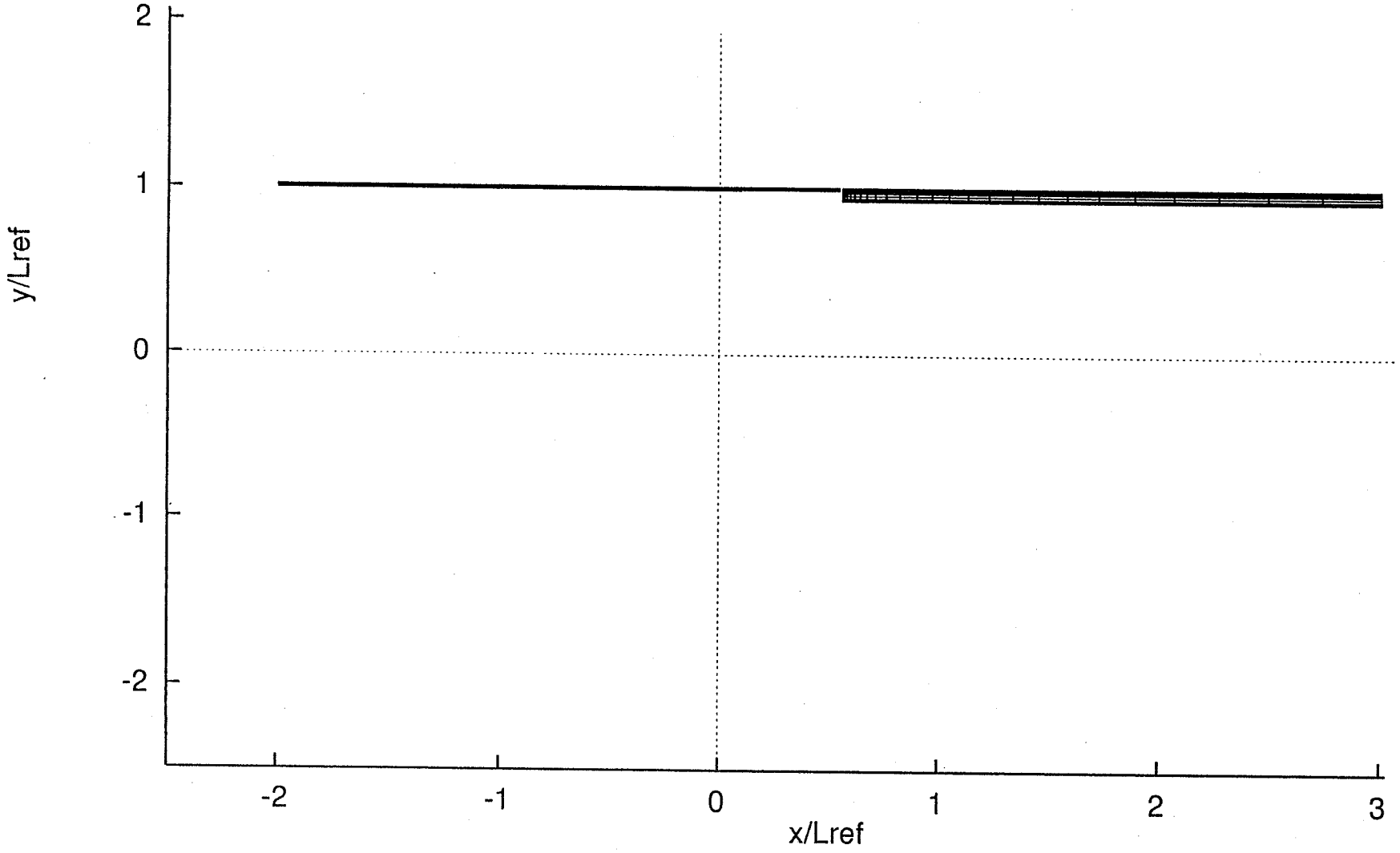

CENTERED SEAL MESH AZIMUTH PLANE

GRID 1

GRID 2

GRID 3

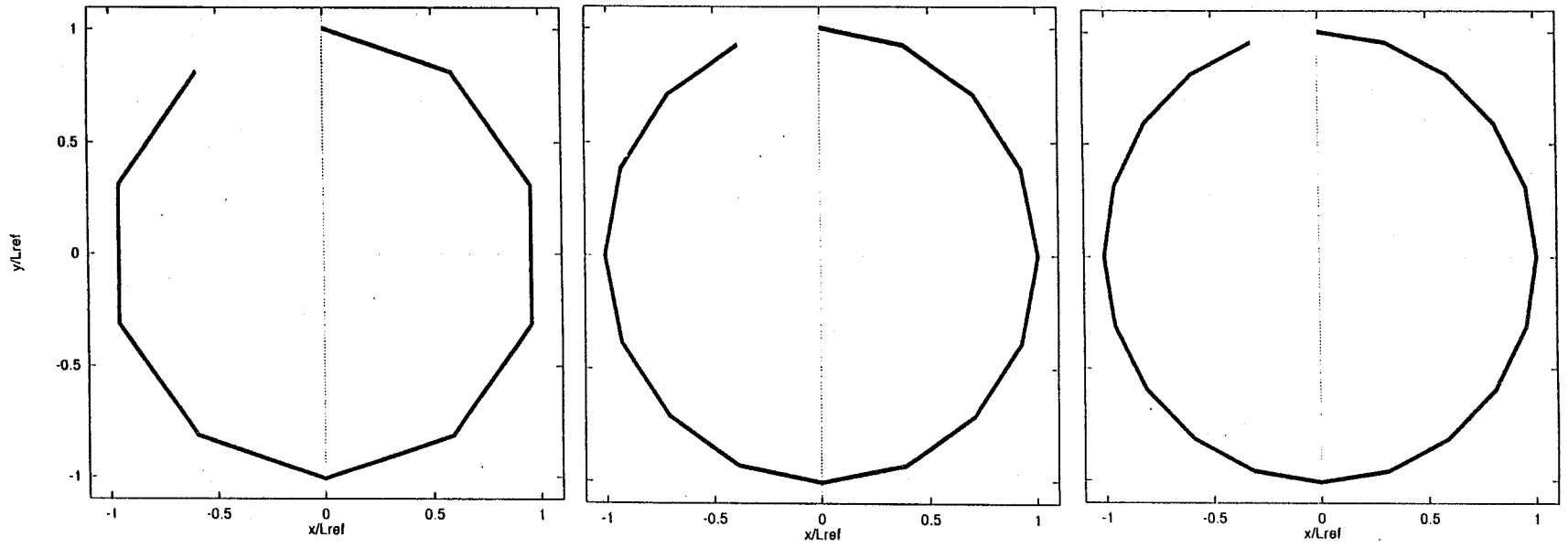

Velocity Contours At Exit Of Centered Seal

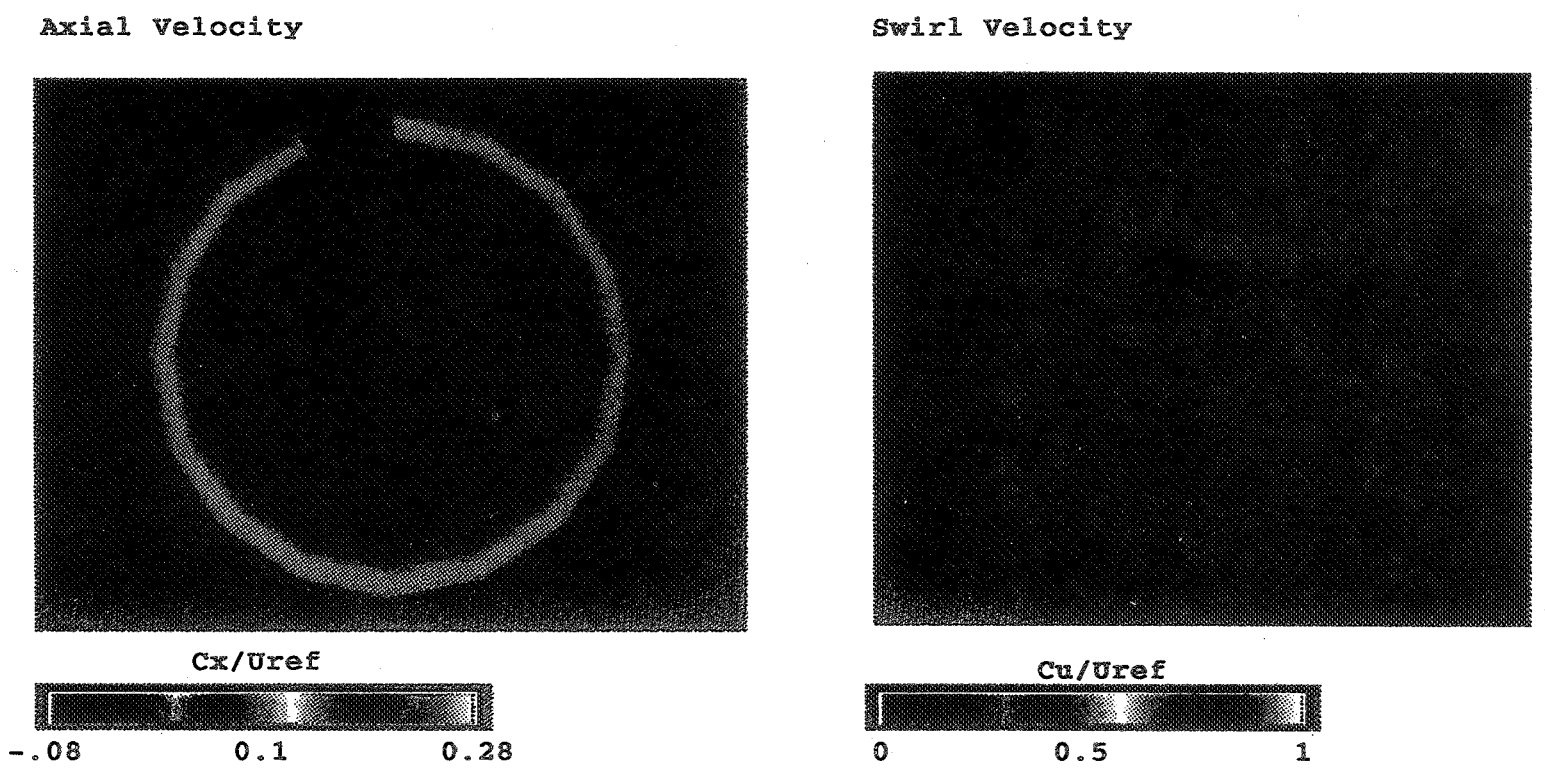

SEAL EXIT AXIAL VELOCITY

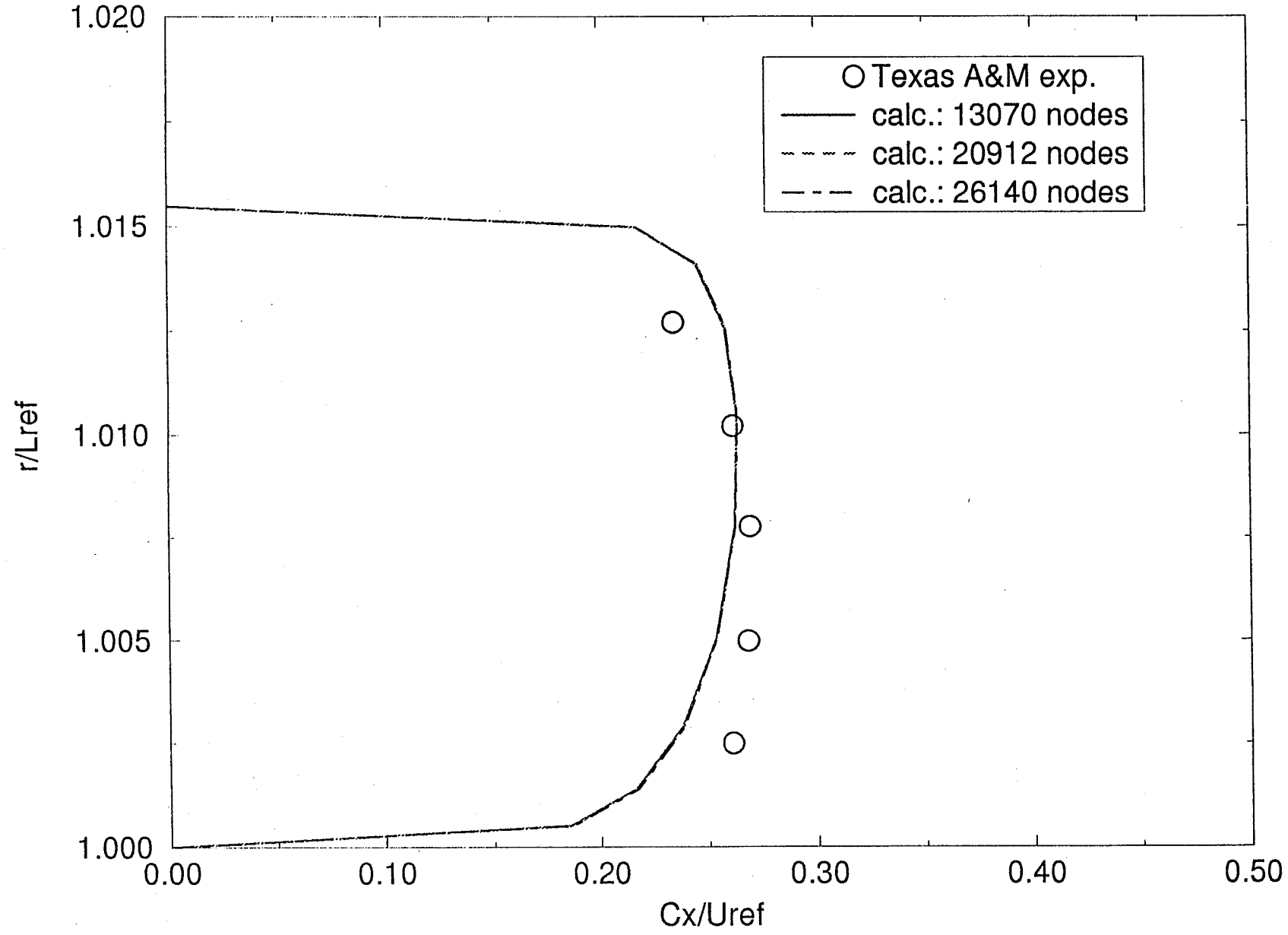

Rockwell Aerospace
Rocketdyne

EXIT SWIRL VELOCITY

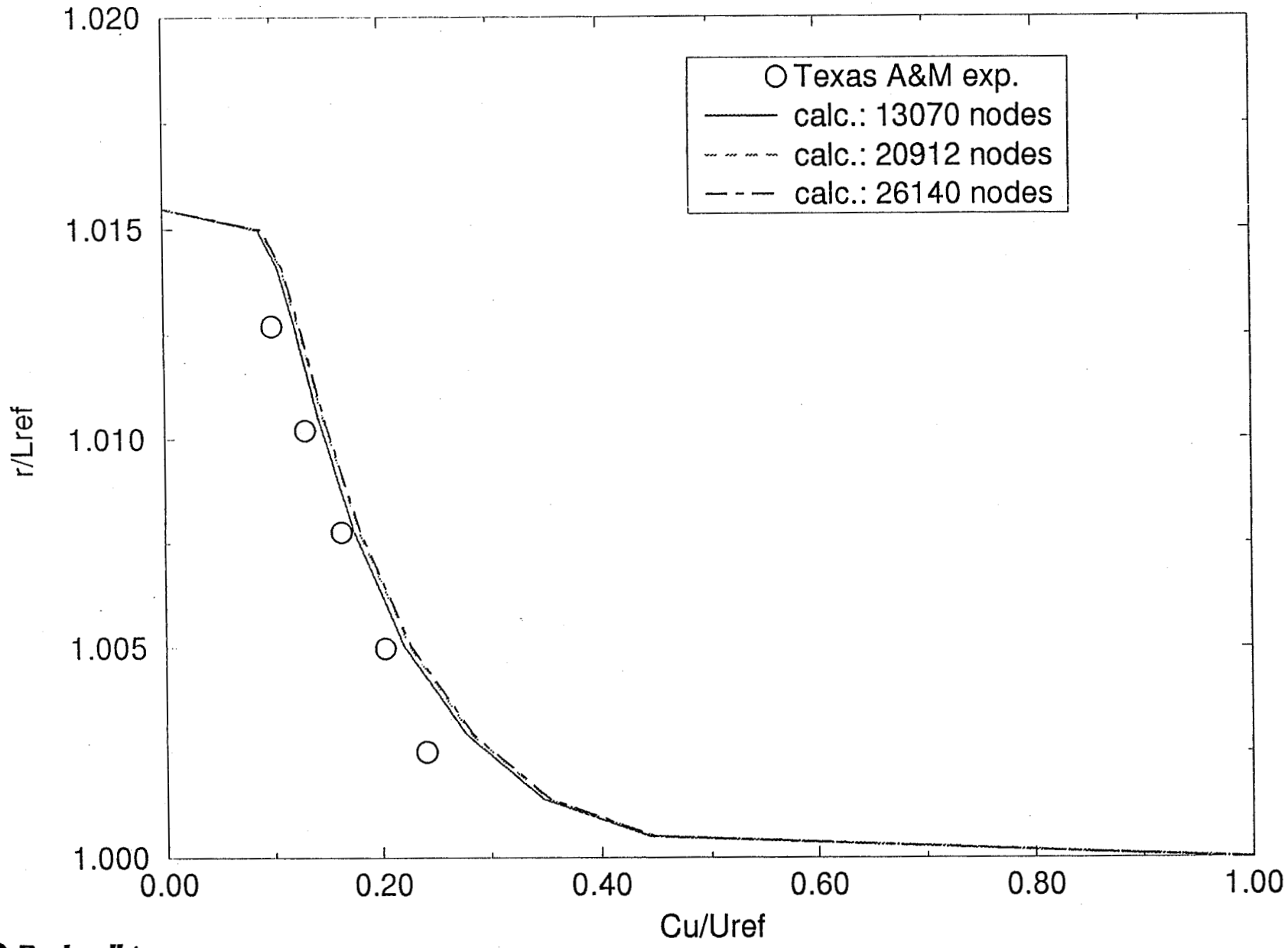

Rockwell Aerospace
Rocketdyne

SEAL WITH 50% STATIC ECCENTRICITY

- **Test Data (Texas A&M)**
  - Overall Geometry Similar To Centered Seal (But Without Plug)
  - Seal Has 50% Static Eccentricity (Nominal Clearance = 1.27mm)
  - Flow Rate = 0.00486 m**3/s
  - Shaft Rotation = 3600 rpm

- **Flow Calculation**
  - 25312 Node Flow Mesh (1 Node per 22.5 Deg. In Azimuth)
  - Steady-State Mode
  - Centered Flow Mesh Created First And Then Rotor Is Moved To Obtain A Flow Mesh For 50% Static Eccentricity
  - Preliminary Results; Need To:
    - Perform Mesh Refinement In Radial Direction
    - Assess The Effect Of Inlet Conditions And Boundary Conditions On Solution;
  - Cx and Cu Compared At Seal Exit
  - In General Compares Well, But Axial Velocity Is Overpredicted At 0 Deg Azimuth And Underpredicted At 180 Deg
  - For Clarity, Contour Plots Shown With Exaggerated Clearance

FLOW GEOMETRY

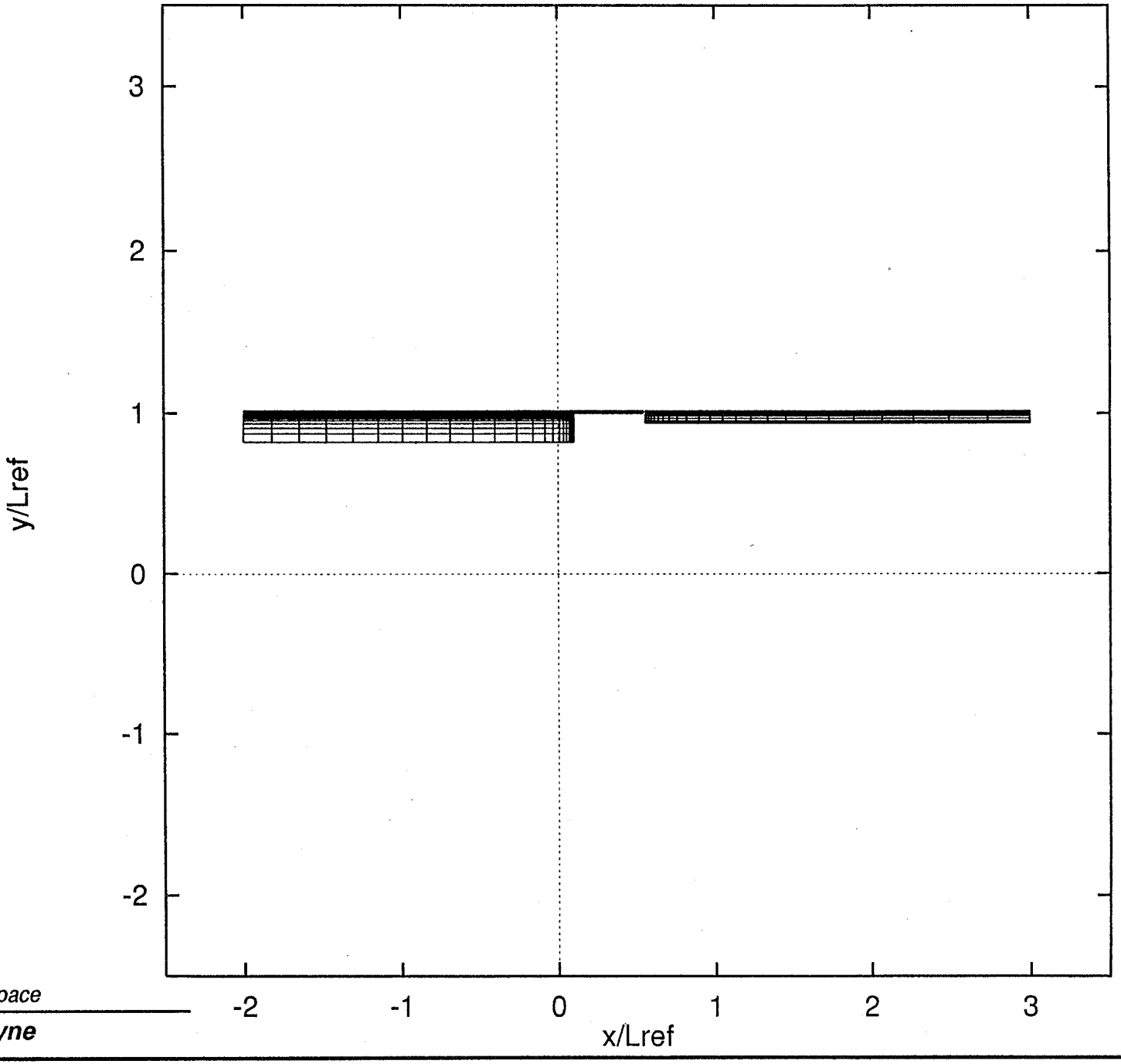

Velocity Contours At Exit Of Seal With 50% Static Eccentricity

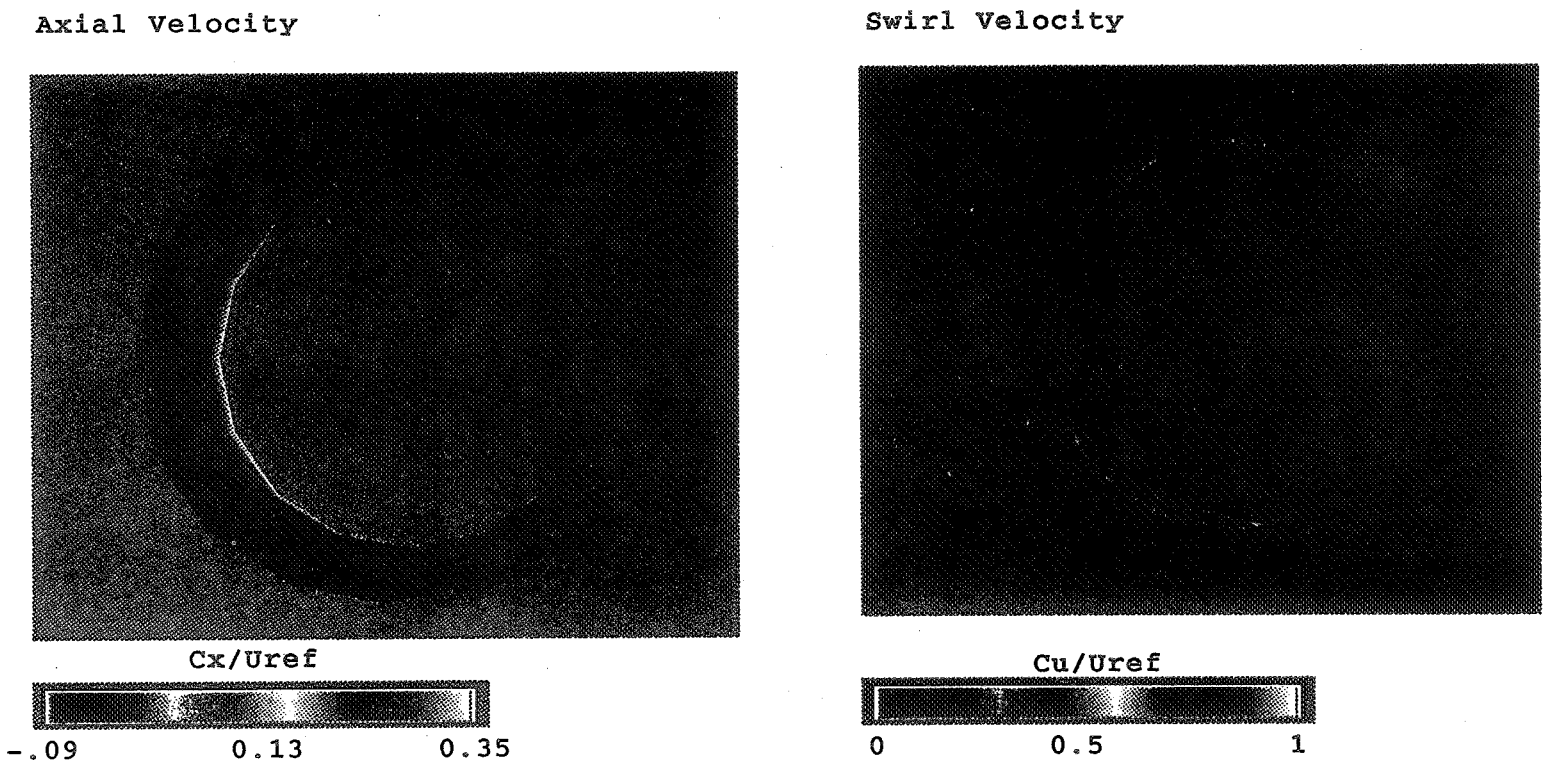

Cx COMPARISON AT SEAL EXIT

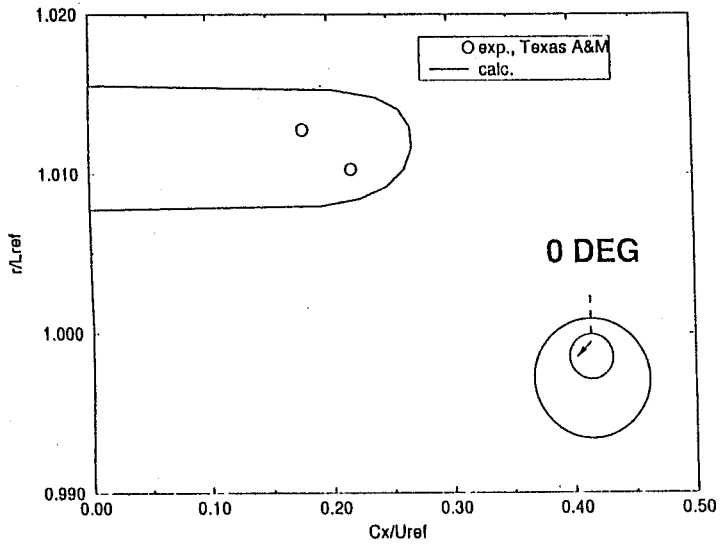

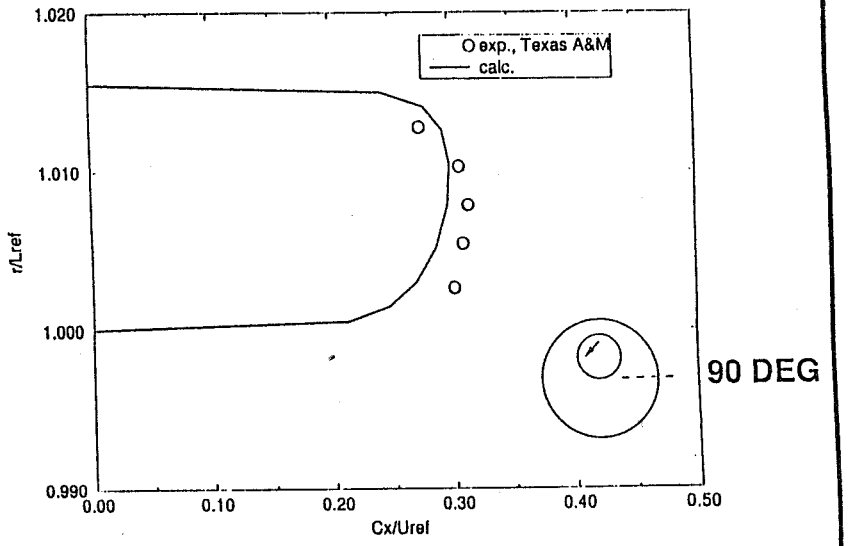

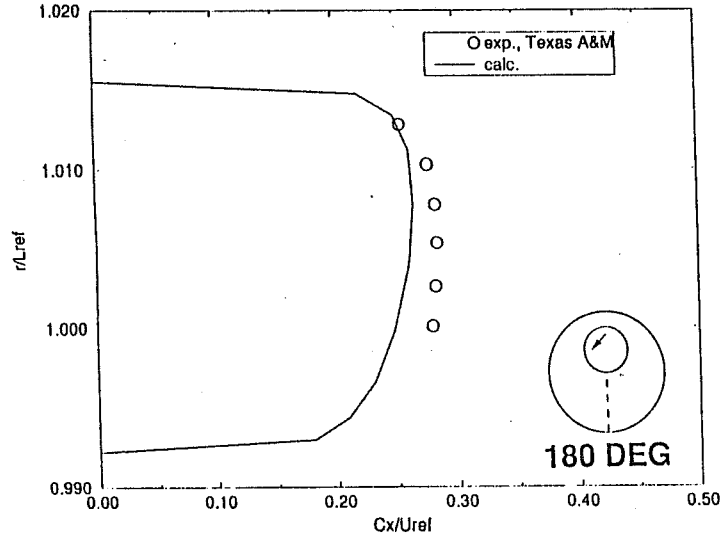

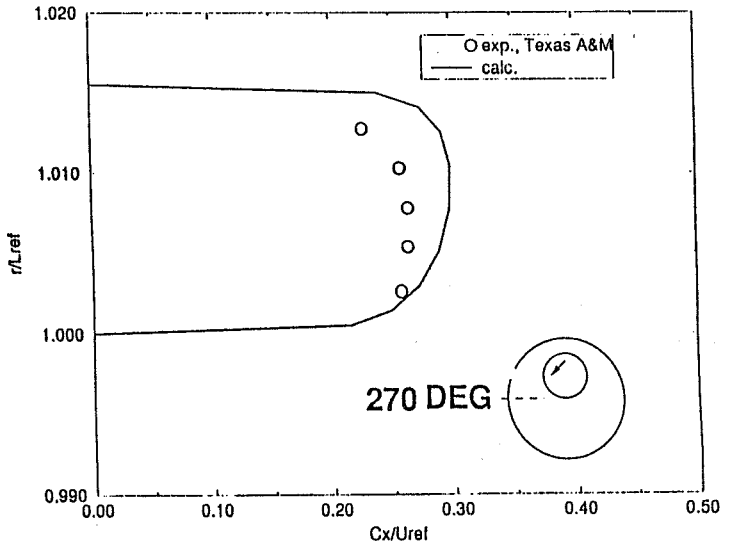

Cu COMPARISON AT SEAL EXIT

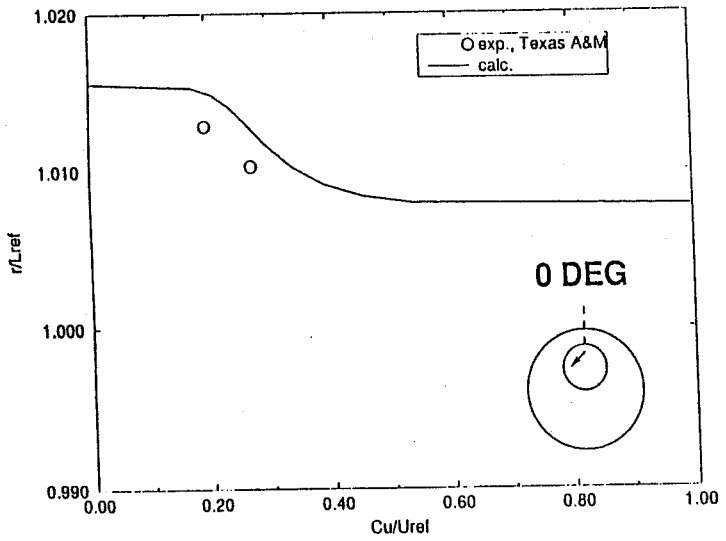

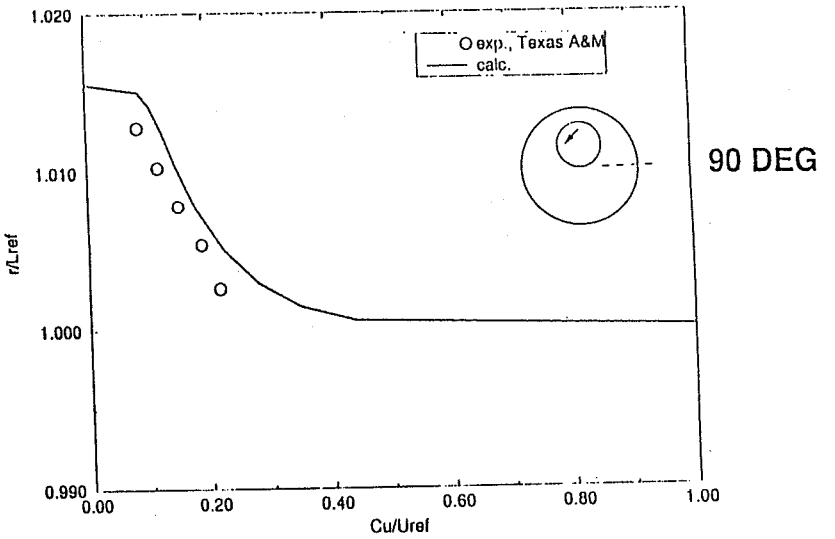

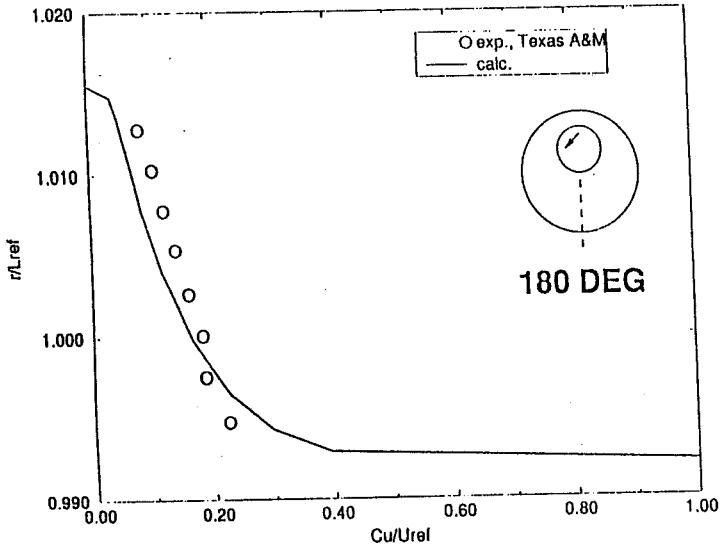

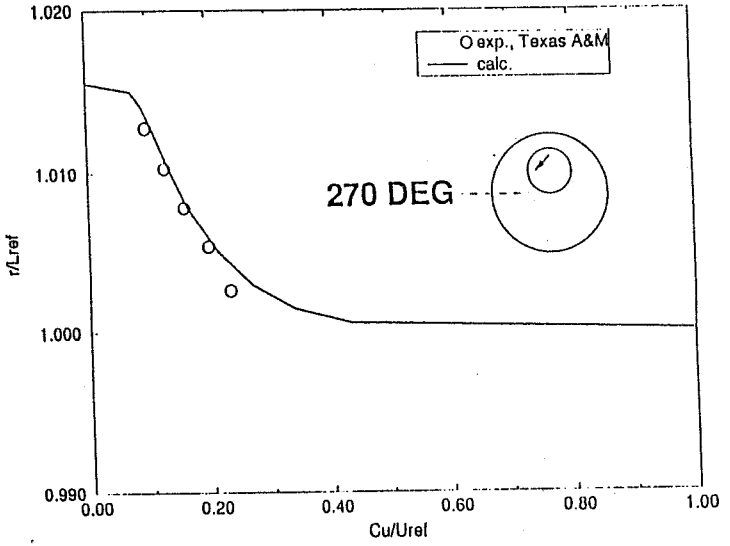

WHIRLING SEAL, 50% DYNAMIC ECCENTRICITY

- **Test Data (Texas A&M)**
  - Geometry Similar To Previous Seal
  - Rotor Was Mounted On Steel Shaft Using A Brass Bushing 0.63mm Eccentric With Respect To The Shaft Axis
  - This Resulted In Eccentric Whirl With A Whirl Ratio = 1
  - Flow Rate = 0.00486
  - 50% Eccentricity Is Quite Large But Ensures That Measured Values Are Not Perturbations Of Noise

MEASUREMENT GRID FOR TEST DATA

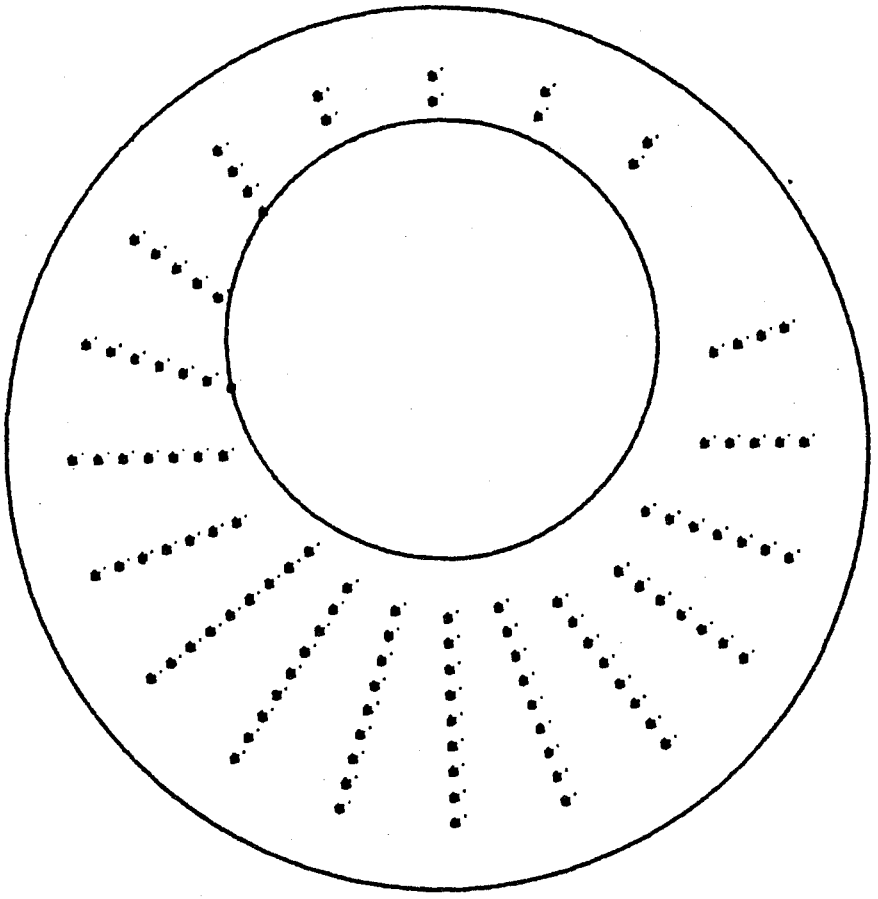

WHIRLING SEAL, 50% DYNAMIC ECCENTRICITY (CONT'D)

- **Flow Calculations**
  - 25312 Node Flow Mesh (1 Node Per 22.5 Deg.); Same As 50% Static Case
  - Unsteady Flow Calculations Started From Steady-State Solution
  - Rotor Whirling With 50% Eccentricity
  - Time Periodic Solution Achieved After Impulsive Start
  - Preliminary Results, Need To:
    - Assess The Effect Of Inflow Conditions And Boundary Conditions On Solution
    - Perform Mesh Refinement In Radial Direction
  - Cx and Cu Velocities Are Compared To Test Data
  - Source Of Radial Offset Between Exp. And Computed Velocities Not Known At This Time; No Such Offset Was Present in the 50% Static Eccentricity Case
  - Swirl Velocities Are In Fair Agreement With Test Data
  - Axial Velocities At 90° and 270° Show Best Agreement With Test Data
    - Compared To Test Data, Large Gap Axial Velocity Underpredicted And Small Gap Axial Velocity Overpredicted
    - This Trend Was Also Evident In 50% Static Eccentricity Case
  - For Clarity, Contour Plots Shown With Exaggerated Clearance

Cx Axial Variation At One Time Slice

Near Inlet

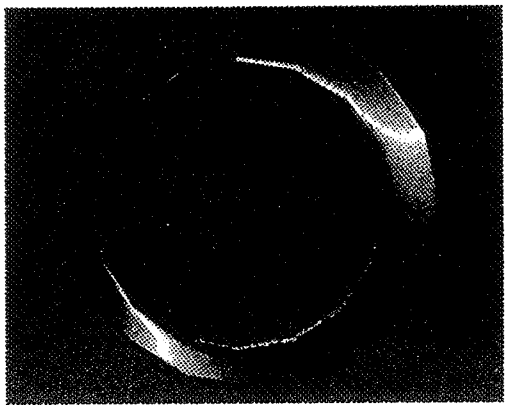

Middle

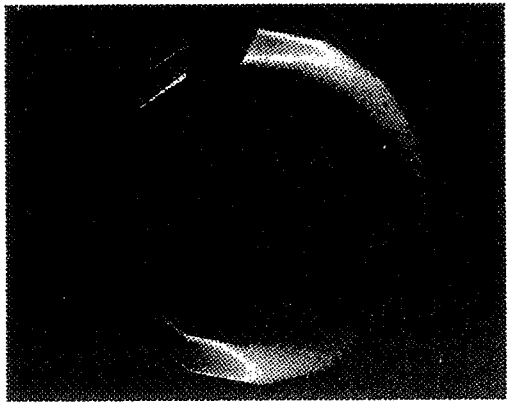

Exit

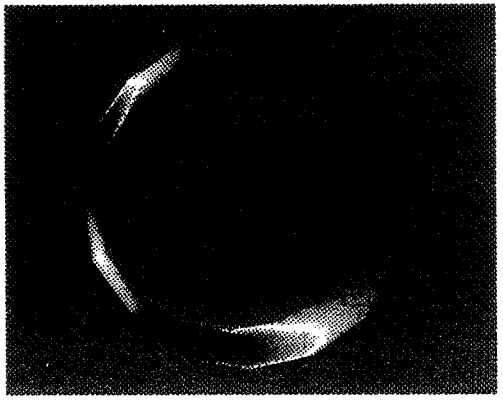

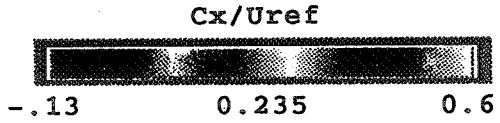

Cx Contours At Seal Exit As A Function Of Time

t/tref = 3.15 = 6.3 = 9.4

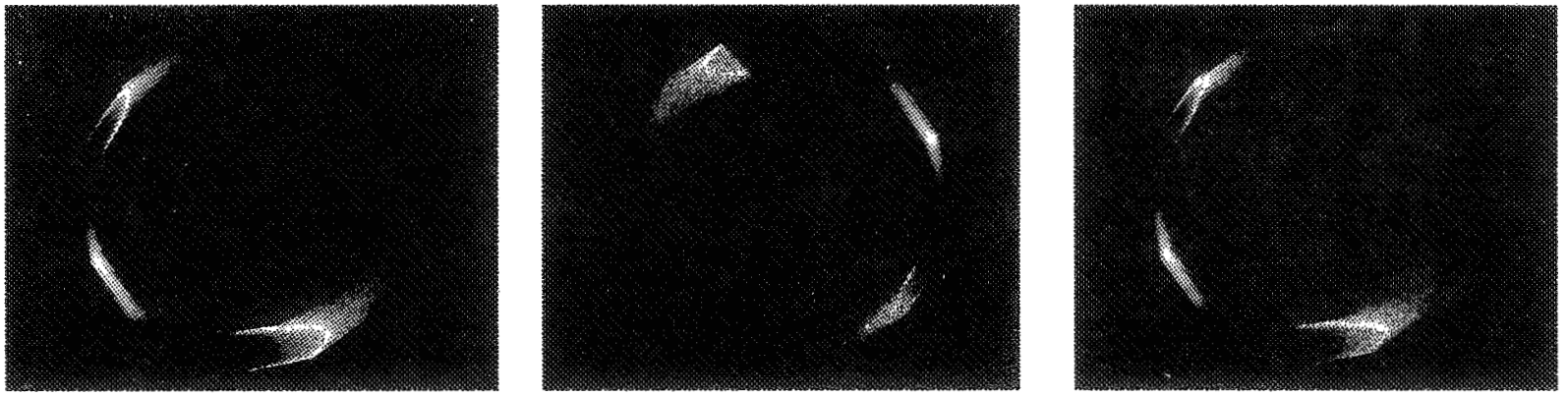

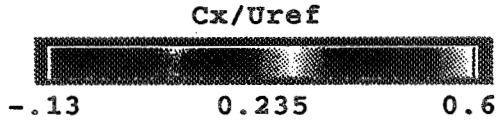

Cu Contours At Seal Exit As A Function Of Time

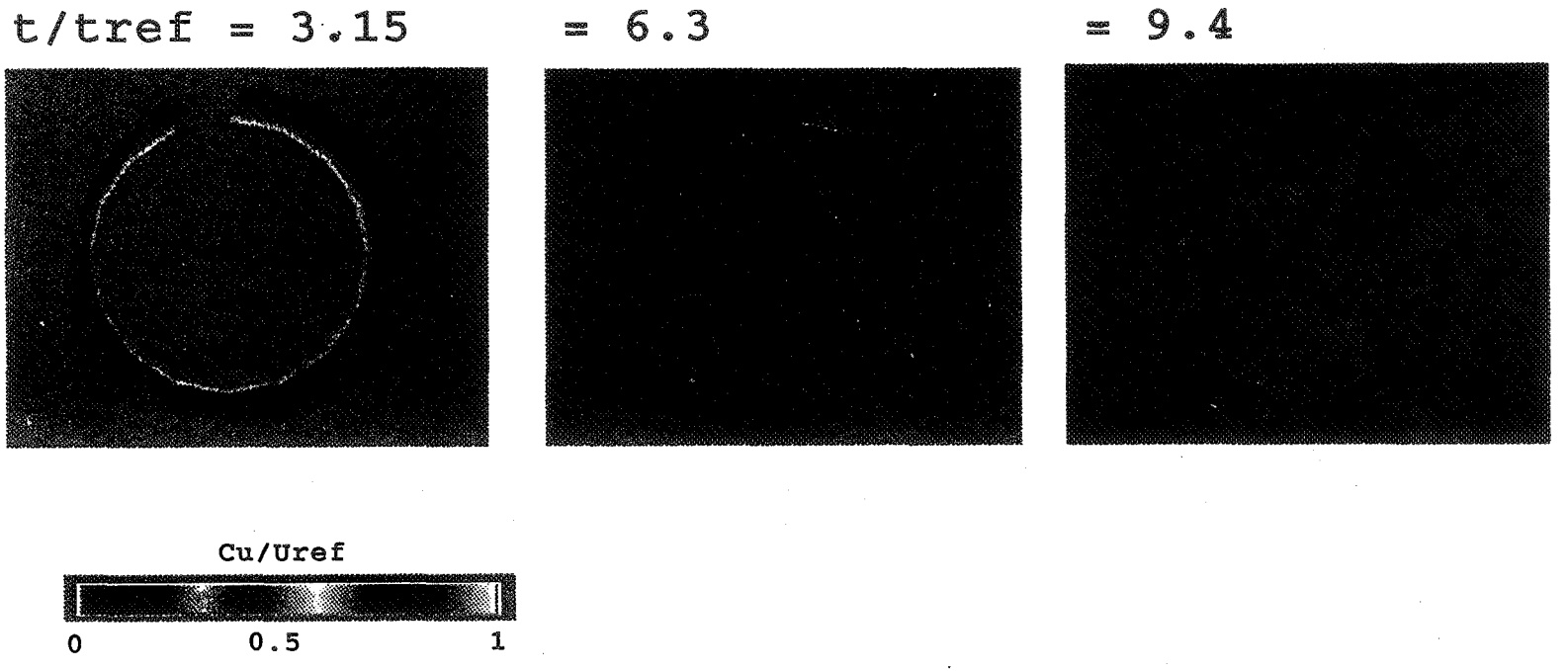

Cx COMPARISON AT SEAL EXIT (WHIRLING SEAL)

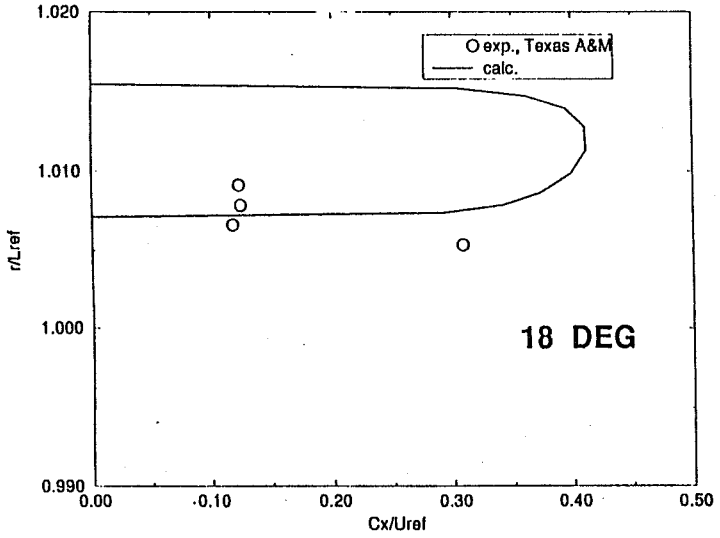

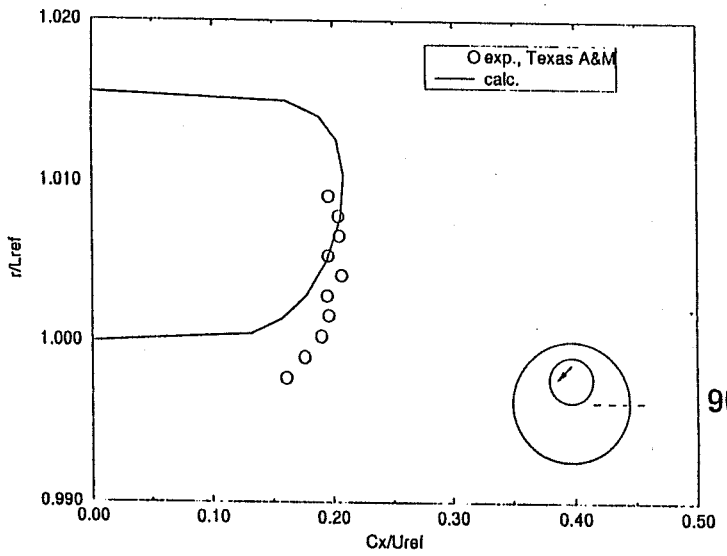

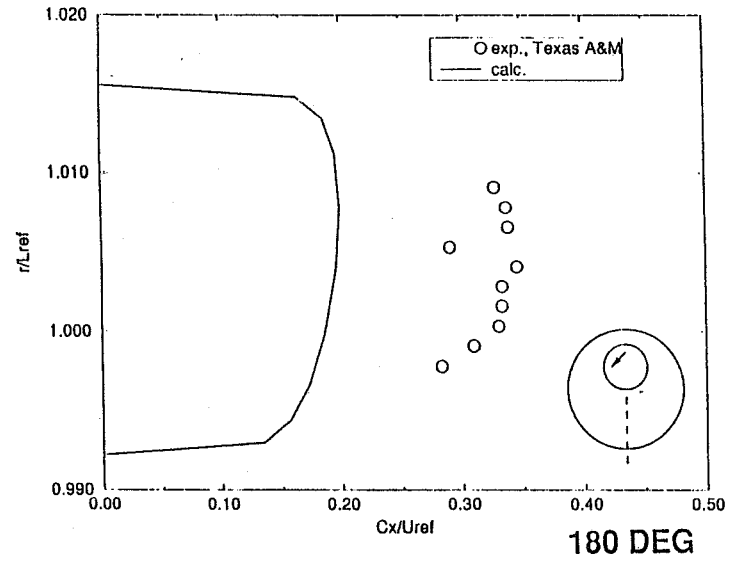

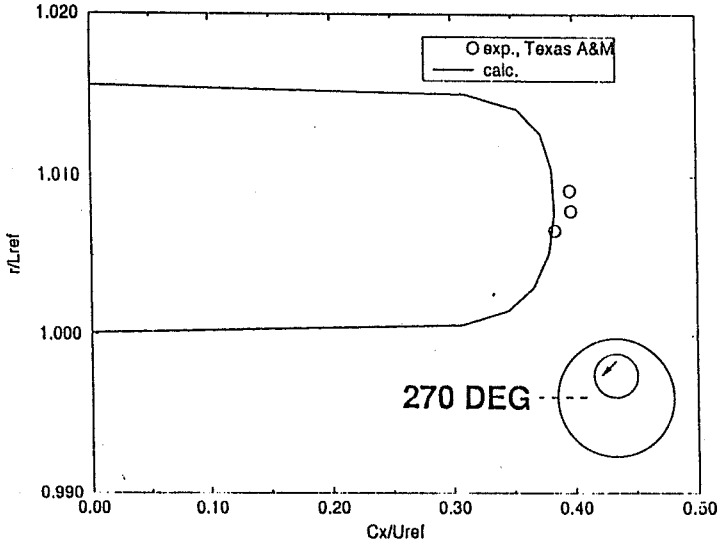

Cu COMPARISON AT SEAL EXIT (WHIRLING SEAL)

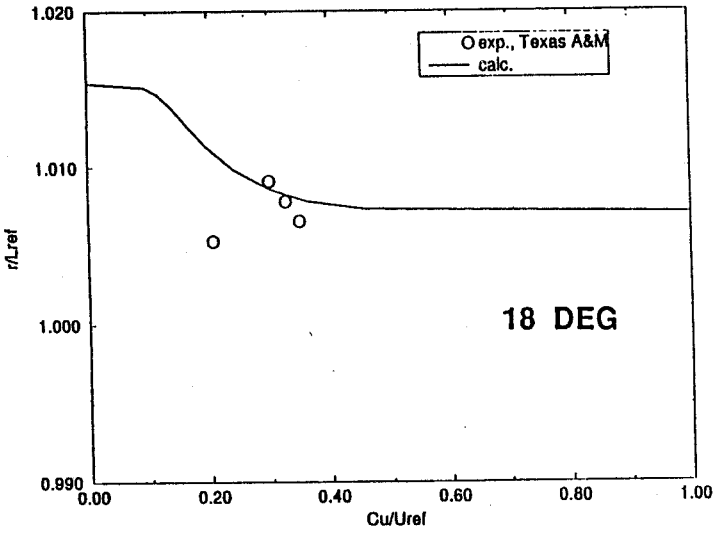

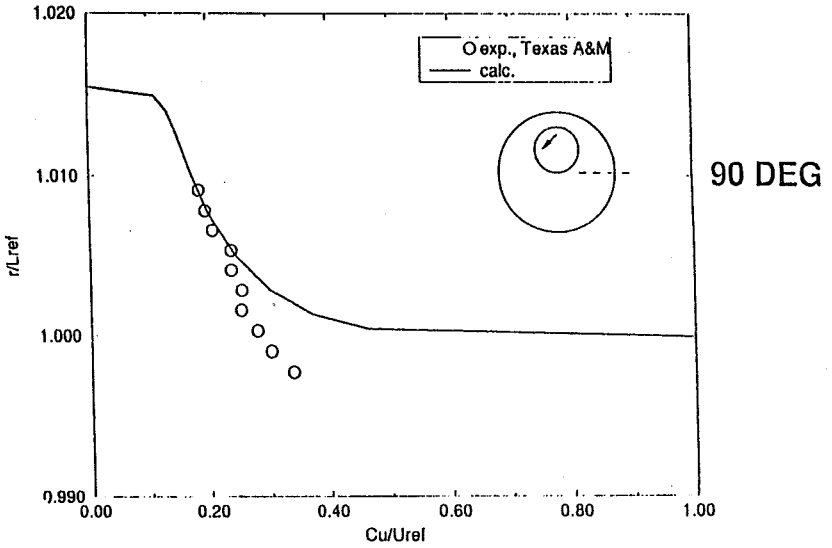

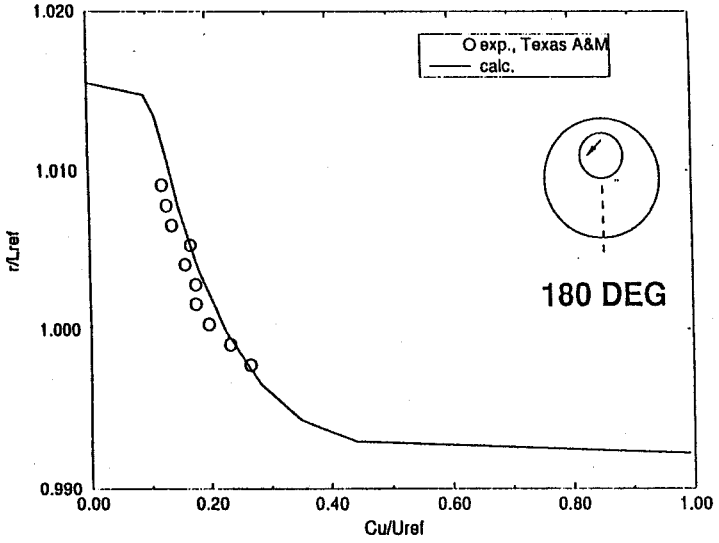

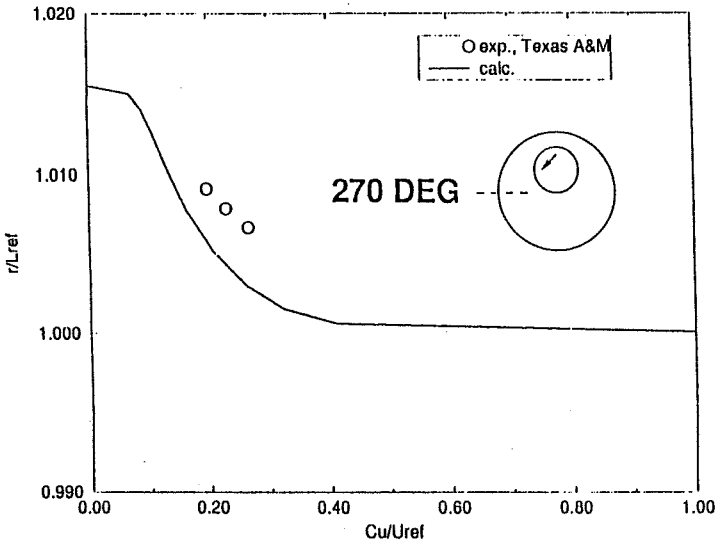

CAL TECH IMPELLER SHROUD

- **Test Data (Cal Tech, Guinzburg et al.)**
  - Working Fluid Is Water
  - Rotating Shroud
  - Normal And Tangential Forces Measured

- **Flow Calculation**
  - 38120 Node Flow Mesh
  - Nominal Clearance = 0.424cm
  - Eccentricity = 0.118cm
  - Shaft Rotation = 500 rpm
  - Flow Rate = 1.892 liter/s
  - Tangential Force Predicted Reasonably Well
  - Normal Force Predicted For Low Whirl Frequencies
    - $\Delta\tau$ and Mesh Refinement Study To Be Performed

IMPELLER SHROUD FLOW GEOMETRY

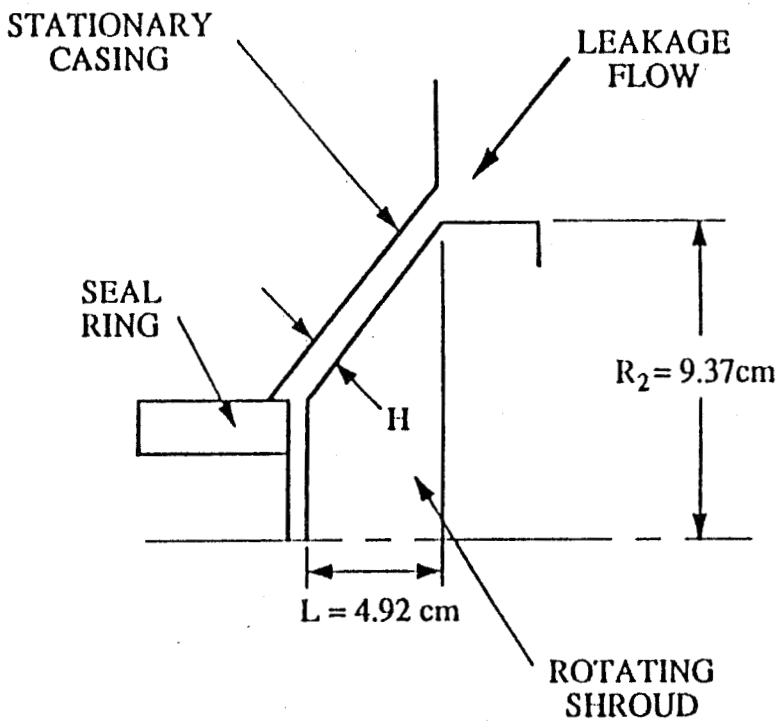

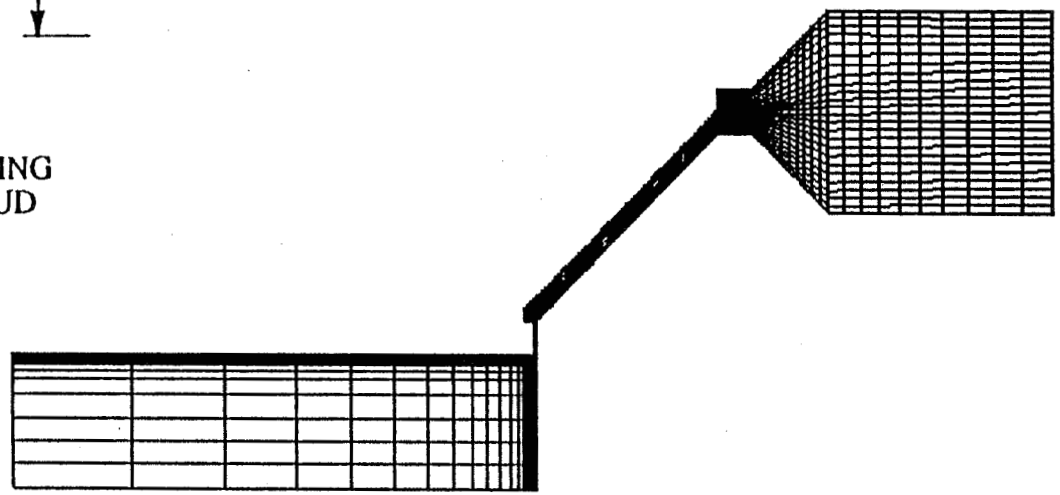

NORMAL AND TANGENTIAL FORCES

Navier-Stokes Based
Rotordynamic Flow
Calculation Methodology
For Impeller Shroud

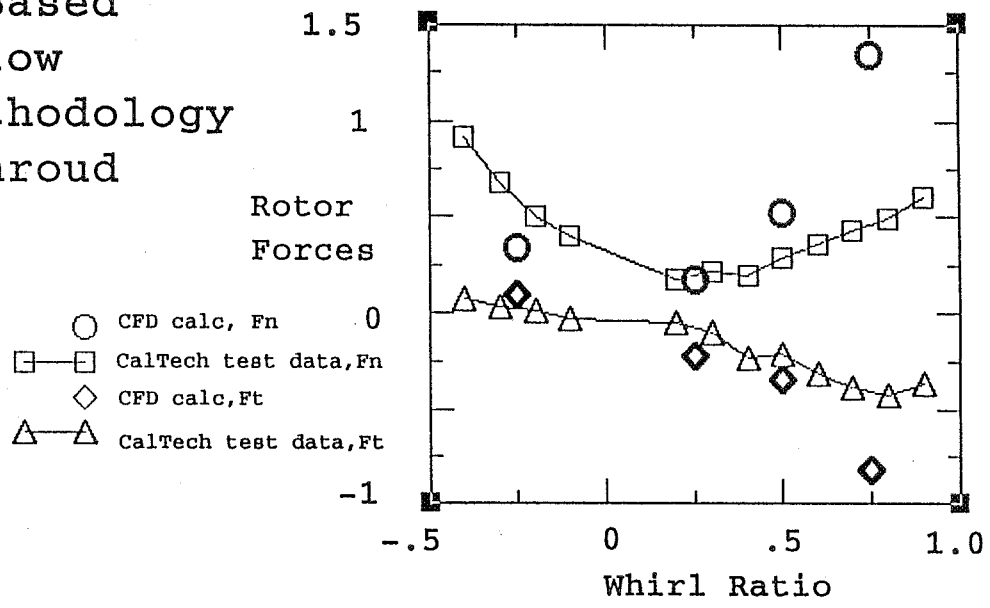

Flow mesh moves with
shaft (counterclockwise).

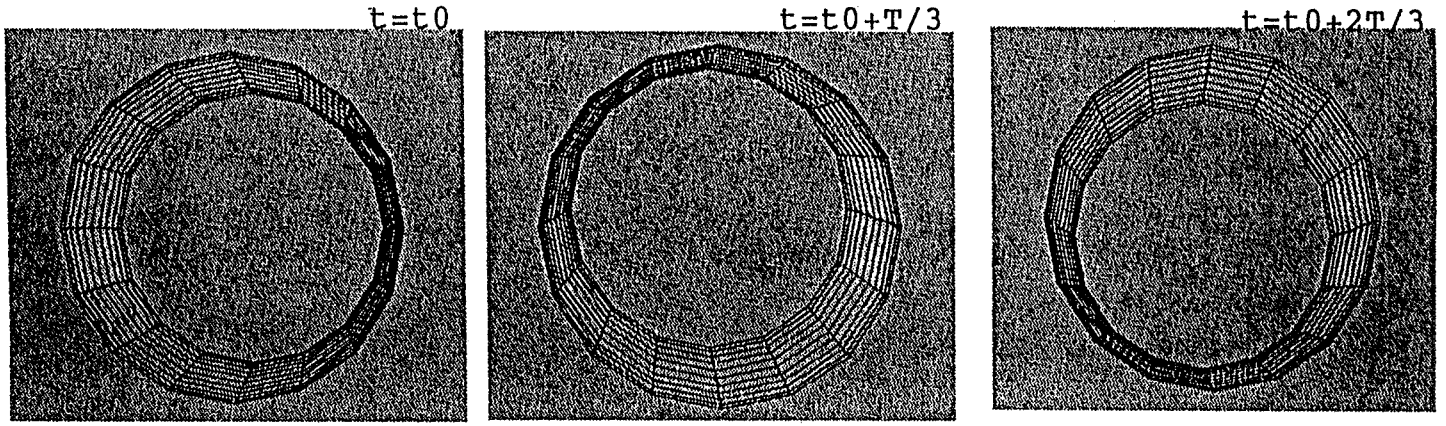

CONCLUDING REMARKS

- Development Of A 3-D Methodology For Rotordynamic Flows Progressing Well
- Computational Prediction Of Rotordynamic Flows Appears To Be Feasible On Workstations
- Careful Assessment Of Boundary Conditions Needs To Be Performed
- Radial Mesh Refinement And Mesh Density Requirements Will Be Investigated
- Will Investigate 3-D Accuracy Needs And Computational Efficiency Issues
- More Validation Underway

Rocketdyne's Turbomachinery Design Process Improvements for RRTT and Future Programs

George H. Prueger, Bruce Kovac, Wei Chen, Edward Ascoli, and D.P. Mondkar
RocketdyneDivision/Rockwell

Abstract

Cost and schedule reductions for turbomachinery designs applicable to the rocket engine market require evaluation of the design process and the development of tools to enable the reductions. A number of tools have been implemented to speed the design and analysis process for turbomachinery components at Rocketdyne. These tools have been linked to provide a framework for consistent geometric representations between the design and analysis functions. These tools include solid model representations of all components, rapid grid generation for CFD analysis, rapid mesh generation for structural and heat transfer analysis, and links between analysis functions to carry boundary conditions directly applicable analysis required.

This paper will present a description of an impeller design and analysis process used to showcase the developed tools and baseline the process time reductions. The process includes preliminary sizing, CFD analysis, CAD model generation, and structural analysis of the impeller. The paper will also present the areas where the process is in use in the RRTT program.

Rocketdyne's Turbomachinery Design Process Improvements For RRTT and Future Programs

Rockwell - Rocketdyne Division

George Prueger, Bruce Kovac, Wei Chen, D.P. Mondkar,
Ed Ascoli

CFD Workshop

April 25, 1995

Rockwell Aerospace
Rocketdyne

Turbomachinery Design Process Goals

- **Reduce Cost**
  - Global competition requires low cost systems
- **Reduce Schedule**
  - Time to market key to companies viability
- **Reduce Design Risk**
  - High performance and low weight required by new rocket engine systems
  - Extended test and development programs no longer tolerated
    - "Get it right the first time" attitude prevails
  - Means - move complex analysis upstream in design process

Turbomachinery Design Process

- **Multi-Function Interaction Dominates**
  - Design, Fluid dynamics, Structural Analysis, Manufacturing
- **Different Types of Models**
  - Design and manufacturing require true representation of hardware
  - Fluid Dynamics requires accurate representation of flow passages
  - Structural Analysis requires geometric representation with suppression of detail design features which increase analysis time and do not significantly affect results
- **Consistent Models Between All Functions Required**
  - Time required for multiple models
  - Quality of multiple models can not be guaranteed
- **Transfer of Data Between Functions**
  - Boundary conditions for analysis
  - Manufacturing requirements definition

Turbomachinery Design Process

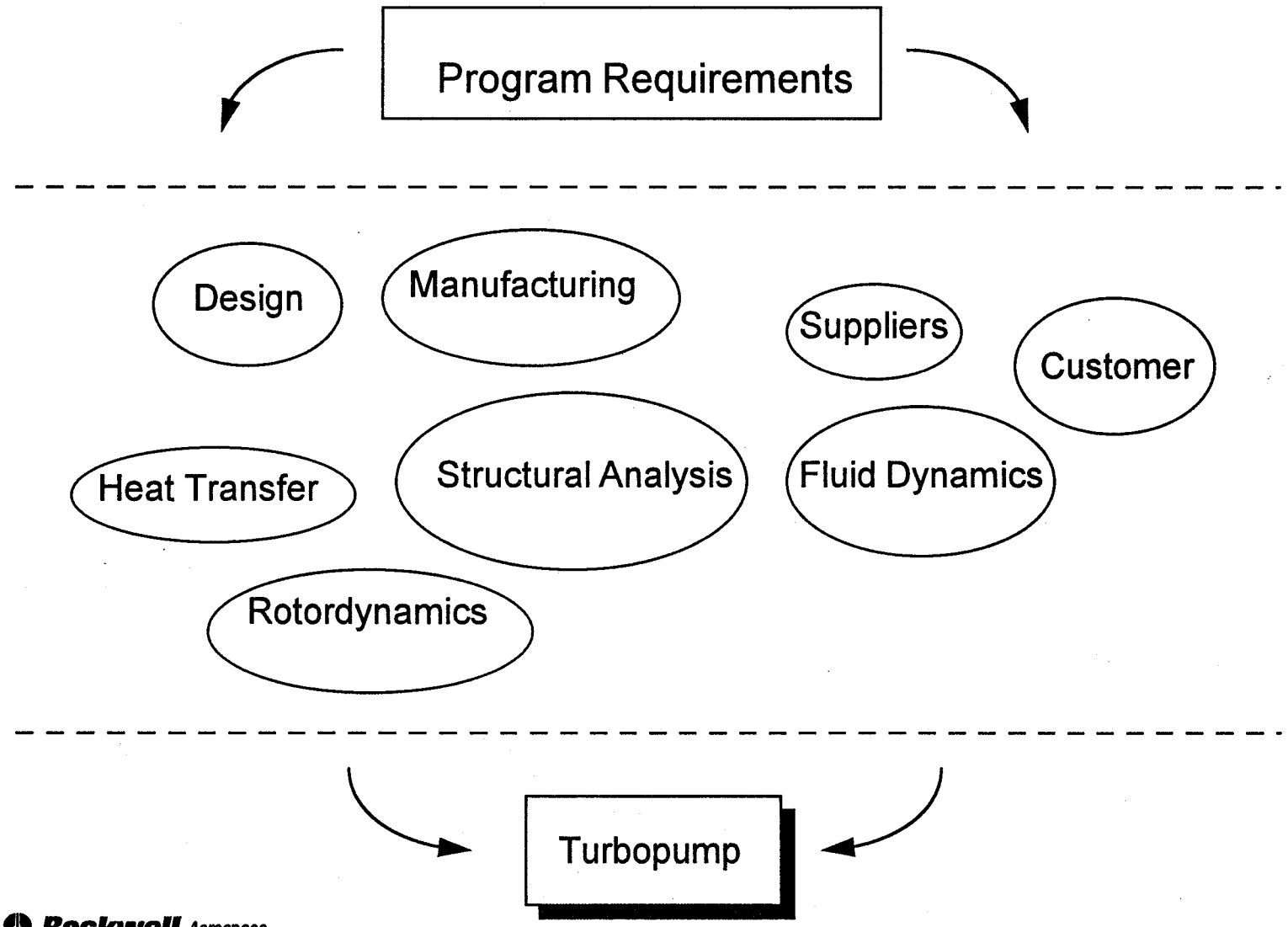

Rockwell Aerospace
Rocketdyne

Design and Manufacturing Models

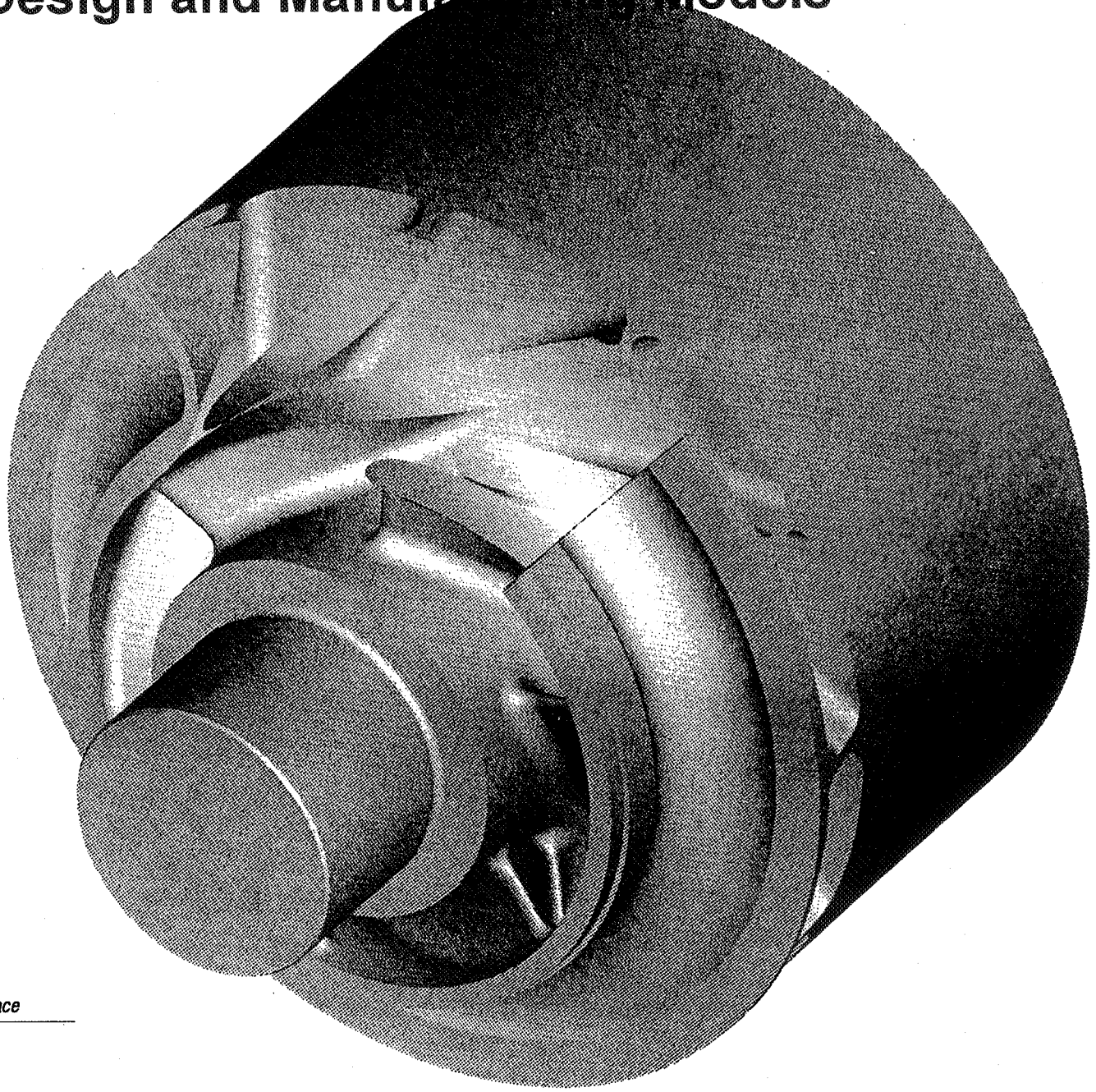

Rockwell Aerospace
Rocketdyne

Fluid Dynamics Flow Passage Model

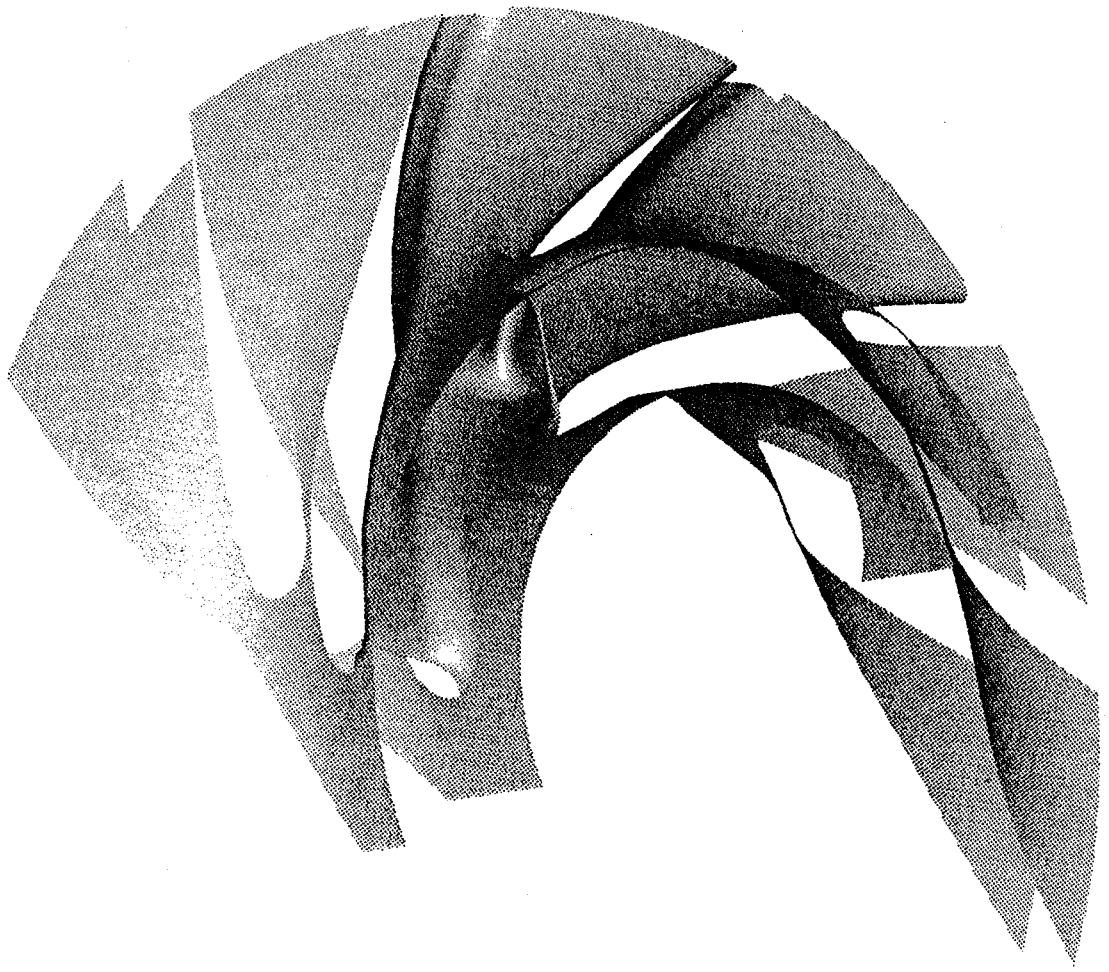

Structural Analysis Model

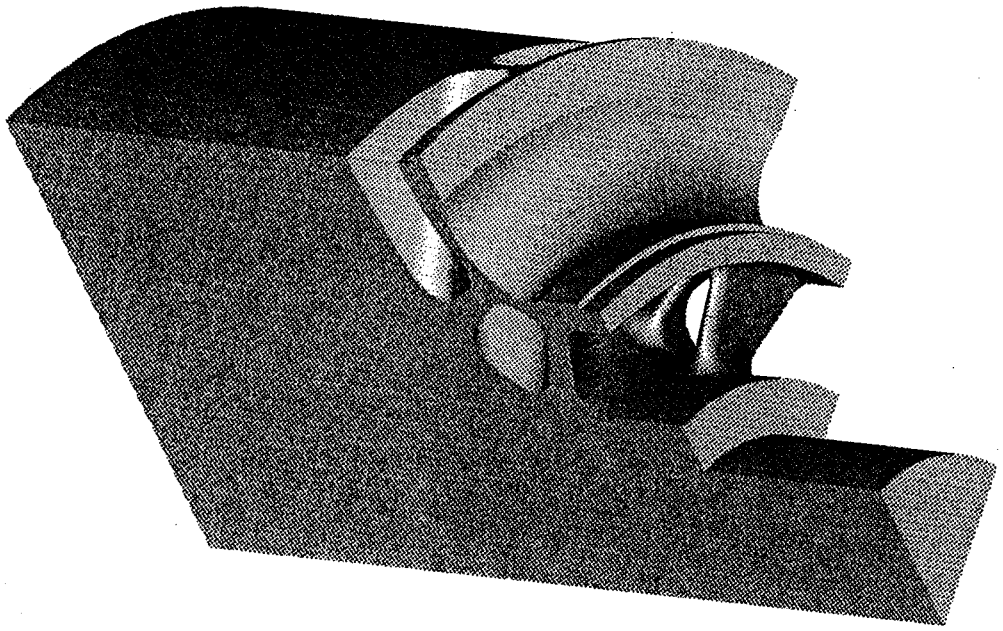

Process Enabling Tools

- **CAD/CAE Tools**
  - Solid Modeling
  - Associative, Parametric, Feature based system
- **Rapid Grid and Mesh Generators**
  - Flow passage gridding for CFD
  - Mesh generation for Structural Analysis
  - Associative to solid model
- **Validated Solver**
  - Quasi-3D solvers and REACT3D
  - Structural Analysis, FEM's and SAFER
  - Heat Transfer
- **Electronic Links**
  - Environment File for transfer of boundary condition data

Impeller Design Process

- **Design Issues**
  - Structural and performance requirements push state of the art
  - Complex 3-Dimensional geometry
  - Minimize blade thickness and fillet radii to meet performance
  - Maintain factors of safety on design
- **Design Process**
  - Fluid Dynamic definition of blade passages
  - Design definition of attachment geometry
  - Structural definition of shroud and blade thickness and fillet radii

Impeller Model Geometry

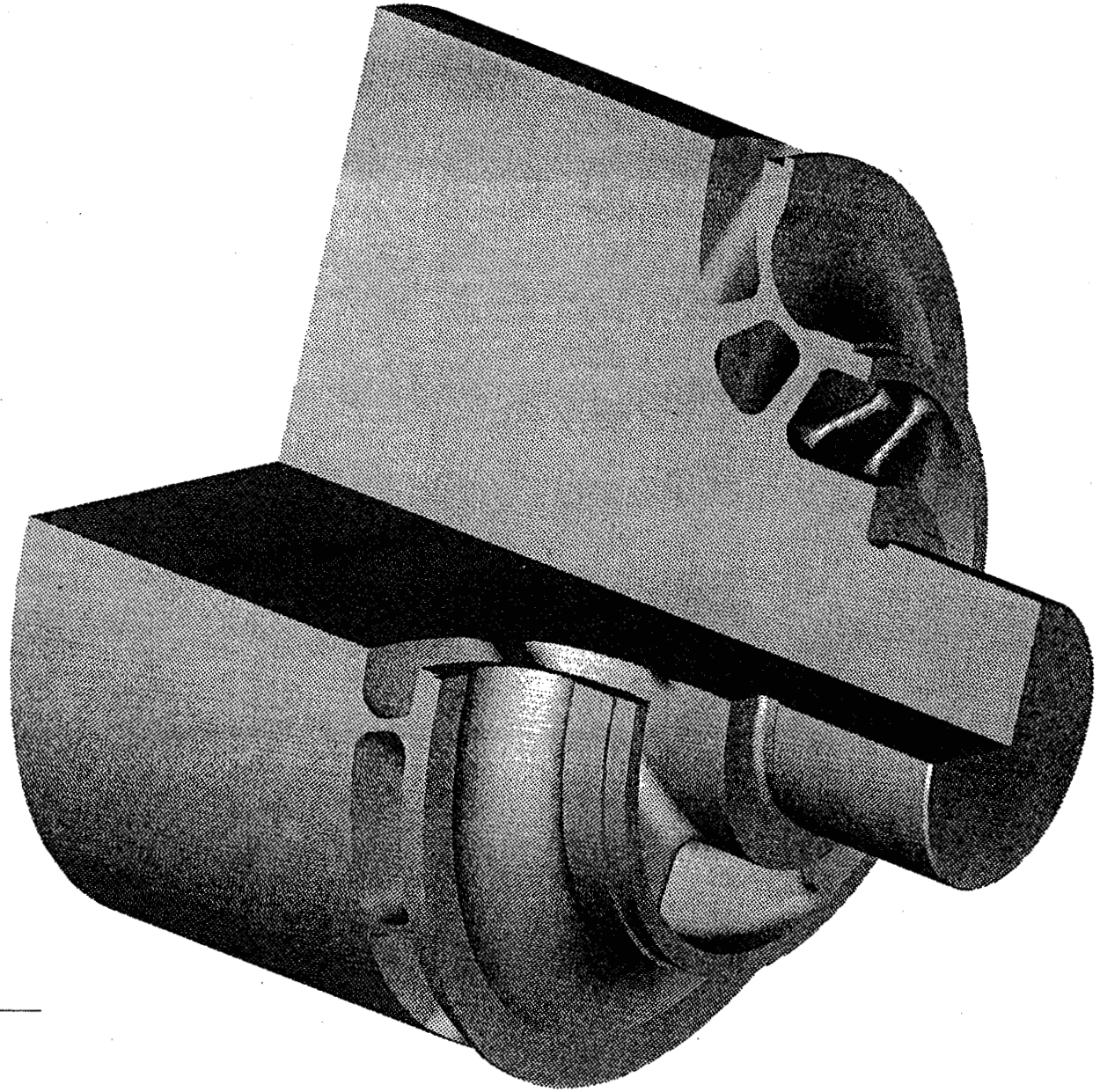

Traditional Impeller Design Process

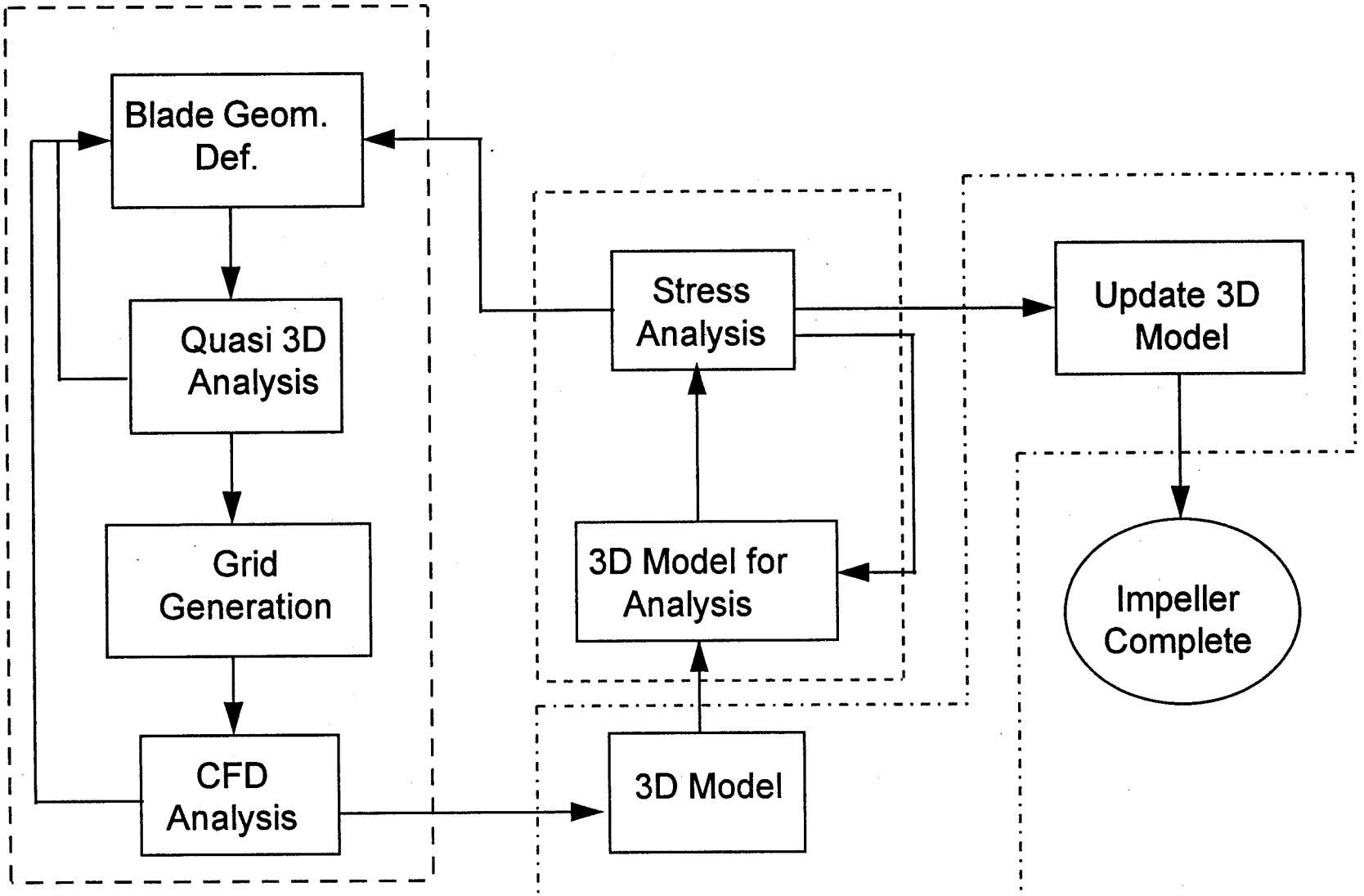

Rockwell Aerospace
Rocketdyne

Impeller Design Process

- **Solution**

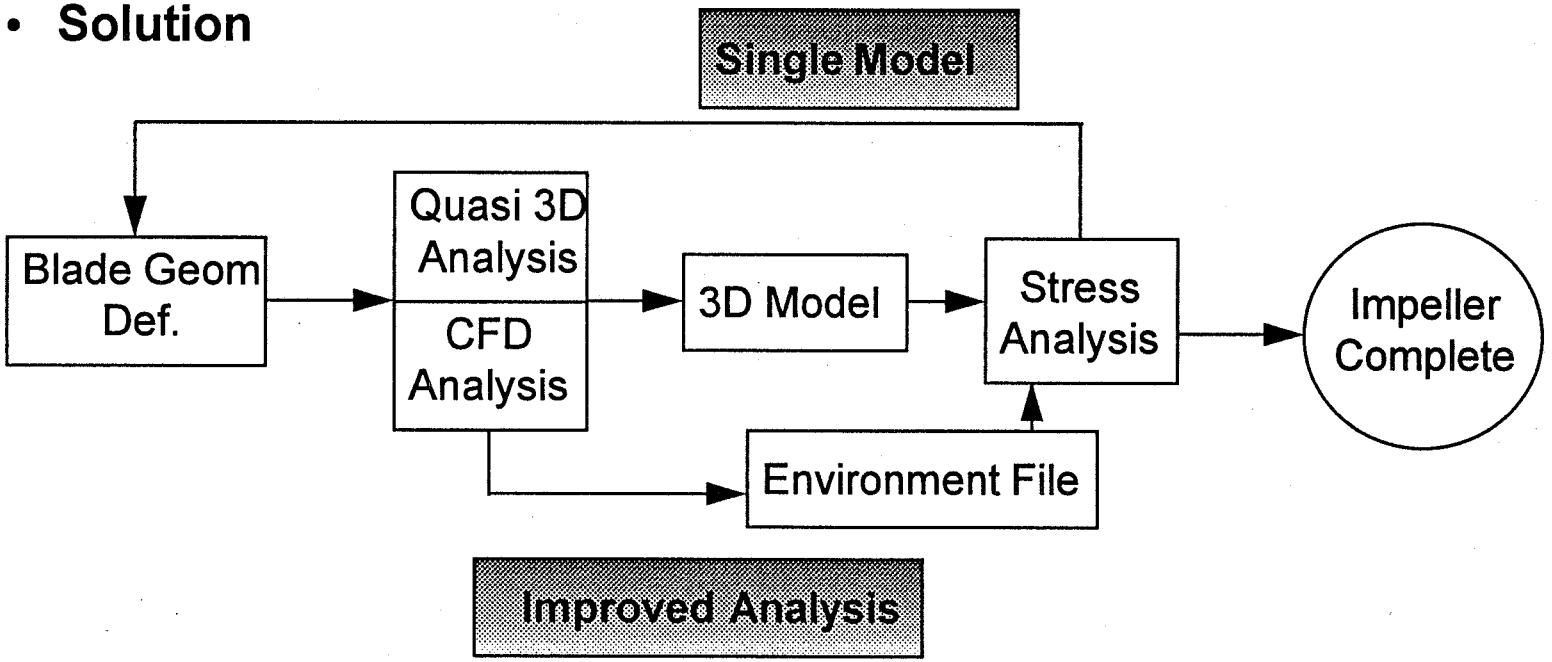

- **Metrics**
  - HPFTP 1360 man-hours reduced to 101 man-hours
  - NLS 6+6 impeller took 700 man-hours versus 85 man-hours for latest designs

RRTT Applications

- **Process Successfully applied to RRTT primary flow path elements**
  - Stator
    - CFD and 3D geometry complete
  - Impeller
    - CFD and 3D geometry complete
  - Diffuser-Volute
    - Flow passage defined
    - Structural analysis of housing in work
  - Turbine Nozzle
    - Multiple iterations between stress and fluid dynmacs underway
    - Casting evaluation started
  - Blisk
    - Fluid dynamic and structural evaluation underway
- **Detailed analysis addressing long lead components early in product definition phase**

Stator Model

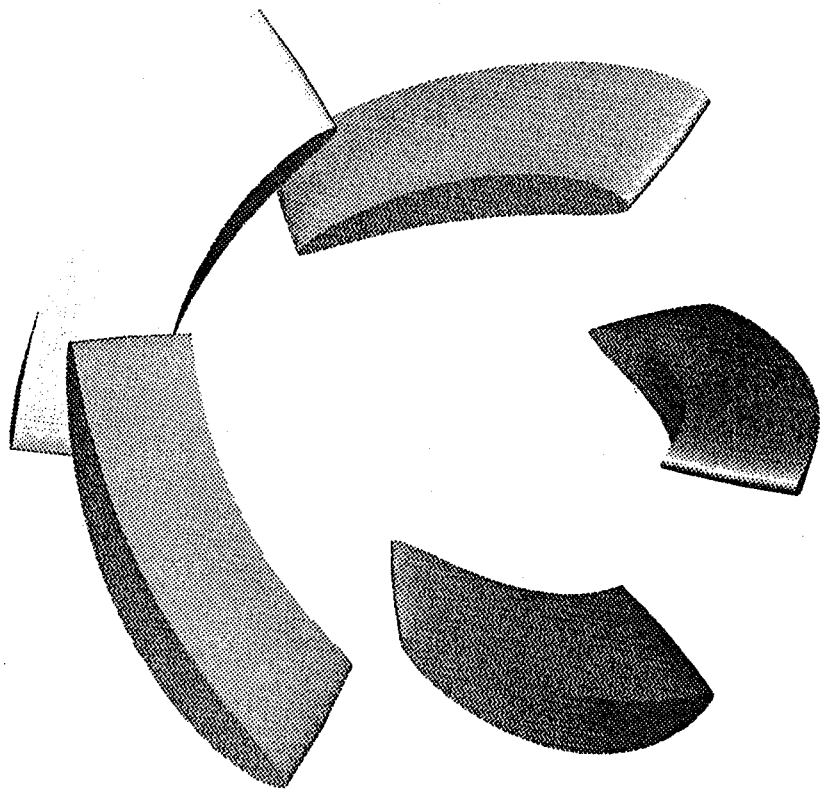

RRTT Stator Velocity Distributions

REACT3D Solution

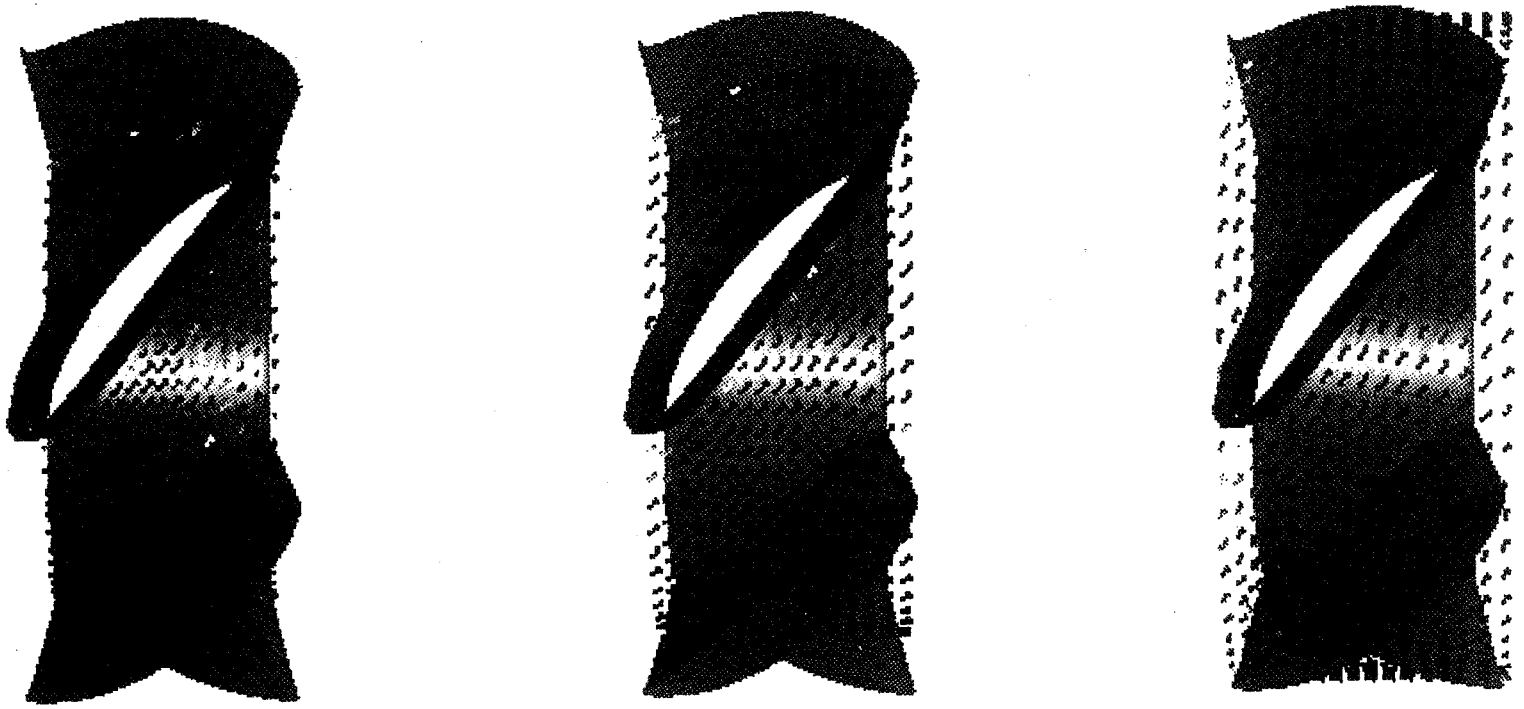

HUB RMS TIP

Impeller Model

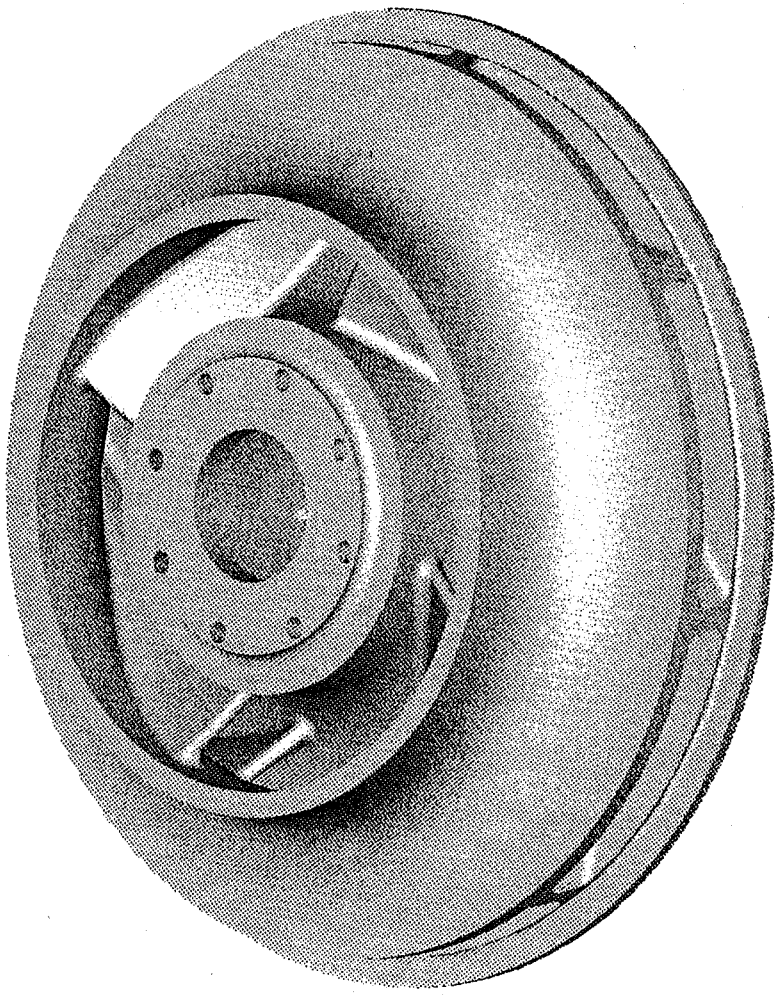

RRTT IMPELLER VELOCITY VECTOR AT MID-SECTION

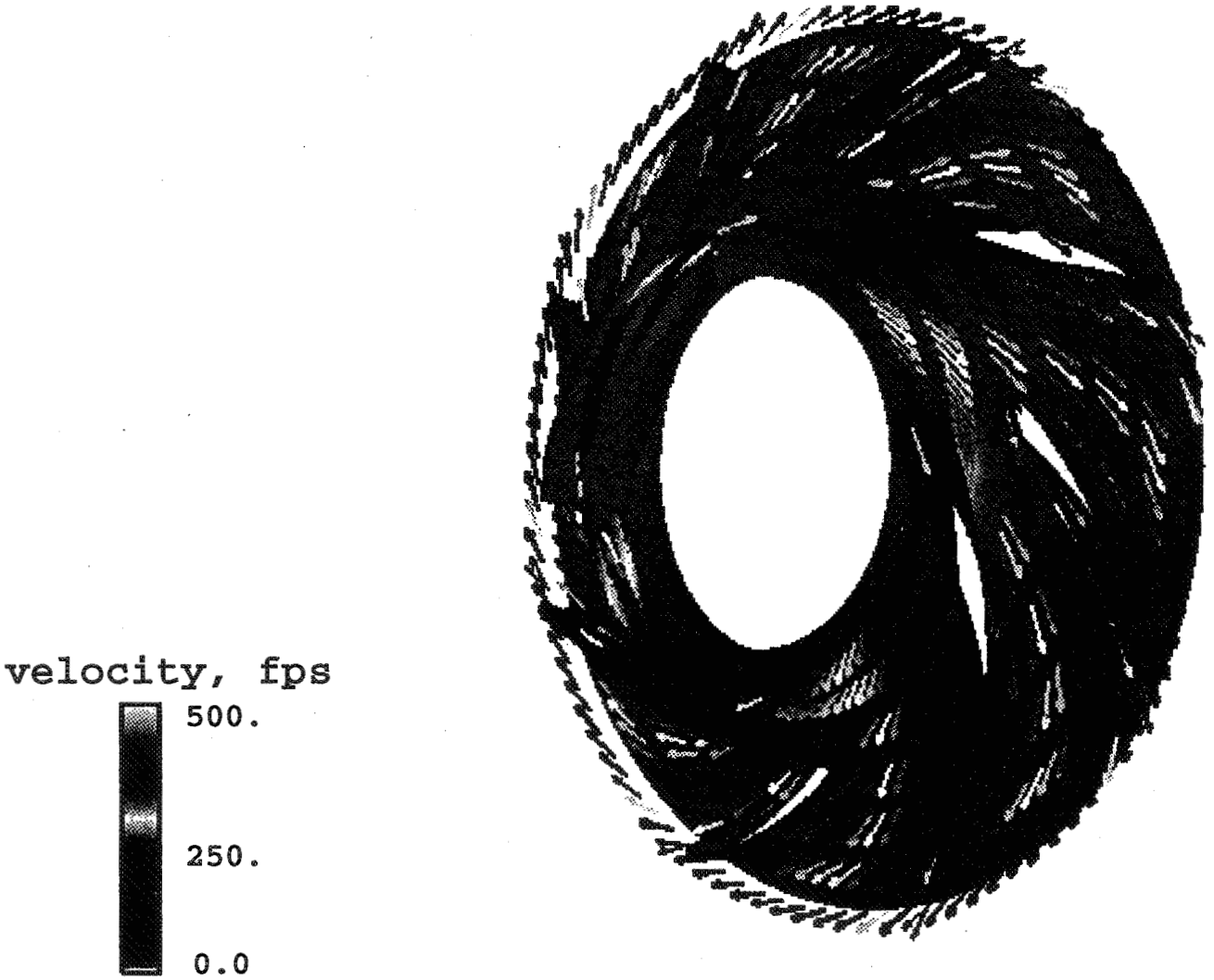

Pump Housing Model

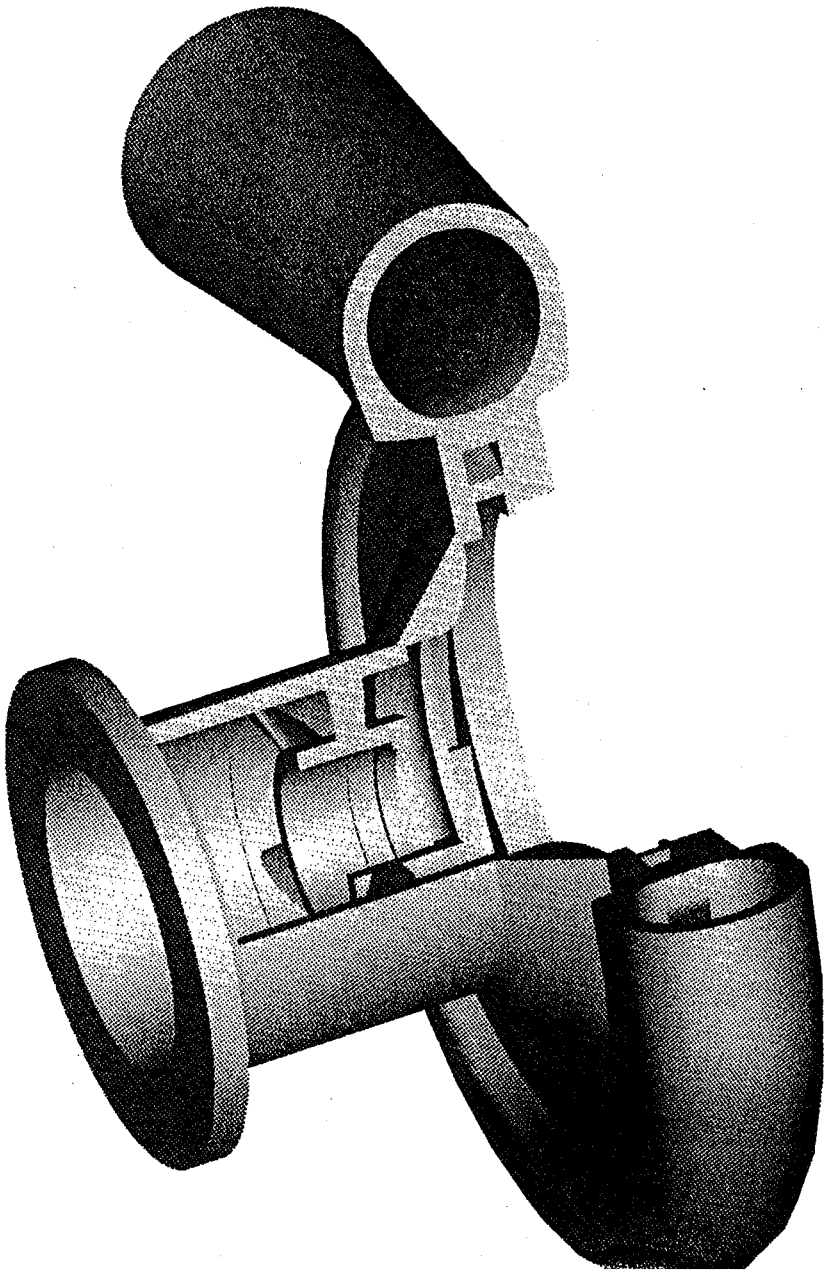

Diffuser and Volute Flow Path

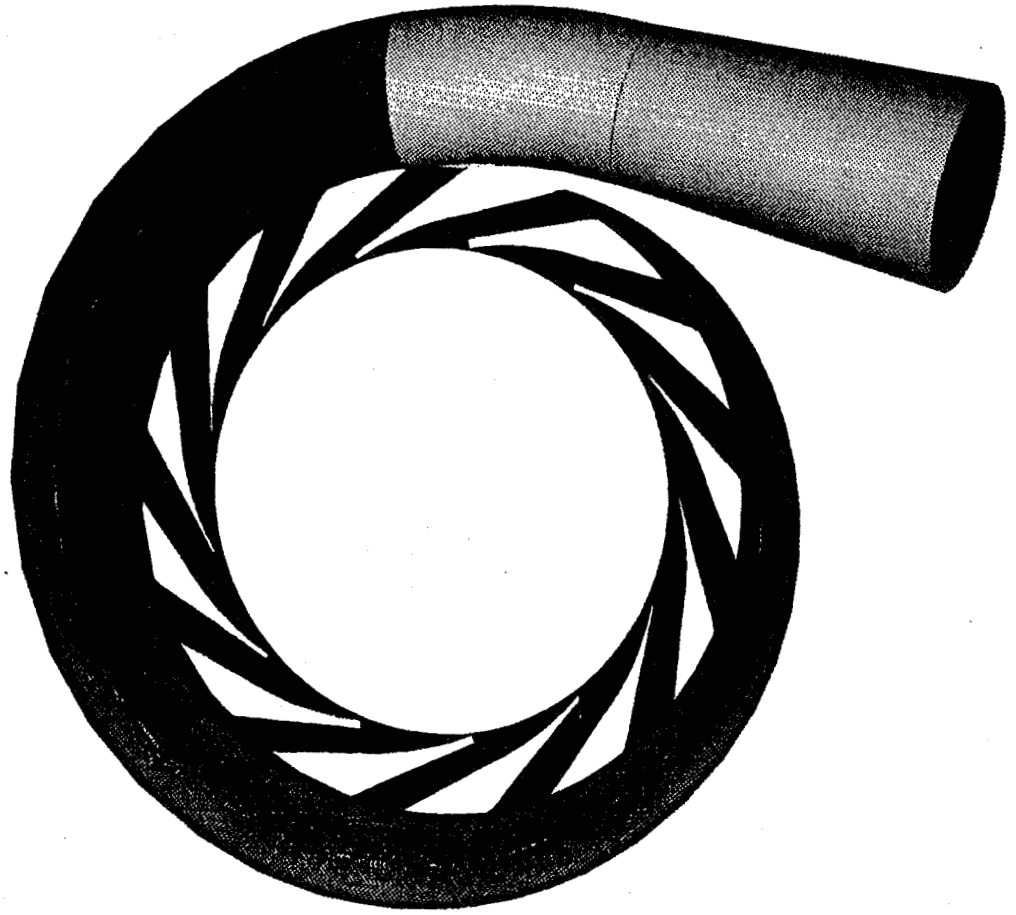

Axisymmetric Structural Model Of RRTT Pump Housing

Turbine Housing Model

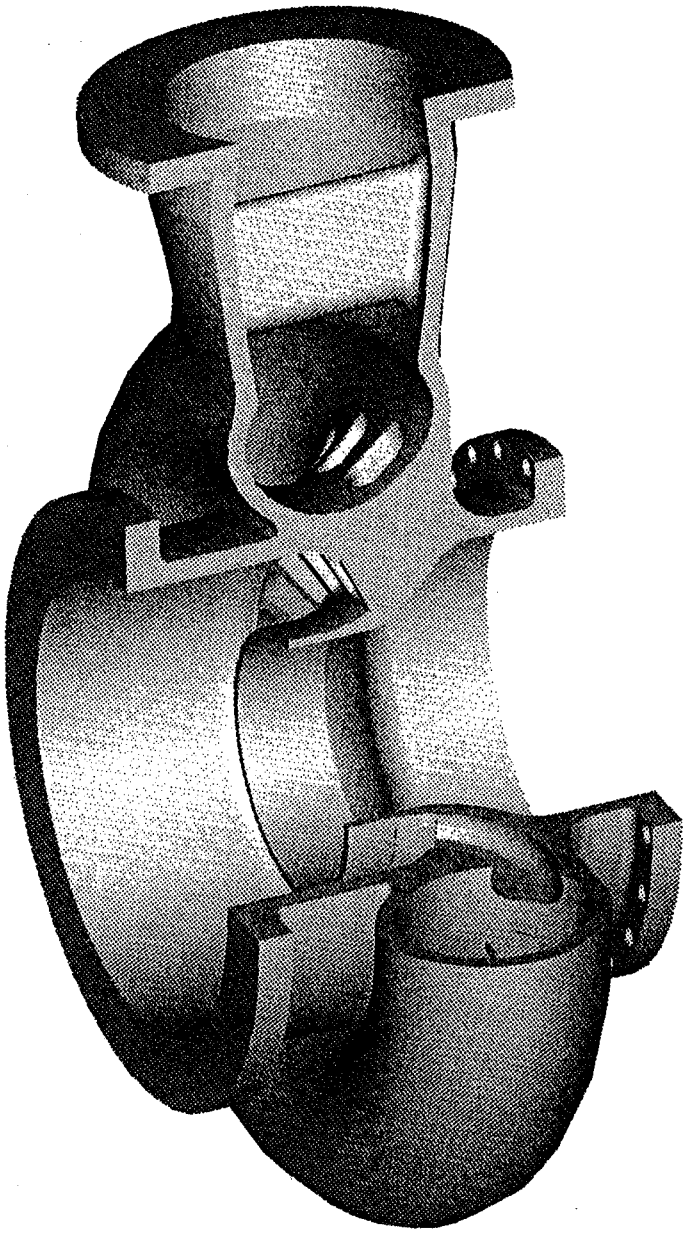

Rockwell Aerospace
Rocketdyne

Axisymmetric Model of Turbine Housing

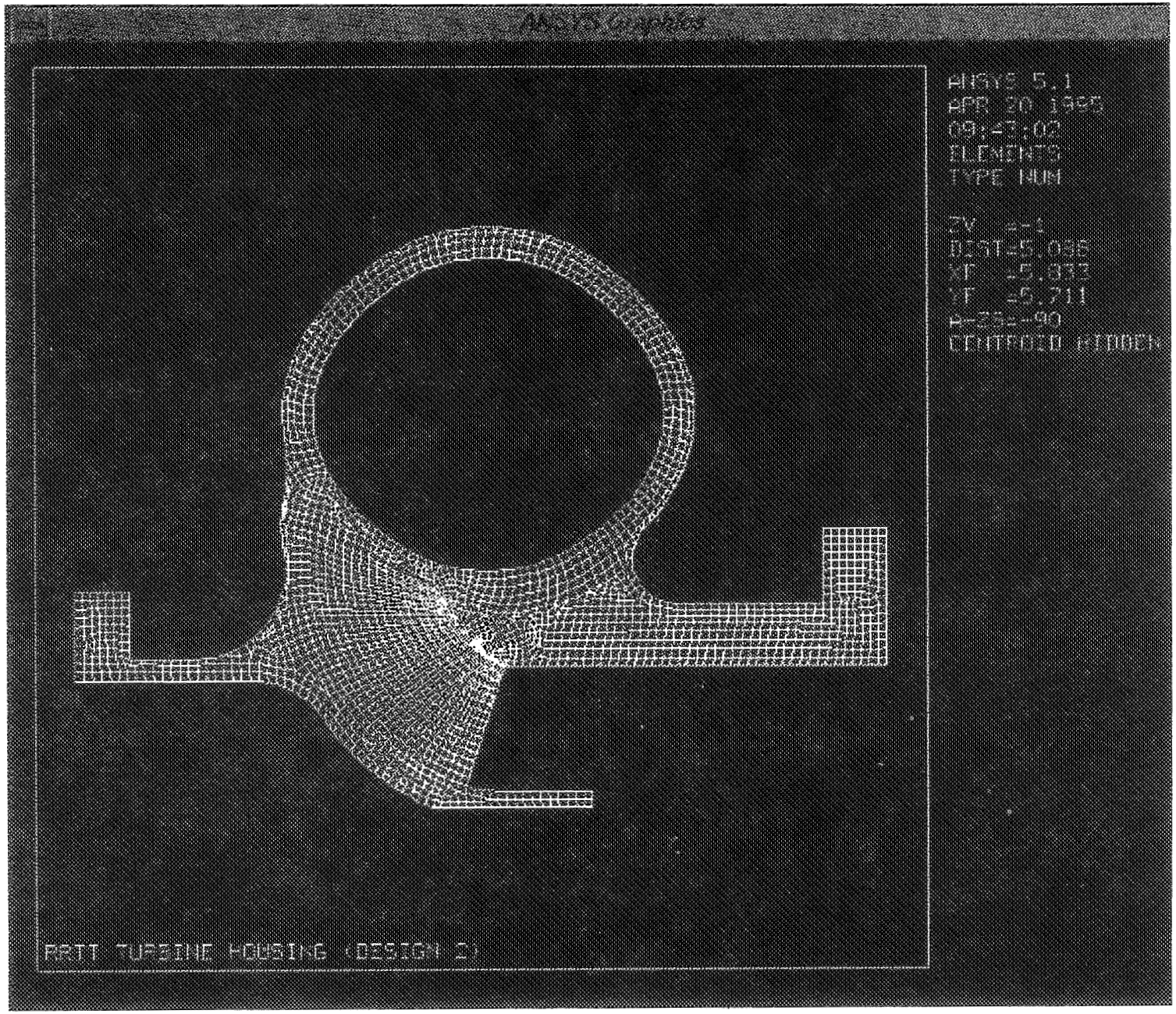

Shaft and Blisk Model

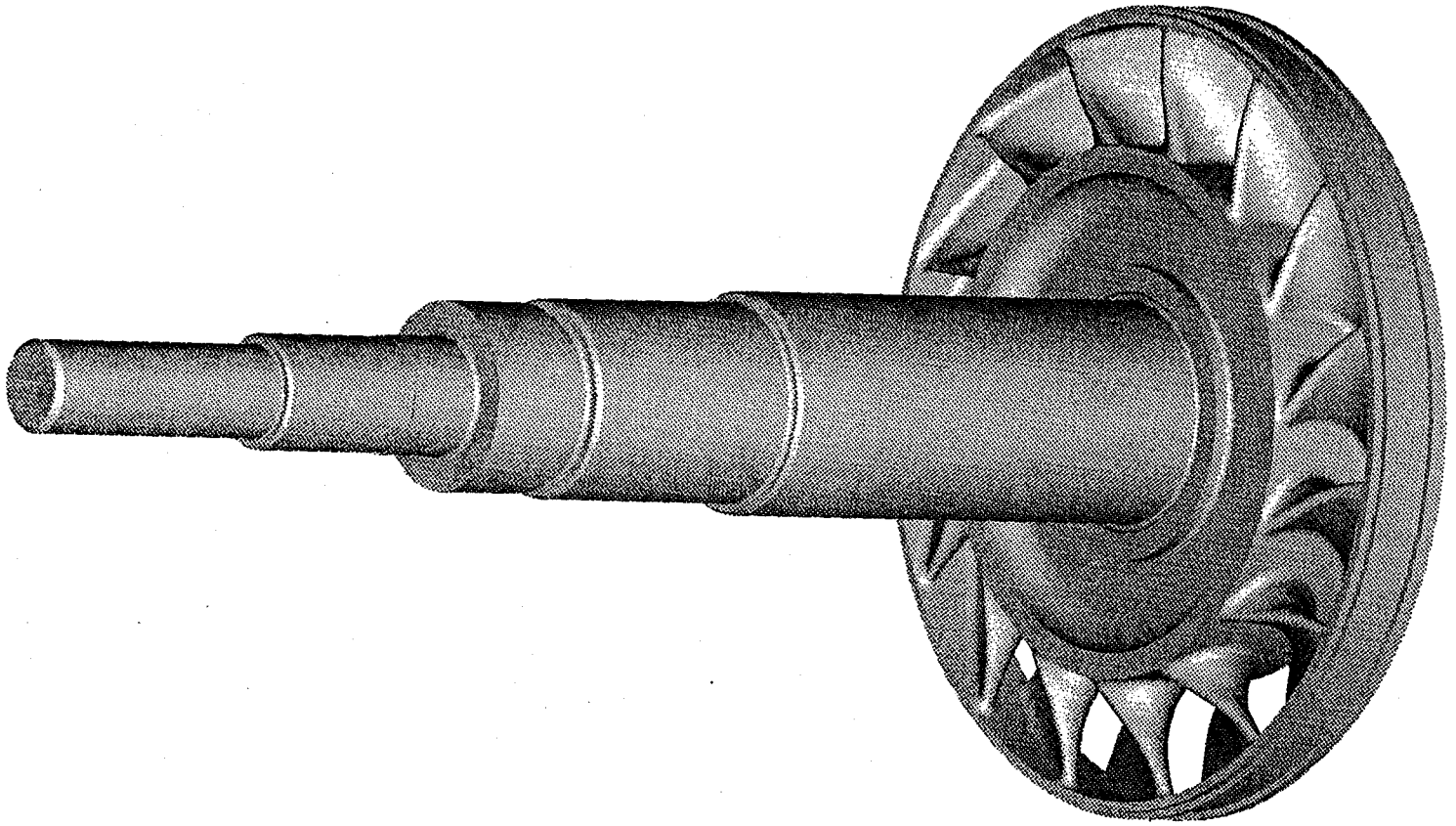

3D Structural Model of Turbine Rotor

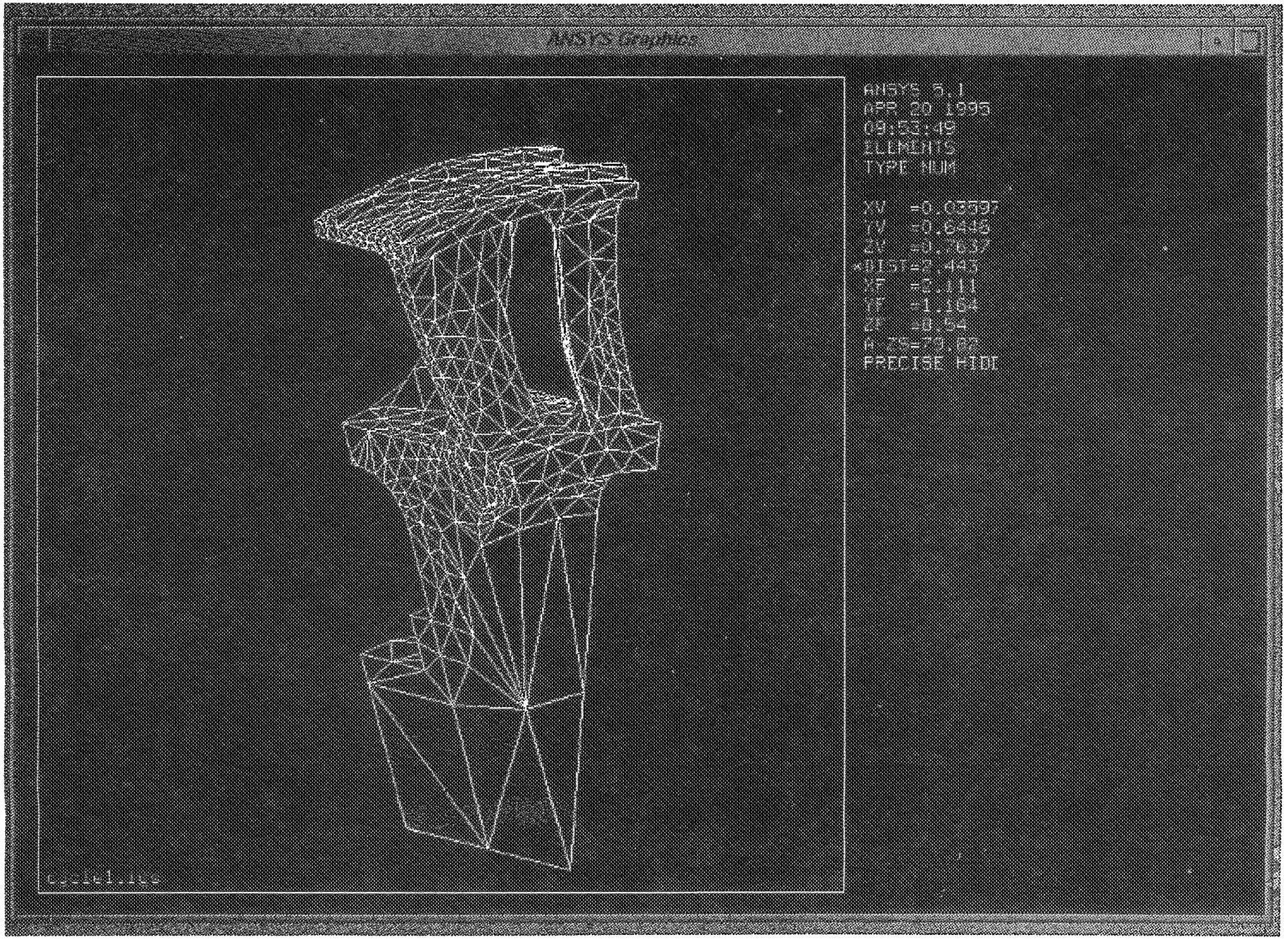

Conclusion

- Process Concentration Key to Success
- Tool Development Required for Information Transfer
- Significant Design Time Reductions Obtained

Three–Dimensional Viscous Flow Analysis for Rocket Propulsion System with Structured and Unstructured Grid Methods

Chunill Hah
NASA Lewis Research Center

James Loellbach and Fu–Lin Tsung
Institute for Computational Mechanics in Propulsion
NASA Lewis Research Center

Objectives

- Establish an unstructured solution capability for 3D viscous turbomachinery flows to compliment an existing structured capability
- Validate the unstructured solver by comparing numerical results with experimental data
- Assess the performance of the unstructured solver by comparing with that of a well–established structured solver
- Identify areas for improvement in the unstructured solver

Motivation

- The present structured solver has limitations:
  - limited choice of topologies
  - difficulty of generating grids for complex geometries

- We desire an alternate solution technique that provides greater geometric flexibility for complex geometries

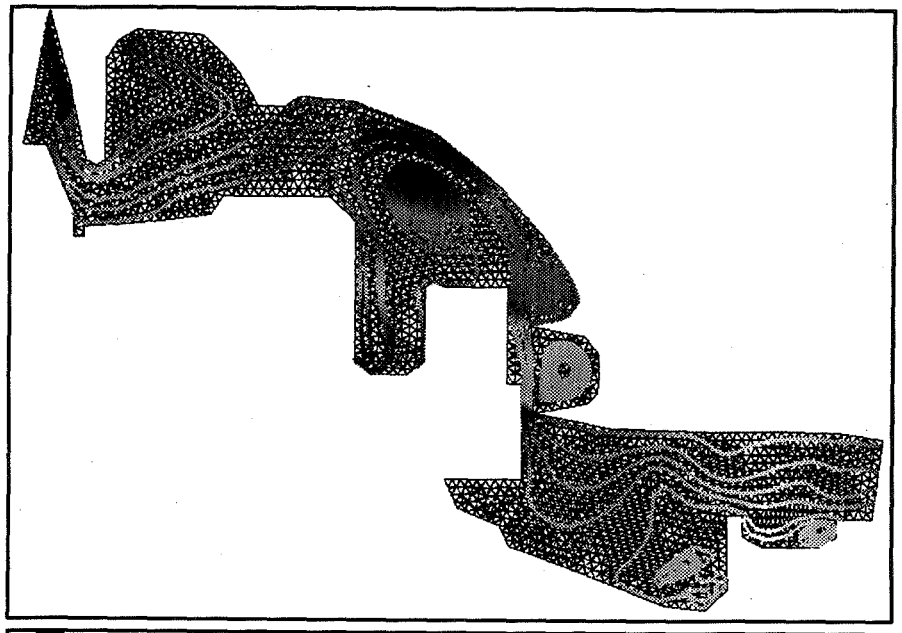

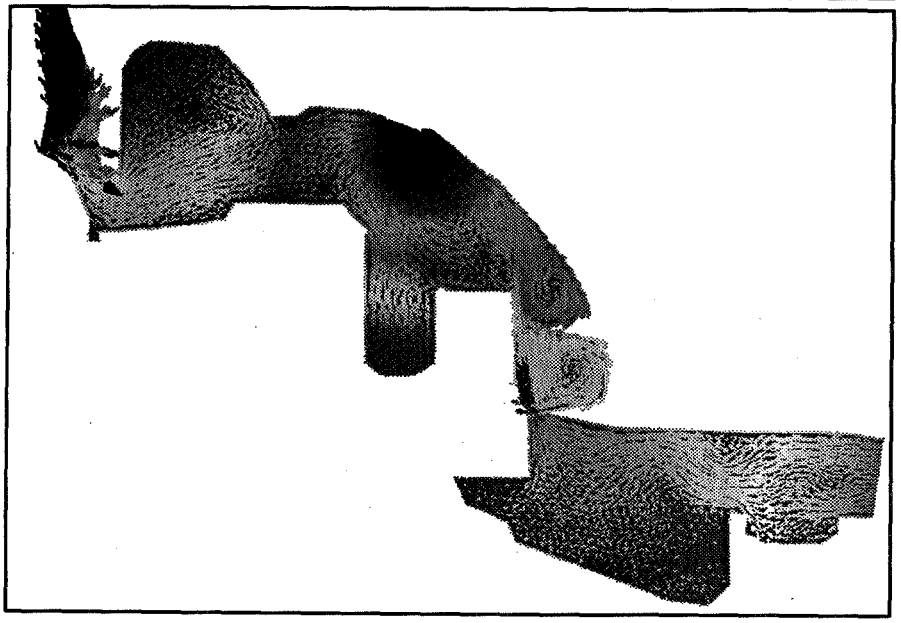

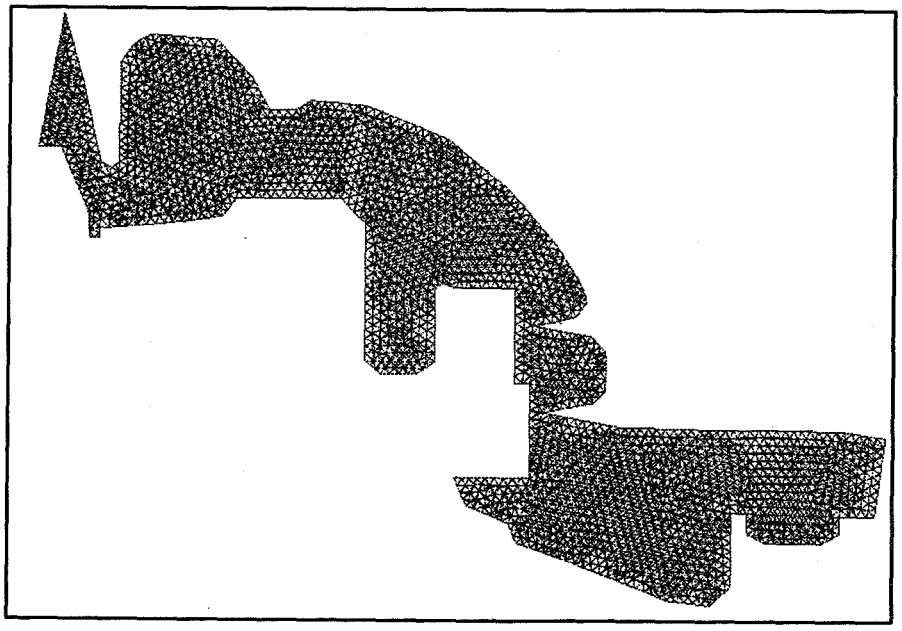

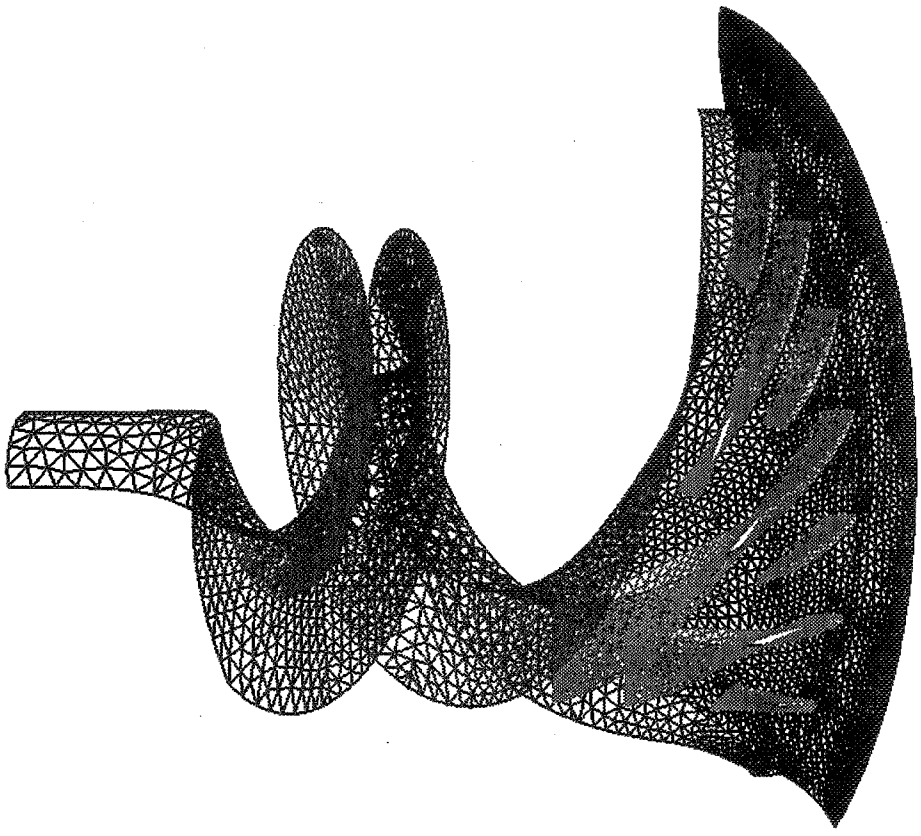

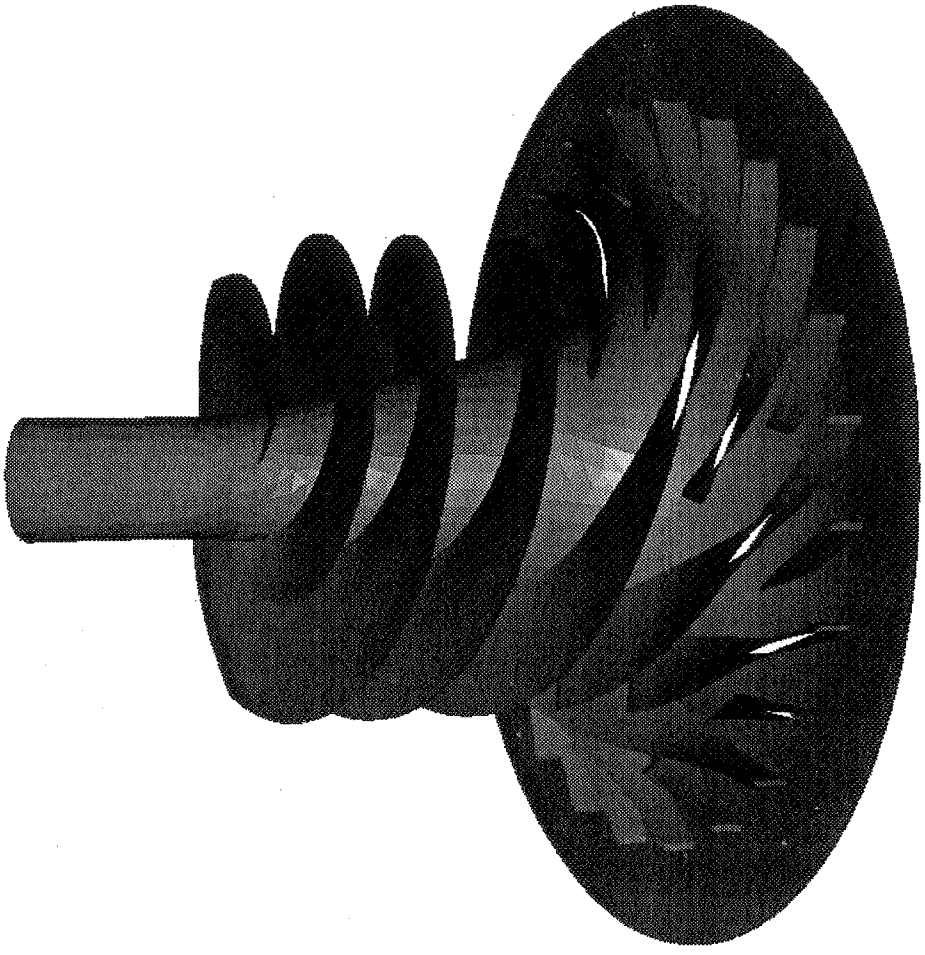

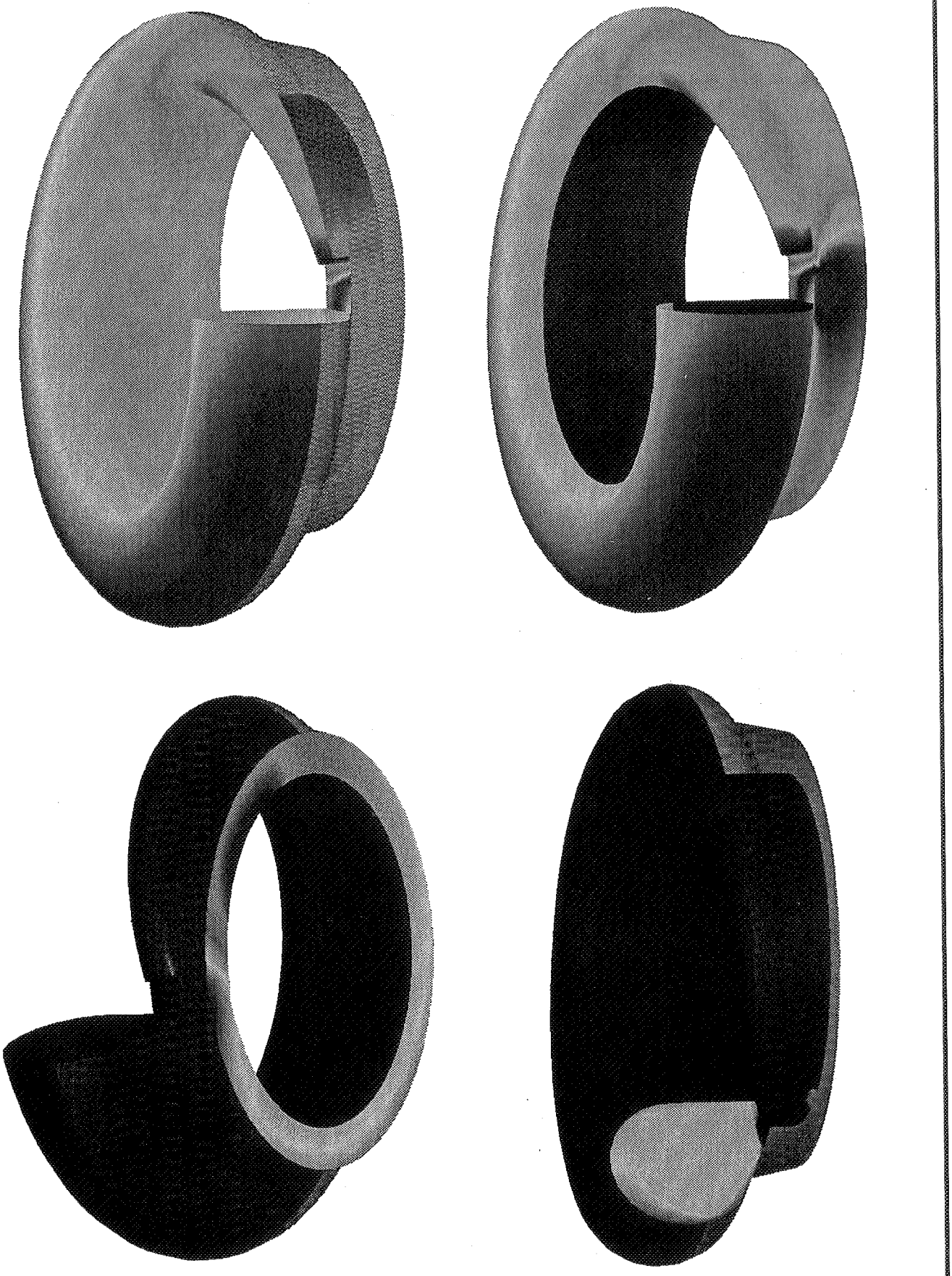

Test Case and Conditions

- DLR Low Speed Annular Turbine Test Rig

- 25–blade turbine stator blade row (annular cascade)
  - Blade aspect ratio = 0.61
  - Constant–radius hub and tip endwalls

- Subsonic flow
- Inlet Mach number = 0.176
- Exit Mach number = 0.74
- Reynolds number = 1.0×10^6

- 5–hole probe traverses at Stations 0 and 4
- Laser velocimetry at Stations 1 through 4

Test Section

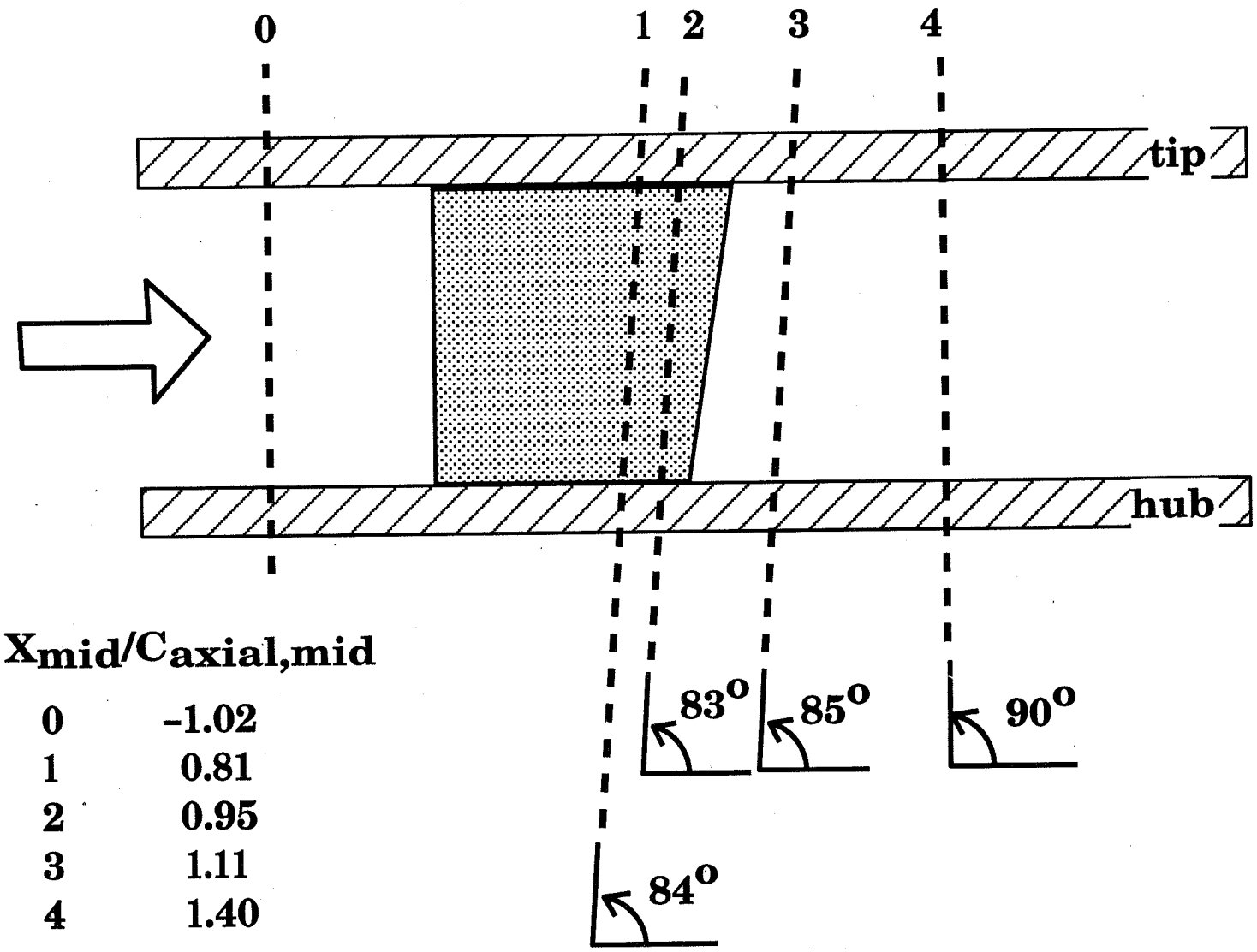

$X_{mid}/C_{axial,mid}$	
0	-1.02
1	0.81
2	0.95
3	1.11
4	1.40

Structured Grid

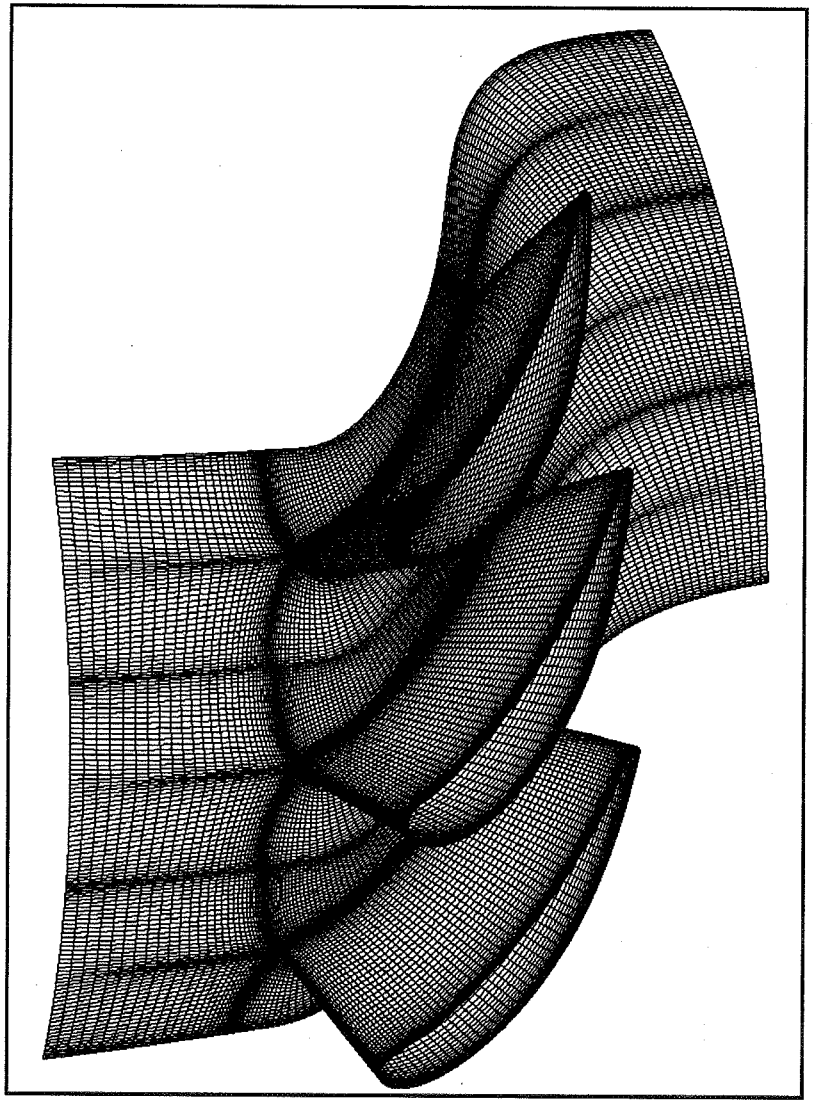

151 x 50 x 51
385050 Nodes
385050 Control Volumes

Numerical Procedures
Structured Solver

- Node–based finite volume method
- Third–order upwind inviscid flux calculation
  Centrally–differenced viscous flux calculation
- Implicit relaxation of steady–state governing equations
- k–e turbulence model
- Automatic switching between wall function and integration to the wall based on y+ of first grid point.

Unstructured Grid

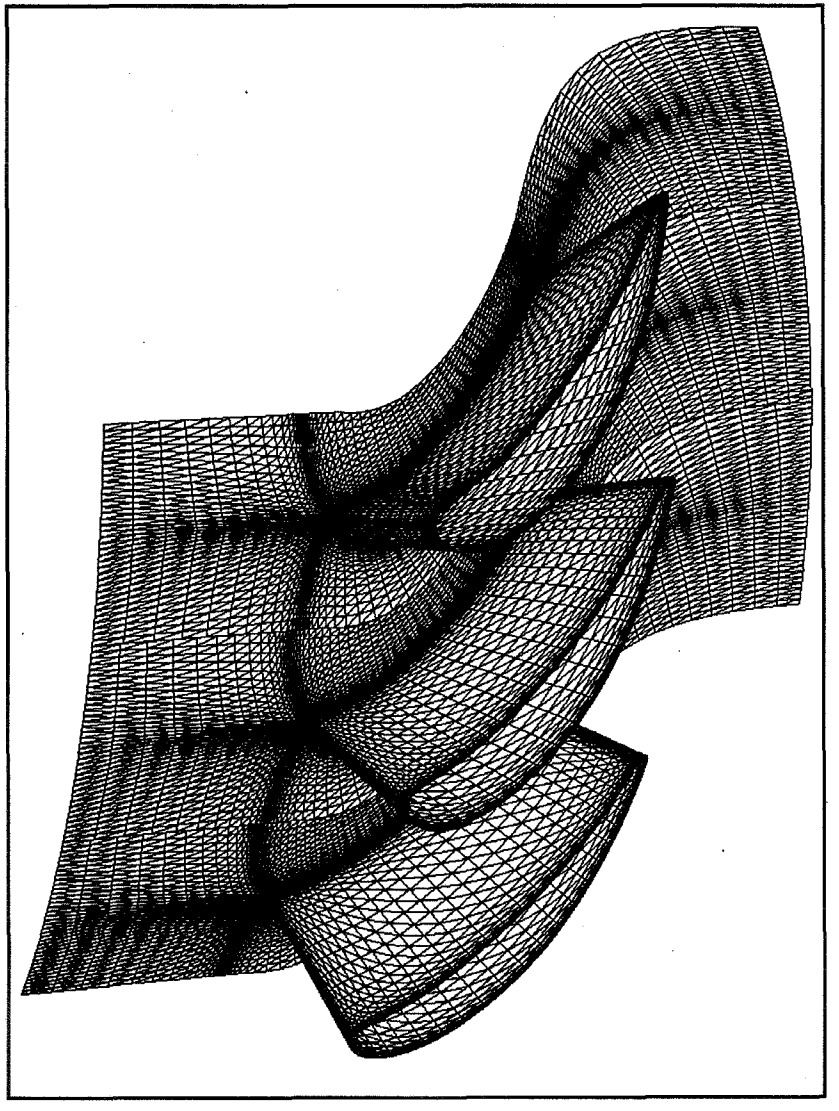

76 x 38 x 25
71150 Nodes
388800 Control Volumes

Numerical Procedures
Unstructured Solver–1

- Based on USM3D unstructured Solver
- Cell–based finite volume method
- Second–order Roe FDS inviscid flux calculation
  Centrally–differenced viscous flux calculation
  (inverse–distance weighted reconstruction from cells to nodes)
- Explicit 3–stage Runge–Kutta time integration of unsteady governing equations
- k–e turbulence model with wall function

Unstructured Grid–2

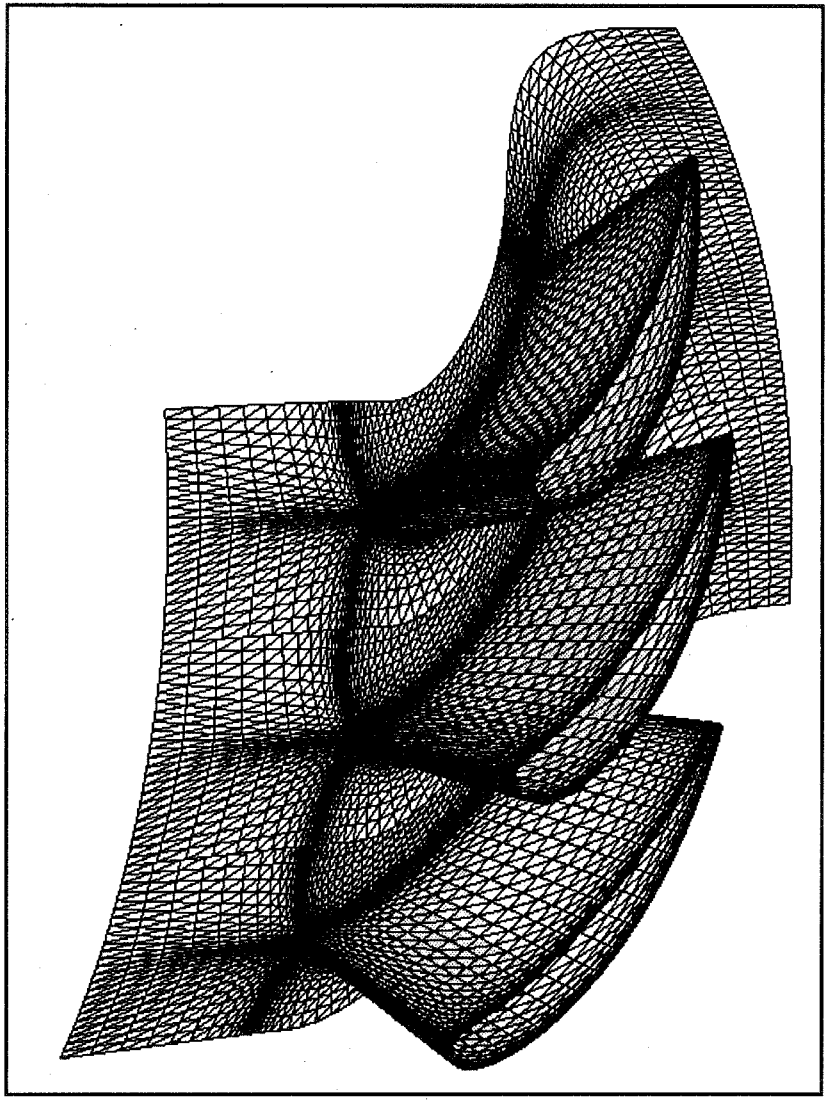

76 x 26 x 25
48375 Nodes
259200 Control Volumes

Numerical Procedures
Unstructured Solver–2

- Based on USM3D unstructured Solver
- Cell–based finite volume method
- Second–order Roe FDS inviscid flux calculation
  Centrally–differenced viscous flux calculation
  (Psudo–Laplacian reconstruction from cell to node)
- Implicit backward Euler time integration
- Spalart–Allmaras turbulence Model

Results

- **Discussion of solution costs**
- **Comparisons of computed and experimental flow properties at Stations 1, 3, and 4**

Axial Velocity Contours at Plane 1

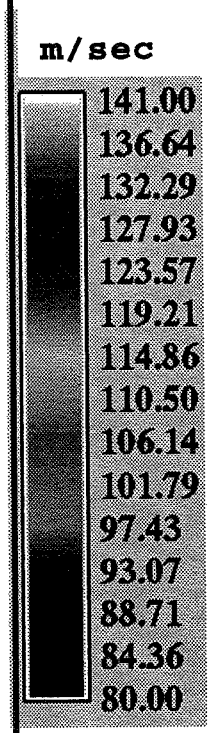

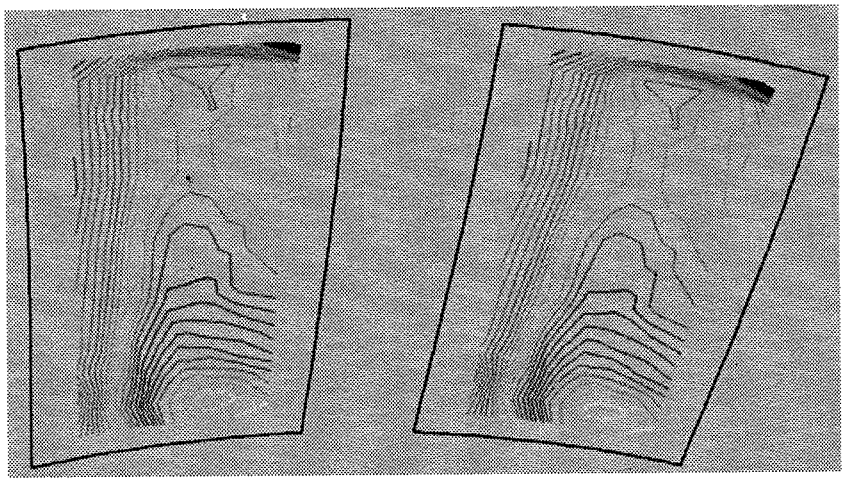

Experiment

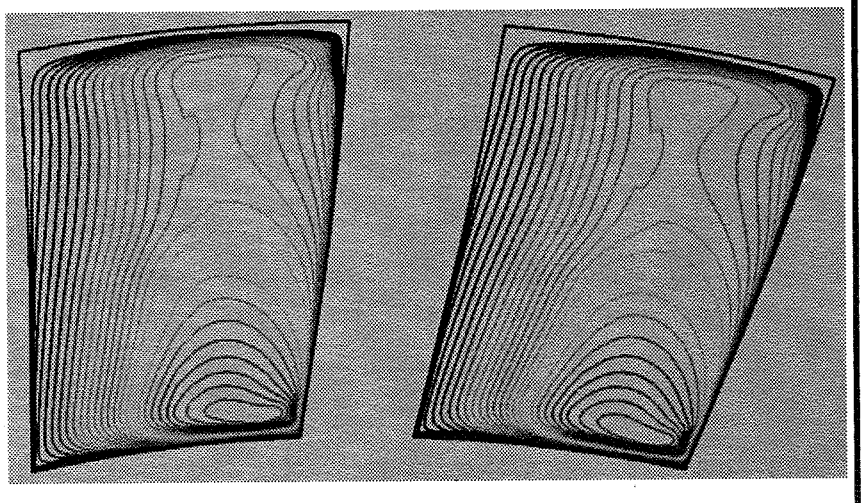

Structured grid

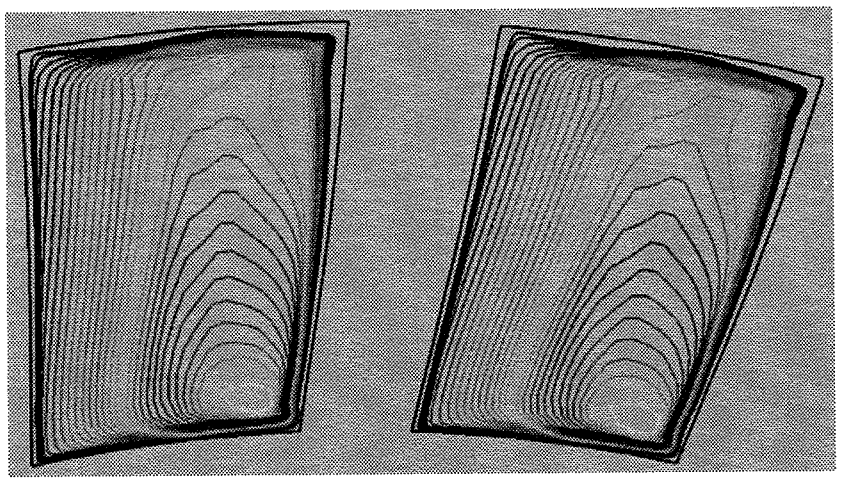

Unstructured–1

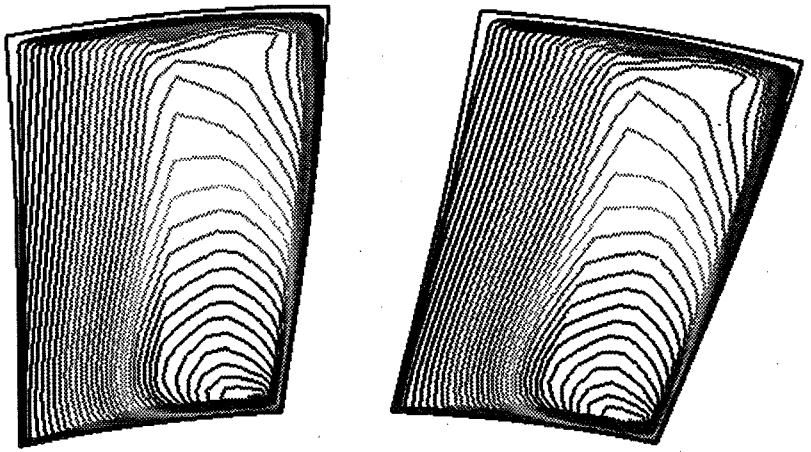

Unstructured–2

Tangential Flow Angle Contours at Plane 1

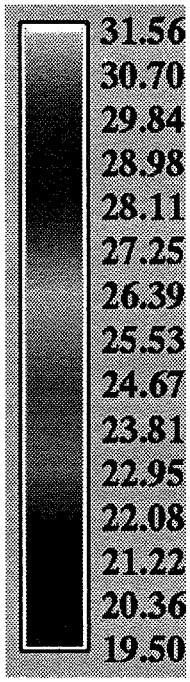

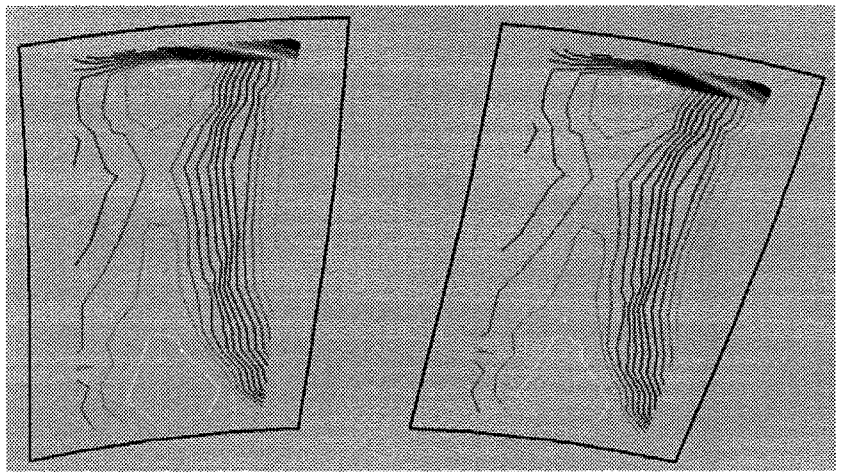

Experiment

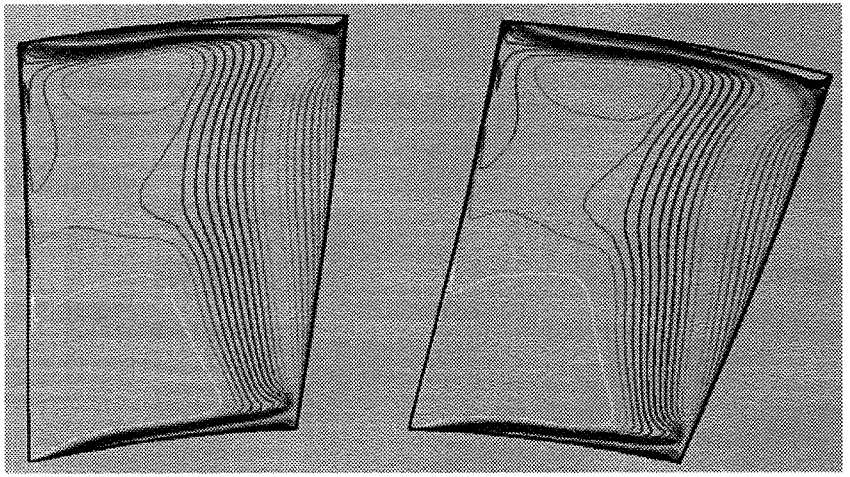

Structured grid

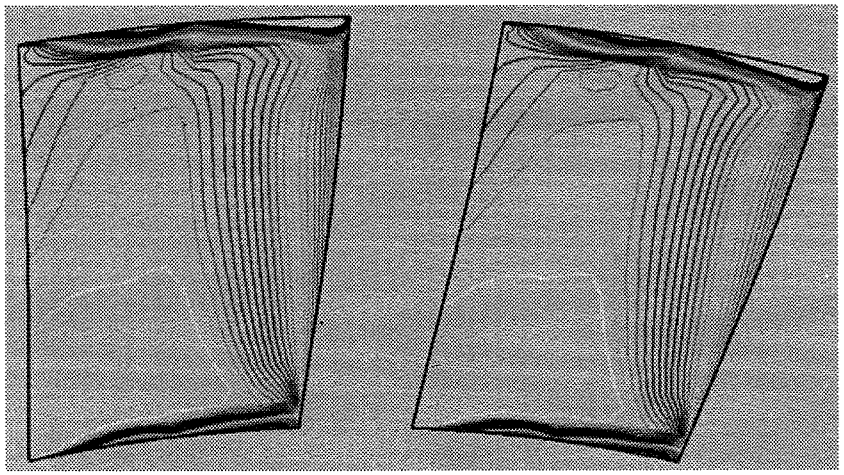

Unstructured–1

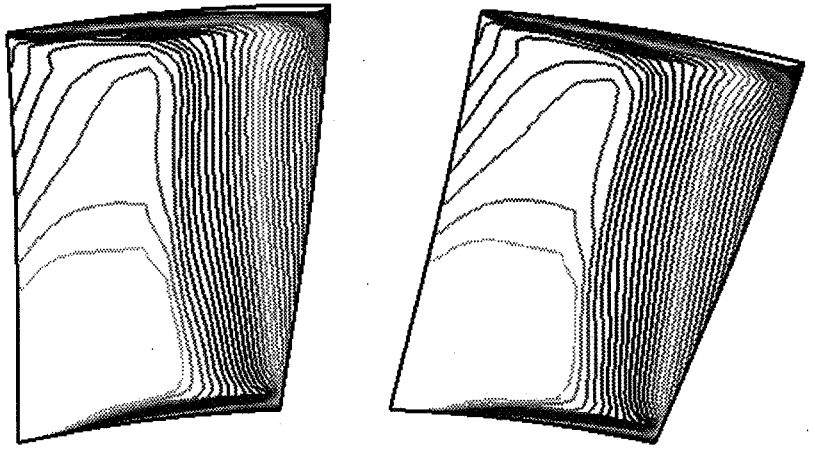

Unstructured–2

Axial Velocity Contours at Plane 3

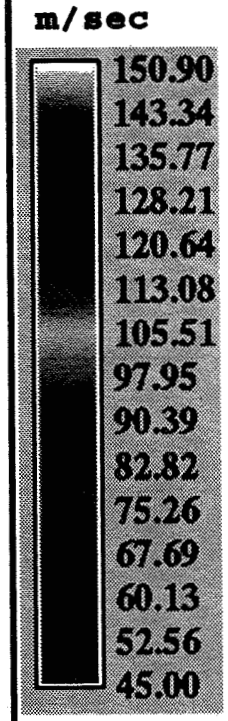

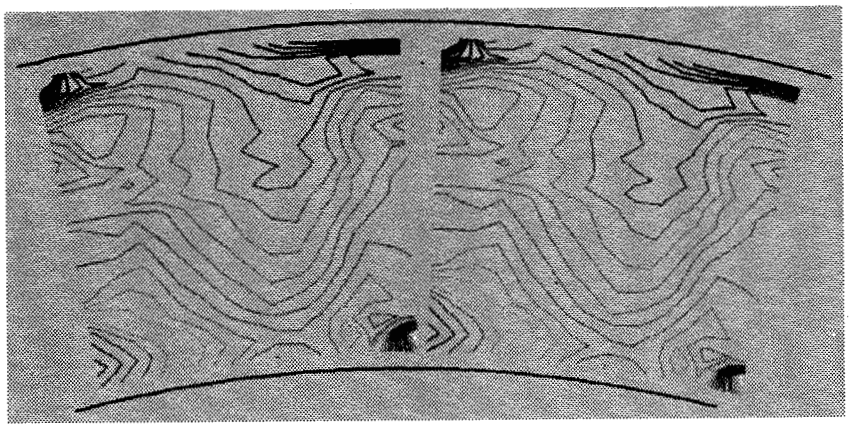

Experiment

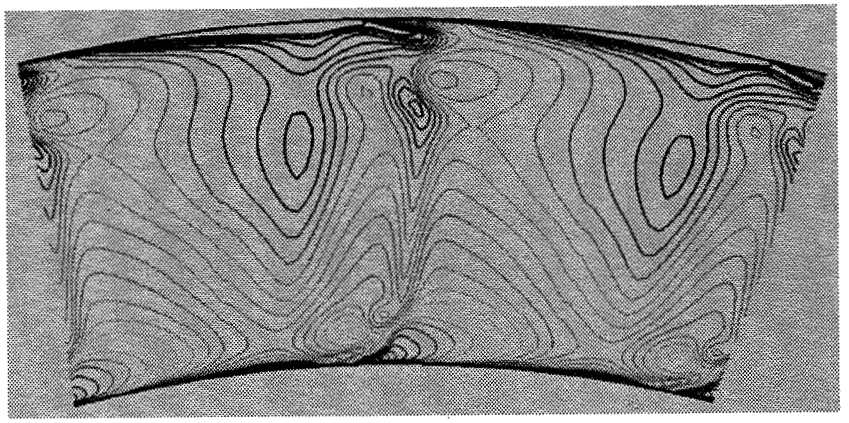

Structured grid

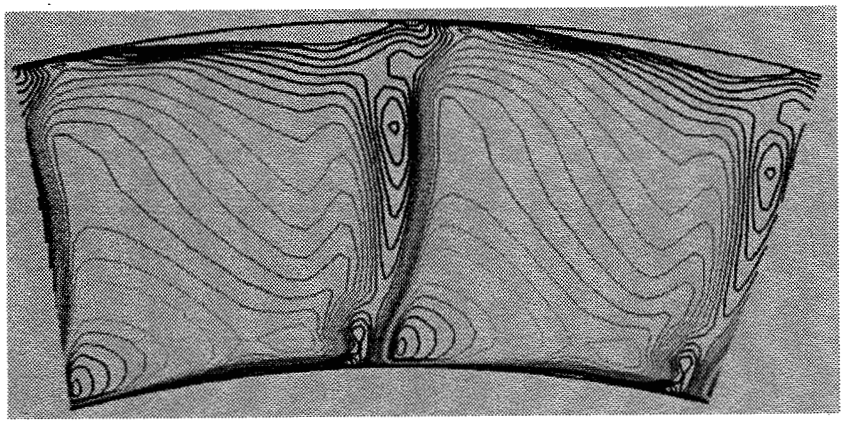

Unstructured–1

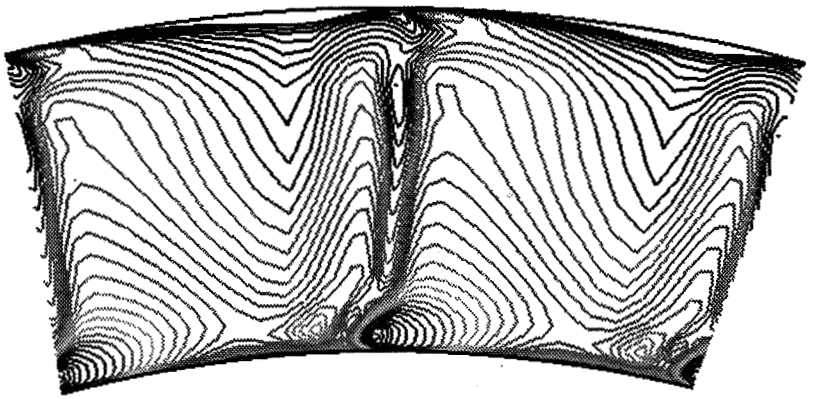

Unstructured–2

Tangential Flow Angle Contours at Plane 3

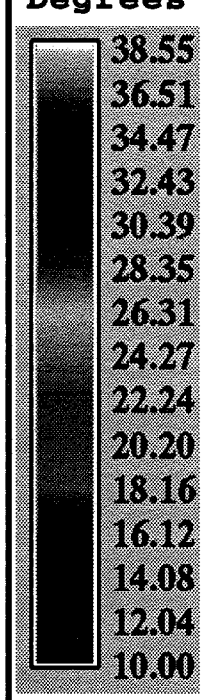

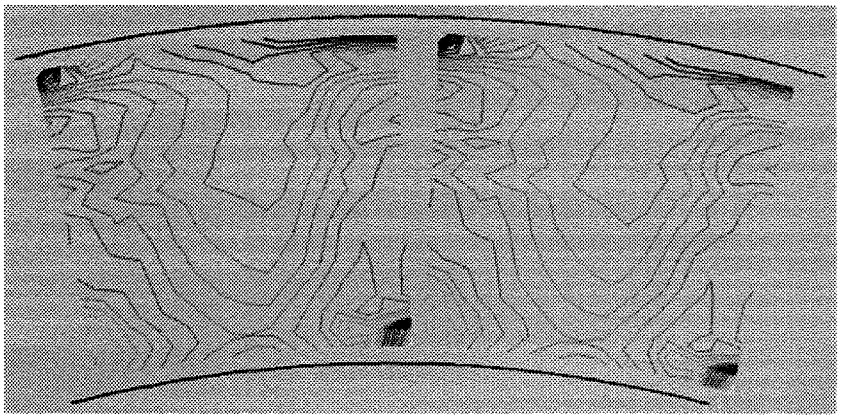

Experiment

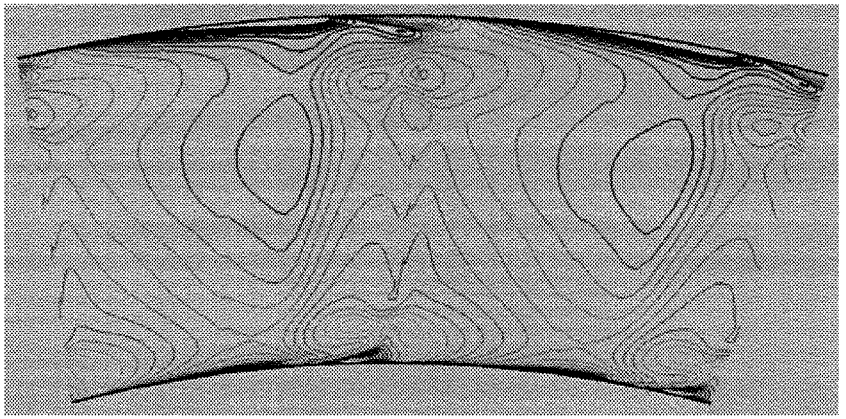

Structured grid

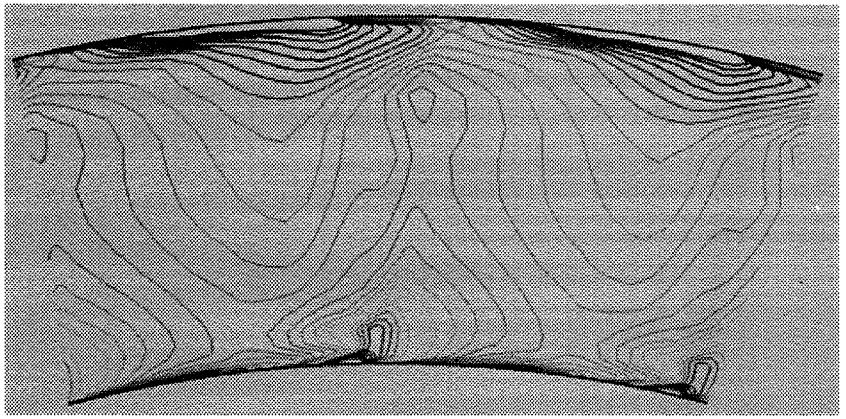

Unstructured–1

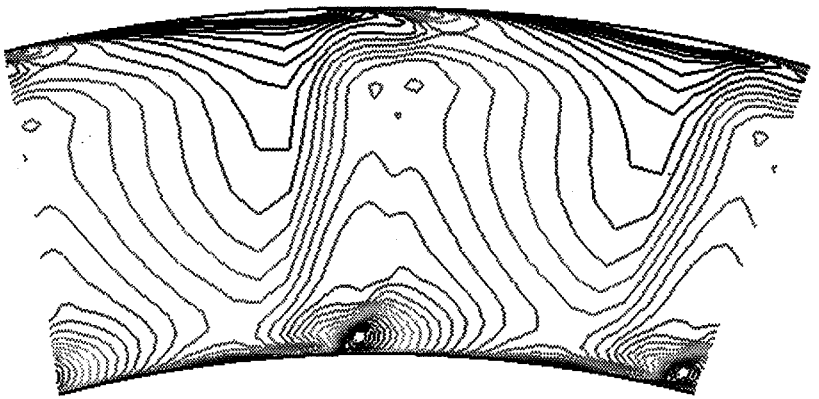

Unstructured–2

Axial Velocity Contours at Plane 4

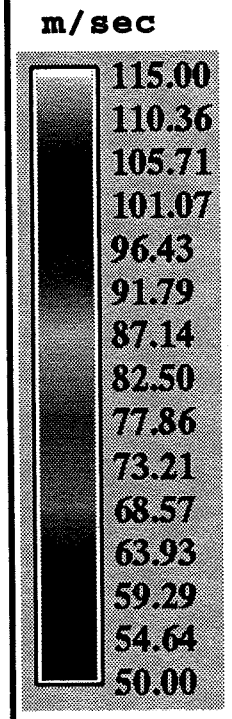

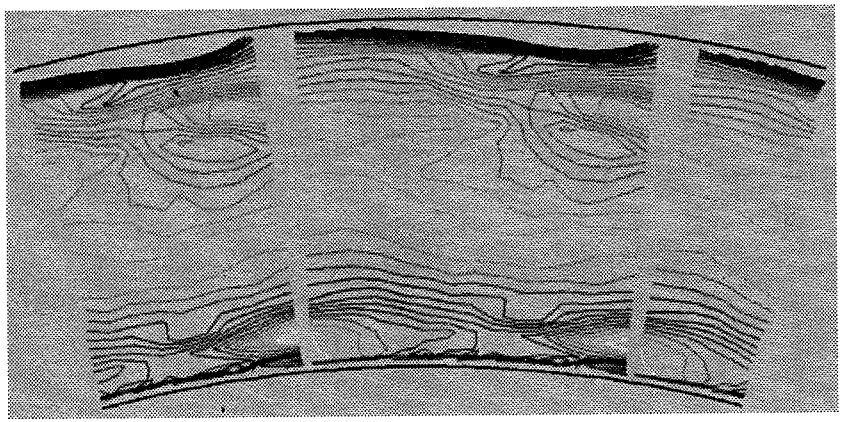

Experiment

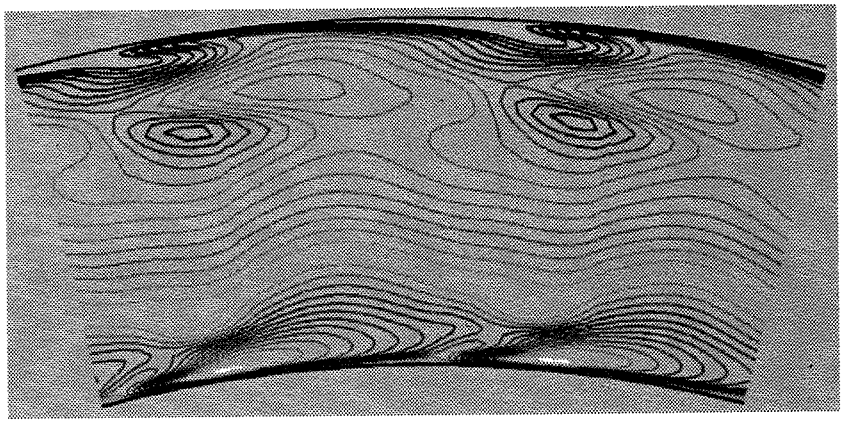

Structured

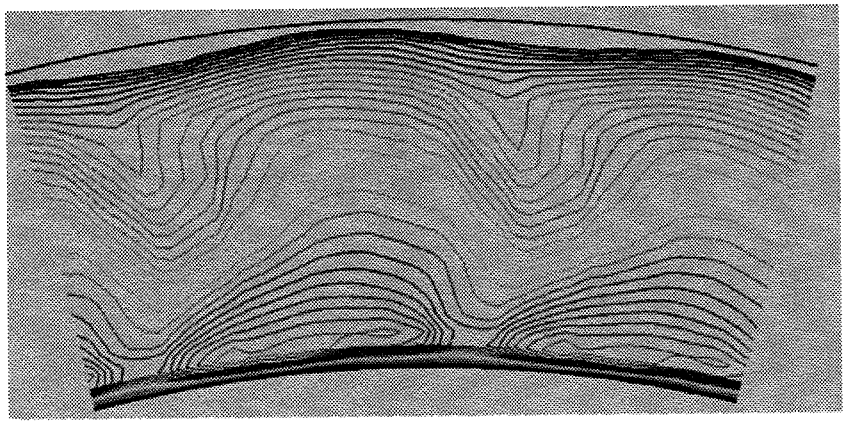

Unstructured–1

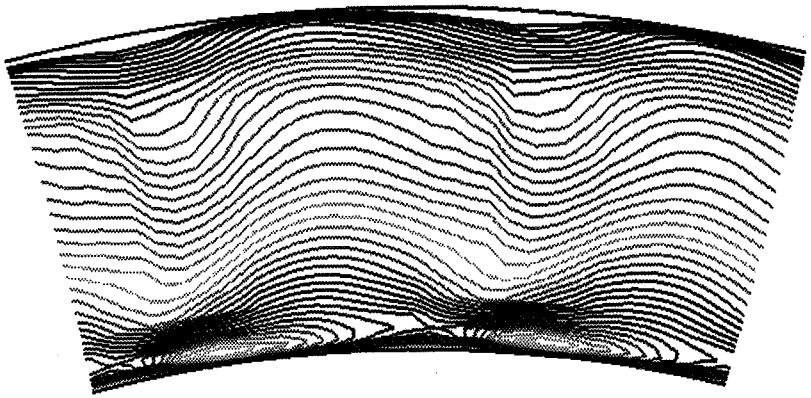

Unstructured–2

Tangential Flow Angle Contours at Plane 4

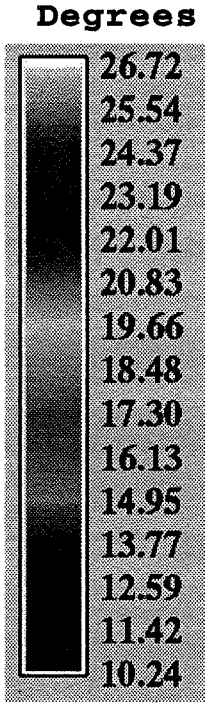

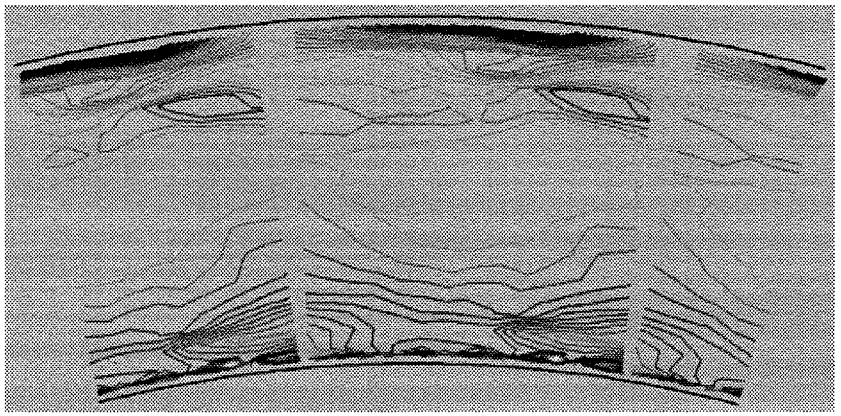

Experiment

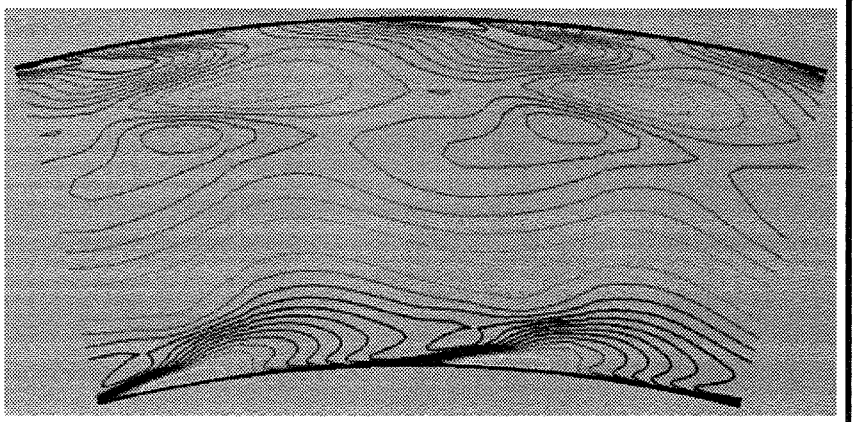

Structured

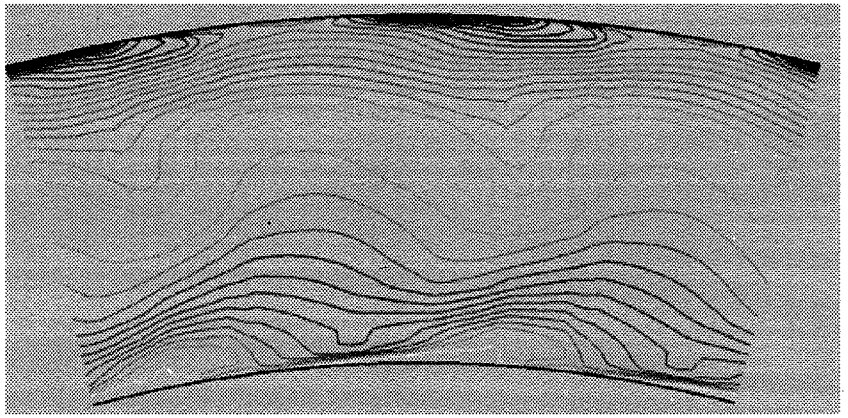

Unstructured–1

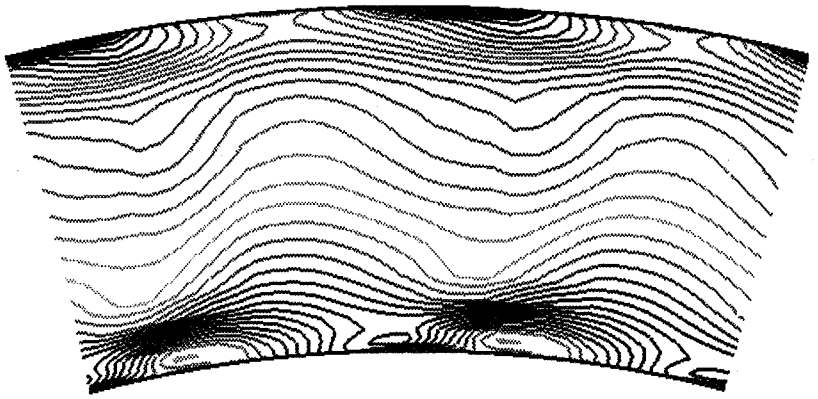

Unstructured–2

Total Pressure Ratio Contours at Plane 4

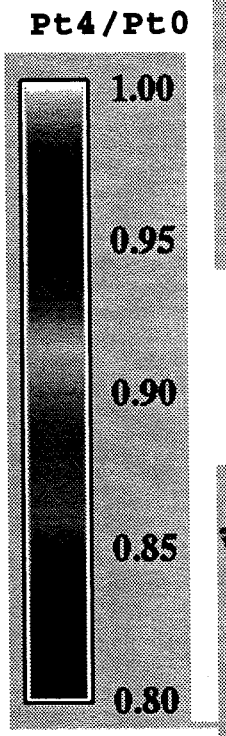

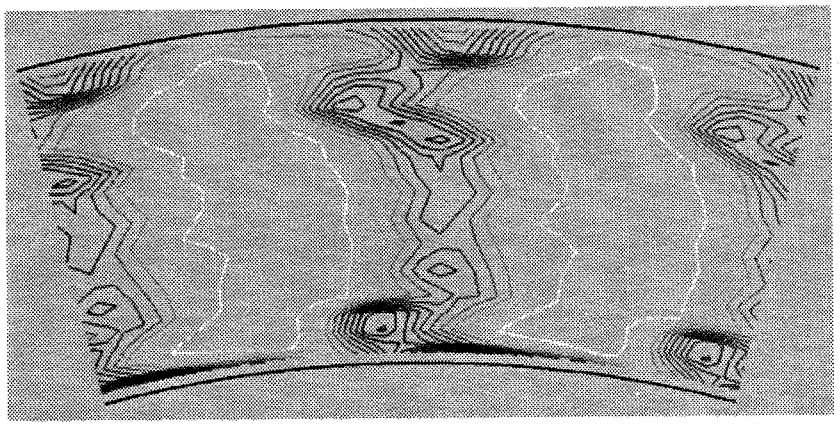

Experiment

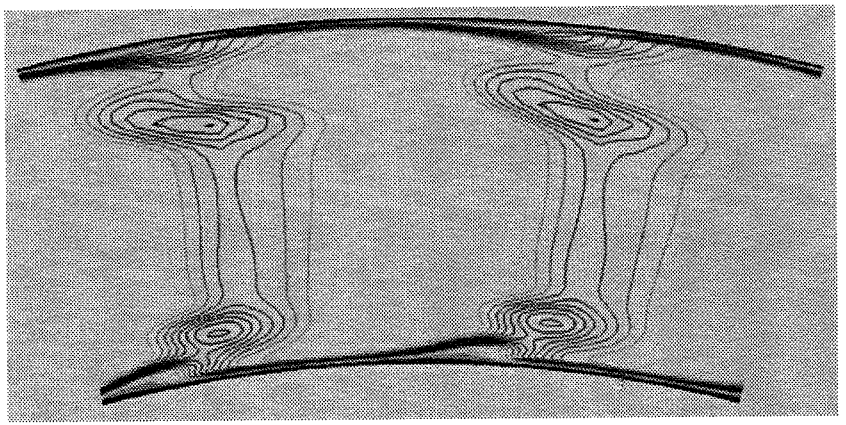

Structured

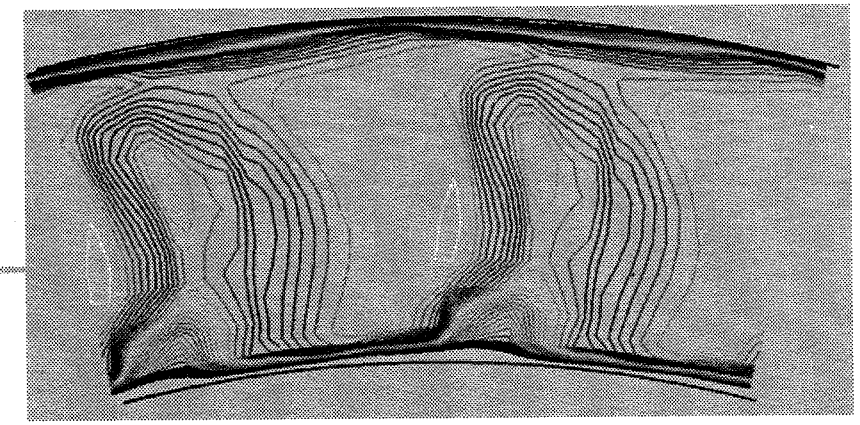

Unstructured–1

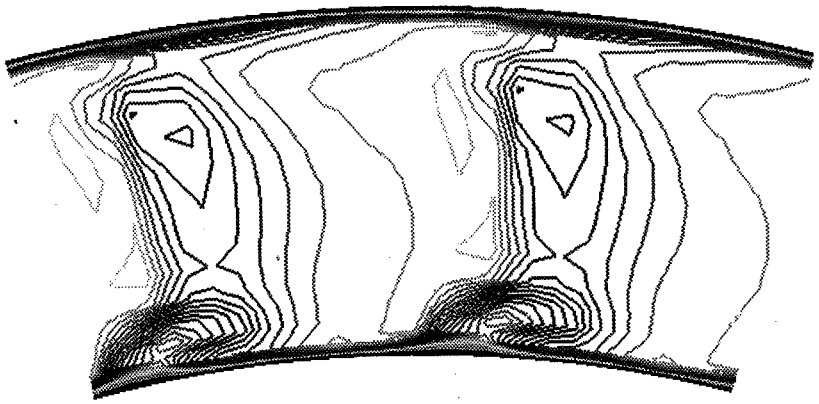

Unstructured–2

2–D Sections for Post Processing

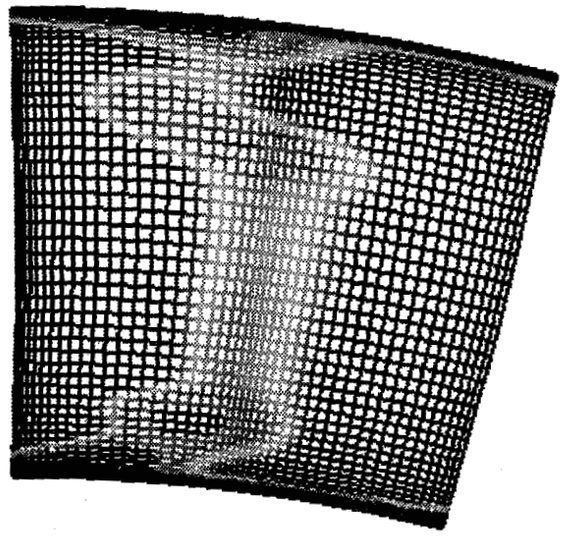

Structured

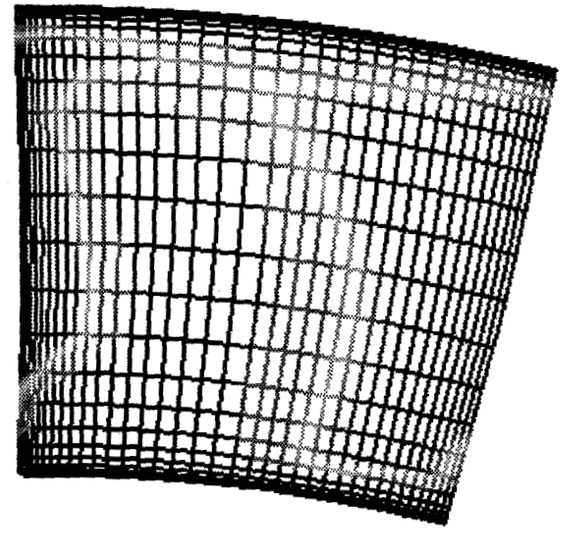

Unstructured–1

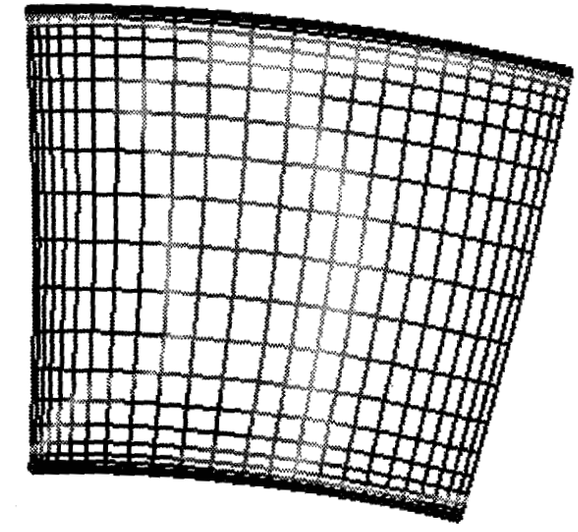

Unstructured–2

Pitch–Averaged Total Pressure Ratio vs. Percent Span at Station 4

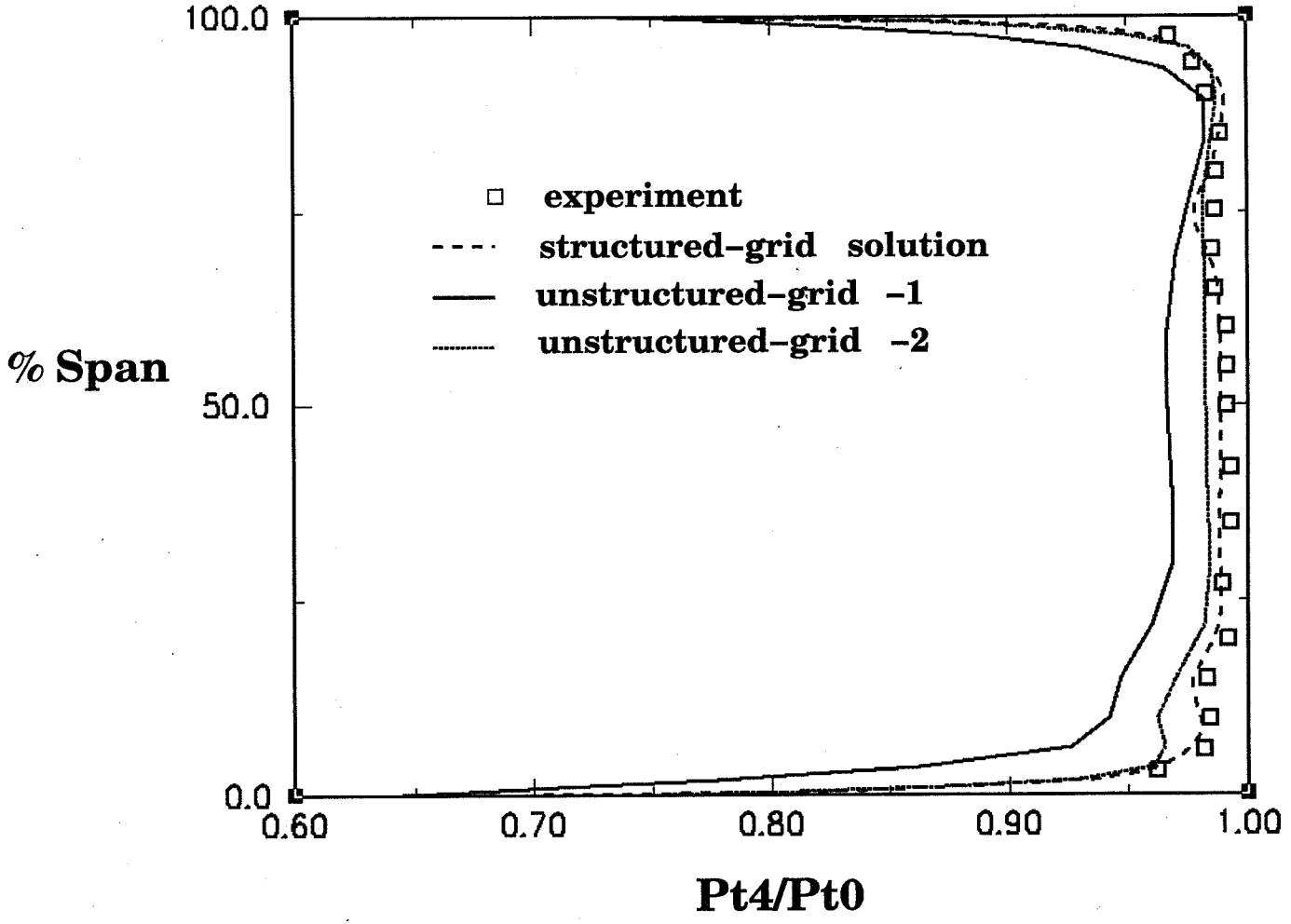

Solution Costs

	Memory(MW)	Iterations	CPU Time (hrs)
Structured	12	3000	2.5
Unstructured–1	25	10000	19.0
Unstructured–2	50	2000	5.8

Unstrctured Solver Comparison

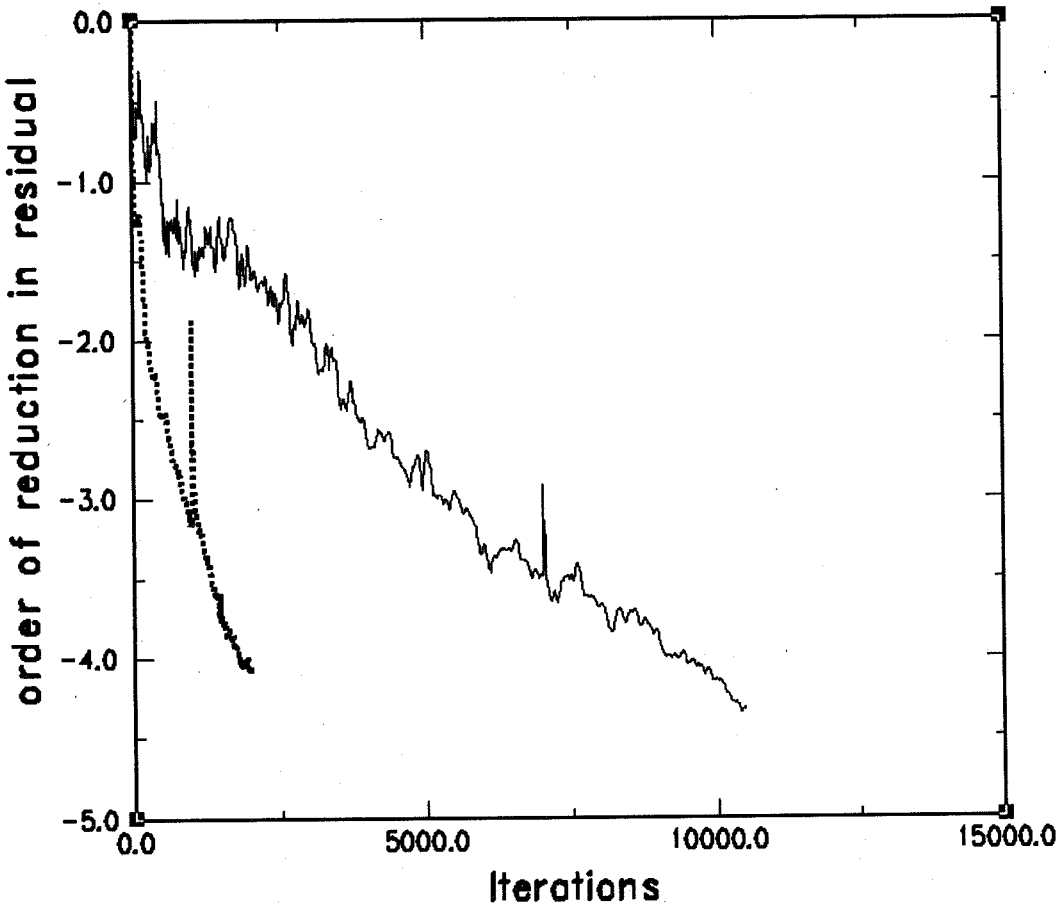

	Explicit	Implicit
Memory		
total	**25MW**	**50MW**
per cell	**64W**	**190W**
CPU		
per cycle	**6.86S**	**10.36S**
per cell	**17.6μS**	**40μS**

Concluding Remarks

Unstructured solver–1 exhibits higher diffusion than the structured solver with the same number of control volumes

- second–order unstructured inviscid flux
- versus third–order structured inviscid flux
- choice of spatial reconstruction scheme
- more random orientation of flux boundaries in structured grid

Unstructured solver–2 produces noticeably better solution then unstructured solver–1

- different viscous construction
- better spatial reconstruction scheme
- different turbulence model

Implicit unstructured solver requires substantially more memory then structured and explicit unstructured solver, but requires much less cpu time then explicit unstructured solver

A Mesh Generation Template for Turbomachinery Blade Passages

Edward P. Ascoli and George H. Prueger
Rocketdyne Division/Rockwell International
6633 Canoga Avenue
Canoga Park, CA 91303

ABSTRACT

Tools were developed which greatly reduced the time required to generate 3-D structured CFD meshes for turbomachinery blade passages. RAGGS (Rockwell Automated Grid Generation System), an existing, general purpose mesh generation and visualization system provided the starting point and framework for tool development. RAGGS provided highly interactive and highly visual mesh generation and visualization. At the same time, nearly every primary gridding tool available in RAGGS interactive mode had a "batch" counterpart. For this effort, batch RAGGS tools were combined and manipulated using UNIX C-shell programming. New RAGGS compatible tools were also developed in FORTRAN as needed. Key intermediates in the meshing process were still easily viewed using RAGGS interactive tools if desired.

Utilities which manipulate and interface with RAGGS tools were developed to 1) facilitate blade geometry inputs from point or CAD representations, 2) automate auxiliary surface creation and 3) streamline and automate edge, surface and subsequent volume mesh generation from minimal inputs. The emphasis of this approach was to maintain all the functionality of the general purpose mesh generator while simultaneously eliminating the bulk of the repetitive and tedious manual steps in the mesh generation process. Artificial intelligence was added to the system whenever possible. For instance, surface and volume meshes were automatically tested for negative areas and volumes respectively. If the system encountered a negative value it automatically attempted elliptic refinement of the corresponding mesh. This approach was demonstrated on a variety of realistic configurations. These configurations included a 3-D turbine nozzle, two inducer configurations as well as an impeller. Using this approach, mesh generation cycle times were reduced from the order of days down to the order of hours.

AUTOMATION OF 3-D STRUCTURED MESH GENERATION FOR TURBOMACHINERY BLADE PASSAGES

CFD WORKSHOP
MARSHALL SPACE FLIGHT CENTER
HUNTSVILLE, AL

APRIL 25-27, 1995

Edward P. Ascoli
CFD Technology Center

George H. Prueger
Advanced Rotating Machinery

INTRODUCTION

GOAL: REDUCE CYCLE TIME FOR CFD ANALYSIS OF TURBOMACHINERY COMPONENTS

- **CFD CYCLE TIME IS CURRENTLY TOO LONG FOR CFD TO IMPACT THE EARLY DESIGN CYCLE**
- **GRID GENERATION CONSUMES A SIGNIFICANT FRACTION (OFTEN THE MAJORITY) OF THE CFD ANALYSIS CYCLE TIME**

FOCUS: DECREASE CFD CYCLE TIME BY REDUCING GRID GENERATION TIME

BACKGROUND

- **TURBOMACHINERY PROBLEMS CHARACTERIZED BY**
  - COMPLEX GEOMETRIES
  - GEOMETRY AVAILABLE IN CAD, OR AS BLADE POINT DATA
  - MANY VARIATIONS ON SAME "BASIC" CONFIGURATION
  - CFD MODELING REQUIRES ADDITIONAL (AUXILIARY) SURFACES TO BOUND THE FLOW DOMAIN

- **EXISTING ENGINEERING LEVEL CFD SOLVERS USE MULTIBLOCK, STRUCTURED MESHES**

FOR THIS EFFORT:

- **WILL FOCUS ON STRUCTURED MESH GENERATION FOR AXIAL, MIXED AND RADIAL BLADE PASSAGE CONFIGURATIONS**

3-D TURBINE NOZZLE
(AXIAL FLOW DEVICE)

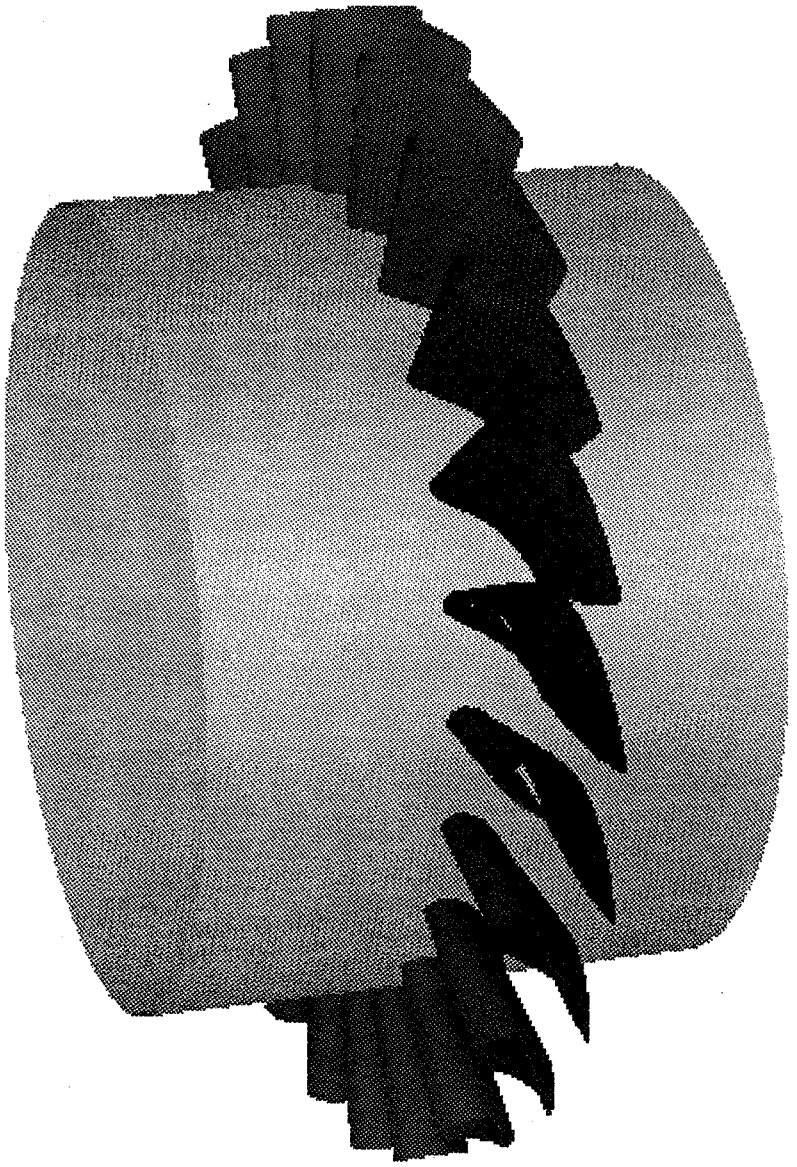

Rockwell Aerospace
Rocketdyne

CFD Technology Center

CFD 95-016-003A/D1/EPA

INDUCER
(AXIAL FLOW DEVICE)

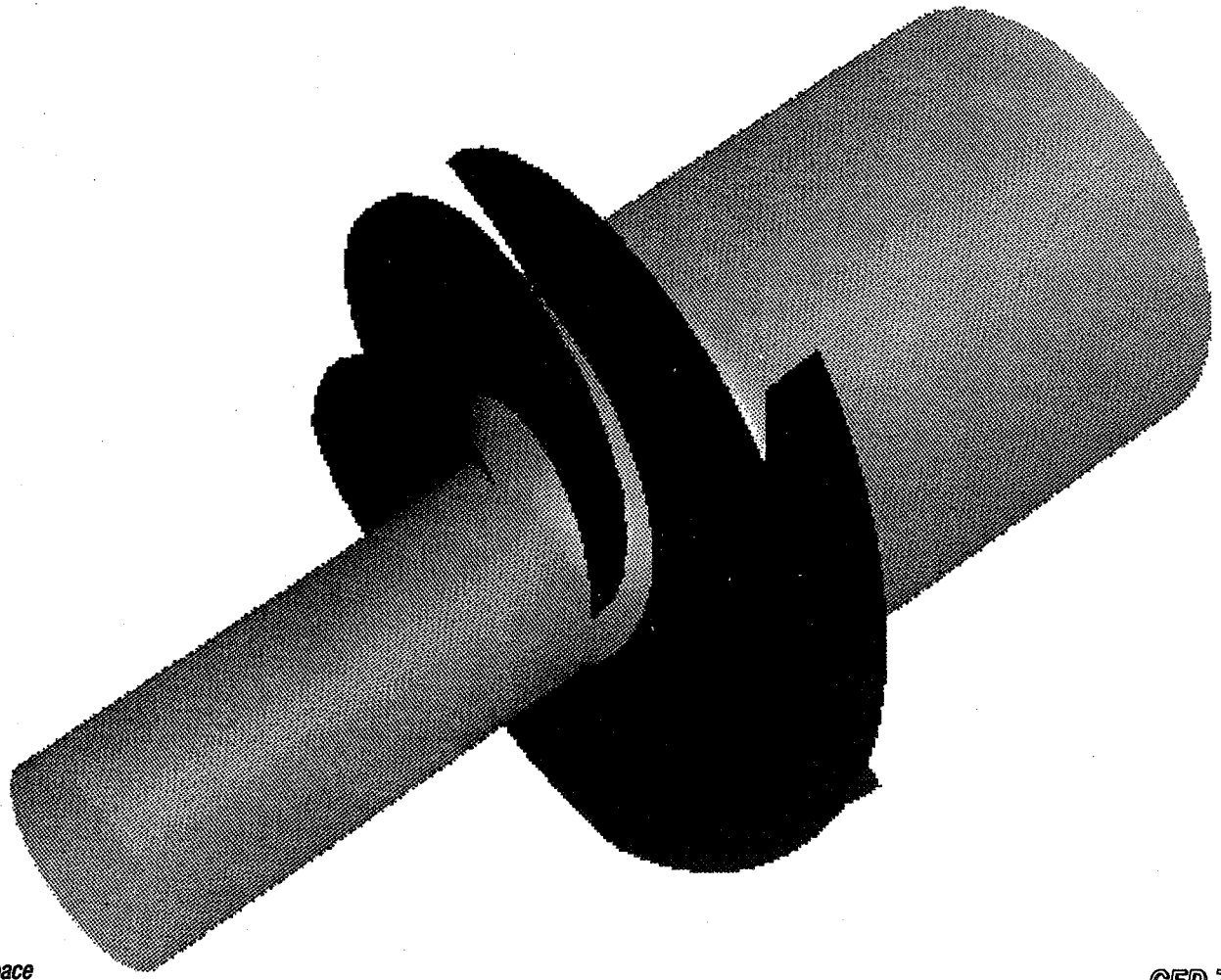

IMPELLER

(RADIAL FLOW DEVICE)

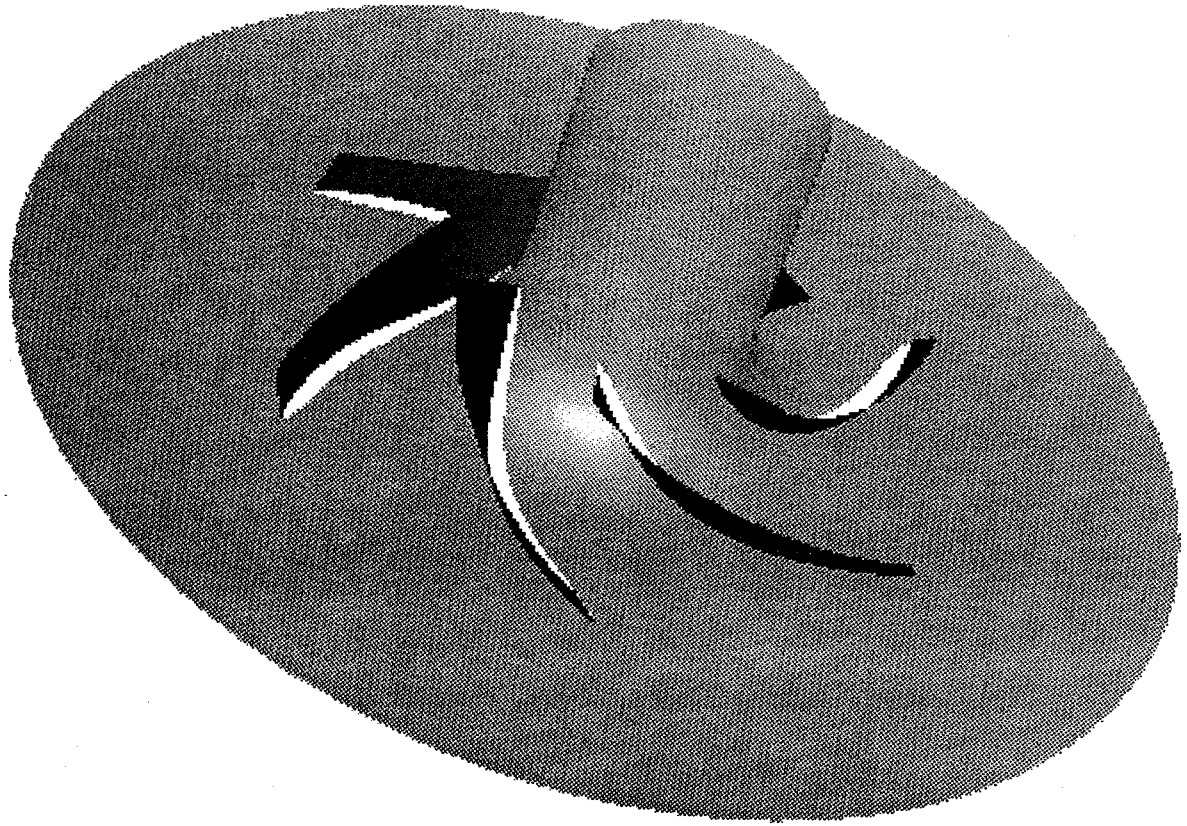

SCHEMATIC OF BLADE PASSAGES

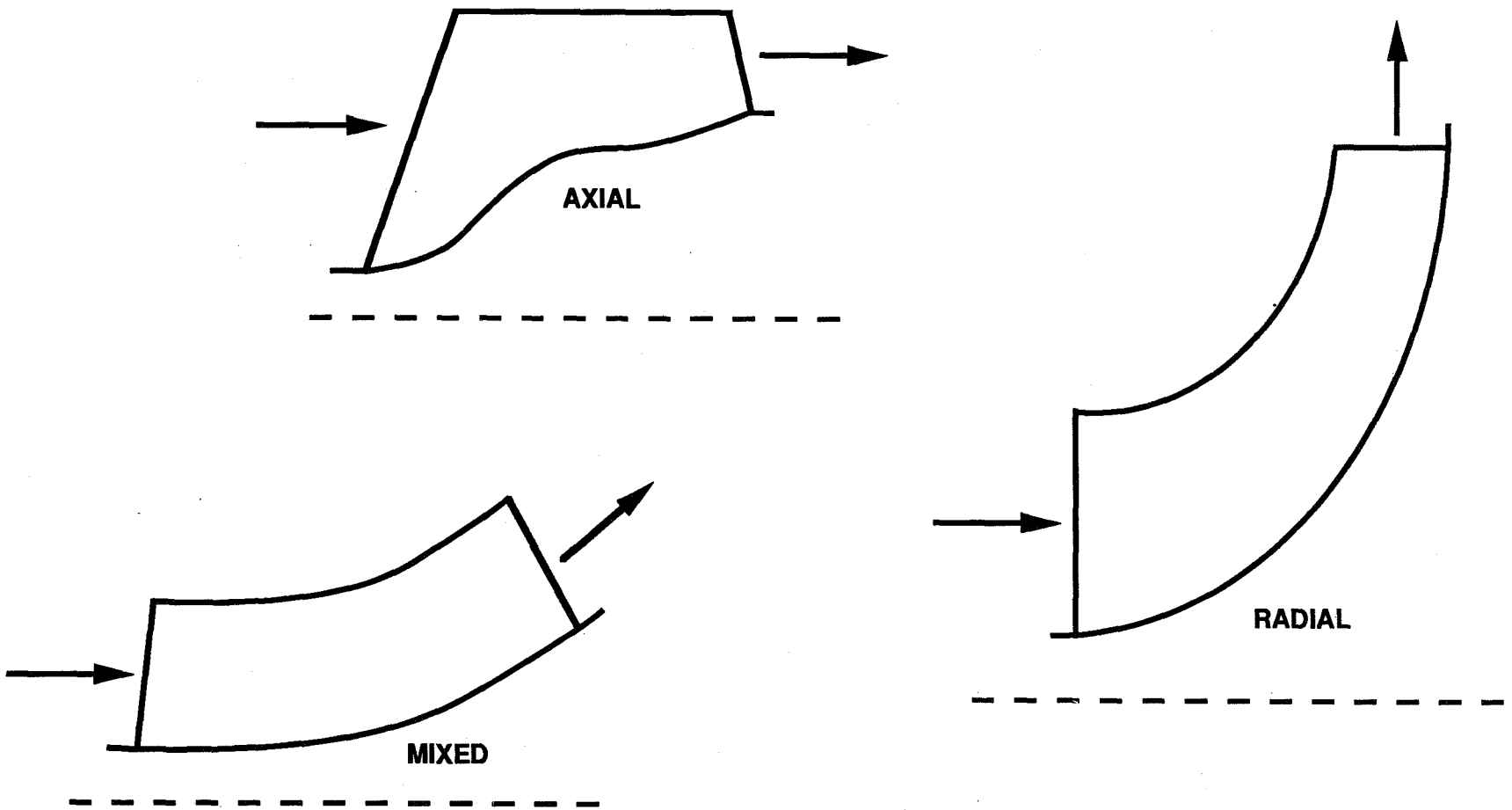

GRID GENERATION APPROACHES

- **GENERAL GRID GENERATOR (e.g., RAGGS, GRIDGEN, PATRAN)**

  PRO: CAN HANDLE HIGHLY COMPLEX PROBLEMS, CAD INPUTS ETC., EXCELLENT FOR FIRST TIME APPLICATIONS

  CON: SIGNIFICANTLY LONGER GRID GENERATION TIMES THAN TEMPLATES (SACRIFICE SOME SPEED AND EFFICIENCY FOR GENERALITY)

- **TEMPLATE TYPE GRID GENERATOR: CUSTOMIZE AND AUTOMATE GRID GENERATION FOR A RESTRICTED GEOMETRICAL CLASS OF PROBLEMS**

  PRO: FAST MESH GENERATION, EXCELLENT FOR PARAMETRICS

  CONS:
  - MAY FAIL IF GEOMETRY ONLY SLIGHTLY DIFFERENT THAN TEMPLATE CLASS
  - MAY BE LIMITED TO SPECIALIZED GEOMETRY INPUTS (e.g., ONLY POINTS OR SPECIAL EQUATIONS)
  - MAY NOT HAVE SUFFICIENTLY GENERAL TOOLS TO HANDLE OCCASIONAL ODD PROBLEMS (e.g., INADEQUATE MESH SMOOTHING ALGORITHMS ETC.)

TEMPLATE APPROACH USED HERE AVOIDS CONS

IDEA: BUILD TEMPLATE "AROUND" GENERAL GRID GENERATION SYSTEM (RAGGS)

- GENERAL GEOMETRY INPUTS (CAD, POINTS)
- GENERAL TOOLS AVAILABLE FOR ODD PROBLEMS
- EXTENSIVE DIAGNOSTIC AND MANIPULATION TOOLS AVAILABLE
- CAN HANDLE GEOMETRIES SLIGHTLY OUTSIDE OF TEMPLATE CLASS

RAGGS BACKGROUND

- **RAGGS (ROCKWELL AUTOMATED GRID GENERATION SYSTEM)**
  - GENERAL GRID GENERATION PACKAGE
  - GEOMETRY INPUTS INCLUDE CAD (IGES) AND POINT ARRAYS
  - TWO MODES OF OPERATION: INTERACTIVE AND BATCH
    - INTERACTIVE: HIGHLY VISUAL, MOUSE AND PANEL GUI
    - BATCH: MULTITUDE OF STANDALONE TOOLS PARALLELING WHAT IS AVAILABLE IN INTERACTIVE MODE

NOTE: BATCH TOOLS ARE CRUCIAL TO TEMPLATE APPROACH

TEMPLATE APPROACH USED HERE (CONT'D)

- **SUPPLEMENT RAGGS BATCH TOOLS WITH TEMPLATE TOOLS WRITTEN (IN FORTRAN) FOR SPECIFIC TEMPLATE TASKS**
  - **E.G., FORTRAN TOOLS WRITTEN TO CREATE AUXILIARY SURFACES**
- **USE UNIX BASED SHELL PROGRAMMING TO CALL RAGGS AND TEMPLATE TOOLS**
  - ALLOWS EASY FILE HANDLING AND I/O
  - ALLOWS "ARTIFICIAL INTELLIGENCE" (LOGICAL BRANCHING AND ERROR HANDLING AVAILABLE)
  - RESULTS IN EASILY EXTENDED, MODULAR PROGRAMS
- **AT ALL TIMES, ENSURE COMPATIBILITY WITH INTERACTIVE RAGGS TOOLS**
  - INTERMEDIATES EASILY VISUALIZED AND CHECKED WITH RAGGS INTERACTIVE VISUALIZATION TOOLS
  - PROBLEMS CORRECTED USING GENERAL TOOLS

GRID GENERATION PROCESS USING TEMPLATE APPROACH

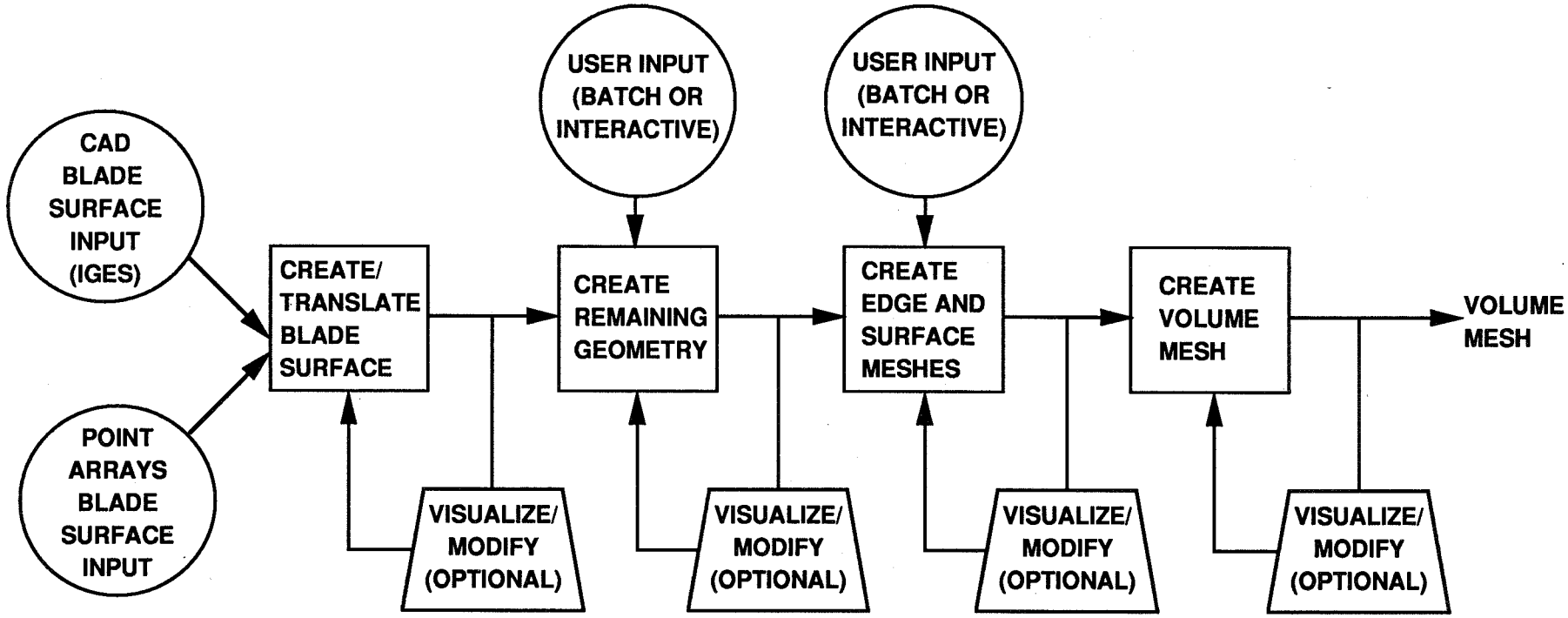

= INPUTS

= USE INTERACTIVE AND GENERAL RAGGS TOOLS (OPTIONAL)

= KEY MODULE IN TEMPLATE

Rockwell Aerospace
Rocketdyne

CFD Technology Center

CFD 95-016-009/D1/EPA

MESH SURFACE FOR 3-D TURBINE NOZZLE

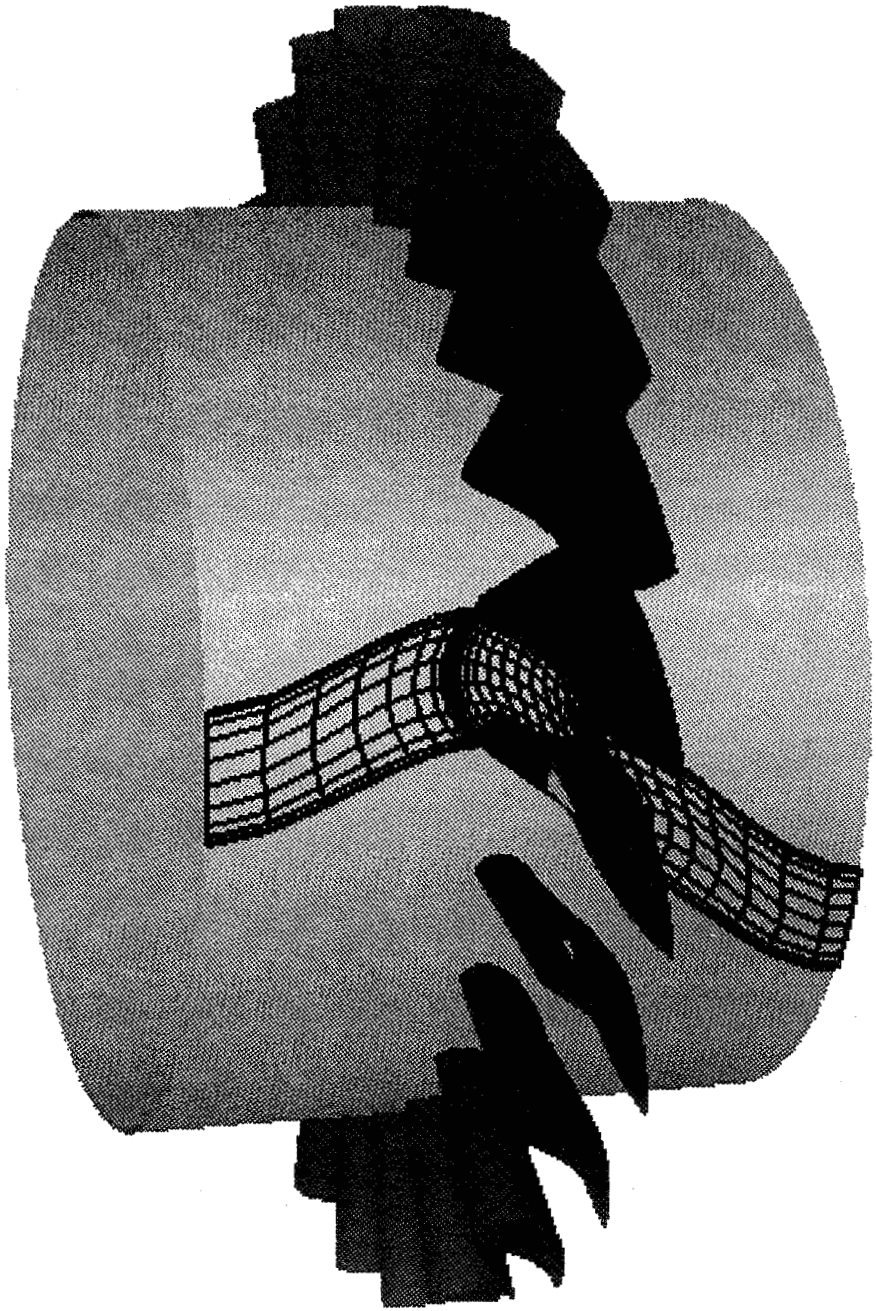

REDUCTION IN MESH GENERATION TIME

FLOW DEVICE	DEVICE TYPE	RAGGS* (MAN HRS) (NO TEMPLATES)	TEMPLATES (MAN HRS)
3-D TURBINE NOZZLE	AXIAL	25-30	5
INDUCER	AXIAL	35	5-6
IMPELLER	AXIAL	35	5

- TEMPLATE MAN HOURS ARE START TO FINISH FOR FIRST GRID
- SUBSEQUENT CHANGES TO POINT DISTRIBUTION AND MINOR CHANGES TO GEOMETRY CAN BE PERFORMED AND A NEW GRID MADE IN UNDER 2 HOURS

*FOR PROPER COMPARISON, RAGGS (NO TEMPLATES) MAN HOURS INCLUDE THE TIME REQUIRED USING A CAD SYSTEM TO CREATE ALL AUXILIARY GEOMETRY WHICH IS CREATED AUTOMATICALLY BY THE TEMPLATES. BOTH TEMPLATE AND NO TEMPLATE HOURS ASSUME THE BLADE GEOMETRY ALREADY EXISTS.

MESH SURFACE FOR INDUCER

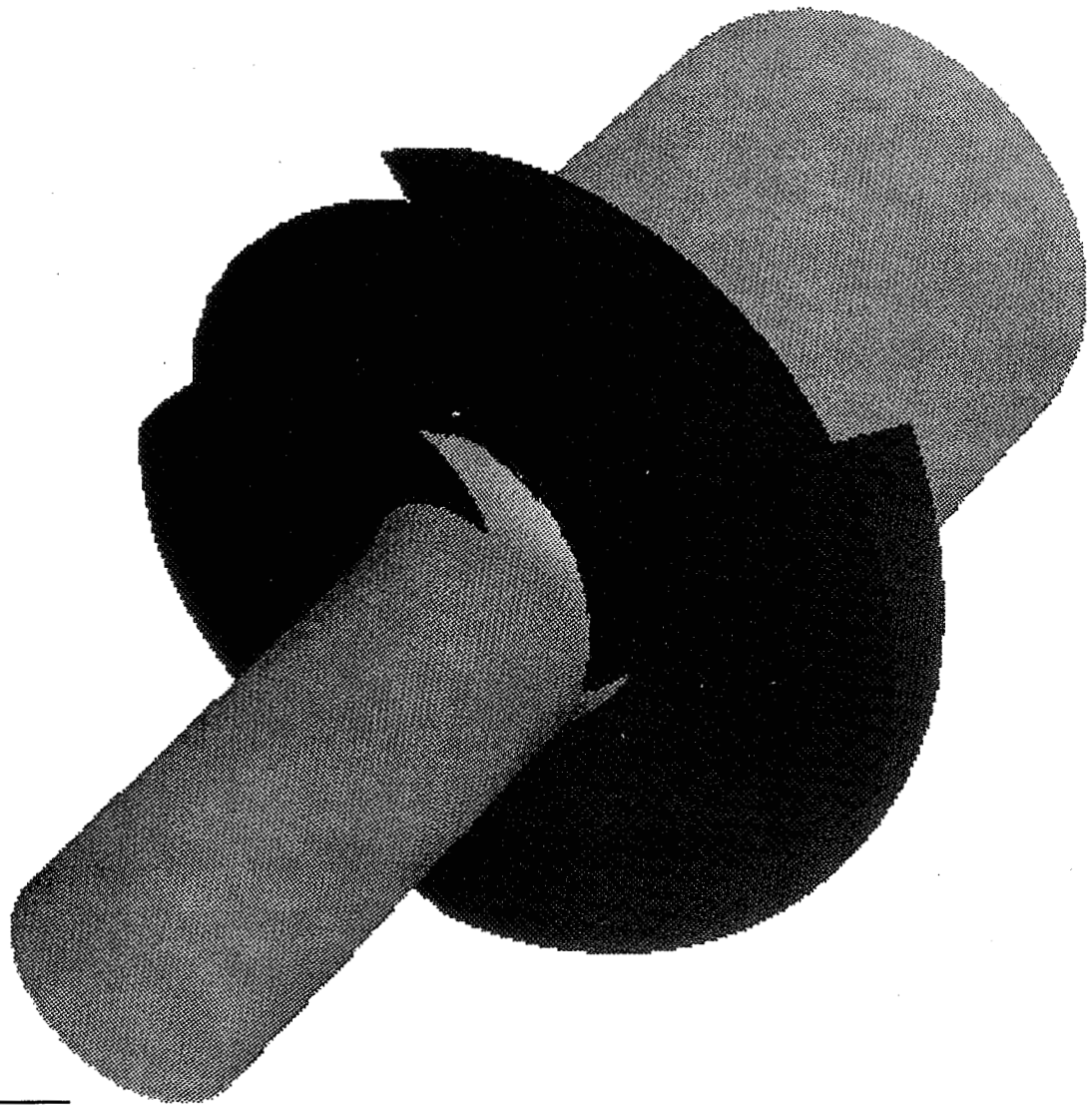

MESH SURFACE FOR IMPELLER

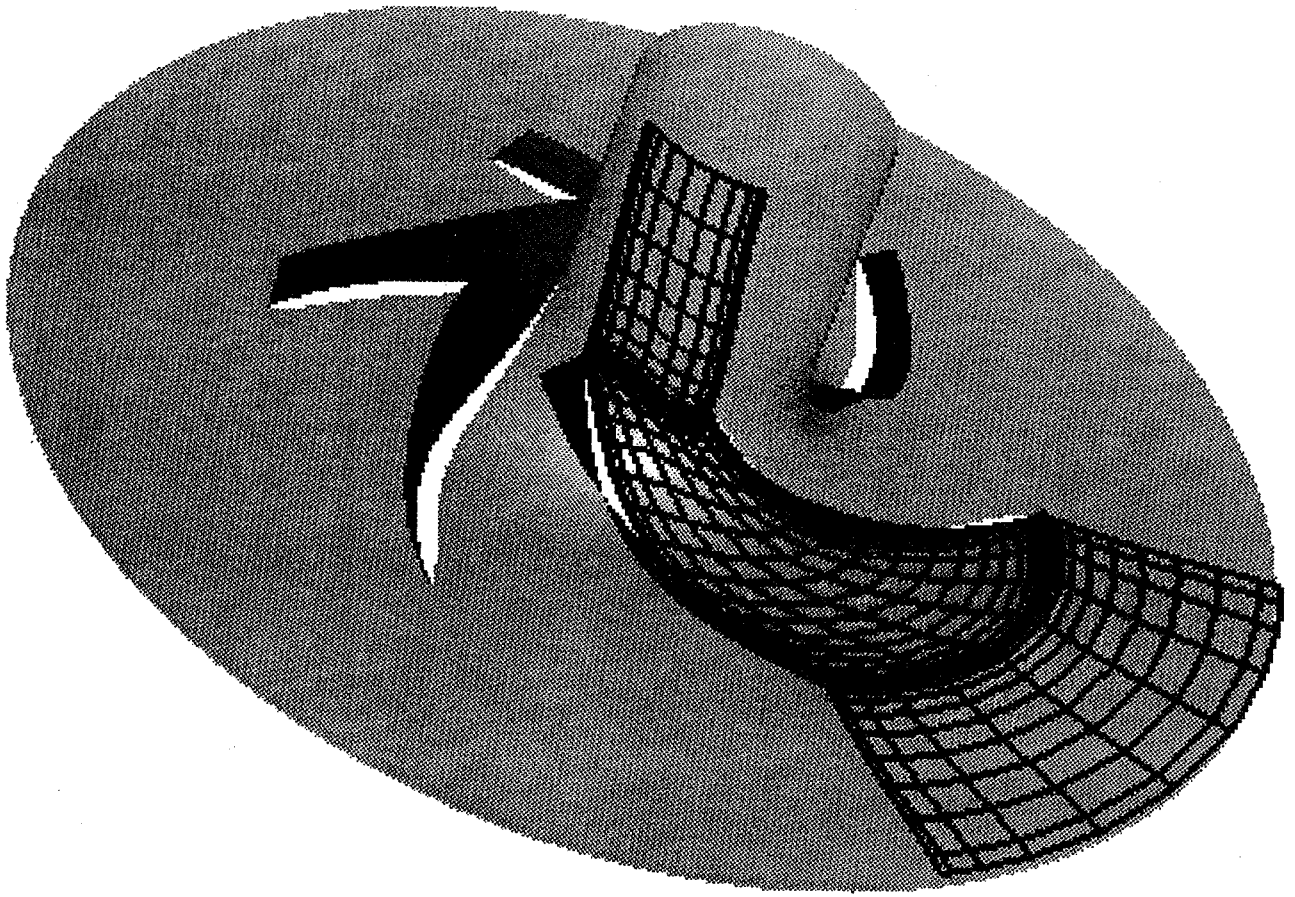

National Aeronautics and
Space Administration

AN ANALYTICAL INVESTIGATION OF THE EFFECTS OF STATOR AIRFOIL CLOCKING ON TURBINE PERFORMANCE

Lisa W. Griffin
NASA/MSFC

Frank W. Huber and Om P. Sharma
Pratt and Whitney

Presented at the Workshop for CFD Applications in Rocket Propulsion and Launch Vehicle Technology
MSFC, AL
April 25 - 27, 1995

National Aeronautics and
Space Administration

An Analytical Investigation of the Effects of Stator Airfoil Clocking on Turbine Performance

OVERVIEW

- **Background**
  - ATD HPFTP Turbine Aerodynamics Tests
  - Modified ATD HPFTP Turbine Airfoil Clocking Tests
- **Analytical Objective**
- **Modified Turbine Description and Test Conditions**
- **Analytical Approach**
  - Numerical Application
  - Code Description
  - Grid System
- **Results**
  - Entropy
  - Velocity
  - Unsteadiness
- **Conclusions**

National Aeronautics and Space Administration

An Analytical Investigation of the Effects of Stator Airfoil Clocking on Turbine Performance

BACKGROUND

- **ATD HPFTP Turbine Aerodynamics Tests**
  - Series of Aerodynamic Rig Tests Conducted at MSFC to Measure the Performance of ATD HPFTP turbine
  - Turbine Efficiency Contours at the Exit of the Turbine Showed:
    - » 54 Cycle Pattern Corresponding to the Second Vane Count
    - » Two Cycle Secondary Pattern of +/- 0.5 Percentage Points
  - Theorized that the Secondary Pattern Due To Airfoil Clocking

- **Modified ATD HPFTP Turbine Clocking Tests**
  - First Stage Vane Count Increased to Equal Second Stage Vane Count
  - Tests Conducted for Six First Vane Clocking Positions
    - » Positions Spaced 1.333° for a Total of 6.667° (1 Vane Pitch)
  - Plot of Efficiency vs Clocking Position Shows a $\Delta\eta$ of +/- 0.4%

An Analytical Investigation of the Effects of Stator Airfoil Clocking on Turbine Performance

FIRST VANE CLOCKING POSITIONS IN RIG

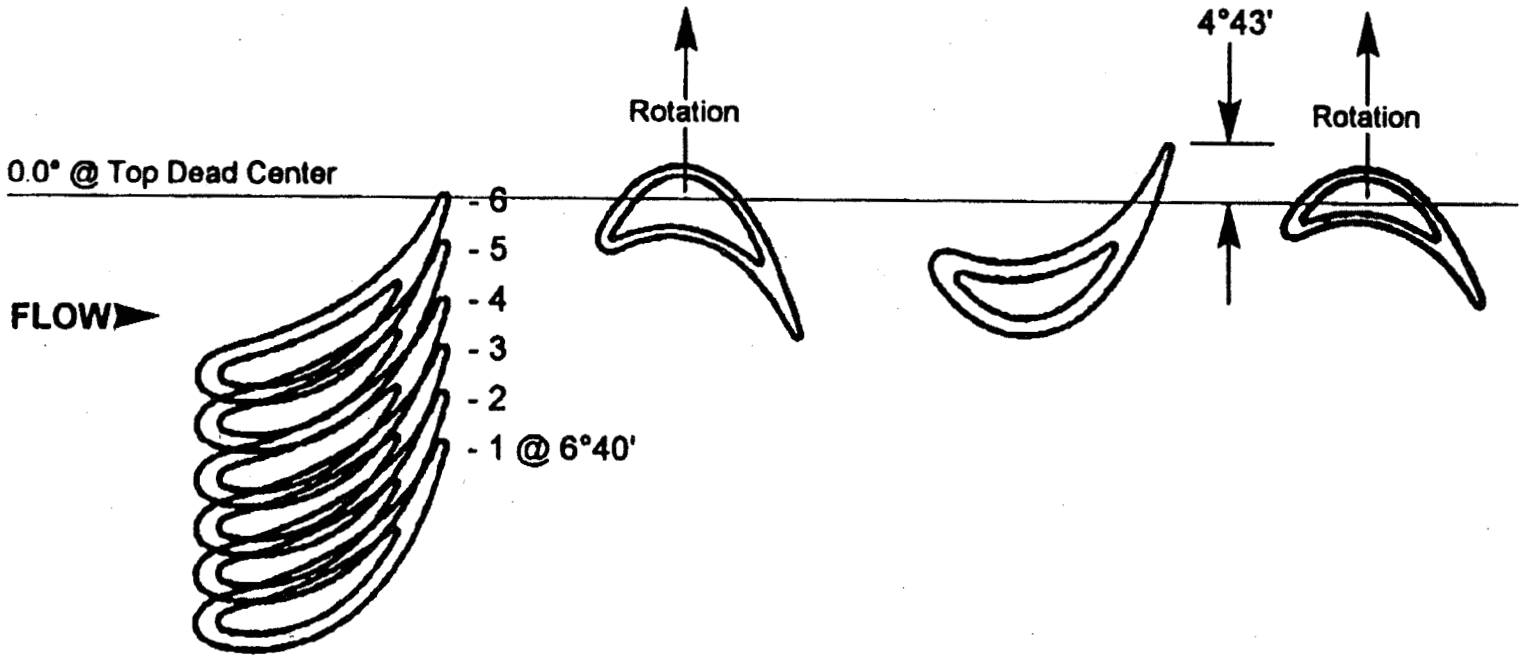

EXPERIMENTALLY OBSERVED EFFICIENCY VS CLOCKING POSITION

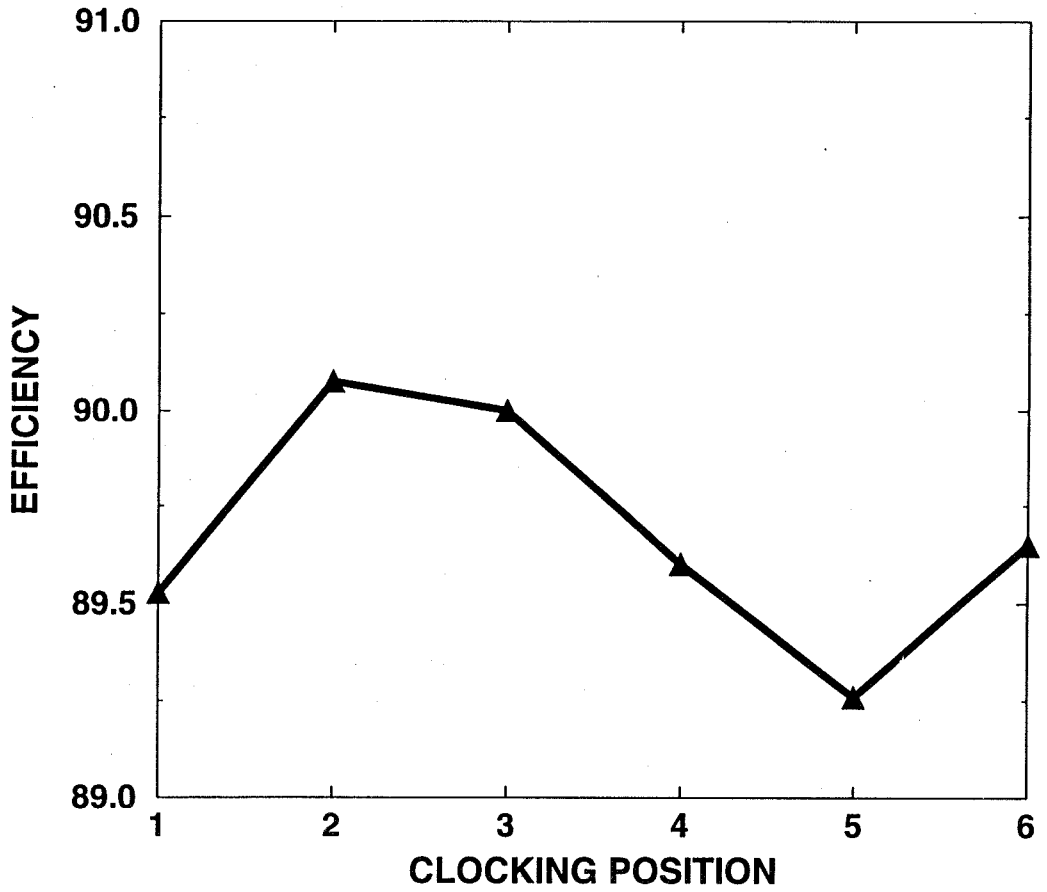

National Aeronautics and
Space Administration

An Analytical Investigation of the Effects of Stator Airfoil Clocking on Turbine Performance

ANALYTICAL OBJECTIVE

- **To Perform Unsteady CFD Analysis to Provide Insights into the Physical Mechanisms of the Changes in Turbine Performance Due to Stator Airfoil Clocking**

National Aeronautics and Space Administration

An Analytical Investigation of the Effects of Stator Airfoil Clocking on Turbine Performance

MODIFIED TURBINE DESCRIPTION AND TEST CONDITIONS

- **Full Scale Model of the ATD HPFTP**
  - Two Stages with Vane:Blade Ratio of 54:50:54:50

- **First Stage Vane Modifications**
  - Count Increased from 52 to 54
  - Restaggered Slightly Open to Maintain Nominal Flow Area

• **Inlet Mach Number**	=	**0.1226**
• **Inlet Total Pressure**	=	**99.6 psi**
• **Inlet Total Temperature**	=	**546 R**
• **Rotational Speed**	=	**6982 RPM**
• **Reynolds Number** (inlet conditions, axial chord)	=	**363,500**

ANALYTICAL APPROACH - Numerical Application

- Apply 2D, Time-Accurate, Viscous Code (STAGE2) to the Turbine Midspan for the Configurations in the Test Series
- Vane to Blade Count Modeled as 1:1:1:1
- For the Test Series, First Vane Clocking Positions Spaced at 1.333° or 20% of the Vane Pitch. For the Analysis, First Vane Clocking Positions set at 20% of the Scaled Vane Pitch or 1.444°
- 1:1:1:1 Model Resulted in 5 Unique Clocking Positions (Positions 1 and 6 are Identical) Rather than 6
- Grid System Density and Distribution, Boundary Conditions, Initial Conditions, and Convergence Criteria Consistent from Case to Case
- Ultimate Convergence Criteria Established to be When Time- and Circumferentially-Averaged Efficiency Stablized for 4 Significant Digits

NUMERICALLY MODELED FIRST VANE CLOCKING POSITIONS

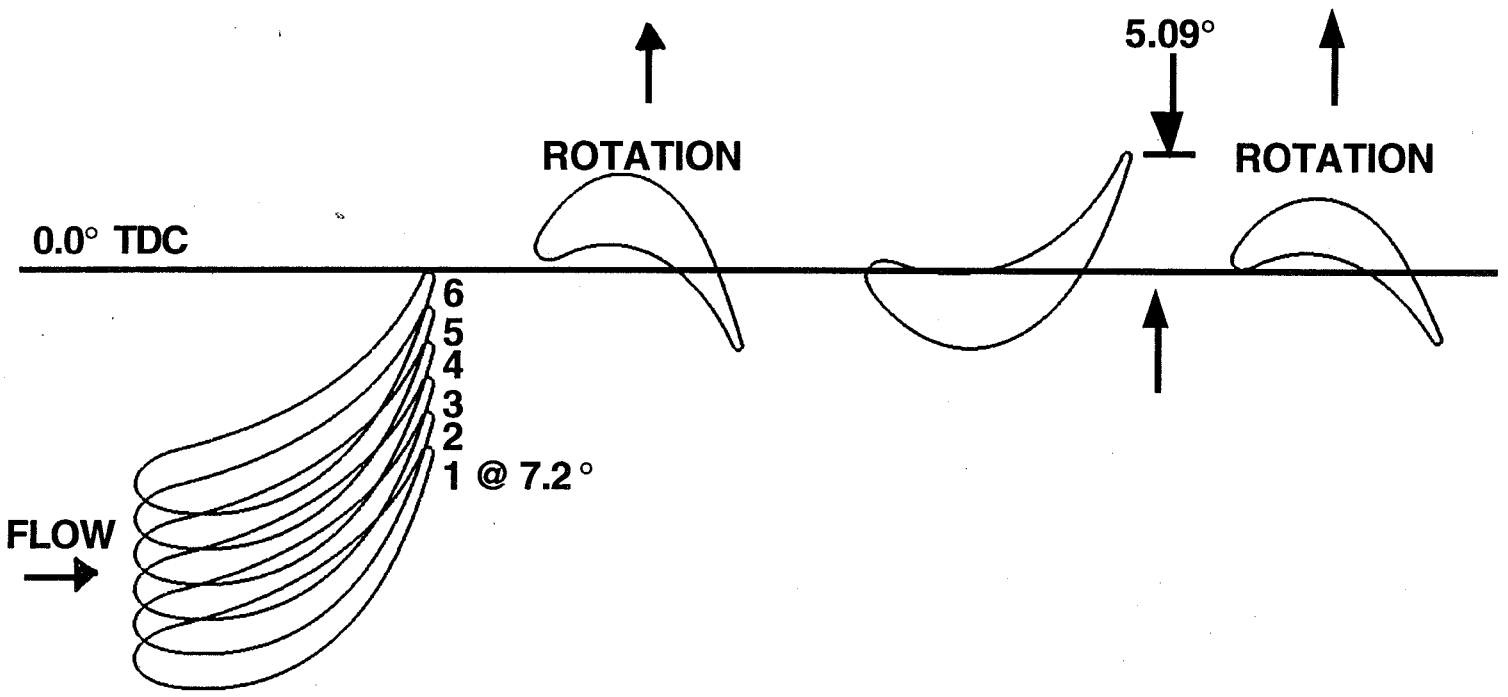

National Aeronautics and Space Administration

An Analytical Investigation of the Effects of Stator Airfoil Clocking on Turbine Performance

ANALYTICAL APPROACH - Code Description
STAGE2

- Solves 2D, Unsteady, Compressible, Thin-Layer Navier-Stokes Equations
- Time-marching, Implicit, Third-order Spatially Accurate, Upwind Finite Difference Scheme
- Flow Field Discretized by O Grids Around Airfoils Overlaid onto H Grids. H Grids Patched Between Blade Rows. Rotor H Grids Slide Past Stator H Grids in Time
- Airfoil Surface Boundary Conditions - No Slip, Adiabatic Walls, Zero Normal Pressure Gradient
- Inlet Boundary Conditions - Specified Flow Angle, Upstream Riemann Invarient, and Average Total Pressure, Extrapolated Downstream Riemann Invarient
- Exit Boundary Conditions - Specified Average Static Pressure, Extrapolated Upstream Riemann Invarient, Tangential Velocity, and Entropy
- Baldwin-Lomax Turbulence Model

National Aeronautics and
Space Administration

An Analytical Investigation of the Effects of Stator Airfoil Clocking on Turbine Performance

ANALYTICAL APPROACH - Grid System

- Each Airfoil O Grid Contains 201 X 51 Points with Average y^+ of 0.8
- Each Airfoil H Grid Contains 97 X 79 Points
- Inflow and Outflow Grids Contain 36 X 79 and 39 X 79 Points and Extend Approximately 15 chord lengths Upstream and Downstream
- Total Number of Grid Points - 77,581

National Aeronautics and Space Administration

An Analytical Investigation of the Effects of Stator Airfoil Clocking on Turbine Performance

MODIFIED ATD FUEL TURBINE GRID

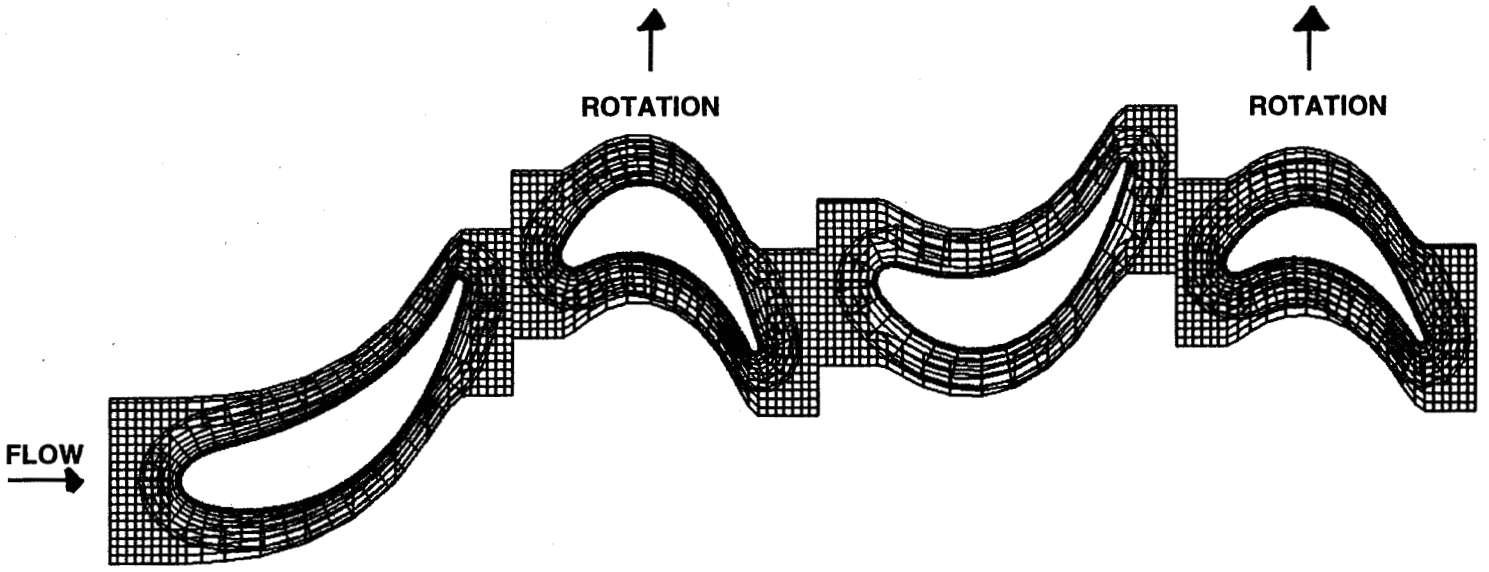

Every 4th Point Shown in Each Direction; Inflow and Outflow Grids Not Shown

National Aeronautics and Space Administration

An Analytical Investigation of the Effects of Stator Airfoil Clocking on Turbine Performance

RESULTS

- **Predicted Average Time- and Circumferentially-Averaged Total-to-Total Efficiency of 94.8% and a Delta of +/- 0.15%**
  - Experimentally Measured Losses Not Truly Midspan Losses (Short Blades and Low Aspect Ratio). Analytically Predicted Midspan Losses are Strictly Midspan Profile Loss. Meanline Analysis with Only Profile Losses Considered Predicts Efficicency of 94.9%.
  - Possible Explanations for Difference Between Observed and Predicted Delta
    - » Numerical Limitations
    - » Clocking Reduces Endwall Losses
- **Predicted 1 1/2 Stage Time- and Circumferentially-Averaged Total-to-Total Efficiency Delta of +/- 0.14%**
  - Indication that Second Vane Performance Major Driver in Turbine Performance for Each Clocking Position

Remainder of this Study Focused on Improved Second Vane Performance

An Analytical Investigation of the Effects of Stator Airfoil Clocking on Turbine Performance

PREDICTED TOTAL-TO-TOTAL EFFICIENCY - 2 STAGE

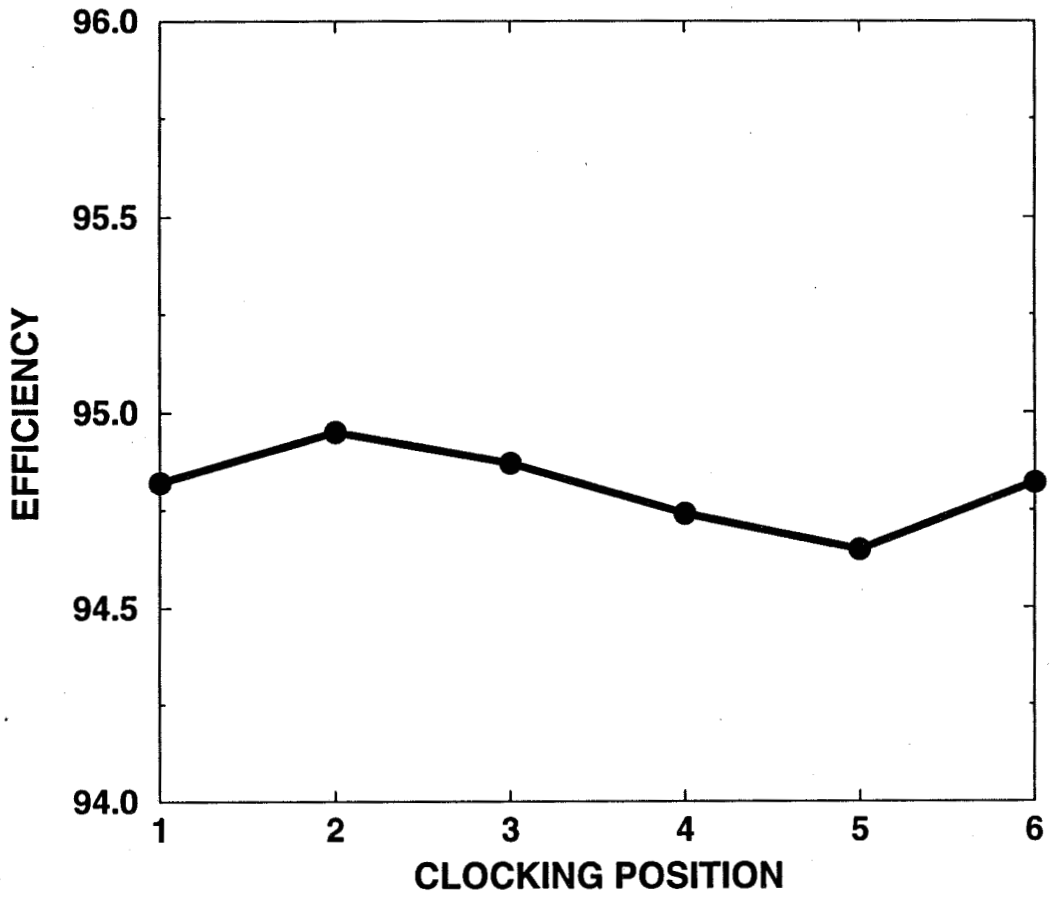

An Analytical Investigation of the Effects of Stator Airfoil Clocking on Turbine Performance

PREDICTED TOTAL-TO-TOTAL EFFICIENCY - 1 1/2 STAGE

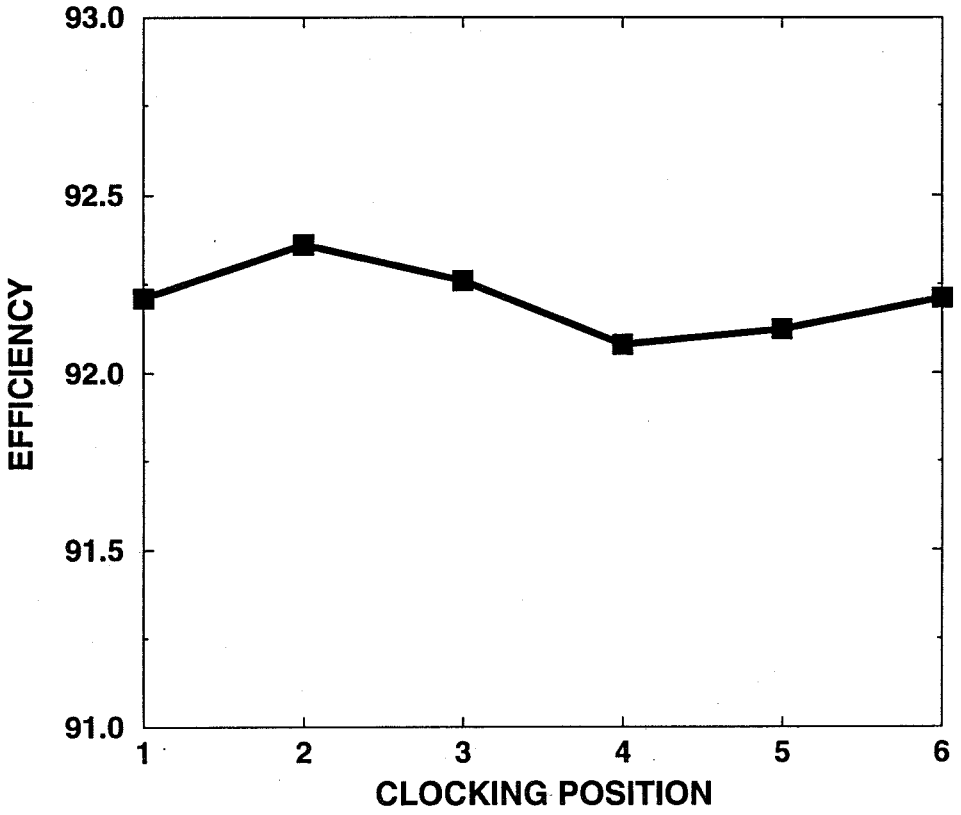

National Aeronautics and
Space Administration

An Analytical Investigation of the Effects of Stator Airfoil Clocking on Turbine Performance

RESULTS - Entropy

- **Entropy Contours Generated to Visualize Airfoil Wakes**
  - First Vane Wakes Appear as a Continuous Stream into the Second Vane
  - For Position 2 (Predicted to Have the Highest Efficiency), the Time-Averaged First Vane Wake Impinges on the Leading Edge of the Second Vane
  - For Position 5 (Predicted to Have the Lowest Efficiency), the Time-Averaged First Vane Wake Passes through the Mid-Channel of the Second Vane

Best Performance is Predicted to be Obtained When the Time-Averaged First Vane Wake is Aligned with the Second Vane Leading Edge

National Aeronautics and
Space Administration

An Analytical Investigation of the Effects of Stator Airfoil Clocking on Turbine Performance

TIME-AVERAGED ENTROPY CONTOURS FOR THE SECOND VANE

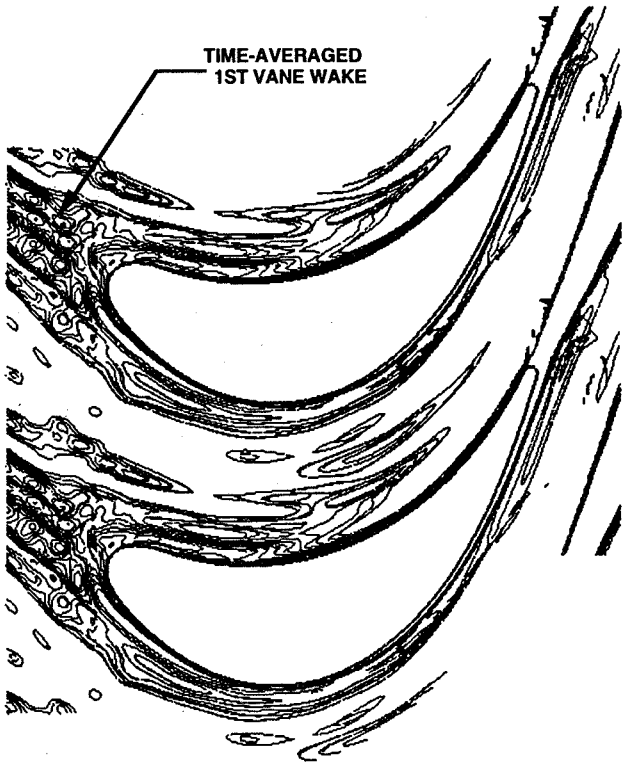

(a)

Position 2

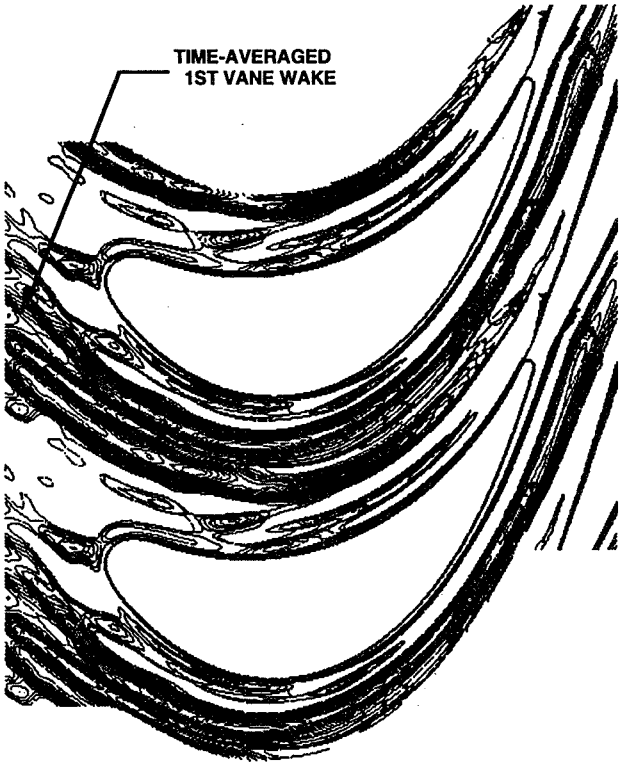

(b)

Position 5

National Aeronautics and
Space Administration

An Analytical Investigation of the Effects of Stator Airfoil Clocking on Turbine Performance

RESULTS - Velocity

- **Surface Velocities on Second Vane are Lower When Vanes are Optimally Indexed**
  - Confirmed by Time-Averaged Pressure Coefficients
  - Average Surface Mach Numbers for the Second Vane for Position 2 Configuration is 0.437; for Position 5 is 0.471

- **Estimating Loss as Proportional to the Difference in u^3 Indicates ReducedLosses Due to Lower Velocities is 73% of the Efficiency Difference**

Reduced Surface Velocities a Potential Reason for Improved Second Vane Performance When Vanes Optimally Clocked

TIME-AVERAGED PRESSURE COEFFICIENTS FOR THE SECOND VANE

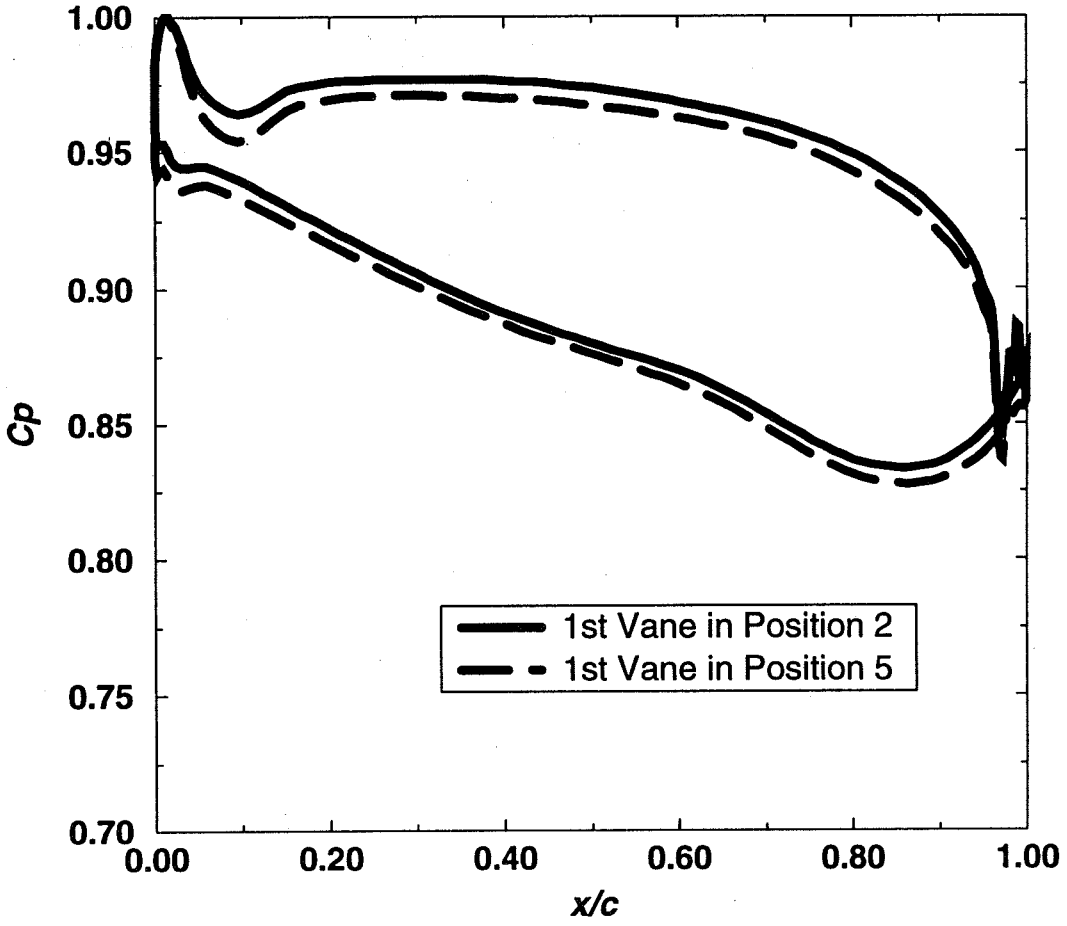

National Aeronautics and Space Administration

An Analytical Investigation of the Effects of Stator Airfoil Clocking on Turbine Performance

RESULTS - Unsteadiness

- **Flow Field Unsteadiness Decreased on Second Vane When Vanes Optimally Aligned**
  - Decrease of 11.8% in Flow Field Unsteadiness on the Pressure Surface of Second Vane When Vanes Optimally Clocked (Position 2) vs Least Optimally Clocked (Position 5)
  - Decrease of 26% in Flow Field Unsteadiness on Suction Surface of Second Vane When Vanes Optimally Clocked vs Least Optimally Clocked
  - Higher Entopy Regions Due to First Vane Wake Fill in Between Rotor Wakes at the Second Vane Leading Edge When Vanes are Optimally Indexed. More Discrete Blade Wakes at Leading Edge of Second Vane When First Vane Clocked to Position 5

Reduced Local Variation in Entropy a Possible Reason for Increased Second Vane Performance When Vanes Optimally Indexed

UNSTEADY PRESSURE COEFFICIENTS AT THE SECOND VANE LEADING EDGE

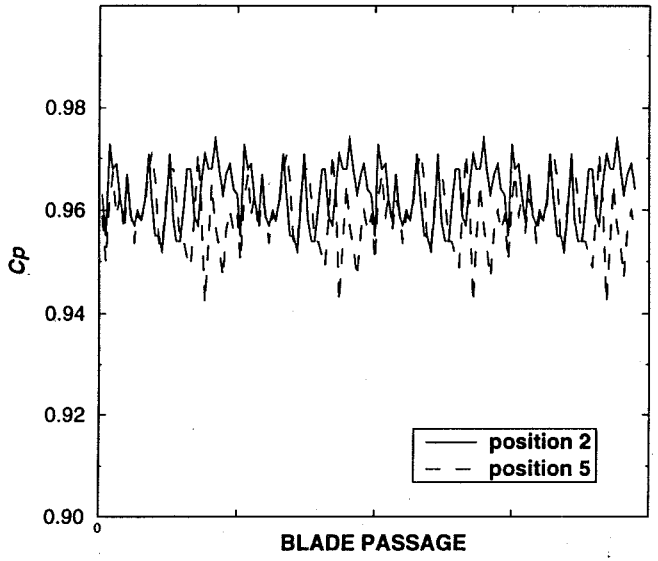

Pressure Surface

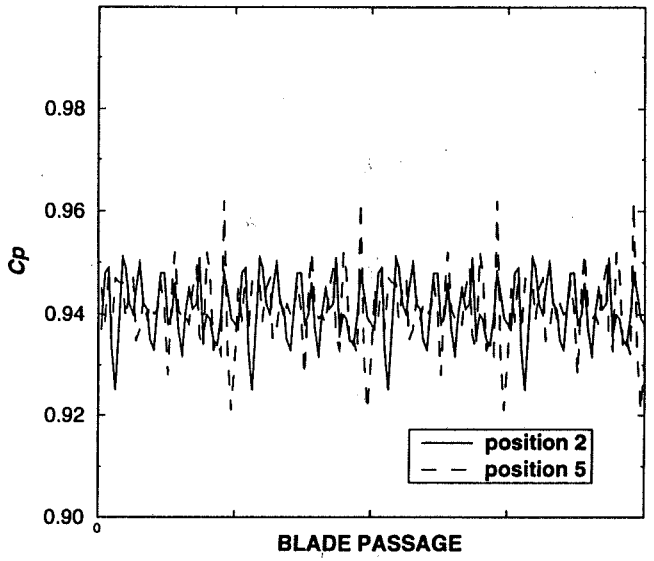

Suction Surface

National Aeronautics and Space Administration

An Analytical Investigation of the Effects of Stator Airfoil Clocking on Turbine Performance

INSTANTANEOUS ENTROPY CONTOURS AT FOUR TIME SLICES

t = 0

t = 1/4 BladePassage

t = 1/2 Blade Passage

t = 3/4 Blade Passage

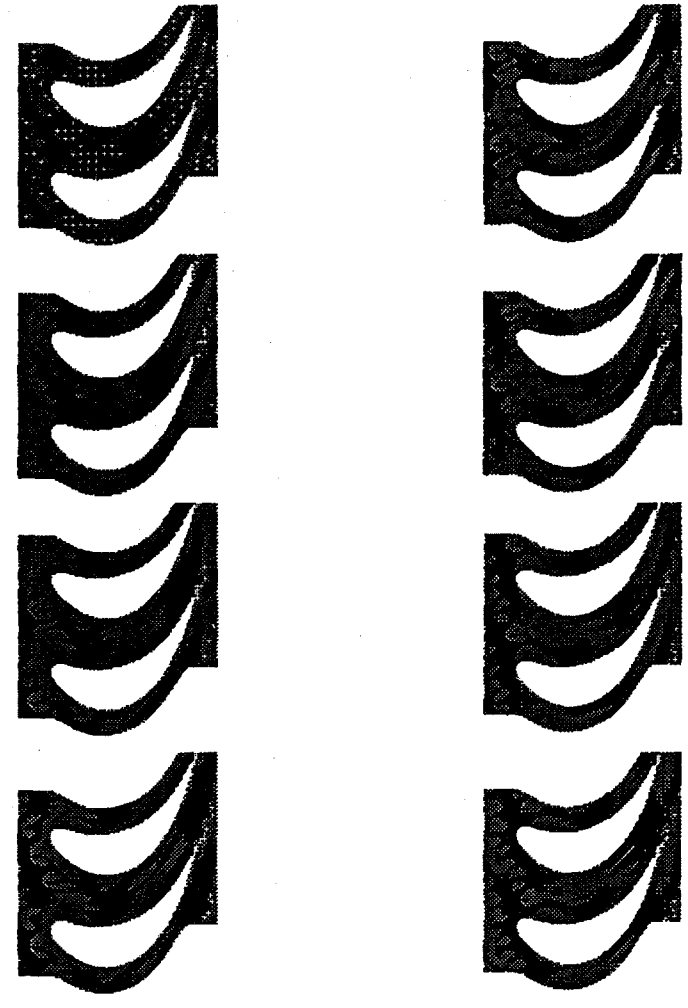

Position 2 Position 5

National Aeronautics and
Space Administration

An Analytical Investigation of the Effects of Stator Airfoil Clocking on Turbine Performance

CONCLUSIONS

- **Two-Dimensional, Time-Accurate, Navier-Stokes Simulations of the Vane Indexing Experiment Performed**
- **Objective of Providing Insights into Physical Mechanisms of Performance Enhancement Due to Airfoil Clocking Achieved (Though the Understanding is Initial; More Work Needs to be Done)**
- **Numerical Analysis Correctly Predicts the Indexing Positions of the First and Second Vanes Required to Produce Maximum Efficiency**
- **Computational Results Indicate Improved Performance of Second Vane Major Contributor to Turbine Efficiency Benefits Achievable Through Airfoil Clocking**
  - Best Performance Achieved When Time-Averaged First Vane Wake Aligned with Second Vane Leading Edge
  - Reduced Velocities and Less Large-Scale Unsteadiness on Second Vane Seen as Possible Reasons for Improved Second Vane Performance
- **Future Work Should Include Further Interrogation of 2D Results and 3D Analysis**

TURBULENCE MODELING AND COMPUTATION OF TURBINE AERODYNAMICS AND HEAT TRANSFER

B. Lakshminarayana & J. Luo
The Pennsylvania State University
Center for Gas Turbine & Power
University Park, PA 16802

The objective of the present research is to develop improved turbulence models for the computation of complex flows through turbomachinery passages, including the effects of streamline curvature, heat transfer and secondary flows.

Advanced turbulence models are crucial for accurate prediction of rocket engine flows, due to existance of very large extra strain rates, such as strong streamline curvature. Numerical simulation of the turbulent flows in strongly curved ducts, including two 180-deg ducts, one 90-deg duct and a strongly concave curved turbulent boundary layer have been carried out with Reynolds stress models (RSM) and algebraic Reynolds stress models (ARSM). The RSM & ARSM models are successful in the prediction of damping effects of convex curvature. However, both models underpredict the turbulence amplification caused by strong concave curvature. In order to capture this amplification of turbulence, the time scale (for spectral energy transfer) in the dissipation rate (ε) equation must be modified. A detailed analysis has been carried out for the modifications to the ε-equation. An improved near-wall pressure-strain correleration has been developed for capturing the anisotropy of turbulence in the concave region.

A comparative study of two modes of transition in gas turbine, the by-pass transition and the separation-induced transition, has been carried out with several representative low-Reynolds-number (LRN) k-ε models. Effects of blade surface pressure gradient, freestream turbulence and Reynolds number on the blade boundary layer development, and particularly the inception of transition are examined in detail. The present study indicates that the turbine blade transition, in the presence of high freestream turbulence, is predicted well with LRN k-ε models employed.

The three-dimensional Navier-Stokes procedure developed by the present authors has been used to compute the three-dimensional viscous flow through the turbine nozzle passage of a single stage turbine. A low Reynolds number k-ε model and a zonal k-ε/ARSM (algebraic Reynolds stress model) are utilized for turbulence closure. The algebraic Reynolds stress model is used only in the endwall region to represent the anisotropy of turbulence. For the turbine nozzle flow, comprehensive comparisons between the predictions and the experimental data obtained at Penn State show that most features of the vortex-dominated endwall flow, as well as nozzle wake structure, have been captured well by the numerical procedure. An assessment of the performance of the turbulence models has been carried out. The two models are found to provide similar predictions for the mean flow parameters, although slight improvement in the prediction of some secondary flow quantities has been obtained by the ARSM model. It's found that the wake profiles inside the endwall boundary layers arepredicted better than those near the mid-span.

TURBULENCE MODELING AND COMPUTATION OF TURBINE AERODYNAMICS AND HEAT TRANSFER*

B. Lakshminarayana and J. Luo

Center for Gas Turbine & Power
The Pennsylvania State University
University Park, PA 16802

CFD Workshop, April 25, 1995, Huntsville, AL

* Sponsored by NASA Marshall Space Flight Center

Objective:

To develop turbulence models for prediction of turbine flow & thermal fields including effects of curvature, rotation and high temperature

Outline:

- Introduction
- Numerical Technique & Turbulence Models
- 3-D Navier-Stokes Comp. of turbine nozzle flow
- Turbulence Modeling for Strongly Curved Shear Flows
- Computation of Turbine Blade Transition and Heat Transfer
- Concluding remarks

3-D NAVIER-STOKES PROCEDURE

- Explicit 4-Stage Runge-Kutta Scheme
- Central differencing + smoothing (eigenvalue & local vel. scaling)
- Turbulence Models:
  - Differential Reynolds stress model (high Re no. & low Re no.)
  - Algebraic Reynolds stress model
  - Nonlinear k-ε model
  - Two eq. models (low & high-Re-no. versions)
  - ε-modification for strong streamline curvature
- Boundary Conditions
  - Characteristic boundary conditions
  - Quasi-3D non-reflecting boundary conditions
- Acceleration Schemes
  - Local time stepping, implicit residual smoothing
  - Implicit treatment of k-ε equations
  - Multigrid

Strongly curved shear flows investigated:

Flow	Author	Re	δ/R
Concave TBL	Barlow & Johnston	3.3×10^4	0.06
90-deg duct	Kim & Patel	2.2×10^5	0.05/0.04
180-deg duct	Monson et al.	1.0×10^5	0.7/0.2
180-deg duct	Sandborn	2.2×10^5	1.0/0.3
180-deg duct	Monson et al.	1.0×10^6	0.7/0.2

Modeling for Curved Shear Flows

- Modeling of curved flows (mostly mild curvature, convex curvature)
  - Mixing-length model: Prandtl's hypothesis $F = 1-\alpha \frac{U/r}{\partial U/\partial n}$
  - k-ε model: Launder et al (1977) $-C_{\varepsilon 2}(1- C_c\, Ri_t)\frac{\varepsilon^2}{k}$, etc.
  - RSM & ARSM: Irvin & Arnot Smith 1975, Gibson & Rodi 1981, etc.

(used in boundary layer codes, mild/convex curved flows)

- Comps. of strongly curved flows, e.g., 180-deg duct flows.
  - Monson et al. (1990);
  - Avva et al. (1990);
  - Shih et al. (1994), etc.

  Agreement not satisfactory

  $\Rightarrow$ Further modeling work on strongly curved flows

Modifications to ε-equation

- **Standard ε equation:**

$$\frac{\partial(\rho\varepsilon)}{\partial t}+\frac{\partial(\rho U_i\varepsilon)}{\partial x_i}=\frac{\partial}{\partial x_j}\left[\left(\mu+\frac{\mu_t}{\sigma_\varepsilon}\right)\frac{\partial\varepsilon}{\partial x_j}\right]+\rho\frac{\varepsilon}{k}\left(C_{\varepsilon 1}P_k-C_{\varepsilon 2}\varepsilon\right)$$

standard values: C_μ=0.09, $C_{\varepsilon 1}$=1.44, $C_{\varepsilon 2}$=1.92, σ_k=1.0, σ_ε=1.3

- **Modification in the sink term (Launder et al. 1977)**

$$C'_{\varepsilon 2}=C_{\varepsilon 2}(1-0.2Ri_t)$$

where $Ri_t=\left(\frac{k}{\varepsilon}\right)^2\frac{U}{r^2}\frac{\partial(Ur)}{\partial n}$

- **Modification of time-scale in the source term (Lumley 1992)**

$$\frac{\partial(\rho\varepsilon)}{\partial t}+\frac{\partial(\rho U_i\varepsilon)}{\partial x_i}=\frac{\partial}{\partial x_j}\left[\left(\mu+\frac{\mu_t}{\sigma_\varepsilon}\right)\frac{\partial\varepsilon}{\partial x_j}\right]+\rho\frac{\varepsilon}{k}\left(C'_{\varepsilon 1}kS-C_{\varepsilon 2}\varepsilon\right)$$

where $C'_{\varepsilon 1}=0.42$, $S=(2S_{ij}S_{ij})^{1/2}$, $S_{ij}=(U_{i,j}+U_{j,i})/2$

Nonliear k-ε model (Shih, Zhu & Lumley 1993)

$$\overline{u_i u_j} = \frac{2}{3}k\delta_{ij} - \nu_t(U_{i,j} + U_{j,i})$$

$$+ \frac{C_{\tau 1}}{A_2 + \eta^3}\frac{k^3}{\varepsilon^2}(U_{i,k}U_{k,j} + U_{j,k}U_{k,i} - \frac{2}{3}U_{i,j}U_{j,i}\delta_{ij})$$

$$+ \frac{C_{\tau 2}}{A_2 + \eta^3}\frac{k^3}{\varepsilon^2}(U_{i,k}U_{j,k} - \frac{1}{3}U_{i,j}U_{i,j}\delta_{ij})$$

$$+ \frac{C_{\tau 3}}{A_2 + \eta^3}\frac{k^3}{\varepsilon^2}(U_{k,i}U_{k,j} - \frac{1}{3}U_{i,j}U_{i,j}\delta_{ij})$$

$$\nu_t = \frac{2/3}{A_1 + \eta}\frac{k^2}{\varepsilon}$$

$$\eta = \frac{k}{\varepsilon}(2S_{ij}S_{ij})^{1/2}$$

$$S_{ij} = (U_{i,j} + U_{j,i})/2$$

ARSM (ALGEBRAIC REYNOLDS STRESS MODELS)

- **Reynolds stress transport eq.:**

$$C_{ij} - D_{ij} = P_{ij} + \phi_{ij} - \varepsilon_{ij}$$

- **ARSM assumption (Rodi, 1976):**

$$C_{ij} - D_{ij} = \frac{\overline{u_i u_j}}{k}(C_k - D_k) = \frac{\overline{u_i u_j}}{k}(P_k - \varepsilon)$$

- **Present ARSM (Derived from Gibson & Launder RSM (1978) for compressible flows)**

$$-\overline{\rho u_i'' u_j''} = -\bar{\rho}\tilde{k}\left[(P_{ij} - 2P\delta_{ij}/3)(1-C_2) + \phi_{ij,w}\right] \Big/ \left[P + \bar{\rho}\tilde{\varepsilon}(C_1 - 1)\right] - \frac{2}{3}\delta_{ij}\bar{\rho}\tilde{k}$$

$$P_{ij} = -\overline{\rho u_i'' u_k''}\,\partial\tilde{u}_j/\partial x_k - \overline{\rho u_j'' u_k''}\,\partial\tilde{u}_i/\partial x_k \quad \text{and} \quad P = P_{ii}/2$$

Low Reynolds-number RSM Models

Shima, 1988

- Based on LRR RSM
- conventional damping function f_w ($f_w = \exp(-(0.015k^{1/2}y/n)^4)$)
- This LRN model reduces to its high-Re version (i.e., LRR model) away from the wall.

Launder & Shima, 1989

- Based on LRR-Gibson-Launder RSM
- Use independent Reynolds stress invariants
- Constants C_1, C_2, C_1' and C_2' are functions of the turbulence anisotropy parameters
- This model may not reduce to its high Re version away from the wall

REYNOLDS-STRESS MODEL (RSM) AND ALGEBRAIC REYNOLDS-STRESS MODEL (ARSM)

- **Reynolds stresss transport equation :**

$$U_k \frac{\partial \overline{u_i u_j}}{\partial x_k} = -\overline{u_i u_k} U_{j,k} - \overline{u_j u_k} U_{i,k} + \overline{\frac{p}{\rho}(u_{i,j} + u_{j,i})} - \frac{\partial}{\partial x_k}\left[\overline{u_i u_j u_k} + \frac{\overline{p u_j}}{\rho}\delta_{ik} + \frac{\overline{p u_i}}{\rho}\delta_{jk} - \nu \frac{\partial \overline{u_i u_j}}{\partial x_k}\right] - 2\nu \overline{\frac{\partial u_i}{\partial x_k}\frac{\partial u_j}{\partial x_k}}$$

i.e., $C_{ij} - D_{ij} = P_{ij} + \phi_{ij} - \varepsilon_{ij}$

- **Models employed in present computations:**

  - **RSM model = LRR Model (Launder,Reece & Rodi, 1975) with Shima near-wall low-Reynolds-number functions**

  - **ARSM model = Algebraic form of LRR model with Gibson-Launder near-wall Pressure-strain correlation**

PERDICHIZZI TURBINE NOZZLE CASCADE

Chord length	55.2 mm
Axial length	34.0 mm
Aspect ratio	1.47
Inlet blade angle	76.1 deg
Outlet blade angle	14.5 deg
Inlet Mach number	0.15
Outlet Mach number	0.70
Reynolds number	0.84×10^6

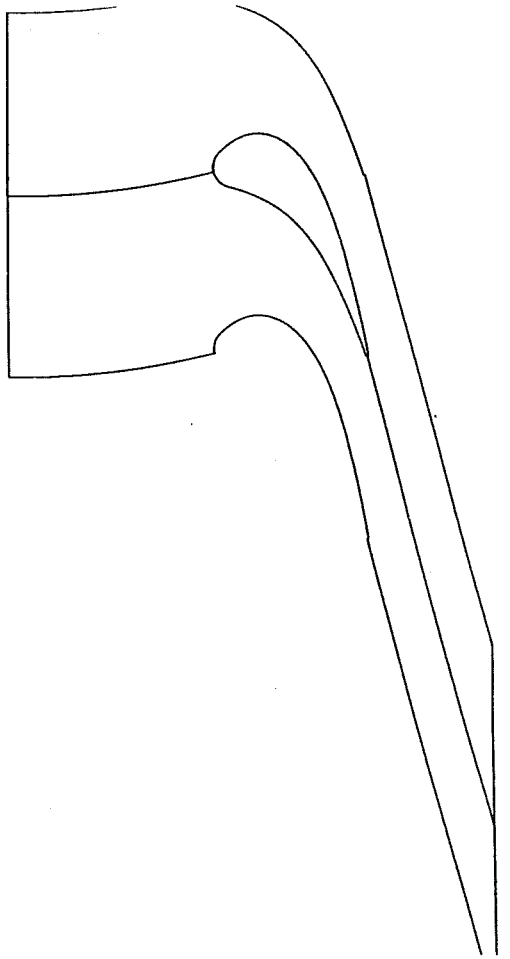

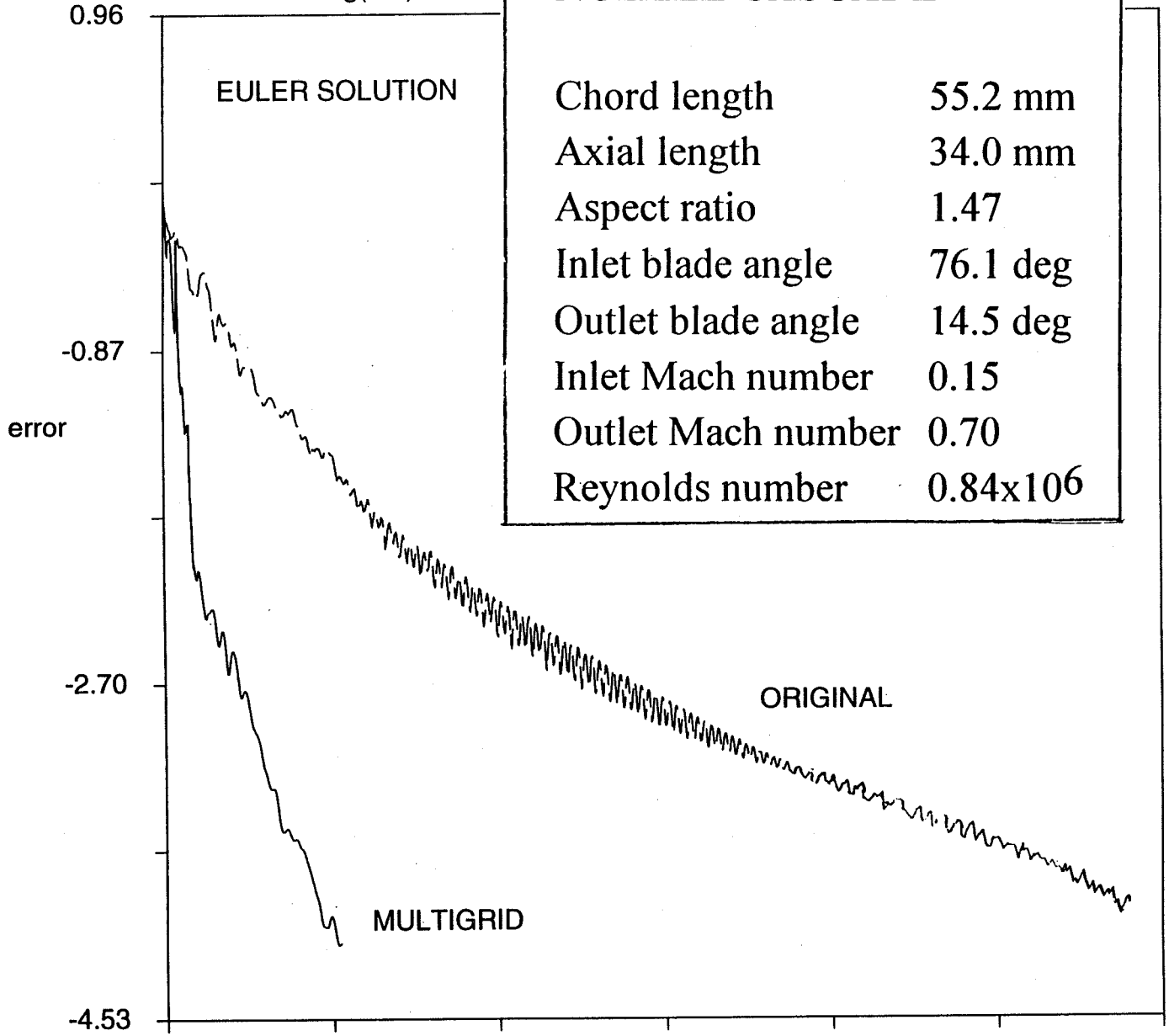

IMPROVEMENT

5 : 1 Convergence Rate

4.3 : 1 CPU Time

24 Apr 95 11:34:01

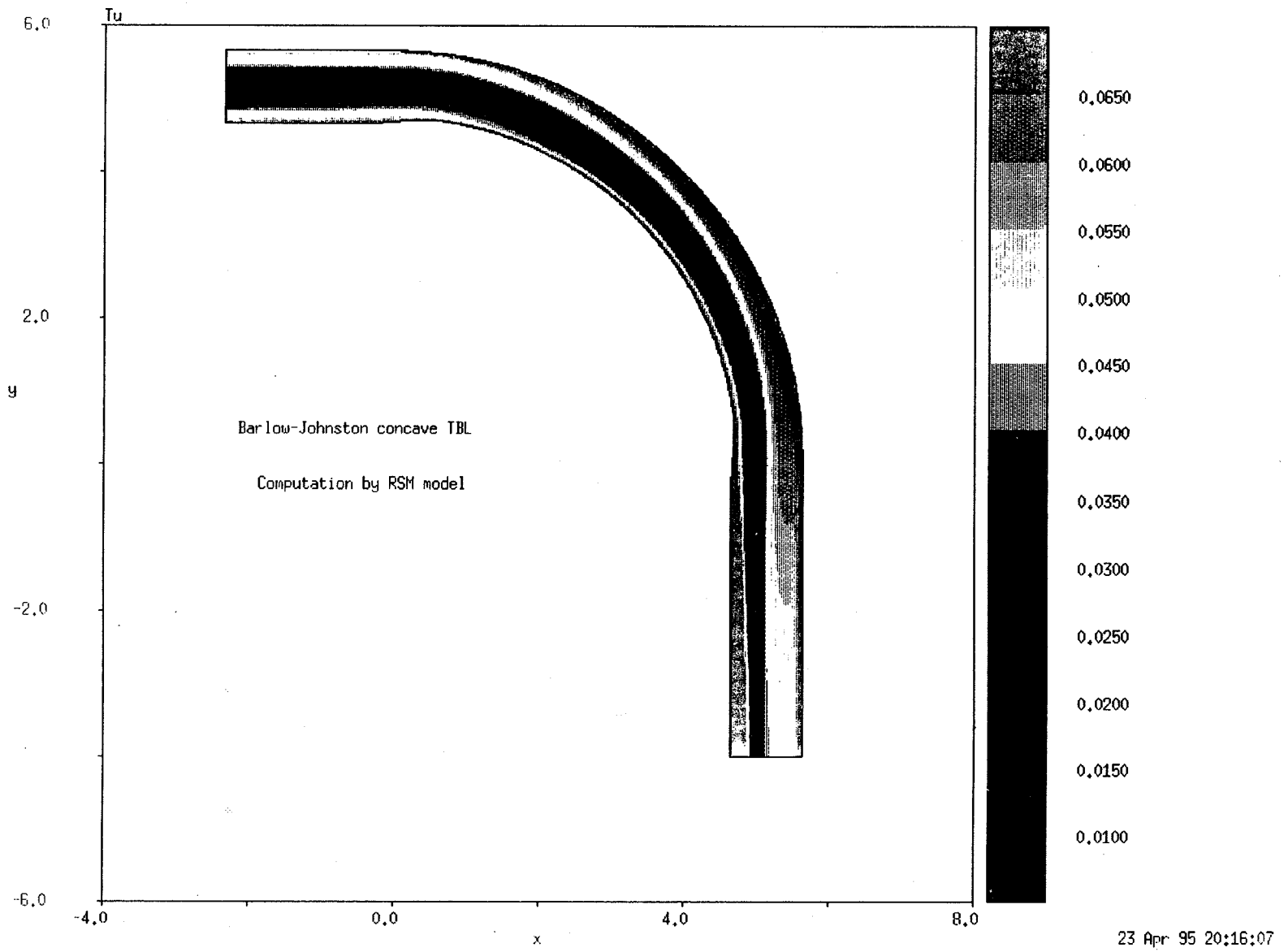
Tu
6.0
2.0
-2.0
-6.0
y
-4.0
0.0
4.0
8.0
x
Barlow-Johnston concave TBL
Computation by RSM model
0.0650
0.0600
0.0550
0.0500
0.0450
0.0400
0.0350
0.0300
0.0250
0.0200
0.0150
0.0100
23 Apr 95 20:16:07

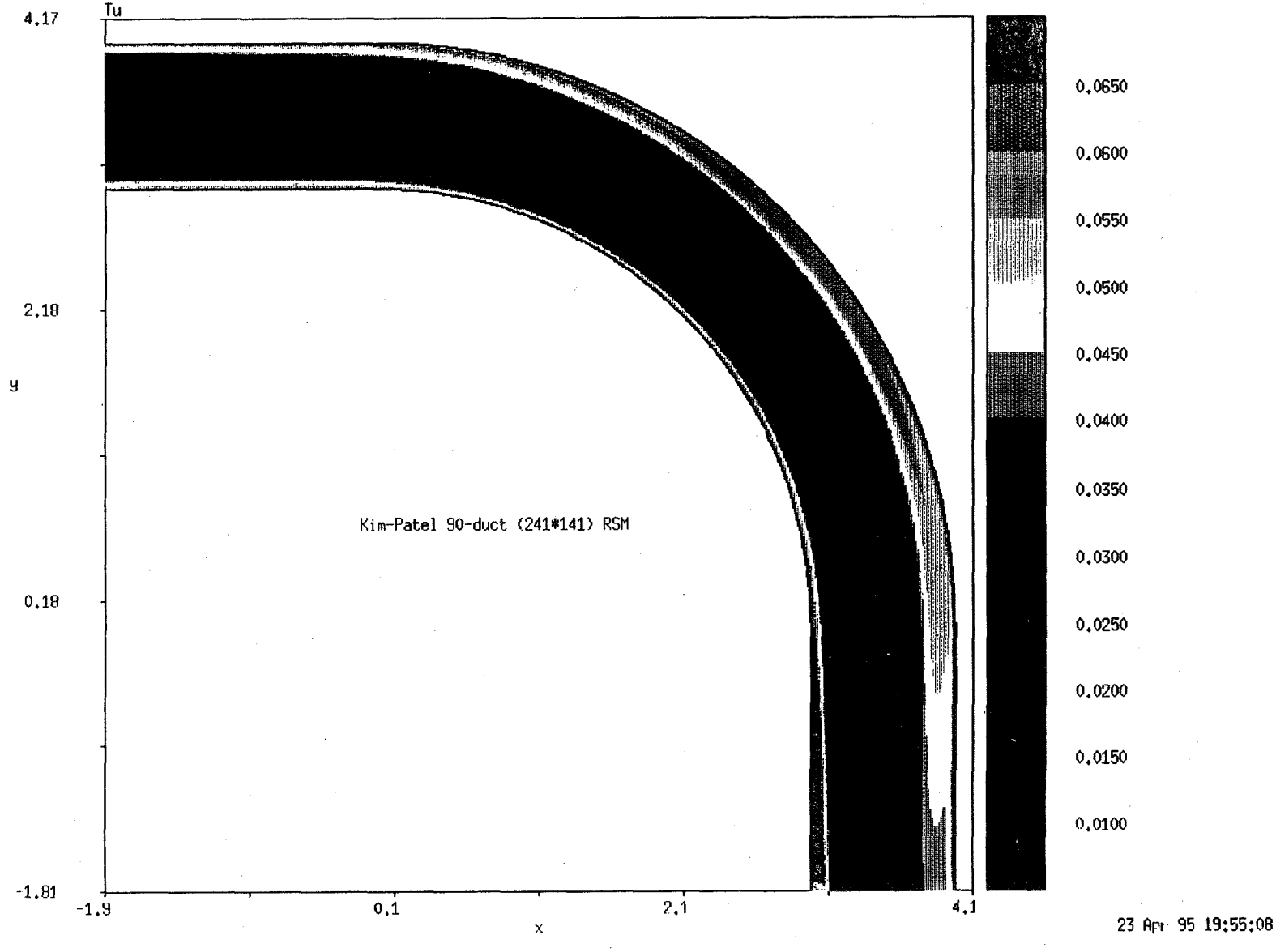
Tu
4.17
2.18
0.18
-1.81
y
-1.9
0.1
2.1
4.1
x
Kim-Patel 90-duct (241*141) RSM
0.0650
0.0600
0.0550
0.0500
0.0450
0.0400
0.0350
0.0300
0.0250
0.0200
0.0150
0.0100
23 Apr 95 19:55:08

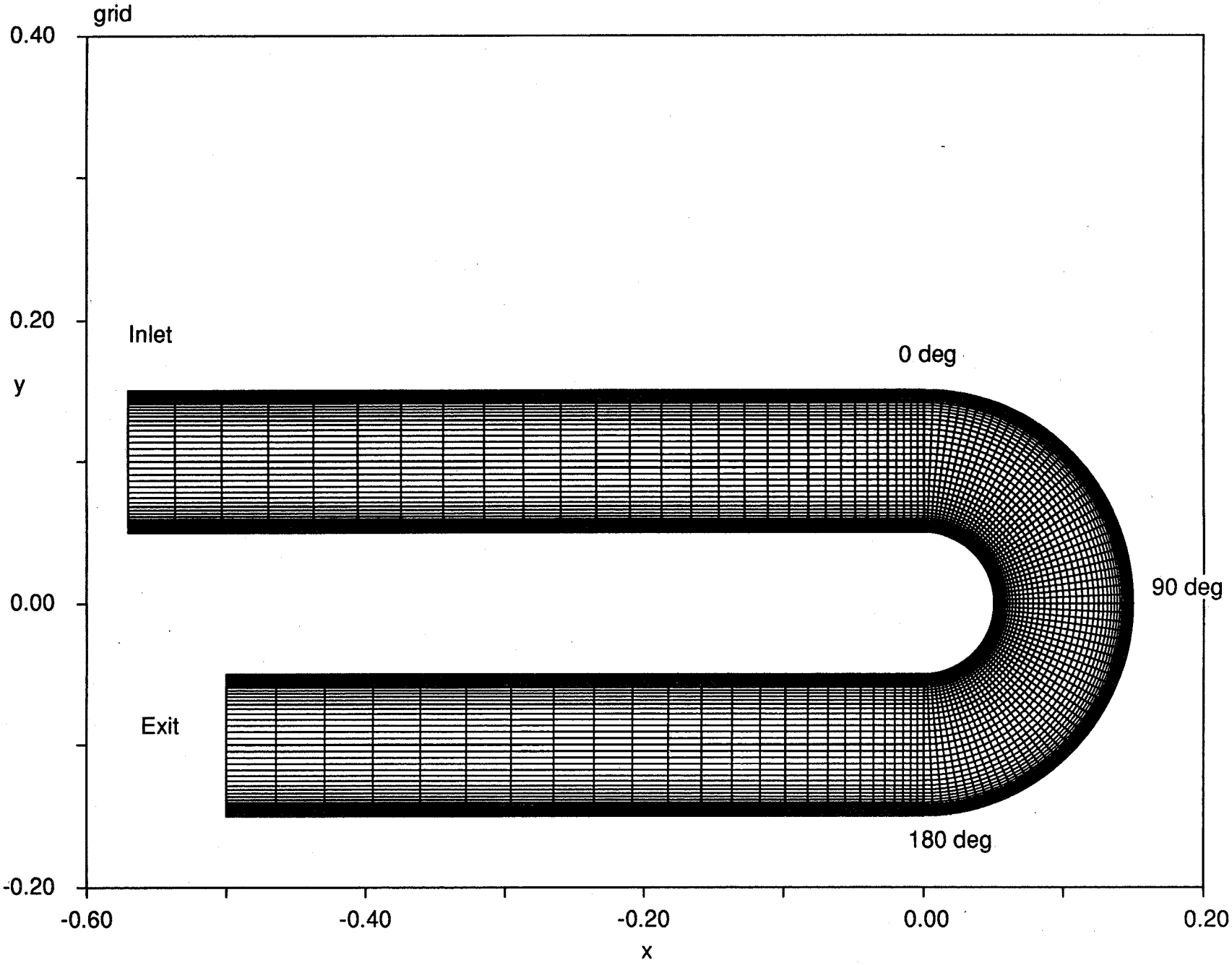
grid
0.40
0.20
0.00
-0.20
y
Inlet
0 deg
90 deg
Exit
180 deg
-0.60
-0.40
-0.20
0.00
0.20
x

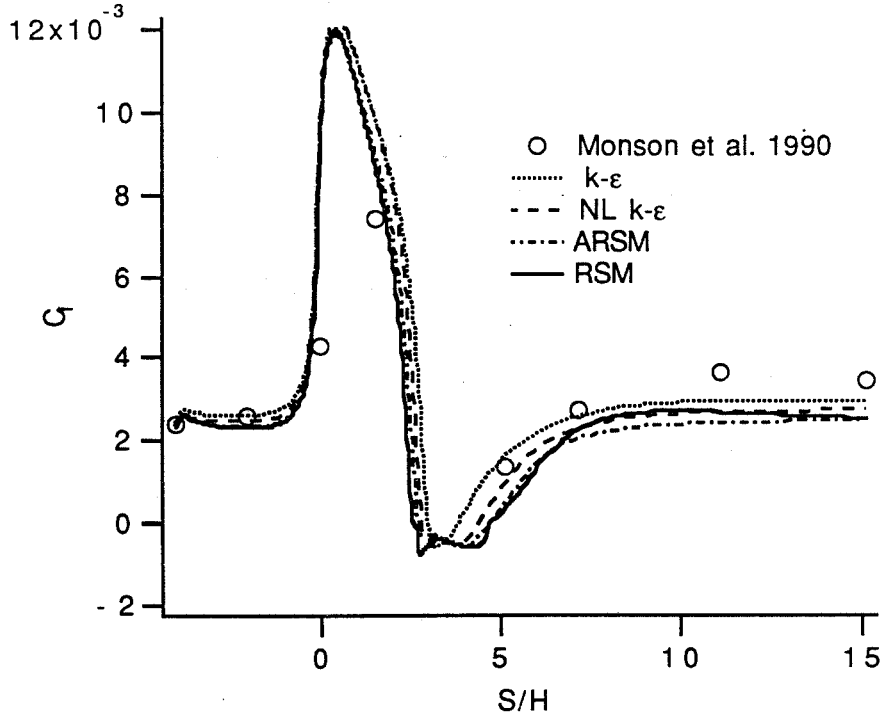

Skin friction on convex wall

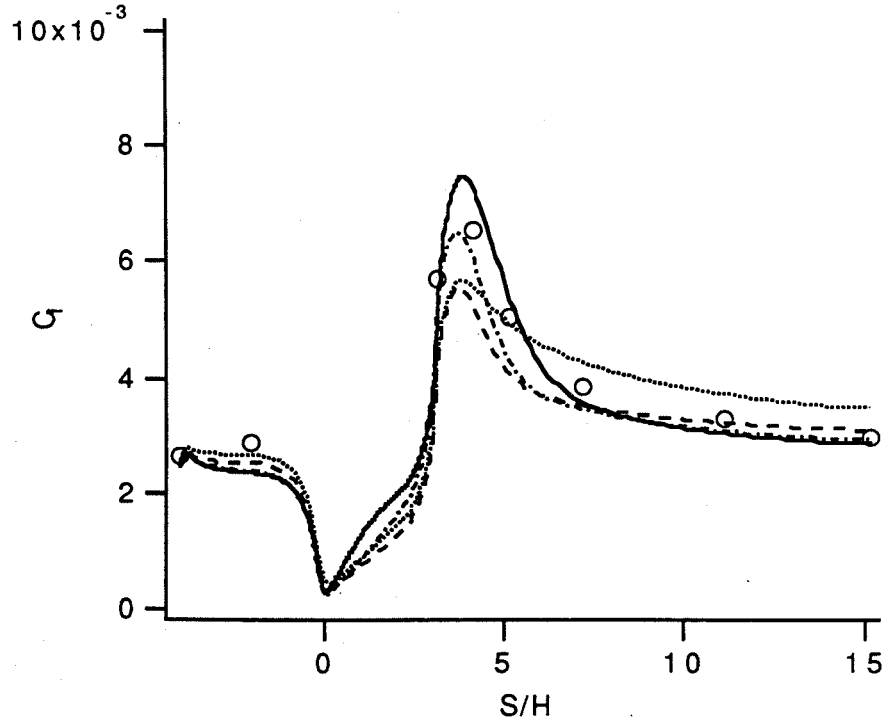

Skin friction on concave wall

Fig. Skin friction for Monson et al. (Re=1x10^6)

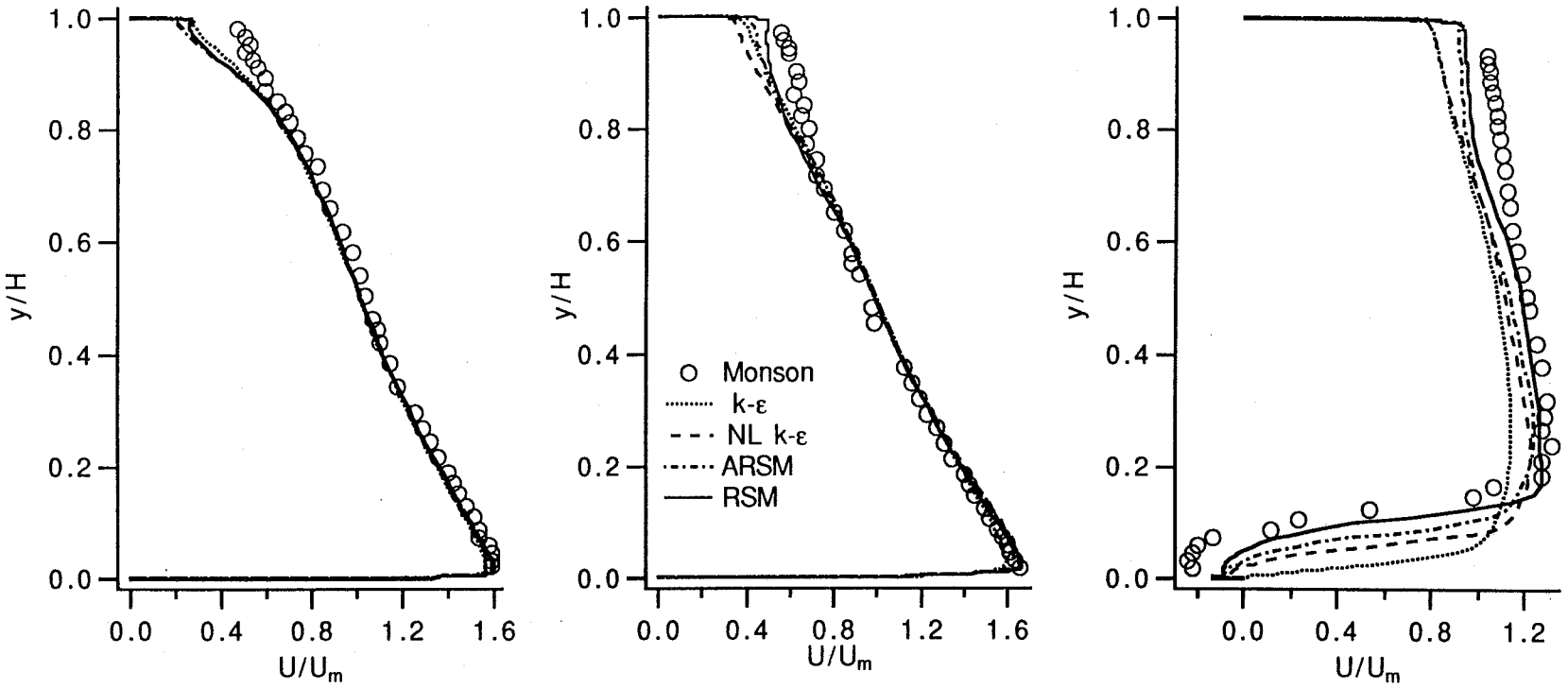

θ=30 deg θ=90 deg θ=180 deg

Fig. Variation of mean velocity profile of 180-deg duct flow

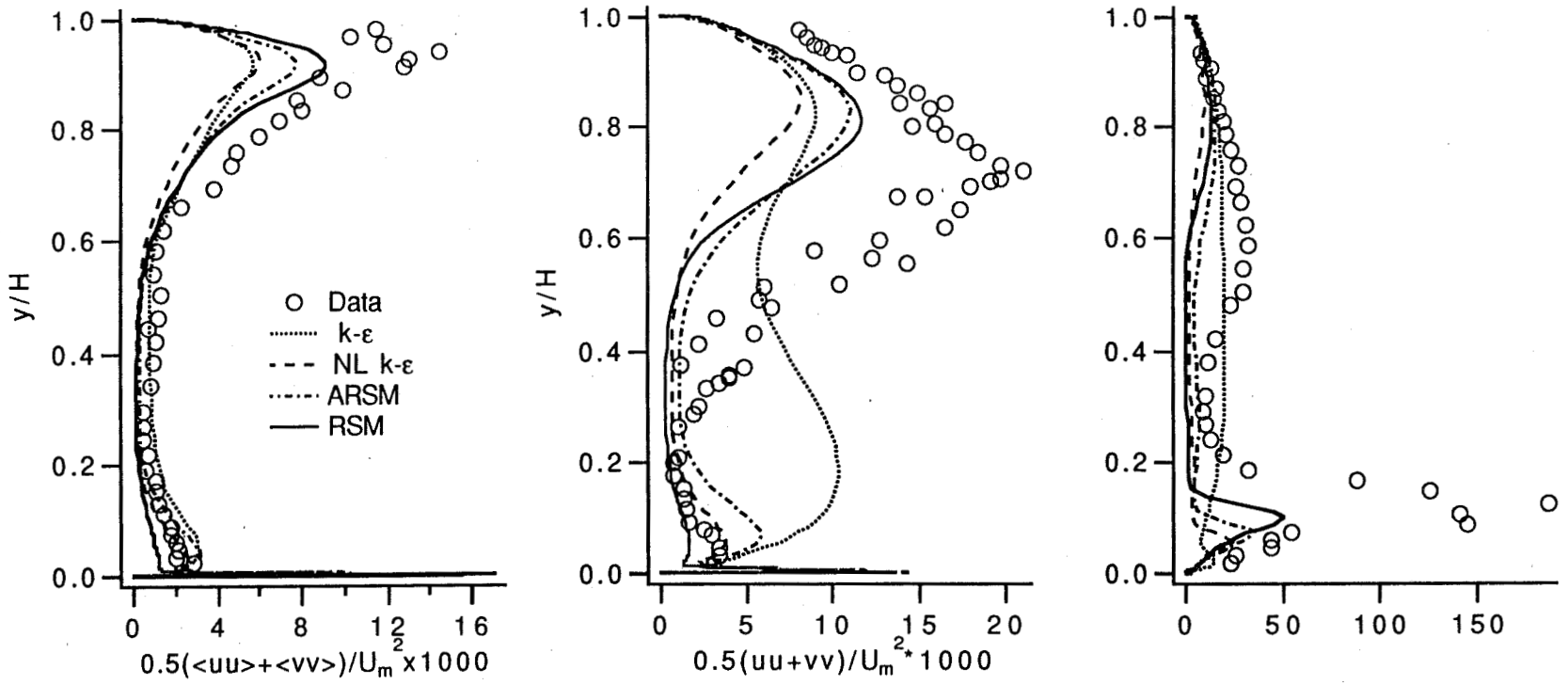

Fig. Variation of 0.5(<uu>+<vv>) profile of 180-deg duct flow

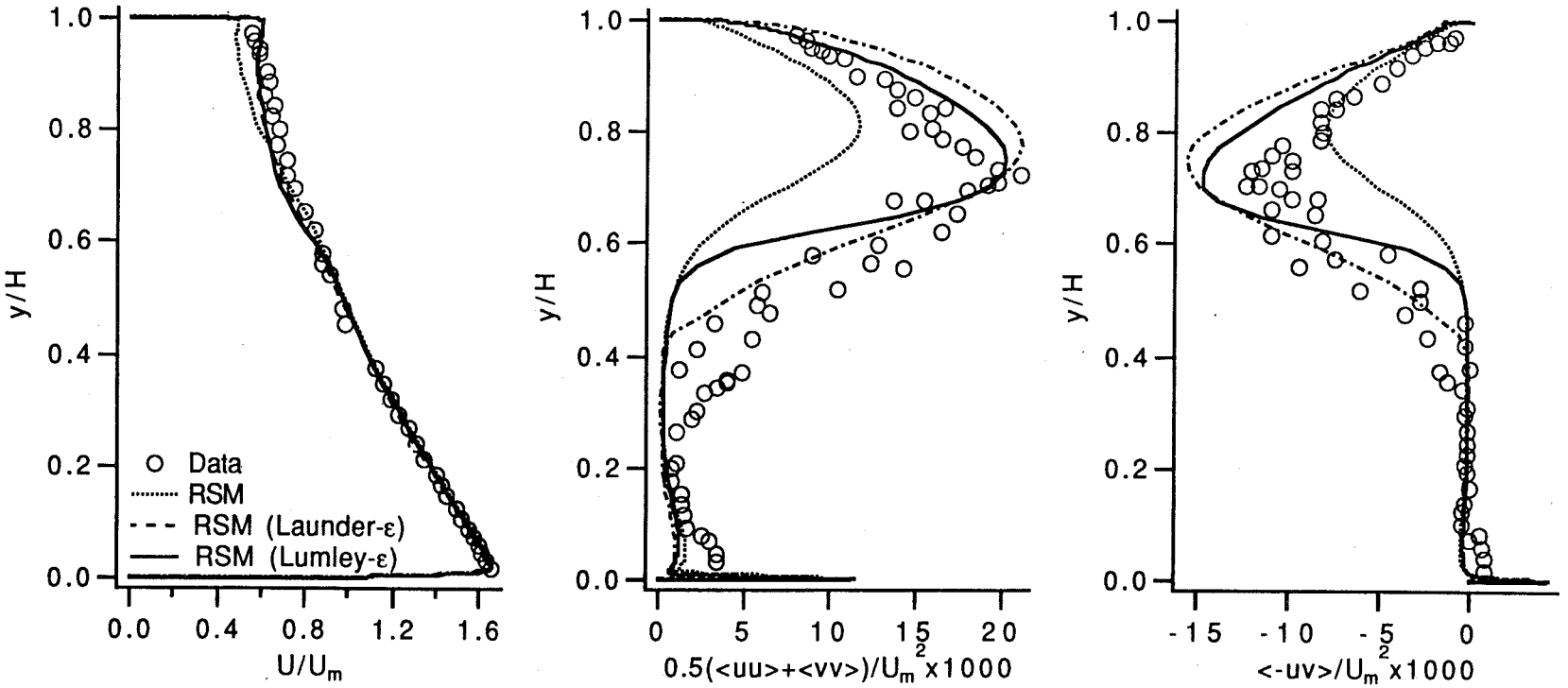

Fig. Profiles at θ=90 deg computed by RSM with modified ε-eq.

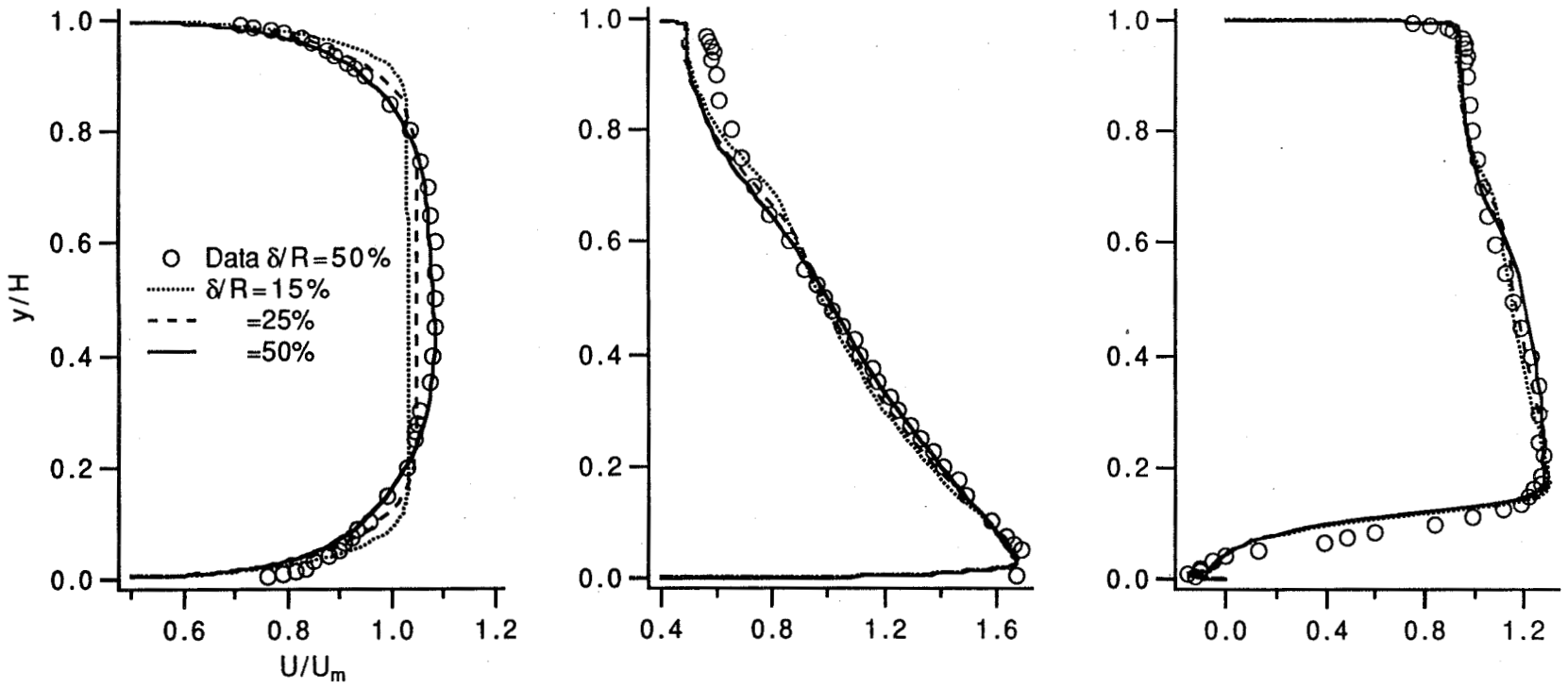

x= -1.73 H **θ=90 deg** **θ=180 deg**

Fig. Effects of δ/R on mean velocity profile of 180-deg duct flow (Simulation by RSM model, data by Sandborn)

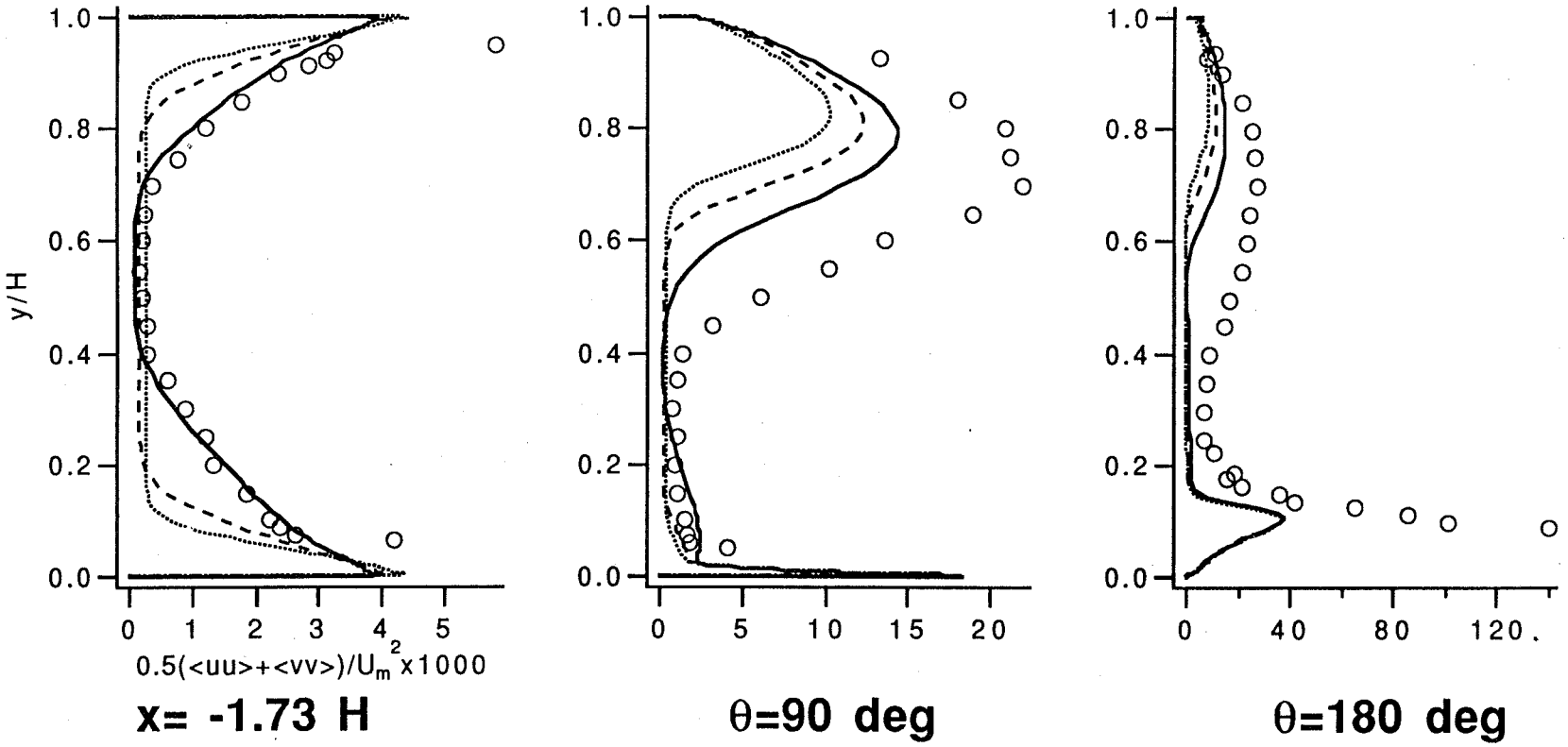

Fig. Effects of δ/R on turbulence energy profile of 180-deg duct flow (Simulation by RSM model, data by Sandborn)

Conclusions on Turbulence Modeling for Strongly Curved Flows

- RSM model provide best predictions for major features of the highly curved duct flows, including major attenuation of turbulence near the convex wall, strong enhancement of turbulence near the concave wall and the extensive separation downstream of the bend.

- Modeling convex curvature effects is different from modeling concave curvature effects, even qualitatively. RSM model is very successful in modeling convex curvature, while still underpredicts concave curvature effect.

- Turbulence damping due to convex curvature are also captured well by ARSM & Nonlinear k-ε model. The isotropic k-ε model fails to account for this effect and underpredicts the extent of separation.

- ARSM model is superior to nonlinear k-ε model for the curved duct flows investigated. The nonlinear k-ε model does not capture any turbulence enhancement in concave region.

- All the models provide too slow a recovery process from separation downstream of the bend, indicating defects in the modeling of turbulent diffusion as well as dissipation terms.

- Simulation studies & data indicate that the flow inside the bend is not sensitive to the upstream inflow conditions, different δ/R leading to only minor variation in downstream velocity profiles.

- To capture concave curvature effect, ε-eq. must be modified:
  - Model of Launder et al. & Lumley provide some improvement.
  - Further improvement of ε-eq. is needed.

Design Features of Penn State Turbine Nozzle

Hub tip ratio	0.7269
Tip radius	0.4582 m
Chord(tip)	0.1768 m
Spacing(tip)	0.1308 m
Turning angle	70 deg
Vane Re(outlet)	(9-10)x10^5
Exit Mach	0.27

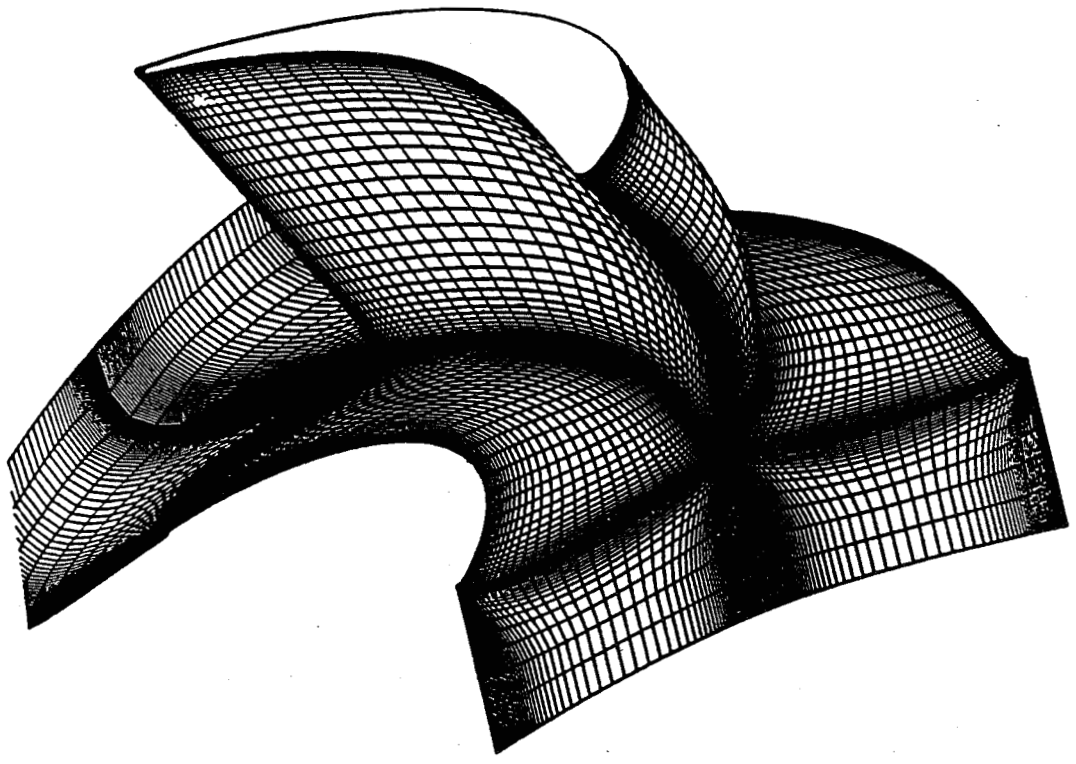

Fig. 3a Computational grid for PSU turbine nozzle

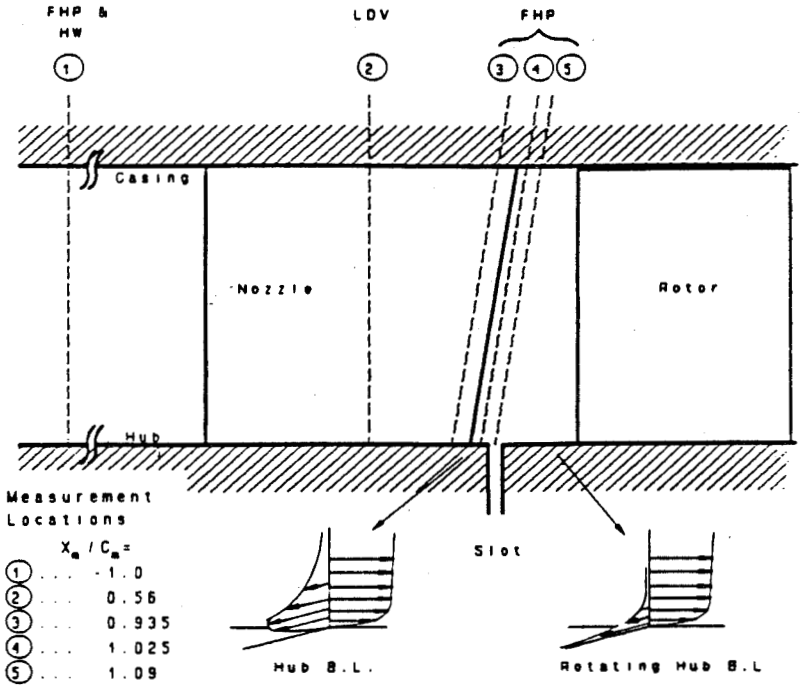

Fig. 3b Measurement locations for the turbine nozzle (FHP: Five hole probe; LDV: Laser doppler velocimeter)

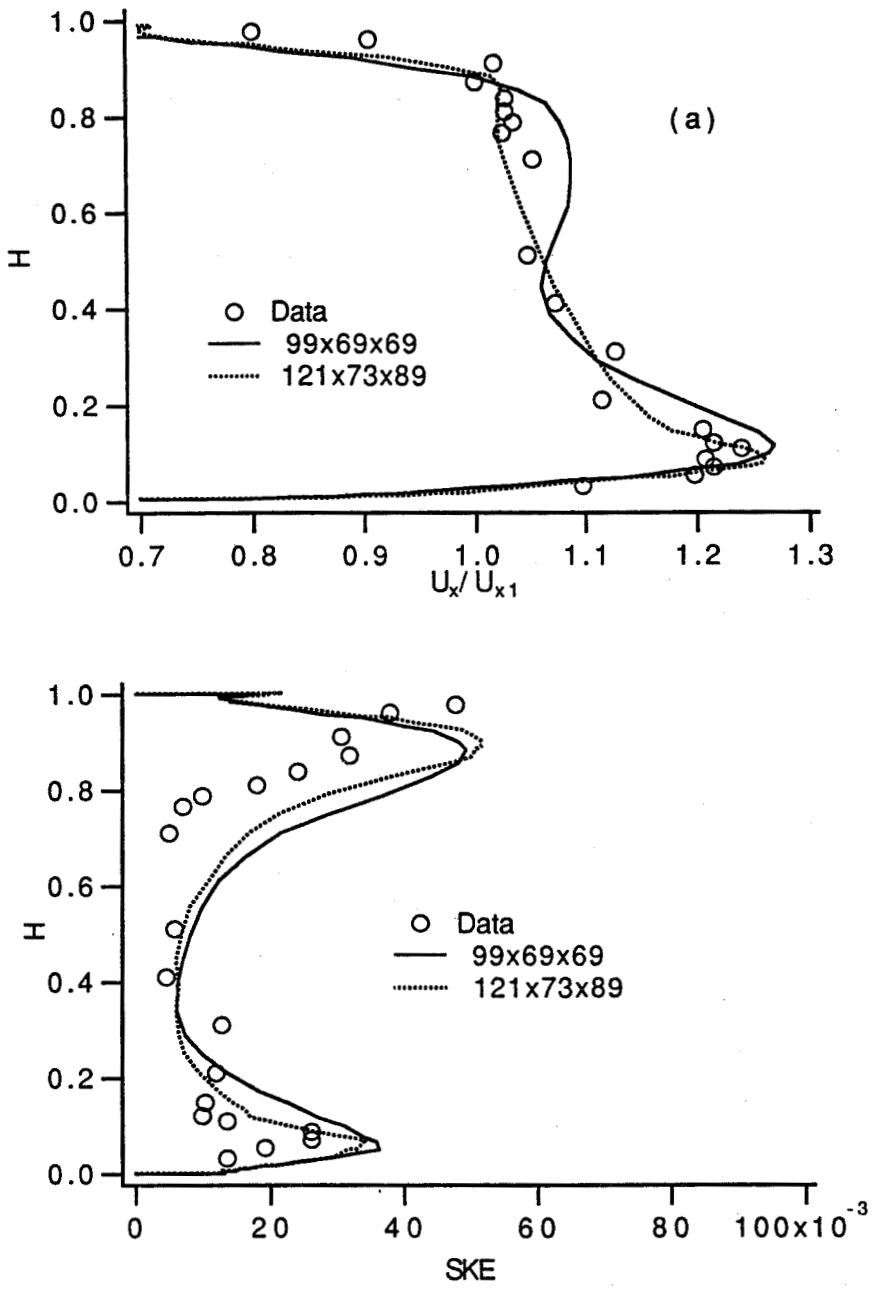

Fig. Pitchwise-mass-averaged parameters (tangential velocity and secondary kinetic energy) predicted using 121x73x89 and 99x69x69 grids with k-ε model

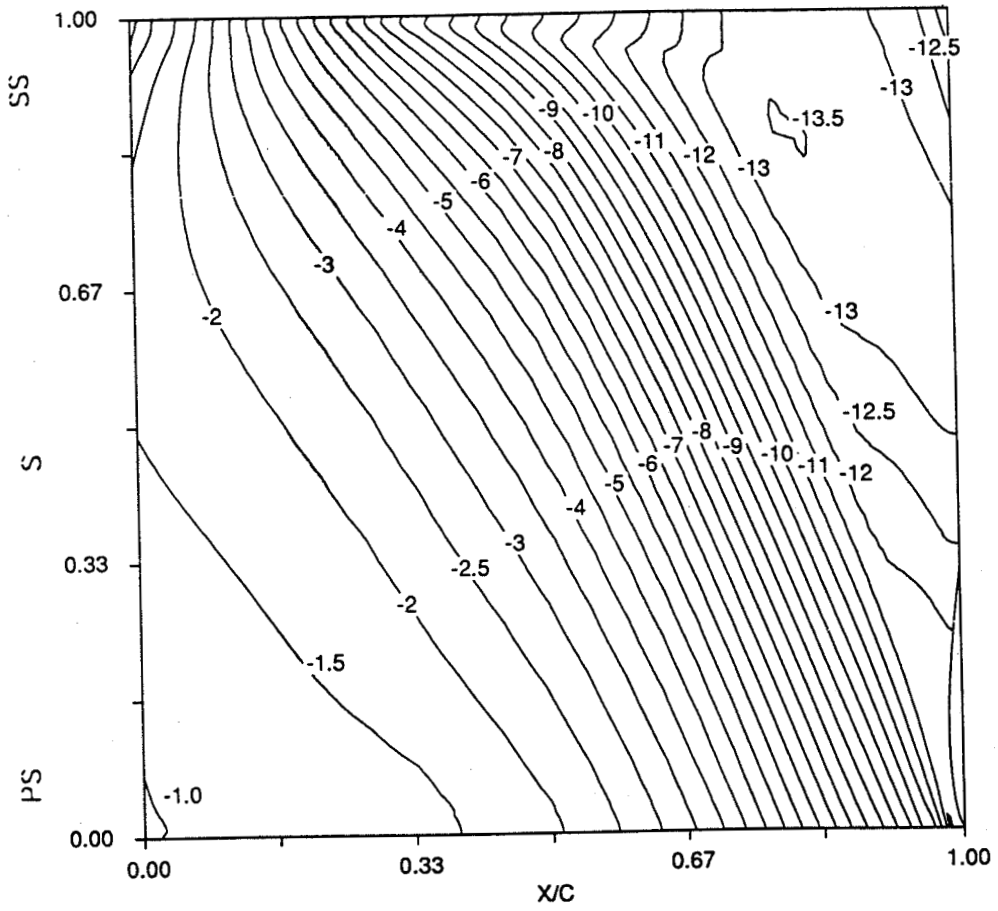

Computation by k-ε/ARSM model

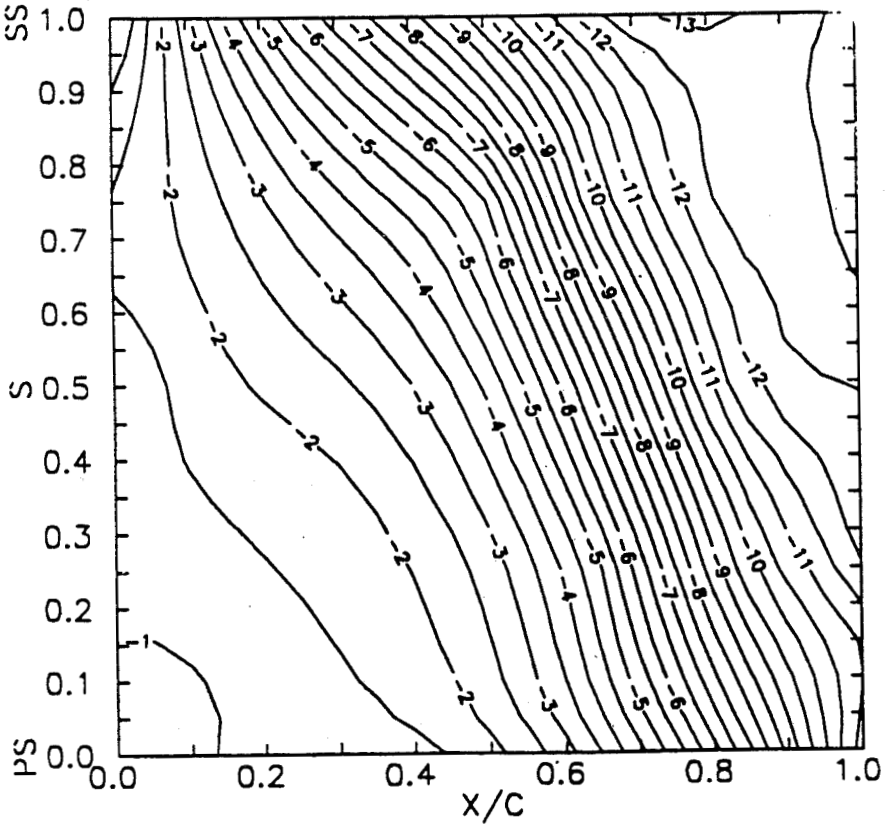

Measurement

Fig. 7 Nozzle hub wall static pressure coeffi. (C_p)

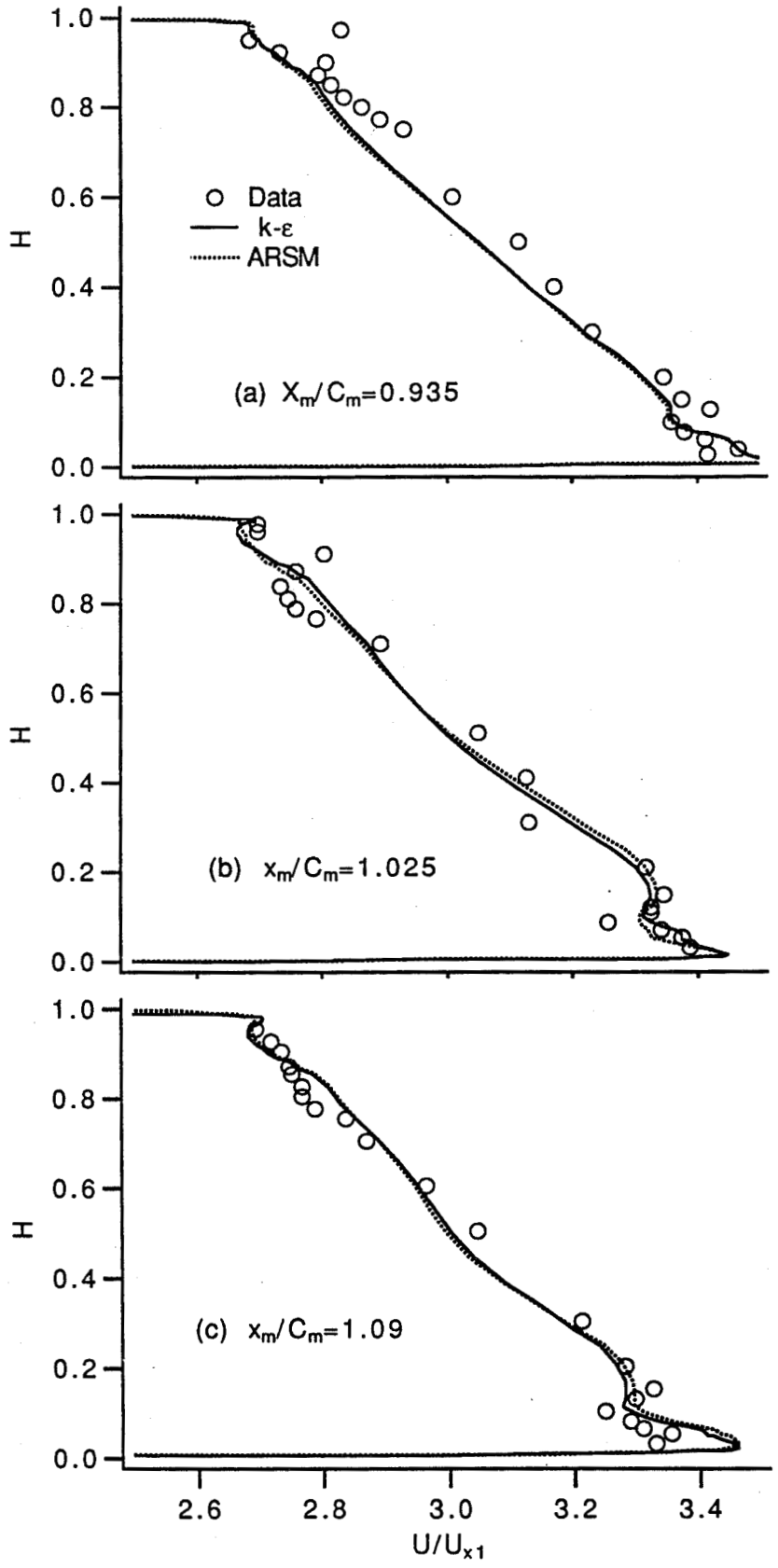

Fig. Pitchwise-averaged total velocity profile

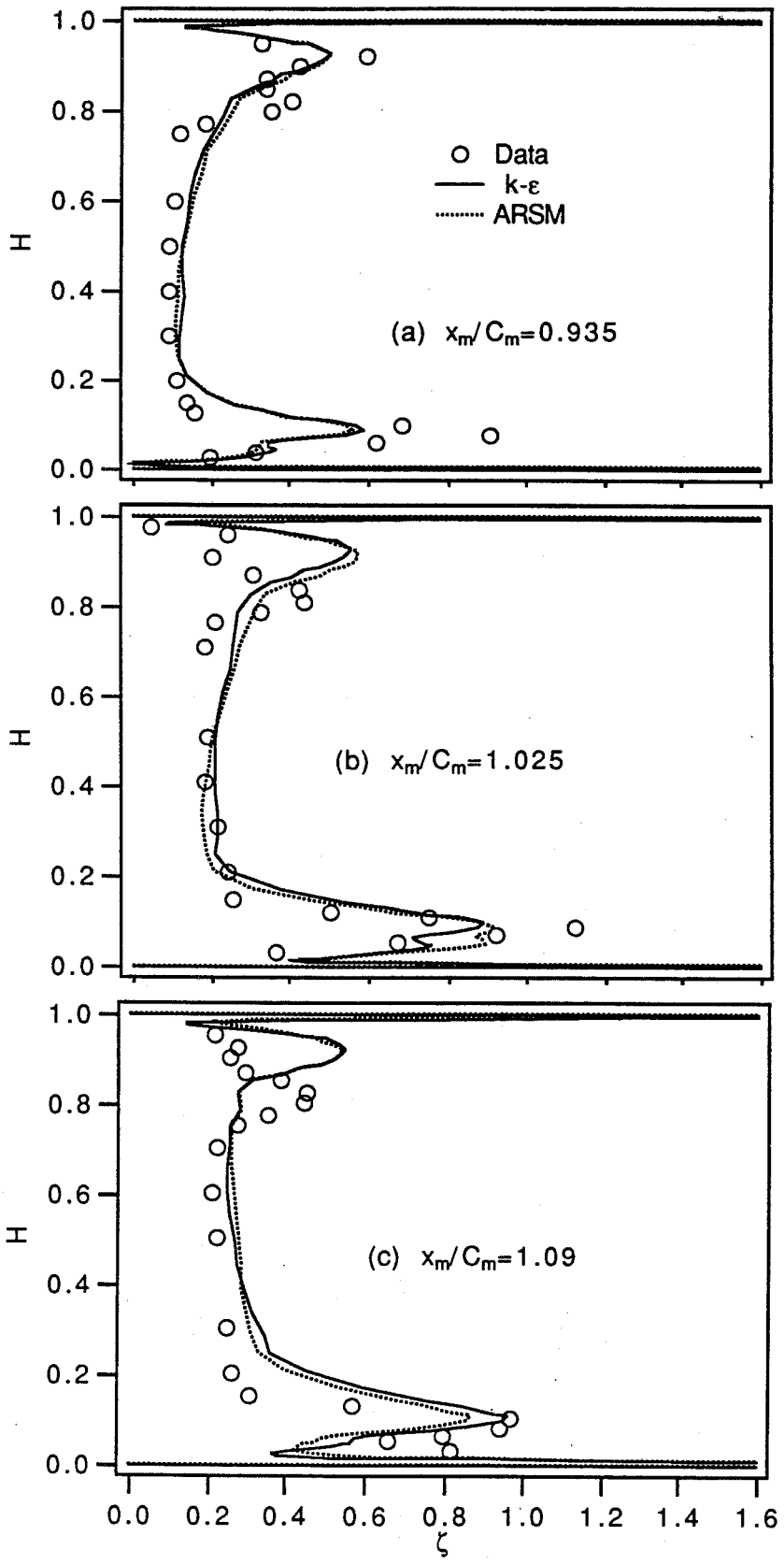

Fig. Pitchwise-averaged total pressure loss coeff.

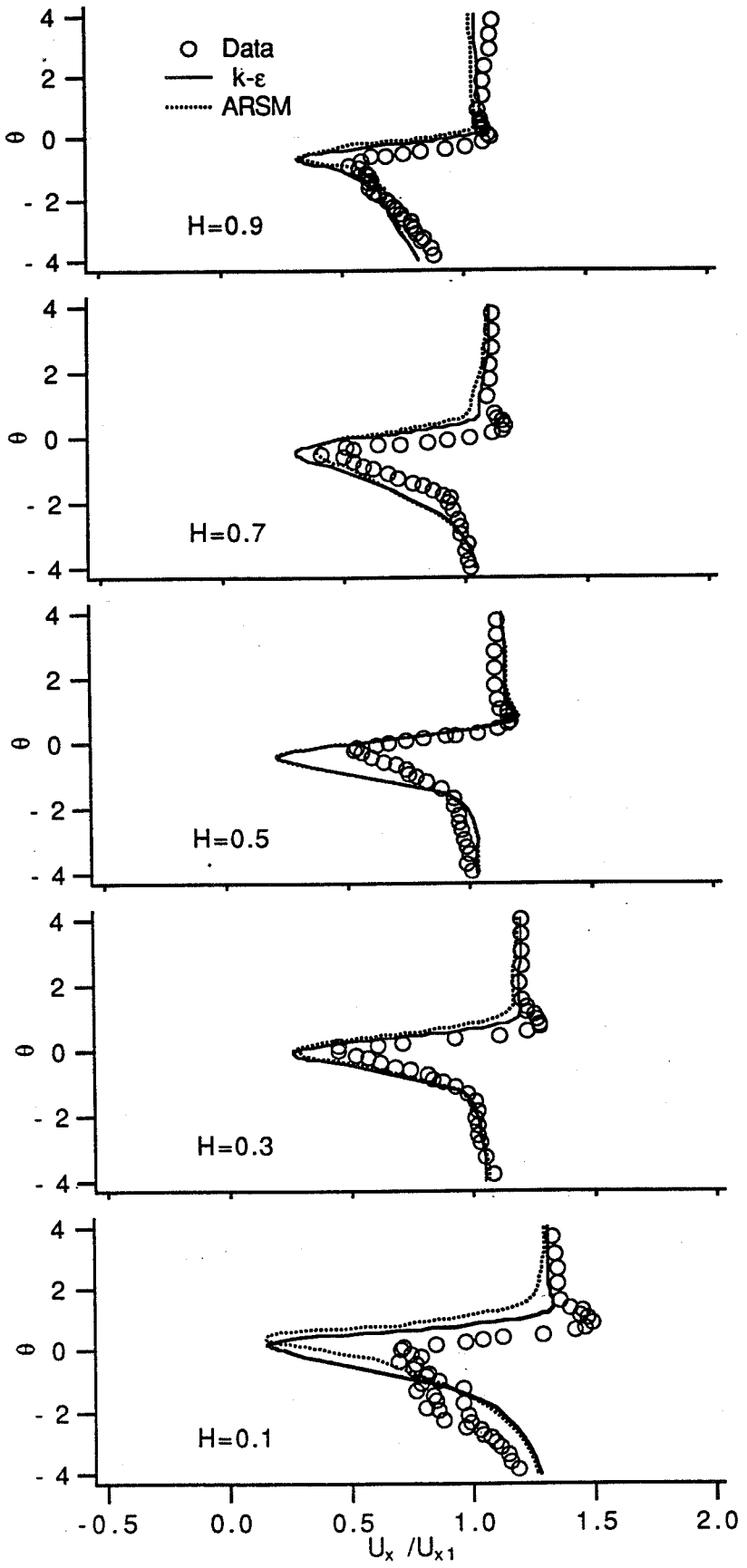

Fig. 18b Axial velocity profile at x_m/C_m=1.025

Conclusions

- Most features of the vortex-dominated endwall flow in the annular turbine nozzle have been captured accurately by the 3-D Navier-Stokes prediction. The passage-averaged properties, particularly the yaw angle and velocity profiles, are captured very well by the present numerical computation.

- The predictions by the anisotropic ARSM model are close to those by the isotropic k-ε model for the mean flow properties, although slight improvement in the prediction of secondary flow (e.g., the secondary kinetic energy) has been obtained by the ARSM model.

- The turbine nozzle secondary flows are primarily driven by pressure gradients. The anisotropy of turbulence becomes important when the secondary flow rolls up into a distinct vortex. Its dissipation and diffusion may only be captured by the ARSM and other anisotropic turbulence models.

• The wake profiles inside the endwall boundary layers are predicted better than those near the mid-span. The width and depth of the wake at the mid-span are overpredicted due to a premature transition predicted by the k-ε model on the blade suction surface in the presence of low freestream turbulence. The discrepancy in the wake profile are also due to the downstream rotor influence.

PSU Rotor (midspan)

- Axial chord = 9.114 cm
- True chord = 11.13 cm
- Flow turning angle = 110 deg
- Re (exit) = 5-7x10^5
- Mach (exit) = 0.27

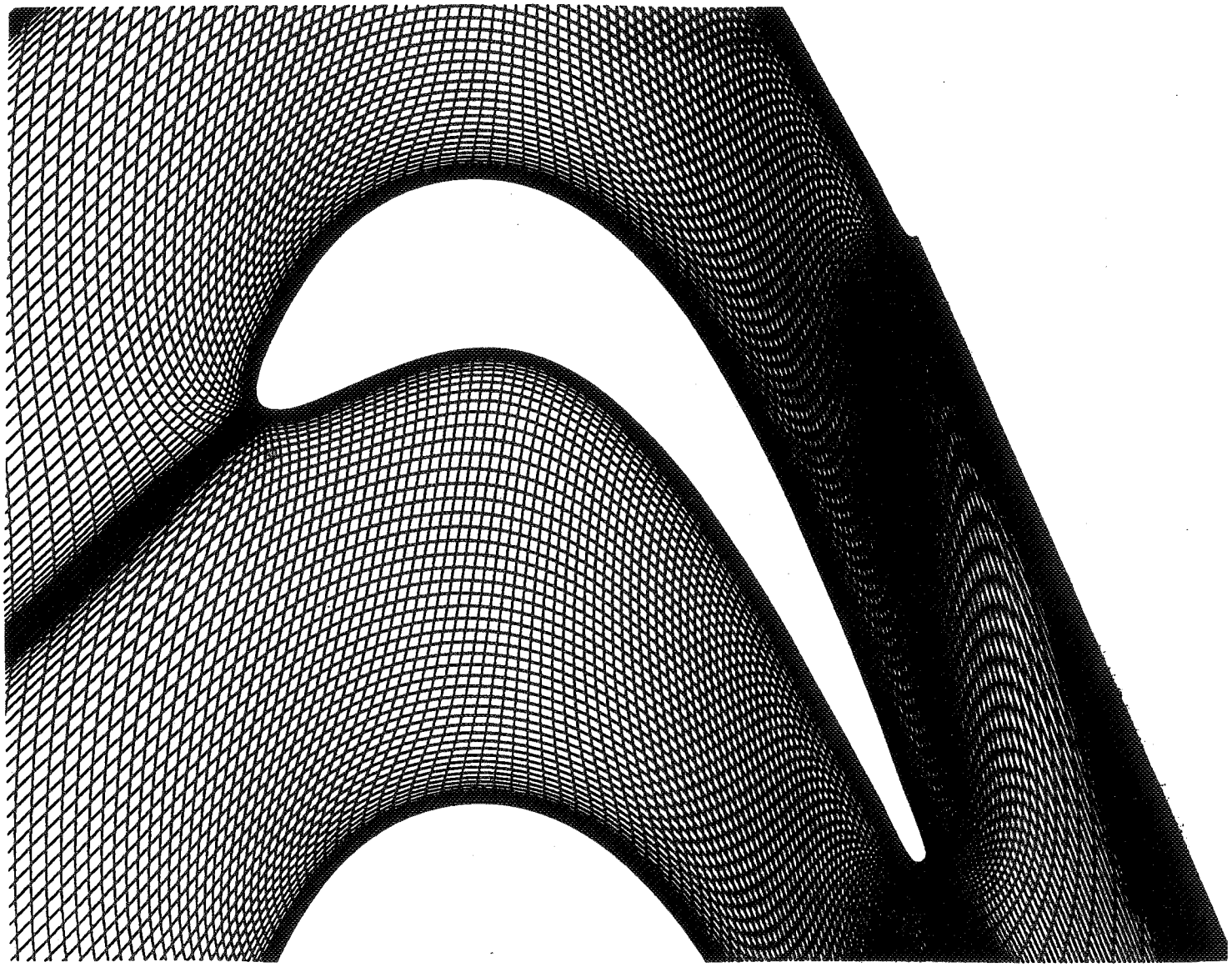

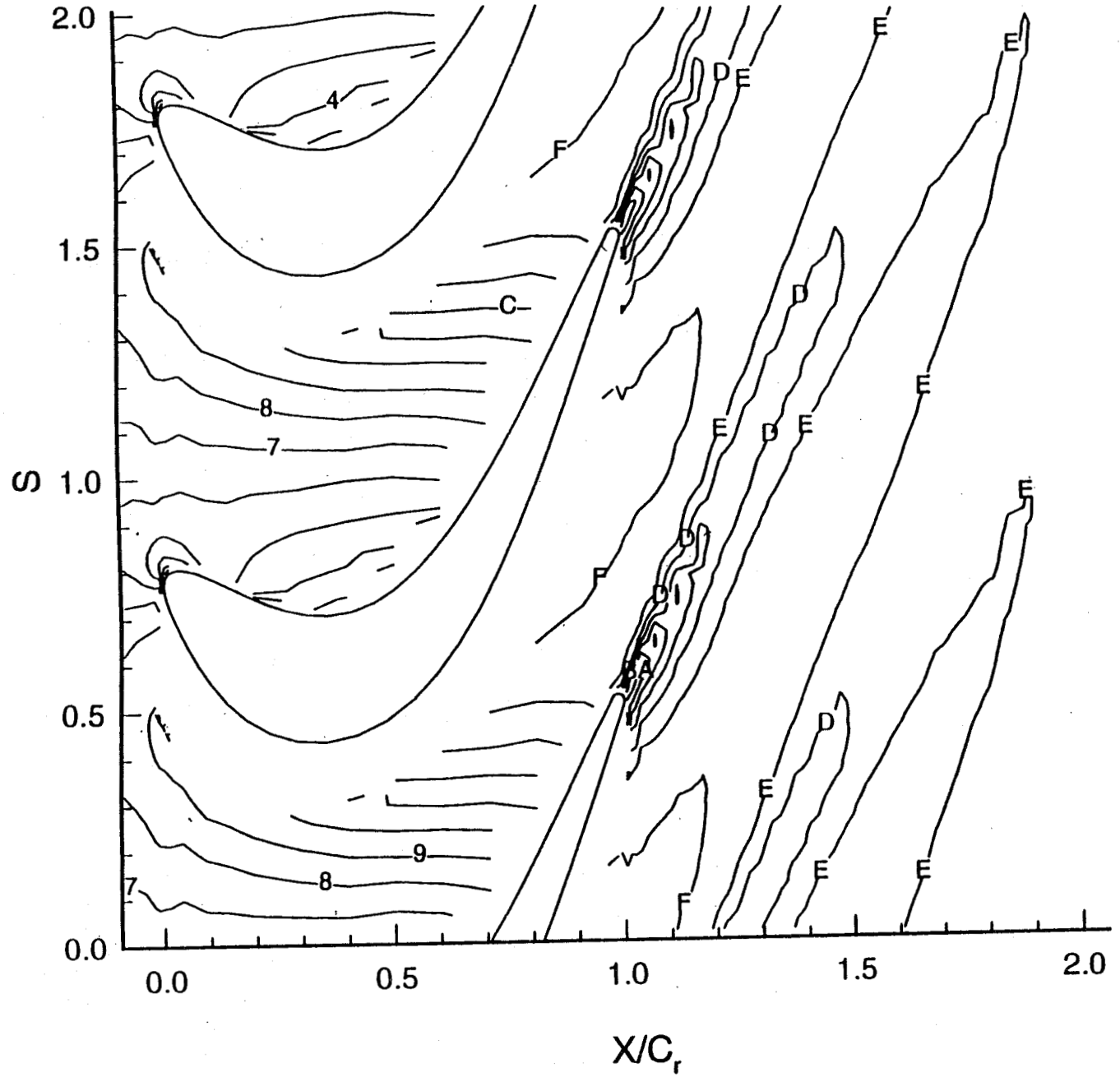

Level	W/U_m
F	1.558
E	1.455
D	1.351
C	1.247
B	1.143
A	1.039
9	0.935
8	0.831
7	0.727
6	0.623
5	0.519
4	0.416
3	0.312
2	0.208
1	0.104

Fig. Total velocity contour of PSU rotor midspan flowfield (Measurement at Penn State)

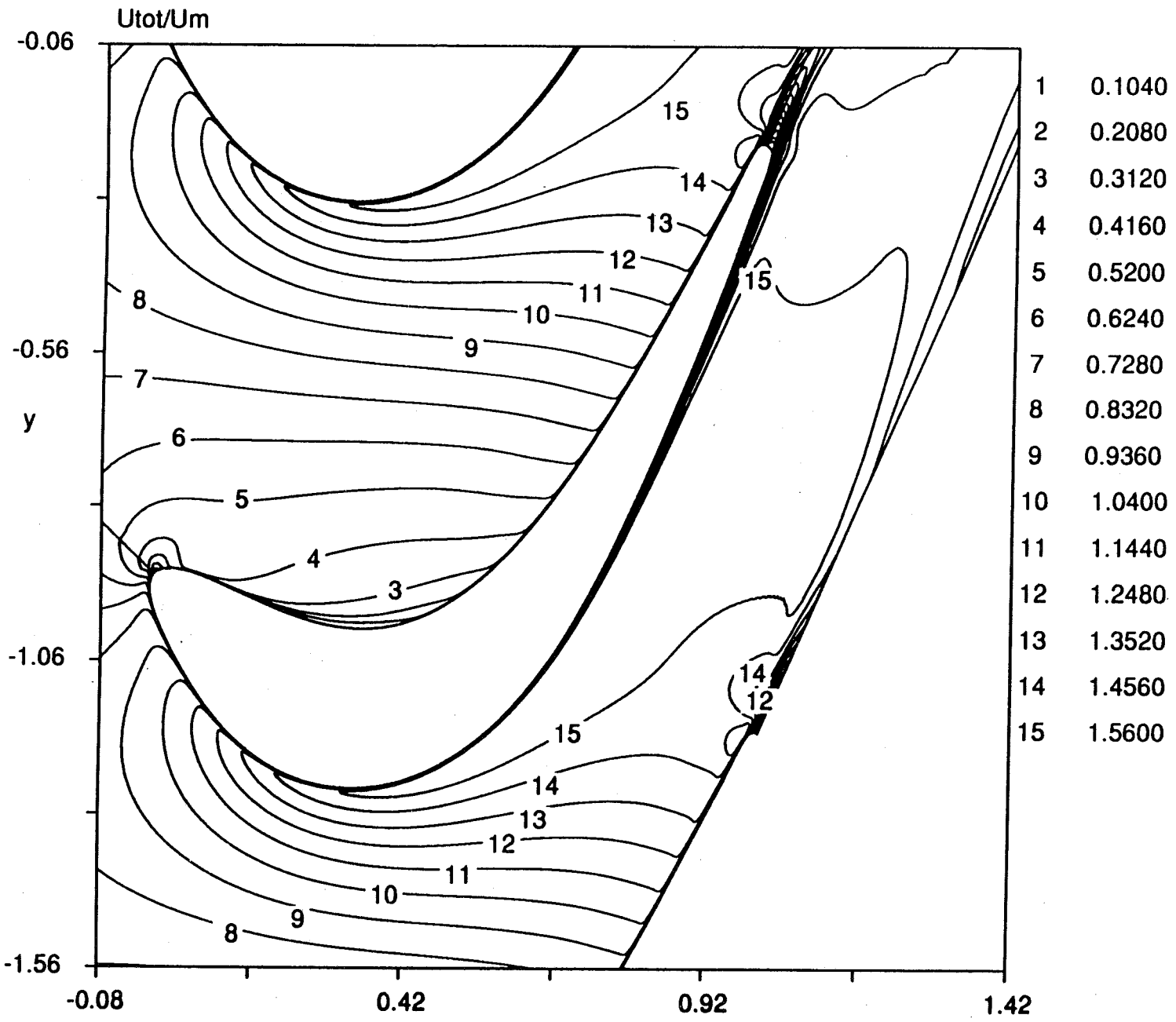

Fig. Total velocity contour of PSU rotor midspan flowfield (computation with k-ε/ARSM model)

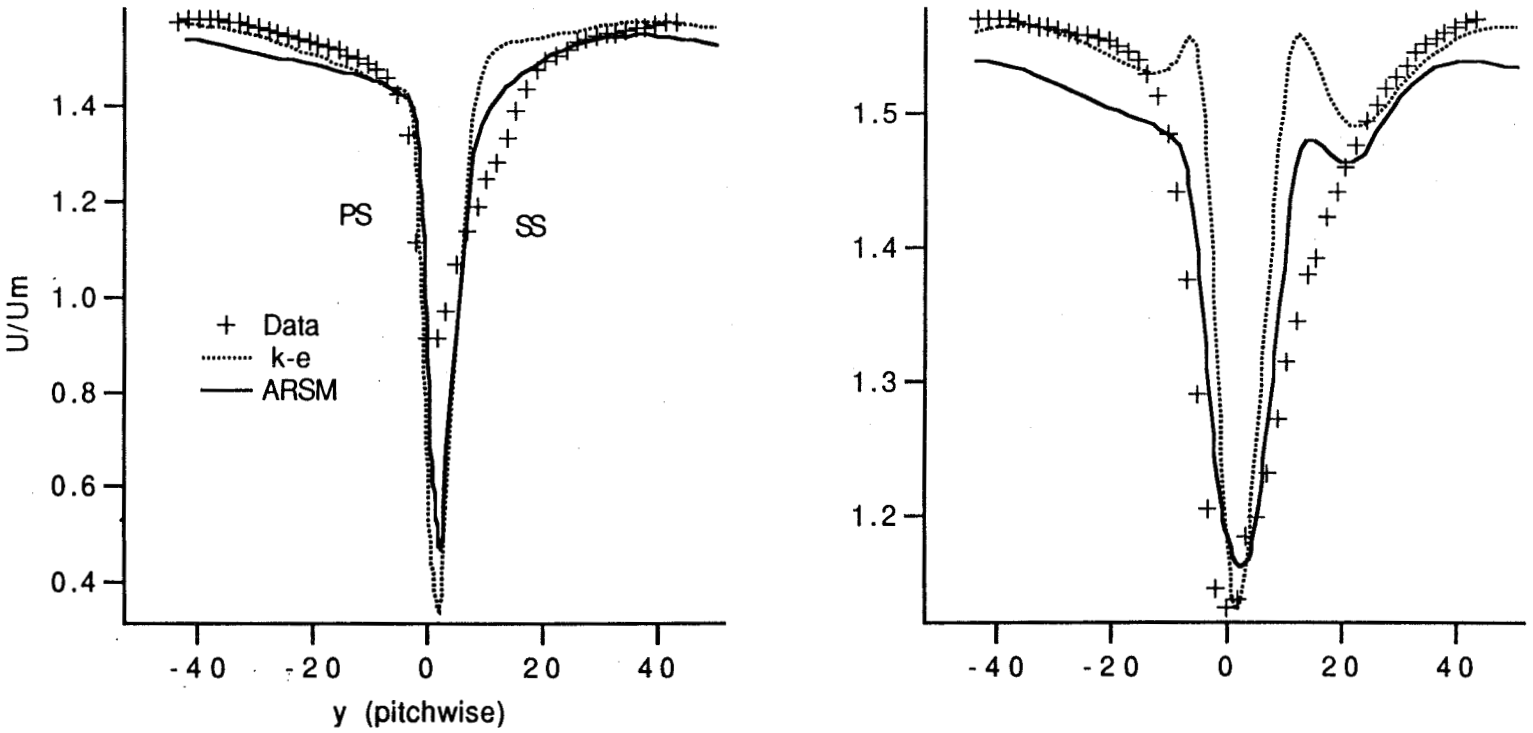

x/C=102% **x/C=112%**

Fig. Wake profile at midspan for PSU rotor flow

Cascade geometries of Mark II and C3X:

	Mark II	C3X
Stagger angle (deg)	63.69	59.89
Air exit angle (deg)	70.96	72.38
Pitch (cm)	12.97	11.77
True chord (cm)	13.62	14.49

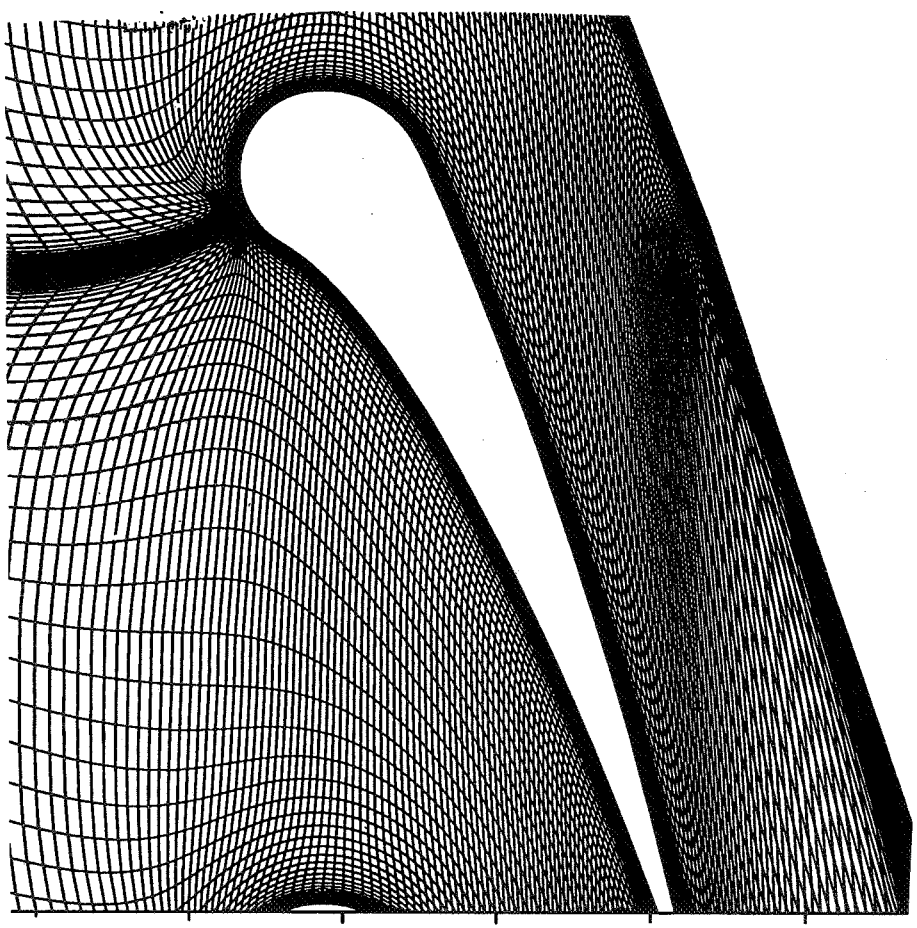

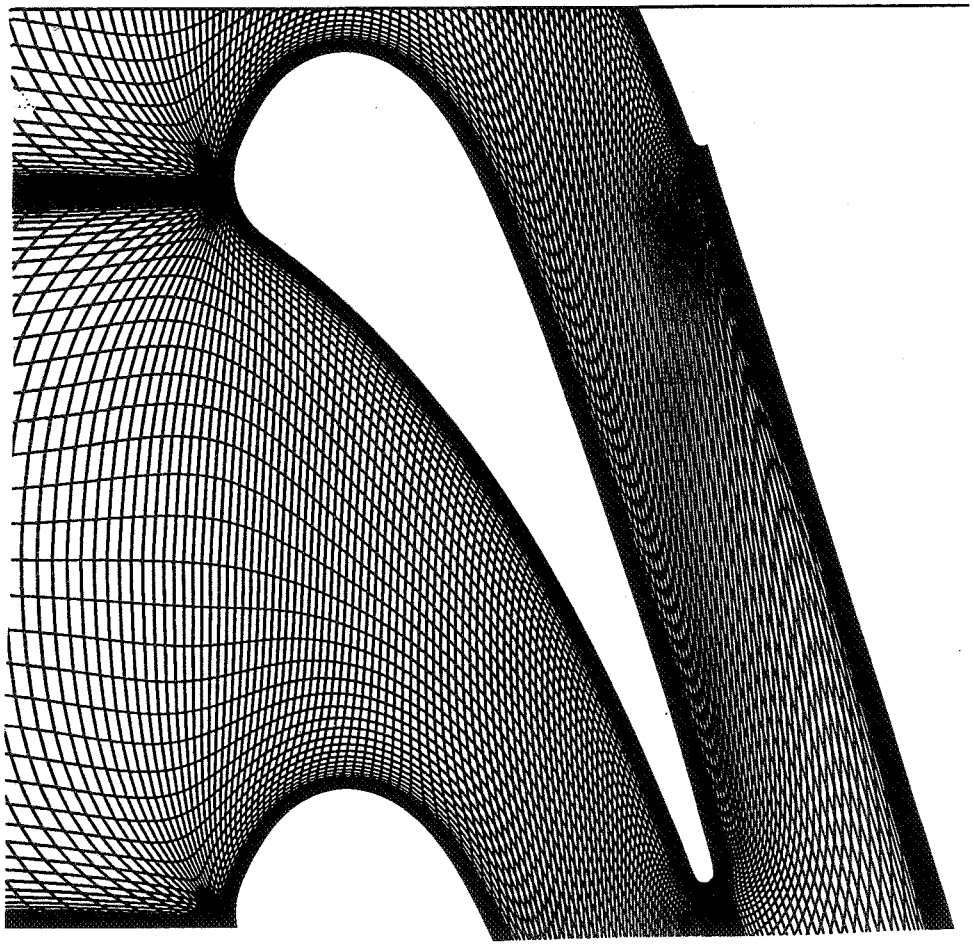

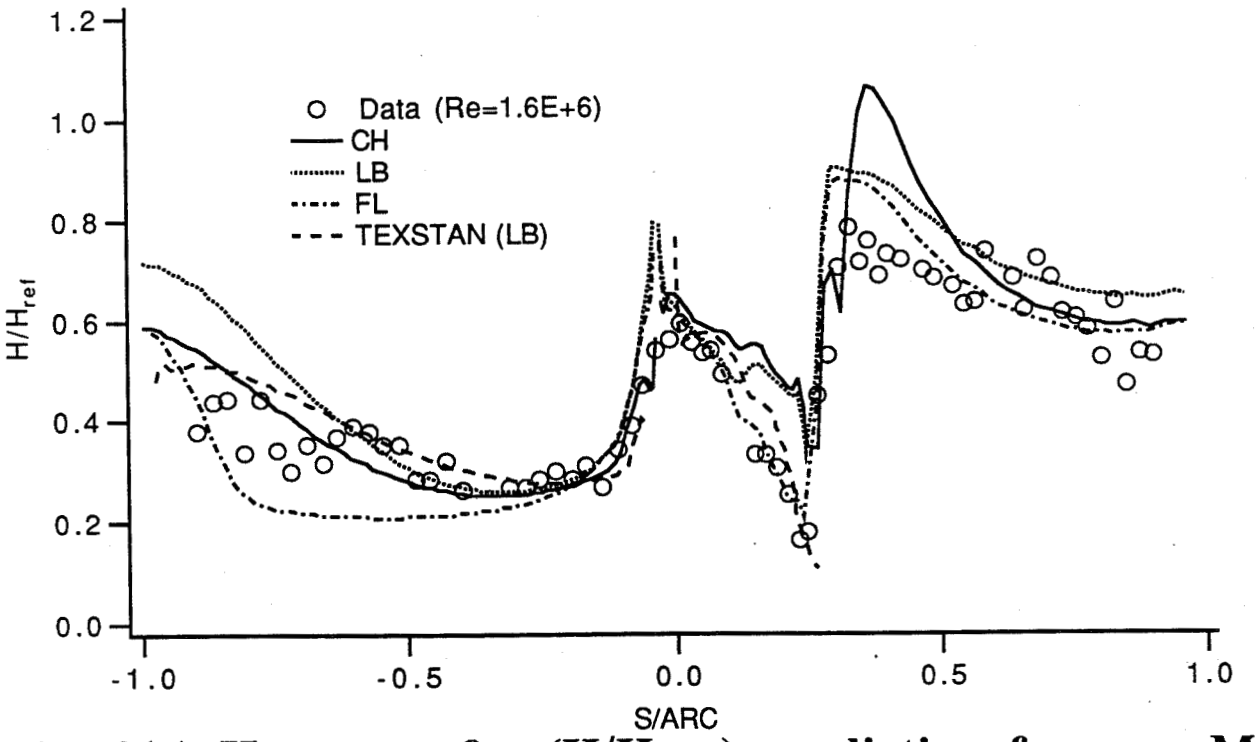

Fig. 3(a) Heat transfer (H/H_{ref}) prediction for case Mark15 (M_{is2}=0.90, Re_{is2}=1.6*10^6, Tu_∞=8.3%)

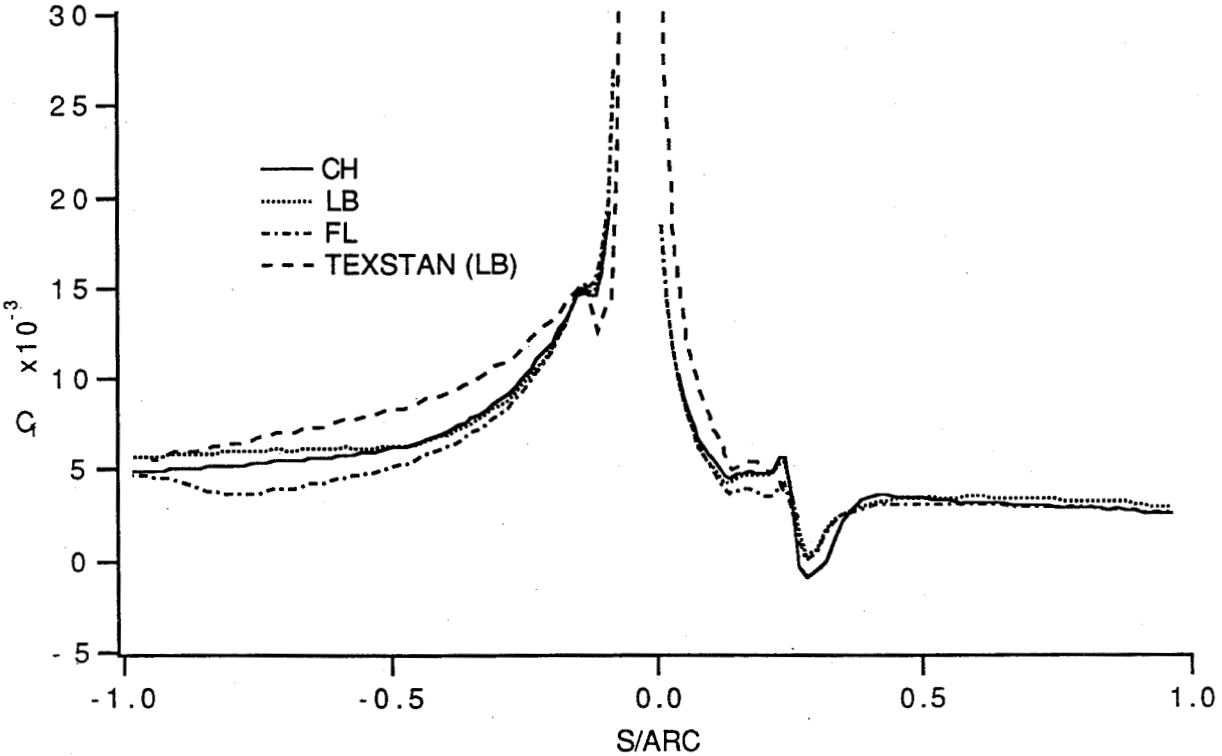

Fig. 3 (b) Skin friction (C_f)prediction for above case

Analysis of Heat Transfer for Mark II & C3X Turbine Nozzle Guide Vanes

with conditions (Re, Tu, T0, Tw) close to real engine conds.

- Preds. with engr. accuracy obtained by CH, LB, FL k-ε models
  - LB prediction appears to be the best
  - CH performs well in fully turbulent region,
    but tends to smear out transition process,
    also not good for separation-induced transition
  - FL yield delayed transitions for accelerating turbine flows

- Separated-flow transition lead to much sharper increase of heat transfer than the nominal by-pass transition

- With minimum smoothing and good LRN k-ε model,
  2-D N-S method provide good pred. of blade boundary layer development, transition & heat transfer under diff. Re, Tu, etc.

Future Efforts

- Turbulence modeling:
  - Investigation of combined effects of curvature & rotation on turbulent flowfield in 3-D rotor flows
  - Modeling the source term in ε-equation to capture strong concave curvature; couple this with RSM
  - Modeling the ε-eq. & turbulent diffusion to improve the prediction of recovery process after re-attachment
- Code Development:
  - Multigrid solution of Reynolds stress transport equations
  - Development & implementation of full 3-D non-reflecting B.C.
- Validation & Simulation:
  - Modeling strong concave curved TBL & duct flows
  - Navier-Stokes simulation of rotor flow with non-reflecting boundary conditions & advanced turbulence models

Optimization Methodology for Unconventional Rocket Nozzle Design

W. Follett
Rocketdyne Division, Rockwell International, Canoga Park, California

Abstract

Several current rocket engine concepts such as the bell-annular tripropellant engine, and the linear aerospike being proposed for the X-33, require unconventional three-dimensional rocket nozzles which must conform to rectangular or sector-shaped envelopes to meet integration constraints. These types of nozzles exist outside the current experience database, therefore, development of efficient design methods for these propulsion concepts is critical to the success of launch vehicle programs.

Several approaches for optimizing rocket nozzles, including streamline tracing techniques, and the coupling of CFD analysis to optimization algorithms are described. The relative strengths and weaknesses of four classes of optimization algorithms are discussed: Gradient based methods, genetic algorithms, simplex methods, and surface response methods. Additionally, a streamline tracing technique, which provides a very computationally efficient means of defining a three-dimensional contour, is discussed.

Gradient based schemes generally rely on a gradient evaluation at the current design point to determine the search direction required for objective function minimization with either constrained or unconstrained design variables. This type of technique is good at rapidly achieving an optimum if the objective function is well behaved. However, it can easily be trapped in local optima or by constraints in a region far from the optimal design.

Genetic algorithms are adaptive search procedures based on the biological concept of evolution. They start with an initial set, or population, of design points and use the genetic operators of selection, crossover and mutation to converge on an optimal design. Since this method searches from a set of designs rather than a single design, it can uncover different "families" of good designs.

Surface response methods utilize a limited number of runs to construct a model of the design space. This model is then used to determine an optimal design. Examples of such methods include Taguchi, neural networks, and regression models. If accurate models of the design space can be constructed, these methods become very attractive for problems where function evaluations are computationally expensive.

Streamline tracing provides a rapid means of determining a nozzle design which exhibits good performance but has an arbitrary exit shape. By using an axisymmetric optimum or ideal nozzle as a baseline, a shape can be inscribed onto the exit plane of the nozzle and numerous streamlines may be traced back to the plenum. These streamlines may then be used to define a nozzle contour, which will exhibit the same inviscid flow characteristics as the nozzle from which it was traced.

The performance of the various optimization methods on thrust optimization problems for tripropellant and aerospike concepts is assessed and recommendations are made for future development efforts.

OPTIMIZATION METHODOLOGY FOR UNCONVENTIONAL ROCKET NOZZLE DESIGN

W. Follett

Rocketdyne Division - Rockwell International

Computational Fluid Dynamics Branch
Fluid Dynamics Division
Structures and Dynamics Laboratory
Science and Engineering Directorate
Marshall Space Flight Center

13th Workshop for CFD
Applications in Rocket Propulsion
Huntsville, Alabama
April 25-28, 1995

Rockwell Aerospace
Rocketdyne

CFD Technology Center

OPTIMIZATION METHODOLOGY FOR UNCONVENTIONAL ROCKET NOZZLE DESIGN

- **WHY OPTIMIZATION?**
  - EFFICIENT AERO DESIGN TOOLS CURRENTLY EXIST FOR 2-D AND AXISYMMETRIC NOZZLES
    - CURRENT ROCKET ENGINE CONCEPTS CAN BENEFIT FROM 3-D NOZZLE DESIGNS
    - A POWERFUL DESIGN TOOL IS BEING CREATED BY COUPLING CFD TO OPTIMIZATION METHODS
- **CHARACTERISTICS OF THRUST OPTIMIZATION PROBLEM:**
  - RELATIVELY LITTLE ROOM FOR IMPROVEMENT (<3%) - NEED ACCURATE FLOWSOLVER
  - MULTIPLE OPTIMA
  - ROUGHNESS

OPTIMIZATION PROBLEMS

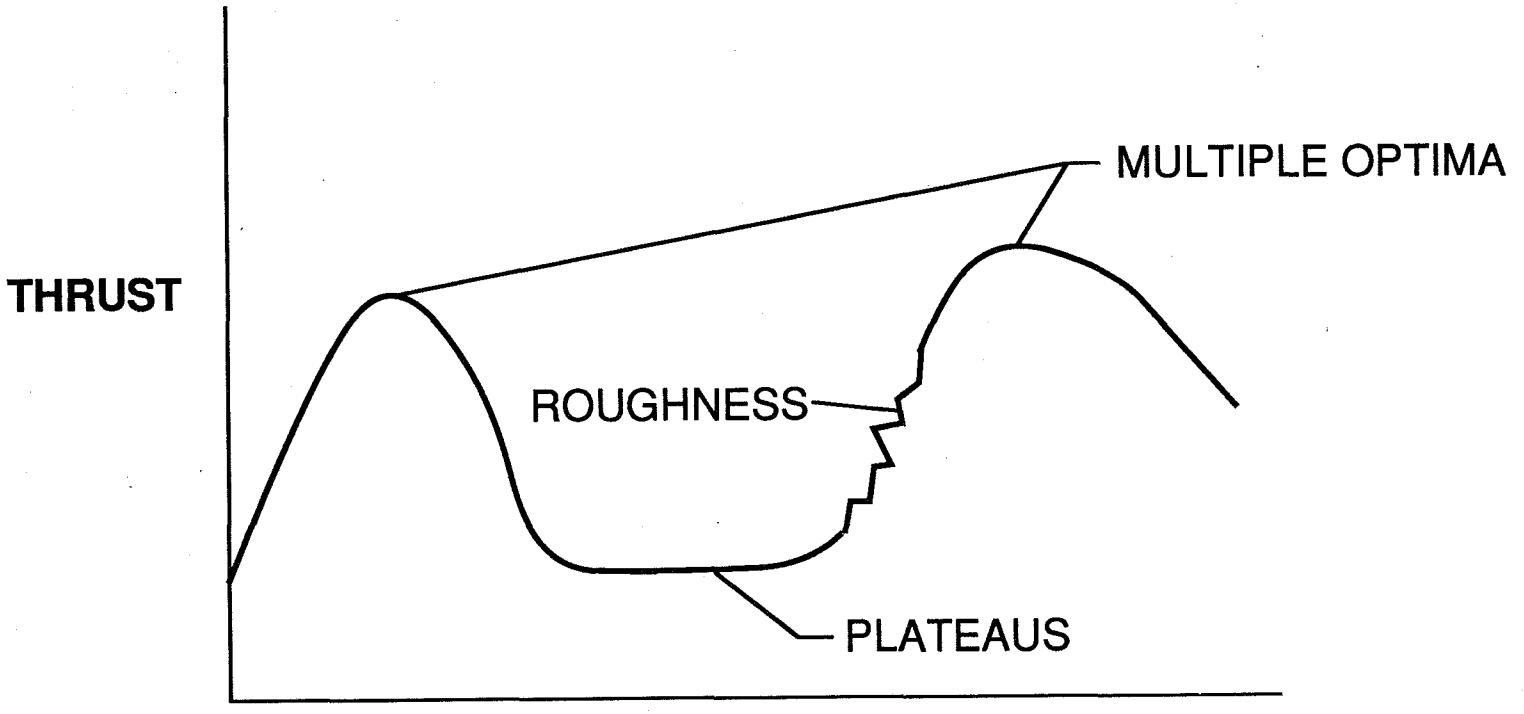

THRUST OPTIMIZATION METHODOLOGY

- **OBJECTIVE**
  - EVALUATE EFFECTIVENESS OF VARIOUS OPTIMIZATION ALGORITHMS WHEN APPLIED TO THRUST PROBLEM
    - GRADIENT BASED METHODS
    - GENETIC ALGORITHMS
    - SIMPLEX METHOD
    - SURFACE RESPONSE METHODS
    - STREAMLINE TRACING

OPTIMIZATION METHODOLOGY DESCRIPTION

- **GRADIENT BASED METHODS**
  - PERTURB EACH DESIGN VARIABLE SLIGHTLY TO GENERATE FINITE DIFFERENCE GRADIENT
  - PROS - RAPID SOLUTION FOR SMOOTH FUNCTIONS
  - CONS - MAY GET TRAPPED IN LOCAL OPTIMA
    - DOES NOT HANDLE ROUGHNESS WELL
- **GENETIC ALGORITHMS**
  - UTILIZE GENETIC OPERATORS OF MUTATION, CROSSOVER, & SELECTION TO EVOLVE TOWARDS OPTIMUM DESIGN
  - PROS - ROBUST METHOD GOOD AT FINDING GLOBAL OPTIMUM AMIDST LOCAL OPTIMA
    - HANDLES ROUGHNESS WELL
    - CAN FIND "FAMILIES" OF GOOD DESIGNS
  - CONS - COMPUTATIONALLY EXPENSIVE

OPTIMIZATION METHODOLOGY DESCRIPTION

- **SIMPLEX METHOD**
  - CONSTRUCT SIMPLEX FROM N+1 POINTS
  - EVALUATE ALL POINTS - MOVE WORST ONE TO OPPOSITE SIDE
  - IF NEW POINT IS STILL WORST, SHRINK SIMPLEX

  - PROS - CAN HANDLE ROUGHNESS
  - CONS - MAY GET TRAPPED IN LOCAL OPTIMA
    - SLOW ON SMOOTH FUNCTIONS
    - NOT NATURALLY PARALLEL

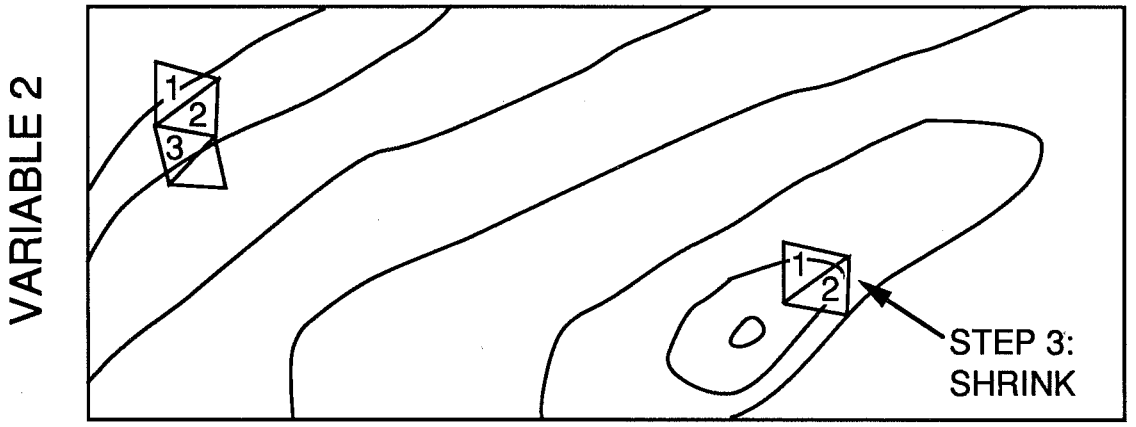

OPTIMIZATION METHODOLOGY DESCRIPTION

- **SURFACE RESONSE METHODS**
  - TAGUCHI METHODS
    - ORTHOGANAL ARRAYS ASSUME GLOBAL LINEARITY
      - EFFECT OF A + EFFECT OF B = EFFECT OF A+B
  - NEURAL NETS
    - GOOD FOR MODELING NONLINEAR RESPONSES
  - REGRESSION MODELS - FIRST ORDER, SECOND ORDER
  - PROS - SIMULATES DESIGN SPACE WITH SMALL NUMBER OF CFD EVALUATIONS
    - CAN FILTER OUT ROUGHNESS
  - CONS - MODEL MAY NOT ACCURATELY SIMULATE DESIGN SPACE

COUPLING CFD TO OPTIMIZATION ALGORITHMS IN THE REAL WORLD

- **CFD AUTOMATION**
  - GRID GENERATION
  - CONVERGENCE CHECKING
  - FLEXIBLE SOLUTION STRATEGY
- **PARALLEL PROCESSING**
  - MOST OPTIMIZATION SCHEMES ARE NATURALLY PARALLEL
  - DISTRIBUTED HETEROGENEOUS ENVIRONMENT
  - FAULT TOLERANCE
- **COPING WITH CODE CRASHES**
  - ASSIGNING PERFORMANCE LEVEL
  - SWITCH OPTIMIZATION ALGORITHMS

COMPARISON OF OPTIMIZATION METHODS FOR NOZZLE DESIGN APPLICATIONS

		GRADIENT BASED	GENETIC ALGORITHM	SIMPLEX	TAGUCHI
ROBUSTNESS	ROUGH SURFACE	-	+	+	+
	HANDLE CODE CRASHES	-	+	+	0
	NONLINEAR VARIABLE INTERACTIONS	0	+	+	-
EFFECT-IVENESS	FINDS GLOBAL OPTIMUM	-	+	-	0
	CAN FIND ALTERNATE OPTIMA	-	+	-	+
EFFICIENCY	EFFICENCY / SPEED IN ROUGH	-	0	+	+
	EFFICIENCY / SPEED ON SMOOTH FCN'S.	+	-	-	0

- NO ALGORITHM IS PERFECT, ALL HAVE STRENGTHS AND WEAKNESSES
- AN INTELLIGENT HYBRID COULD TAKE ADVANTAGE OF THE BEST ASPECTS OF EACH TECHNIQUE

3-D THRUST CELL OPTIMIZATION

- **OBJECTIVE**
  - MAXIMIZE: $\frac{\text{THRUST(THRUSTER ONLY)}}{\text{SYSTEM WEIGHT}}$
  - MINIMIZE PEAK HEAT LOAD
- **OPTIMIZATION METHODS**
  - TAGUCHI L32 & L64 MATRICES
  - GENETIC ALGORITHM
  - 15-21 DESIGN VARIABLES
- **3-D MOC EVALUATIONS**
  - 460 FOR TAGUCHI
  - 1000 FOR GENETIC
- **IMPROVEMENT OVER BASELINE**
  - 4.6% IN THRUST / WEIGHT

Thrust Cell Taguchi Optimum
Mach Number Contours

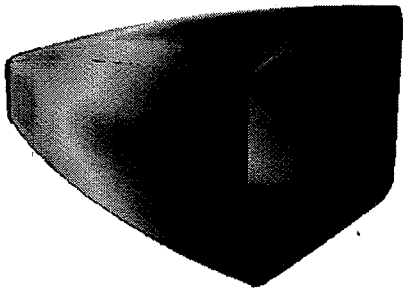

Mach Number Minimum = 1.0
Mach Number Maximum = 4.0

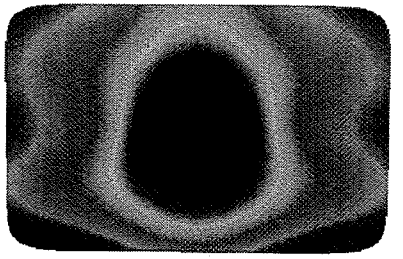

Mach Number Minimum = 3.0
Mach Number Maximum = 4.0

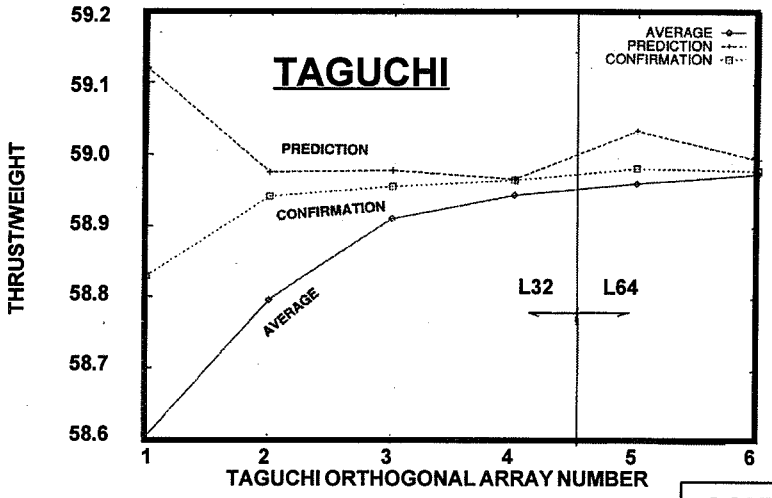

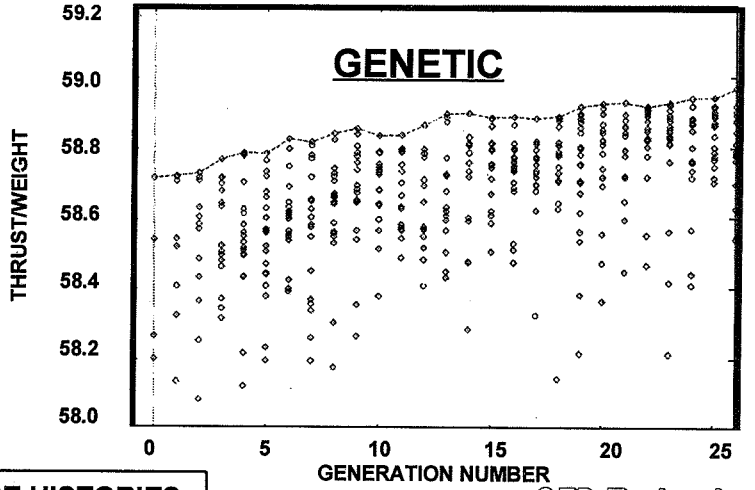

CONVERGENCE HISTORIES

Rockwell Aerospace
Rocketdyne

CFD Technology Center

OPTIMIZATION METHODOLOGY FOR UNCONVENTIONAL ROCKET NOZZLE DESIGN

CONCLUSIONS

- **THRUST OPTIMIZATION IS DIFFICULT DUE TO MULTIPLE LOCAL OPTIMA AND ROUGHNESS OF THE OBJECTIVE FUNCTION**
  - GRADIENT BASE METHODS HAVE PROVEN INEFFECTIVE
  - SIMPLEX METHODS ARE MEDIOCRE
  - GENETIC ALGORITHMS ARE ROBUST, BUT COSTLY
  - SURFACE RESPONSE METHODS CAN DRASTICALLY REDUCE NUMBER OF CFD RUNS REQUIRED, BUT ONLY IF MODEL IS ACCURATE
- **NO SINGLE SCHEME IS A "MAGIC BULLET"**
  - CURRENTLY INVESTIGATING FILTERING METHODS FOR GRADIENT BASED METHODS, INTELLIGENT HYBRID SCHEMES
- **MULTI-DISCIPLINARY OPTIMIZATION IS ESSENTIAL**

Combustor Modeling Under GOX-Rich Conditions

Manish Deshpande, Doug Schwer, Hsin-Hua Tsuei
S. Venkateswaran, Charles L. Merkle

Propulsion Engineering Research Center
Department of Mechanical Engineering
Penn State University

CFD Workshop on Applications in Rocket Propulsion
NASA MSFC
April 26, 1995

PENNSTATE

Motivation

- OX-Rich Conditions Characteristic of Rocket Engine Preburners.
- CFD can Serve as a Valuable Design Tool. Integrate into Design Process.
- Enables Analysis/Study of Important Physical Phenomena in Combustion Process (e.g. Flame Holding)
- GOX Analyses Form Validation Step for Eventual LOX Calculations.

Objective

- GOAL : Computational Analysis of GOX/H Combustion over range of O/F Ratios.
- Understand Combustion Characteristics at High O/F Ratios.
- Validate with Experimental Data and Develop Predictive Capability.
- Approach :
  - Premixed Laminar Flames
  - Shear Layers
  - Unielement injector

Numerical Formulation

$$\Gamma \frac{\partial Q_v}{\partial \tau} + \frac{\partial E_v}{\partial x} + \frac{\partial F_v}{\partial y} = H + L(Q_v)$$

$$Q_v = (p, u, v, T, k, \varepsilon, w, Y_1, ..., Y_N)$$

- **Navier Stokes + k-ε + Species**
- **Density-based, Preconditioned, Time-Marching**
- **Uniform Convergence**
  - **All Mach Numbers**
  - **All Reynolds Numbers**
  - **All Aspect Ratios**

Numerical Formulation

- Implicit ADI Solution Technique.
- Central Difference/ Upwind Capability.
- k-e Equations : Chien Low-Reynolds Model used.
- Chemistry Model : 9 Species/18 Reactions.
- Parallel Implementation.

Results

- Laminar Flame Speed Calculations.
- Reacting Shear Layer Validation.
- Shear Layer Calculations : O/F Ratio Variation, Flame Holding
- Unielement Injector Validation.
- Unielement Injector : O/F Ratio Variation
- Effect of Swirl

Premixed Laminar Flames

- Objective
  - Important in Many Combustion Devices
  - Provides Means of Validating Chemical Mechanisms
- Research Goals
  - One-dimensional Adiabatic Flames
    - Complex Chemistry
    - Diffusion Effects
  - CFD-Premixed Flame Code Comparisons
    - Validate CFD Model
    - Extend Studies to Include Other Effects
- H2/O2 Combustion under Oxygen Rich Conditions

Premixed laminar flame characteristics
Hydrogen/oxygen flames

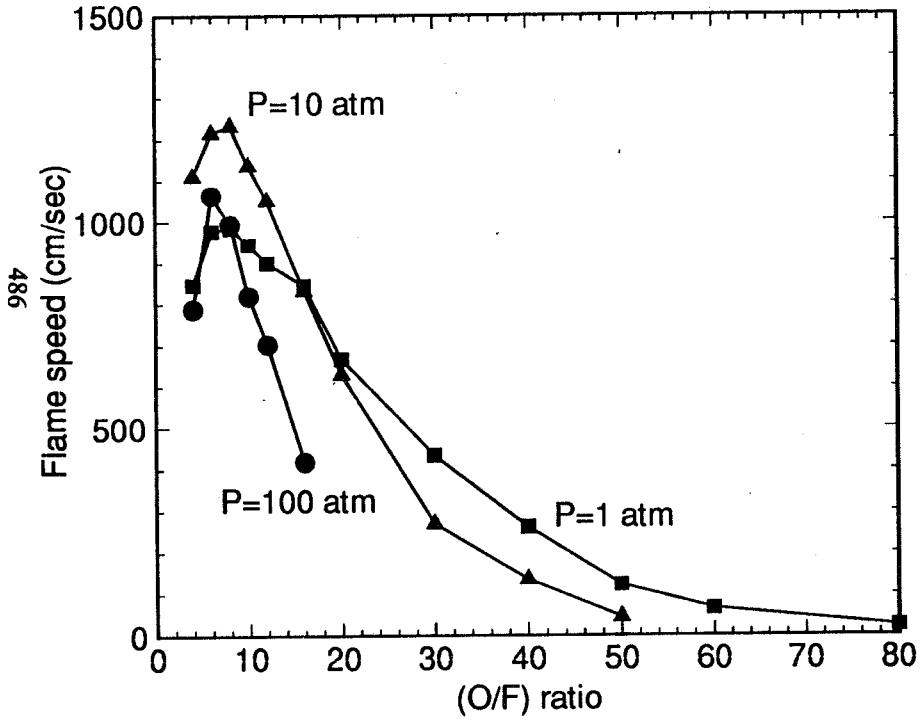

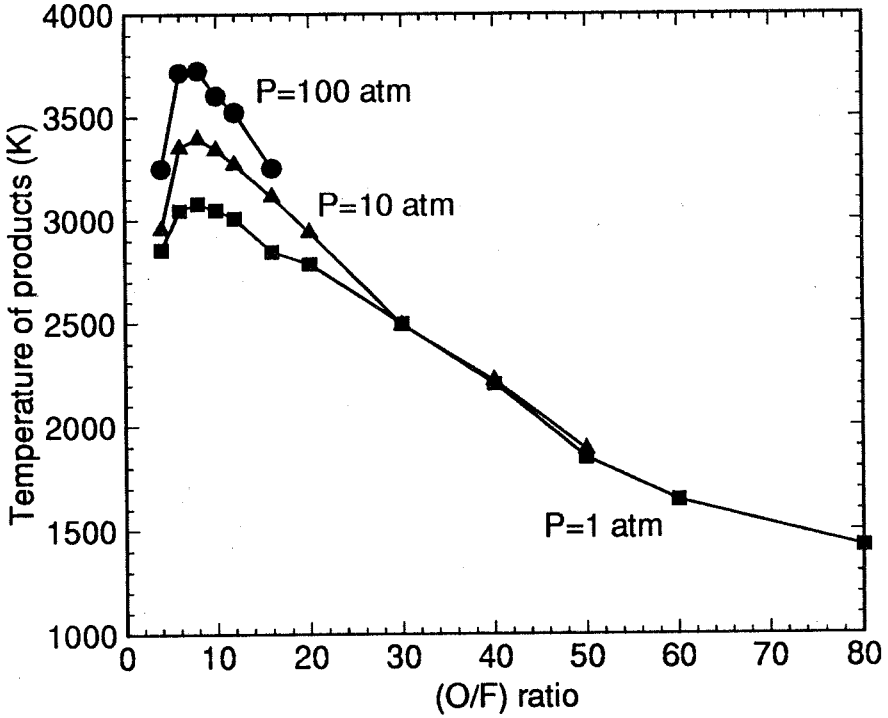

Reacting Planar Shear Layer

Schematic and Mesh

Reacting Configuration

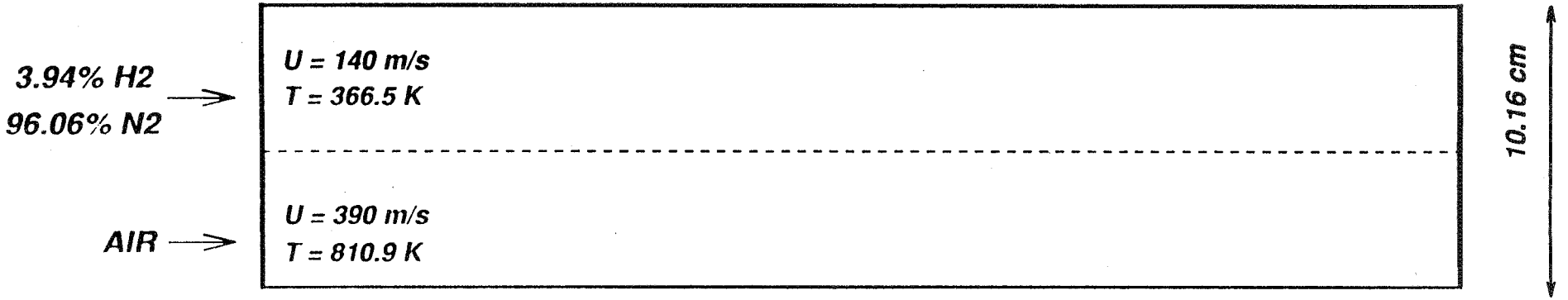

Ignition Source : 1.3% H2, 21%O2, 77.7% N2, T=1250 K -0.1 < y < 0

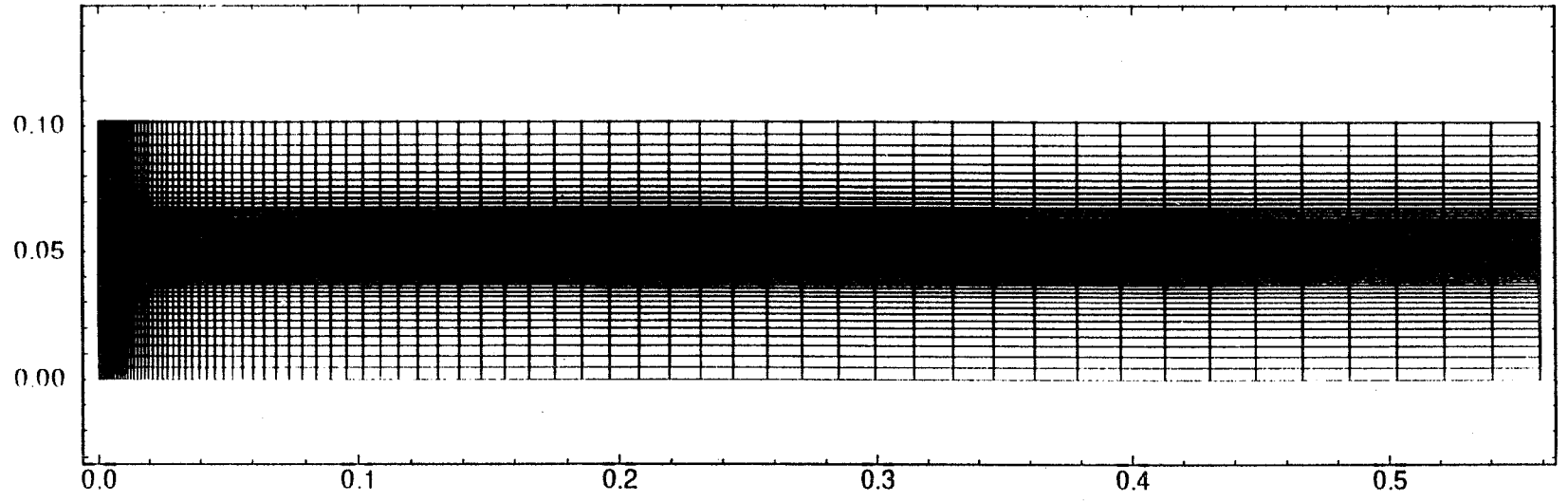

Reacting Planar Shear Layer

Velocity and Tke Contours

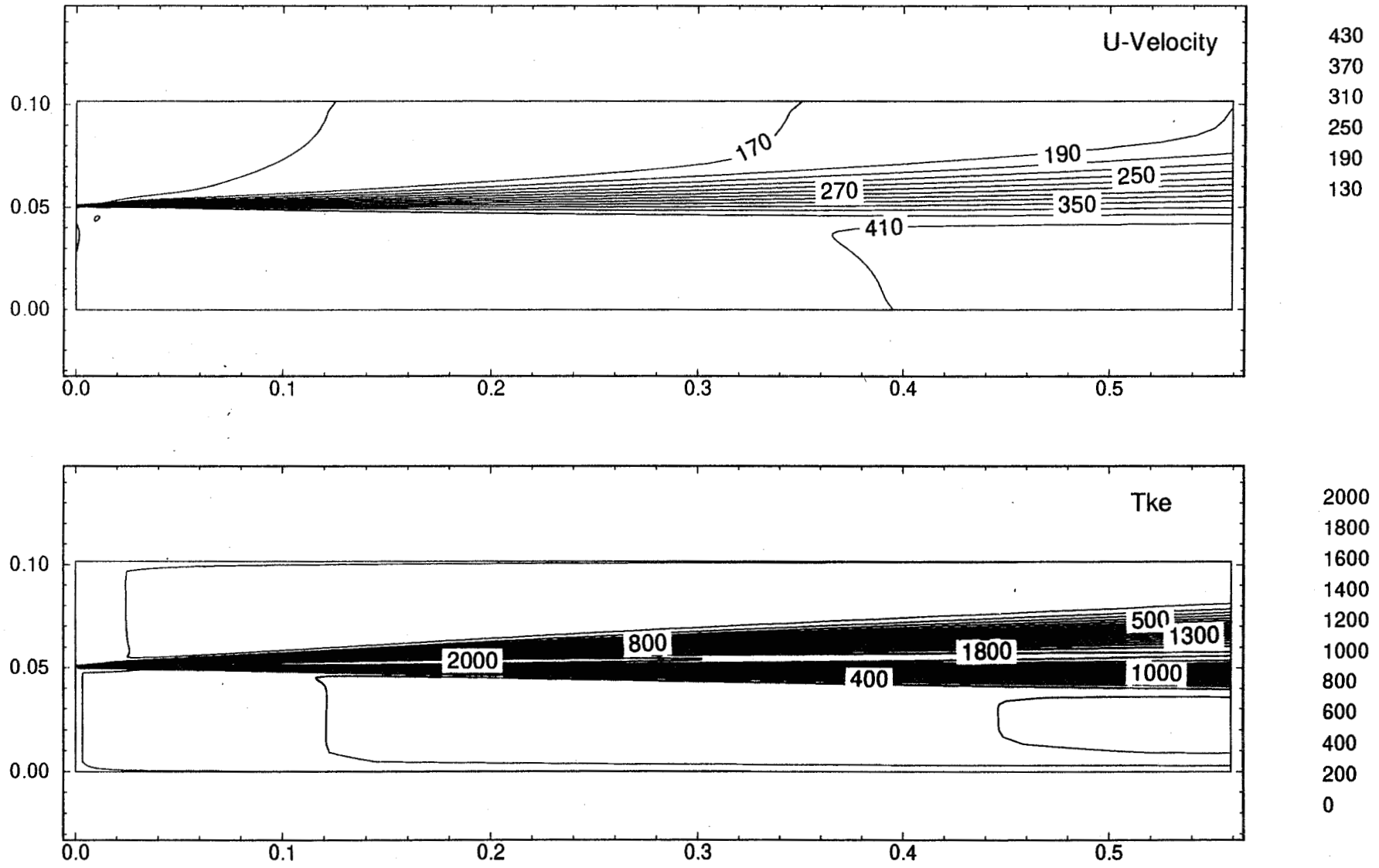

Reacting Planar Shear Layer

Temperature and OH contours

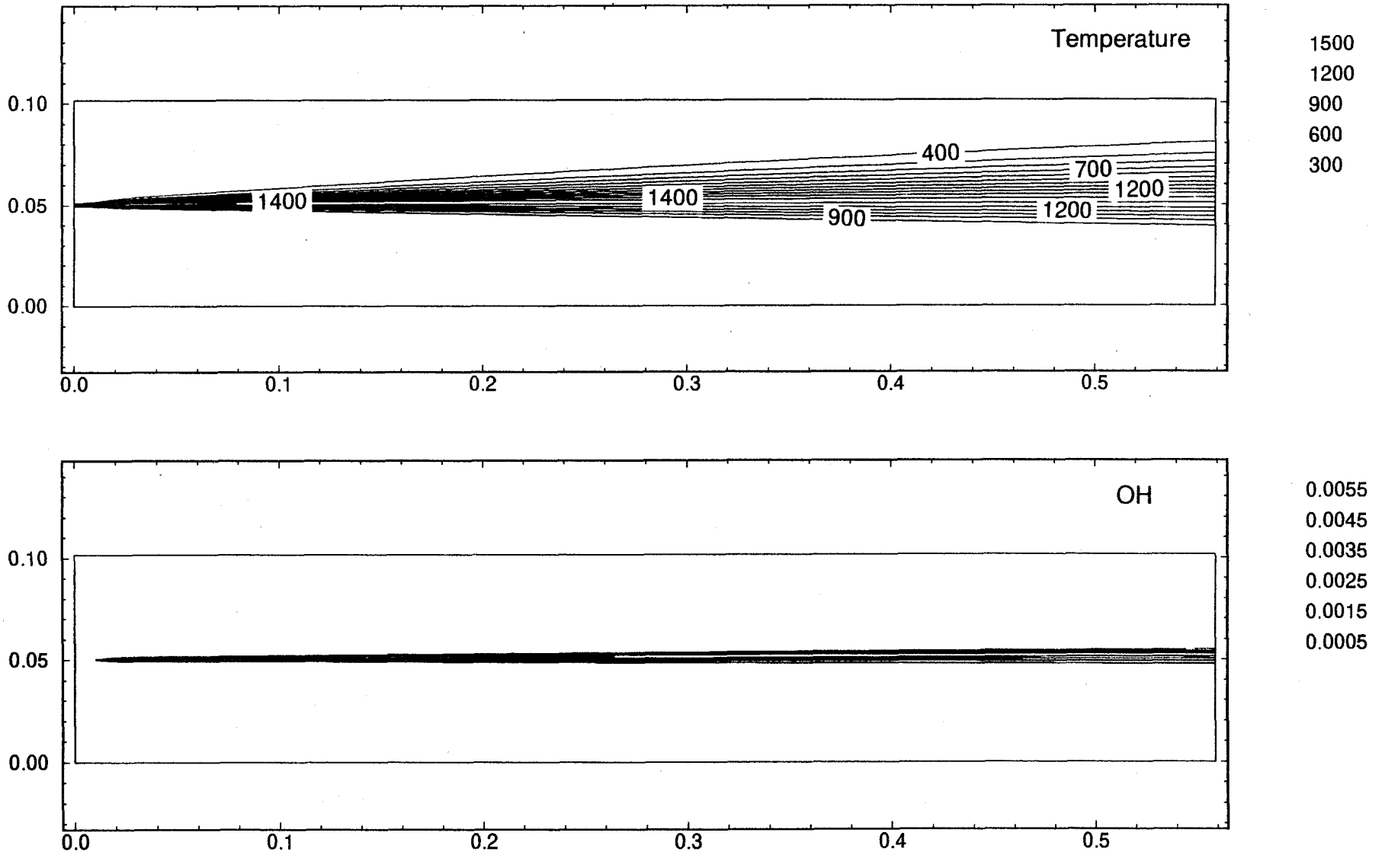

Reacting Planar Shear Layer

Velocity Profiles, Comparison with Experiment

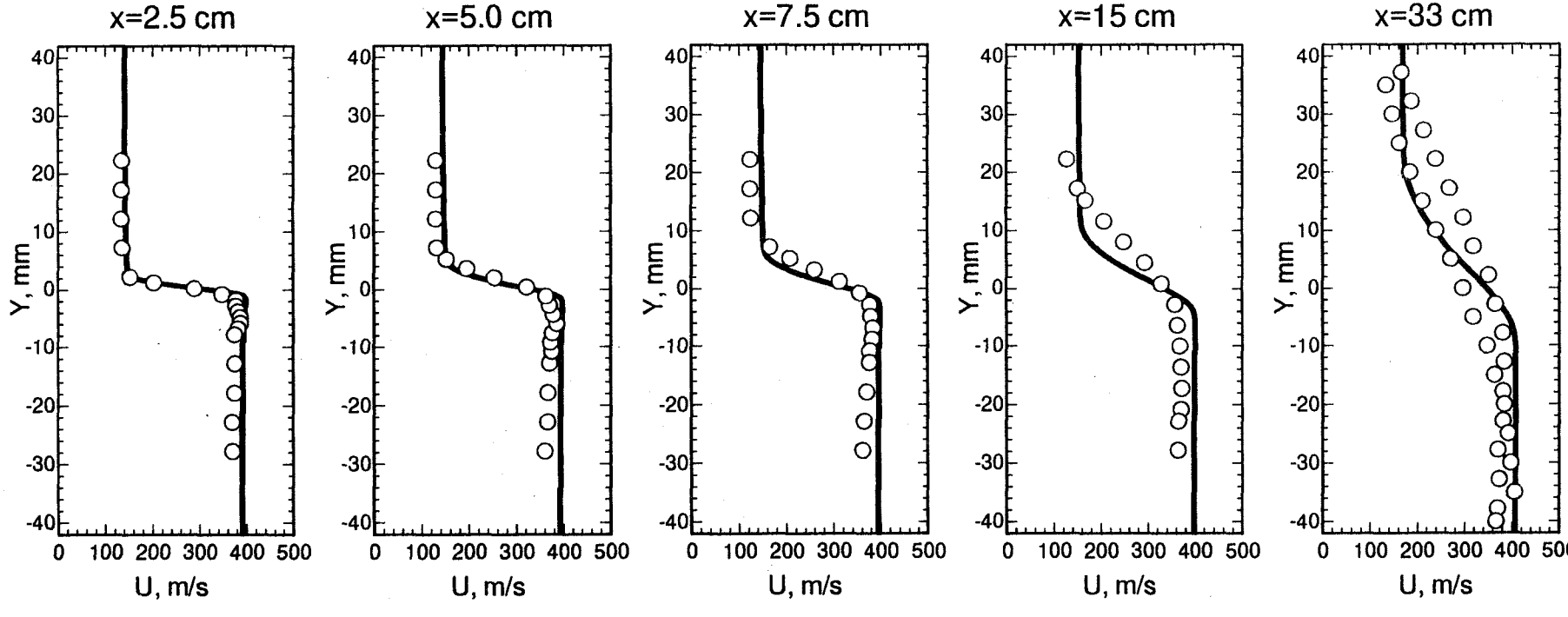

Reacting Planar Shear Layer

Tke Profiles, Comparison with Experiment

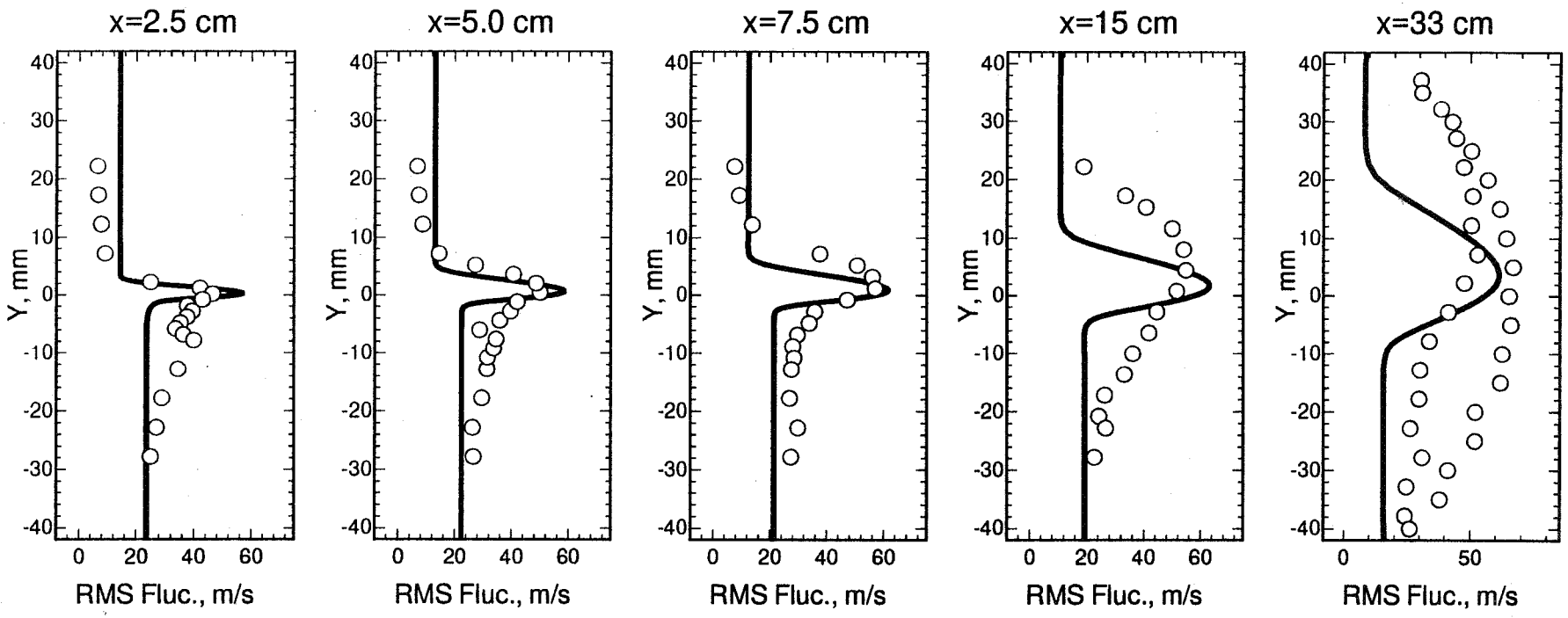

Reacting Planar Shear Layer

Temperature Profiles

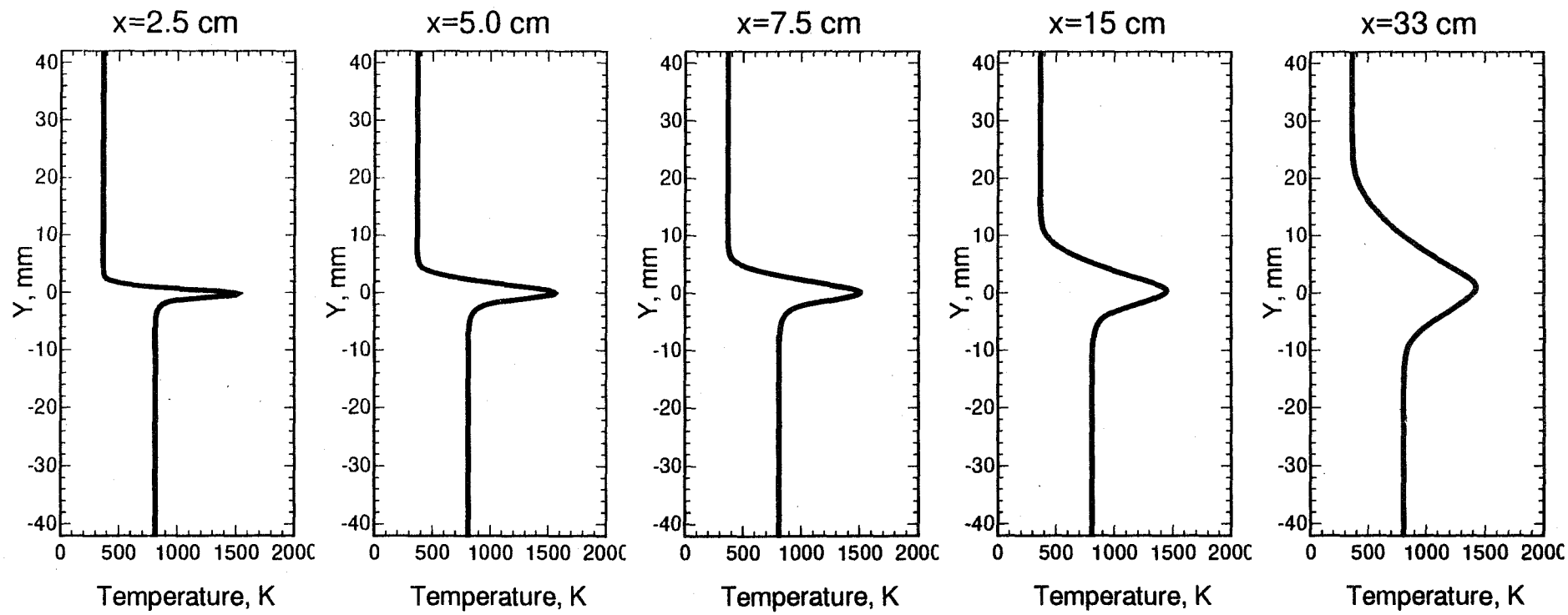

Reacting Shear Layer - O/F Ratio Variation

Schematic and Mesh

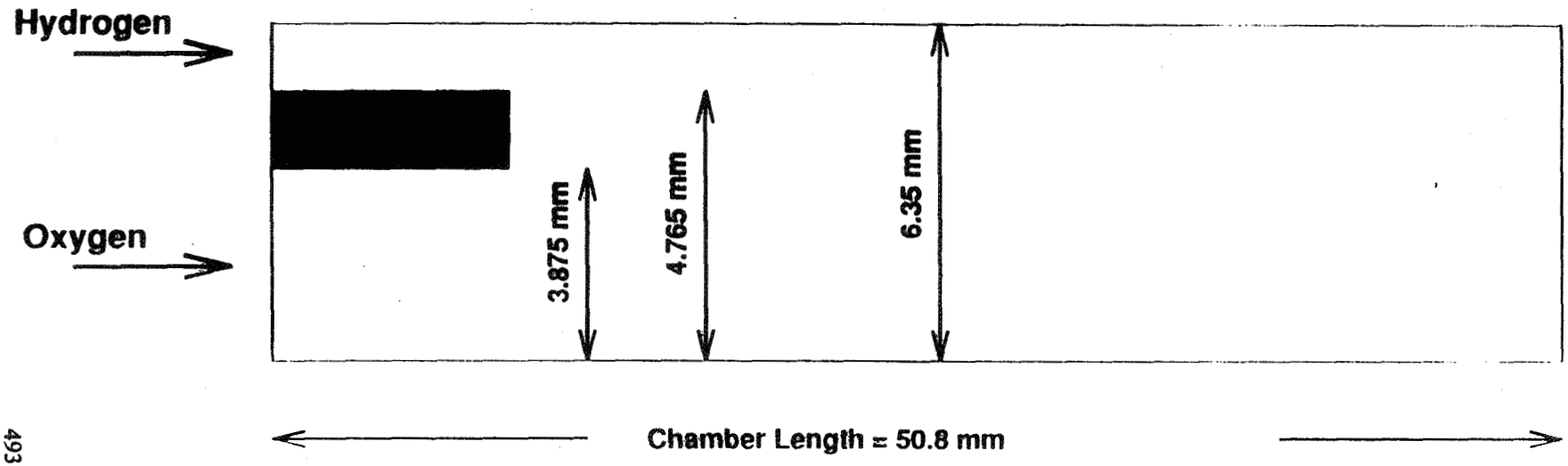

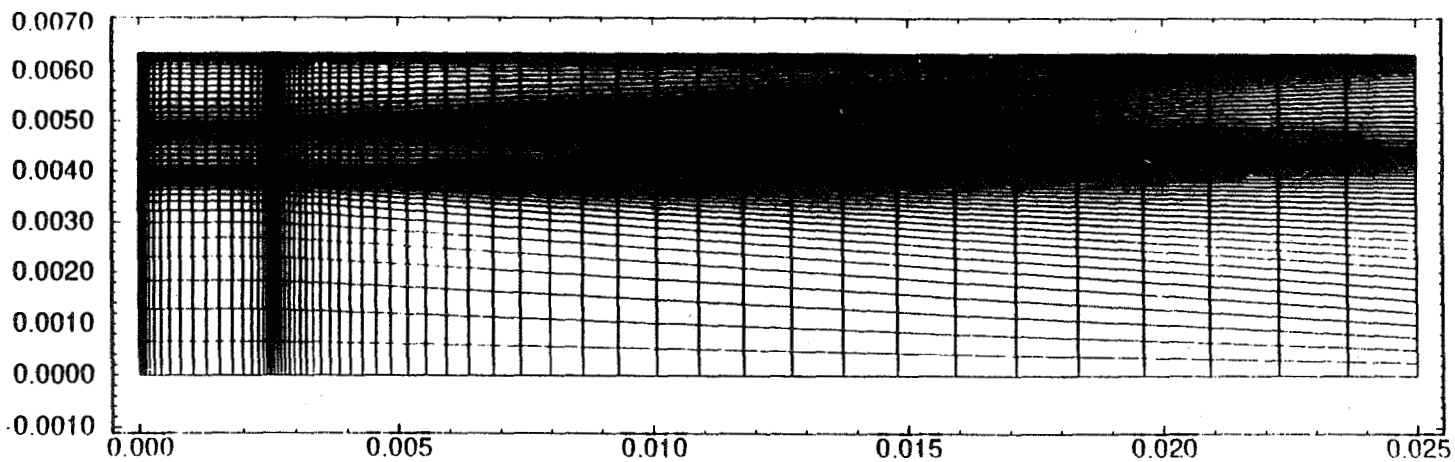

Reacting Shear Layer - O/F Ratio Variation

Velocity and Tke Contours

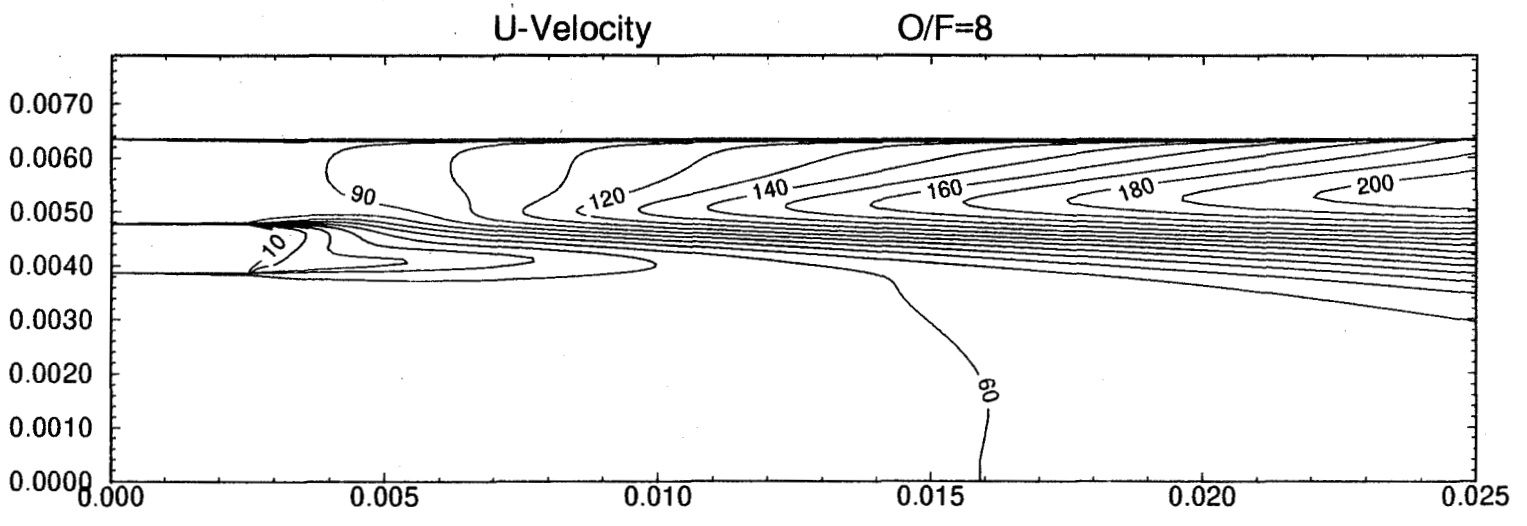

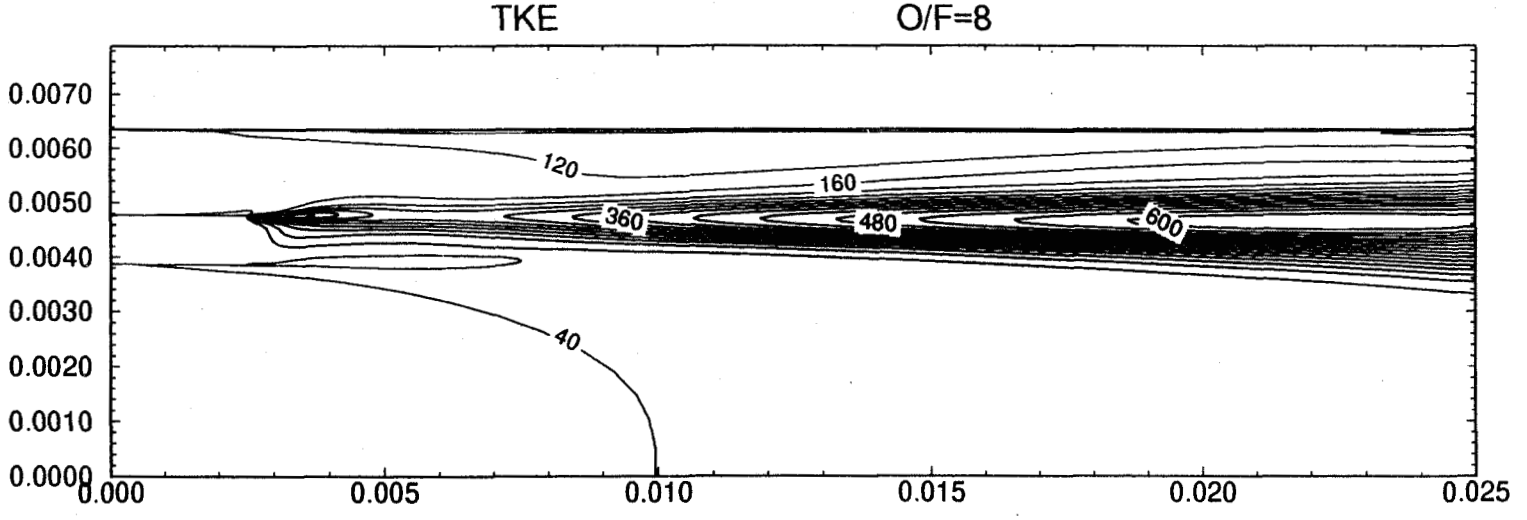

Reacting Shear Layer - O/F Ratio Variation

Temperature and OH Contours

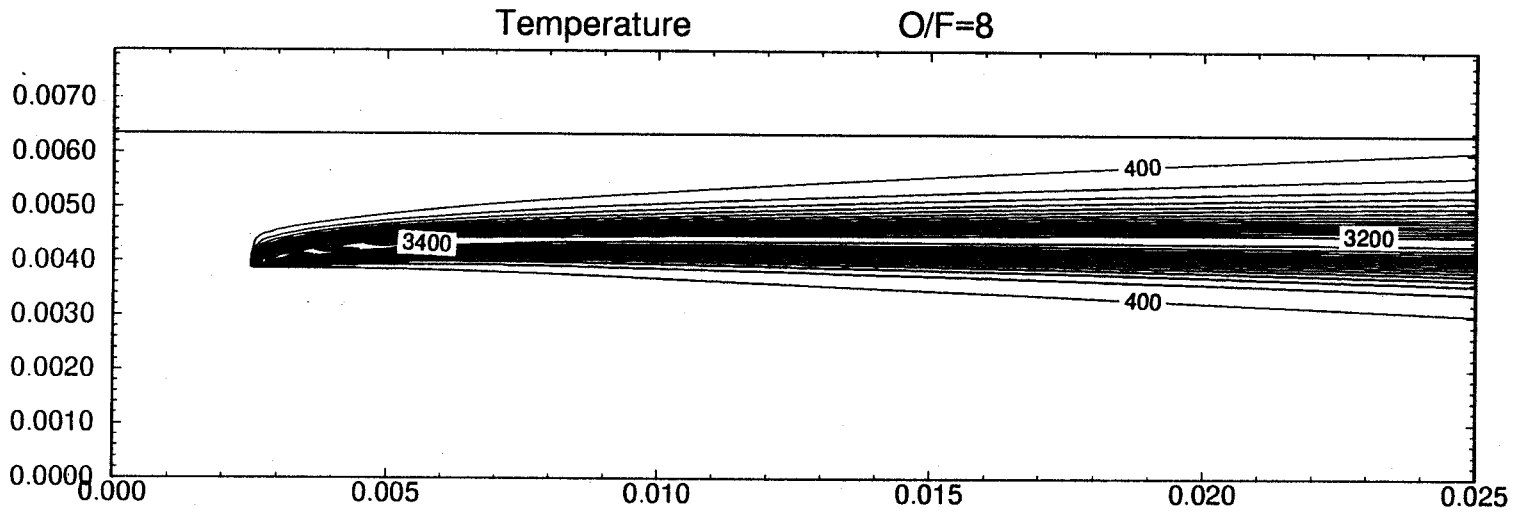

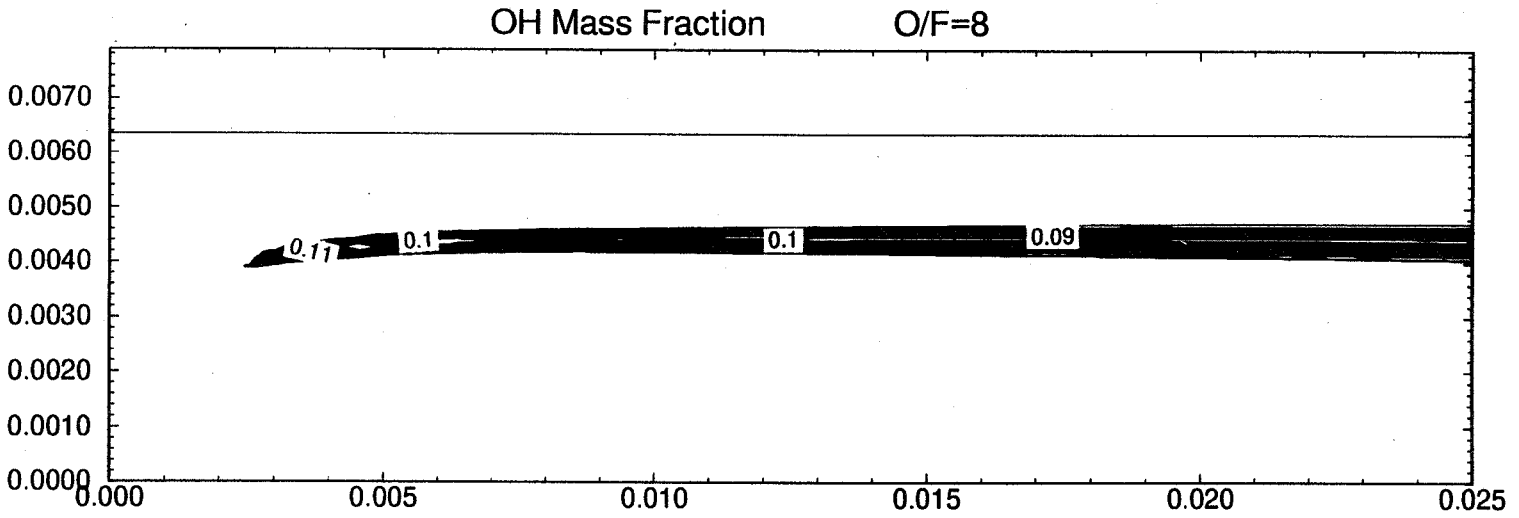

Turbulent Reacting Shear Layer

Temperature

O/F=4

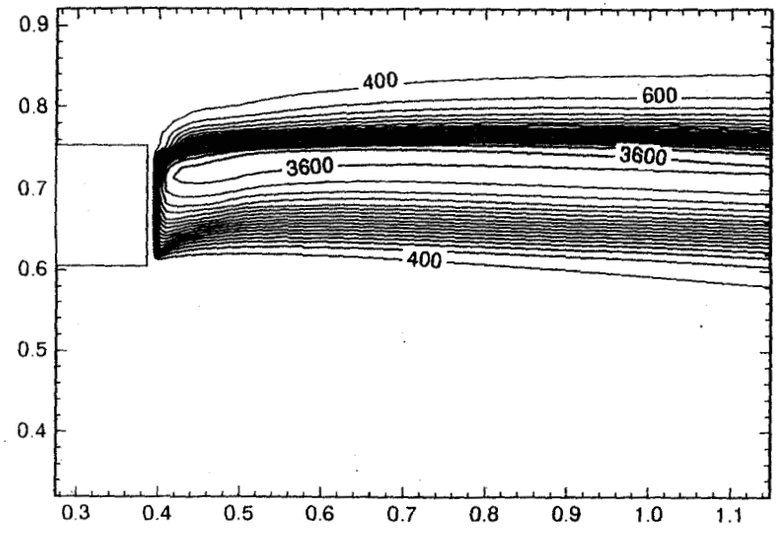

O/F=8

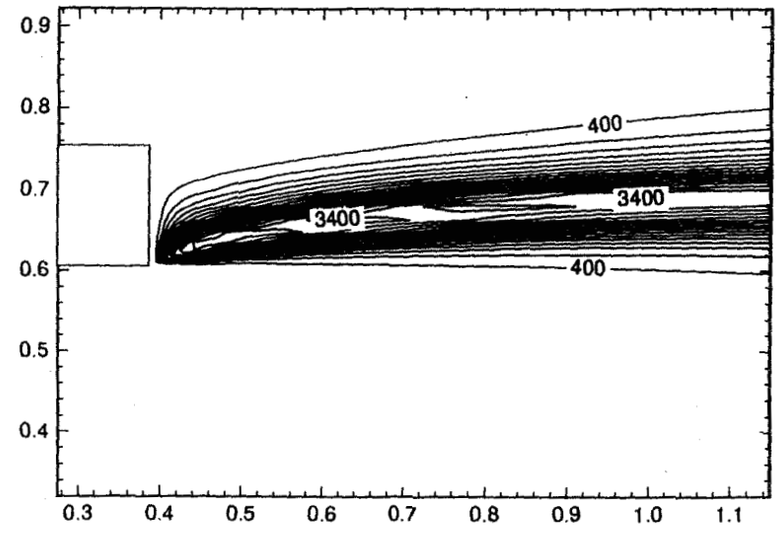

O/F=16

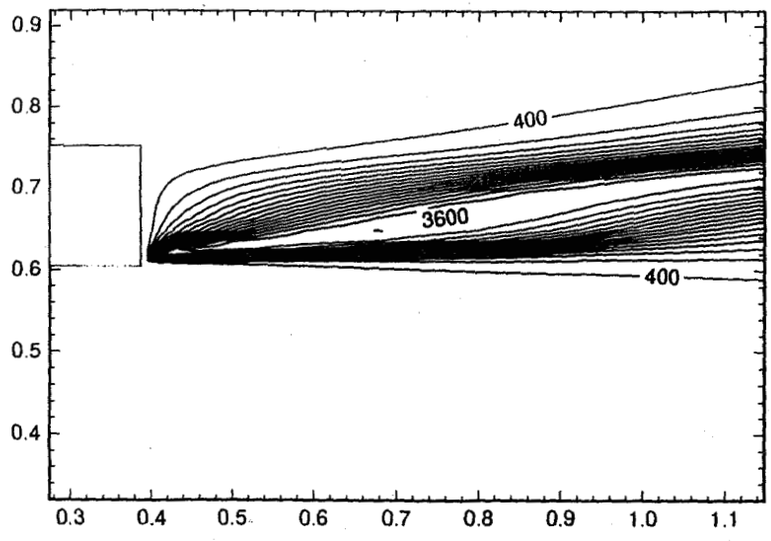

O/F=100

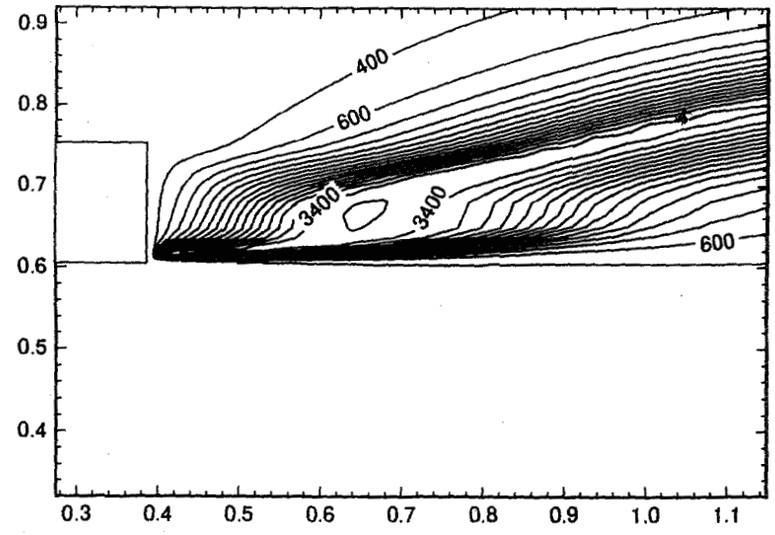

Shear Layer - O/F Ratio Variation

Radial Temperature Profiles

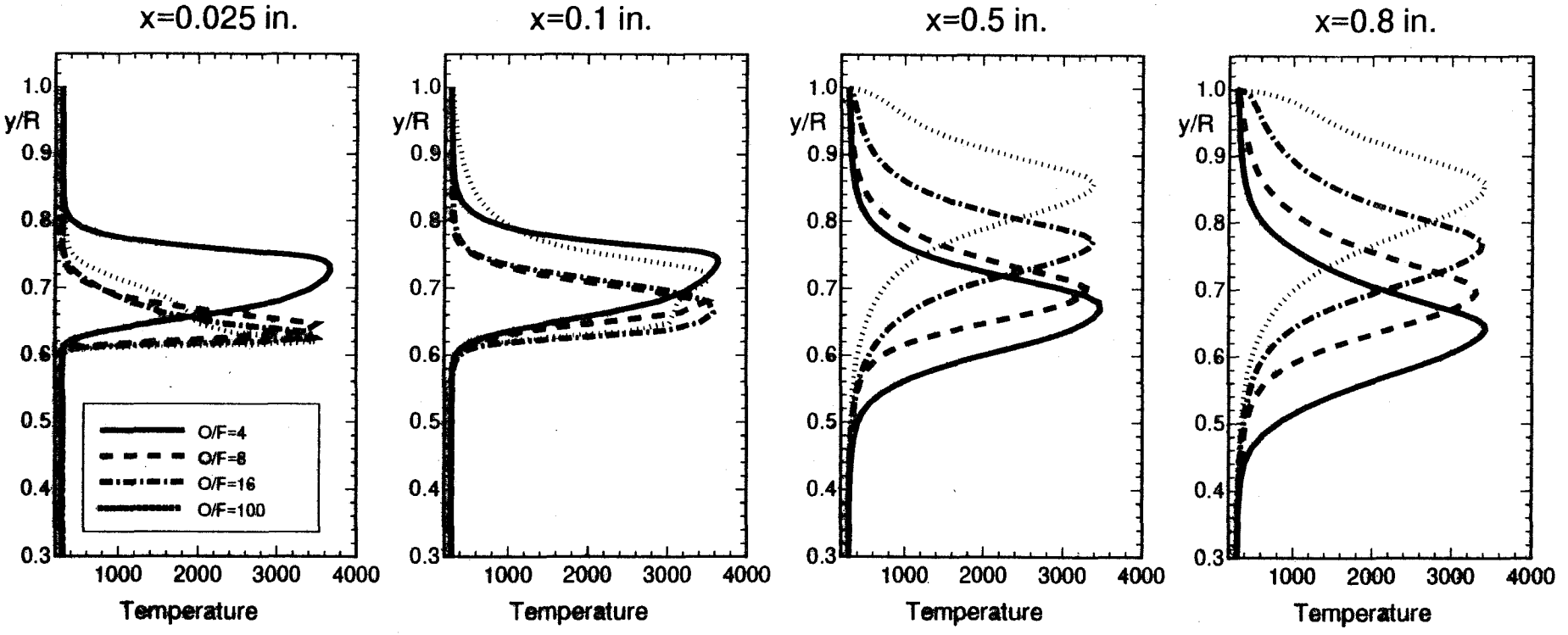

Turbulent Reacting Shear Layer

H_2O Mass Fraction

O/F=4

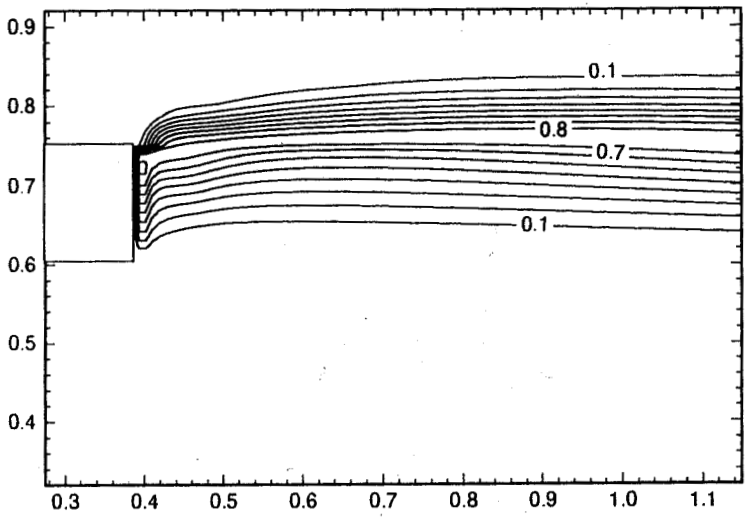

O/F=8

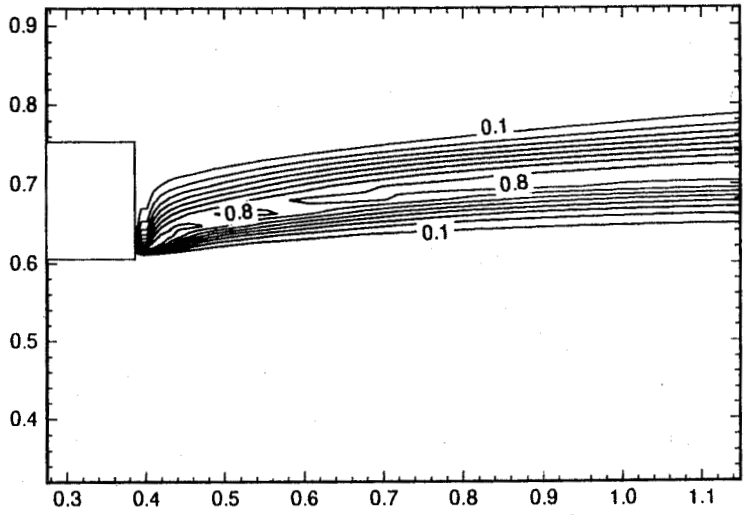

O/F=16

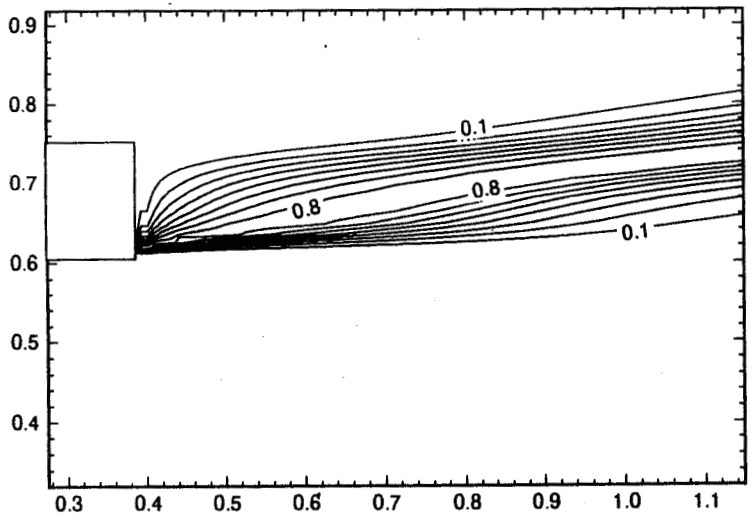

O/F=100

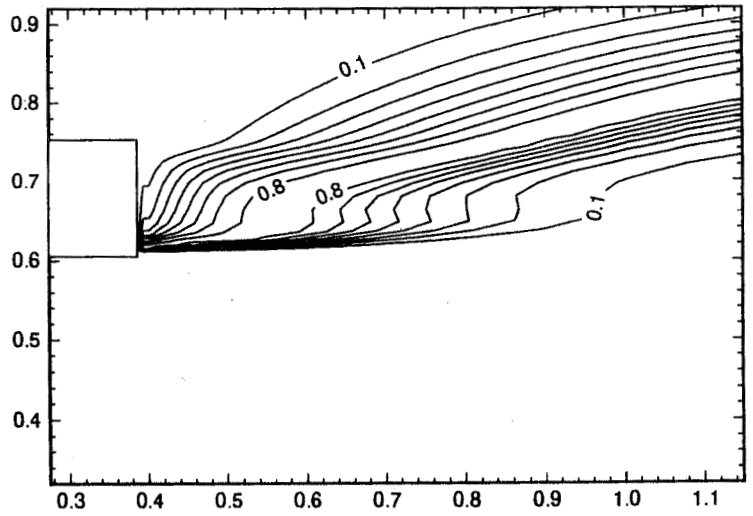

Shear Layer - O/F Ratio Variation

H_2O Mass Fraction Profiles

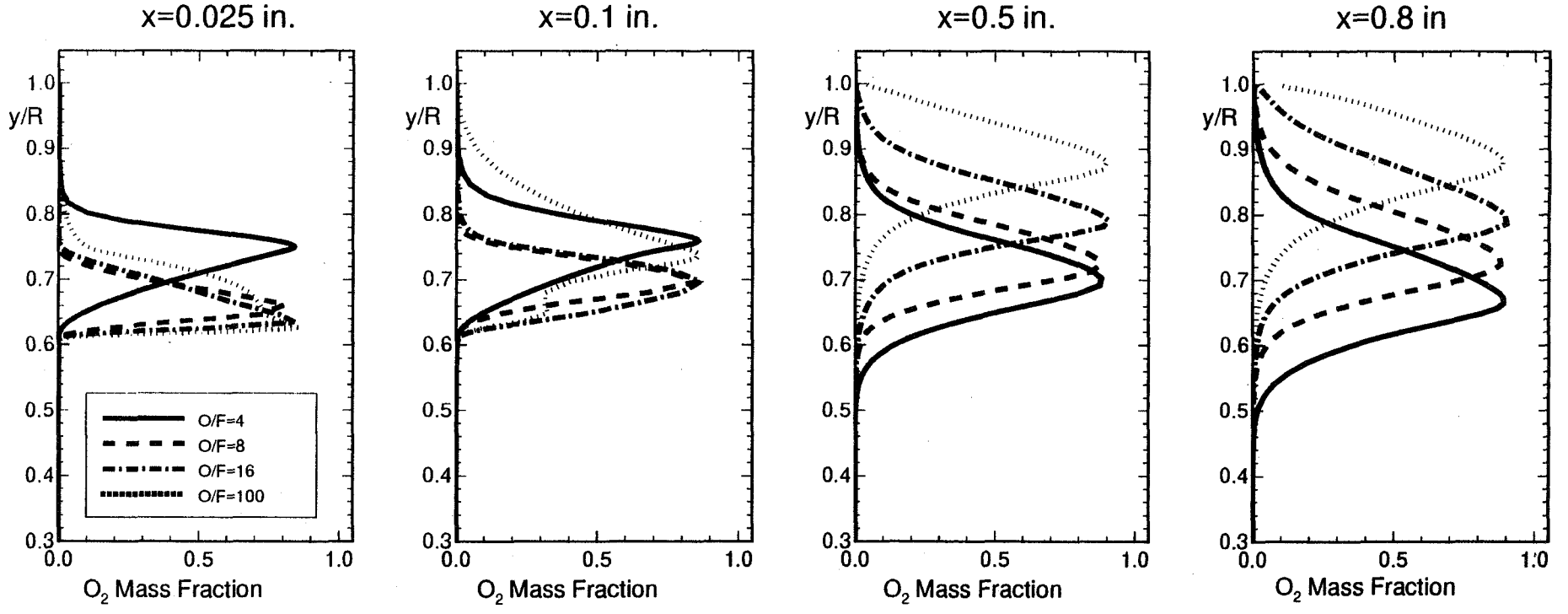

Shear Layer - O/F Ratio Variation

OH Mass Fraction Profiles

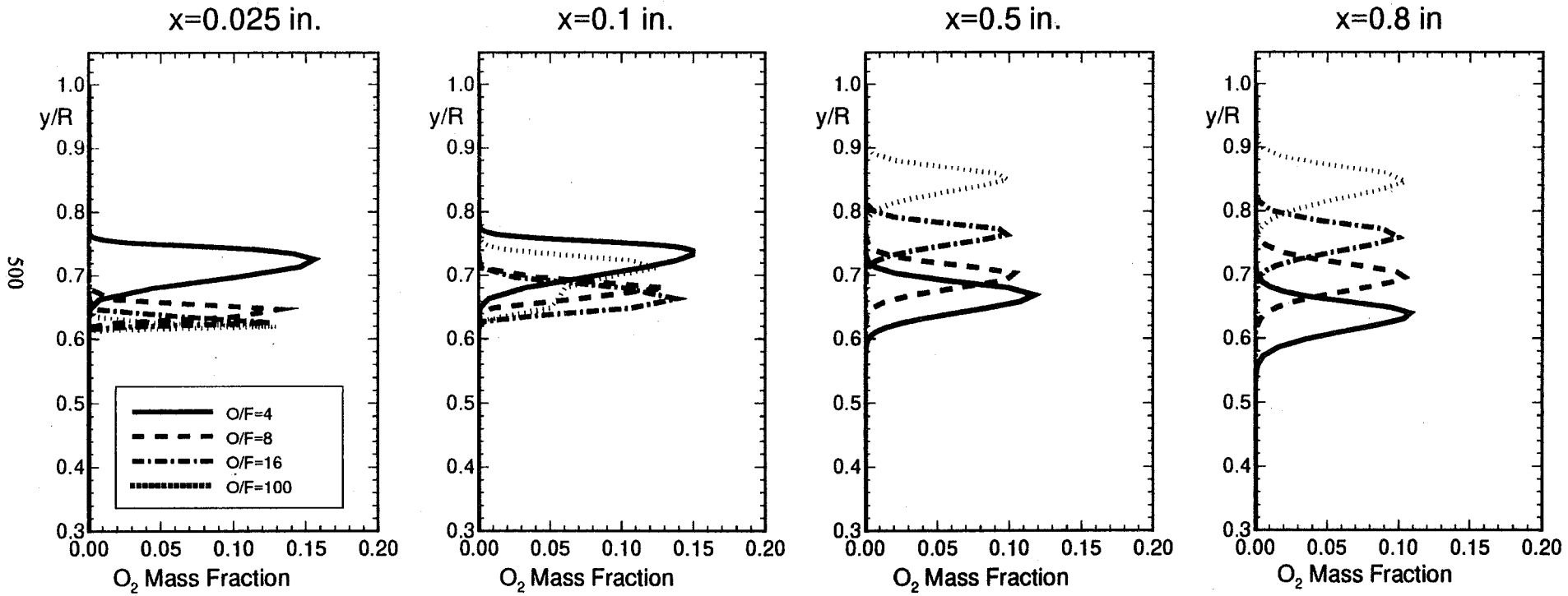

Unielement Injector

Schematic and Representative Mesh

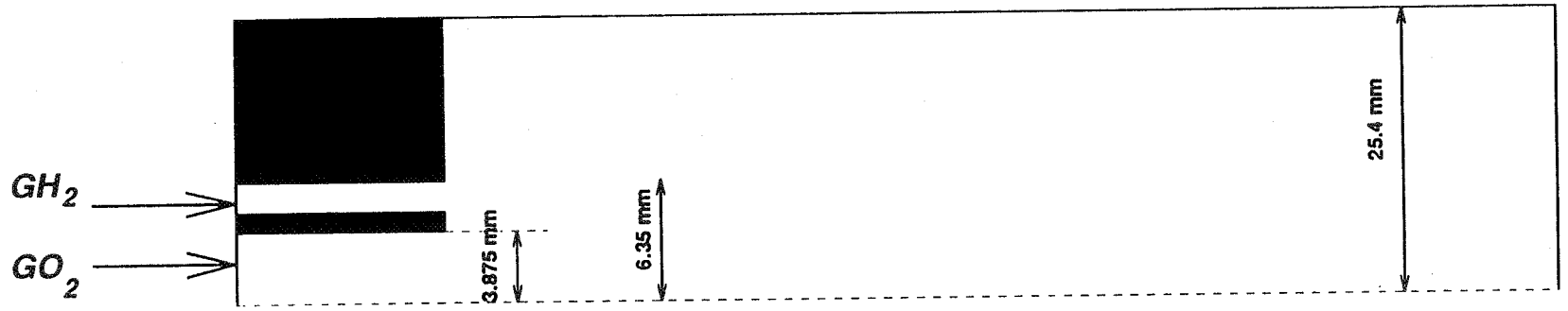

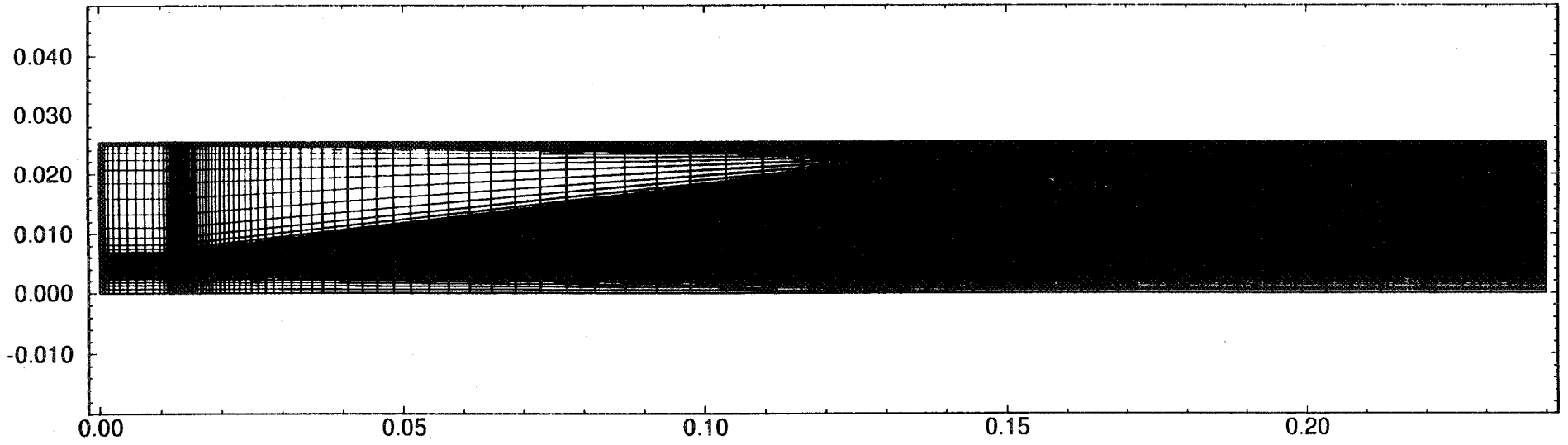

Optically Accessible Rocket

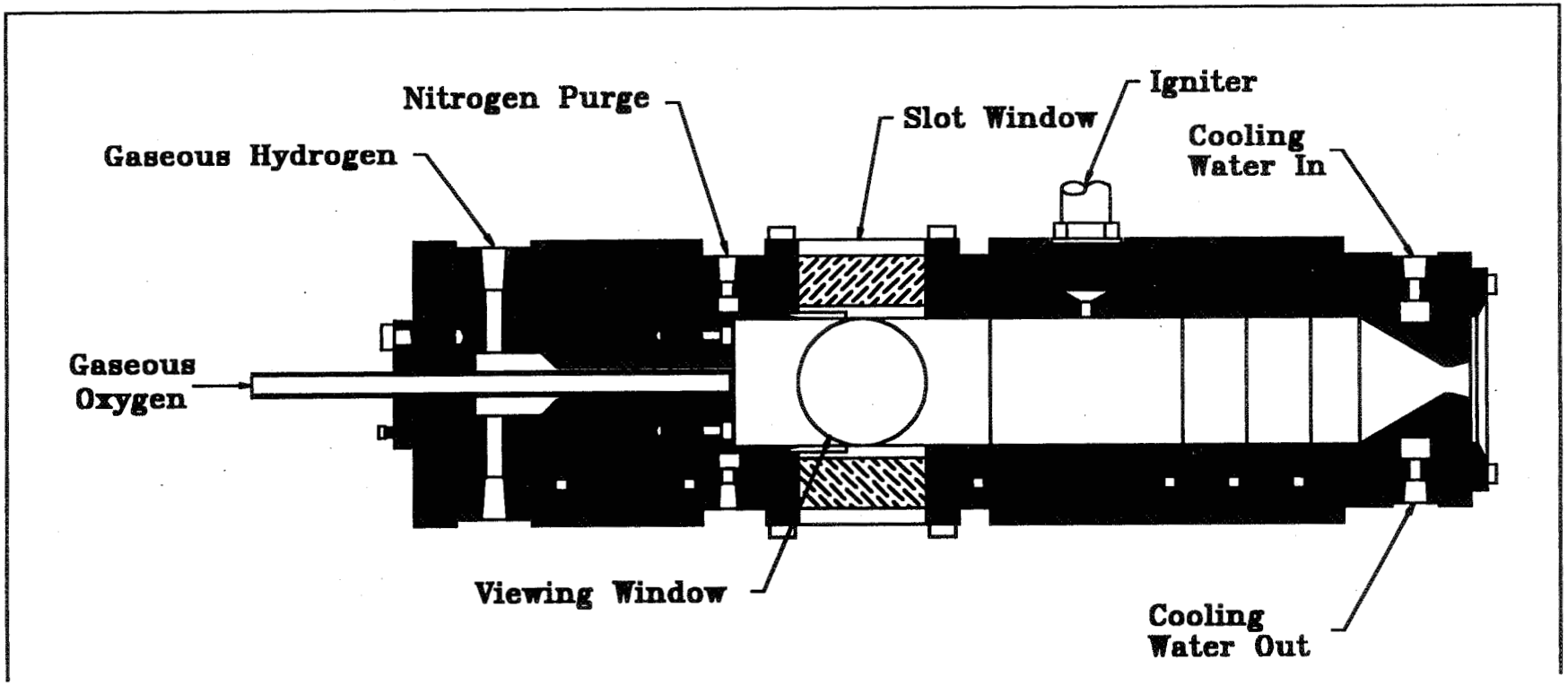

Unielement Injector - GO_2/GH_2

Mean Velocity Profiles - Comparison with Experiment

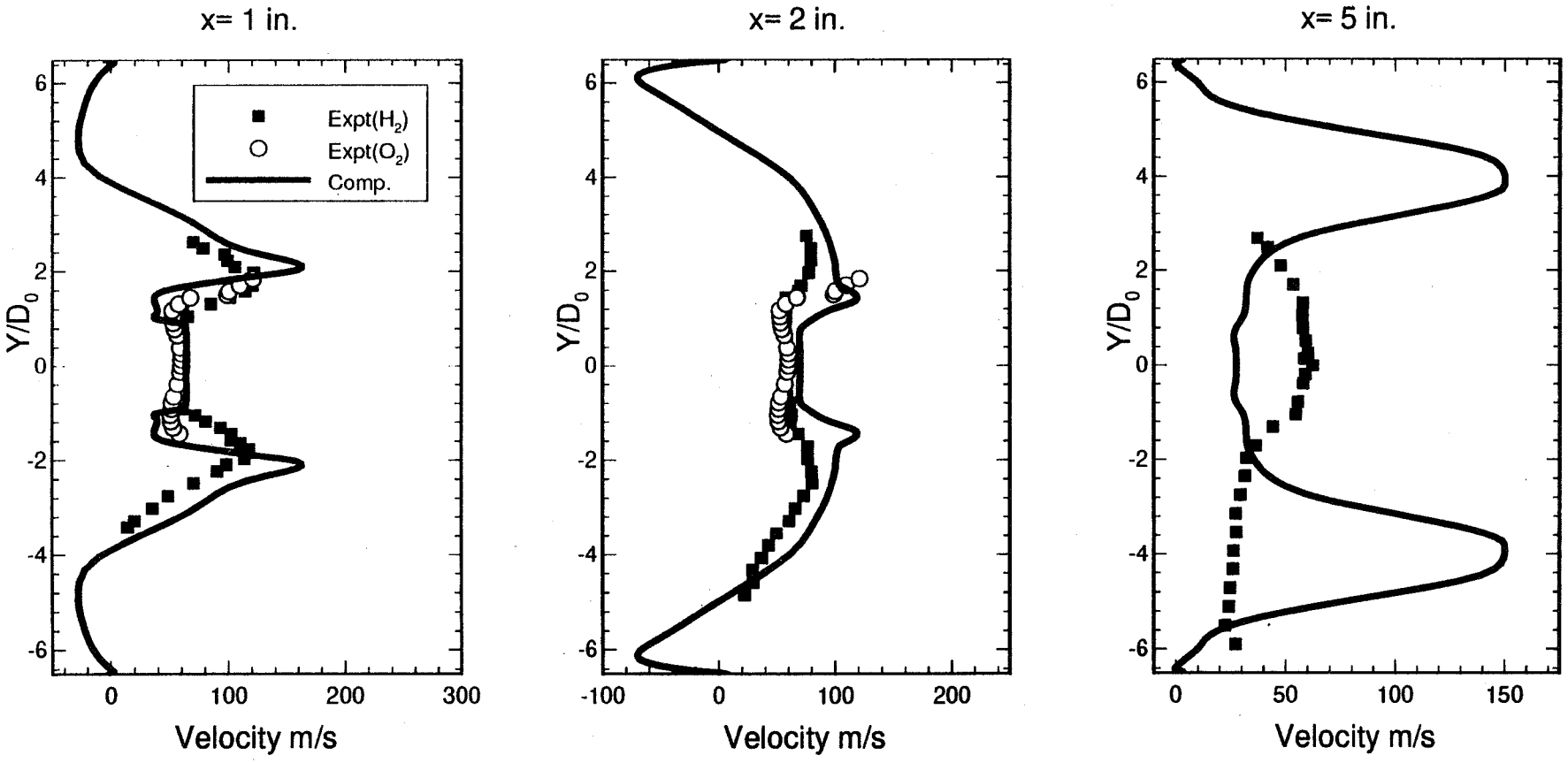

Unielement Injector - GO_2/GH_2

Hydrogen Mole Fraction - Comparison with Experiment

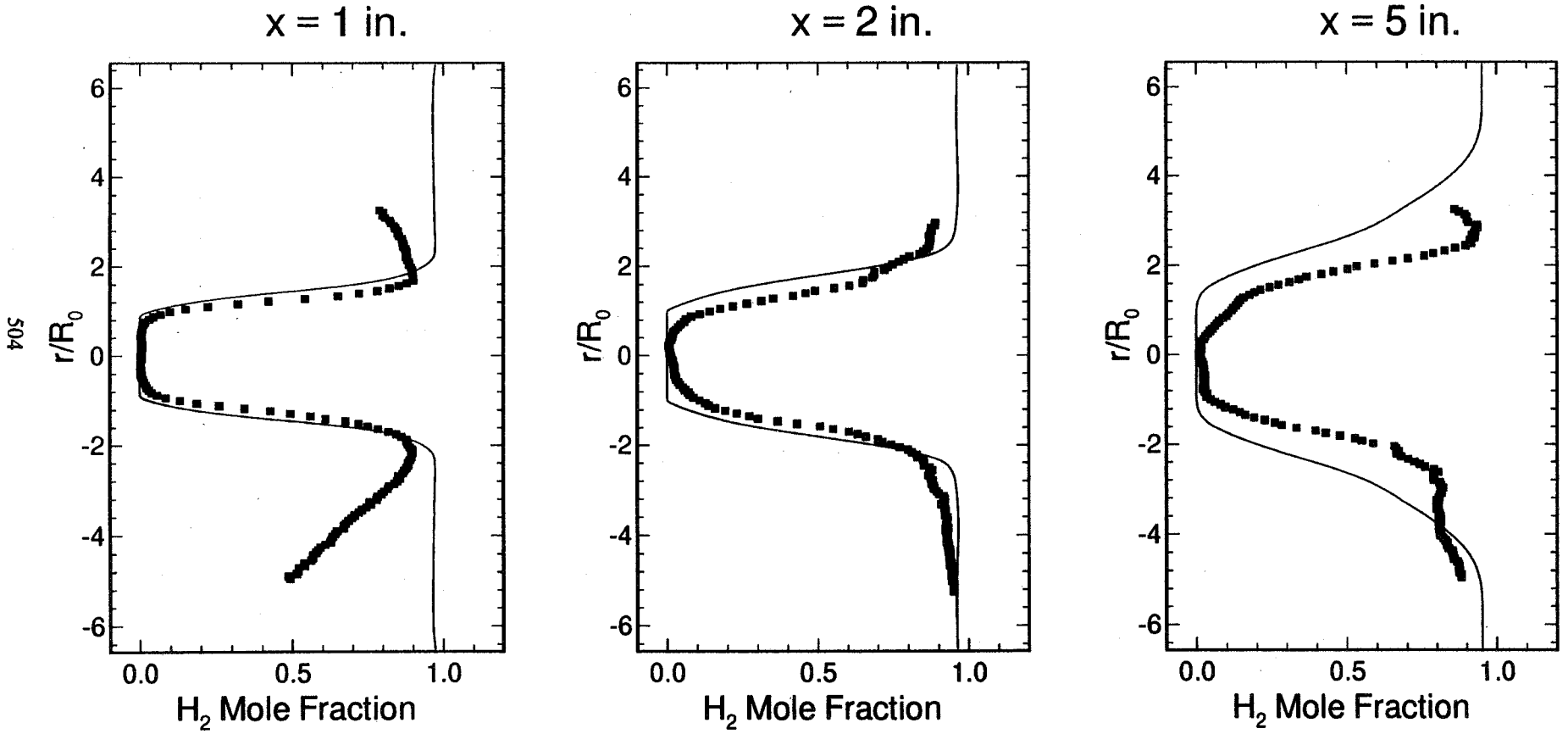

Unielement Injector - GO_2/GH_2

Oxygen Mole Fraction - Comparison with Experiment

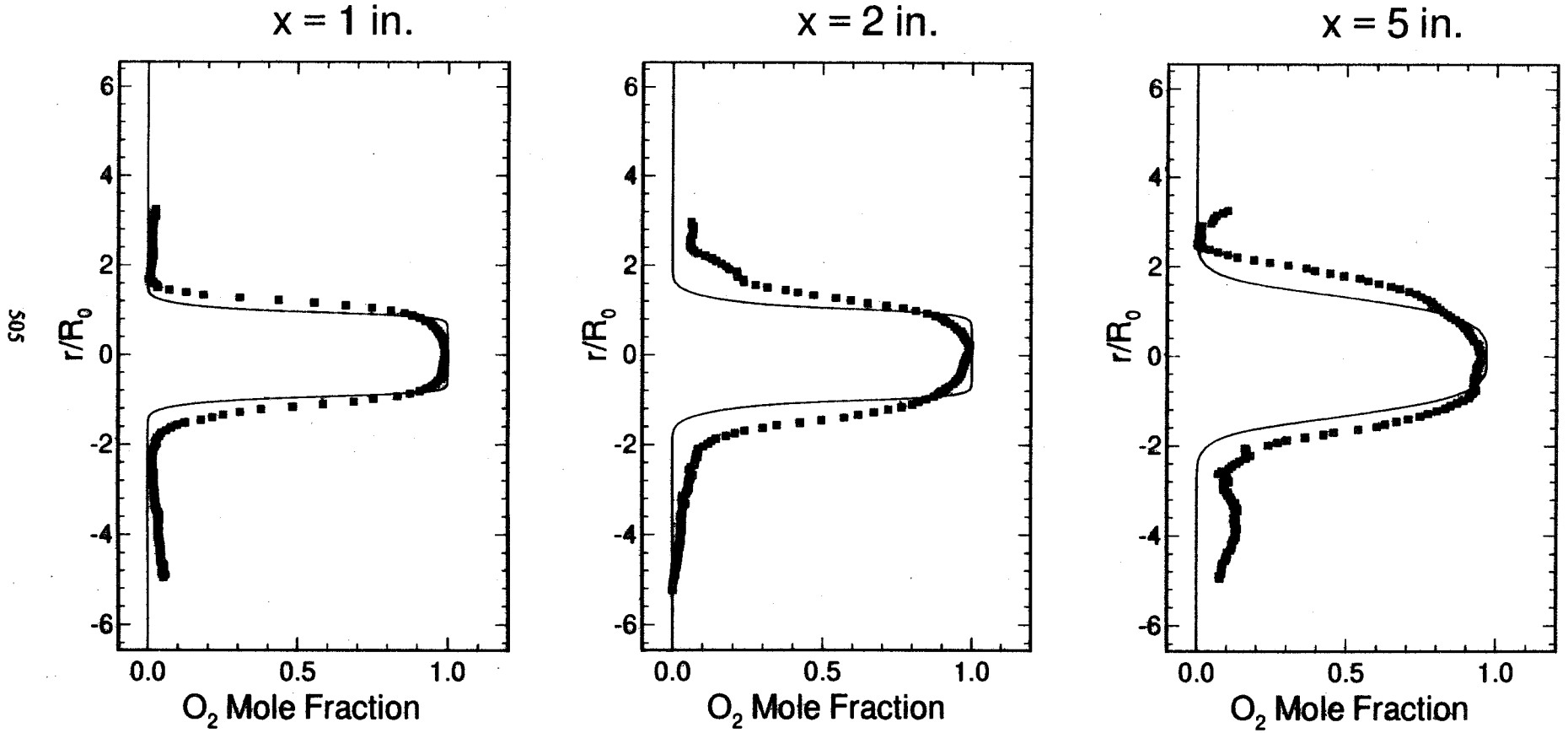

Unielement Injector - GO_2/GH_2

OH Mass Fraction Profiles - O/F Ratio Variation

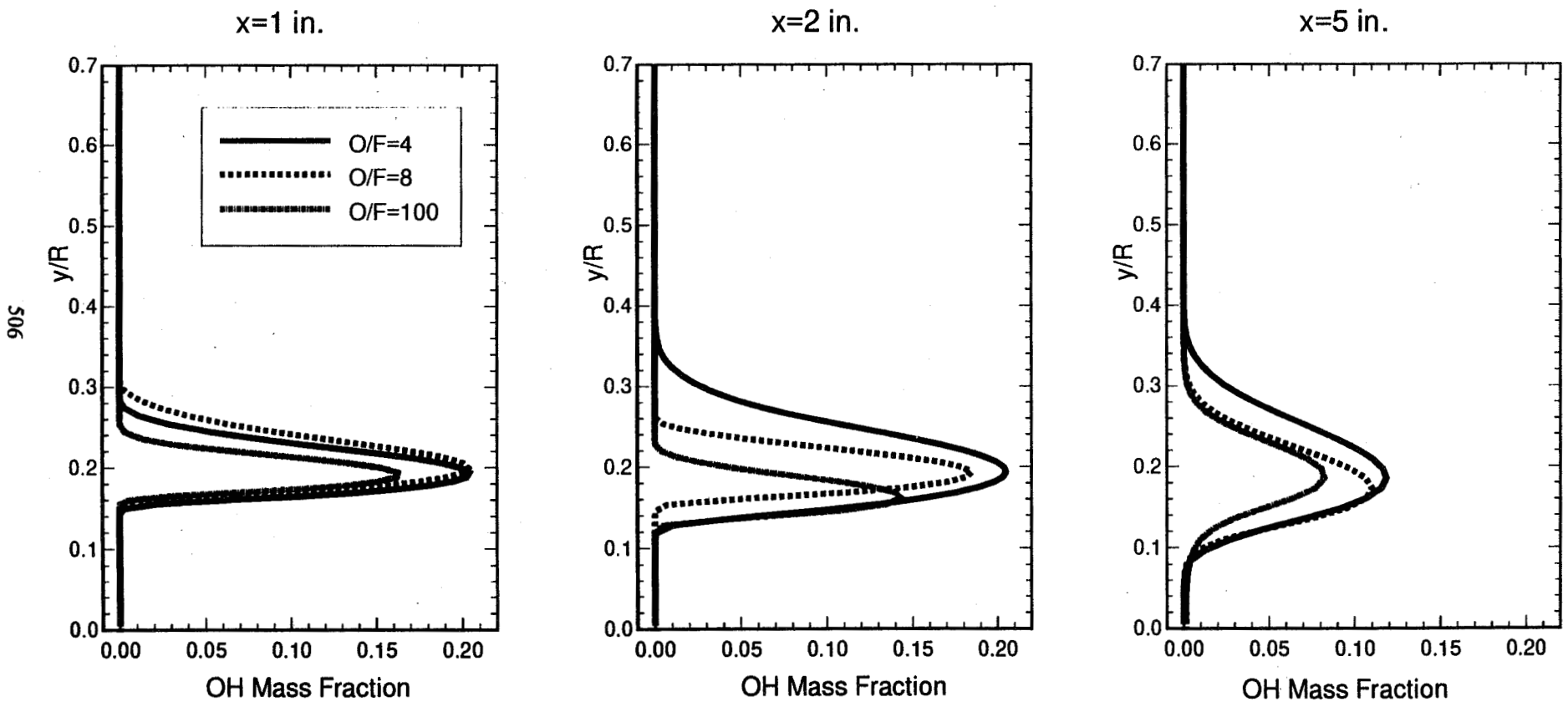

Unielement Injector - GO_2/GH_2

Temperature Profiles - O/F Ratio Variation

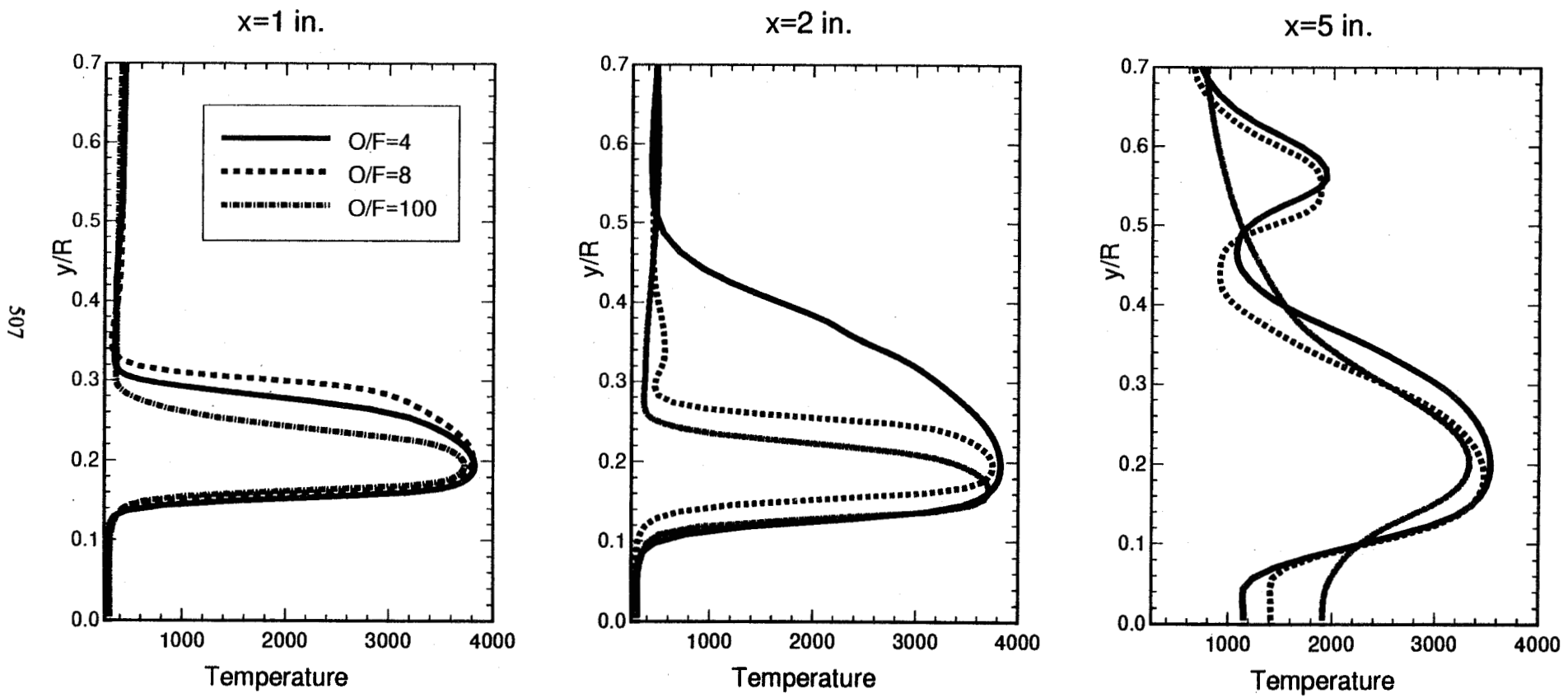

Unielement Injector - GO_2/GH_2

Temperature Contours - Effect of Swirl

No Swirl

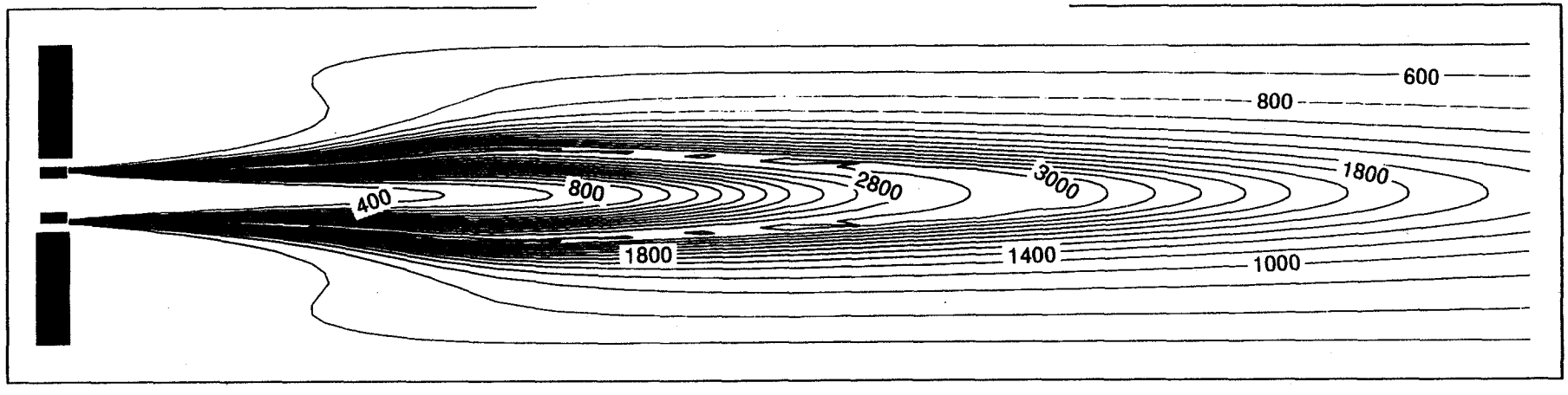

Nominal Swirl (35°)

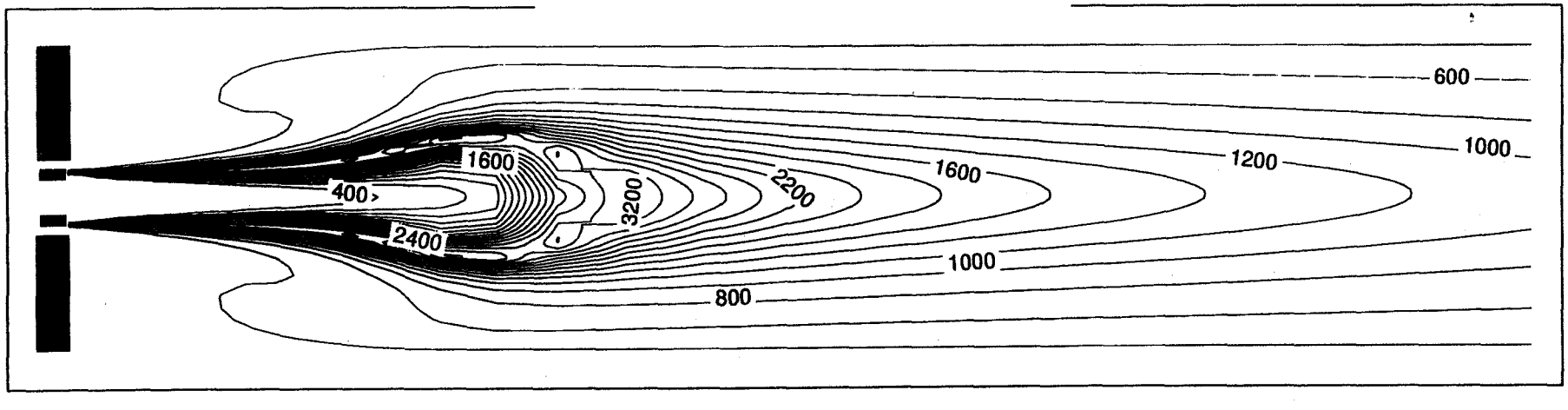

Unielement Injector - GO_2/GH_2

Temperature Contours - Effect of Swirl

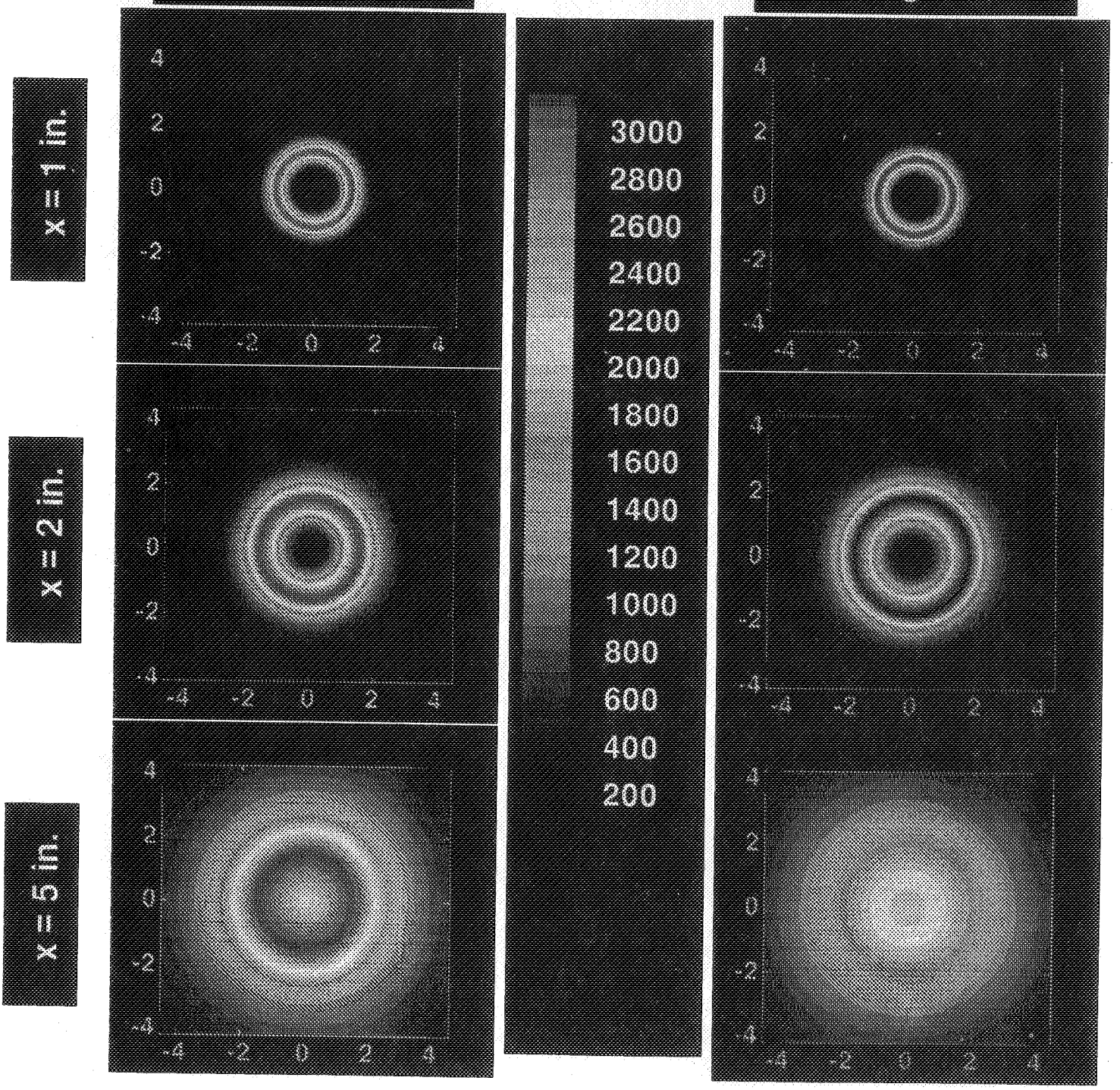

Unielement Injector - GO_2/GH_2

O_2 Mass Fraction Contours - Effect of Swirl

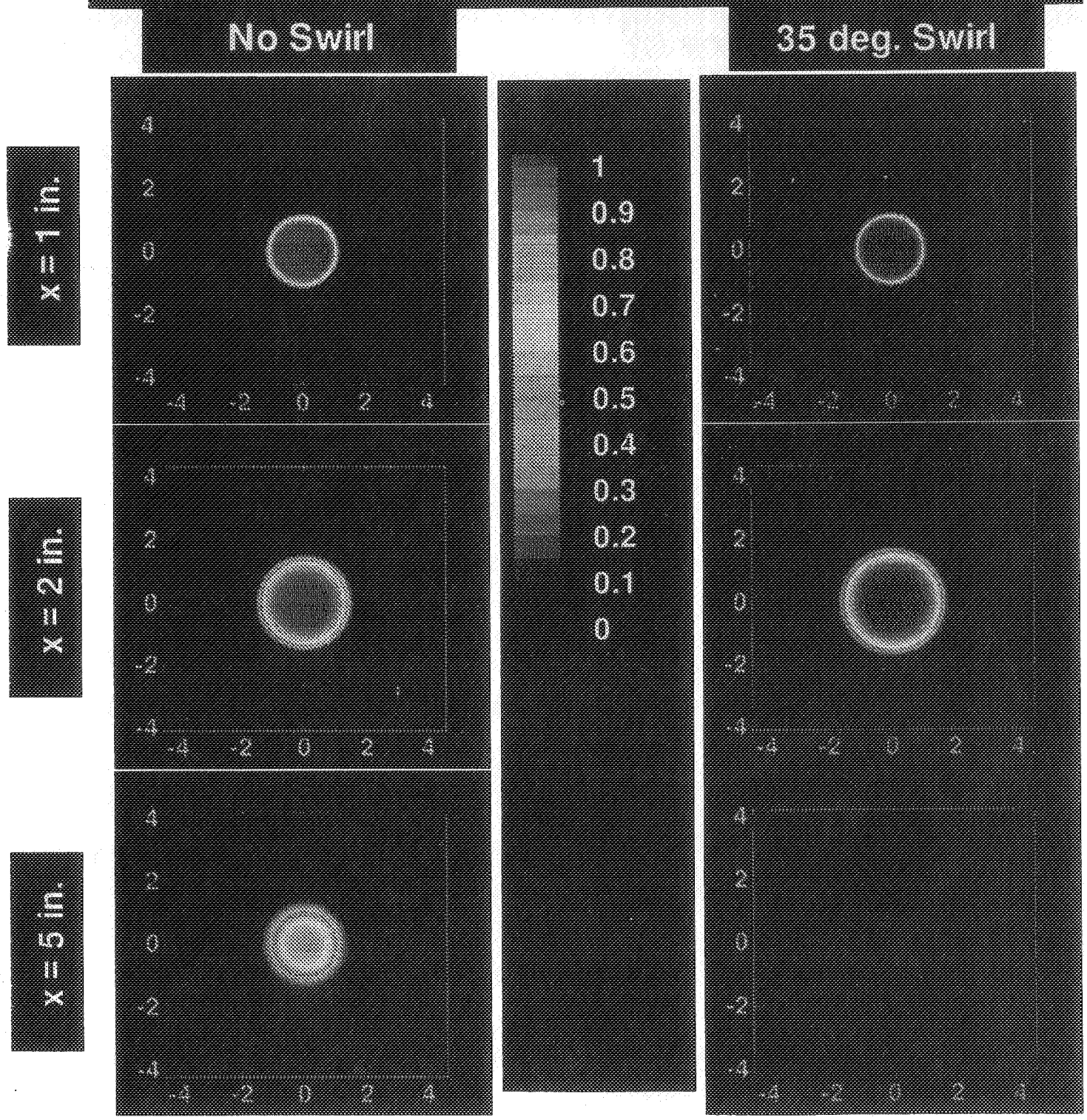

Unielement Injector - GO_2/GH_2

H_2O Mass Fraction Contours - Effect of Swirl

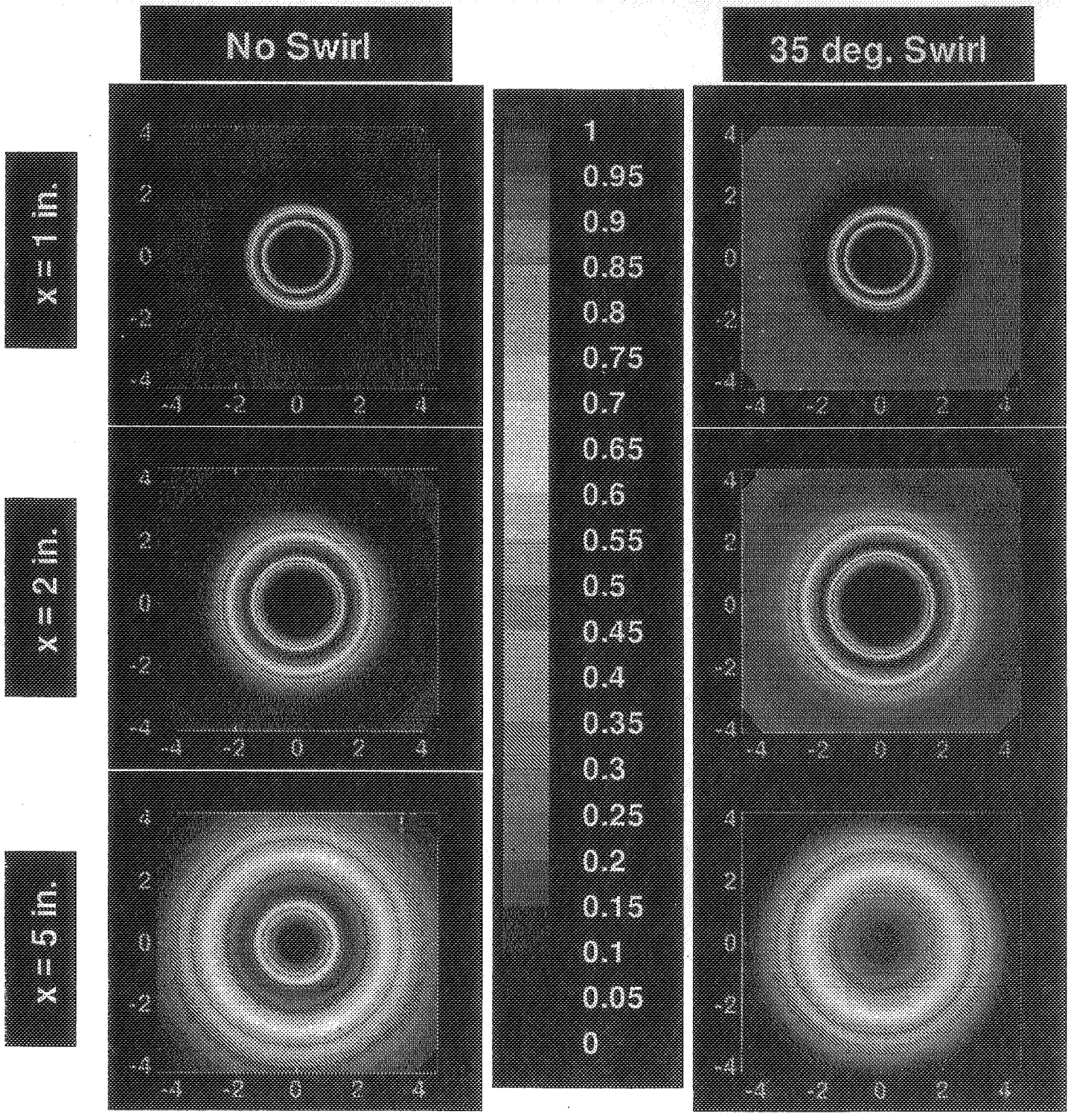

SUMMARY

- **CFD Analysis of GO2 / GH2 Combustion at Wide O / F Ratios**

- **Premixed Flame Calculations**

  - **Rapid Overall Look at Combustion Characteristics**
  - **Compare Various Kinetic Models at Wide O / F Ratios**
  - **Validation Of CFD Code**

- **Chang - Marek Shear Layer Experiment**

  - **Diluted H2 / N2 - Air Shear Layer**
  - **Rapid Spread in Velocity and TKE Suggests Unsteadiness in Experiment**
  - **CFD Calculations in Reasonable Agreement with Data, but Underpredict Spread Rate**

SUMMARY (CONT'D)

- **Injector - Scale shear Layer Calculations**
  - **Base Region Is Effective Flame - Holder**
  - **Flame Attaches to Upper / Lower Corner of Base as O / F Changes**
  - **Good Flame Stability over all O / F Ratios**
  - **Location of Flame Shifts with O / F Ratio**
- **Unielement Injector Validation**
  - **Good Qualitative Comparison with Data**
  - **CFD Recirc ulation Zone Appears to be Shorter than Experiment**
  - **Experiment Mixes Slower than Computation**
- **Swirl Calculations Show Improved Mixing and Temperature Uniformity**

Oxygen-Rich Combustion Experiments in a LOX/GH_2 Uni-element Rocket

S. A. Rahman, H. M. Ryan, S. Pal, R. J. Santoro

Propulsion Engineering Research Center
and
Department of Mechanical Engineering
The Pennsylvania State University
University Park, PA 16802

Background

Combustion characteristics of a LOX/GH_2 swirl coaxial injector element have been examined up to very high oxidizer to fuel ratios in a research rocket chamber at Penn State University's Cryogenic Combustion Lab. The single-element tests demonstrate that, for injector element flowrates comparable to those of booster engine injectors, ignition, stable combustion, and good performance can be achieved with LOX at O/F ratios as high as 170.

Operation of injectors at such high O/F ratios is a highly desirable element of candidate cryogenic propulsion systems for next-generation Reusable Launch Vehicles (RLV). Oxygen-rich preburners, supplying low temperature exhaust gases to the turbine drives, have the potential to minimize cost, weight, and operational complexity of advanced rocket engines. Fundamental data at the single-element level, such as that reported here, is a component of an industry-wide oxygen-rich combustion technology program for RLV propulsion. Recent progress is summarized in this presentation.

Research Objectives

Research efforts are directed towards understanding specific technical issues that must be resolved to minimize the risk and cost associated with developing oxygen-rich rocket preburners. The experiments concentrate on hot-fire uni-element tests to demonstrate concepts which can be incorporated into hardware design and development. Two concepts under consideration are direct injection of propellants at high O/F, and stoichiometric injection followed by downstream injection of LOX to achieve the high O/F. The specific results given here address the performance, ignition, combustion stability, and wall heat transfer aspects of a direct-injection swirl coaxial element design operating at high O/F.

Current Progress

Experiments with direct-injection at high O/F have been conducted in an optically-accessible uni-element rocket test chamber of 2 inch square cross-section (1.1 ft. length) with LOX/GH_2 propellants. A swirl coaxial injector element, characterized under both cold-flow and hot-fire, was used to atomize the LOX. LOX flowrates were held constant in the experiments while O/F ratio was achieved by varying the hydrogen fuel flowrate. A gaseous hydrogen/oxygen torch was used to ignite the main flow.

A series of experiments has been completed where O/F ratio was varied from 5 to 170, while simultaneous measurements were made of high frequency pressure oscillations and wall heat transfer. Chamber pressures for this series were nominally 300 psia, and data was obtained at both upstream and downstream locations within the rocket chamber. The results show that wall heat transfer is greatly reduced for high O/F combustion. Pressure oscillations are also at a low level, approximately 1% of chamber pressure, for the entire range of O/F.

Further characterization of the direct-injection high O/F scheme is planned, and will involve non-intrusive measurement of spray penetration and the spray flame temperature.

Acknowledgment

The oxygen-rich studies are sponsored by NASA Marshall Space Flight Center under NASA Agreement No. NCC8-46. The swirl coaxial injector design/characterization work is supported by Dr. Mitat Birkan of the Air Force Office of Scientific Research, Air Force Systems Command, under grant number F49620-93-1-0365.

OXYGEN-RICH COMBUSTION EXPERIMENTS IN A LOX/GH_2 UNI-ELEMENT ROCKET

S. Rahman, H. Ryan, S. Pal & R. Santoro

PENNSTATE

1855

Department of Mechanical Engineering

and

Propulsion Engineering Research Center

13th Workshop for CFD Applications in
Rocket Propulsion and Launch Vehicle Technology
Huntsville, AL
April 25 - 27, 1995

ACKNOWLEDGEMENTS

- **Dr. Mitat Birkan**
  - Air Force Office Of Scientific Research
- **G. Cox and D. Hautman**
  - United Technologies
- **J. Hulka**
  - Aerojet Propulsion Division
- **C. Dexter, J. Hutt**
  - NASA Marshall Space Flight Center
- **M. Moser, L. Schaaf, M. Foust**
  - Penn State University

OPTICALLY ACCESSIBLE ROCKET CHAMBER

- Heat-Sink Copper Chamber
- Modular / Interchangeable Chamber Sections
- 51 x 51 mm Cross-Section (2 in. square)
- 51 mm (2 in.) Round Viewing Windows
- 51 mm (2 in.) long Slot Windows on top/bottom
- Gaseous H_2/O_2 Torch Ignitor

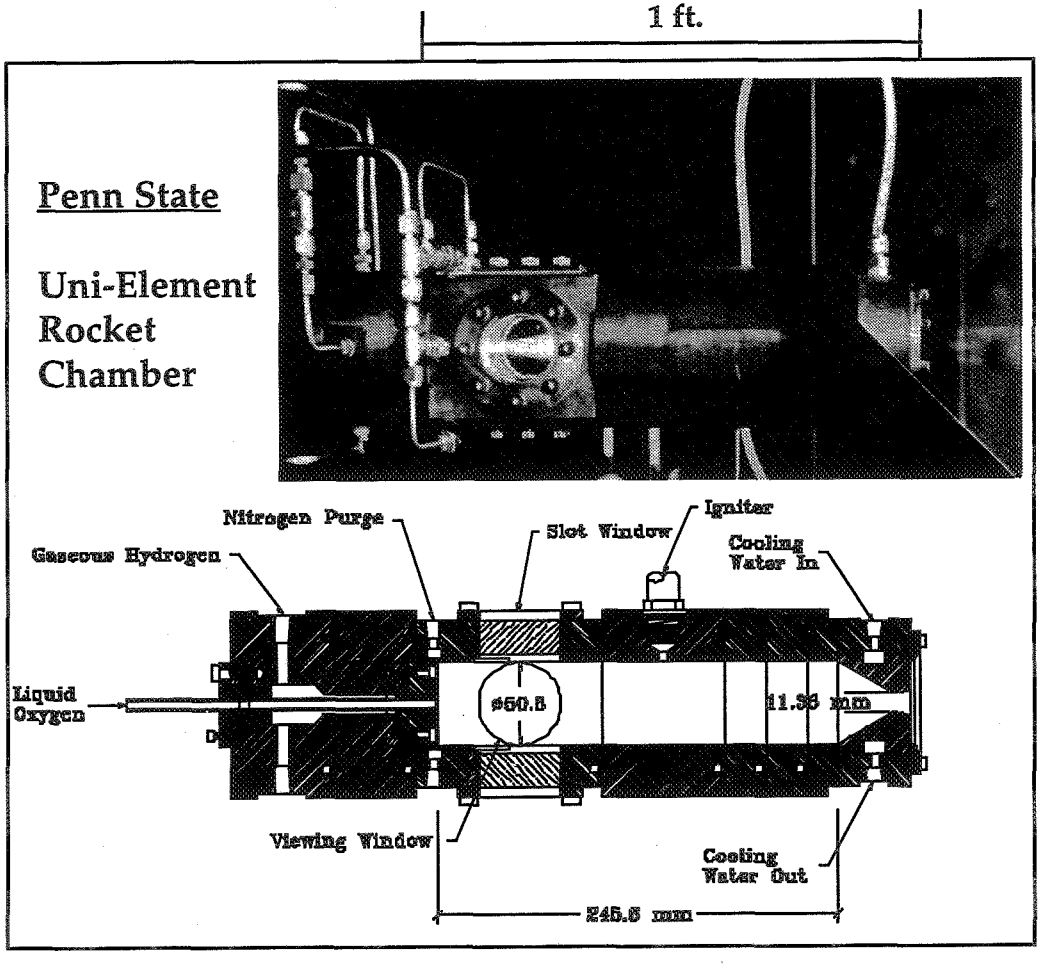

SWIRL COAXIAL INJECTOR

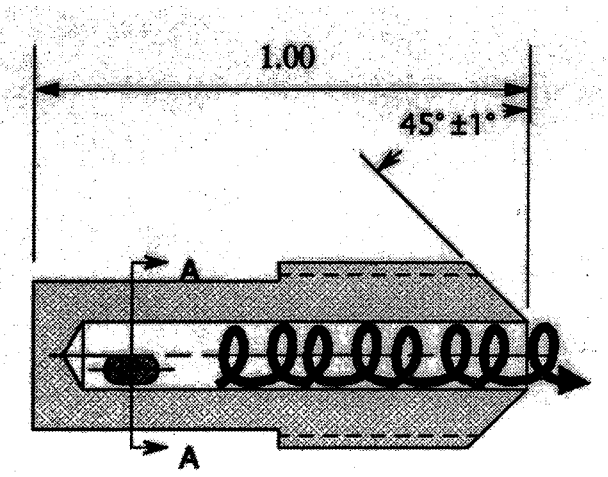

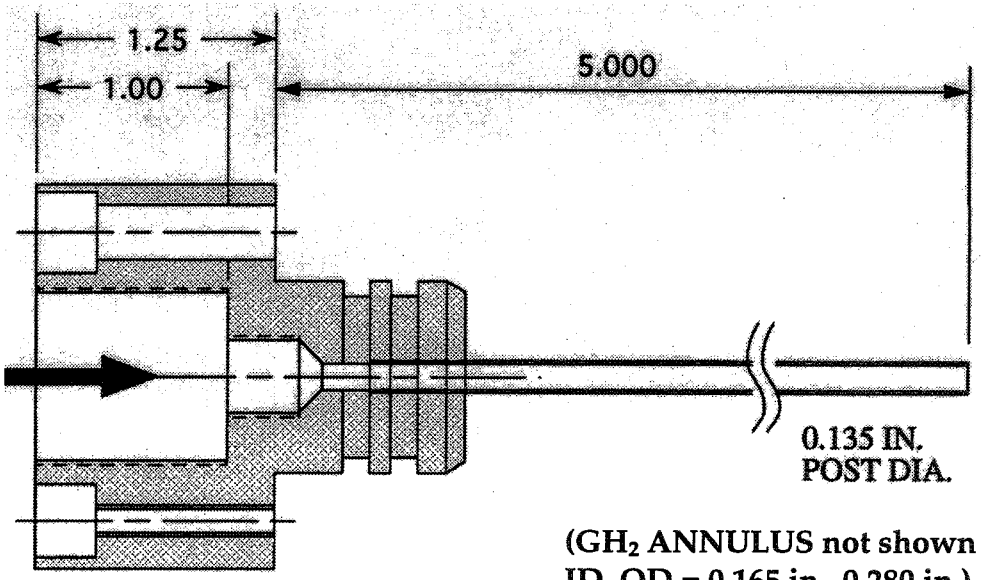

(GH_2 ANNULUS not shown
ID, OD = 0.165 in., 0.280 in.)

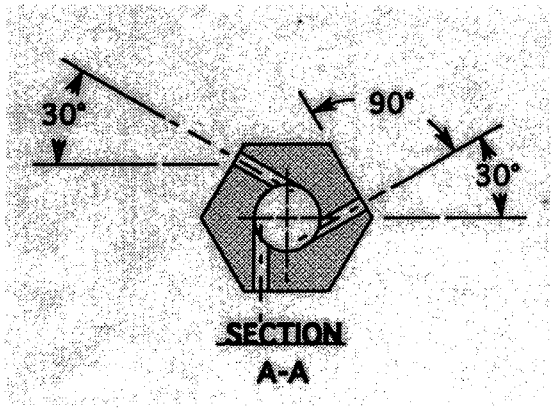

- **LOX/GH_2 Injector Design is Based on Industry Practice**
  - **2 Injectors (0.135 in. & 0.277 in. POST ID)**
  - **Injector shown is similar to RL10A-4-1**
  - **Design Derived from STME Studies by Aerojet, Pratt & Whitney, MSFC**

Ref.: Rahman et al. '95, AIAA Paper No. 0381

OBJECTIVE & MOTIVATION

- **Augment Limited Experimental Data Base on Oxygen-Rich Combustion**
  - **Demonstrate Ignition/Combustion**
  - **Identify High O/F Limit of Combustion**
- **RLV Propulsion Technology Issues to be Addressed**
  - **LOX/GH_2 Preburner Operation at High O/F**
  - **Full Face Injection vs. Stoich. Injection + Dilution**

OVERVIEW & STATUS

- Hot-Fire with LOX/GH_2 Swirl Coaxial Injector (0.135 in. POST ID)
  - LOX Flowrates 0.25 - 0.4 lbm/s
  - P_c 150 - 500 psia
  - O/F 5 - 170
- High O/F Studies (P_c = 300 psia nom.)
  - Meaurements Completed
    - » Chamber Wall Heat Transfer
    - » High Frequency Pressure
    - » C* Efficiency
- High O/F Studies (P_c = 800 psia nom.)
  - Repeat Above Measurements
  - Testing in Progress

HOT-FIRE ... FLOWFIELD

LOX/GH_2, O/F = 5.7, P_c = 440 psia

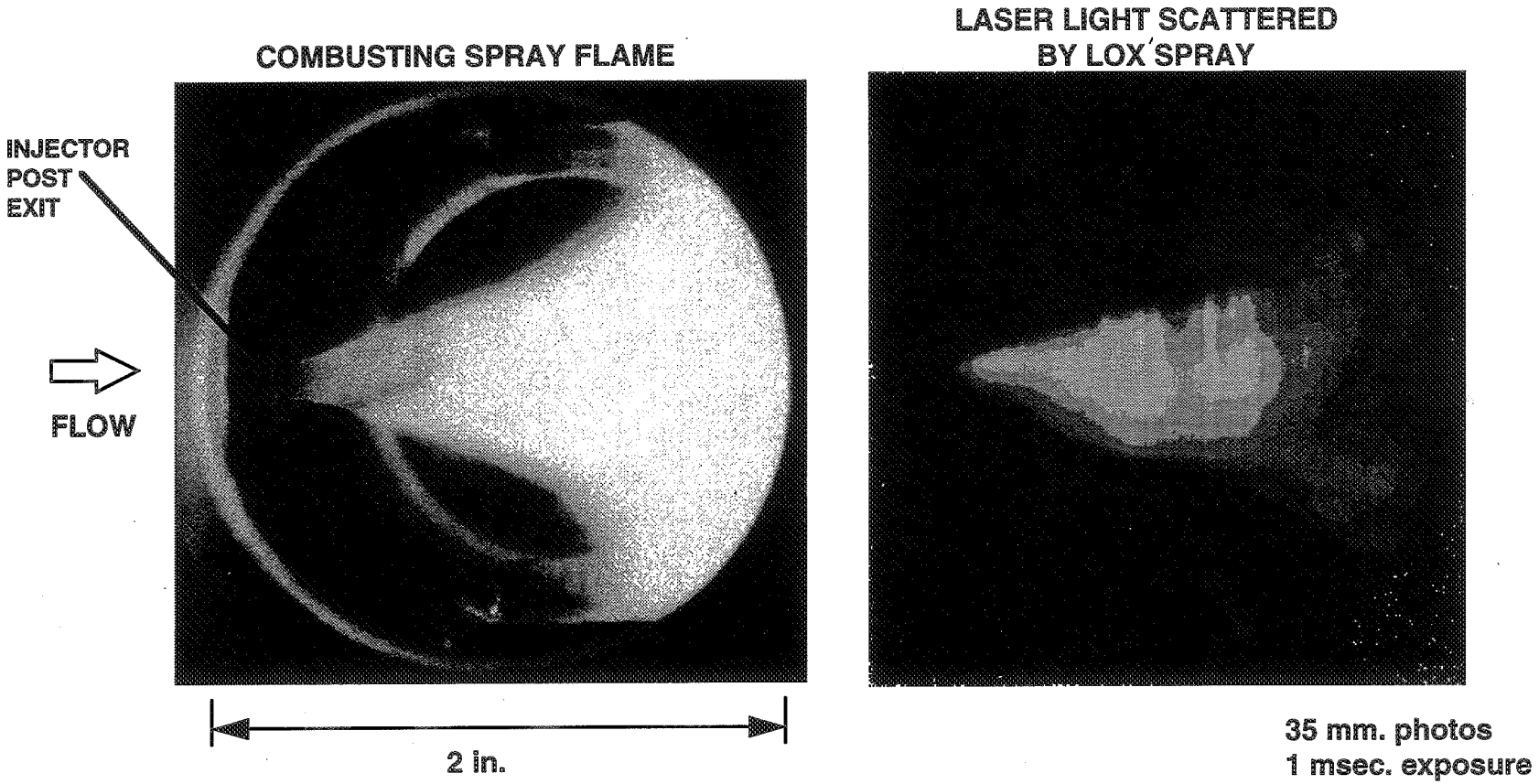

- Conical Flame Zone Attached to LOX Post (left)
- Laser-Light Scattered by LOX Drops in Flame (right)

HIGH O/F COMBUSTION

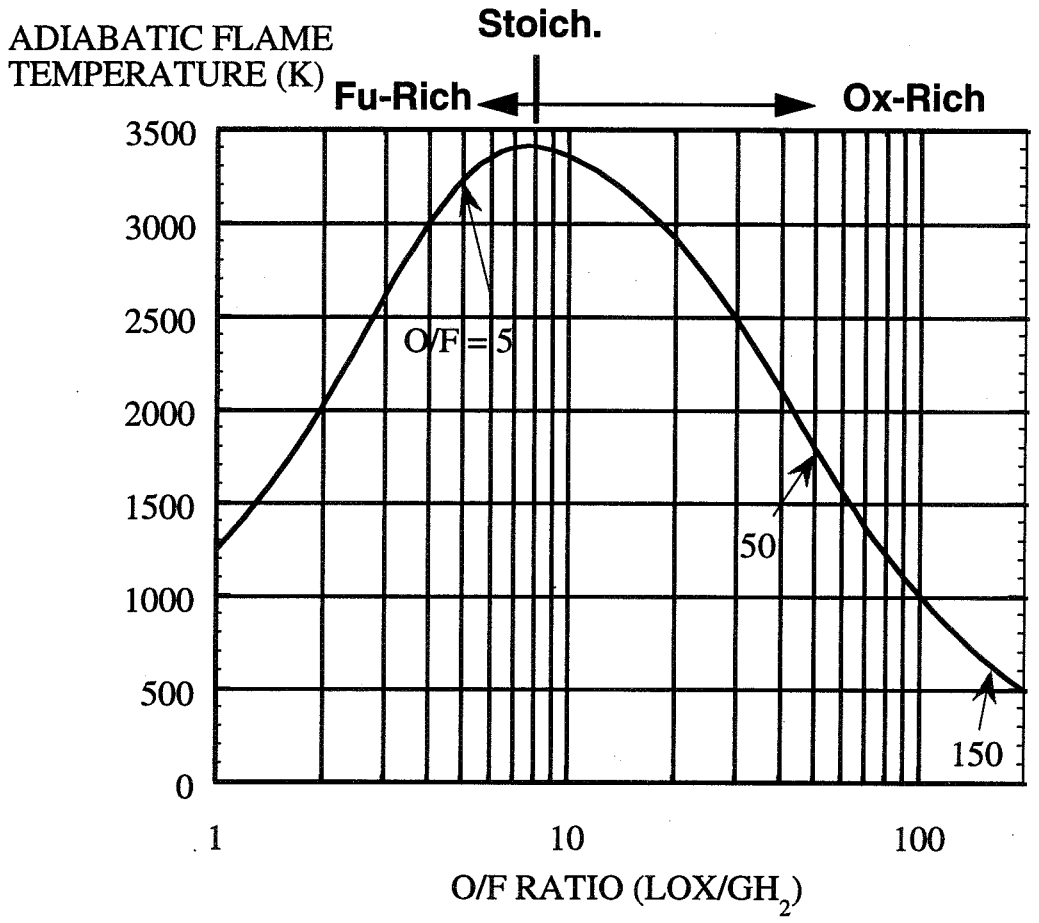

- **Adiabatic Flame Temperature Decreases with O/F Ratio**

C* EFFICIENCY AT HIGH O/F

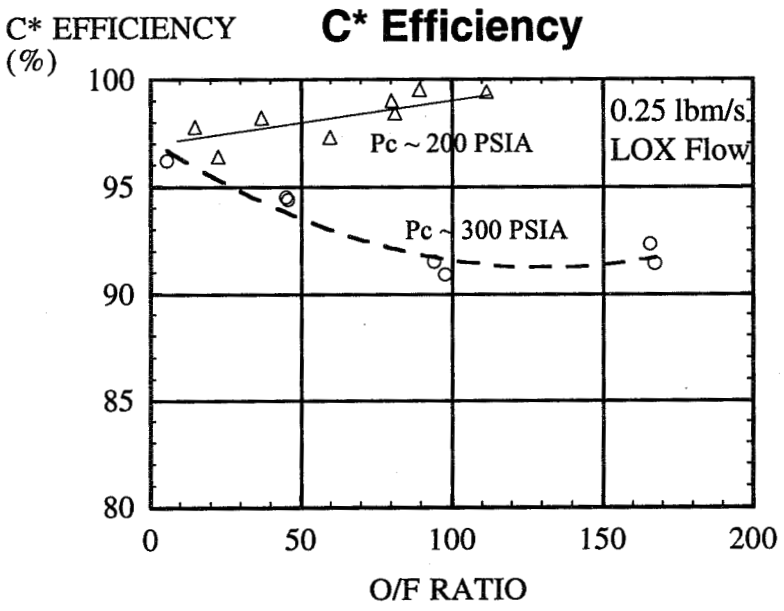

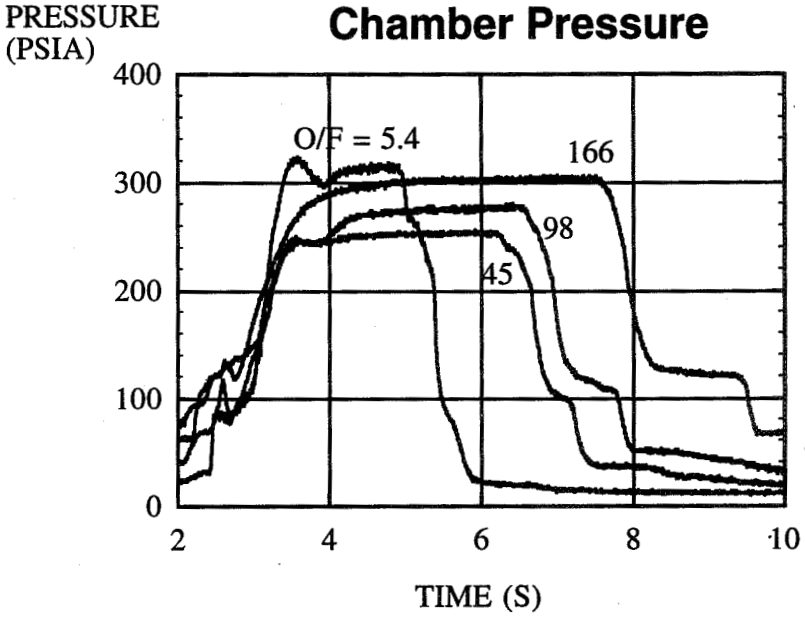

- **Tests Demonstrate Ignition/Combustion for O/F Ratio = 5 to 170**
  - **P_c = 200 - 300 psia**
  - **Swirl Coaxial Injector**
  - **LOX/GH_2 Propellants**
  - **0.25 lbm/s LOX Flow**
  - **Some Tests with Larger LOX Injector**
  - **93% C* Efficiency for (O/F = 125 - 140, LOX Flow = 0.9 lbm/s)**

TEST INSTRUMENTATION

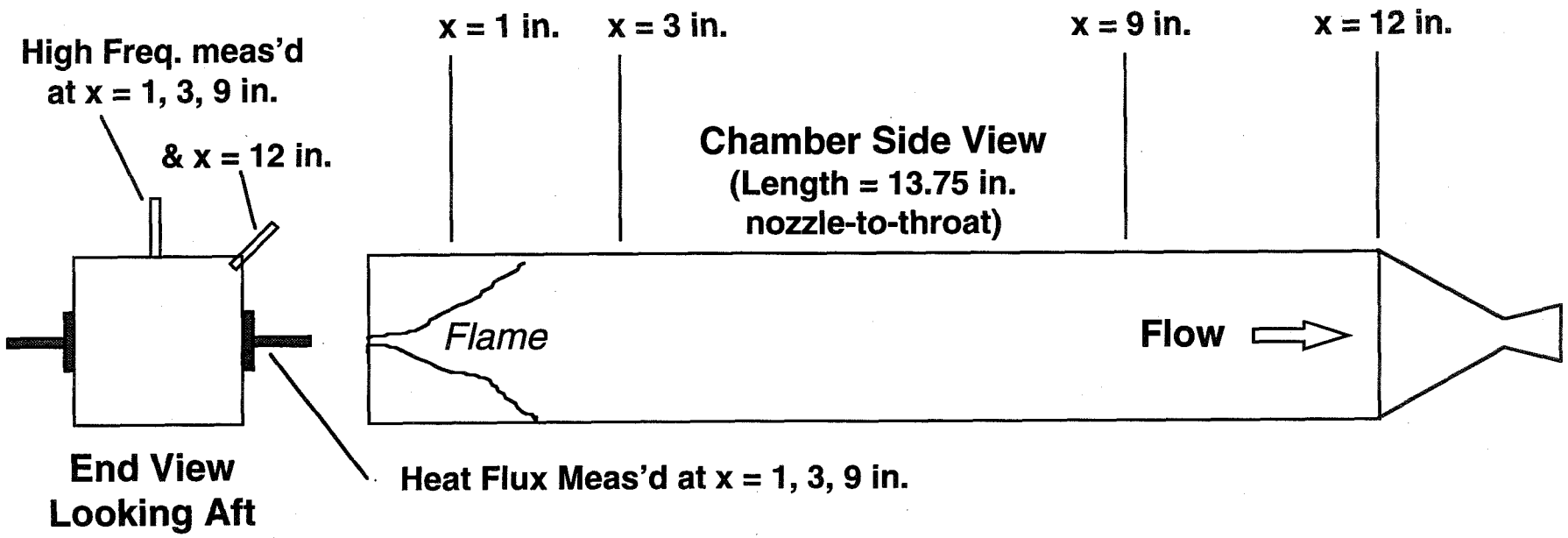

- 2 Heat Flux Gauges
- 2 High Freq. Pressure Gauges (PCB Model 113A24)
- 2 Chamber Pressure Gauges (Setra Model 204)
- Flow Metering with Calibrated Venturi Orifices

HEAT FLUX MEASUREMENT

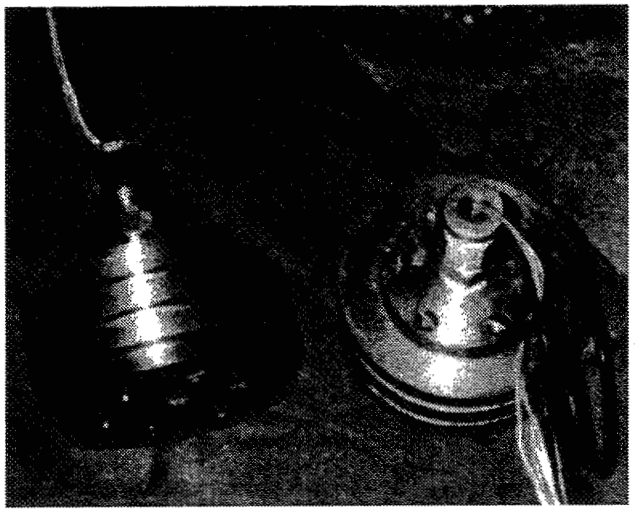

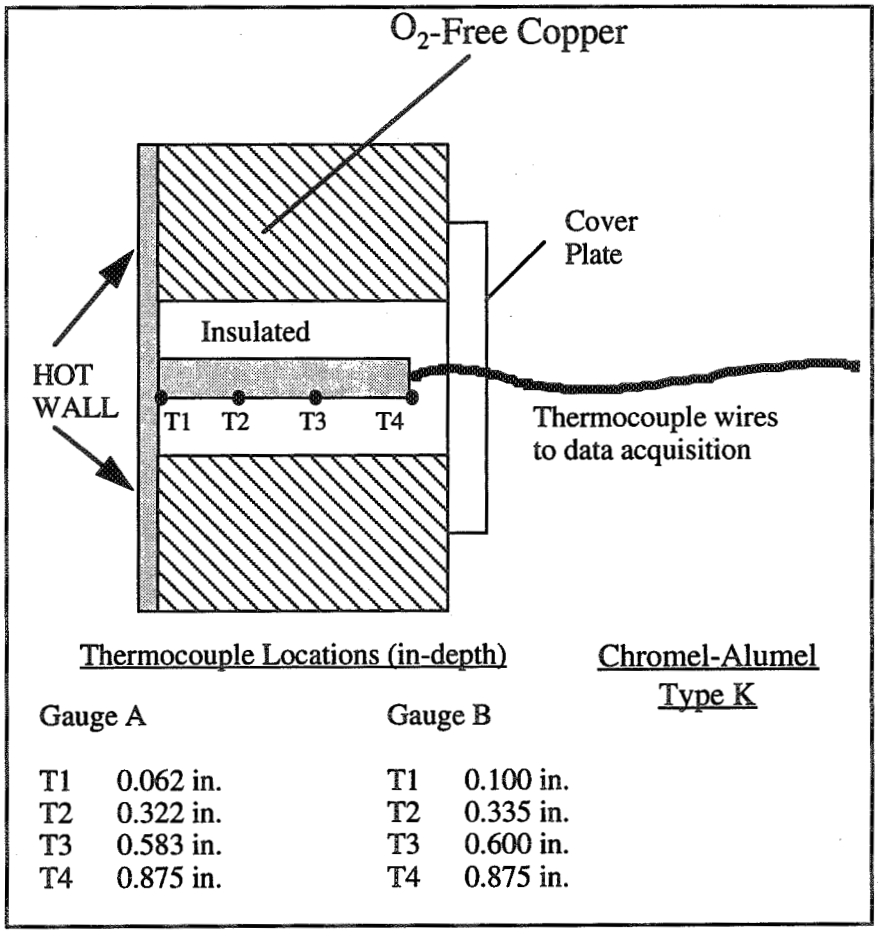

- 2 Heat Flux Gauges Used
  - On Opposing Sidewalls of Rocket
  - Heat Xfer. Computed from Temps. T1, T2, T3, T4
  - Technique by NASA LeRC, Ref: Liebert '88, NASA-TP-2840
- Transient Heat Flux Obtained

HIGH-FREQUENCY PRESSURE GAUGE

- **PCB Gauge Model 113A24**
  (500 kHz Natural Freq., 1 μsec response)
- **50 kHz Sampling Employed**
- **0.02 psi Resolution**
- **Gauge Mounted almost flush with Chamber Inner Wall**

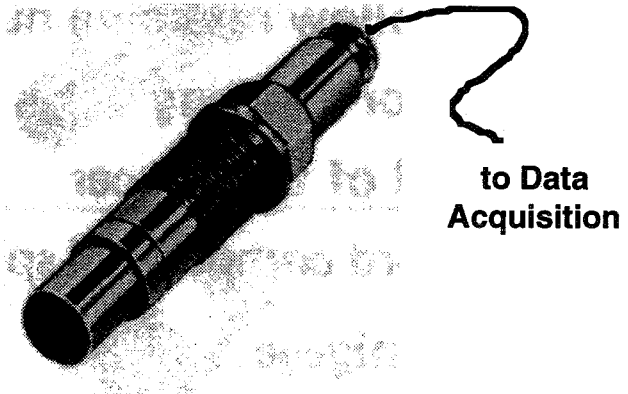

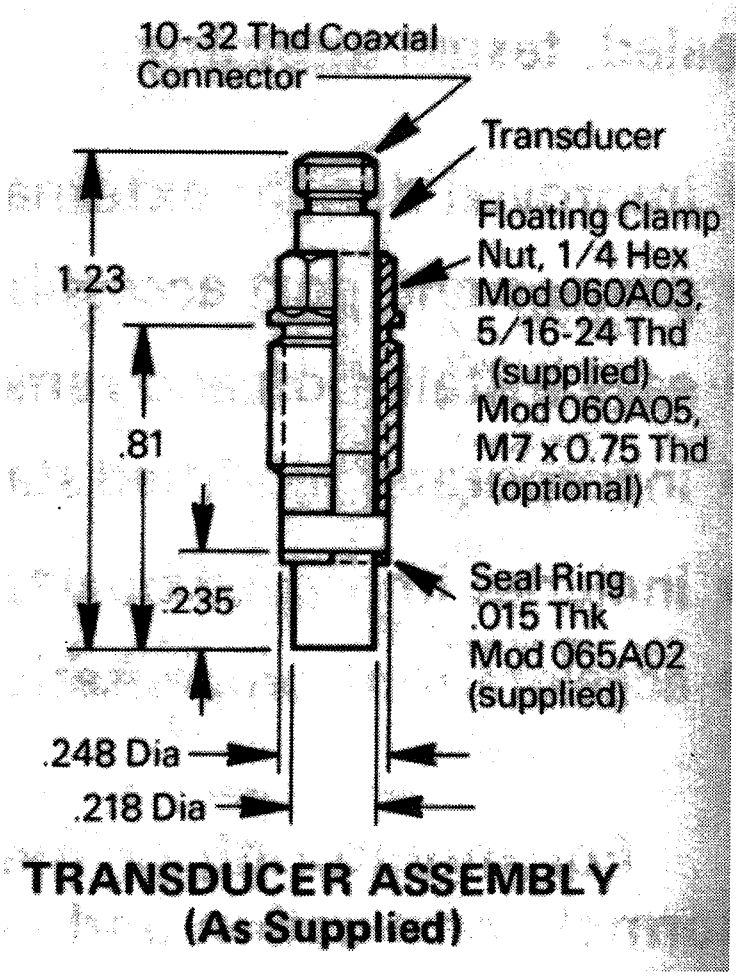

TRANSDUCER ASSEMBLY
(As Supplied)

[redacted] HIGH O/F HOT-FIRE MATRIX

LOX Flow (lbm/s)	Hydrogen Flow (lbm/s)	**O/F Ratio**	Chamber Pressure (psia)	Estimated Flame Temp. (deg R)	**C*-Eff.** (%)	**Instrument Locations** Heat Flux Gauges A & B x = 1in.	x = 3 in.	x = 9 in.	High Frequency Pressure Xdcrs. x = 1in.	x = 3 in.	x = 9 in.	x = 12 in.
0.256	0.04197	**6.1**	295	6160	95.6	x			x			x
0.256	0.00552	**46.4**	262	3435	94.9	x			x			
0.26	0.00252	**103**	249	1765	84.3	x			x			
0.261	0.00157	**166**	301	1100	90.3	x			x			
0.258	0.04859	**5.31**	336	6010	100		x			x		x
0.257	0.00552	**46.6**	258	3425	93.2		x			x		
0.257	0.00266	**96.5**	277	1880	91.5		x			x		
0.257	0.00153	**168**	302	1085	92.7		x			x		
0.259	0.04868	**5.32**	315	6015	95.7			x			x	x
0.246	0.00557	**44.2**	254	3555	93.5			x			x	
0.257	0.00271	**94.8**	264	1910	86.5			x			x	
0.265	0.00155	**171**	308	1060	92.7			x			x	

- **LOX Flowrate Held Constant at 0.25 lbm/s**
- **GH_2 Flow Varied to Achieve Ox-Rich Conditions**

WALL HEAT FLUX ... x = 1 in.

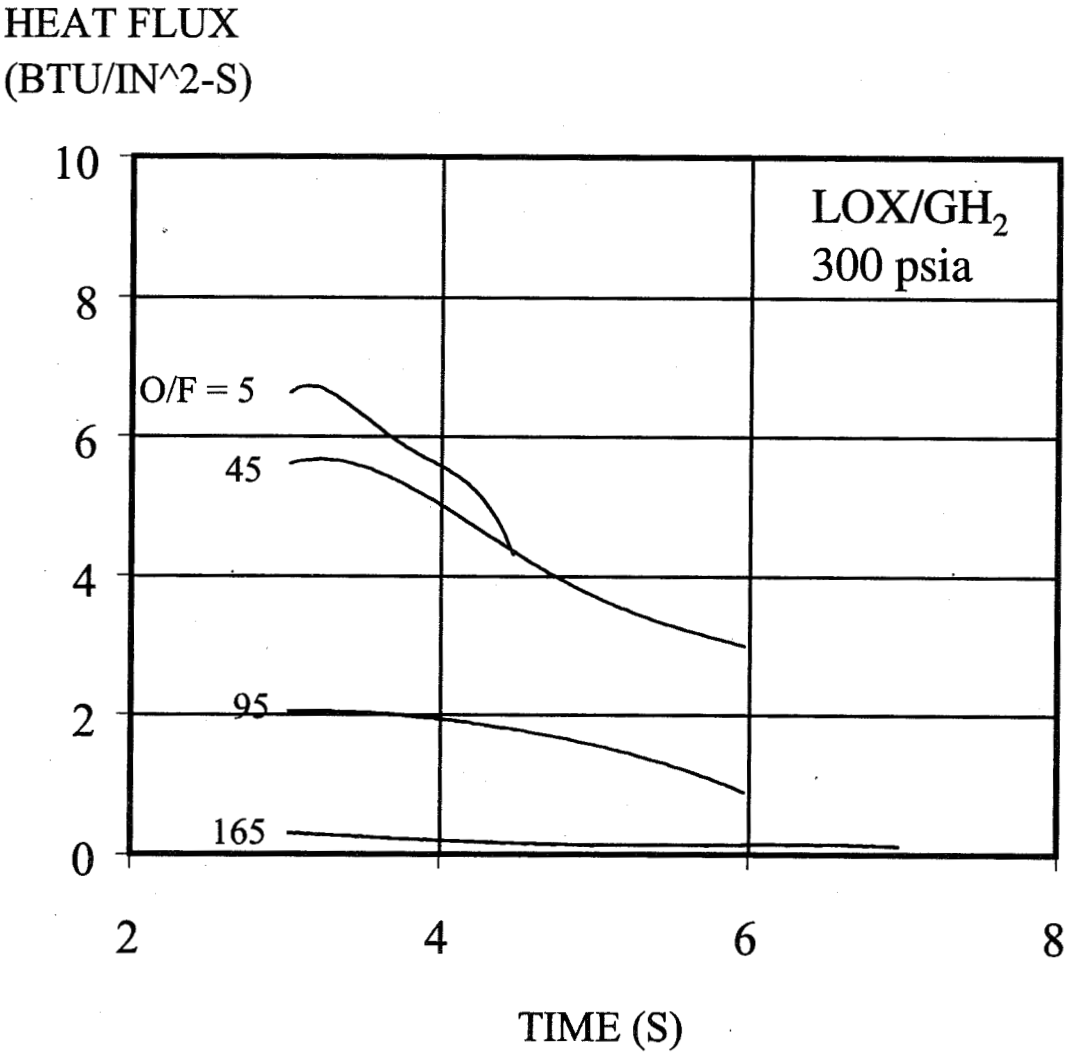

Data is for Steady-State firing period (ignition/shutdown transients excluded)

WALL HEAT FLUX ... x = 9 in.

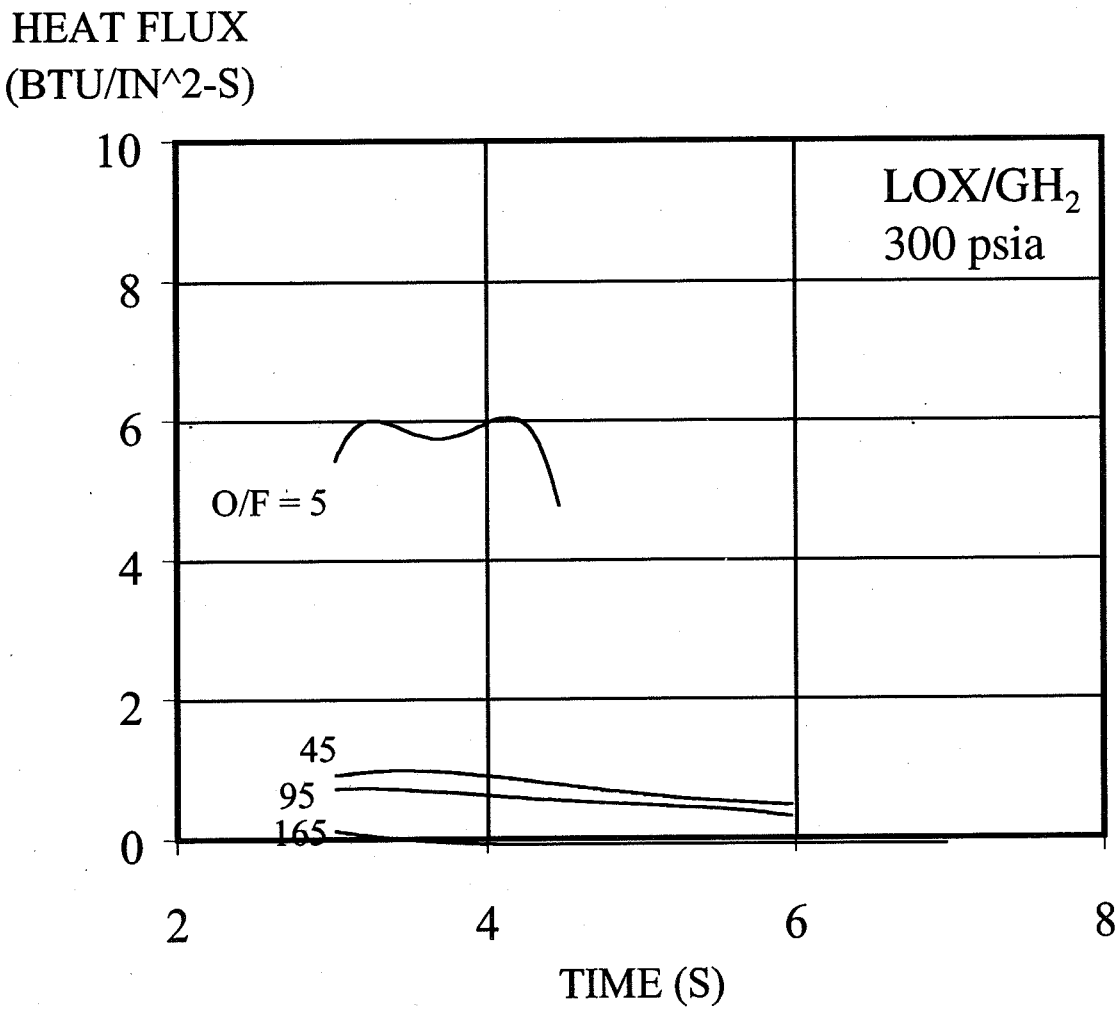

WALL HEAT FLUX vs. O/F

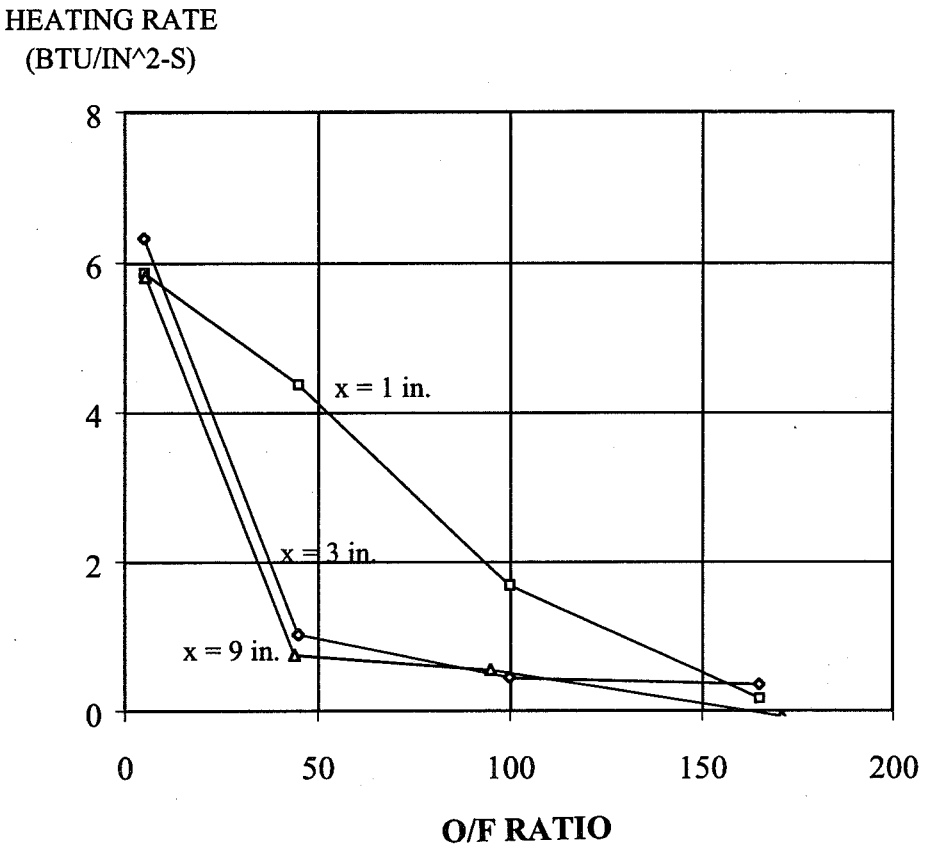

Data Points are Time-Average Values of Heat Flux

- **Heat Flux Decreases with Increasing O/F**
- **Near-Injector Heating Significantly Greater (O/F of 45, 100)**

HEAT FLUX ... Other Work

	PENN STATE	AEROJET ('73)	PRATT & WHITNEY ('91)
INJECTOR	Swirl Coax 1 Element	Swirl Coax 42 Elems.	Swirl Coax 60 Elems.
PROPELLANTS & O/F	LOX/GH_2 5.3	GOX/GH_2 4	LOX/GH_2 6
LOX FLOW (lbm/s)	0.25	n/a	1
P_c (psia)	300	300	1780
HEAT FLUX (Btu/in^2-s)	6	7.5	25

- Chamber Heat Flux Compared to Other Work
  - Compares to Aerojet Result
  - Penn State Heat Flux Scales With Element Flowrate to 18 Btu/in^2-s for 1 lbm/s Element (25 Btu/in^2-s for P&W)

HIGH FREQ. PRESSURE DATA

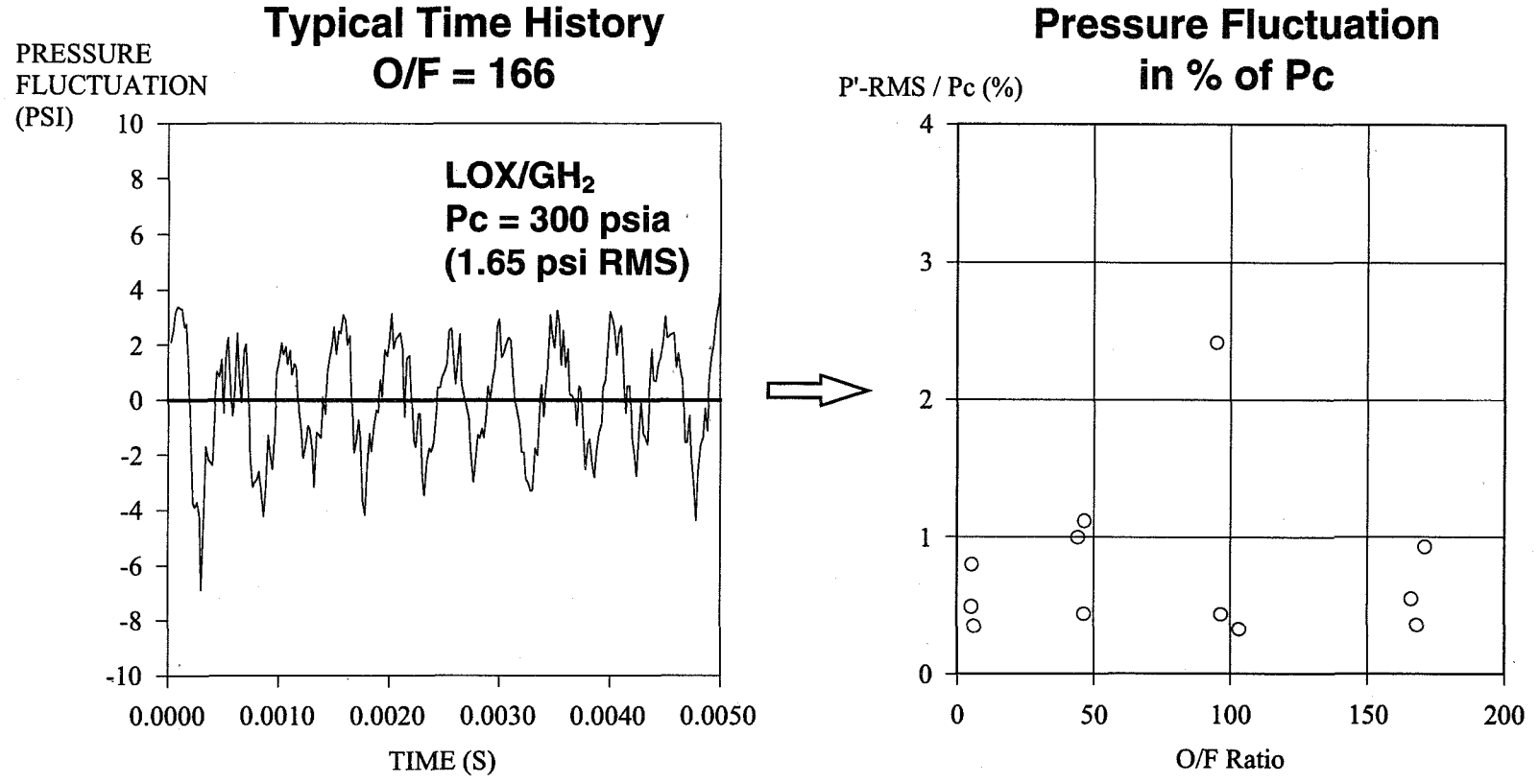

- **Low-Level Pressure Fluctuations Observed for all O/F**
  - **RMS Less Than 1% of Pc**
  - **Longitudinal Modes (Low Freq. < 3000 Hz Typ.)**

[redacted] CHAMBER RESONANT FREQS.

O/F Ratio	P'-rms Pc (%)	Resonant Frequency Observed (Hz) at Different Positions				Predicted Freq. (Hz)
		x = 1 in.	x = 3 in.	x = 9 in.	x = 12 in.	
6.1	0.35	6476			none	2360 (1L)
5.31	0.49		6534		-	7140 (3L)
5.32	0.80			**6580**	-	
46.4	0.44	1279			1279	
46.6	1.12		**1291**		-	1240 (1L)
44.2	1.00			**1309**	-	
103	0.33	931			931	
96.5	0.44		1154		1154	910 (1L)
94.8	**2.42**			**1740, 1975, 5081**	-	
166	0.55	2032			2032	690 (1L)
168	0.36		2029		-	2070 (3L)
171	0.93			**1987**	-	

- **1st and 3rd Longitudinal Modes Observed**

SUMMARY

- **Uni-Element Hot-fire Results (LOX/GH_2)**
  - **Oxygen-Rich Ignition/Combustion Achieved with LOX in Uni-Element Rocket: $5 < O/F < 170$**
  - **Observed Flameholding at LOX Post**
  - **LOX Region Visualized in Flame at O/F = 5.7**
  - **Oxygen-Rich: C*-Efficiency > 92%**
  - **Near-Stoich.: C*-Efficiency > 96%**
  - **Chamber Heat Flux Characterized at P_c = 300 psia (800 psi Tests in Progress)**
  - **Smooth Combustion in Uni-Element Rocket, Fluctuations ~ 1% of P_c for 300 psia tests**

Computational Fluid Dynamic Analyses of of Oxygen-Rich Preburners Utilizing Secondary Dilution

Jeffrey M. Grenda and Charles L. Merkle

Propulsion Engineering Research Center
Department of Mechanical Engineering
The Pennsylvania State University

POTENTIAL FULL-FLOW PREBURNER DESIGNS

- Direct Injection
  - Fuel Burned with Full Oxidizer Flow Rate
  - High O/F Combustion
- Downstream Dilution
  - Fuel Burned at Near-Stoichiometric Conditions
  - Remaining Oxidizer Injected Downstream
- Design Issues:
  - Geometry and Method of Downstream Dilution
  - Mixing and Uniformity of Exit Flow
  - Ensure Vaporization of All Liquid
  - Effects of Operating Conditions

PRE-BURNER SCHEMATIC

- Near Stoichiometric Combustion Produces High Temperatures
- Diluted By Injection of Liquid Oxidizer Downstream

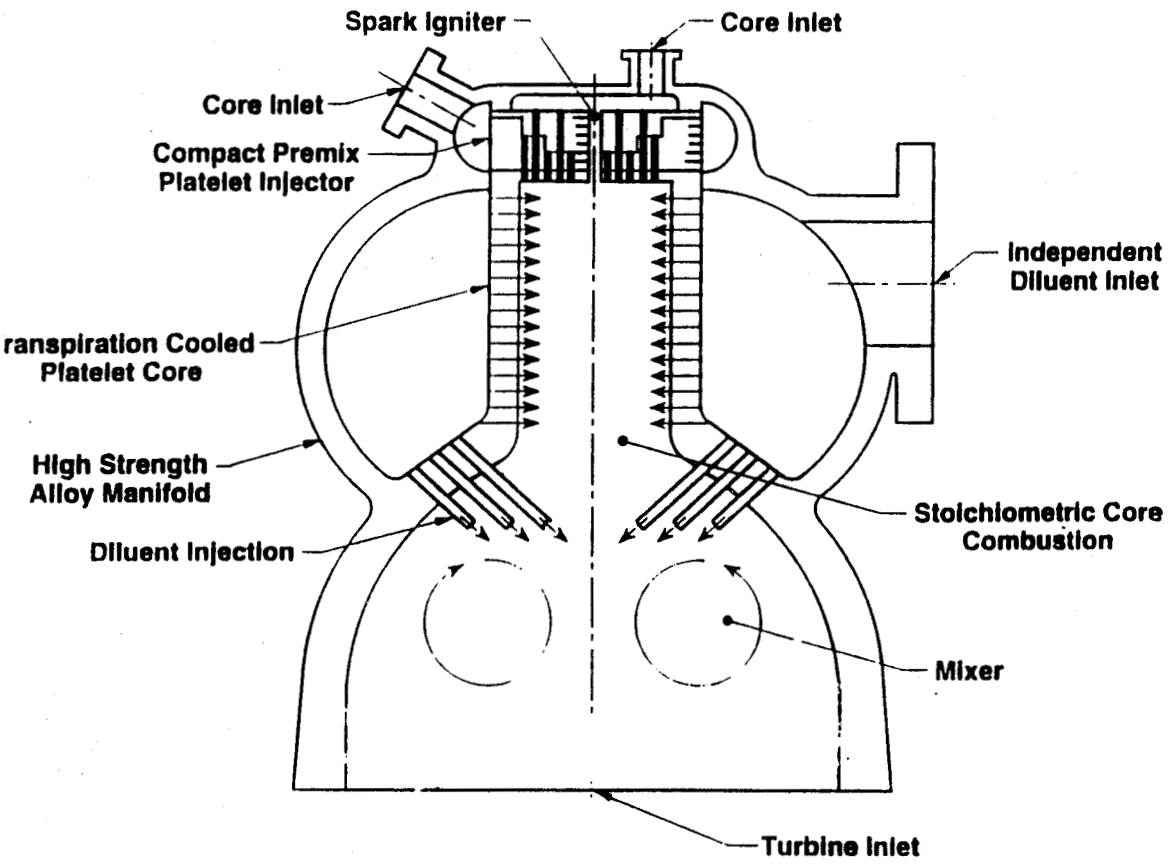

RESEARCH GOALS

- Use CFD as Preliminary Design Tool
  - Screen Various Geometrical Configurations
  - Identify Appropriate Parameter Ranges
  - Define Subscale Experiments
    - Geometrical Configuration
    - Parameter Ranges

- Validation of CFD Procedure
  - Compare Vaporization Predictions with Measurements
  - Assess Reliability of CFD Predictions

- Predict Full-Scale Performance
  - Address Experimental Scale-Up Issues
  - Project Pros and Cons of Various Configurations
  - Identify Important Design Parameters
  - Define Appropriate Operating Regimes

PRESENT STATUS

- Configurations Considered:
  - Axial Injection From Faceplate
  - Radial Injection From Outer Wall
  - Recessed Stoichiometric Core/Chamber

- Operating Conditions Tested:
  - O/F Ratio Variations
  - Liquid Injection Characteristics
  - Gas Phase Composition and Character
  - Chamber Length/Radius

BASIC PRE-BURNER GEOMETRIES

- **Radial Injection From Outer Wall:**

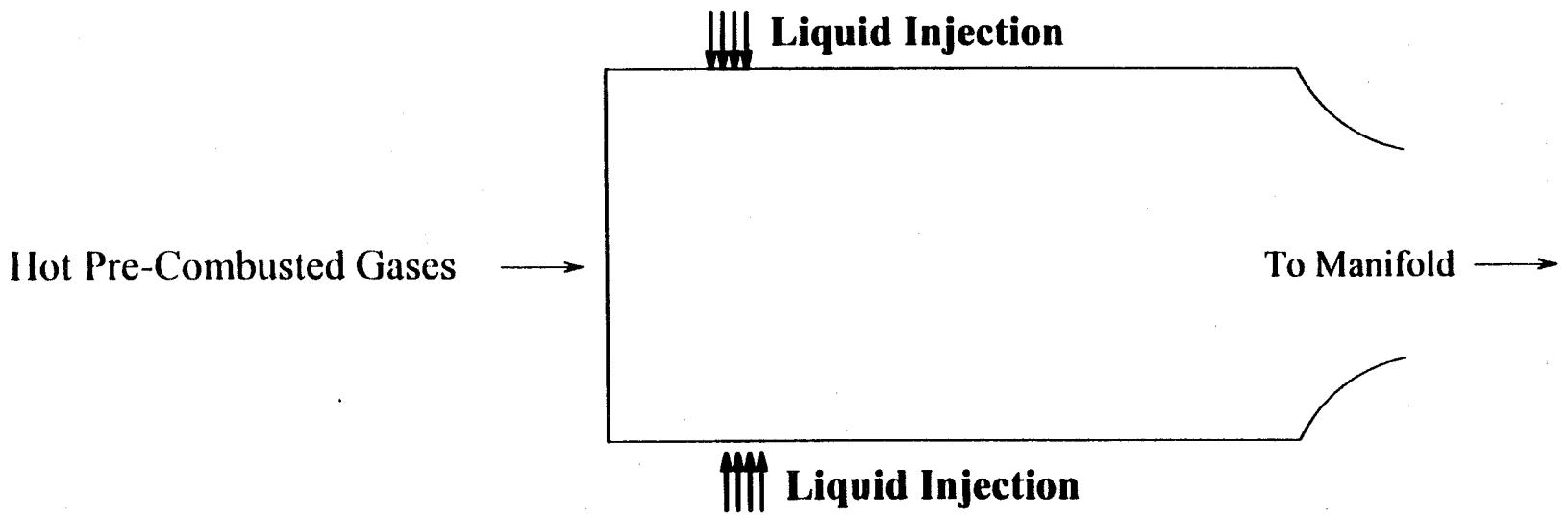

- **Liquid Injected Inward From Wall Injectors**
  - Liquid Injected Either Perpendicular or Canted
  - Initial Drop Sizes and Velocities Stochastic

BASIC PRE-BURNER GEOMETRIES

- **Axial Injection Geometry:**

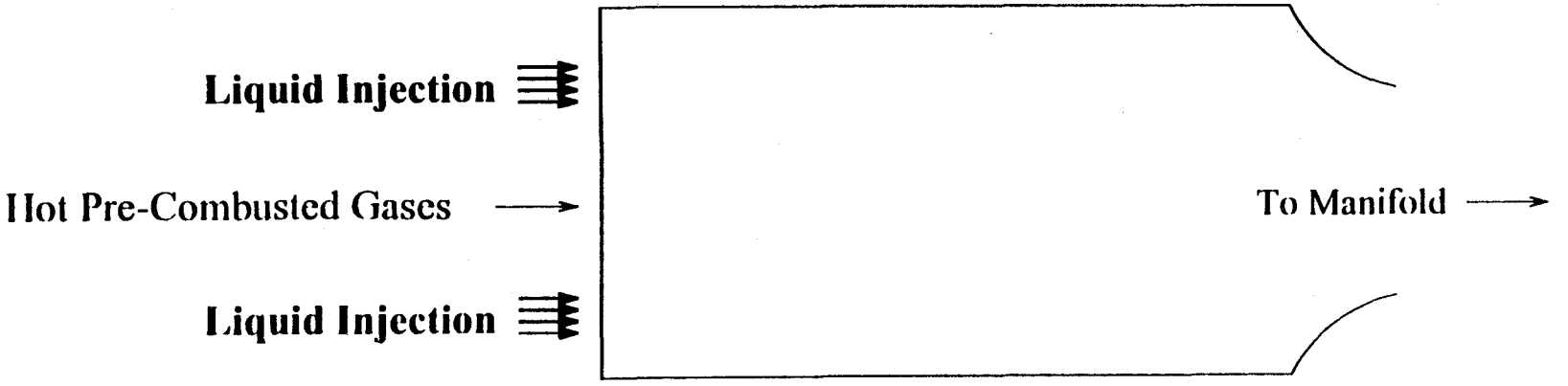

- **Liquid Injected Axially From Injector Faceplate**
  - Atomization is Treated Empirically (Mean Drop Size)
  - Initial Drop Sizes and Velocities Stochastic

BASIC PRE-BURNER GEOMETRIES

- **Axial Injection Including Detailed Core Region:**

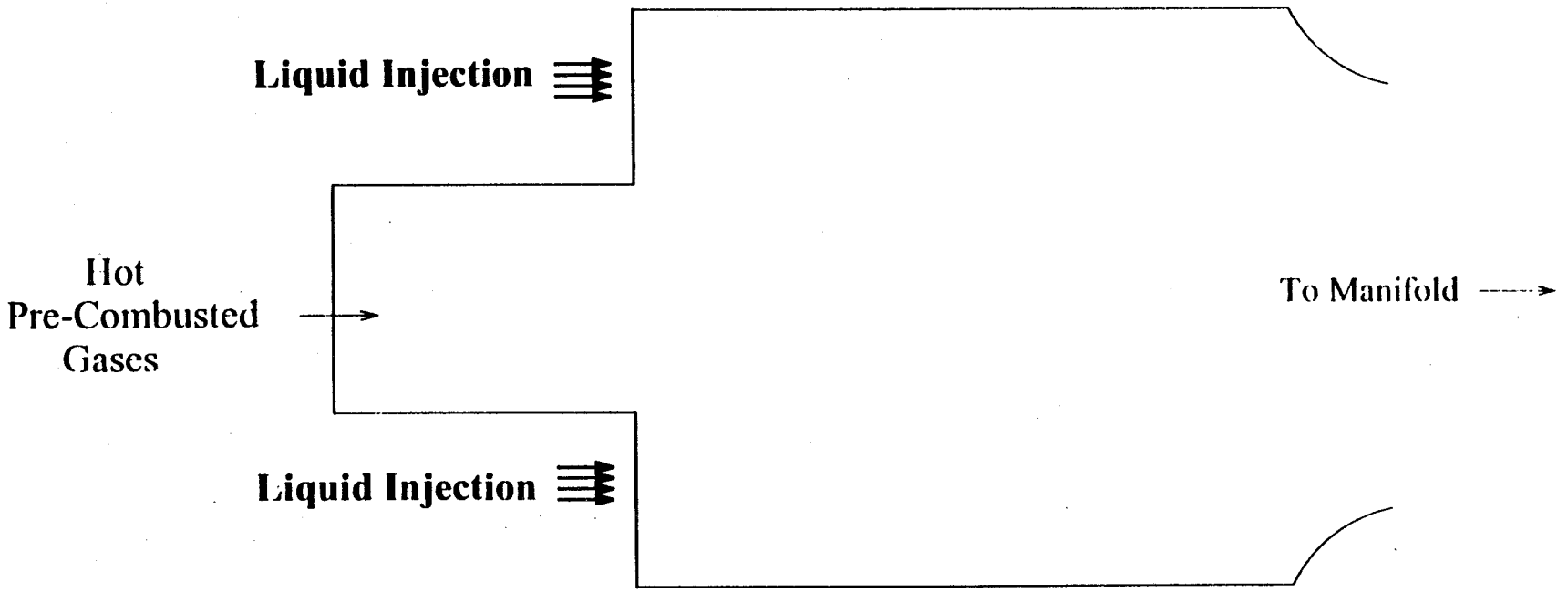

- **Main Chamber Forms an Equivalent Backstep**
  - **Liquid Injected Either Axially or Canted**
  - **Initial Drop Sizes and Velocities Stochastic**

GAS PHASE MODELING

- Gas Phase Treated in Eulerian Fashion
  - Preconditioned Navier-Stokes Equations/Species Transport
  - k-e Turbulence Modeling

$$\Gamma \frac{\partial Q}{\partial t} + \frac{\partial E}{\partial x} + \frac{1}{r}\frac{\partial Fr}{\partial y} = H_{gas} + H_{liq} + L(Q_v)$$

- Requires Liquid Phase Coupling Source Terms
- Solved Implicitly for Robustness (ADI or LGS Algorithm)
- Gas Phase Solution Procedure Well-Validated Against Experimental and Analytical Solutions

DESCRIPTION OF LIQUID PHASE PROCESSES

- Injection
  - Distributed Over Finite Region
  - "Axisymmetric" Injector; 3-D Drop Velocities
  - Injector "Cone" Angle Specified
- Atomization
  - Specify Droplet Size
    - Mean: Experimental Observations; Δp
    - Distribution: Upper Limit
  - Specify Droplet Velocity
    - Mean: Determined by Injector Δp
    - Distribution: Random Function--Experimental Observation

      Typical: $u = \bar{u} \pm 10\% \bar{u}$

      $v = \pm 10\% \bar{u}$

      $w = \pm 10\% \bar{u}$

DROPLET DISTRIBUTION FUNCTIONS:

- **Droplet Size Distribution is Represented by Several Models:**
  - **Upper-Limit Distribution Function**
  - **Experimental Measurements**
- **Number Distribution f(d) and Mass Distribution g(d)**
- **Liquid Partitioned into Various Droplet Sizes**

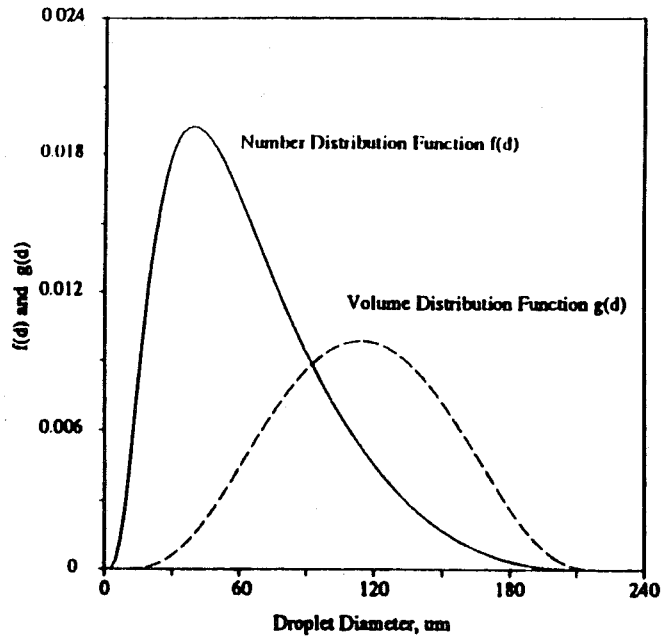

LIQUID PHASE VALIDATION:

- **Trajectories Validated By Comparison With Analytical Solutions**

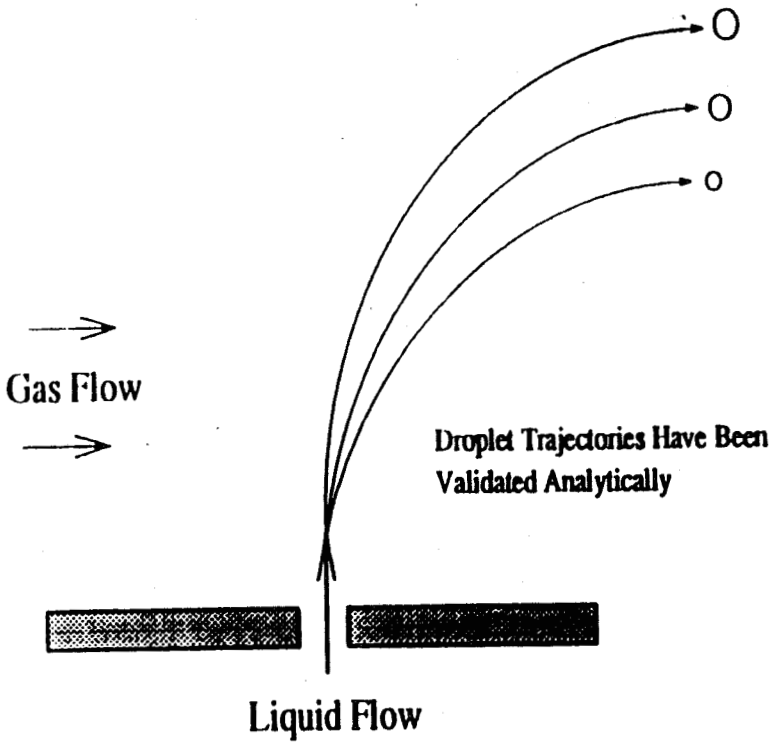

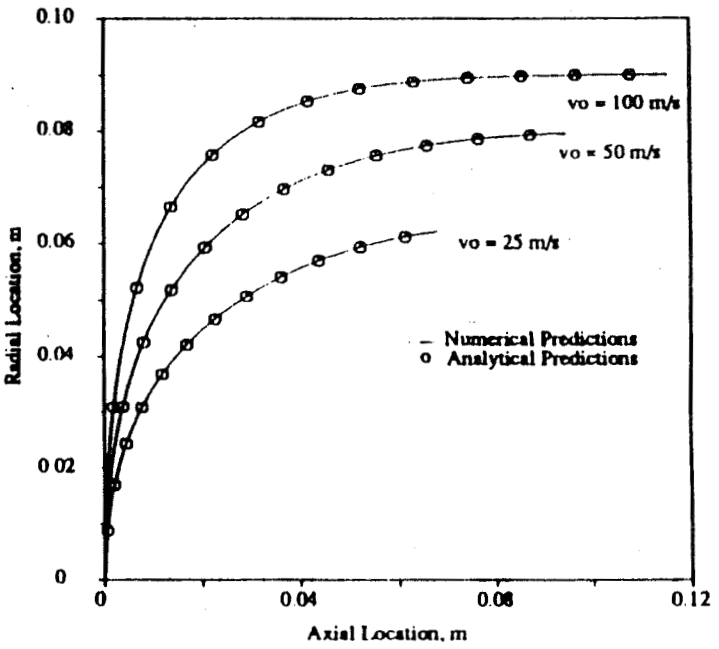

LIQUID PHASE VALIDATION:

- **Droplet Vaporization Rate Validated by Comparison With Detailed Numerical Solutions for Single Droplet**

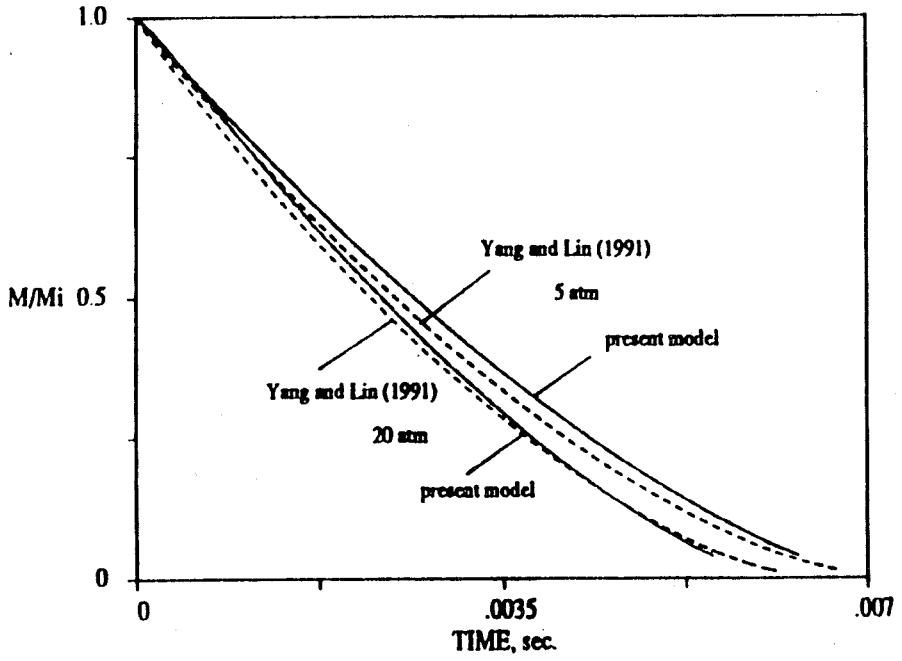

LIQUID PHASE VALIDATION:

- **Droplet Vaporization Rate Compares Well With Experiments**

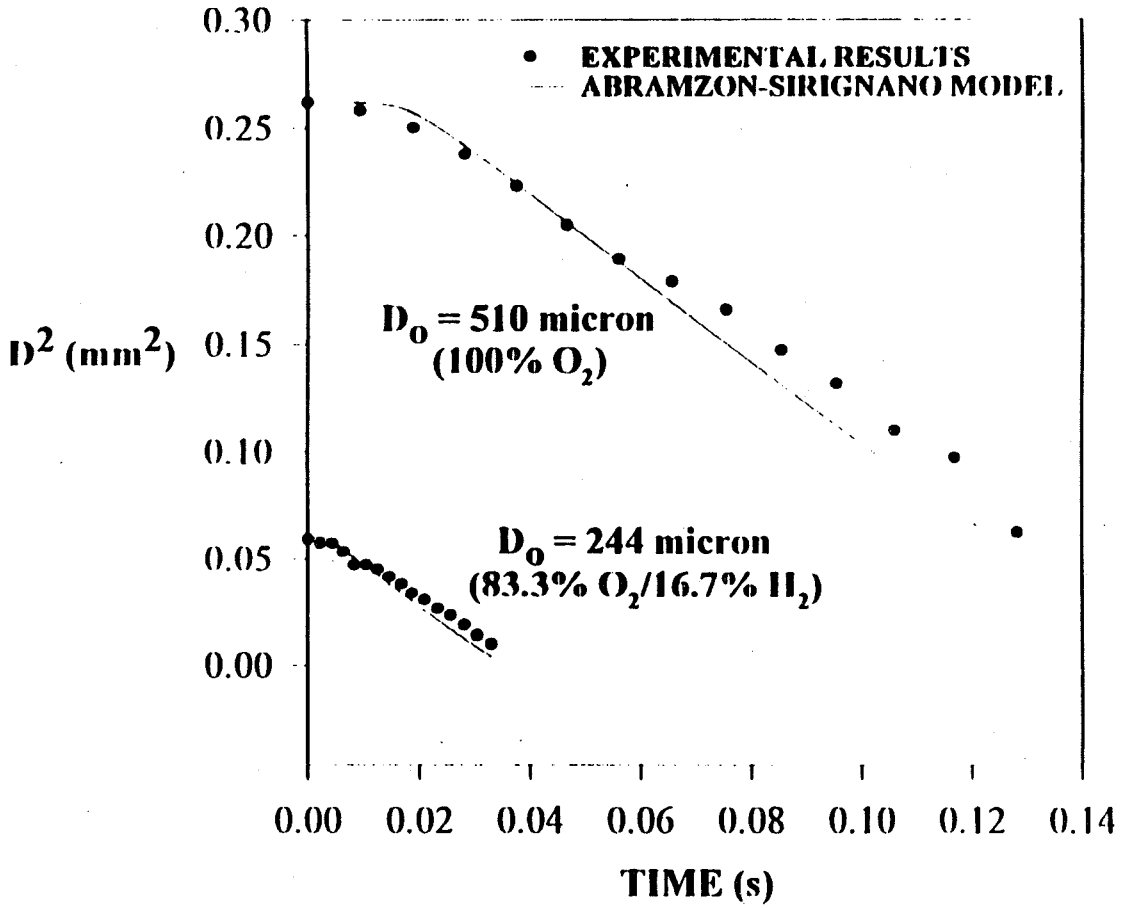

BASIC PRE-BURNER GEOMETRIES

- **Radial Injection From Outer Wall:**

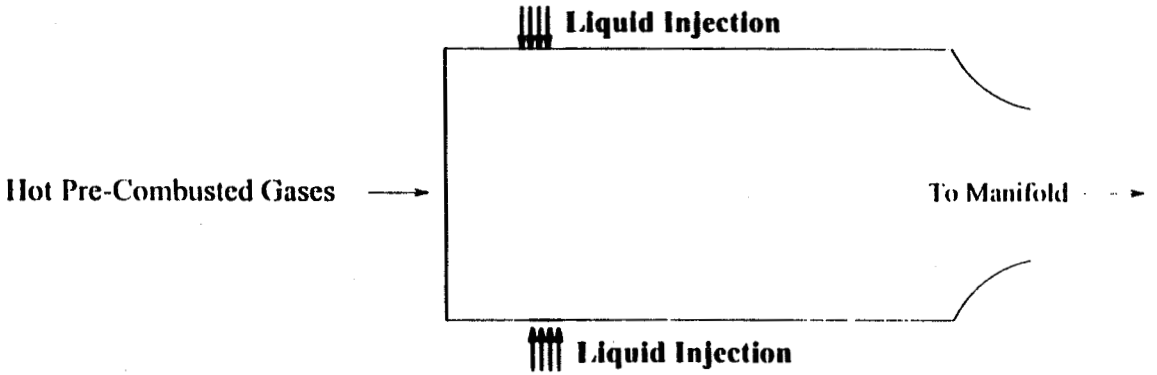

- **Axial Injection Geometry:**

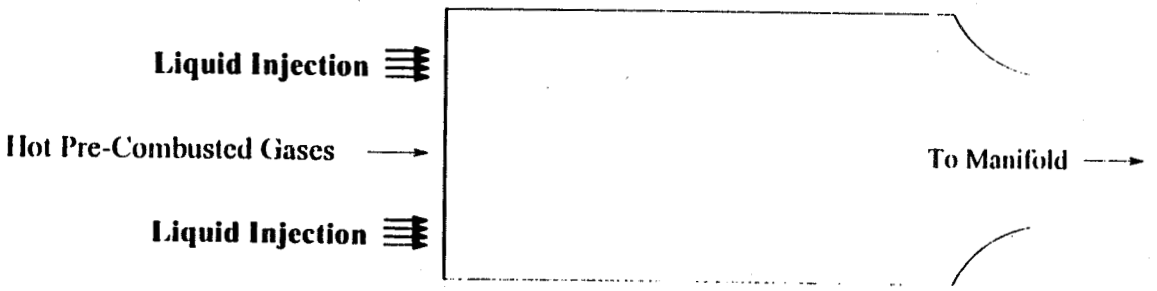

- **Axial Injection Including Detailed Core Region:**

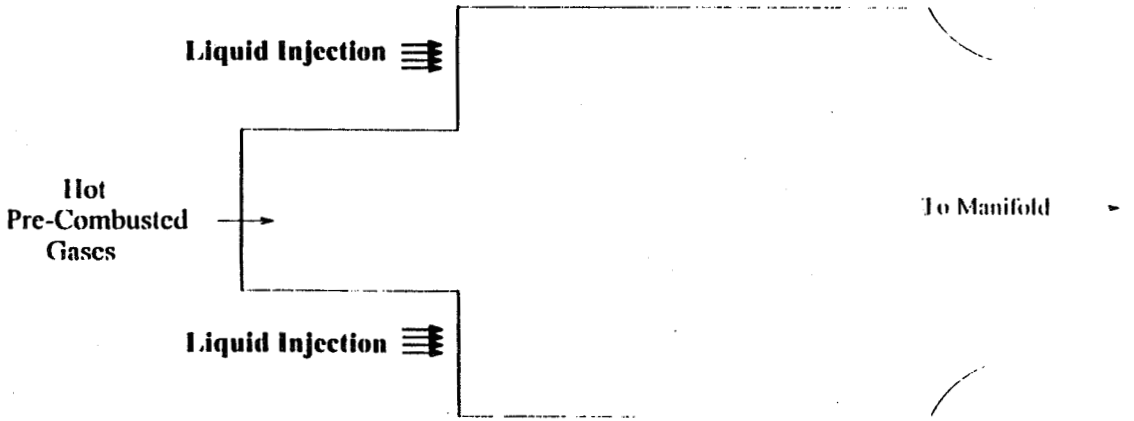

NOMINAL CONDITIONS:

- **Operating Conditions:**
  - Chamber Diameter of 9"
  - Injector O/F Ratio 10 (3365 K)
  - Core Mass Flow Rate 8.5 kg/sec
  - Average Gas Velocity 100 m/s
- **Design Parameters Considered:**
  - Overall Dilution O/F Ratio
  - Liquid Injection Velocity
  - Injected Droplet Diameter
  - Gas Phase Mass Flow Rate/Velocity
  - Liquid Injection Spray Angle

• PARAMETRIC RESULTS—RADIAL INJECTION

O/F Vinj	80	150	180
80	x	x x (Vjet = 50)	x
100		x x (d32 = 100)	x
100		x x (d32 = 100)	x

VARIATION IN O/F RATIO:

- Operating Conditions:
  - Injector O/F Ratio: 10 (3365 K)
  - Inlet Gas Velocity: 100 m/s
  - Mean Droplet Diameter: 150 um
  - Liquid Injection Velocity: 80 m/s (20% dP)
- Vary Parameter:
  - Downstream O/F: 80 to 180
- Exit Flowfield Similar for All O/F Ratio
  - Colder Near Walls
  - Uniformity Increases With Axial Distance

Gas Temperature for LOX-Rich Preburner (Peripheral Injection Geometry)

Overall O/F = 150
V_{inj} = 80 m/s
d_{32} = 150 μm
U_{gas} = 50 m/s

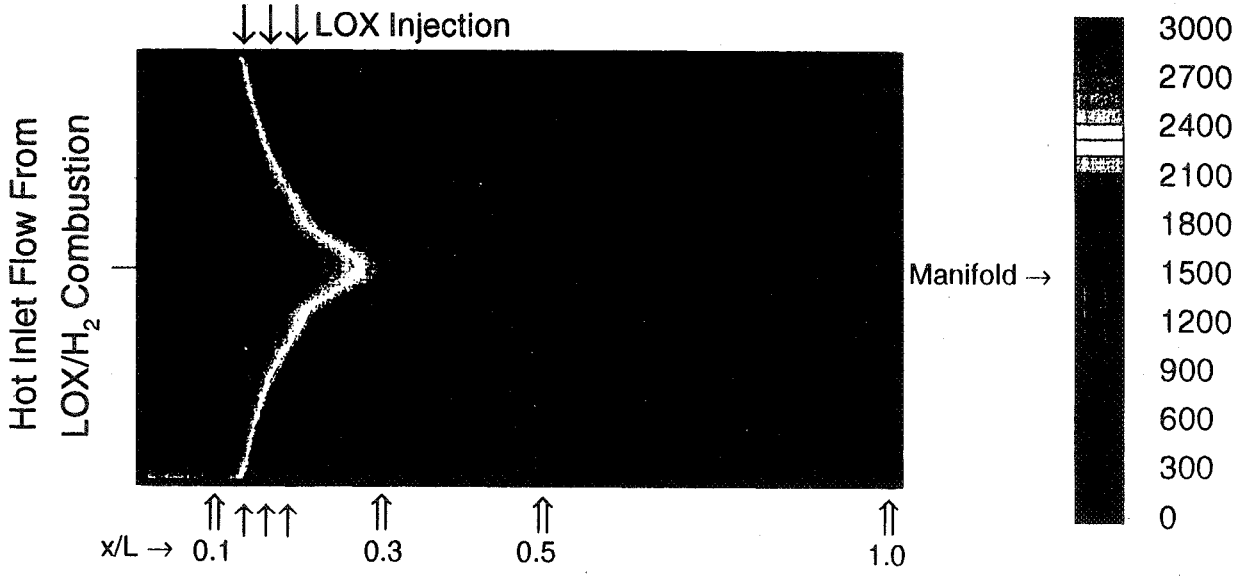

Cross-Sections of Gas Temperature

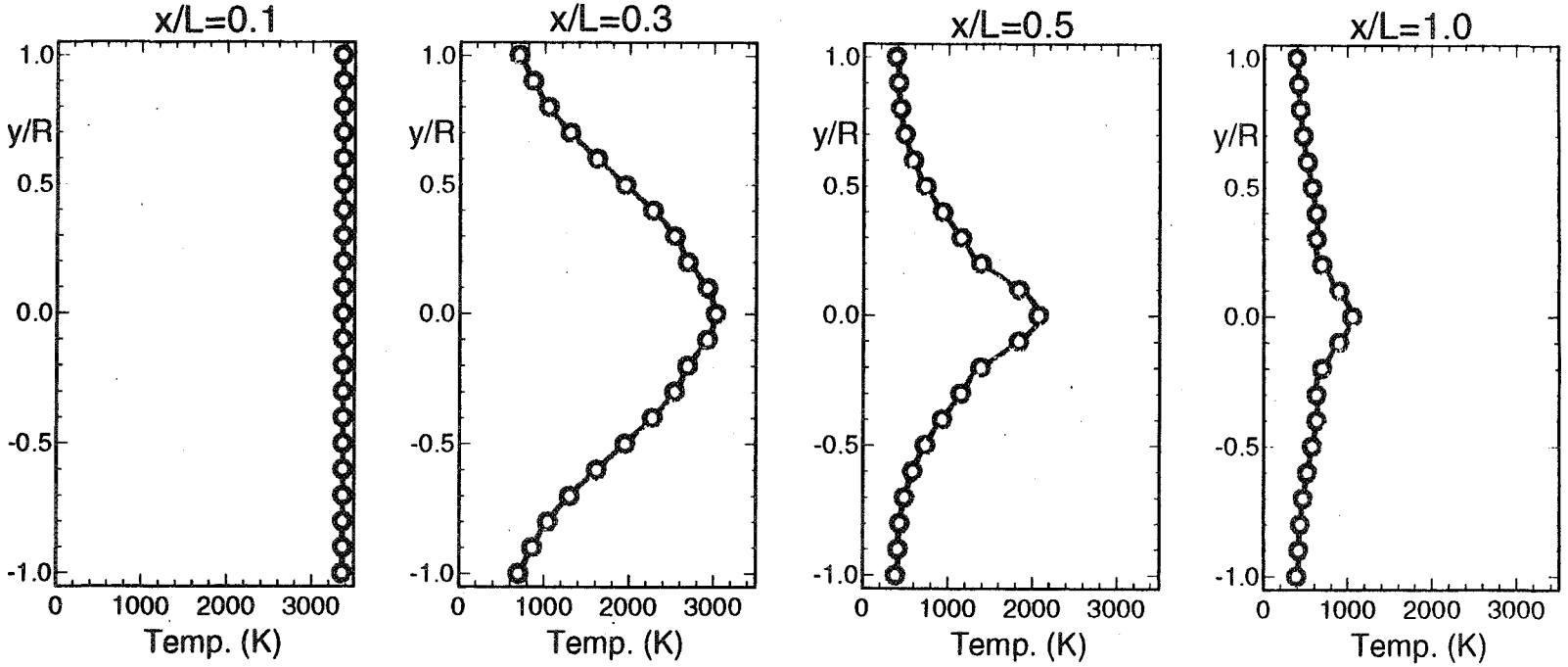

Gas Temperature for LOX-Rich Preburner (Peripheral Injection Geometry)

Overall O/F = 150
V_{inj} = 80 m/s
d_{32} = 150 μm
U_{gas} = 100 m/s

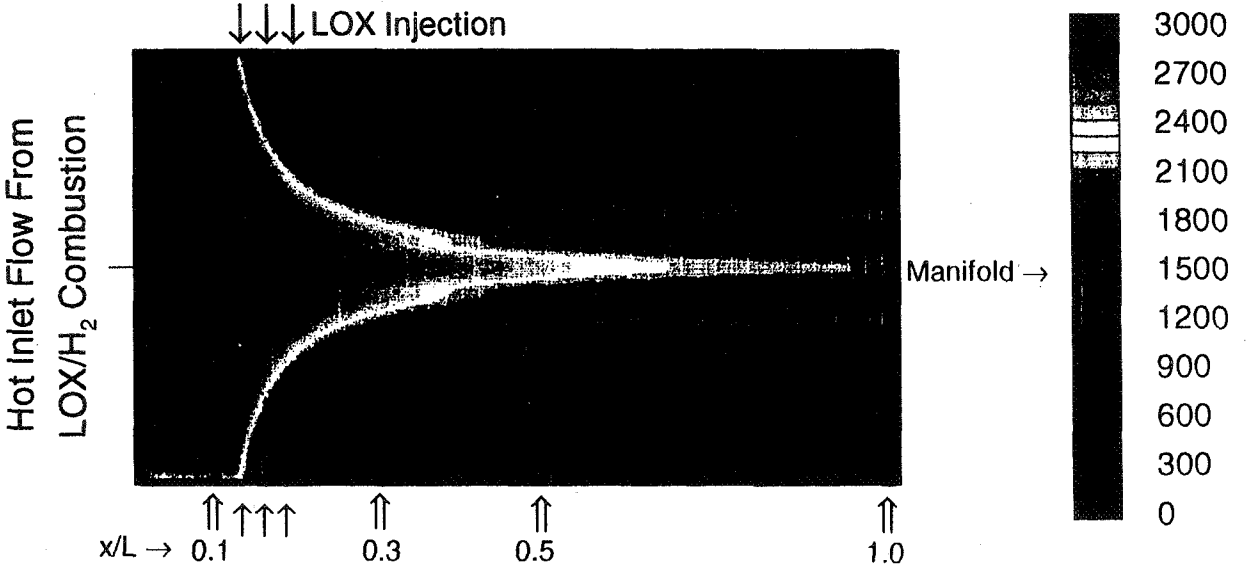

Cross-Sections of Gas Temperature

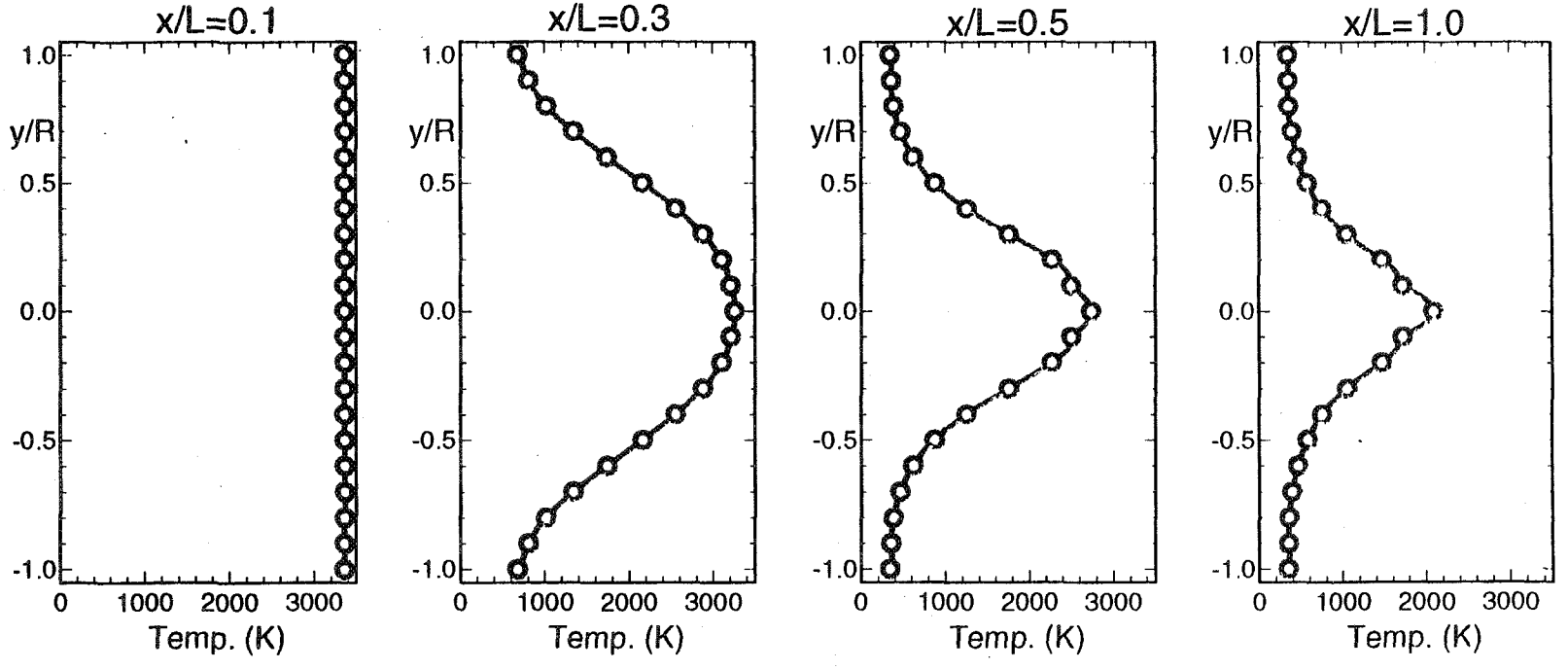

RADIAL INJECTION SUMMARY

	O/F	Vinj	d32
Best Case	**180**	**120**	**150**
Worst Case	**150**	**100**	**100**

Gas Temperature for LOX-Rich Preburner (Peripheral Injection Geometry)

Overall O/F = 180

V_{inj} = 120 m/s

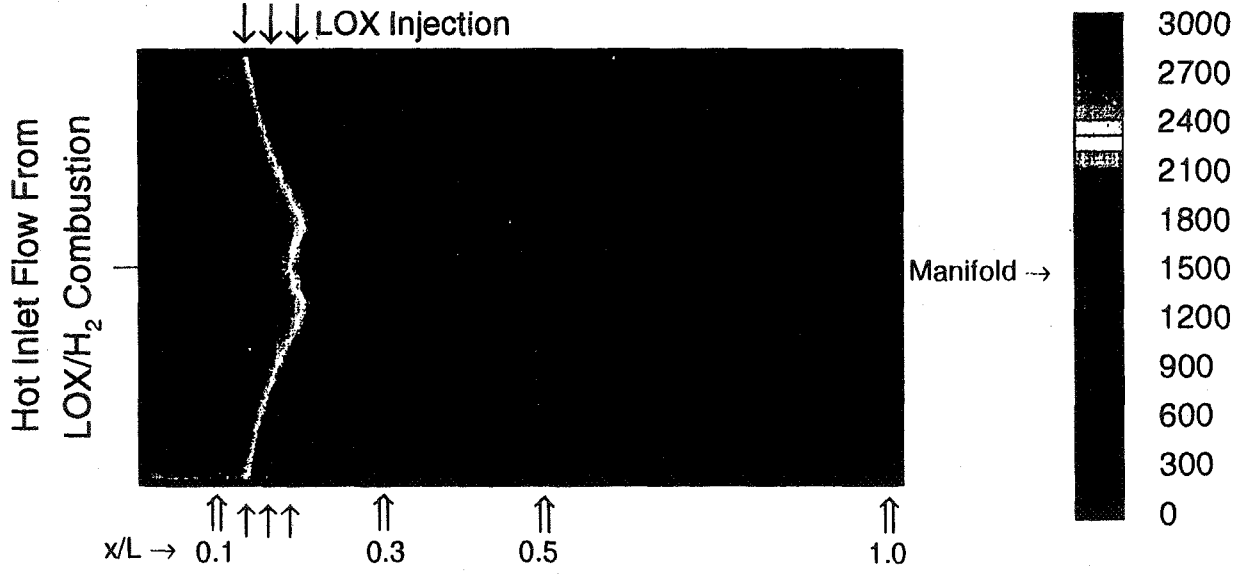

Cross-Sections of Gas Temperature

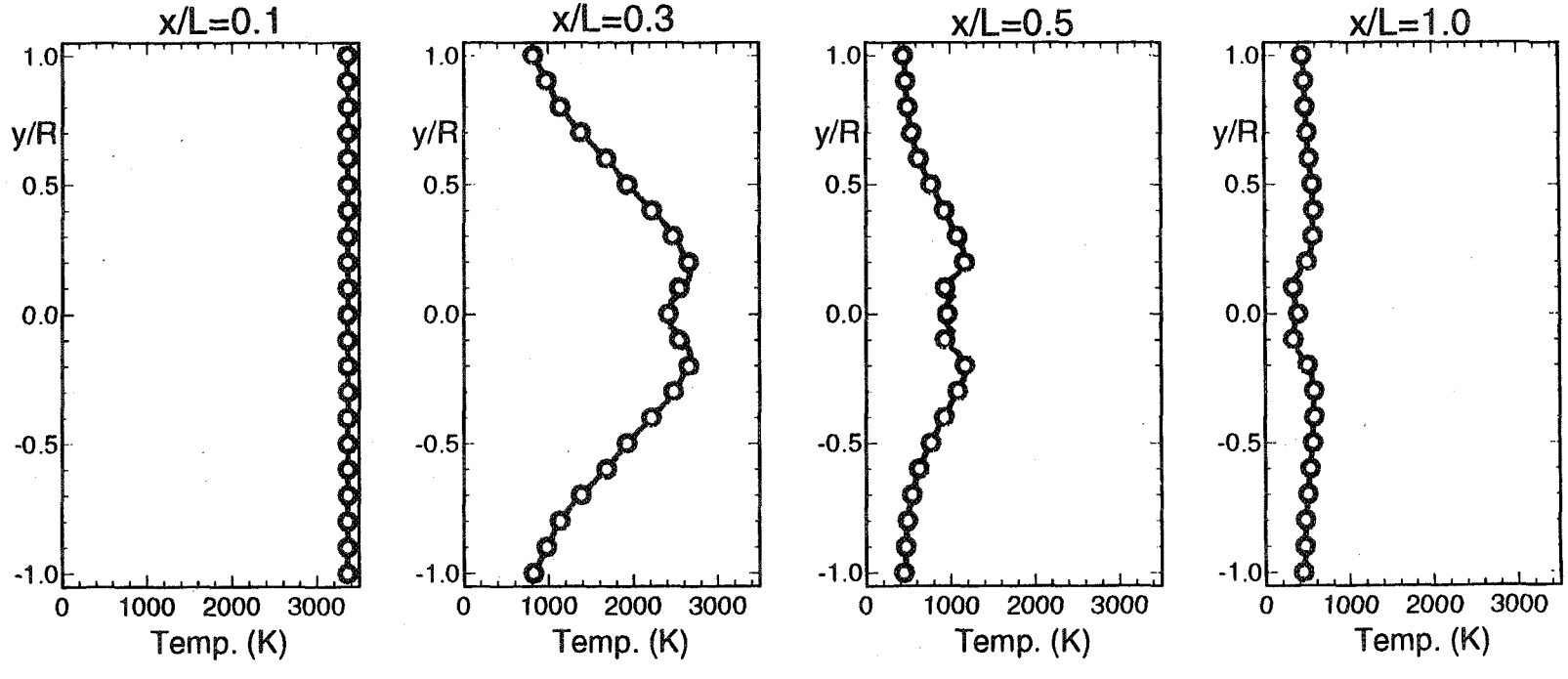

Gas Temperature for LOX-Rich Preburner (Peripheral Injection Geometry)

Overall O/F = 150

V_{inj} = 100 m/s

d_{32} = 100 μm

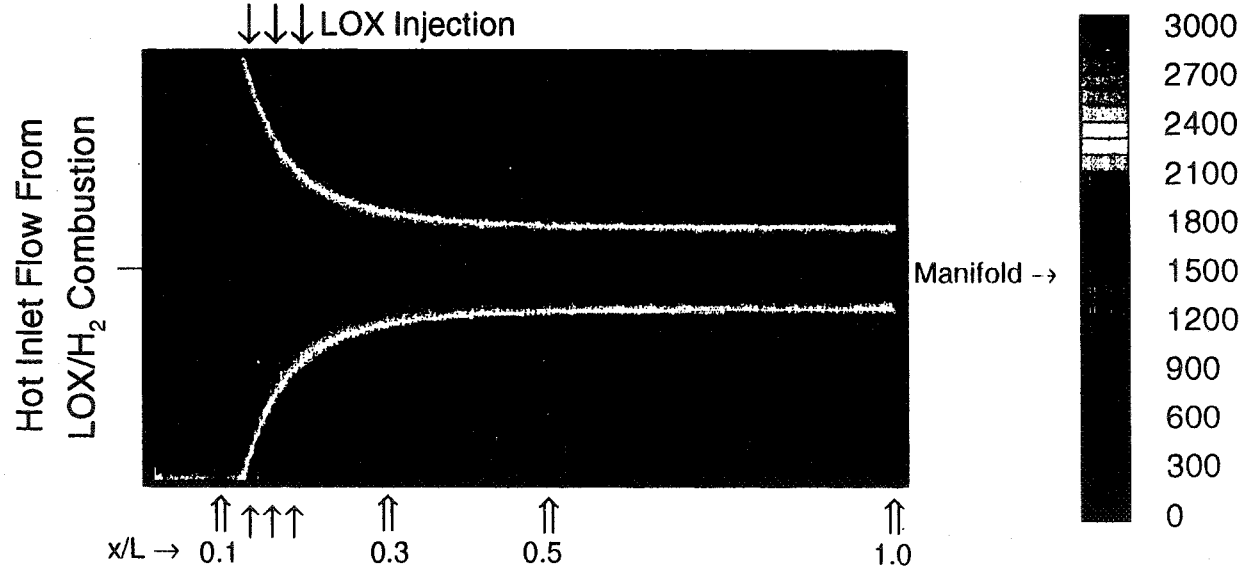

Cross-Sections of Gas Temperature

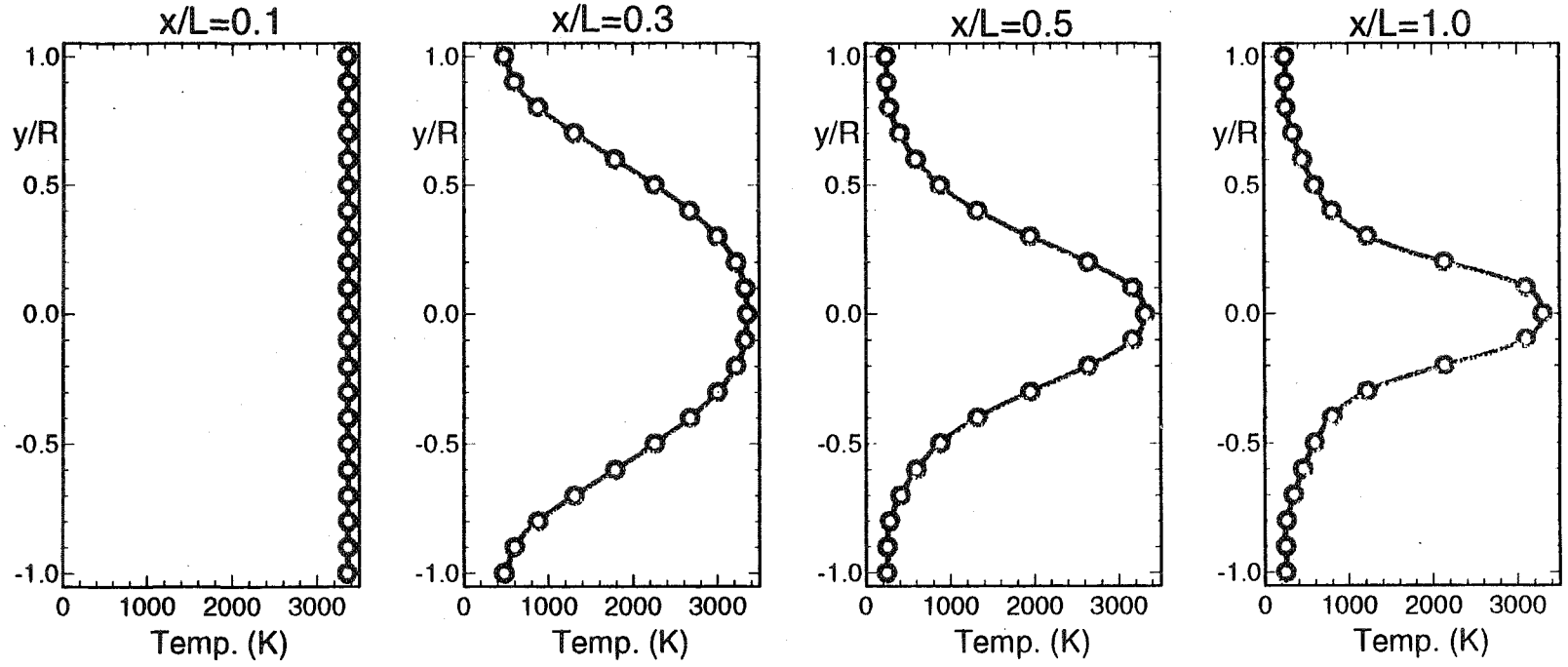

Schematic of Preburner Geometry

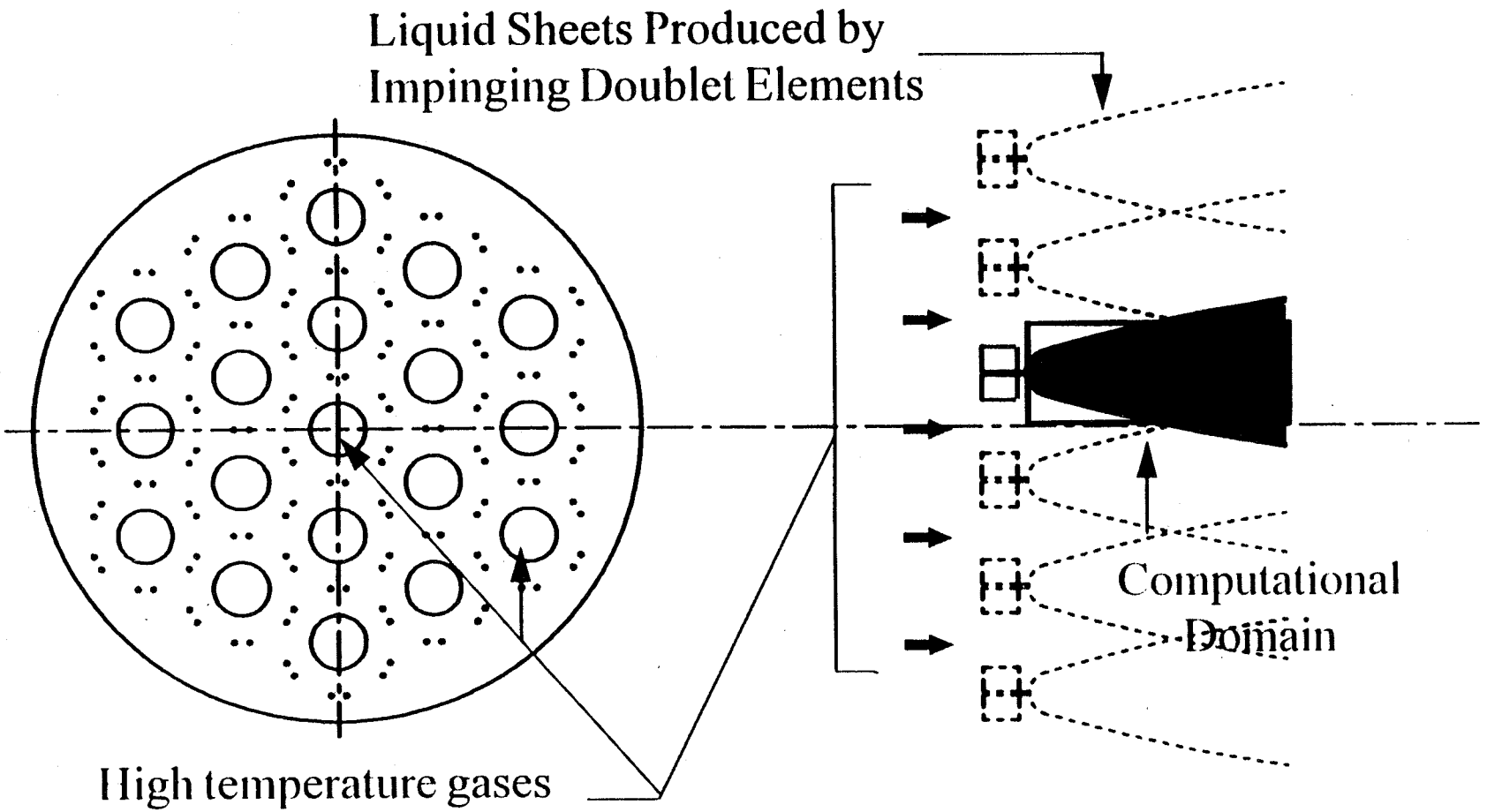

AXIAL INJECTION SUMMARY

	O/F	Vinj	Angle
Best Case	**120**	**60**	**45**
Worst Case	**80**	**30**	**30**

Gas Temperature for LOX-Rich Preburner (Axial Injection Geometry)

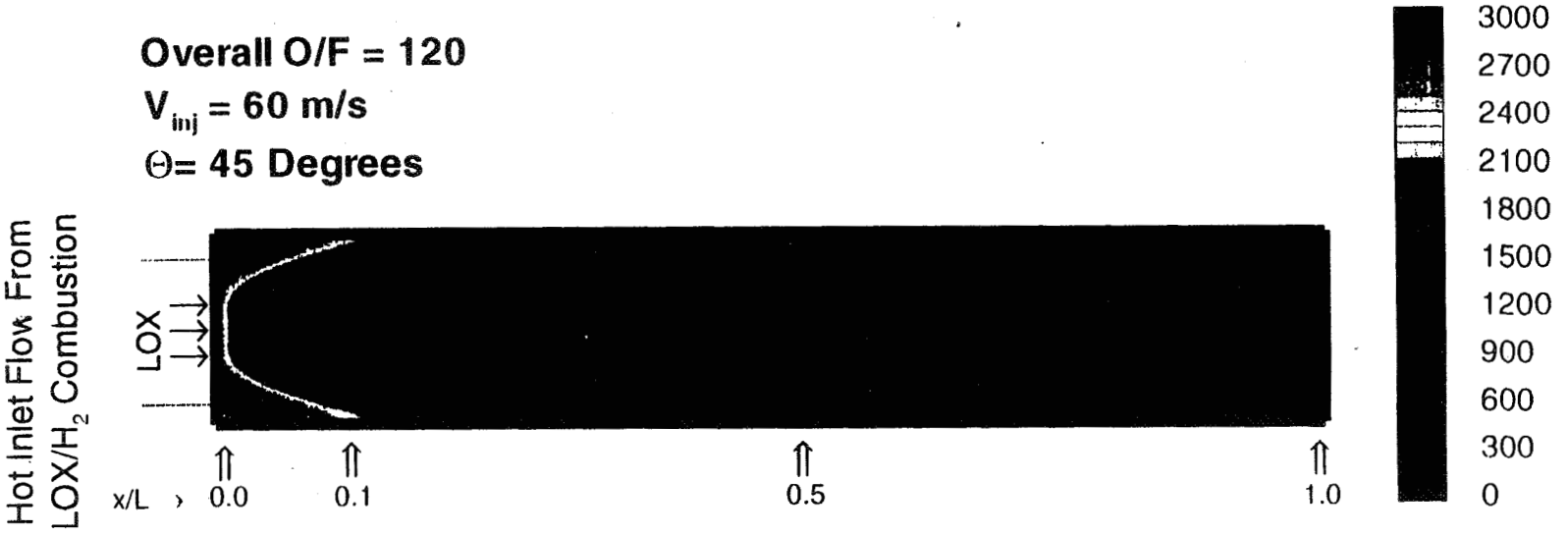

Cross-Sections of Gas Temperature

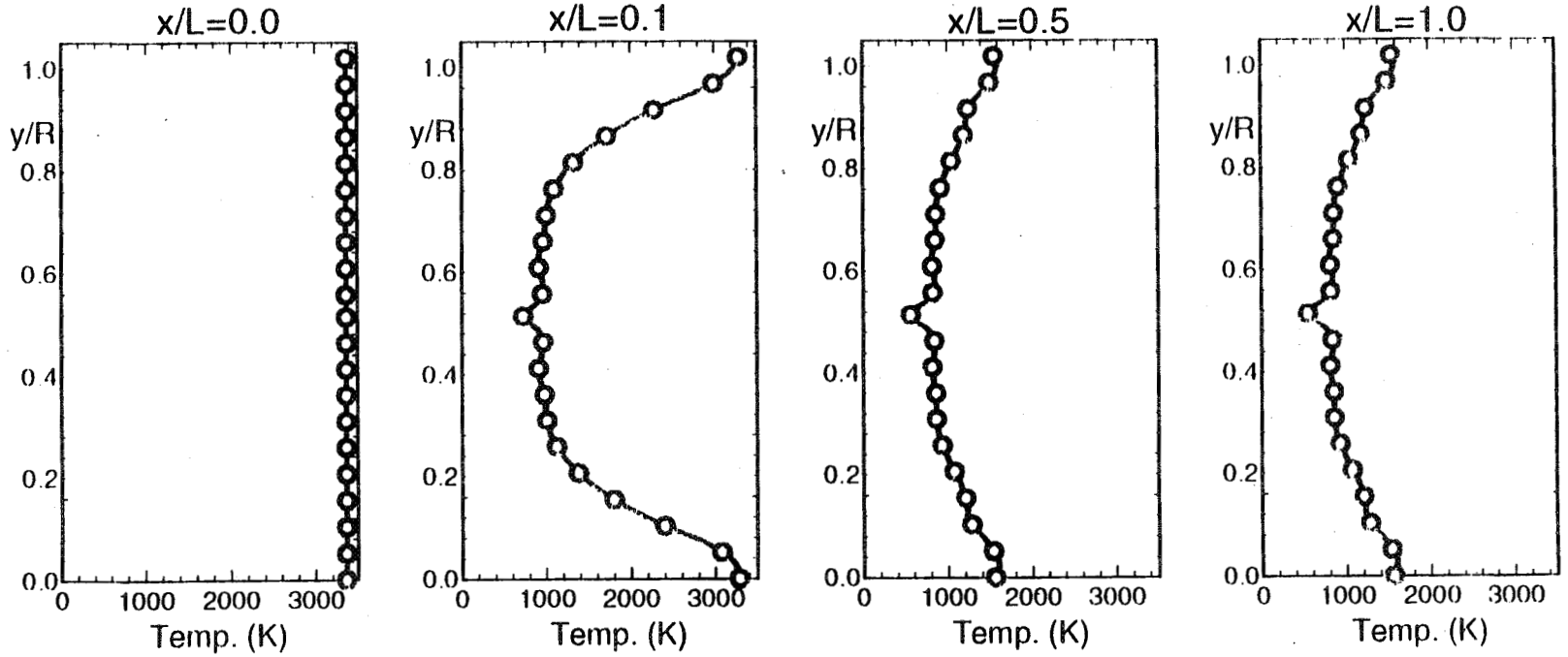

Gas Temperature for LOX-Rich Preburner (Axial Injection Geometry)

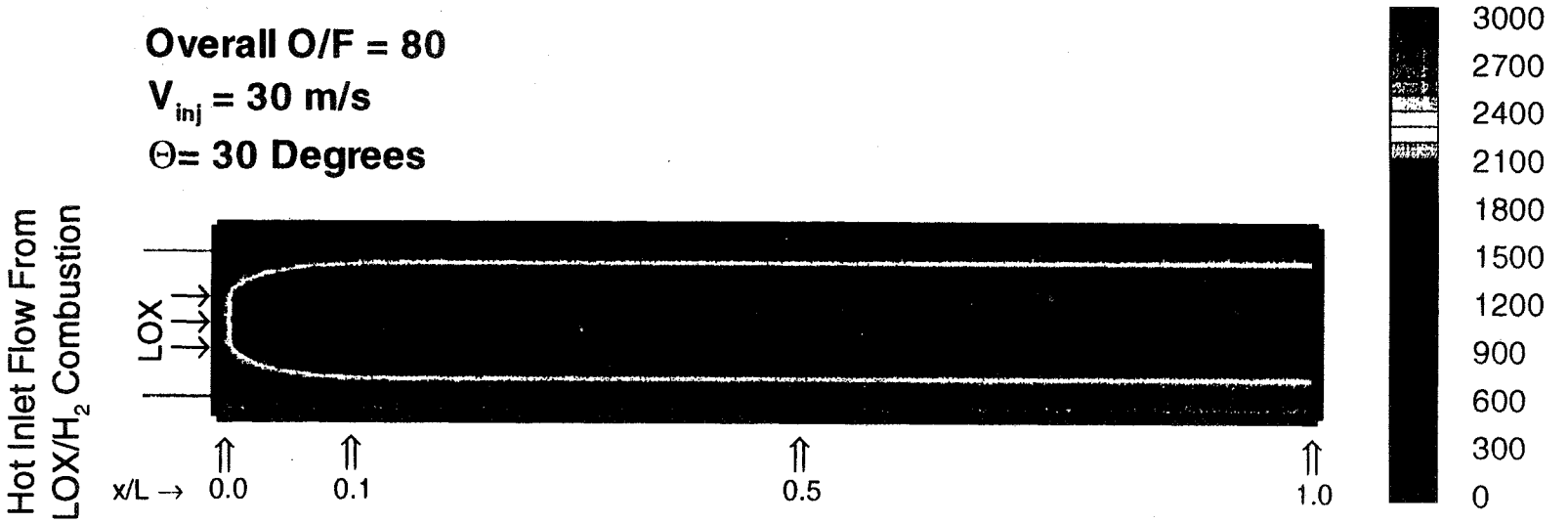

Cross-Sections of Gas Temperature

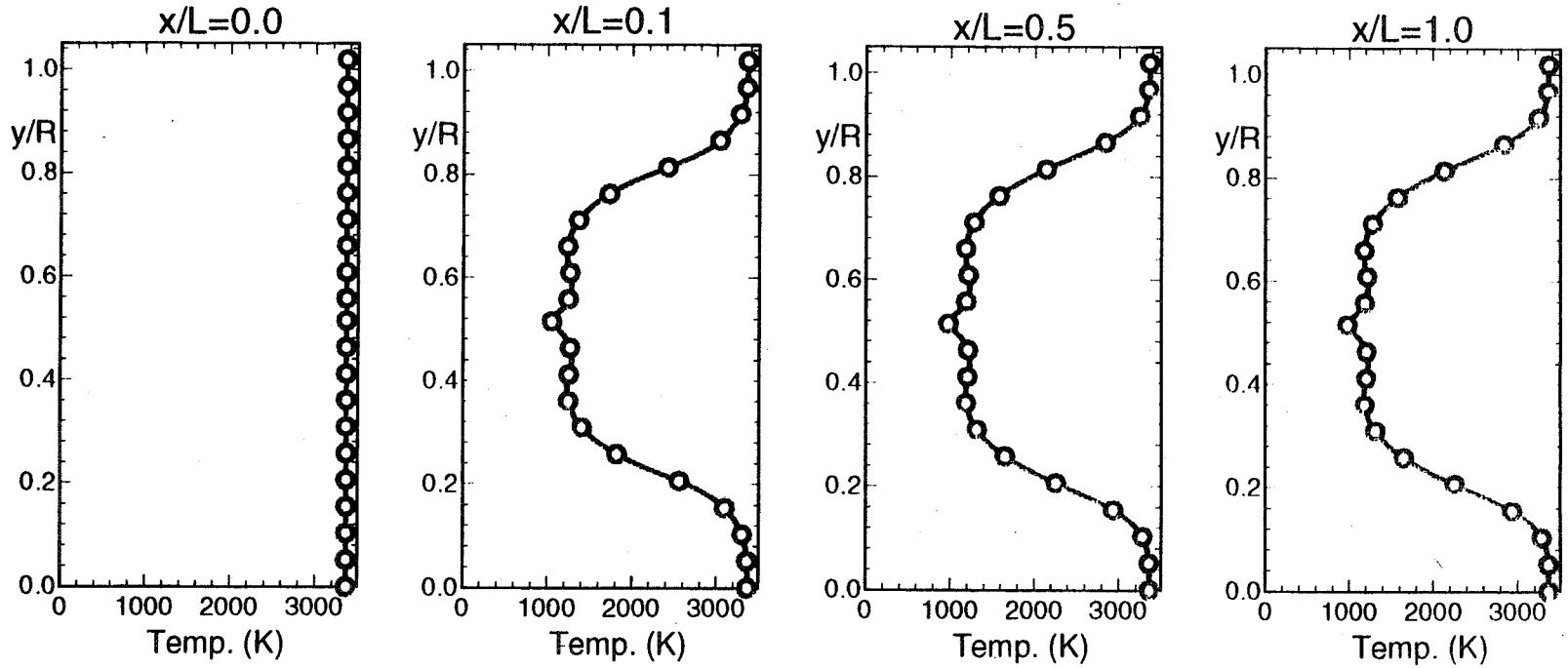

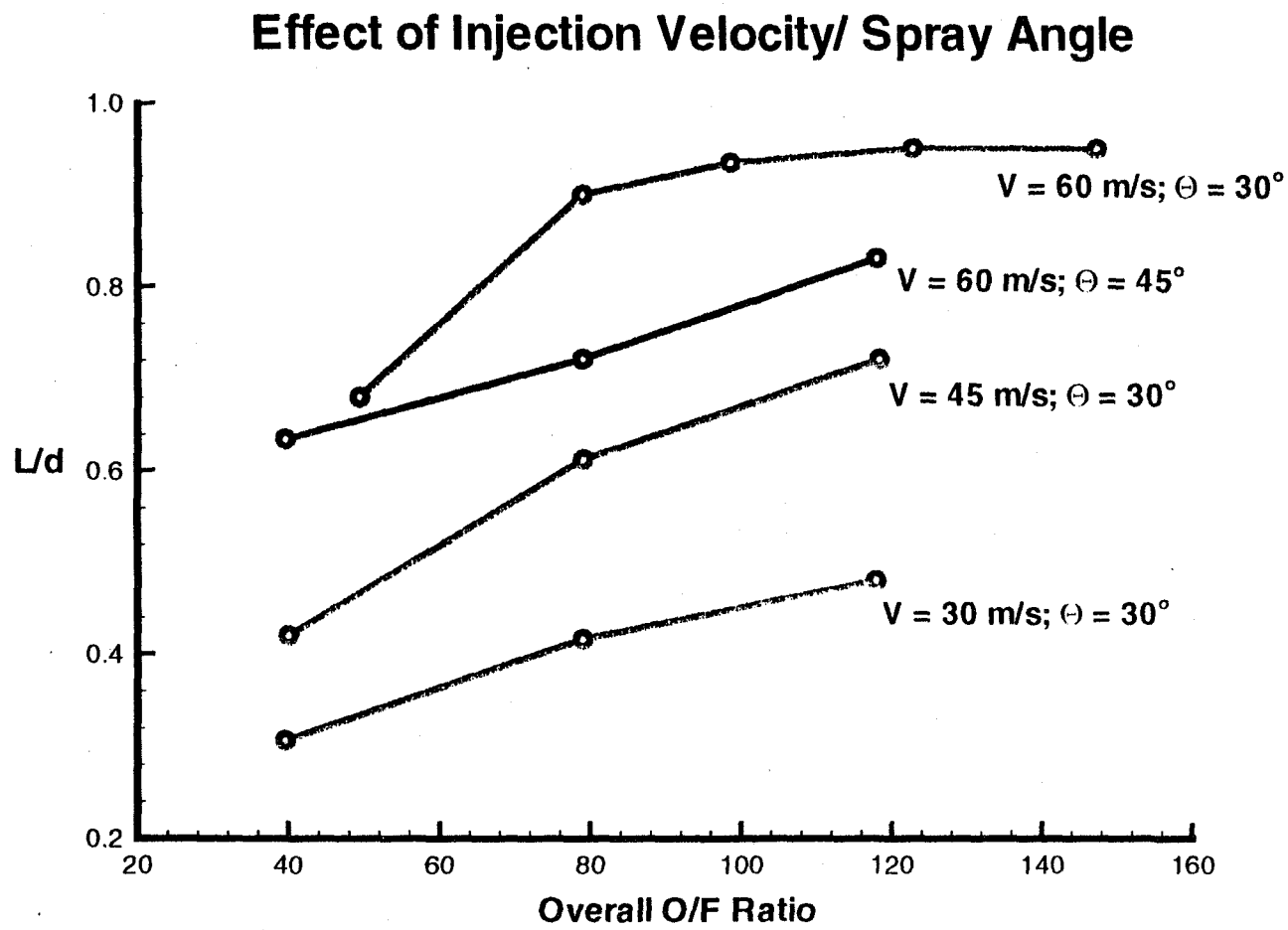
Effect of Injection Velocity/ Spray Angle
L/d
1.0
0.8
0.6
0.4
0.2
20
40
60
80
100
120
140
160
Overall O/F Ratio
V = 60 m/s; Θ = 30°
V = 60 m/s; Θ = 45°
V = 45 m/s; Θ = 30°
V = 30 m/s; Θ = 30°

CONCLUDING REMARKS

- Radial Injection is Most Effective
  - Requires Matching Between:
    - Injector Δp (Droplet Size/Velocity)
    - PreBurner Diameter
    - Mean Flow Velocity
  - Representative Δp's Match Expected PreBurner Sizes Well
  - Appropriate Control Available to Provide Acceptable Outflow Profiles
  - Viable Candidate for Downstream Dilution PreBurners
- Axial Face Plate Injection
  - Results in Acceptable Vaporization Lengths
  - Outflow Uniformity is Marginal

CONCLUDING REMARKS
(continued)

- Axial Face Plate Injection (continued)
  - Can Be Simulated in Unielement Injector
    - Useful Verification of Model Validation
  - Useful Unielement Test Configuration

- Recessed Stoichiometric Core
  - Backstep is an Aid in Mixing
  - Use With Single or Dual Axial Injection
  - Potentially Viable Candidate for Downstream Dilution PreBurners

54-25
51373
132505
26 P.

SPRAY COMBUSTION MODELING WITH VOF AND FINITE-RATE CHEMISTRY

Yen-Sen Chen, Huan-Min Shang and Paul Liaw
Engineering Sciences, Inc., 1900 Golf Road, Suite D, Huntsville, AL 35802
and
Ten-See Wang
NASA/Marshall Space Flight Center, ED32, NASA/MSFC, AL 35812

ABSTRACT

A spray atomization and combustion model is developed based on the volume-of-fluid (VOF) transport equation with finite-rate chemistry model. The gas-liquid interface mass, momentum and energy conservation laws are modeled by continuum surface force mechanisms. A new solution method is developed such that the present VOF model can be applied for all-speed range flows. The objectives of the present study are: (a) to develop and verify the fractional volume-of-fluid (VOF) cell partitioning approach into a predictor-corrector algorithm to deal with multiphase (gas-liquid) free surface flow problems; (b) to implement the developed unified algorithm in a general purpose computational fluid dynamics (CFD) code, Finite Difference Navier-Stokes (FDNS), with droplet dynamics and finite-rate chemistry models; and (c) to demonstrate the effectiveness of the present approach by simulating benchmark problems of jet breakup/spray atomization and combustion. Multiphase fluid flows involving free surface fluids can be found in many space transportation and propulsion systems such as injector atomization in Space Shuttle Main Engine (SSME) combustors, cavitation in liquid rocket pump operations, handling of cryogenic liquids in a micro-gravity environment and the operation of cryogenic propellants on board spacecraft. Modeling these types of flows poses a significant challenge because a required boundary must be applied to a transient, irregular surface that is discontinuous, and the flow regimes considered can range from incompressible to high-speed compressible flows. The flow-process modeling is further complicated by surface tension, interfacial heat and mass transfer, spray formation and turbulence, and their interactions.

The major contribution of the present method is to combine the novel feature of the Volume of Fluid (VOF) method and the Eulerian/Lagrangian method into a unified algorithm for efficient non-iterative, time-accurate calculations of multiphase free surface flows valid at all speeds. The proposed method reformulated the VOF equation to strongly couple two distinct phases (liquid and gas), and tracks droplets on a Lagrangian frame when spray model is required, using a unified predictor-corrector technique to account for the non-linear linkages through the convective contributions of VOF. The discontinuities within the sharp interface will be modeled as a volume force to avoid stiffness. Formations of droplets, tracking of droplet dynamics and modeling of the droplet breakup/evaporation, are handled through the same unified predictor-corrector procedure. Thus the new algorithm is non-iterative and is flexible for general geometries with arbitrarily complex topology in free surfaces. The FDNS finite-difference Navier-Stokes code is employed as the baseline of the current development.

Benchmark test cases of shear coaxial LOX/H2 liquid jet with atomization/combustion and impinging jet test cases are investigated in the present work. Preliminary data comparisons show good qualitative agreement between data and the present analysis. It is indicative from these results that the present method has great potential to become a general engineering design analysis and diagnostics tool for problems involving spray combustion.

SPRAY COMBUSTION MODELING WITH VOF AND FINITE-RATE CHEMISTRY

Y. S. Chen, H. M. Shang and P. Liaw
Engineering Sciences, Inc., Huntsville, Alabama

and

T.S. Wang
NASA/Marshall Space Flight Center, NASA/MSFC, Alabama

Workshop for Computational Fluid Dynamics Applications in Rocket Propulsion and Launch Vehicle Technology
April 25 - 27, 1995

Overview

- INTRODUCTION
- THEORETICAL APPROACH
- NUMERICAL METHOD
- SHEAR COAXIAL INJECTOR TEST CASES
- IMPINGING INJECTOR TEST CASES
- FUTURE WORK

INTRODUCTION

- FLUID DYNAMICS PROBLEMS WITH MULTI-PHASE INTERFACE ARE IMPORTANT IN MANY ENGINEERING DESIGN APPLICATIONS SUCH AS INJECTOR SPRAY BREAKUP/ ATOMIZATION, SPRAY COATING, CRYOGENIC FLUID MANAGEMENT, MATERIAL PROCESSING, CRYSTAL GROWTH, CHEMICAL VAPOR DEPOSITION AND CAVITATION/ CONDENSATION, ETC.

- MAJOR DIFFICULTIES IN NUMERICAL MODELING INVOLVE LARGE DENSITY JUMP ACROSS INTERFACE, CALCULATION OF SURFACE TENSION FORCE IN 3-D SPACE AND IMPORTANT EFFECTS OF MATERIAL PROPERTY VARIATIONS.

- VOLUME OF FLUID (VOF) METHOD USES FLUID VOLUME TRANSPORT EQUATION ON EULERIAN FRAMEWORK -- RESOLUTION OF THE INTERFACE IS AN IMPORTANT ISSUE. VOF METHOD IS GENERAL AND CAN BE APPLIED TO COMPLEX INTERFACE GEOMETRY PROBLEMS.

- WITH VOF INTERFACE MODELING, LAGRANGIAN PARTICLE TRACKING METHOD AND FINITE-RATE CHEMISTRY MODELS, SPRAY ATOMIZATION/ COMBUSTION PROCESSES CAN BE SIMULATED. A SPRAY COMBUSTION MODEL DEVELOPED BASED ON THESE FEATURES CAN BE VERY USEFUL IN THE ANALYSIS OF INJECTOR/COMBUSTION CHAMBER DESIGN AND DIAGNOSIS ISSUES.

THEORETICAL APPROACH

- CONSERVATION EQUATIONS FOR THE LIQUID, WHICH IS INCOMPRESSIBLE, AND FOR THE GAS FLOW WHICH IS COMPRESSIBLE.
- VOLUME OF FLUID TRANSPORT EQUATION USED TO PREDICT THE INTERFACE DYNAMICS.
- CONTINUUM SURFACE FORCE MODEL IS EMPLOYED TO MODEL THE SURFACE TENSION FORCE.
- LAGRANGIAN PARTICLE TRACKING METHOD FOR TREATING THE DYNAMICS AND HEAT/MASS TRANSFER OF PARTICLE PARCELS IN STATISTICAL SENSE.
- MULTI-COMPONENT FINITE-RATE CHEMISTRY MODEL BASED ON POINT IMPLICIT AND PENALTY FUNCTION APPROACH.

Transport Equations

For flow variables:

$$\frac{\partial \rho \phi}{\partial t} + \frac{\partial \rho \left(u - u_g\right)_i \phi}{\partial x_i} = D_\phi + S_\phi$$

and for VOF equation:

$$\frac{\partial \alpha}{\partial t} + \left(u - u_g\right)_i \frac{\partial \alpha}{\partial x_i} = S_\alpha$$

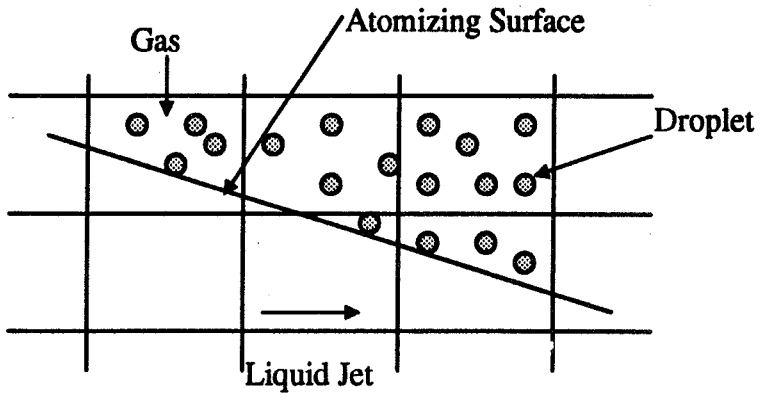

Implementation of atomization and spray model

where $\alpha = 1$ stands for liquid and $\alpha = 0$ is for gas. The interface is located at $1 > \alpha > 0$.

For a given solution of α field, the governing equations can be recast as:

$$\frac{\partial \rho_m \phi}{\partial t} + \frac{\partial \rho_m \left(u - u_g\right)_i \phi}{\partial x_i} = D_\phi + S_\phi, \quad \alpha < 0.05 \quad \text{--------} \quad \text{for compressible gas}$$

$$\rho_m \frac{\partial \phi}{\partial t} + \rho_m \left(u - u_g\right)_i \frac{\partial \phi}{\partial x_i} = D_\phi + S_\phi, \quad \alpha \geq 0.05 \quad \text{--------} \quad \text{for interface and liquid}$$

where

$$\rho_m = (1-\alpha)\rho_g - \alpha\rho_l$$

where ρ_g and ρ_l denote gas and liquid density respectively. u_g represents the grid speed components used to simulate moving domain effects.

Continuum Surface Force Model

Surface Tension Forces:

$$F_x = -\sigma\left(\nabla \hat{n}\right)\alpha_x$$

$$F_y = -\sigma\left(\nabla \hat{n}\right)\alpha_y + \left(\frac{|\alpha_y|}{y}\right)_{\textit{for 2D axisymetric only}}$$

$$F_z = -\sigma\left(\nabla \hat{n}\right)\alpha_z\ , \quad \textit{--- for 3D case only}$$

where

σ = surface tension constant

$$\nabla \hat{n} = \hat{\alpha}_{xx} + \hat{\alpha}_{yy} + \hat{\alpha}_{zz}$$

Spray Atomization Model

- Reitz & Diwakar Wave Instability Atomization Model
- CICM (Coaxial Injector Combustion Model) Atomization Model (Liang & Jensen)
- Mass Stripping Rates Applied to the VOF Equation Along the Interface for the Liquid Core Prediction

Pressure Sensitivity Analysis

- Case D of Penn State Experiment:

Pc = 443 psia;
injector diameter = 3.43 mm;
gas velocity = 840 m/s;
liquid velocity = 18 m/s;
gas temperature = 300 K;
liquid temperature = 106 K; and
gas density = 2.48 kg/m**3.

Table 1. Comparisons of Spray Atomization Models

	Mean Droplet Size (μm)			
P (ATM)	10	20	40	300
Reitz Model	0.122	0.0636	0.0334	0.0054
CICM Model	3.22	2.03	1.28	0.334

NUMERICAL METHOD

- PREDICTOR-CORRECTOR TIME MARCHING ALGORITHM BASED ON FDNS
  - -- UNIFIED SOLUTION FOR INCOMPRESSIBLE LIQUID AND COMPRESSIBLE GAS
- SECOND-ORDER ARTIFICIAL DISSIPATION SCHEMES OR THIRD-ORDER UPWIND TVD SCHEMES
- CENTRAL DIFFERENCING FOR DIFFUSION, SOURCE AND SURFACE TENSION FORCE TERMS
- TURBULENCE-PARTICLE INTERACTION BASED ON THE TKE SOLUTION AND A GAUSSIAN FILTERED RANDOM NUMBER GENERATOR
- HIGH-ORDER TVD SCHEME FOR VOF TRANSPORT EQUATION FOR GOOD INTERFACE RESOLUTION

COAXIAL INJECTOR TEST CASES

- COAXIAL LIQUID JET ATOMIZATION
  - KEROSENE/O2 INJECTOR ELEMENT AT 1 ATM
  - STEADY-STATE AND TRANSIENT APPROACH
  - WAVE INSTABILITY ATOMIZATION MODEL (Reitz & Diwakar)
- UNI-ELEMENT COMBUSTOR SIMULATION
  - LOX/H2 COAXIAL INJECTOR (CASE D CONDITIONS OF THE PENN STATE EXPERIMENT): Real Fluid Property (NBS Table) for LOX Used.
  - O/F RATIO OF 5.2 (Ignition initiated about the same location as the experiment)
  - FINITE-RATE CHEMISTRY COMPUTATIONS (2-Step and 7-Step Model)

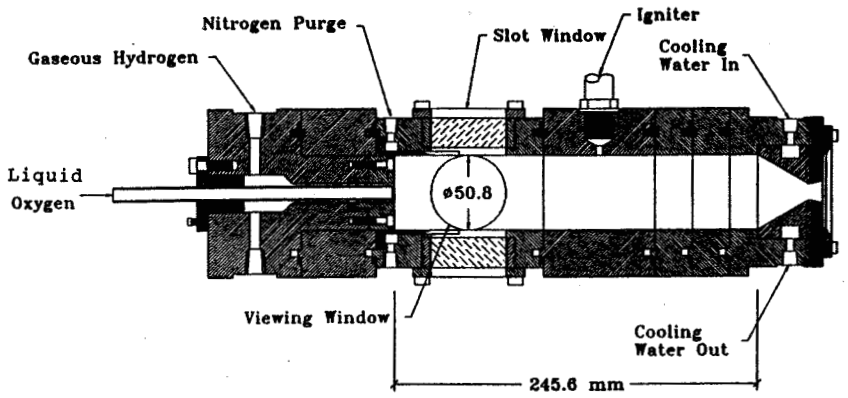

Cross-sectional view of the combustion chamber.

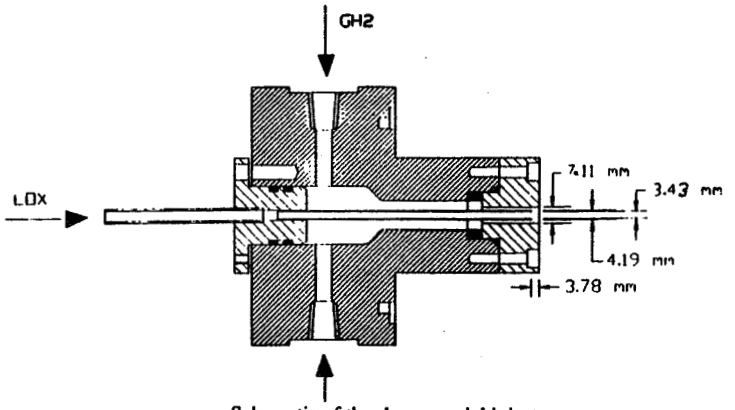

Schematic of the shear coaxial injector.

COAXIAL INJECTOR SIMULATION (1 atm, Steady-State Approach)

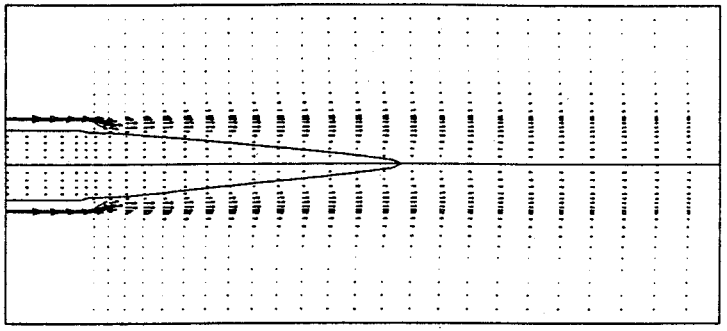

(a) Flowfield

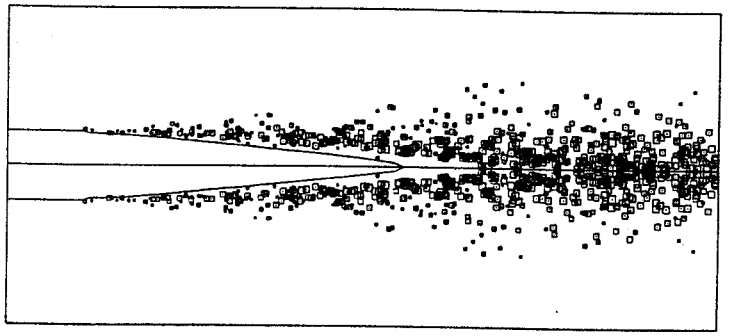

(c) t = 0.9 ms

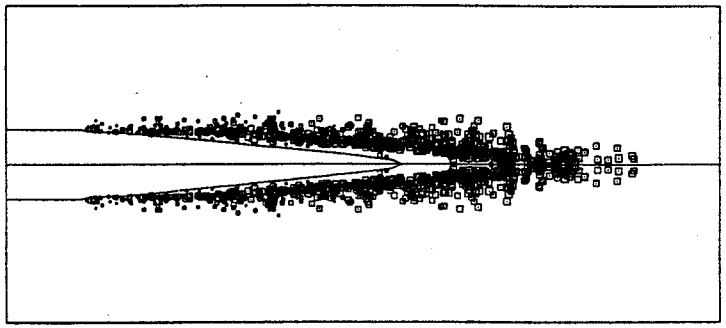

(b) t = 0.3 ms

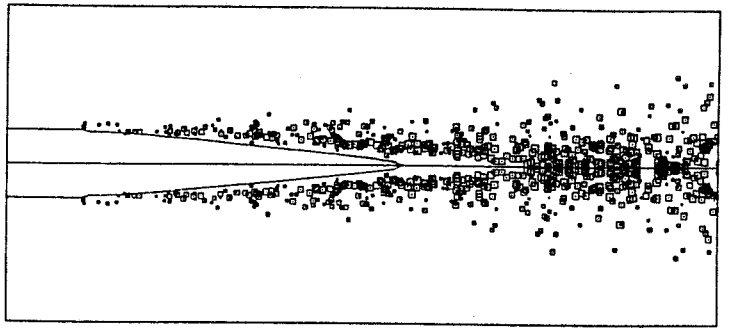

(d) t = 1.2 ms

COAXIAL INJECTOR SIMULATION (1 atm, Transient Approach)

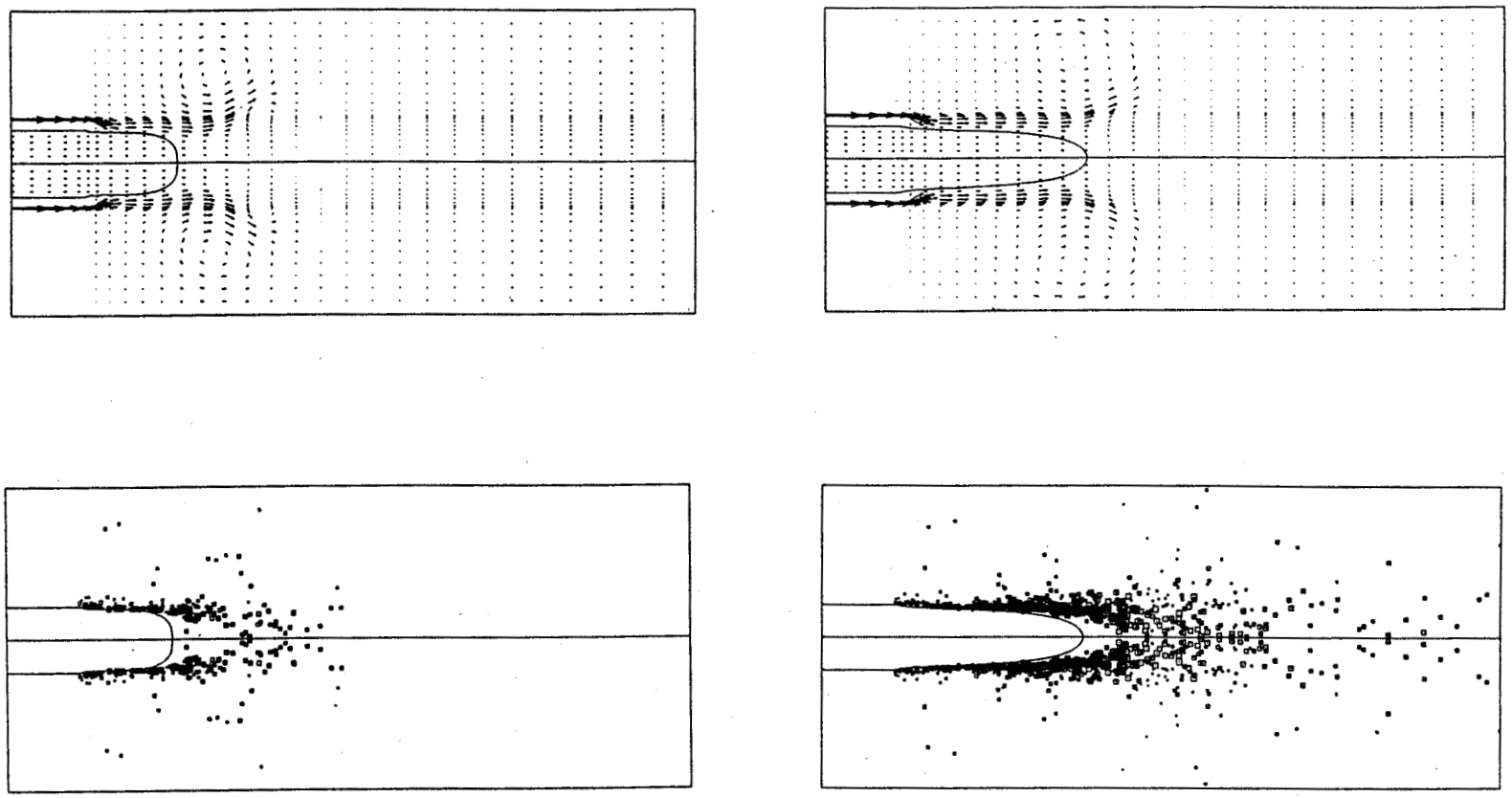

(a) t = 0.3 ms

(b) t = 0.6 ms

COAXIAL INJECTOR SIMULATION (1 atm, Transient Approach)

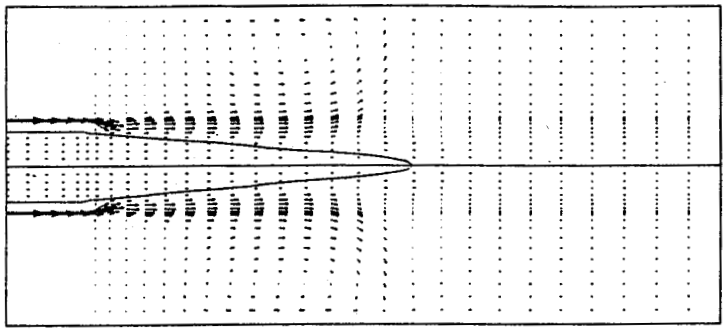

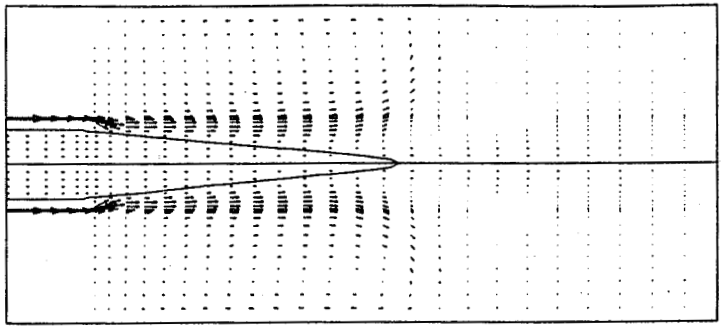

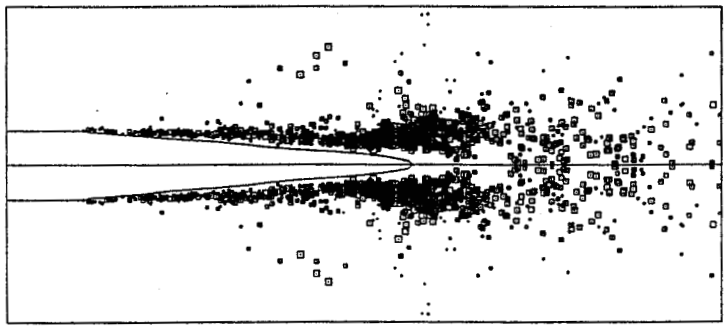

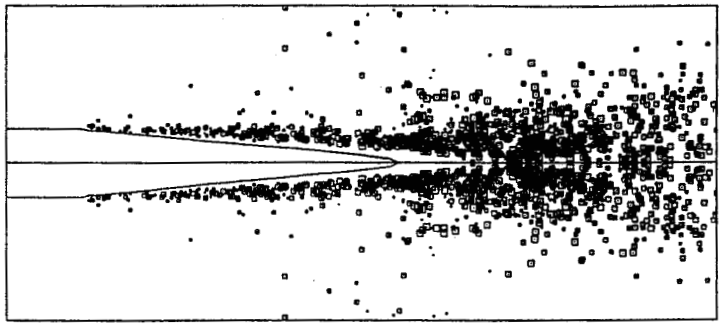

(c) t = 1.08 ms

(d) t = 1.5 ms

UNI-ELEMENT COMBUSTOR SIMULATION (30 atm, 2-Step Model)

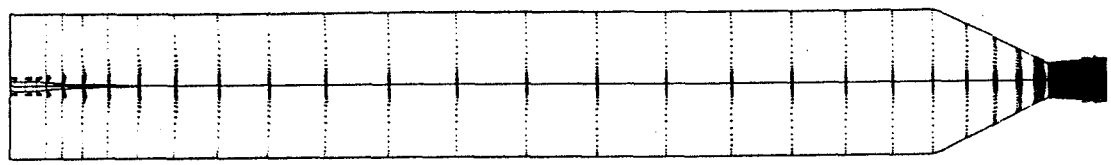

LOX Interface and Velocity Vectors

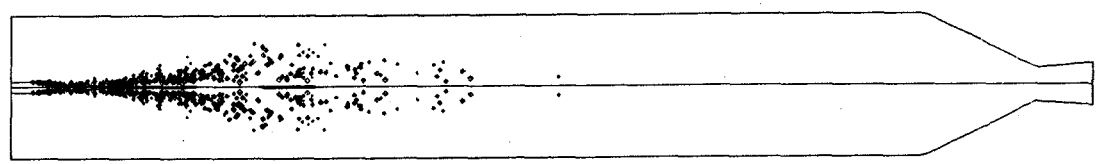

LOX Particle Plot

UNI-ELEMENT COMBUSTOR SIMULATION (30 atm, 2-Step Model)

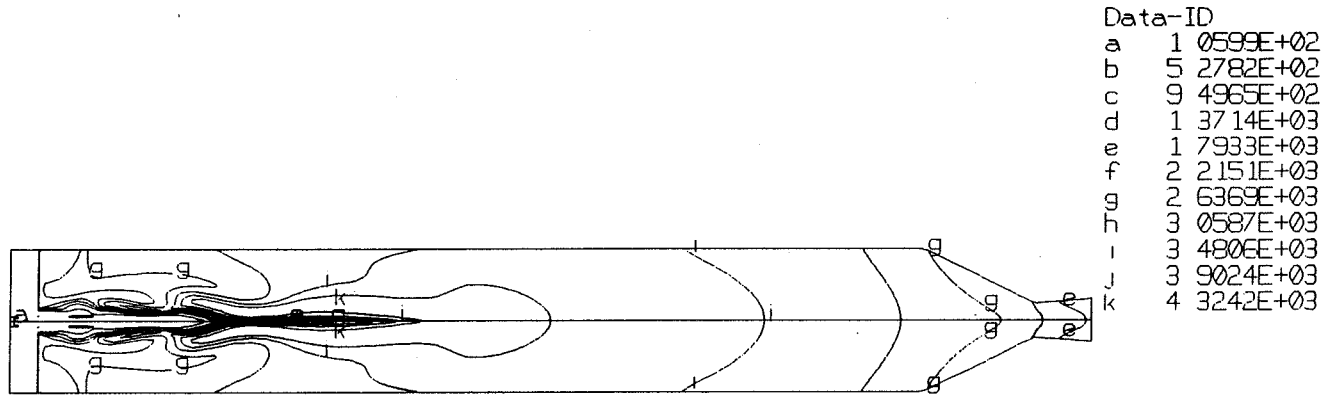

Temperature Contours (K)

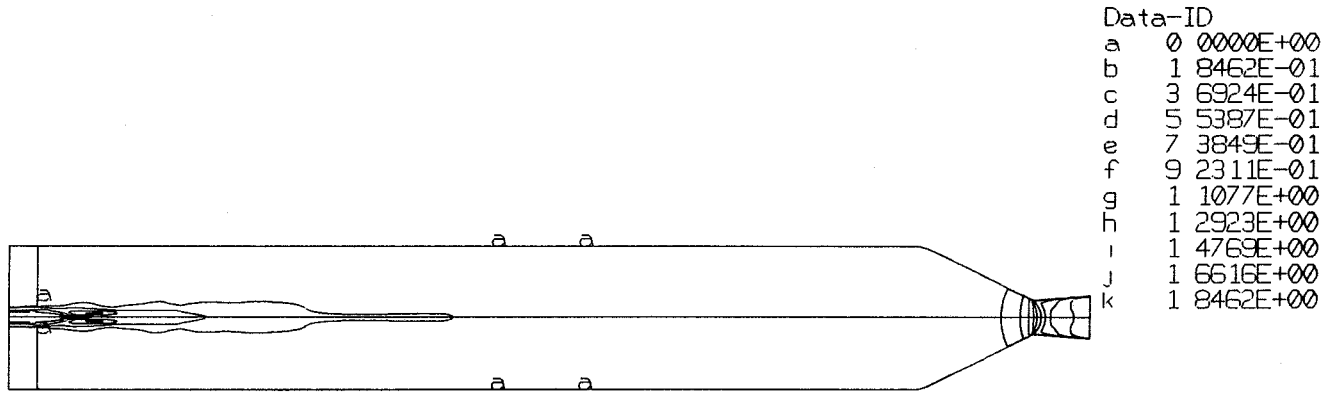

Mach Number Contours

UNI-ELEMENT COMBUSTOR SIMULATION (30 atm, 7-Step Model)

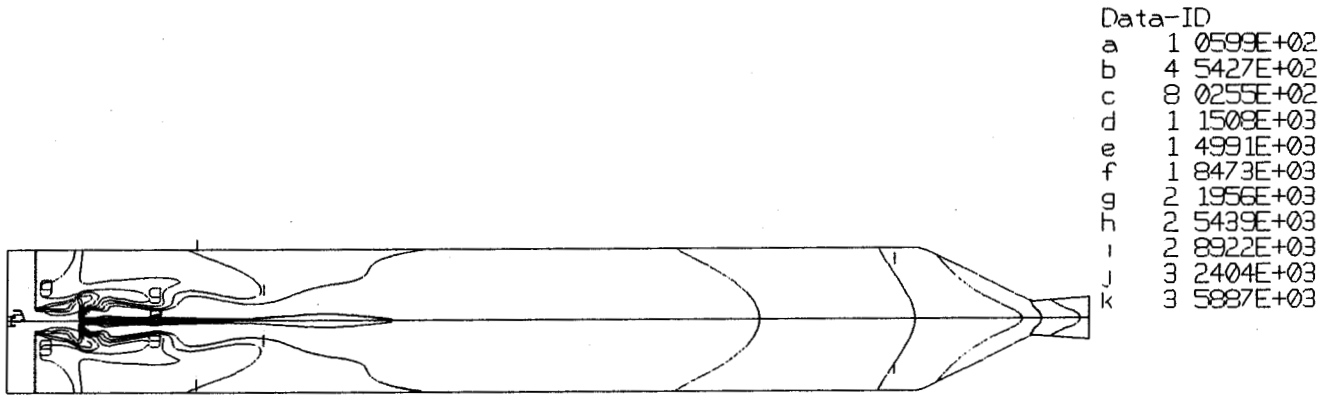

Temperature Contours (K)

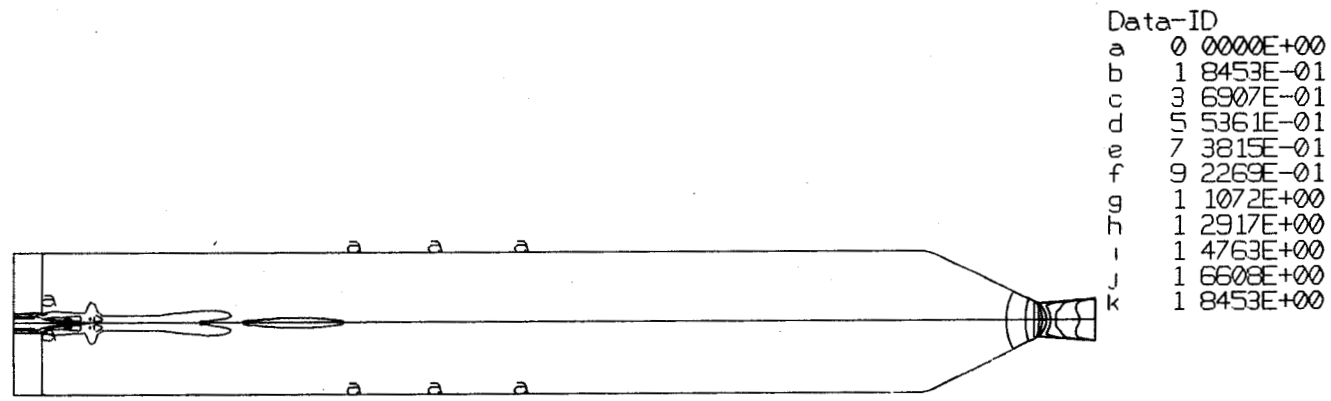

Mach Number Contours

IMPINGING INJECTOR TEST CASES

- LAMINAR JET CONDITIONS FOR THEORETICAL COMPARISONS
- JET IMPINGEMENT HALF ANGLE OF 30, 60 AND 90 DEGREES
- THEORETICAL SOLUTION OF LIQUID SHEET THICKNESS DISTRIBUTION FUNCTION:

$$\frac{h * r}{R^2} = \frac{\mathrm{Sin}^2\theta}{(1 - \mathrm{Cos}\phi\mathrm{Cos}\theta)^2}$$

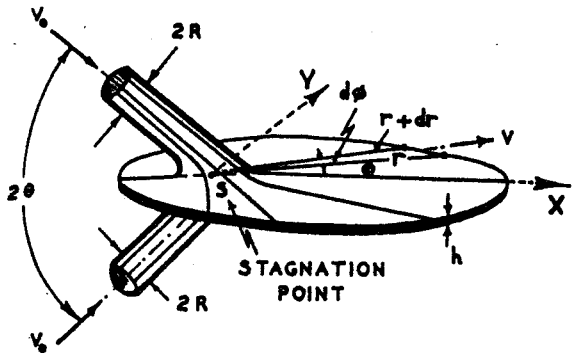

Fig. 1. Equal thickness contour of sheet formed by impinging jets.

LIQUID SHEET SURFACE ($\theta = 30°$)

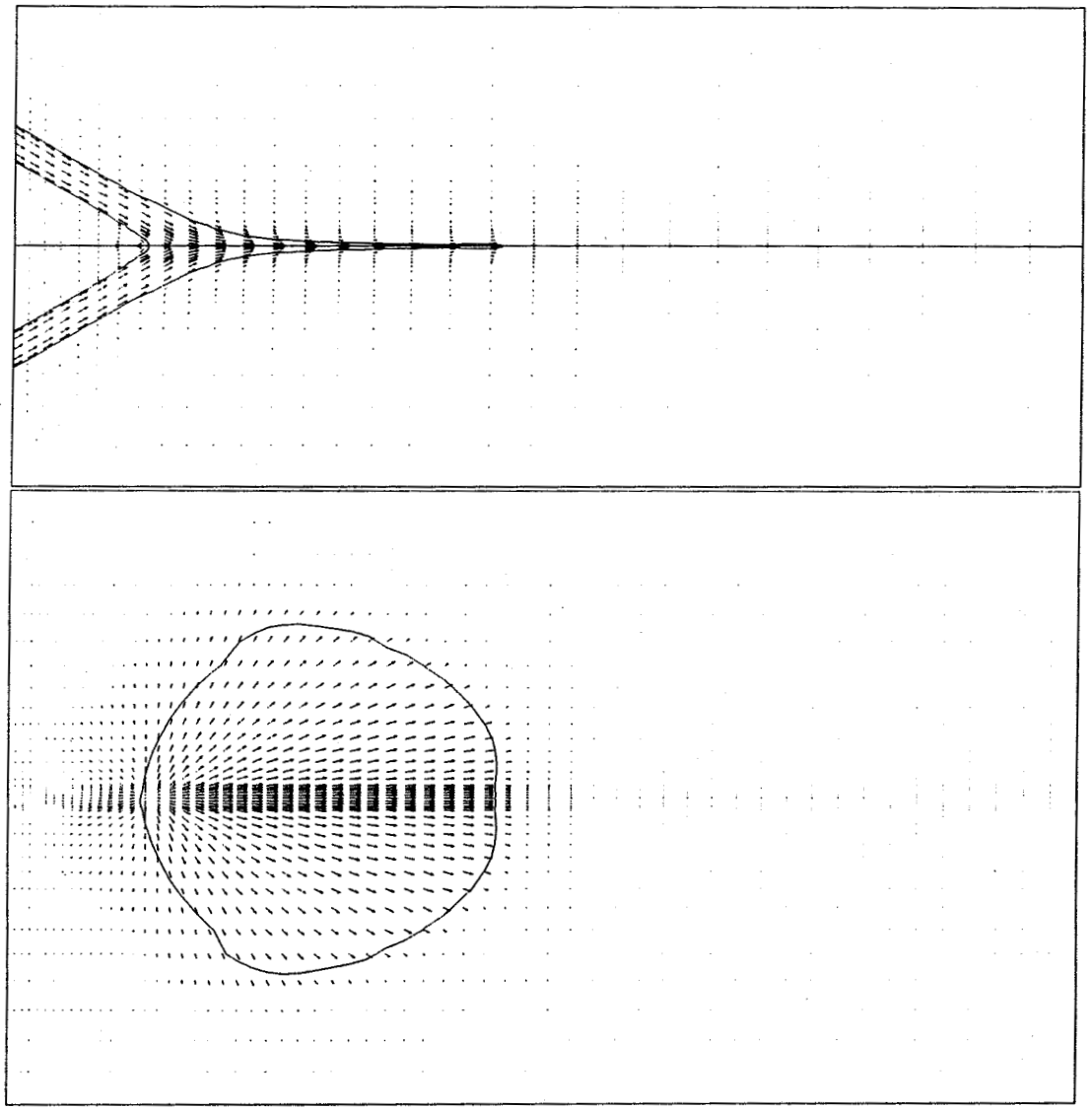

LIQUID SHEET THICKNESS COMPARISONS ($\theta = 30°$)

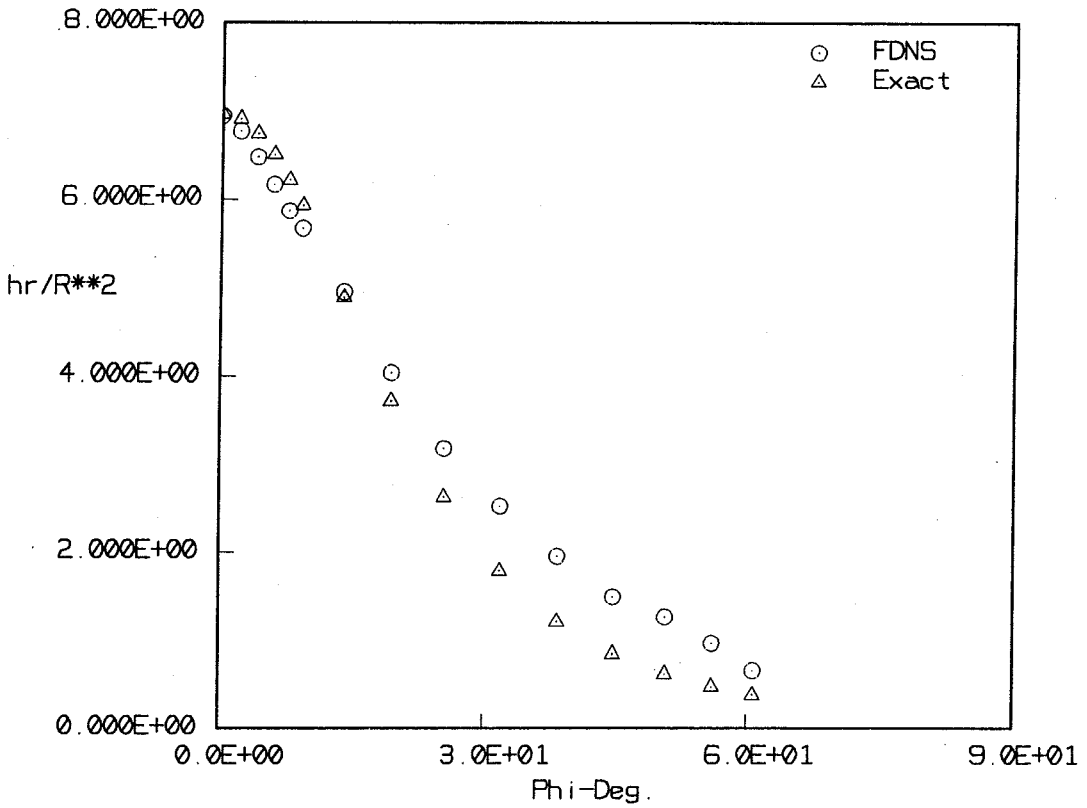

Liquid Sheet Thickness Distributions. (Theta = 30 deg.)

LIQUID SHEET SURFACE ($\theta = 45°$)

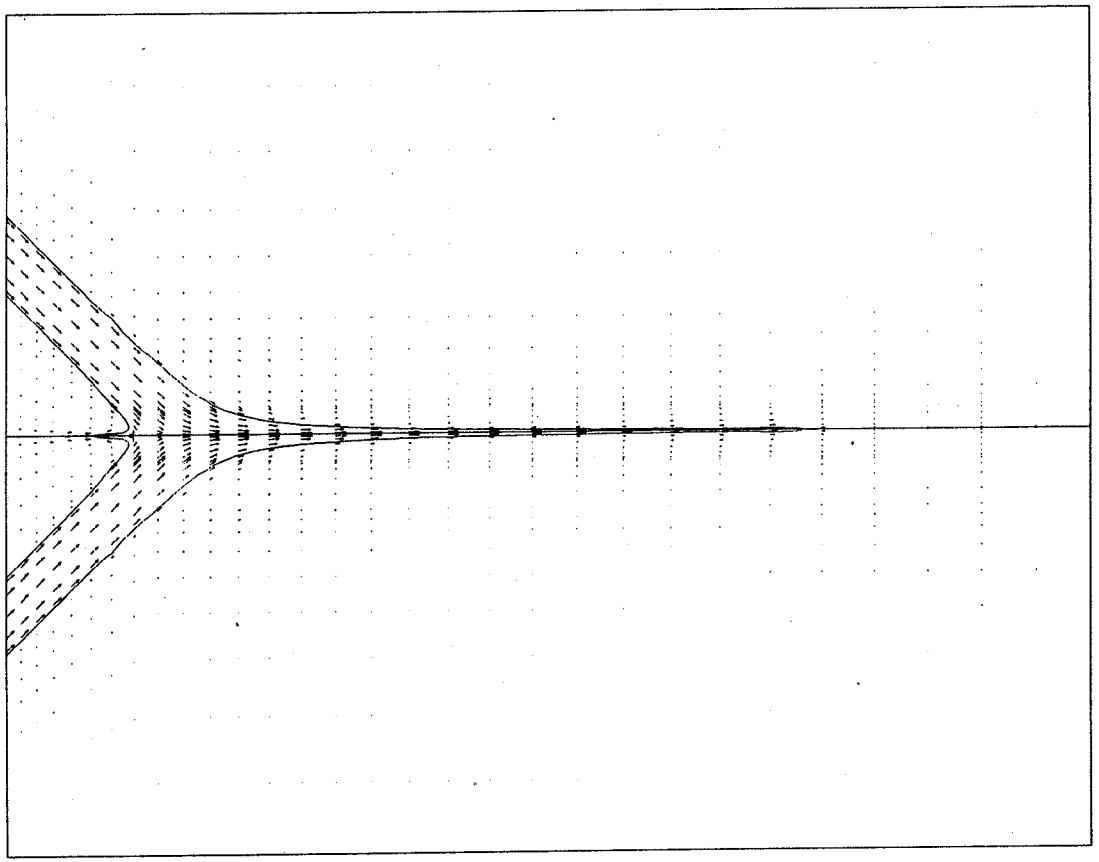

Liquid Sheet Surface. (Theta = 45 deg.)

LIQUID SHEET THICKNESS COMPARISONS (θ = 45°)

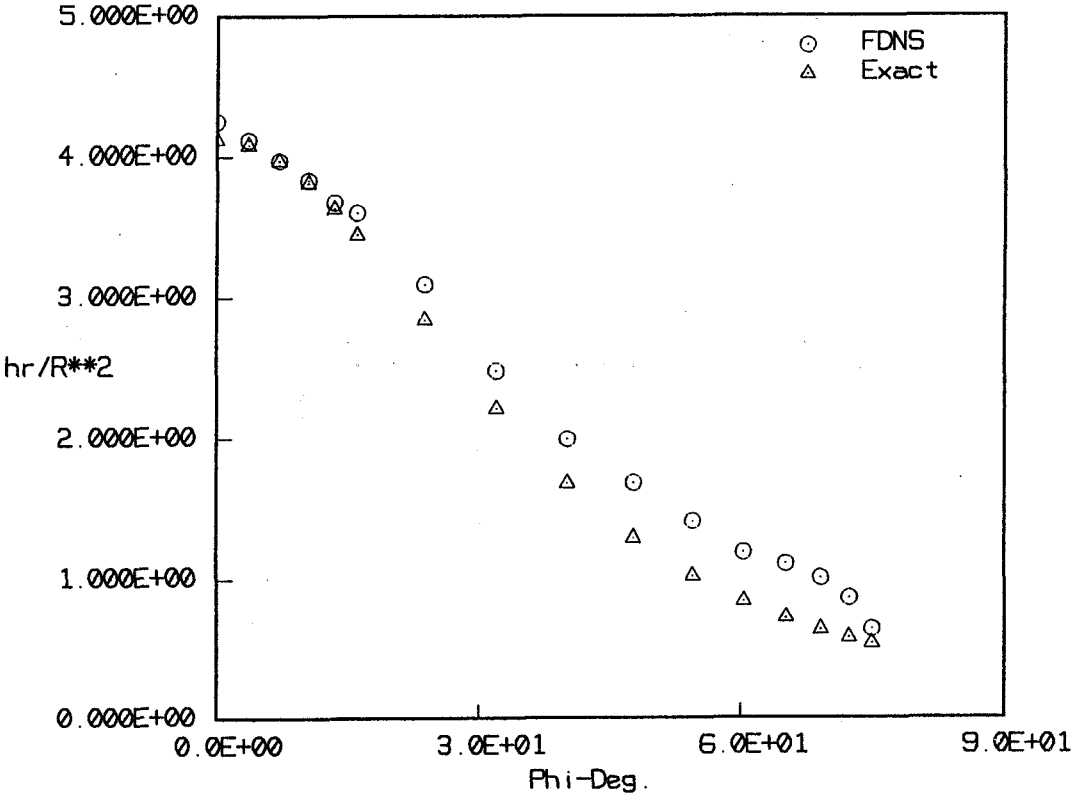

Liquid Sheet Thickness Distributions. (Theta = 45 deg.)

LIQUID SHEET SURFACE ($\theta = 60°$)

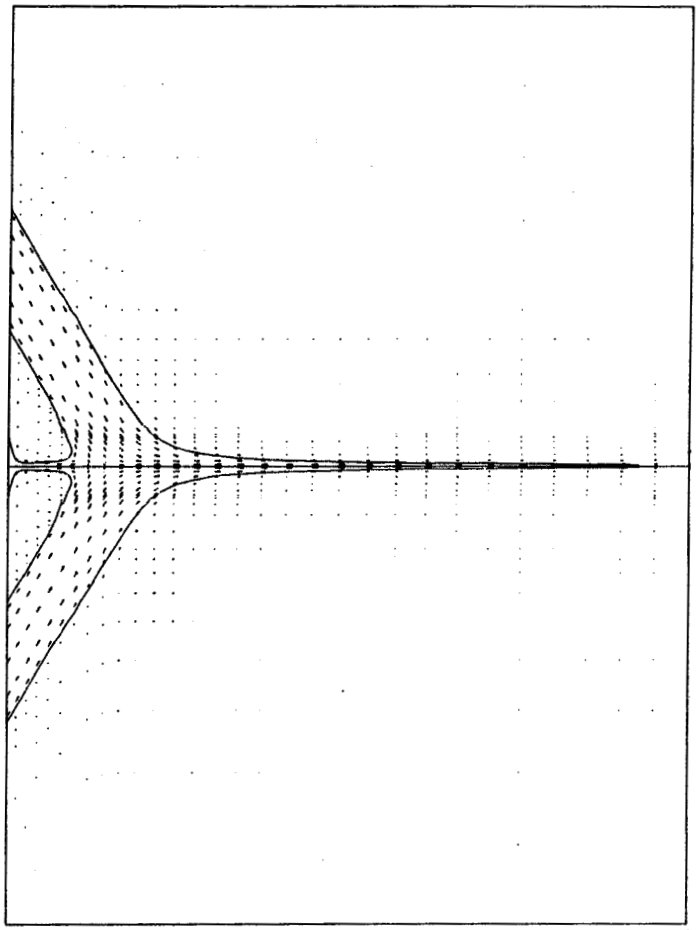

Liquid Sheet Surface. (Theta = 60 deg.)

LIQUID SHEET THICKNESS COMPARISONS (θ = 60°)

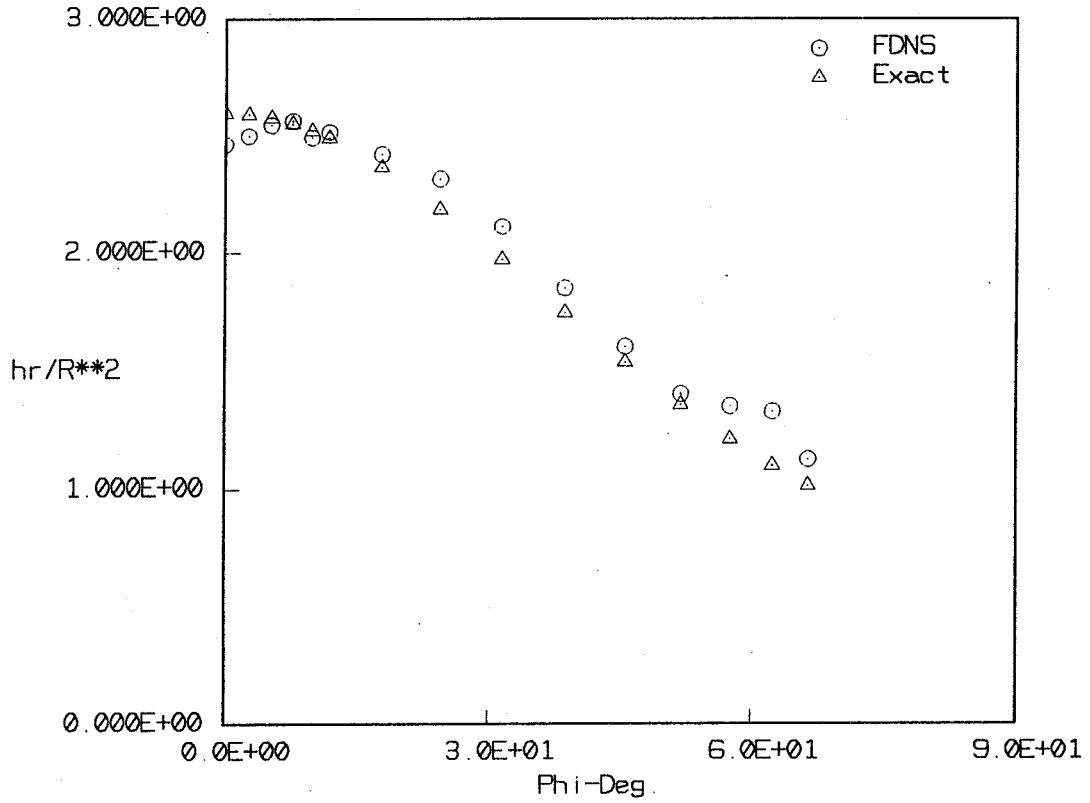

FUTURE WORK

- A GENERAL SPRAY COMBUSTION MODEL WITH VOF AND FINITE-RATE CHEMISTRY MODELS IS DEVELOPED AND BENCHMARK VALIDATION CASES ARE BEING STUDIED

- THE UNIQUENESS OF THE PRESENT METHOD IS IN ITS ALL-SPEED CAPABILITY WHICH EXPANDS THE VERSATILITY OF THE CLASSICAL VOF APPROACH

- FURTHER DEVELOPMENTAL WORK TO INCLUDE IMPINGING JETS ATOMIZATION MODEL AND VOF INTERFACE VAPORIZATION PROCESSES IN THE FDNS CODE

Progress Towards an Efficient and General CFD Tool for Propulsion Design/Analysis

C. F. Cox, P. Cinnella, and S. Westmoreland
Engineering Research Center for Computational Field Simulation
Mississippi State University
Mississippi State, MS 39762

The simulation of propulsive flows inherently involves chemical activity. Recent years have seen substantial strides made in the development of numerical schemes for reacting flowfields, in particular those involving finite-rate chemistry. However, finite-rate calculations are computationally intensive and require knowledge of the actual kinetics, which are not always known with sufficient accuracy. Alternatively, flow simulations based on the assumption of local chemical equilibrium are capable of obtaining physically reasonable results at far less computational cost.

The present study summarizes the development of efficient numerical techniques for the simulation of flows in local chemical equilibrium, whereby a "Black Box" chemical equilibrium solver is coupled to the usual gasdynamic equations. The generalization of the methods enables the modelling of any arbitrary mixture of thermally perfect gases, including air, combustion mixtures and plasmas. As demonstration of the potential of the methodologies, several solutions, involving reacting and perfect gas flows, will be presented. Included is a preliminary simulation of the SSME startup transient. Future enhancements to the proposed techniques will be discussed, including more efficient finite-rate and hybrid (partial equilibrium) schemes. The algorithms that have been developed and are being optimized provide for an efficient and general tool for the design and analysis of propulsion systems.

MISSISSIPPI STATE UNIVERSITY / National Science Foundation

Progress Towards an Efficient and General CFD Tool for Propulsion Design/Analysis

Carey F. Cox, Pasquale Cinnella and Shawn Westmoreland

Workshop for Computational Fluid Dynamic Applications in Rocket Propulsion and Launch Vehicle Technology
April 25-27, 1995
Huntsville, AL

ENGINEERING RESEARCH CENTER FOR
COMPUTATIONAL FIELD SIMULATION
COMPLEX GEOMETRY / COMPLEX PHYSICS

Purpose

- Provide an overview of the development of a solver for reacting gas flows, which

  utilizes EFFICIENT numerical techniques

  and is

  capable of handling ARBITRARY mixtures.

MOTIVATIONS

- Finite-rate chemistry is COMPLICATED and EXPENSIVE

  Chemical kinetics, actual reaction path are required.

  N species continuity equations.

  Finite-rate equations are extrememly stiff for near equilibrium flows.

- Why not curvefits?

  Limited to a particular mixture and range.

APPROACH

- Chemical equilibrium "Black Box" solver coupled to the "usual" gasdynamic equations

  5 equations, not the N+4 equations required for finite-rate chemistry.

- An "off-the-shelf" multi-block flow solver is modified to handle "real gas" effects

  Unstructured Block Implicit solver

BLACK BOX

- Provides chemical composition and thermodynamic properties
- Capable of handling ARBITRARY mixtures

  10 chemistry models available including air, combustion and plasma mixtures, as well as perfect gas.

- Variety of computational options

  2 Solution Methods: Mass Constraint & Degree of Advancement

  2 Rate Coefficient Models: Curvefit & Consistent

  2 Thermodynamic Models: Vibrational & Curvefit

- EFFICIENT and ROBUST

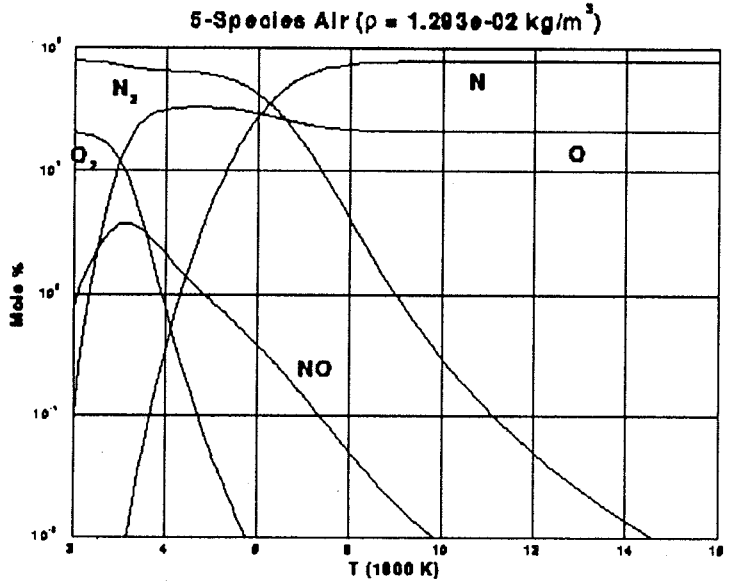
5-Species Air (ρ = 1.293e-02 kg/m³)
N₂
O₂
N
O
NO
Mole %
T (1000 K)

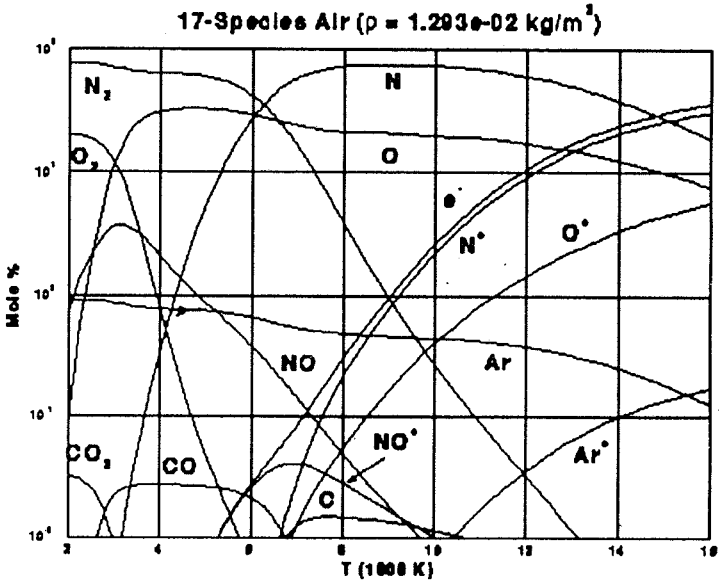
17-Species Air (ρ = 1.293e-02 kg/m³)
N₂
O₂
N
O
e⁻
N⁺
O⁺
NO
Ar
CO₂
CO
NO⁺
C
Ar⁺
Mole %
T (1000 K)

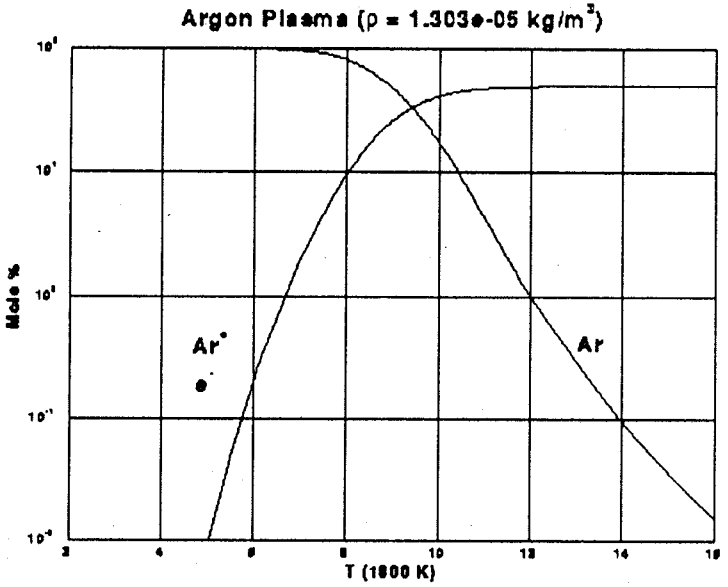
Argon Plasma (ρ = 1.303e-05 kg/m³)
Ar⁺
e⁻
Ar
Mole %
T (1000 K)

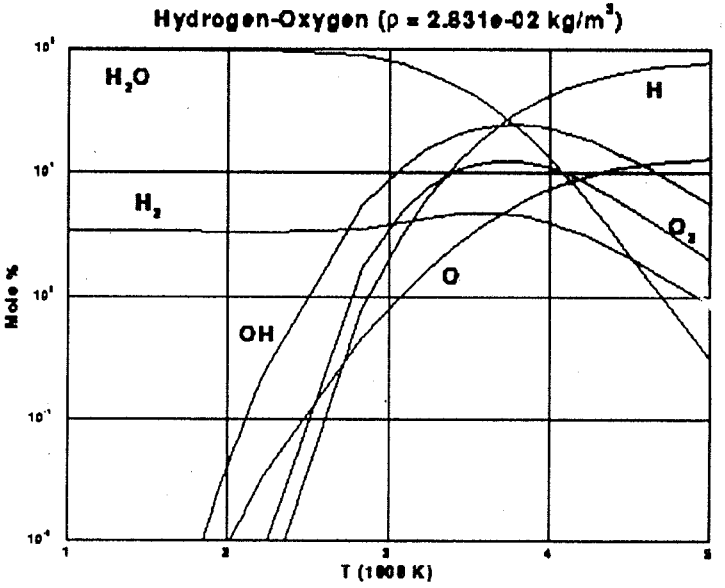
Hydrogen-Oxygen (ρ = 2.831e-02 kg/m³)
H₂O
H
H₂
O₂
O
OH
Mole %
T (1000 K)

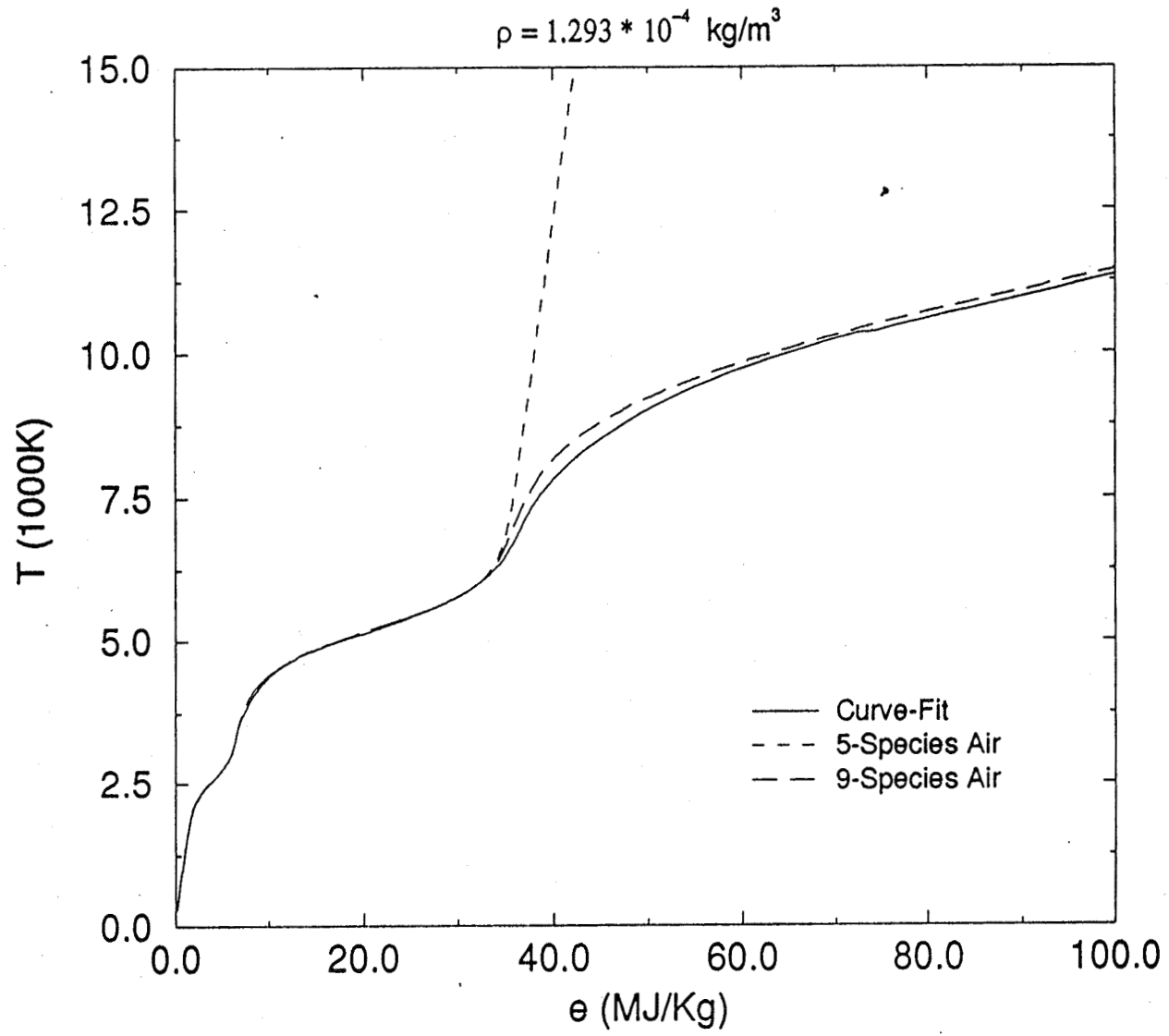
Temperature vs Internal Energy
ρ = 1.293 * 10^-4 kg/m^3
T (1000K)
15.0
12.5
10.0
7.5
5.0
2.5
0.0
0.0
20.0
40.0
60.0
80.0
100.0
e (MJ/Kg)
Curve-Fit
5-Species Air
9-Species Air

Isentropic Index vs Temperature

$\rho = 1.293 * 10^{-4}$ kg/m^3

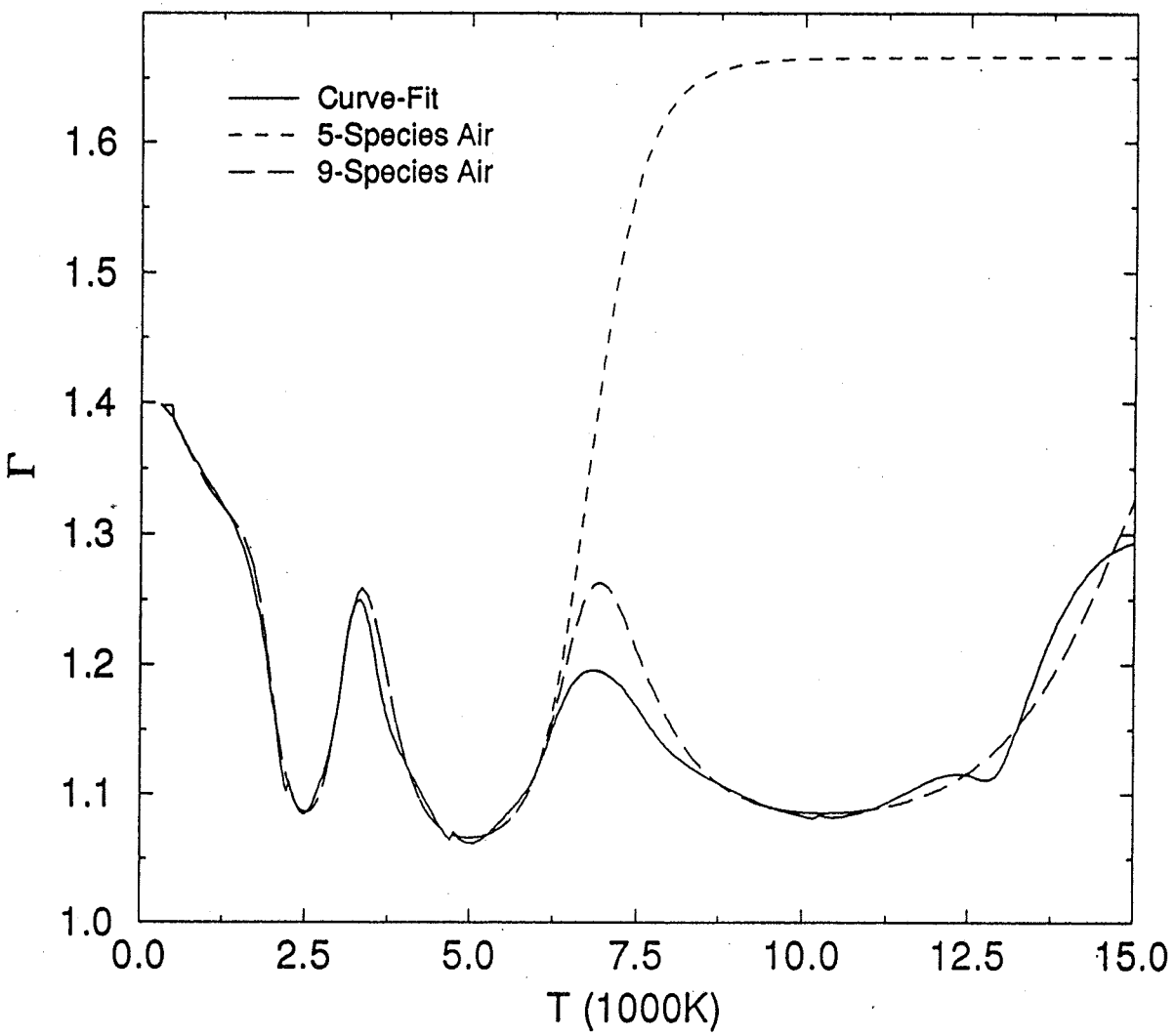

FLOW SOLVER

- Implicit, finite–volume, high–order TVD scheme.
- Modified 2–Pass solution algorithm
- Steger–Warming FVS used on LHS
- Approximate Riemann Solver used on RHS
- Unstructured multi–block capability using ...
  - "ribbon vector" storage,
  - block–structured grids, and
  - extraction–injection for block–to–block communication.

BLUNT CONE

- 9 degree half angle, 2.5 in. nose radius

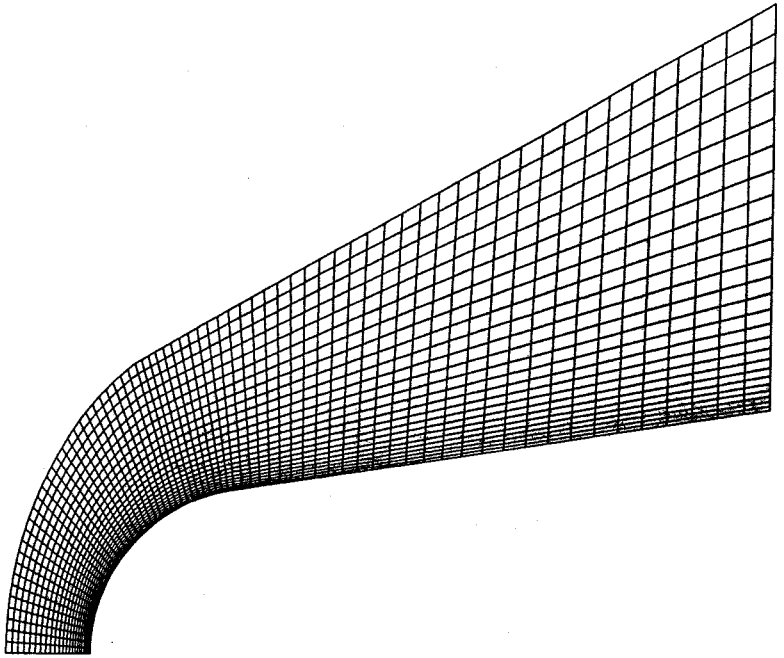

- Flow conditions:

$T_\infty = 223\ K$ $\qquad$ $M_\infty = 10$

$p_\infty = 26.5\ kPa$ $\qquad$ $\alpha_\infty = 0\ degrees$

Black Box - Curvefit Comparison

(Blunt Cone, Surface , Temperature)

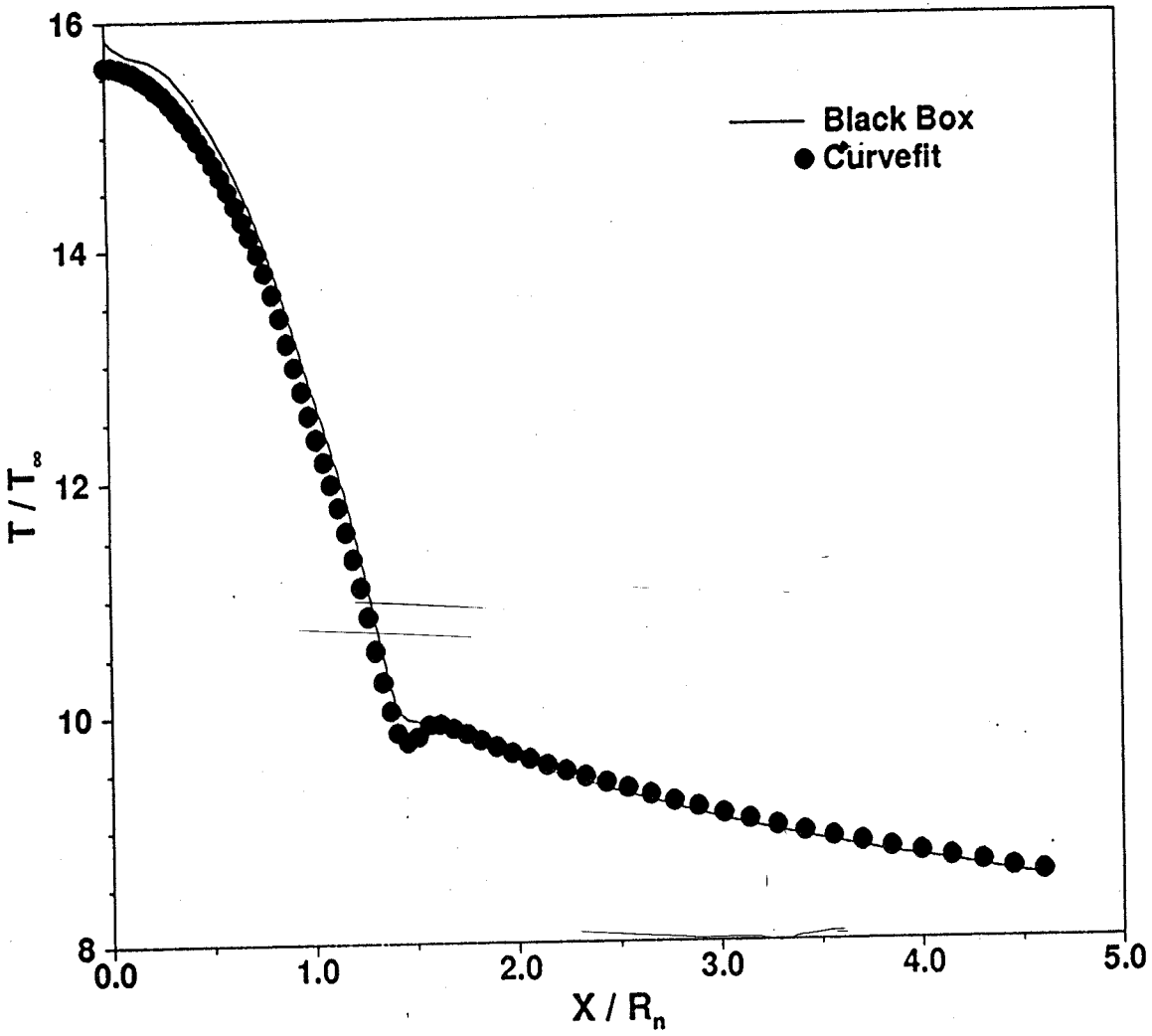

Timing Comparisons for Multi-Block Solver

(Blunt Cone, M_∞ = 10, Cray-YMP)

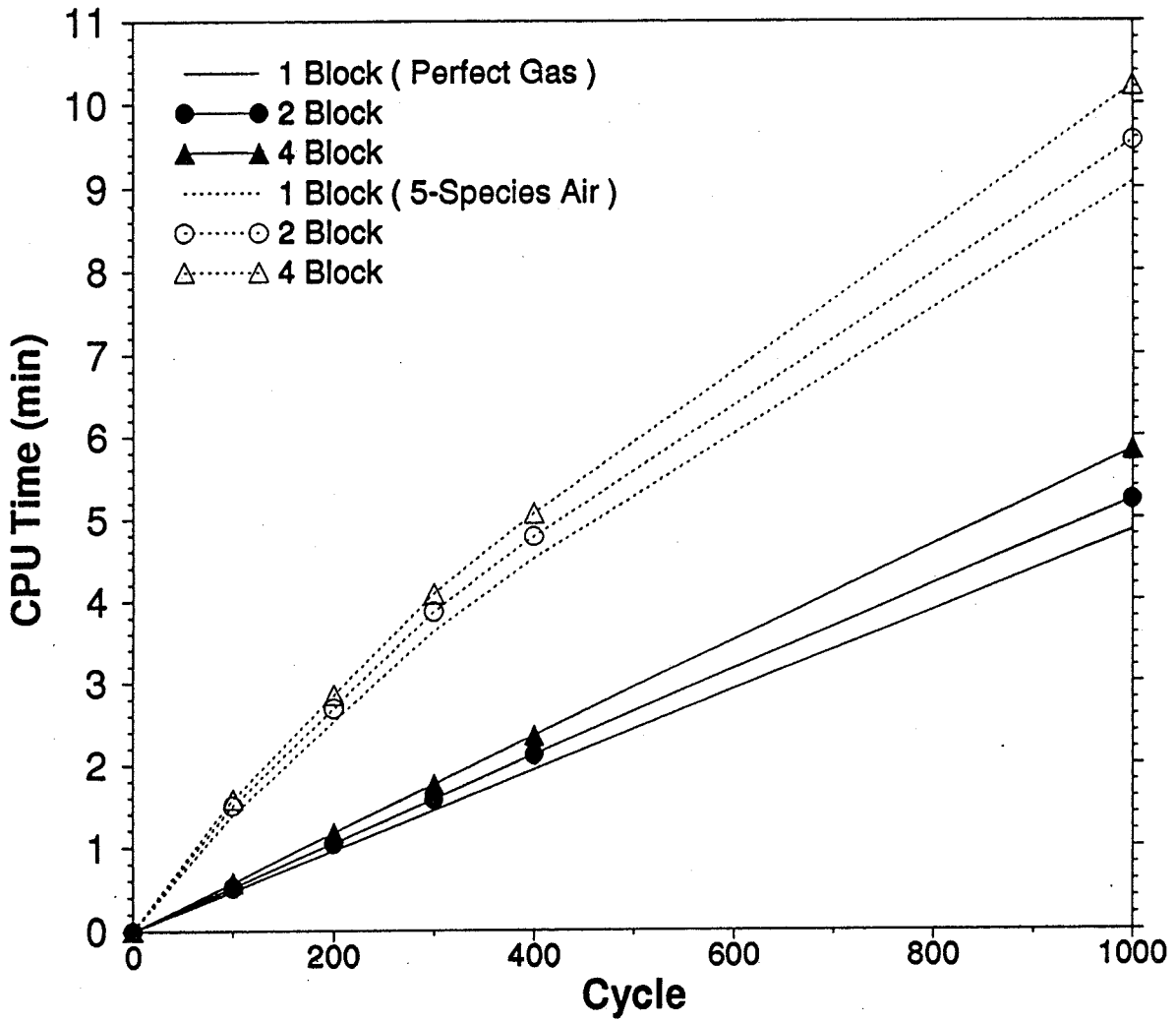

SSME NOZZLE

- 100% power @ sea level, mixture ratio 6:1

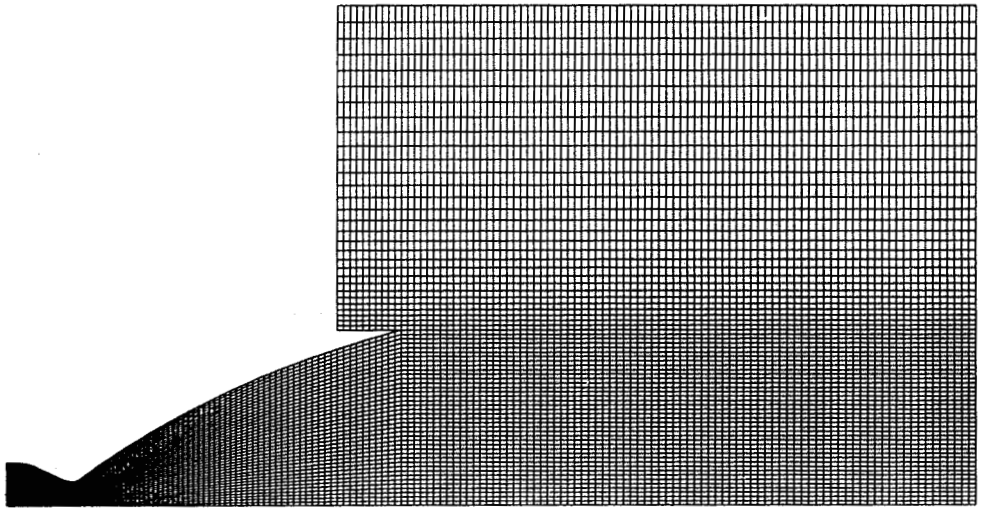

- Chamber conditions:

$T_c = 3639\ K$ $\qquad$ $M_c = 0.2$

$p_c = 20.24\ MPa$

Mach Number Profiles

(SSME Nozzle)

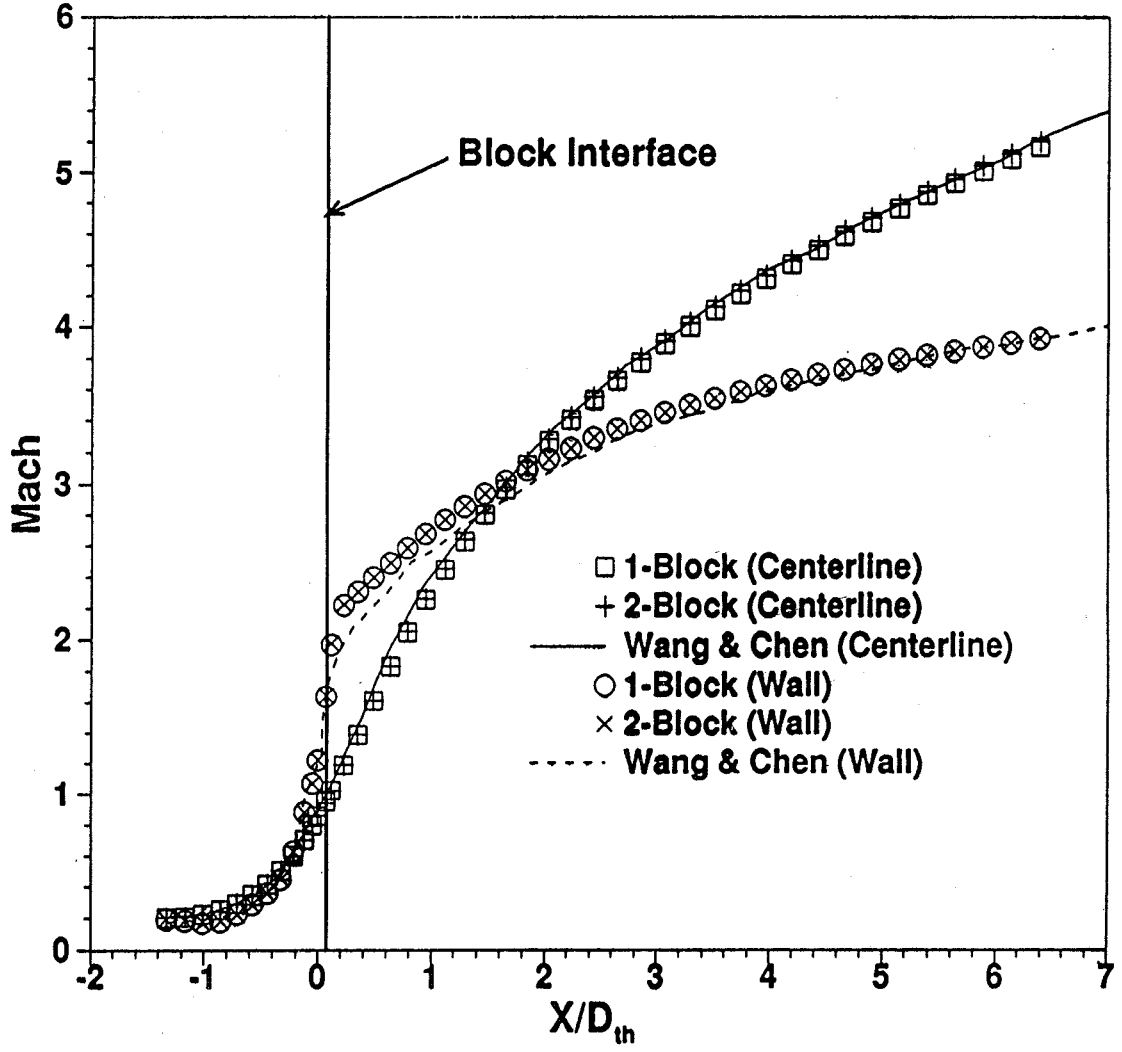

HYPERSONIC INLET

- 10 deg. lower and 20 deg. upper ramp

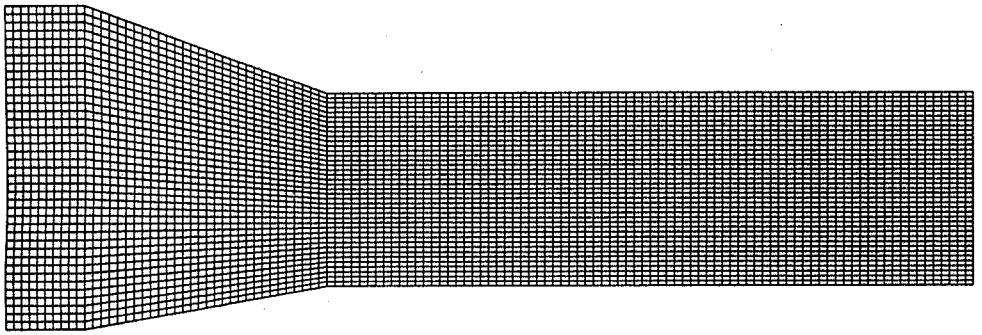

- Flow conditions:

$M_\infty = 5 \qquad p_\infty = 6.52\ kPa$

$\varrho_\infty = 1.293 \times 10^{-2}\ kg/m^3$

Pressure Contours

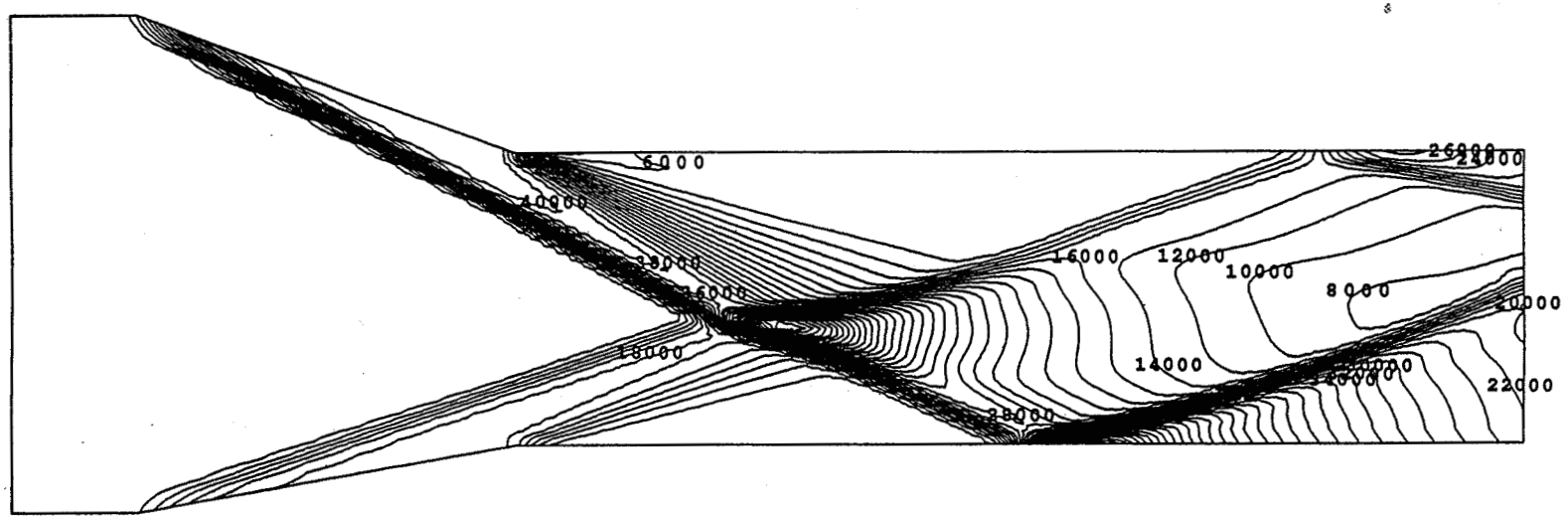

WORK IN PROGRESS

- Viscous terms added
  - **Parabolized Navier-Stokes (Turbulent)**
  - **Full Navier-Stokes (Laminar)**
- Finite-rate chemistry
  - **Improved numerical techniques**
- Hybrid chemistry (partial equilibrium)
  - **Elemental species continuity equations (allows for diffusion)**
  - **Kinetic species continuity equations coupled with "Black Box"**
- Pre-conditioning for low-speed flows
- Parallelization

CONCLUSIONS

- An EFFICIENT and GENERAL solver for reacting gas flows has been developed, which...

  can handle arbitrary mixtures,

  uses efficient numerical techniques,

  and

  is applicable to propulsion design/analysis.

NUMERICAL MODELING OF SPRAY COMBUSTION WITH AN UNSTRUCTURED-GRID METHOD

H.M. Shang, Y.S. Chen, P. Liaw and M.H. Shih
Engineering Sciences, Inc., Huntsville, AL
and
T.S. Wang
NASA/Marshall Space Flight Center, Huntsville, AL

ABSTRACT

The present unstructured-grid method follows strictly the basic finite volume forms of the conservation laws of the governing equations for the entire flow domain. High-order spatially accurate formulation has been employed for the numerical solutions of the Navier-Stokes equations. A two-equation k-ε turbulence model is also incorporated in the unstructured-grid solver. The convergence of the resulted linear algebraic equation is accelerated with preconditioned Conjugate Gradient method. A statistical spray combustion model has been incorporated into the present unstructured-grid solver. In this model, spray is represented by discrete particles, rather than by continuous distributions. A finite number of computational particles are used to predict a sample of total population of particles. Particle trajectories are integrated using their momentum and motion equations and particles exchange mass, momentum and energy with the gas within the computational cell in which they are located. The interaction calculations are performed simultaneously and eliminate global iteration for the two-phase momentum exchange. A transient spray flame in a high pressure combustion chamber is predicted and then the solution of liquid-fuel combusting flow with a rotating cup atomizer is presented and compared with the experimental data. The major conclusion of this investigation is that the unstructured-grid method can be employed to study very complicated flow fields of turbulent spray combustion. Grid adaptation can be easily achieved in any flow domain such as droplet evaporation and combustion zone. Future applications of the present model can be found in the full three-dimensional study of flow fields of gas turbine and liquid propulsion engine combustion chambers with multi-injectors.

NUMERICAL MODELING OF SPRAY COMBUSTION WITH AN UNSTRUCTURED GRID METHOD

H.M. Shang, Y.S. Chen, P. Liaw and M.H. Shih
Engineering Sciences, Inc.

T.S. Wang
NASA-Marshall Space Flight Center

Presented At

13*th* Workshop for CFD Applications in Rocket Propulsion

NASA-MSFC, April 25-27, 1995

OUTLINE

- INTRODUCTION
- MOTIVATION AND OBJECTIVE
- UNSTRUCTURED GRID FLOW SOLVER
- PHYSICAL MODELS AND NUMERICAL APPROACHES
- COMPUTATIONAL RESULTS
- CONCLUSIONS

INTRODUCTION

- APPLICATION OF SPRAY COMBUSTION
  - LIQUID-FUELED ROCKET ENGINES
  - GAS-TURBINE COMBUSTORS
  - INDUSTRIAL FURNACES
  - DIESEL ENGINES
- MODELING IN LIQUID-FUELED ROCKET ENGINES
  - COAXIAL, IMPINGING JETS AND SWIRLING INJECTORS ...
  - ATOMIZATION PROCESS
  - DROPLET VAPORIZATION, DISPERSION AND COLLISION
  - TURBULENT COMBUSTION

INTRODUCTION . . .

- STRUCTURED GRID
  - BODY-FITTED COORDINATES, MULTI-ZONE
  - AUTOMATIC INDEXING
  - HIGH EFFICIENCY AND LESS MEMORY
  - TIME-CONSUMING GRID GENERATION FOR COMPLEX GEOMETRY
- UNSTRUCTURED GRID
  - SIMULATION OF ANY COMPLEX GEOMETRIES
  - FLEXIBLE SOLUTION ADAPTIVITY
  - LESS GRID GENERATION EFFORTS
  - HIGH MEMORY AND COMPUTATION EFFORT

MOTIVATION AND OBJECTIVE

- SIMULATE MULTI-INJECTOR COMPLEX SPRAY COMBUSTION PROCESS IN ROCKET PROPULSION ENGINES
- A MAJOR STRUCTURED GRID CAN BE GENERATED ABOUT THE MAIN COMBUSTION CHAMBER
- EACH INJECTOR REGION CAN BE A SUBDOMAIN (A HOLE IN MAJOR GRID) WHERE STRUCTURED OR UNSTRUCTURED GRID CAN BE GENERATED
- THE OVERLAPPED REGION OR GAP BETWEEN MAJOR- AND SUB-GRID CAN BE FILED UP WITH UNSTRUCTURED GRIDS
- TAKE THE ADVANTAGE OF GRID FLEXIBILITY OF UNSTRUCTURED GRID METHOD
- DEVELOP AND INCORPORATE ADVANCED SPRAY COMBUSTION MODEL IN UNSTRUCTURED CODE

UNSTRUCTURED GRID FLOW SOLVER

- CELL-CENTERED FINITE VOLUME ALGORITHM
- HYBRID UNSTRUCTURED CELL
  - TRIANGLE AND QUADRANGLE FOR 2D
  - PRISM, TETRAHEDRAL AND HEXAHEDRAL FOR 3D
- PRESSURE-CORRECTION ALGORITHM
- CONJUGATE GRADIENT SQUARED (CGS) MATRIX SOLVER
- VISCOUS OR INVISCID, LAMINAR OR TURBULENT, INCOMPRESSIBLE OR COMPRESSIBLE FLOW
- HIGH-ORDER SCHEME WITH FLUX LIMITER
- STEADY STATE OR TRANSIENT FLOW

2D UNSTRCTURED CELLS

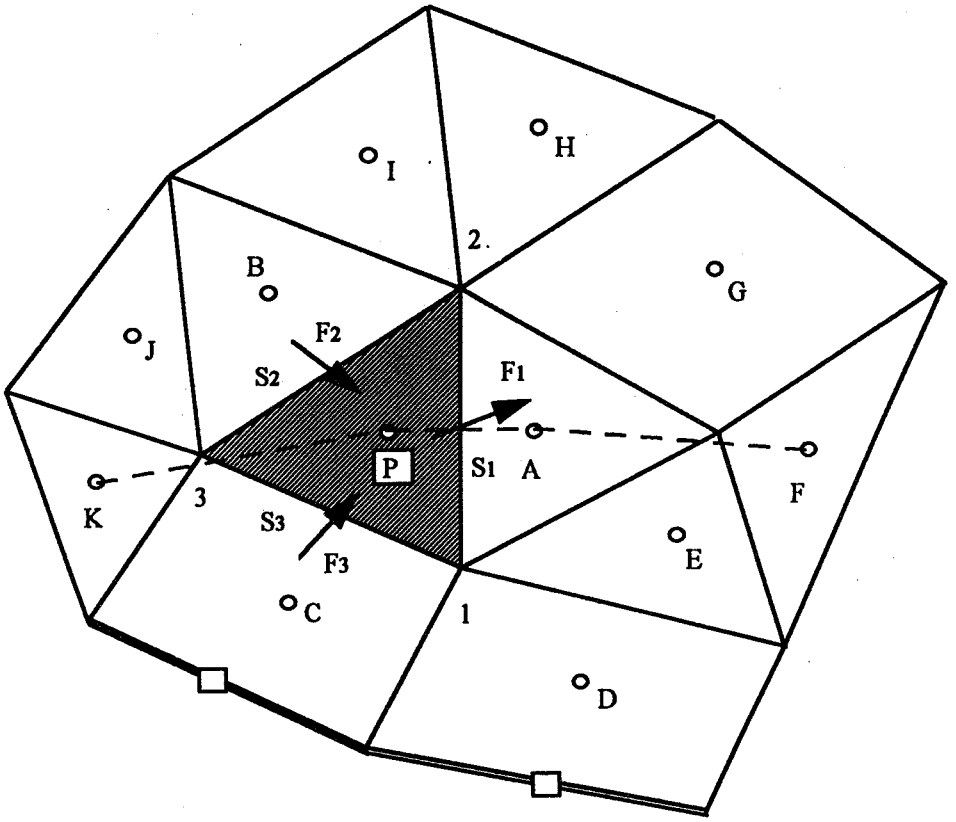

- Main Point
- Boundary Point
- 1,2,.. Node Point
- F Flux
- S Cell Surface

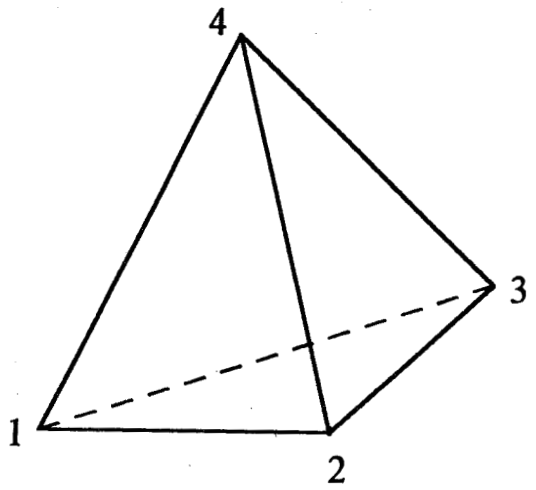

Face	Nodes			
1	1	2	4	
2	2	3	4	
3	3	2	1	
4	1	4	3	

Tetrahedron

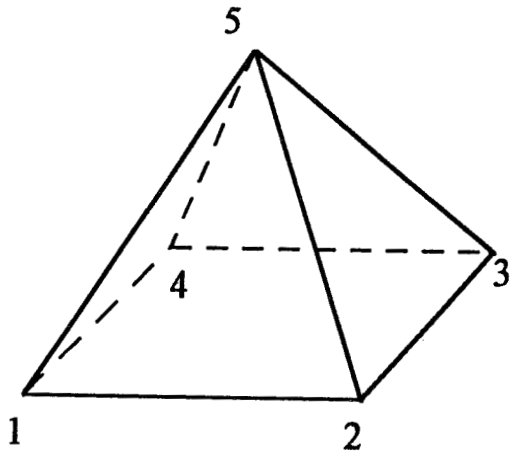

Face	Nodes				
1	1	2	5		
2	2	3	5		
3	3	4	5		
4	4	1	5		
5	3	2	1	4	

Pyramid

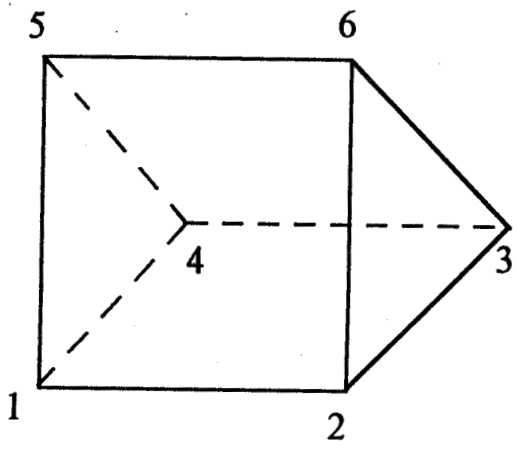

Face	Nodes				
1	1	2	6	5	
2	2	3	6		
3	3	4	5	6	
4	4	1	5		
5	3	4	1	2	

Prism

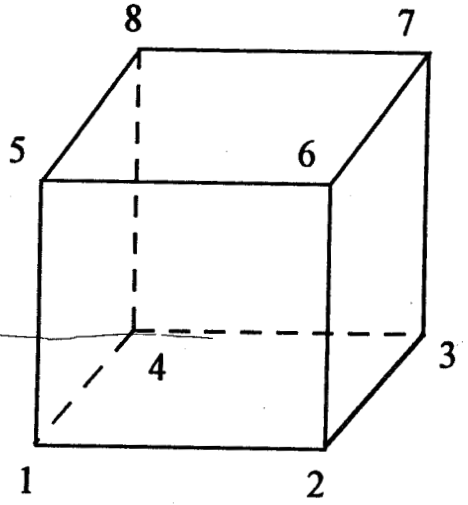

Face	Nodes				
1	1	2	6	5	
2	2	3	7	6	
3	3	4	8	7	
4	4	1	5	8	
5	3	2	1	4	
6	6	7	8	5	

Hexahedron

JOINT HYBRID CELLS

Hexahedron: 1 2 3 4 5 6 7 8
Prism: 2 3 9 6 10 7
Pyramid: 5 6 7 8 11
Tetrahedron: 6 10 7 11

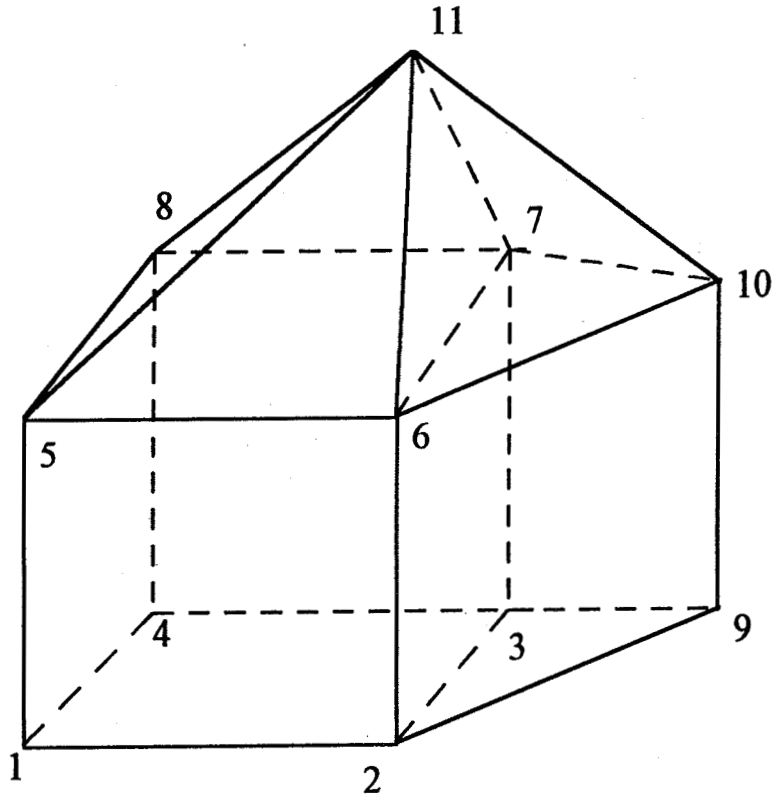

DOUGLAGS MULTI-ELEMENT AIRFOIL

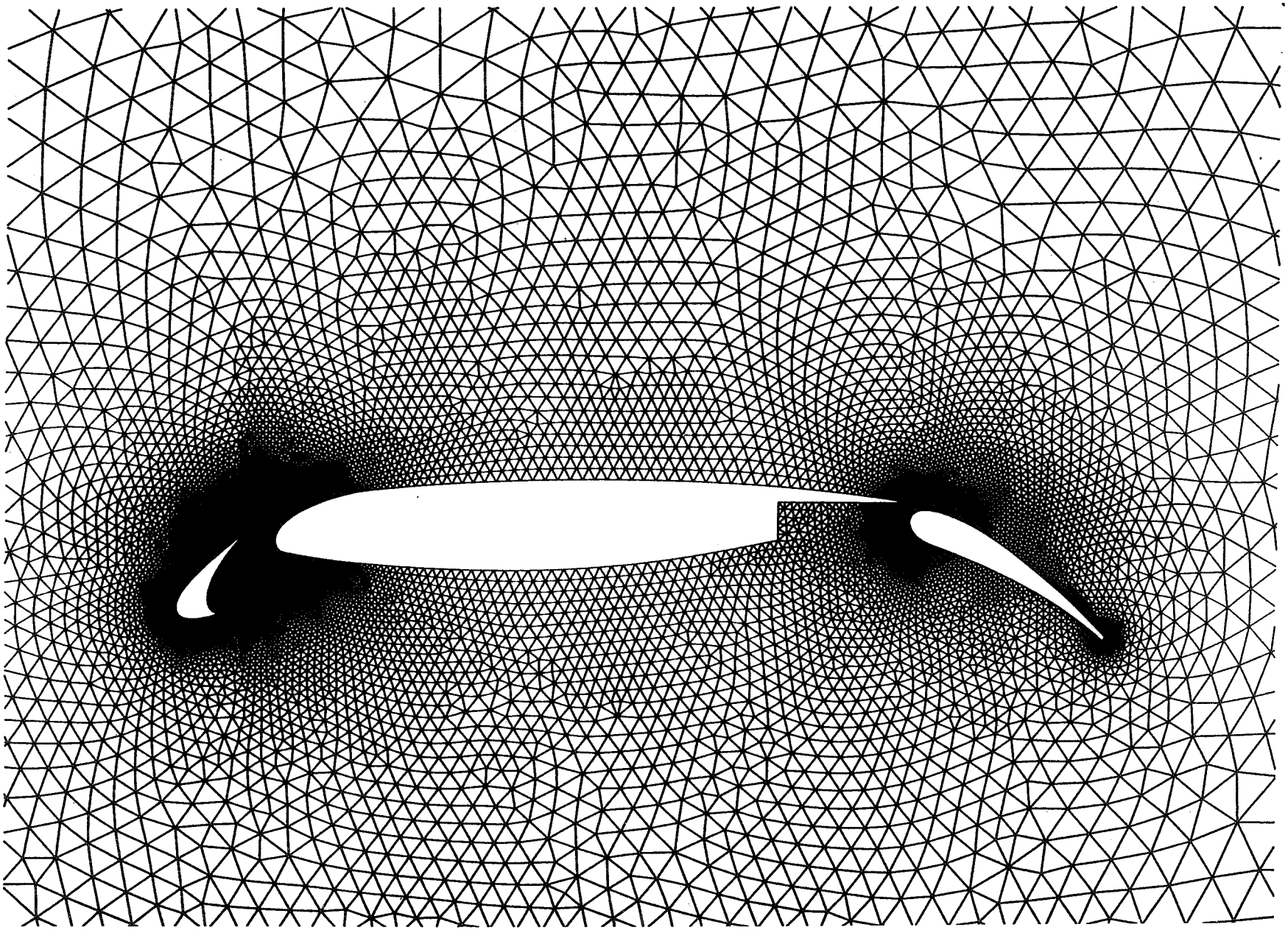

GOUGLAS MULTI-ELEMENT AIRFOIL

PRESSURE CONTOUR

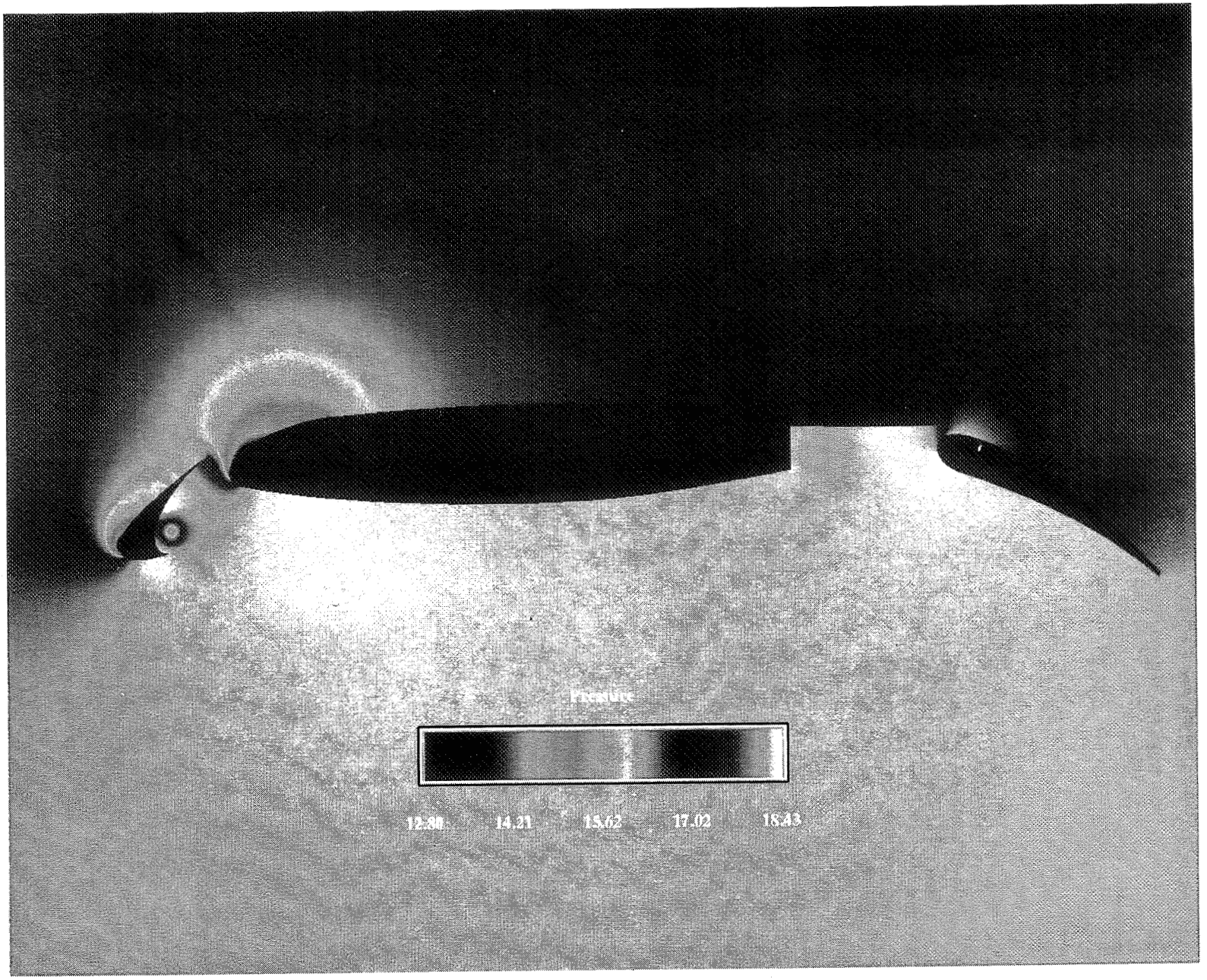

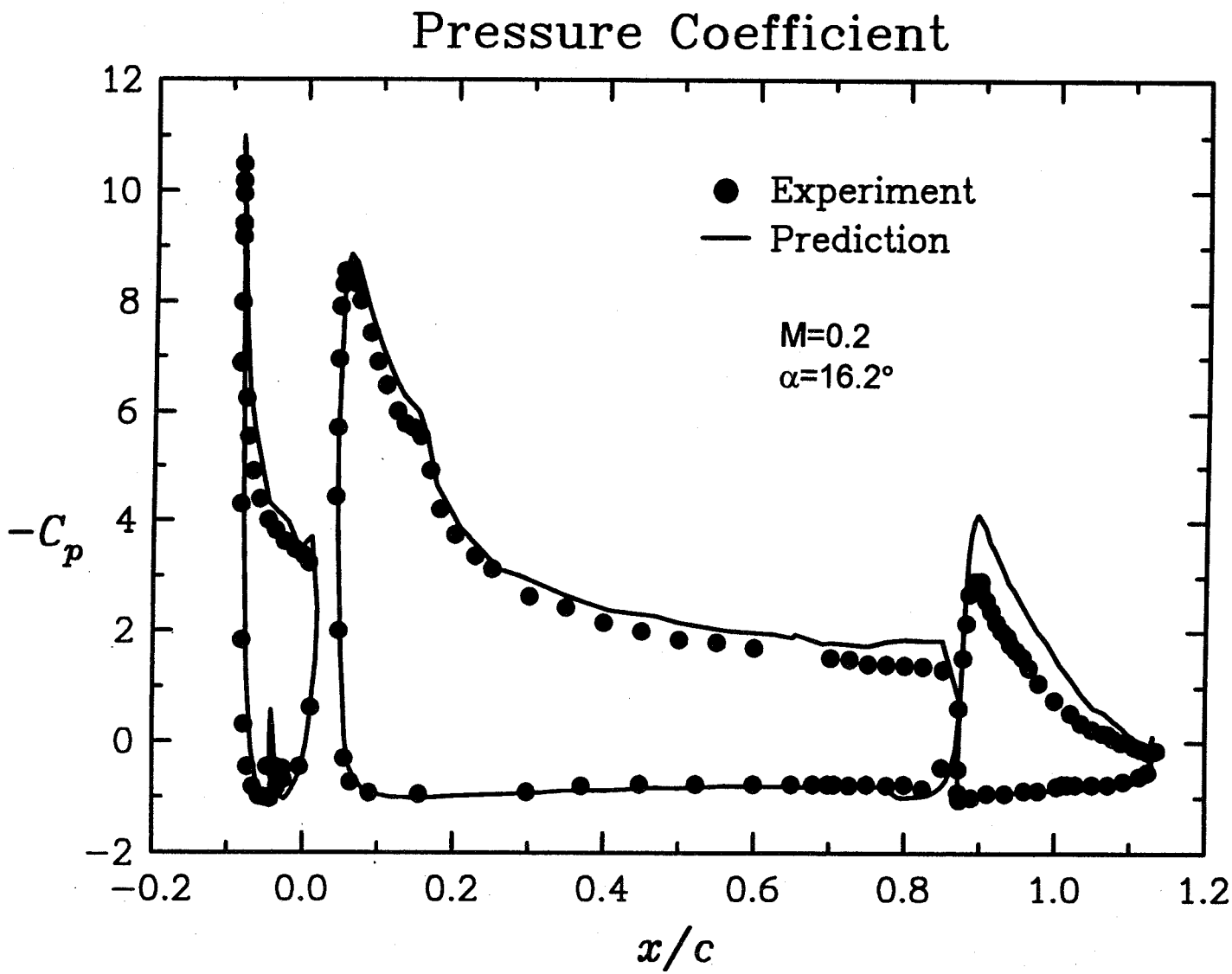
Pressure Coefficient
Experiment
Prediction
M=0.2
α=16.2°
$-C_p$
x/c
12
10
8
6
4
2
0
−2
−0.2
0.0
0.2
0.4
0.6
0.8
1.0
1.2

BOEING 747 AIRPLANE

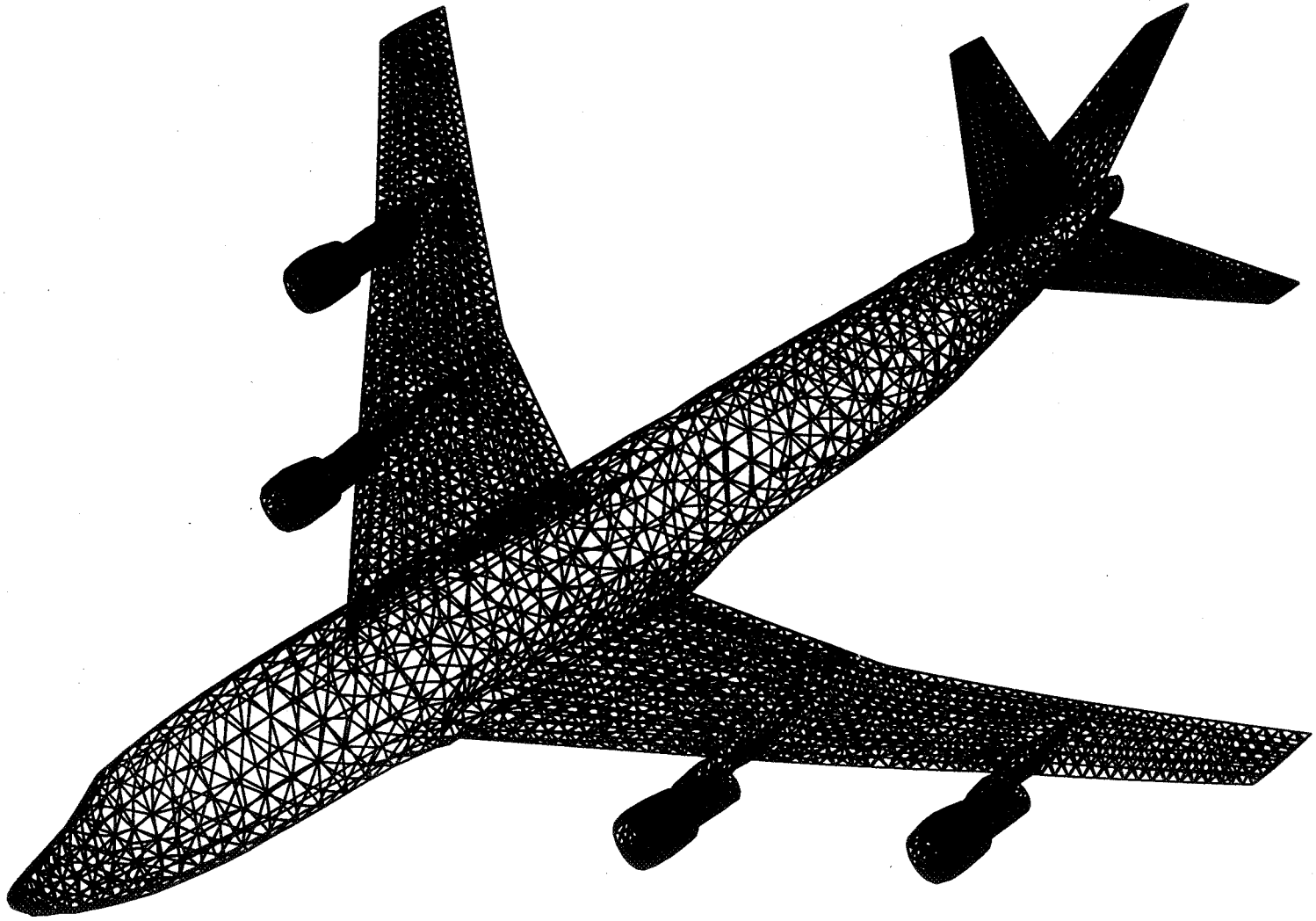

BOEING 747 AIRPLANE

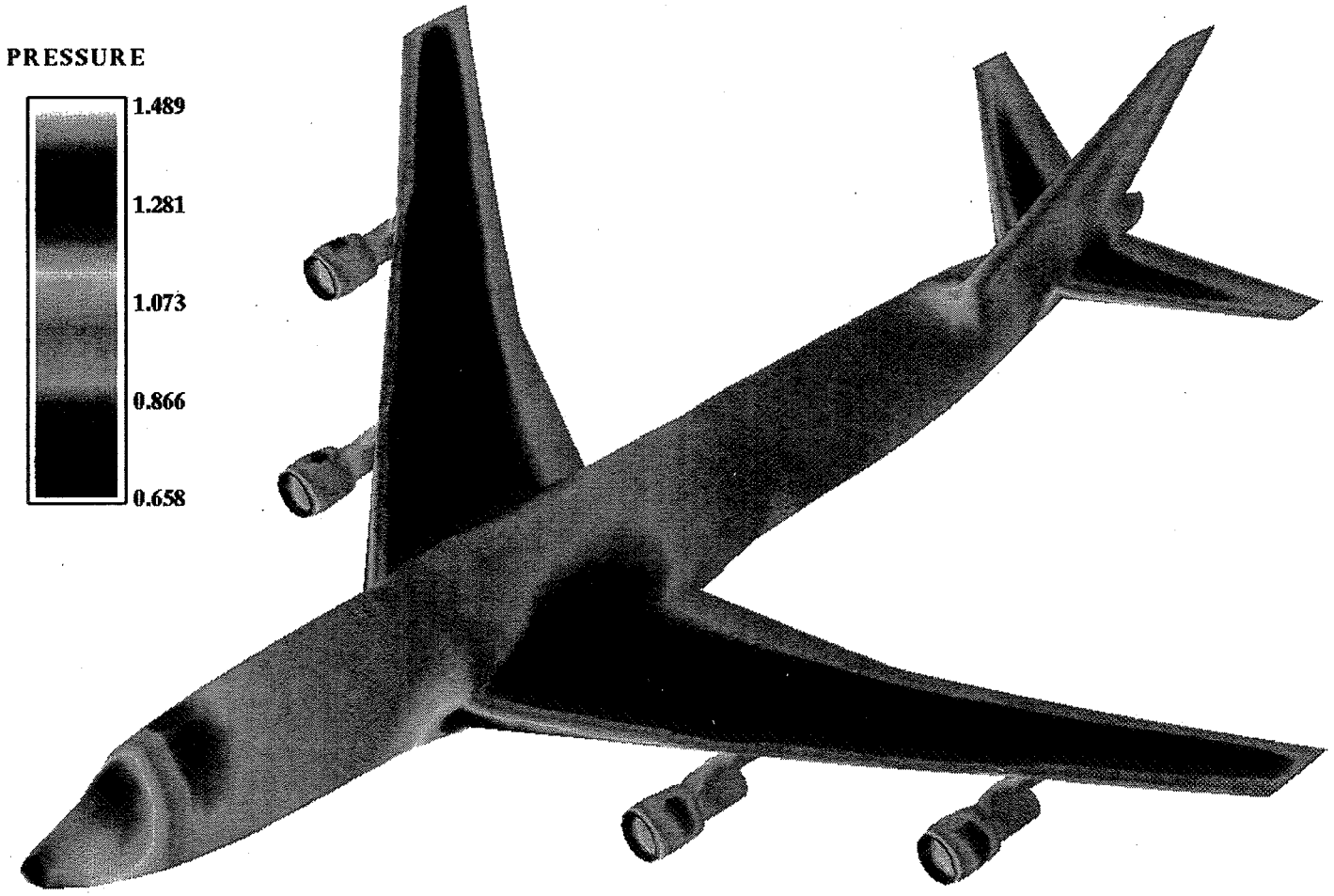

PHYSICAL MODELS AND NUMERICAL APPROACHES

- STRONGLY-COUPLED EULERIAN-LAGRANGIAN TWO-PHASE FLOW APPROACH
- STOCHASTIC SEPARATED FLOW (SSF) MODEL FOR PARTICLE TURBULENT DISPERSION
- DROPLET BREAK-UP, EVAPORATION AND COLLISION MODEL
- LIQUID JET ATOMIZATION MODEL
- VOF (VOLUME OF FLUID) MODEL FOR COAXIAL OR IMPINGING JETS INJECTORS
- K-ε TWO-EQUATION TURBULENCE MODEL
- INSTANEOUS, FINITE-RATE AND EQUILIBRIUM CHEMISTRY MODEL

COMPUTATIONAL RESULTS

- TRANSIENT SPRAY COMBUSTION
  - EXPERIMENT OF YOKOTA ET AL.
  - LIQUID FUEL TRIDECANE ($C_{13}H_{28}$) INJECTED INTO HIGH-PRESSURE (3.0 MPA) AND TEMPERATURE (900 K) AIR CHAMBER
  - SINGLE STEP AND EDDY-BREAK-UP COMBUSTION MODEL
  - FIVE SPECIES WERE CONSIDERED: $C_{13}H_{28}$, O_2, N_2, CO_2 AND H_2O
  - THE IGNITION DELAY AND TRANSIENT CONFIGURATION OF THE SPRAY FLAME ARE REASONABLY PREDICTED

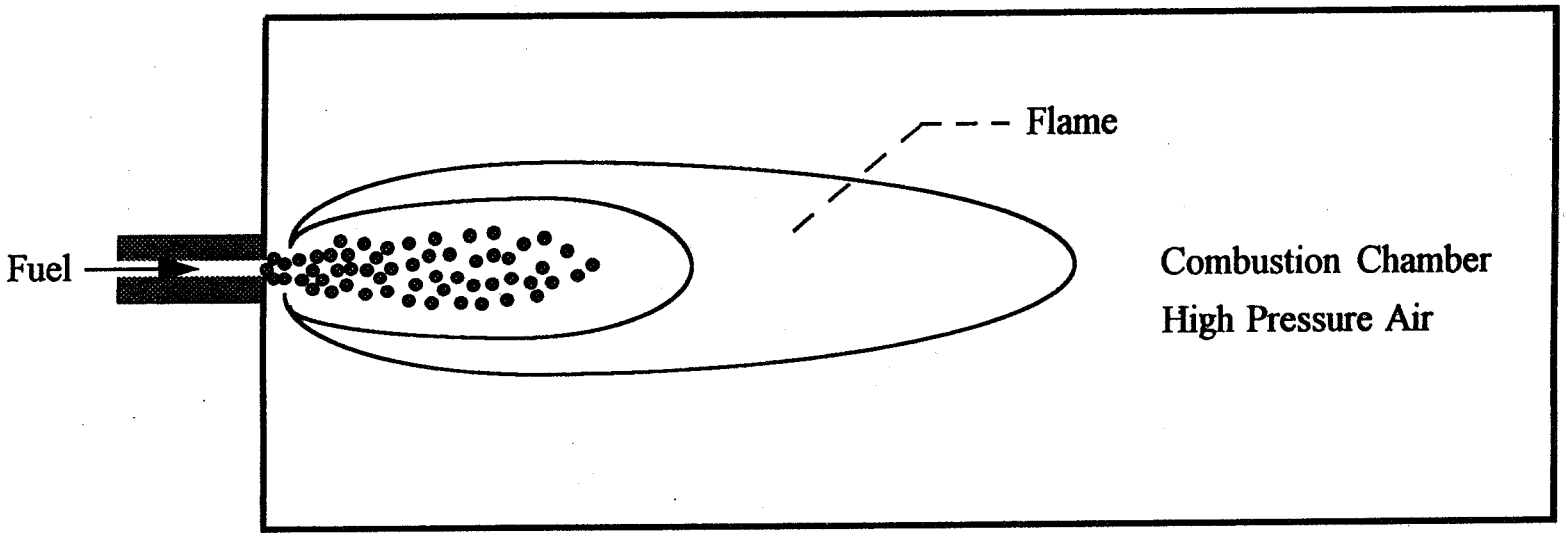
Flame
Fuel
Combustion Chamber
High Pressure Air

TRANSIENT SPRAY COMBUSTION

TEMPERATURE CONTOUR

t=1.0 ms

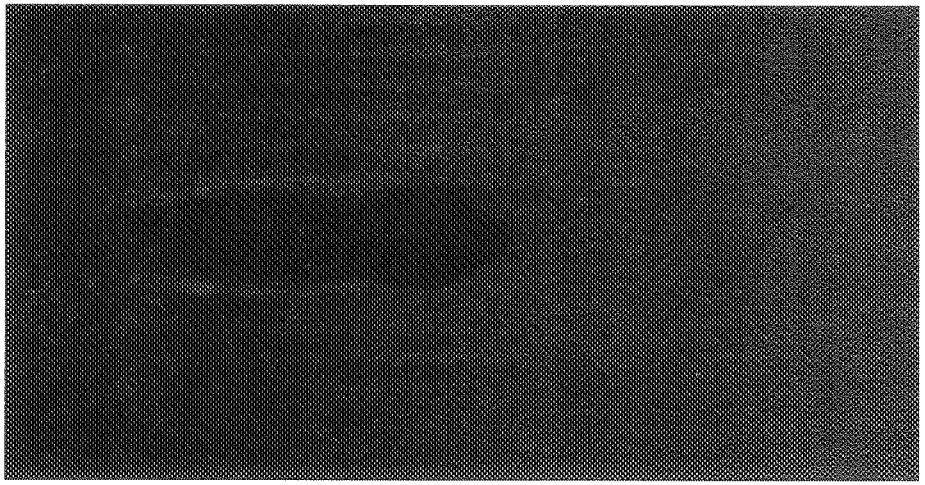

t=2.6 ms

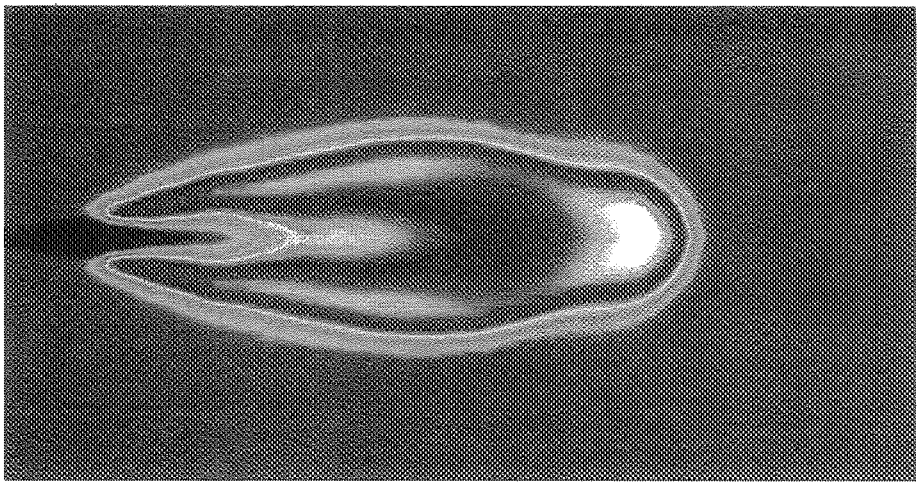

t=1.4 ms

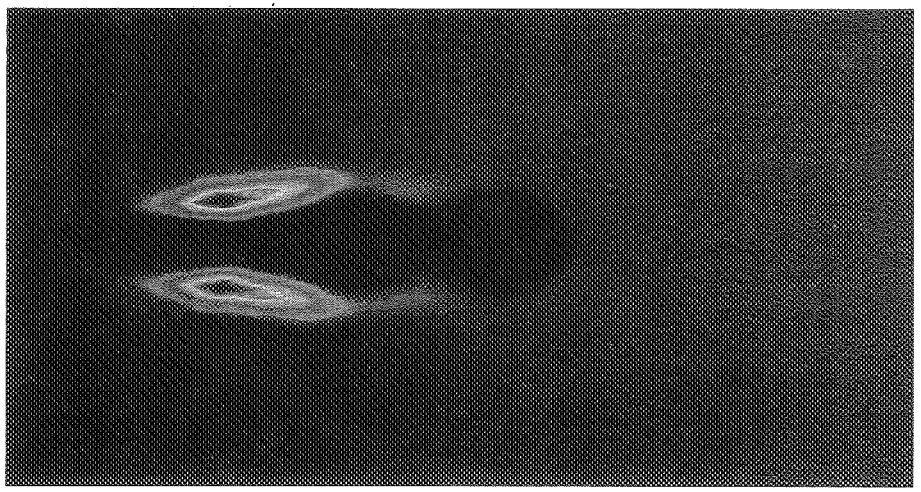

t=3.8 ms

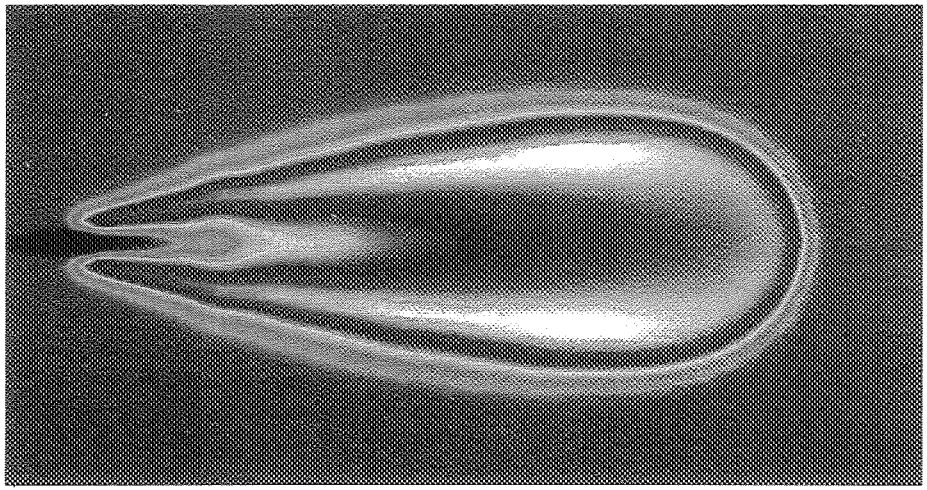

TRANSIENT SPRAY COMBUSTION

t=3.8 ms

FUEL MASS FRACTION

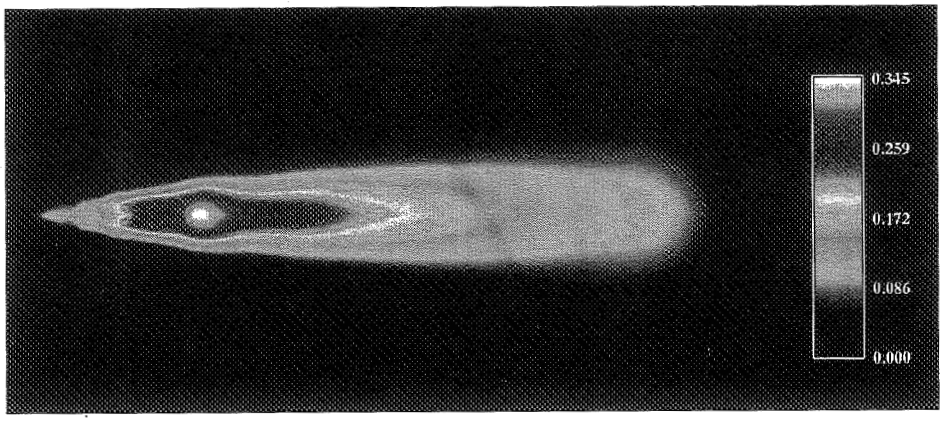

CO2 MASS FRACTION

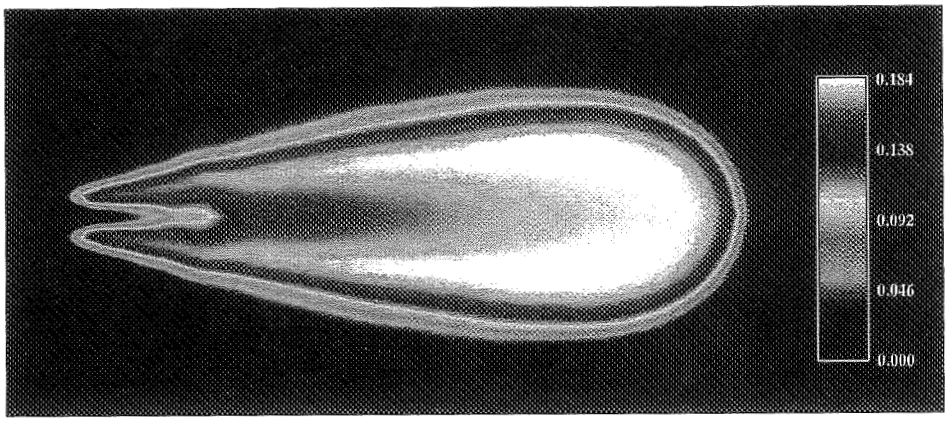

O2 MASS FRACTION

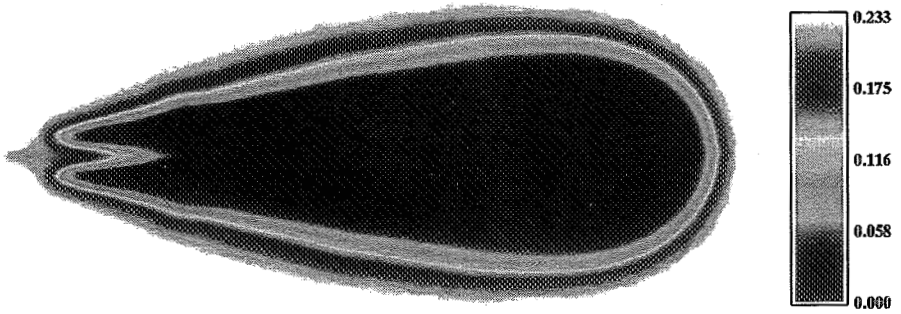

TEMPEATURE

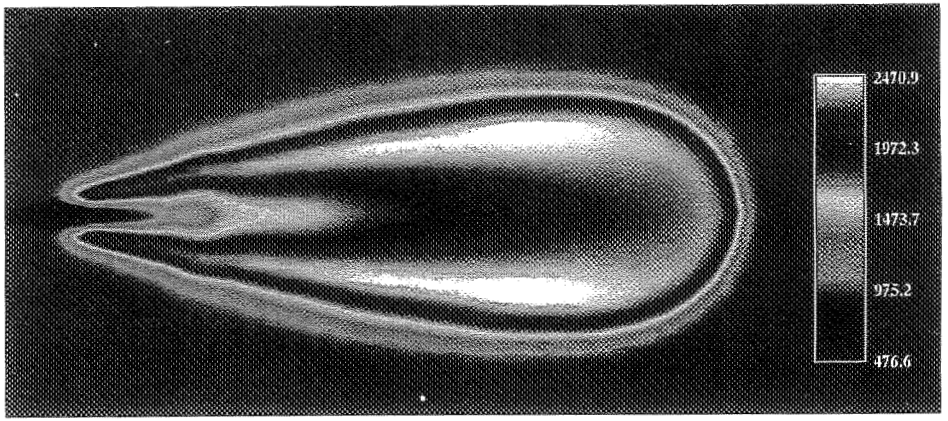

TRANSIENT SPRAY COMBUSTION

SPRAY + GRIDS + TEMPERATURE CONTOUR

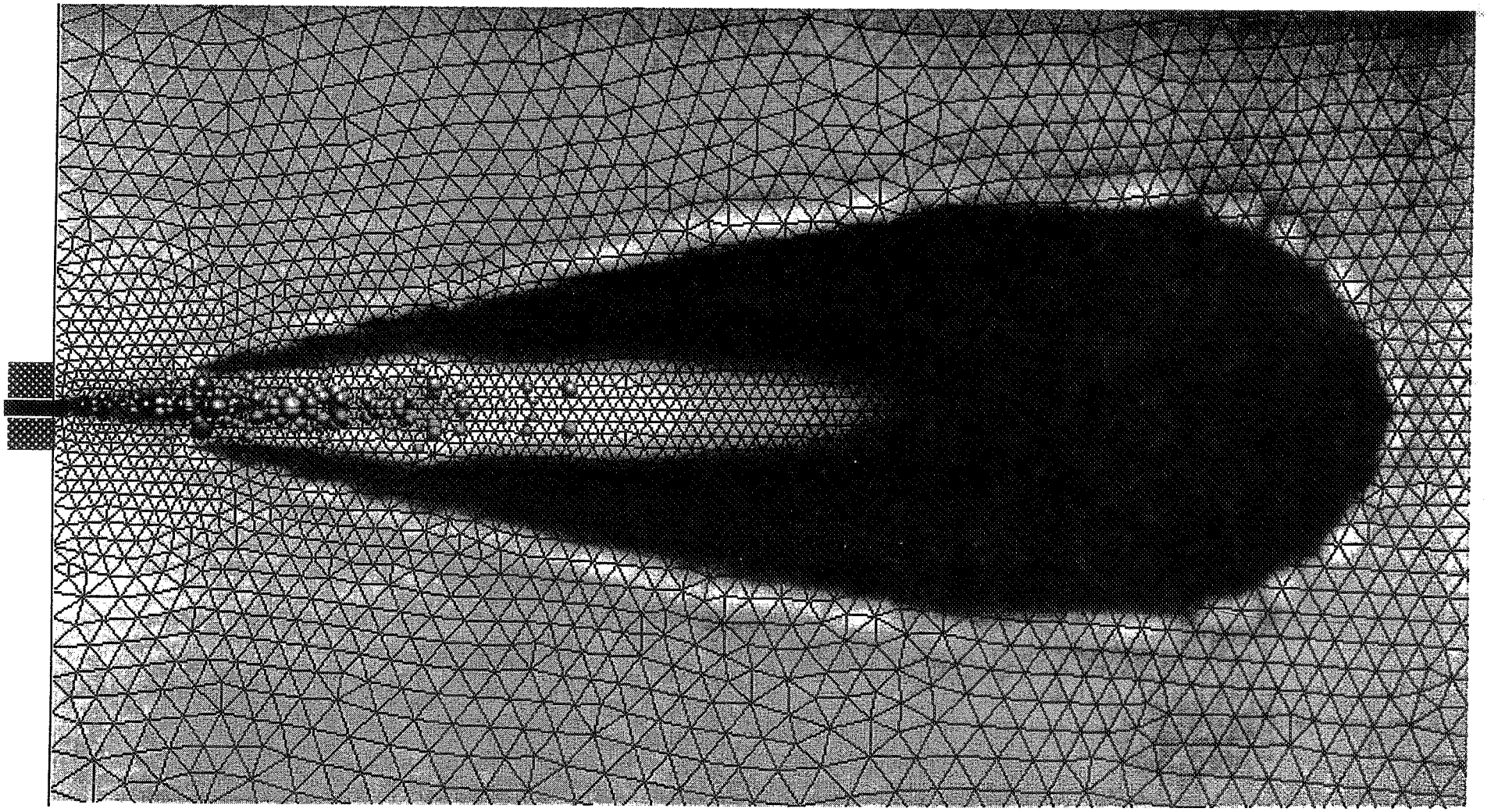

COMPUTATIONAL RESULTS . . .

- SPRAY FLAME IN A COMBUSTION CHAMBER
  - EXPERIMENT OF EL-BANHAWY AND WHITELAW
  - MONO-SIZED (D=47μM) LIQUID KEROSENE INJECTED AT ROOM TEMPERATURE WITH FLOW RATE 1.32×10^{3} KG/S
  - AIR INLET SWIRL NUMBER 1.2 WITH FLOW RATE 0.0556 KG/S
  - SINGLE STEP AND EDDY-BREAK-UP COMBUSTION MODEL
  - FIVE SPECIES WERE CONSIDERED: $C_{13}H_{28}$, O_2, N_2, CO_2 AND H_2O
  - FAVORABLE AGREEMENT WITH EXPERIMENTAL MEASUREMENT
  - HIGHER TEMPERATURE PREDICTED DUE TO THE LACK OF RADIATION HEAT TRANSFER MODEL AND DISSOCIATION OF CHEMICAL RADICALS AND SOOT

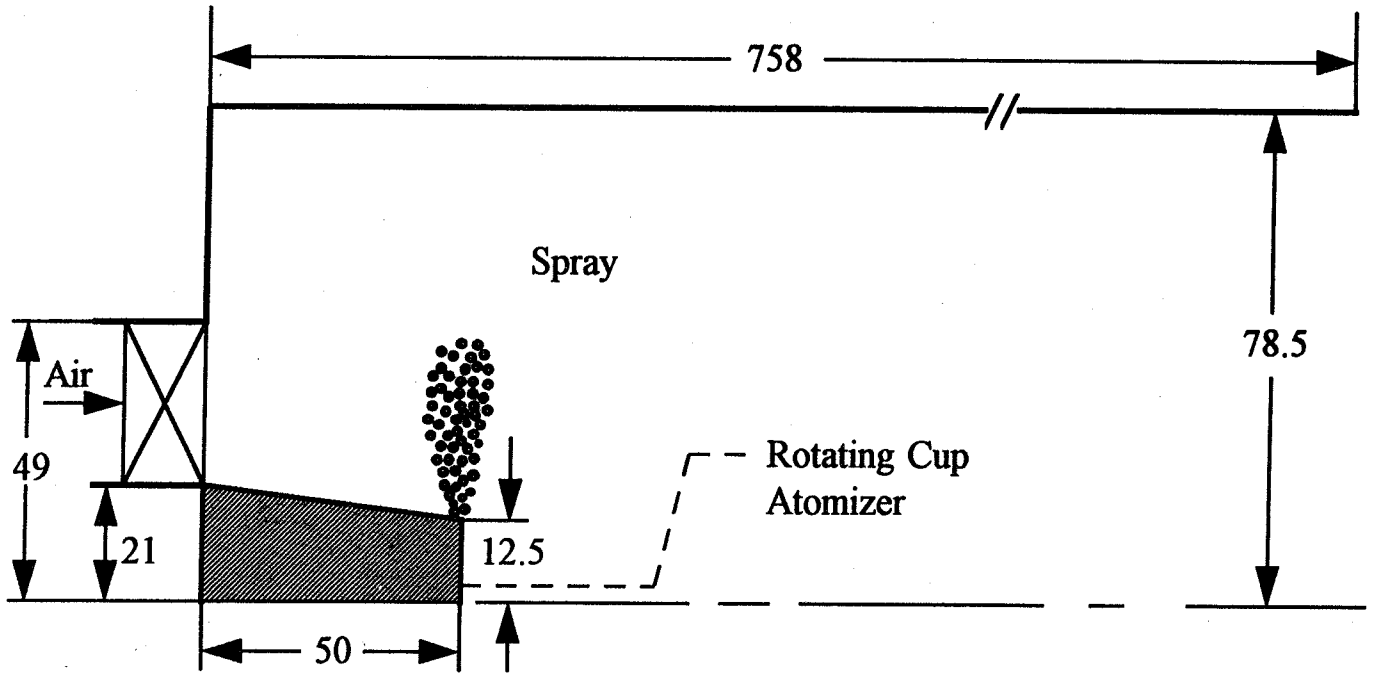
758
Spray
78.5
Air
49
21
12.5
Rotating Cup
Atomizer
50

SPRAY FLAME IN A COMBUSTION CHAMBER

FUEL MASS FRACTION

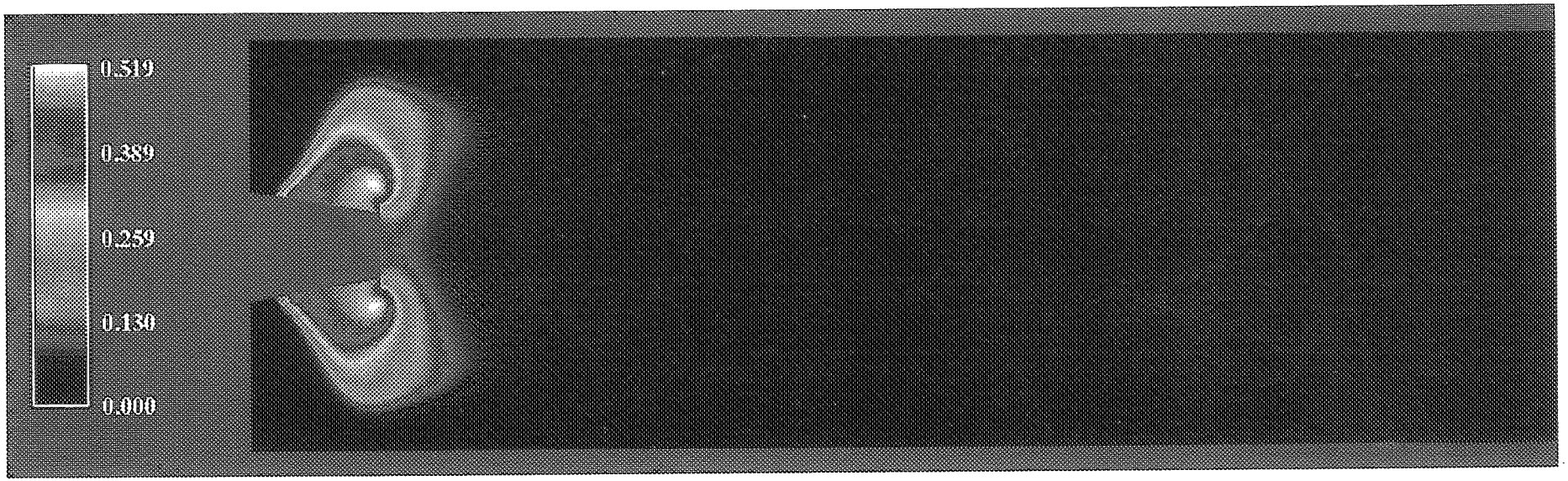

O2 MASS FRACTION

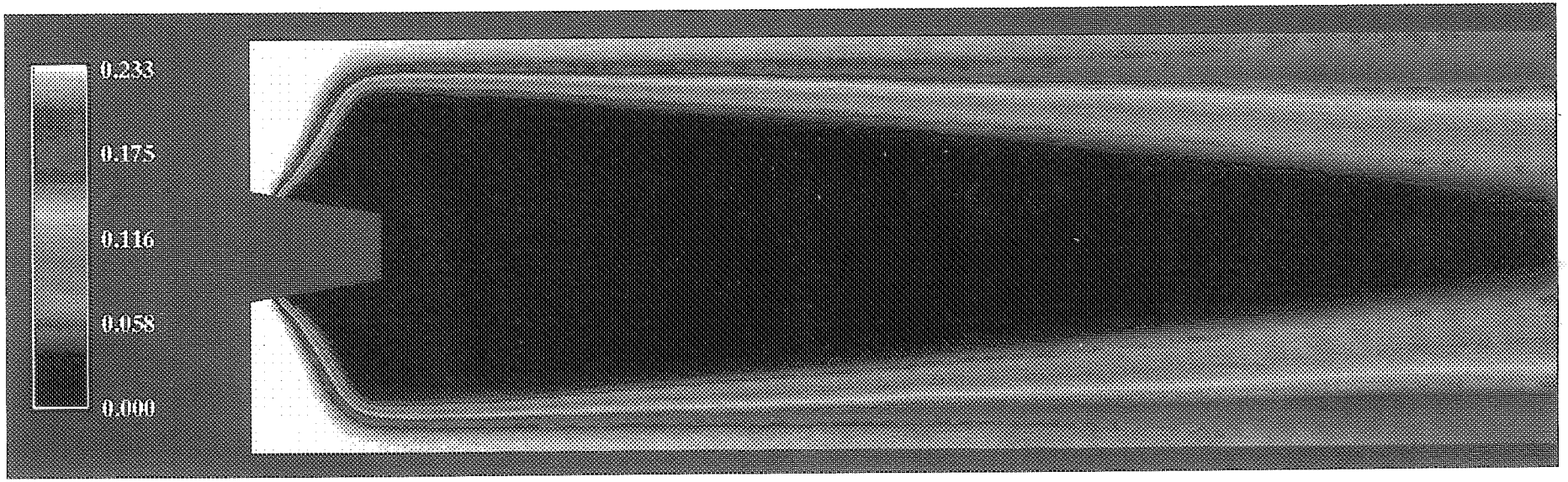

SPRAY FLAME IN A COMBUSTION CHAMBER

CO2 MASS FRACTION

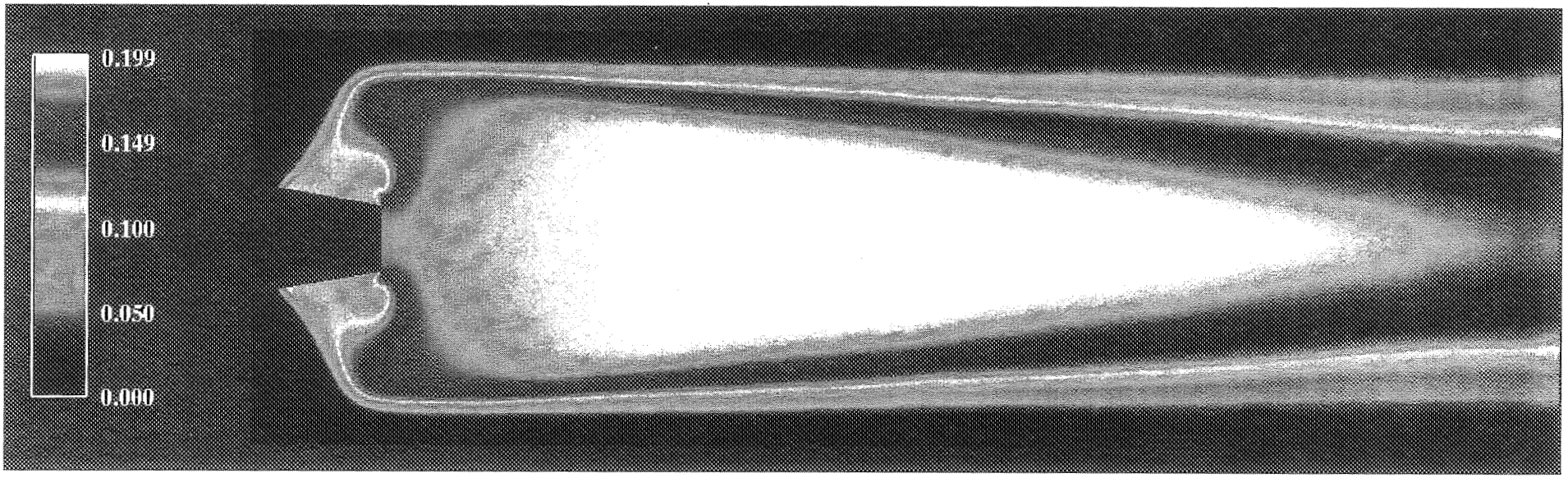

TEMPERATURE

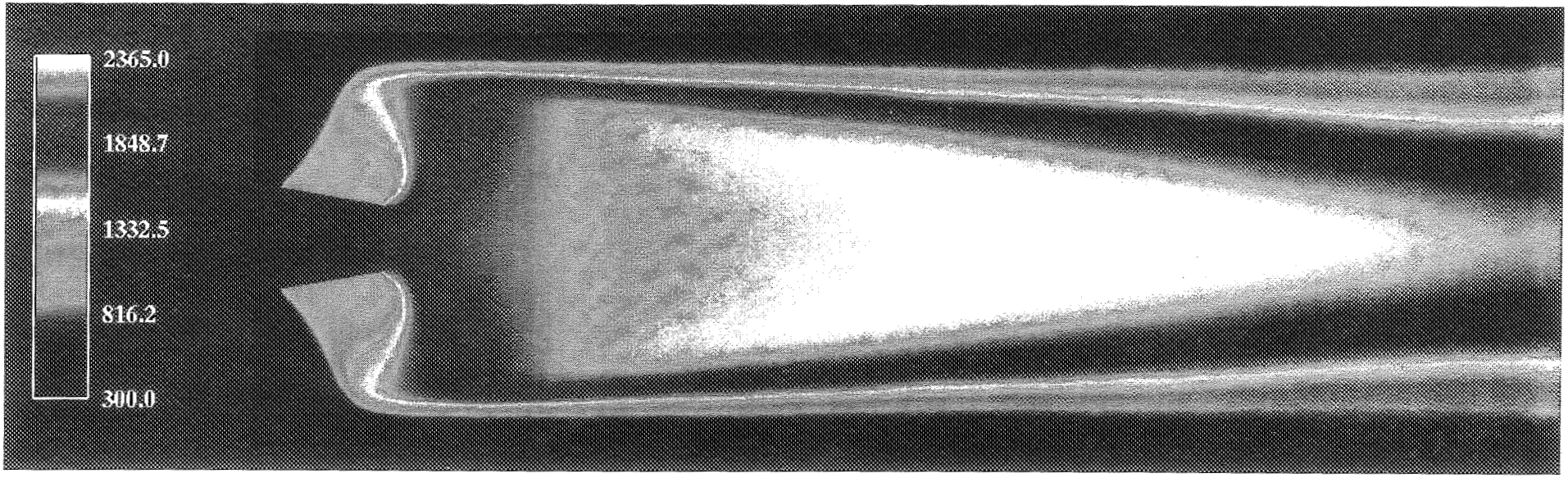

SPRAY FLAME IN A COMBUSTION CHAMBER

SPRAY+GRIDS

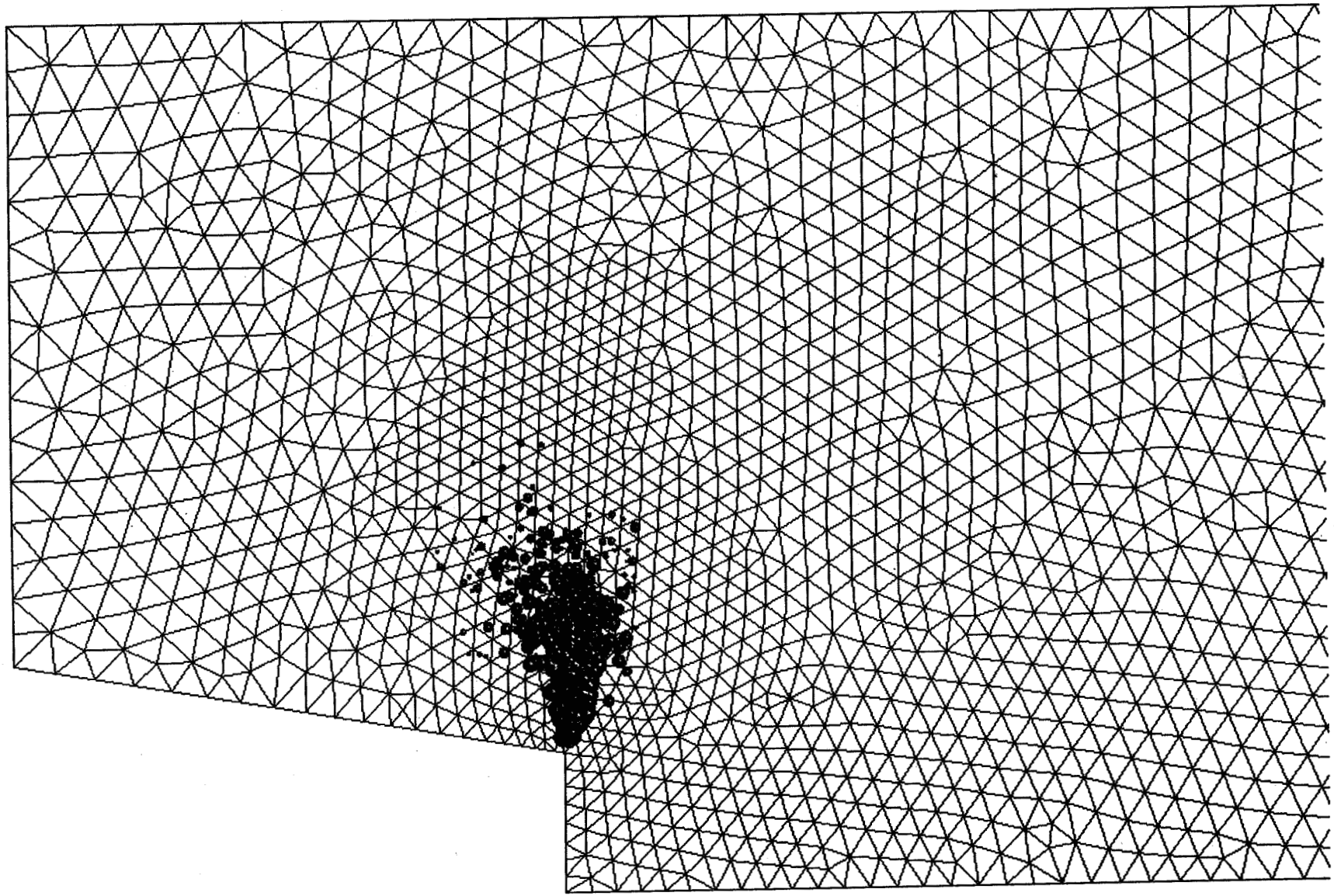

CONCLUSIONS

- A SPRAY COMBUSTION MODEL HAS BEEN INCORPORATED IN A PRESSURE-BASED HYBRID UNSTRUCTURED GRID CODE
- FAVORABLE AGREEMENT WITH EXPERIMENTAL RESULTS HAS BEEN ACHIEVED
- CONTINUE VALIDATE AND EXTEND THE CURRENT MODEL IN 3D MULTI-INJECTOR COMBUSTION MODELING
- DEVELOP HYBRID UNSTRUCTURED GRID GENERATION TECHNIQUE
- RADIATION HEAT TRANSFER EFFECT MUST BE INCLUDED IN FUTURE DEVELOPMENT FOR HYDROCARBON COMBUSTION

Numerical investigation of two-phase turbulent flow of charged droplets in electrostatic field

S.-W. Kim
Resident research associate
NASA Lewis Research Center
Cleveland, Ohio 44135

CONTENTS

I. Introduction

1.1 Development of a numerical procedure to solve chemically reacting two-phase turbulent flows for *aerospace propulsion* applications (vaporization and combustion of multi-component liquid fuels in sub- and super-critical pressure and temperature) is in progress.

Calculation of a two-phase turbulent flow of charged droplets in electrostatic field is presented herein.

The governing equations presented herein include finite rate chemistry and vaporization of multi-component liquid fuels for aerospace propulsion applications.

1.2 The numerical method is based on a finite volume method that includes an incremental pressure equation for conservation of mass.

Turbulence field is described using multiple-time-scale turbulence equations.

1.3 Applications of charged droplets

Industrial applications

spray painting,
aerosols,
fabrication of solar panels,
dust collecting mechanisms.

Combustion applications

control of dispersion of chraged fuel droplets in liquid fuel combustors.

uniform dispersion of charged fuel droplets due to Coulomb force.

charge induced secondary atomization in flames.

II. Theoretical analysis

2.1 Gas phase conservation equations in axisymmetric coordinates

(a) Favre-averaged conservation of mass equation

$$\frac{\partial \bar{\rho}}{\partial t}+\frac{\partial}{\partial x}\left(\bar{\rho}\tilde{u}\right)+\frac{1}{r}\frac{\partial}{\partial r}\left(r\bar{\rho}\tilde{v}\right)=\dot{m}$$

(b) Favre-averaged conservation of momentum equations

$$\frac{\partial}{\partial t}\left(\bar{\rho}\tilde{u}\right)+\frac{\partial}{\partial x}\left(\bar{\rho}\tilde{u}\tilde{u}\right)+\frac{1}{r}\frac{\partial}{\partial r}\left(r\bar{\rho}\tilde{u}\tilde{v}\right)-\frac{\partial}{\partial x}\left(\tau_{xx}\right)-\frac{1}{r}\frac{\partial}{\partial r}\left(r\tau_{xr}\right)=-\frac{\partial \tilde{p}}{\partial x}+F_x$$

$$\frac{\partial}{\partial t}\left(\bar{\rho}\tilde{v}\right)+\frac{\partial}{\partial x}\left(\bar{\rho}\tilde{u}\tilde{v}\right)+\frac{1}{r}\frac{\partial}{\partial r}\left(r\bar{\rho}\tilde{v}\tilde{v}\right)-\frac{\partial}{\partial x}\left(\tau_{rx}\right)-\frac{1}{r}\frac{\partial}{\partial r}\left(r\tau_{rr}\right)=\frac{\rho\tilde{w}^2}{r}-\frac{\tau_{\theta\theta}}{r}-\frac{\partial \tilde{p}}{\partial r}+F_r$$

$$\frac{\partial}{\partial t}\left(\bar{\rho}\tilde{w}\right)+\frac{\partial}{\partial x}\left(\bar{\rho}\tilde{u}\tilde{w}\right)+\frac{1}{r}\frac{\partial}{\partial r}\left(r\bar{\rho}\tilde{v}\tilde{w}\right)-\frac{\partial}{\partial x}\left(\tau_{\theta x}\right)-\frac{1}{r^2}\frac{\partial}{\partial r}\left(r^2\tau_{\theta r}\right)=-\frac{\bar{\rho}\tilde{v}\tilde{w}}{r}+F_\theta$$

Stress tensor

$$\underline{\underline{\tau}} = \begin{bmatrix} 2\mu_e \dfrac{\partial \tilde{u}}{\partial x} + \beta(\nabla \cdot \tilde{\mathbf{v}}) & \mu_e\left(\dfrac{\partial \tilde{u}}{\partial r} + \dfrac{\partial \tilde{v}}{\partial x}\right) & \mu_e \dfrac{\partial \tilde{w}}{\partial x} \\ & 2\mu_e \dfrac{\partial \tilde{v}}{\partial r} + \beta(\nabla \cdot \tilde{\mathbf{v}}) & r\mu_e \dfrac{\partial}{\partial r}\left(\dfrac{\tilde{w}}{r}\right) \\ (sym) & & 2\mu_e \dfrac{\tilde{v}}{r} + \beta(\nabla \cdot \tilde{\mathbf{v}}) \end{bmatrix}$$

Interphase forces

$$\int_{t=t^n}^{t=t^{n+1}} \int_{\Delta V} F_i \, d\mathbf{x} dt = \sum_{k=1}^{Np} \left[n_k \int_{t=t^n}^{t=t^{n+1}} \left\{ \frac{1}{2} c_D \rho \left| \mathbf{v} - \mathbf{v}_\ell \right| \left(u_i - u_i^\ell \right) \pi r_s^2 \right\}_k dt \right]$$

$$+ \sum_{k=1}^{Np} \left[n_k \int_{t=t^n}^{t=t^{n+1}} \dot{m}_k u_i^\ell \, dt \right]$$

(c) Conservation of energy equation

$$\frac{\partial}{\partial t}\left(\overline{\rho}\tilde{h}\right)+\frac{\partial}{\partial x}\left(\overline{\rho}\tilde{u}\tilde{h}\right)+\frac{1}{r}\frac{\partial}{\partial r}\left(r\overline{\rho}\tilde{v}\tilde{h}\right)-\frac{\partial}{\partial x}\left(\alpha_e\frac{\partial\tilde{h}}{\partial x}\right)-\frac{1}{r}\frac{\partial}{\partial r}\left(r\alpha_e\frac{\partial\tilde{h}}{\partial r}\right)$$

$$=\frac{Dp}{Dt}+\mu_e\Phi+\frac{\partial}{\partial x}\left[\sum_{k=1}^{N_S}\tilde{h}_k\left\{\overline{\rho}\left(D_k+D_{kt}\right)-\alpha_e\right\}\frac{\partial\tilde{Y}_k}{\partial x}\right]$$

$$+\frac{1}{r}\frac{\partial}{\partial r}\left[\sum_{k=1}^{N_S}r\tilde{h}_k\left\{\overline{\rho}\left(D_k+D_{kt}\right)-\alpha_e\right\}\frac{\partial\tilde{Y}_k}{\partial r}\right]+H$$

Dissipation function

$$\Phi=\left[2\left(\frac{\partial\tilde{u}}{\partial x}\right)^2+2\left(\frac{\partial\tilde{v}}{\partial r}\right)^2+2\left(\frac{\tilde{v}}{r}\right)^2+\left(\frac{\partial\tilde{u}}{\partial r}+\frac{\partial\tilde{v}}{\partial x}\right)^2\right]-\frac{2}{3}(\nabla\cdot\tilde{\mathbf{v}})^2+\left(\frac{\partial\tilde{w}}{\partial x}\right)^2+\left\{r\frac{\partial}{\partial r}\left(\frac{\tilde{w}}{r}\right)\right\}^2$$

Inter-phase energy exchange term

$$\int_{t=t^n}^{t=t^{n+1}}\int_{\Delta V}H\,d\mathbf{x}dt=\sum_{k=1}^{N_p}\left\{n_k\left\{\Delta\left(m_{\ell,k}h_{\ell,k}\right)-\left(\Delta m_{\ell,k}\right)L_H\right\}\right\}$$

(d) Conservation of chemical species

$$\frac{\partial}{\partial t}\left(\bar{\rho}\tilde{Y}_k\right)+\frac{\partial}{\partial x}\left\{\bar{\rho}\left(\tilde{u}+\tilde{U}_k\right)\tilde{Y}_k\right\}+\frac{1}{r}\frac{\partial}{\partial r}\left\{r\bar{\rho}\left(\tilde{v}+\tilde{V}_k\right)\tilde{Y}_k\right\}=\dot{\tilde{w}}_k+\dot{m}\Psi_k$$

Chemical reaction terms

$$\dot{\tilde{w}}_k=\sum_{i=1}^{N_r}M_k\left(\nu''_{k,i}-\nu'_{k,i}\right)\tilde{\omega}_i$$

$$\tilde{\omega}_i=k_{f,i}\prod_{j=1}^{N_S}\tilde{c}_j^{\,\nu'_{j,i}}-k_{b,i}\prod_{j=1}^{N_S}\tilde{c}_j^{\,\nu''_{j,i}}$$

Inter-phase source terms

$$\Psi_k=Y_{vsk}+\left(1-Y_{vs}\right)\frac{Y_{vsk}-Y_{v\infty k}}{Y_{vs}-Y_{v\infty}}$$

2.2 Equations of motion for discrete phase

(a) Lagrangian description of droplet equations of motion

$$\frac{d\mathbf{x}_d}{dt} = \mathbf{v}_d$$

$$m_d \frac{du_d}{dt} = \frac{1}{2} c_D \rho |\mathbf{v} - \mathbf{v}_d| (u - u_d) \pi r_s^2 + m_d b_x$$

$$m_d \frac{dv_d}{dt} = \frac{1}{2} c_D \rho |\mathbf{v} - \mathbf{v}_d| (u - u_d) \pi r_s^2 + m_d \frac{w_d^2}{y_d} + m_d b_y$$

$$m_d \frac{dw_d}{dt} = \frac{1}{2} c_D \rho |\mathbf{v} - \mathbf{v}_d| (u - u_d) \pi r_s^2 - m_d \frac{v_d w_d}{y_d} + m_d b_z$$

Electrostatic and Coulomb Forces

$$\mathbf{b} = \begin{Bmatrix} b_x \\ b_y \\ b_z \end{Bmatrix} = -q\nabla\phi + \sum_{\substack{k=1 \\ k\neq j}}^{N_p} \frac{1}{4\pi\varepsilon_o} \frac{q_j q_k}{R_{jk}^3} \mathbf{R}_{jk}$$

where

$$\mathbf{R}_{jk} = \mathbf{x}_j - \mathbf{x}_k$$

$$R_{jk} = \left|\mathbf{R}_{jk}\right|$$

(b) Conservation equations for droplets

Droplet regression rate

$$\frac{d}{dt}\left(\frac{4}{3}\pi r_s^3 \rho_\ell\right) = -f(R_{e\ell}, P_n)\dot{m}_\ell$$

Conservation of Energy equation

$$\frac{\partial}{\partial t}(\rho_\ell h_\ell) - \frac{1}{r^2}\frac{\partial}{\partial r}\left\{r^2 \alpha_\ell \frac{\partial h_\ell}{\partial r}\right\} = 0$$

B.C. on droplet surface

$$4\pi r^2 \alpha_\ell \frac{\partial h_\ell}{\partial r} = 4\pi r^2 c_h\left(T_\infty - T_{s^-}\right) - \dot{m}_\ell L_H \text{ at } r = r_s^-$$

Conservation of liquid species

$$\frac{\partial}{\partial t}(\rho_\ell Y_{\ell k}) - \frac{1}{r^2}\frac{\partial}{\partial r}\left\{r^2 D_\ell \frac{\partial}{\partial r}(\rho_\ell Y_{\ell k})\right\} = 0$$

B.C. on droplet surface

$$4\pi r^2 \rho_\ell D_\ell \frac{\partial Y_{\ell k}}{\partial r} = \dot{m}_\ell Y_{\ell k} - \dot{m}_\ell \Psi_k \text{ at } r = r_s-$$

The volatility of different liquid phase chemical species can be resolved by solving the conservation equations of the liquid species.

For *aeropropulsion applications,* vapor-liquid equilibrium in sub- and super-critical environments needs to be considered to resolve the vaporization of liquid species correctly.

III. Two-Phase Turbulent Flow of Charged Droplets in Electrostatic Field[*1]

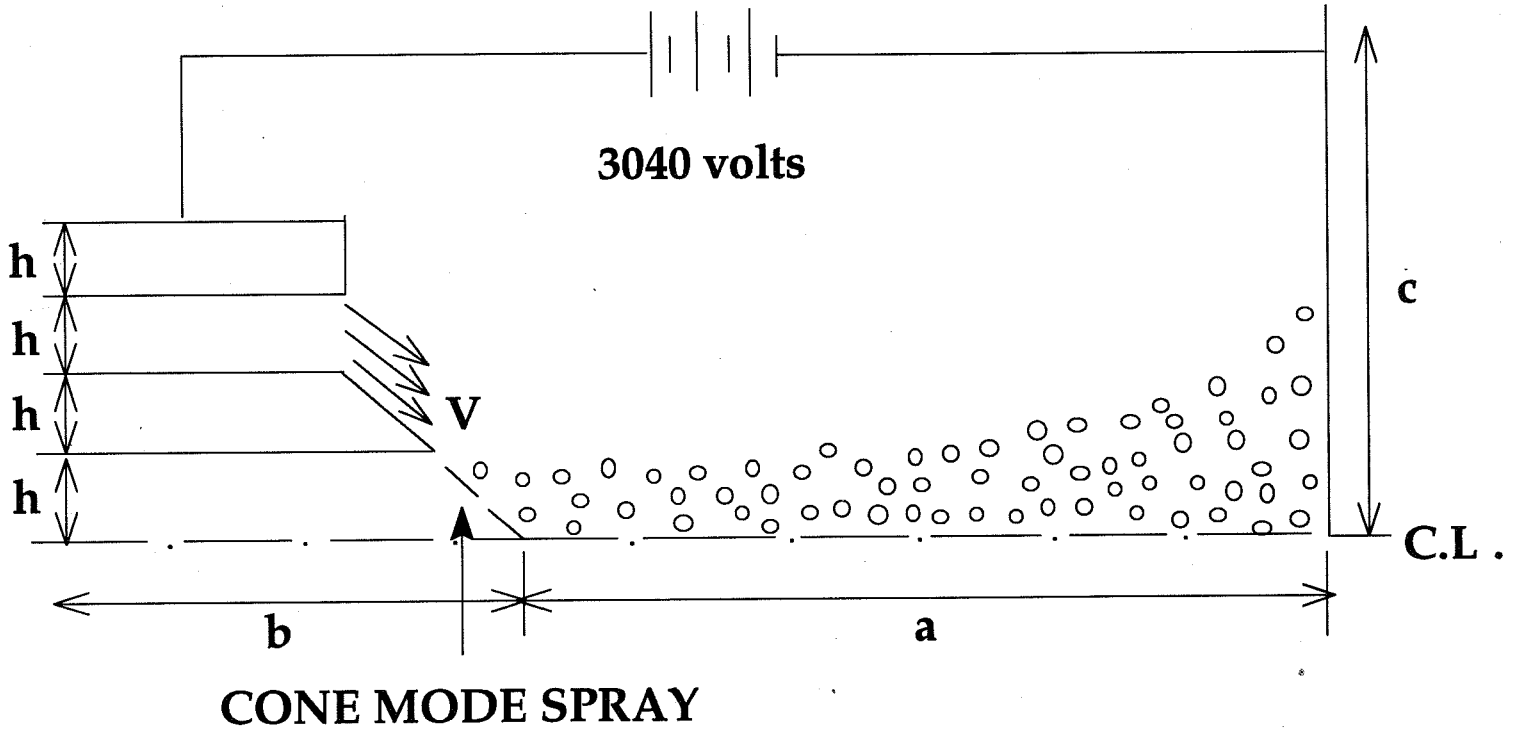

*1 Ganan-Calvo, A. M. et al., J. Aerosol Sci., vol. 25, 00.1121-1142, 1994

3.1 Charged Droplets

Mean diameter (d):	**40 μm**
Standard deviation (RMS) in sizes:	**0.20**
Sauter mean diameter (SMD)	**45 μm**
Volumetric flow rate of liquid	**2.3×10^{-9} m^3/sec**
Inner diameter of injection needle	**0.00025 m**
Length of Injection needle	**0.028 m**
Initial injection velocity (Droplets are accelerated by airjet*1)	**0.0117 m/sec**
Applied electric potential difference	**3040 volts**
Total current by charged droplets (I)	**4.3×10^{-8} Ampere**
Mean charge ($\bar{q}$=I/number flow rate)	**6.74×10^{-13} Coul**
Charge for a droplet*2	$q_j = \bar{q}\left(d_j / \bar{d}\right)^3$

***1 Ganan-Calvo, A. M., Private communication, 1995.**

***2 Gomez, A. and Tang, K., *Physics of Fluids*, vol. 6, pp. 404-414, 1994.**

3.2 Quasi 3-dimensional analysis of droplets

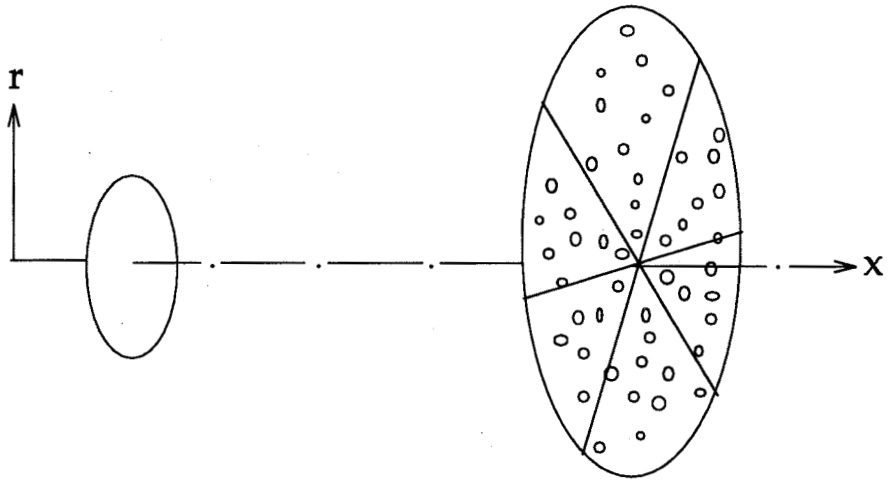

Due to the Coulomb force between charged droplets, axisymmetric representation of the discrete phase is not applicable.

Injection of numerical droplets

1. Deterministic injection

Charged droplets are injected at 6 circumferential sectors and 25 injection locations per circumferential sector based on guessed statistical distribution.

2. Injection using random number generator

Injection locations (x_{inj}, r_{inj}, and θ_{inj}) injection velocity of particles (V_{inj}) are calculated using a random number generator.

3.3 Particle number flow rates at injection locations

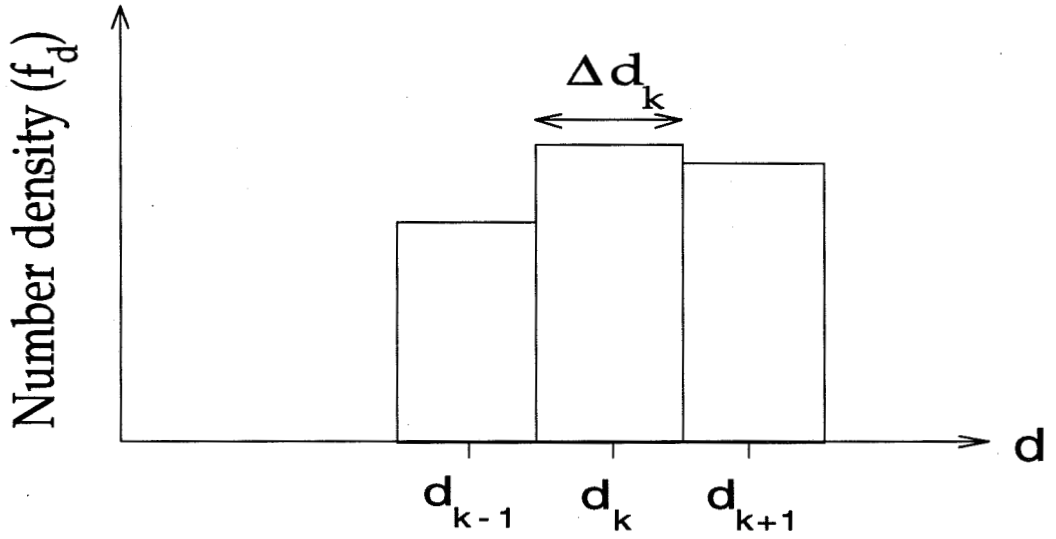

Normalized number flow rate for droplets (or particles) for size d_k

$$\hat{N}_k = f_d(d_k)\Delta d_k$$

Total number flow rate of droplets (or particles) for size d_k

$$N_{k,t} = \hat{N}_k \left(V_{fr} / V_{ns} \right)$$

where

$$V_{ns} = \sum_{k=1}^{N_s} \left\{ \pi (d_k / 6)^3 \hat{N}_k \right\}$$

V_{fr}: **total volumetric flow rate of discrete pahse**

N_s: **number of size groups**

Number flow rate of drop size d_k at injection location r_j $\left(N_{k,j}\right)$

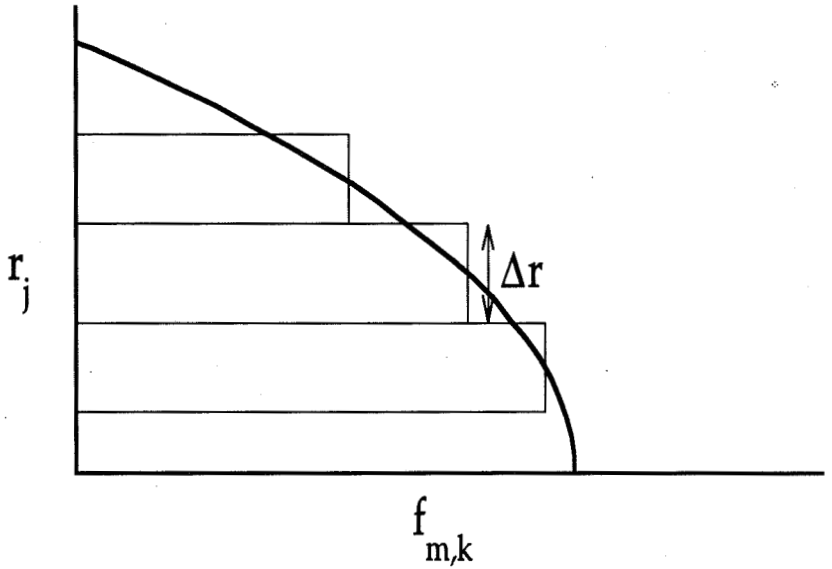

$f_{m,k}$: **mass flow rate of** d_k **across the inlet boundary**

$$N_{k,j} = \frac{2\pi r_j \Delta r_j f_{m,k}(r_j)}{\sum_{i=1}^{N_{inj}} 2\pi r_i \Delta r_i f_{m,k}(r_i)} N_{k,t}$$

N_{inj}: **number of injection locations across the inlet boundary**

3.4 Computational domain

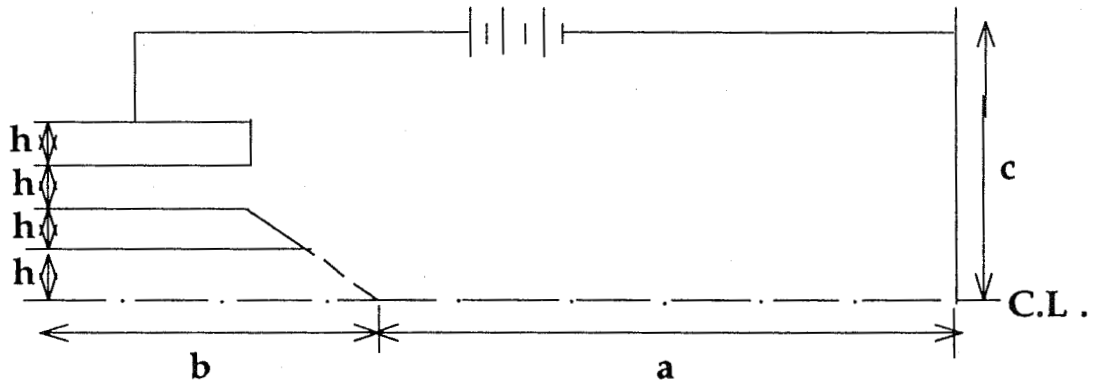

a: 0.0254 m
c: 0.0254 m
h: 0.00025 m

(a) Electrostatic potential field (81x67 mesh)

b: 0.014 m

(b) Flow domain with charged droplets (101x67 mesh)

b: 0.001 m

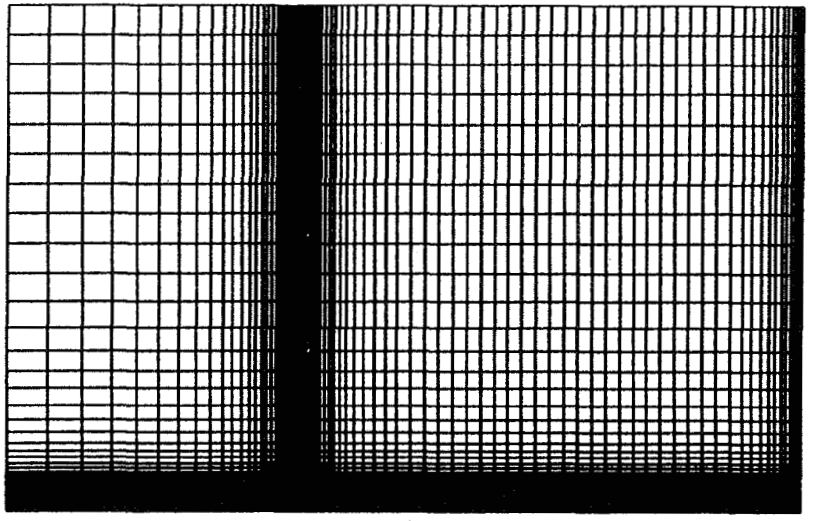

Computational domain for electrostatic field

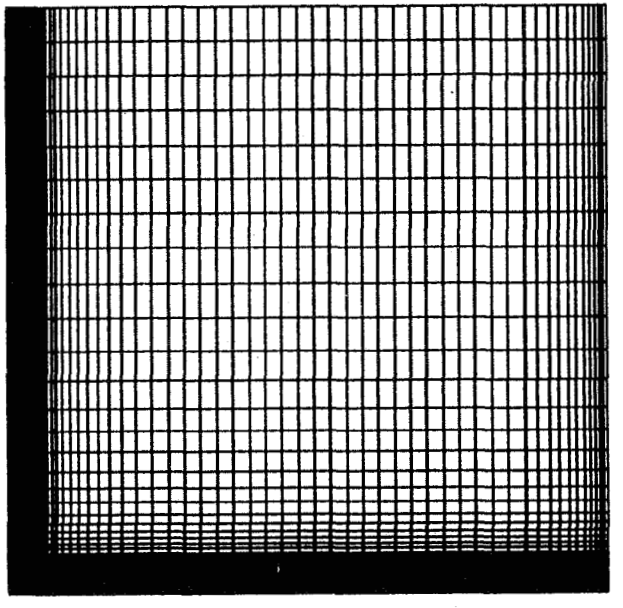

Computational domain for two-phase turbulent flow

Calculated Electrostatic potential field (With $\partial\phi / \partial n = 0$ boundary condition on west side)

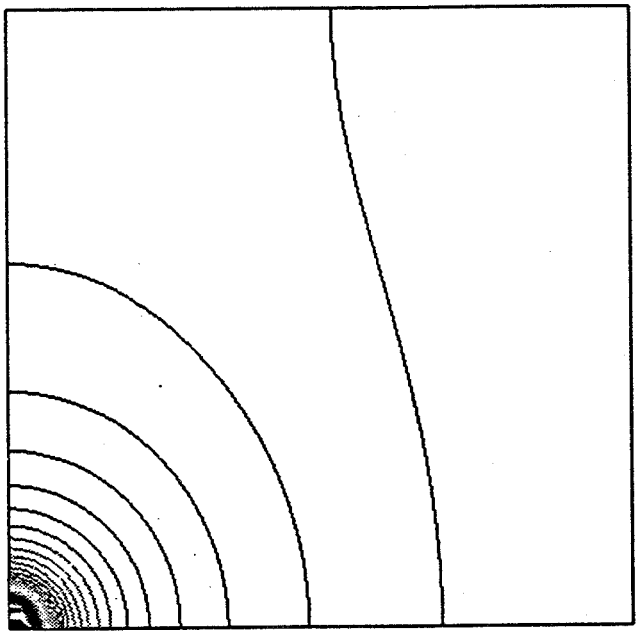

(a) Incorrect computational domain

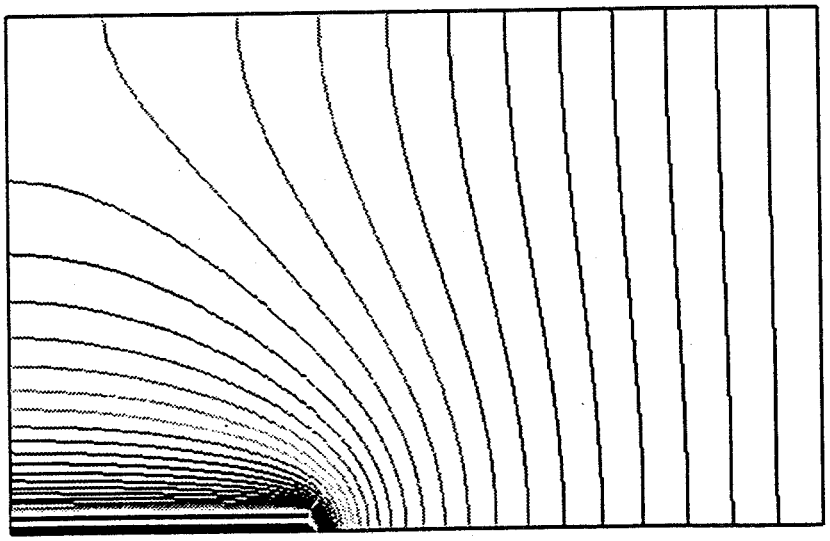

(b) Correct computational domain

Domain dependence of the electrostatic potential field

Consider

$$\nabla^2\phi = 0 \text{ in } \Omega \qquad \textbf{(a)}$$

with b.c.'s $\phi = \bar{\phi}$ in $\partial\Omega_1$ **and** $\partial\phi/\partial n = q$ in $\partial\Omega_2$**.The solution is given as**

$$\phi(\xi)\big|_{\xi\in\Omega} = \int_{\partial\Omega_1\cup\partial\Omega_1} \left(\phi^* \frac{\partial\phi}{\partial n} - \phi\frac{\partial\phi^*}{\partial n}\right) d\Omega \qquad \textbf{(b)}$$

where ϕ^* **is a fundamental solution of** $\nabla^2\phi^* = -\delta\left(\vec{x} - \vec{\xi}\right)$.*1

Eq. (b) indicates that a correct $\partial\phi/\partial n$ **needs to be prescribed at the west side boundary. However,** $\partial\phi/\partial n$ **is not known a priori. In case** $\partial\phi/\partial n = 0$ **b.c. is prescribed on the west side boundary, it needs to be located at the middle of the needle.**

*1 S.-W. Kim, *Int. J. Numer. Fluids,* vol. 3, pp. 481-491, 1983.

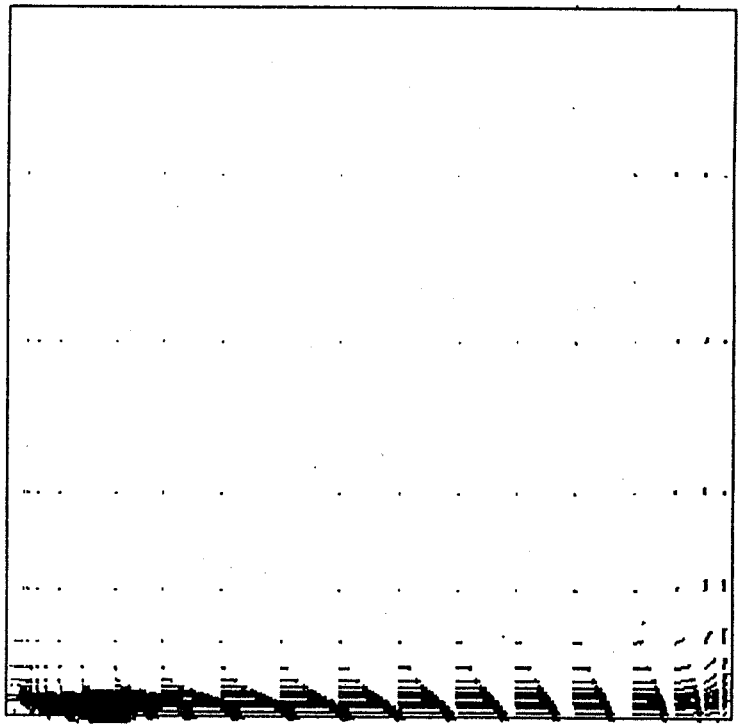

Calculated velocity vectors for airjet injected parallel to x-axis (b.c.'s for airjet is not known)

Dispersion of charged droplets in turbulent flow (superposition of 6 snap shots)

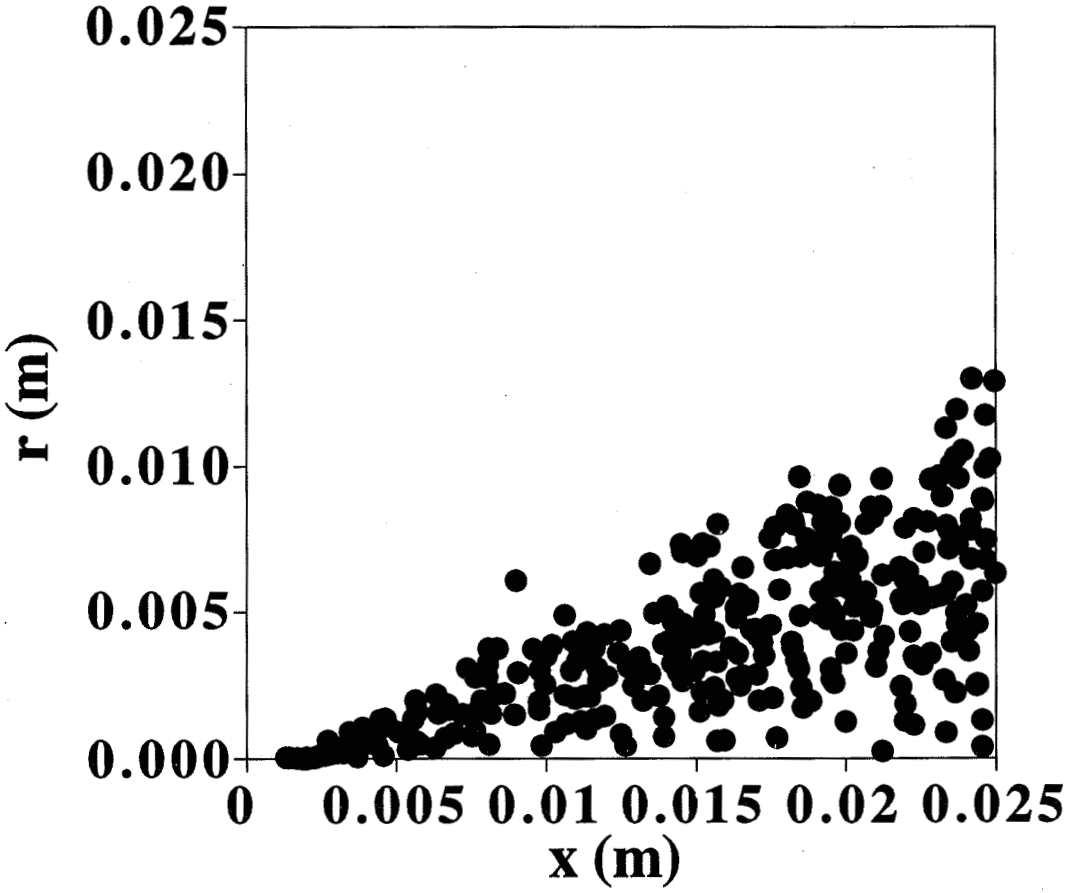

diameter of droplets (μm)

• 33.6, • 36.8, • 40.0, • 43.2, • 46.4

IV. Conclusions and discussion

Successfully developed a numerical method to solve two-phase turbulent flows with charged particles.

Calculated results show that the extent of particle dispersion is mostly determined at and near the injection location. (Particle dispersion is strongly influenced by the Coulomb force.)

Detailed measured data are necessray for further theoretical investigation of two-phase, reacting and nonreacting, turbulent flows with charged droplets.

Gas/Gas Injector Technology Program

699

Kevin Tucker/MSFC
Bryan Palaszewski/LeRC
Bob Santoro/Penn State
Shahram Farhangi/Rocketdyne
April 26, 1995

National Aeronautics and
Space Administration

Gas/Gas Injector Technology Program

Computational Fluid Dynamics Branch
Fluid Dynamics Division
Structures and Dynamics Laboratory
George C. Marshall Space Flight Center

Overview

- Introduction
- Objectives
- Approach
  - Guidelines
  - Technical Issues
    - Gas/Gas Injector Issues
    - Test Program Logic
    - Team Participants/Responsibilities
    - Measurements
    - Numerical Modeling/Code Validation
    - Test Hardware
    - Test Facilities
  - Programmatic Issues
    - Contractual Vehicles
    - Funding
- Summary

INTRODUCTION

- **Why gas/gas injectors?**
  - Requirement to reduce launch costs led to Single Stage to Orbit selection for RLV
  - Staged combustion used to meet performance requirements
  - Mixed (Ox-rich & fuel-rich) preburners for:
    - Lower cost pumps
    - Lower temperatures (Ox-rich)
    - Longer turbine life
  - These needs lead to full-flow staged combustion cycle with gas/gas main injector

INTRODUCTION

- **Key gas/gas technology issues**
  - Mixing/performance
  - Injector face cooling
  - Injector/manifold sizing
  - Injector material/hot-oxidizer compatibility (covered in current NRA)
  - Stability

- **Current database for gas/gas injectors is limited**
  - Aerojet (uni- & multi-elements in subscale chamber)-1973
  - Rocketdyne Advanced Engine Aerospike
  - Rocketdyne Advanced Maneuvering Propulsion Technology
  - Penn State uni-element coax for CFD validation (ETO funded)

Gas/Gas Injector Technology Program

Computational Fluid Dynamics Branch
Fluid Dynamics Division
Structures and Dynamics Laboratory
George C. Marshall Space Flight Center

OBJECTIVES

The overall program objective is to increase the ability of the rocket engine community to design efficient, high-performance, durable gas/gas injectors relevant to RLV requirements. Specifically:

- Provide Rocketdyne with data on preliminary gas/gas injector designs which will enable discrimination among candidate injector designs in a timely manner for design & testing in 40k gas/gas demonstrator.

- Enhance the national gas/gas injector database by obtaining high-quality data that:
  - Increases the understanding of gas/gas injector physics
  - Is suitable for CFD code validation for gas/gas injectors

- Validated CFD codes for future gas/gas injector design in the RLV program

APPROACH

• Guidelines

- Meet the above-noted program objectives in a timely manner without additional funding
- Redirect existing tasks to focus on gas/gas technology
- Leverage Rocketdyne IR&D

APPROACH

•Technical Issues

- Gas/Gas Injector Issues

•Mixing

- Proper injector design is key to high performance
- Gas/gas injector mixing correlations are limited
- Limited available data indicates 96-98% C* efficiency is possible
- Injector element & pattern configuration studies req'd to develop high-performance injector

•Injector Face Cooling

- Previous gas/gas injectors produced high head end heat flux
- Injector face will require special cooling attention

NOTE: As usual, there is a trade-off between mixing/efficiency and head end heat flux.

APPROACH

- **Technical Issues**
  - Test Program Logic

    - **Multi-element screening**
      - Both intra- and inter-element mixing are important
      - 4-6 elements to be tested in realistic pattern relevant to RLV
      - No geometric or condition parametrics

    - **Single-element parametrics**
      - Select best performers from multi-element screening
      - Obtain detailed measurements of baseline designs
      - Make measurements of several geometric and condition parametrics

    - **Multi-element optimization**
      - Test "best" candidate from single parametric studies in multi-element configuration
      - Rocketdyne will use information to design injector for 40k demonstrator

Gas/Gas Injector Technology Program

Computational Fluid Dynamics Branch
Fluid Dynamics Division
Structures and Dynamics Laboratory
George C. Marshall Space Flight Center

APPROACH

- **Technical Issues**
  - Participants/Responsibilities

- **Marshall Space Flight Center**
  - Project Technical Lead
  - Numerical modeling
  - Possible cold flow testing

- **Rocketdyne**
  - Design & fab of Rkdn injectors
  - Diagnostics support @ LeRC & PSU
  - Supply windowed combustor

- **Lewis Research Center**
  - Multi-element injector testing
  - Team injector design
  - Team injector fabrication

- **Penn State University**
  - Single-element injector testing
  - Team injector design
  - Team injector fabrication

Gas/Gas Injector Technology Program

Computational Fluid Dynamics Branch
Fluid Dynamics Division
Structures and Dynamics Laboratory
George C. Marshall Space Flight Center

APPROACH

- **Technical Issues**
  - Single Element Testing at Penn State

- **Test Conditions**
  - 1000 psi P_c
  - total flow rate = 0.25 lb/sec
  - ambient O_2 and H_2
  - main stage duration 4 sec.
  - standard test data to be taken-flow rates, pressures, temperatures

- **Diagnostics**
  - Ultraviolet imaging--measures OH radical & thus indicates combustion zone location
  - Schlieren imaging--gives qualitative information on mixing
  - Raman spectroscopy--maps species location & thus quantifies mixing
  - LDV --maps mean and fluctuating velocities over entire flowfield
  - Temperature on injector face--thermocouple on injector face

APPROACH

- **Technical Issues**
  - Multi-Element Testing at LeRC

- **Test Conditions**
  - 1000 psi P_c
  - total flow rate = 4 lb/sec
  - ambient O_2 and H_2
  - main stage duration 2 sec.
  - standard test data to be taken-flow rates, pressures, temperatures

- **Diagnostics**
  - Ultraviolet imaging--measures OH radical & thus indicates combustion zone location
  - Schlieren imaging--gives qualitative information on mixing
  - Raman spectroscopy--maps species location & thus quantifies mixing
  - Temperature on injector face--thermocouple on injector face

APPROACH

•Technical Issues

- Numerical Modeling/Code Validation @ MSFC

•Selected single- & multi-element cases will be modeled by ED32

•Based on preliminary benchmark cases, the FDNS code has been selected for the numerical modeling/code validation. The FDNS code is currently being used in-house & has the following relevant capabilities:

- Pressure-based, time accurate, all speed flow solver
- 2D/3D, multi-zonal, general curvilinear coordinates
- High order spatial discretization schemes
- Four 2-equation turbulence models
- Multi-species, chemically combusting
- Conjugate heat transfer
- Ideal gas, real gas

APPROACH

•Technical Issues

- Test Hardware

•Single-element testing to be done in Penn State optically accessible modular rocket

•Multi-element testing to be done in Rocketdyne windowed combustor (to be loaned to LeRC)

•Injectors

- 2 proprietary Rocketdyne injectors
- 3 Team, or public domain, injectors. Current candidates include:
  - F-O-F triplet
  - O-F-O triplet
  - Swirl coax
  - Shear coax
  - Counter-rotating swirl triax

Gas/Gas Injector Technology Program

Computational Fluid Dynamics Branch
Fluid Dynamics Division
Structures and Dynamics Laboratory
George C. Marshall Space Flight Center

APPROACH

- **Technical Issues**
  - Test Facilities

    - **Single-element Testing @ PSU**
      - PERC Cryogenic Combustion Laboratory
      - Essentially no facility modifications required

    - **Multi-element Testing @ LeRC**
      - Rocket Test Facility (Cell 32)
      - Facility modifications include:
        - Line to allow use of GO_2 from portable trailer
        - High-pressure H_2O cooling system for nozzle cooling
        - H_2 burn-off igniters
        - H_2 and O_2 regulators and miscellaneous seals

Gas/Gas Injector Technology Program

Computational Fluid Dynamics Branch
Fluid Dynamics Division
Structures and Dynamics Laboratory
George C. Marshall Space Flight Center

APPROACH

- **Programmatic Issues**

  - Contractual Vehicles
    - Rocketdyne Participation - modification of Cooperative Agreement
    - Penn State Participation - redirection of existing RLV Core Technology task
    - LeRC Use of Rocketdyne hardware - Space Act Agreement

  - Funding
    - Rocketdyne - IR&D
    - Penn State - MSFC RLV Core Technology
    - LeRC - Headquarters Code X (Office of Space Access and Technology)

National Aeronautics and Space Administration

Gas/Gas Injector Technology Program

Computational Fluid Dynamics Branch
Fluid Dynamics Division
Structures and Dynamics Laboratory
George C. Marshall Space Flight Center

SUMMARY

- A Gas/Gas Injector Technology Team has been formed
- Identified the relevant gas/gas injector technology issues
- Devised a test strategy to make appropriate, discriminating measurements in both single- and multi-element hot-fire environments. If the program plan is completed, the data obtained will meet the program objectives and fit the assigned program guidelines.
- Most scaling issues have been resolved
- Element selection and preliminary element design is complete
- Final design on Rocketdyne element is complete
- Data has been taken on shear coax element at PSU

REPORT DOCUMENTATION PAGE

Form Approved
OMB No. 0704-0188

1. AGENCY USE ONLY (Leave Blank)	2. REPORT DATE	3. REPORT TYPE AND DATES COVERED
	March 1996	Conference Publication

4. TITLE AND SUBTITLE

Thirteenth Workshop for Computational Fluid Dynamic Applications in Rocket Propulsion and Launch Vehicle Technology

5. FUNDING NUMBERS

6. AUTHOR(S)

R.W. Williams, Compiler

7. PERFORMING ORGANIZATION NAME(S) AND ADDRESS(ES)

George C. Marshall Space Flight Center
Marshall Space Flight Center, Alabama 35812

8. PERFORMING ORGANIZATON REPORT NUMBERS

9. SPONSORING/MONITORING AGENCY NAME(S) AND ADDRESS(ES)

National Aeronautics and Space Administration
Washington, DC 20546-0001

10. SPONSORING/MONITORING AGENCY REPORT NUMBER

NASA CP-3332
Volume I

11. SUPPLEMENTARY NOTES

Prepared by Structures and Dynamics Laboratory, Science and Engineering Directorate.

12a. DISTRIBUTION/AVAILABILITY STATEMENT

Unclassified-Unlimited
Subject Category 34

12b. DISTRIBUTION CODE

13. ABSTRACT *(Maximum 200 words)*

This conference publication includes various abstracts and presentations given at the 13th Workshop for Computational Fluid Dynamic Applications in Rocket Propulsion and Launch Vehicle Technology held at the George C. Marshall Space Flight Center April 25-27, 1995. The purpose of the workshop was to discuss experimental and computational fluid dynamic activities in rocket propulsion and launch vehicles. The workshop was an open meeting for government, industry, and academia. A broad number of topics were discussed including computational fluid dynamic methodology, liquid and solid rocket propulsion, turbomachinery, combustion, heat transfer, and grid generation.

14. SUBJECT TERMS	15. NUMBER OF PAGES
computational fluid dynamics, rocket propulsion, launch vehicle technology, liquid rocket, solid rocket, turbopump, turbomachinery, combustion, methodology, impeller, inducer, heat transfer, grid generation, nozzle, plume spray, injector	689
	16. PRICE CODE A99

17. SECURITY CLASSIFICATION	18. SECURITY CLASSIFICATION OF THIS PAGE	19. SECURITY CLASSIFICATION OF ABSTRACT	20. LIMITATION OF ABSTRACT
Unclassified	Unclassified	Unclassified	Unclassified

National Aeronautics and
Space Administration
Code JTT
Washington, DC
20546–0001

Official Business
Penalty for Private Use, $300

Postmaster: If Undeliverable (Section 158 Postal Manual), Do Not Return